ISOTOPE TECHNIQUES IN GROUNDWATER HYDROLOGY 1974

PROCEEDINGS OF A SYMPOSIUM
VIENNA, 11-15 MARCH 1974

VOL.II

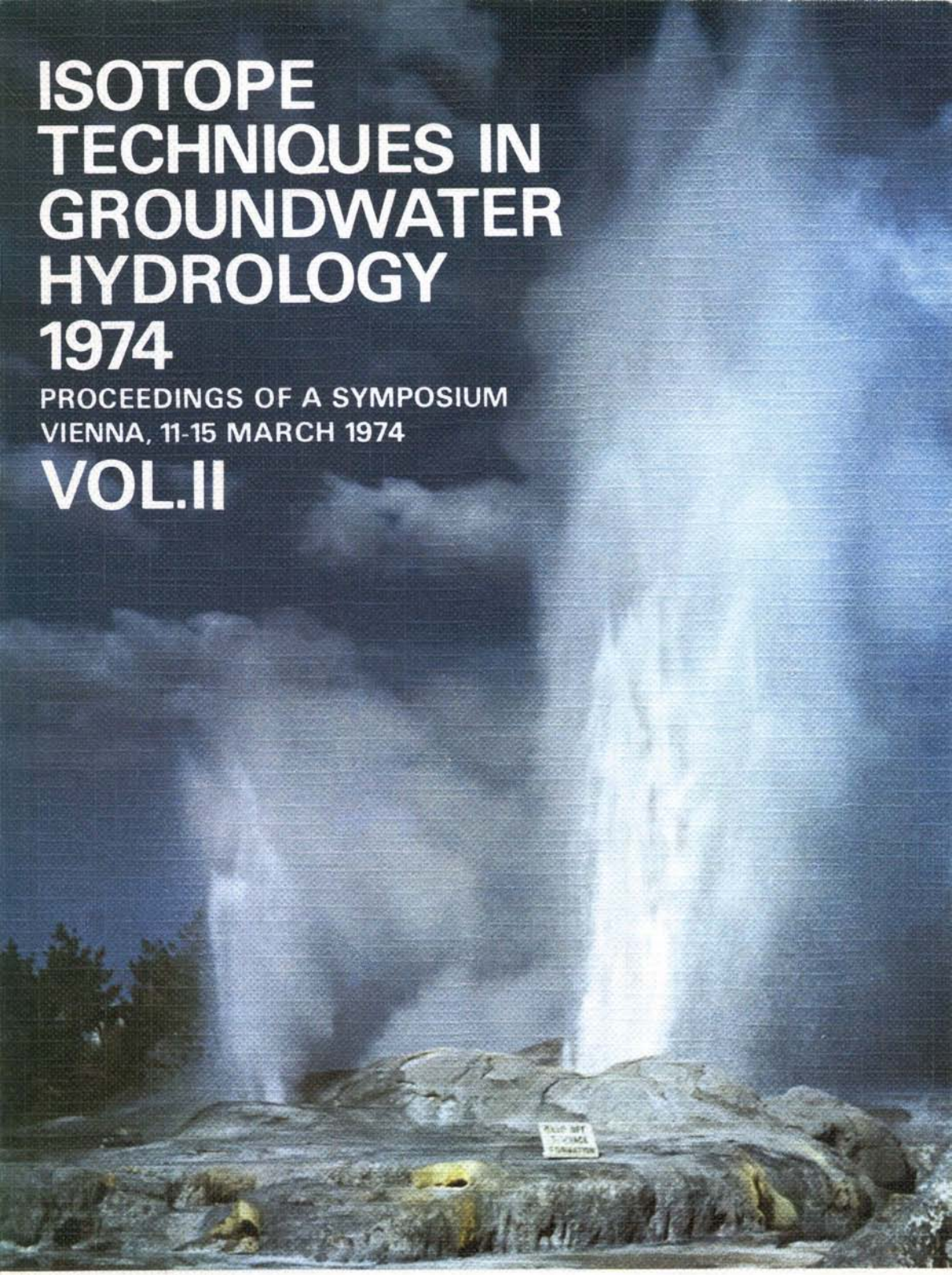

INTERNATIONAL ATOMIC ENERGY AGENCY, VIENNA, 1974

SYMPOSIUM ON ISOTOPE TECHNIQUES IN
AN: 048990-V.002
UN: 551.49 S989

00000380911

48990

38091

ISOTOPE TECHNIQUES IN GROUNDWATER HYDROLOGY 1974

VOL. II

The following States are Members of the International Atomic Energy Agency:

AFGHANISTAN
ALBANIA
ALGERIA
ARGENTINA
AUSTRALIA
AUSTRIA
BANGLADESH
BELGIUM
BOLIVIA
BRAZIL
BULGARIA
BURMA
BYELORUSSIAN SOVIET SOCIALIST REPUBLIC
CAMEROON
CANADA
CHILE
COLOMBIA
COSTA RICA
CUBA
CYPRUS
CZECHOSLOVAK SOCIALIST REPUBLIC
DENMARK
DOMINICAN REPUBLIC
ECUADOR
EGYPT, ARAB REPUBLIC OF
EL SALVADOR
ETHIOPIA
FINLAND
FRANCE
GABON
GERMAN DEMOCRATIC REPUBLIC
GERMANY, FEDERAL REPUBLIC OF
GHANA
GREECE
GUATEMALA
HAITI
HOLY SEE
HUNGARY
ICELAND
INDIA
INDONESIA
IRAN
IRAQ
IRELAND
ISRAEL
ITALY
IVORY COAST
JAMAICA
JAPAN
JORDAN
KENYA
KHMER REPUBLIC
KOREA, REPUBLIC OF
KUWAIT
LEBANON
LIBERIA
LIBYAN ARAB REPUBLIC
LIECHTENSTEIN
LUXEMBOURG
MADAGASCAR
MALAYSIA
MALI
MEXICO
MONACO
MONGOLIA
MOROCCO
NETHERLANDS
NEW ZEALAND
NIGER
NIGERIA
NORWAY
PAKISTAN
PANAMA
PARAGUAY
PERU
PHILIPPINES
POLAND
PORTUGAL
ROMANIA
SAUDI ARABIA
SENEGAL
SIERRA LEONE
SINGAPORE
SOUTH AFRICA
SPAIN
SRI LANKA
SUDAN
SWEDEN
SWITZERLAND
SYRIAN ARAB REPUBLIC
THAILAND
TUNISIA
TURKEY
UGANDA
UKRAINIAN SOVIET SOCIALIST REPUBLIC
UNION OF SOVIET SOCIALIST REPUBLICS
UNITED KINGDOM OF GREAT BRITAIN AND NORTHERN IRELAND
UNITED STATES OF AMERICA
URUGUAY
VENEZUELA
VIET-NAM
YUGOSLAVIA
ZAIRE, REPUBLIC OF
ZAMBIA

The Agency's Statute was approved on 23 October 1956 by the Conference on the Statute of the IAEA held at United Nations Headquarters, New York; it entered into force on 29 July 1957. The Headquarters of the Agency are situated in Vienna. Its principal objective is "to accelerate and enlarge the contribution of atomic energy to peace, health and prosperity throughout the world".

Printed by the IAEA in Austria
September 1974

PROCEEDINGS SERIES

ISOTOPE TECHNIQUES IN GROUNDWATER HYDROLOGY 1974

PROCEEDINGS OF A SYMPOSIUM
ORGANIZED BY THE
INTERNATIONAL ATOMIC ENERGY AGENCY
AND HELD IN VIENNA,
11-15 MARCH 1974

In two volumes

VOL. II

INTERNATIONAL ATOMIC ENERGY AGENCY
1974 -12 10
LIBRARY

INTERNATIONAL ATOMIC ENERGY AGENCY
VIENNA, 1974

ISOTOPE TECHNIQUES IN GROUNDWATER HYDROLOGY 1974
IAEA, VIENNA, 1974
STI/PUB/373

FOREWORD

This symposium, held in Vienna on 11-15 March, 1974, was the fourth on the subject of isotope hydrology organized by the International Atomic Energy Agency. However, this one was limited to groundwater hydrology in view of the general increase of interest and activity in isotope hydrology since the previous meeting in 1970.

The proceedings of this symposium are a good indicator of the present world status of these techniques. Thus one notes that many of the studies are in the developing areas of the world. Furthermore, there has been a shift to using these techniques as an additional applied tool in specific problems of development of water resources. Examples of such applications also give evidence of the closer collaboration between isotope specialists, who originally developed the methods, and hydrogeologists and geochemists.

It is hoped that these proceedings will contribute to a wider appreciation of the potential use of isotope techniques to hydrological problems associated with the development of groundwater for agriculture, community water supply and industry.

EDITORIAL NOTE

The papers and discussions incorporated in the proceedings published by the International Atomic Energy Agency are edited by the Agency's editorial staff to the extent considered necessary for the reader's assistance. The views expressed and the general style adopted remain, however, the responsibility of the named authors or participants.

For the sake of speed of publication the present Proceedings have been printed by composition typing and photo-offset lithography. Within the limitations imposed by this method, every effort has been made to maintain a high editorial standard; in particular, the units and symbols employed are to the fullest practicable extent those standardized or recommended by the competent international scientific bodies.

The affiliations of authors are those given at the time of nomination.

The use in these Proceedings of particular designations of countries or territories does not imply any judgement by the Agency as to the legal status of such countries or territories, of their authorities and institutions or of the delimitation of their boundaries.

The mention of specific companies or of their products or brand-names does not imply any endorsement or recommendation on the part of the International Atomic Energy Agency.

CONTENTS OF VOL. II

GEOTHERMAL WATERS (Session 5, Part 2)

Oxygen and hydrogen isotope studies of the Larderello (Italy) geothermal system (IAEA-SM-182/27) 3
C. Panichi, R. Celati, P. Noto, P. Squarci, L. Taffi, E. Tongiorgi
Discussion 28
Hot springs of the igneous terrain of Swaziland: Their noble gases, hydrogen, oxygen and carbon isotopes and dissolved ions (IAEA-SM-182/28) 29
E. Mazor, B.T. Verhagen, E. Negreanu
Discussion 45

PROBLEMS IN USING ENVIRONMENTAL ISOTOPES FOR GROUNDWATER STUDIES (Session 6)

Local variability of the isotope composition of groundwater (IAEA-SM-182/29) 51
J.R. Gat
Discussion 58
Sampling of lysimeters for environmental isotopes of water (IAEA-SM-182/51) 61
G. Sauzay
Discussion 67
Problems in ^{14}C dating of water from aquifers of deltaic origin: An example from the New Jersey coastal plain (IAEA-SM-182/31) 69
I.J. Winograd, G.M. Farlekas
Discussion 91
^{14}C evidence for the origin of arid region groundwater, Northeastern Province, Kenya (IAEA-SM-182/32) 95
F.J. Pearson, Jr., W.V. Swarzenki
Discussion 108
Radiocarbon, ^{13}C and tritium in water samples from basaltic aquifers and carbonate aquifers on the island of Oahu, Hawaii (IAEA-SM-182/33) 111
T.H. Hufen, L.S. Lau, R.W. Buddemeier
Discussion 126

ENVIRONMENTAL ISOTOPES, OTHER THAN HYDROGEN, OXYGEN AND CARBON ISOTOPES, IN GROUNDWATER STUDIES (Session 7, Part 1)

^{234}U and ^{238}U in the Carrizo sandstone aquifer of South Texas (IAEA-SM-182/35) 131
J.B. Cowart, J.K. Osmond
Discussion 148
$^{234}U/^{238}U$ disequilibrium in waters of the Judea group (Cenomanian-Turonian) aquifer in Galilee, northern Israel (IAEA-SM-182/34) 151
E. Wakshal, F. Yaron
Discussion 176
^{39}Ar dating of groundwater (IAEA-SM-182/37) 179
H. Oeschger, A. Gugelmann, H. Loosli, U. Schotterer, U. Siegenthaler, W. Wiest
Discussion 189
Distribution of sulphur isotopes of sulphates in groundwaters from the principal artesian aquifer of Florida and the Edwards aquifer of Texas, United States of America (IAEA-SM-182/39) 191
C.T. Rightmire, F.J. Pearson, Jr., W. Back, R.O. Rye, B.B. Hanshaw
Discussion 206
Utilisation des variations naturelles d'abondance de l'azote-15 comme traceur en hydrogéologie — Premiers résultats (IAEA-SM-182/40) 209
R. Létolle, A. Mariotti
Discussion 219

AQUIFER CHARACTERISTICS STUDIES (Session 7, Part 2; Session 8)

Utilisation des techniques isotopiques pour la résolution de problèmes hydrologiques en génie civil — Etude de trois cas précis (IAEA-SM-182/43) 223
P.Ch. Lévêque, J.Cl. Gros, Catherine Maurin, J. Sévérac, Cl. Viguier
Discussion 238
Application of single borehole methods in groundwater research (IAEA-SM-182/12) 241
W. Drost, F. Neumaier
Discussion 253
Modelos matemáticos simplificados para interpretación de resultados por el método de marcación de toda la columna piezométrica (IAEA-SM-182/44) 255
H.A. Múnera
Discussion 274
Theoretical possibilities of the two-well pulse method (IAEA-SM-182/45) 277
A. Zuber
Discussion 294

Determination of effective porosities by the two-well pulse method (IAEA-SM-182/46) 295
A. Kreft, A. Lenda, B. Turek, A. Zuber, K. Czauderna
Discussion 311
Investigations of effective porosity of till by means of a combined soil-moisture/density gauge (IAEA-SM-182/47) 313
L. Nordberg, S. Modig
Discussion 339
Hydrodynamic dispersion as aquifer characteristic: model experiments with radioactive tracers (IAEA-SM-182/42) 341
D. Klotz, H. Moser
Discussion 355

THEORETICAL AND EXPERIMENTAL STUDIES OF TRACER MOVEMENT IN GROUNDWATER (Session 9)

Радиоиндикаторные исследования молекулярной и конвективной диффузии в насыщенных и ненасыщенных (песчано-глинистых) породах (IAEA-SM-182/54) 359
В.Т. Дубинчук, З.Г. Колесниченко, О.Ф. Лаптева, В.С. Гончаров
Discussion 375
Analyse des informations fournies par les traceurs naturels ou artificiels dans l'étude des systèmes aquifères en hydrogéologie (IAEA-SM-182/48) 377
J. Guizerix, R. Margrita, B. Gaillard, P. Corompt, M. Alquier
Méthode pour la détermination de caractéristiques de transfert de substances polluantes dans les nappes aquifères (IAEA-SM-182/41) 405
P. Corompt, B. Gaillard, J. Guizerix, R. Margrita, J. Molinari, R. Corda, N. Crampon, D. Olivier
Discussion 421
Some conceptual mathematical models and digital simulation approach in the use of tracers in hydrological systems (IAEA-SM-182/49) 425
K. Przewłocki, Y. Yurtsever
Discussion 448
Application of digital modelling to the prediction of radioisotope migration in groundwater (IAEA-SM-182/50) 451
J.B. Robertson
Discussion 477

Chairmen of Sessions and Secretariat of the Symposium 479
List of participants 481
Author index 497

GEOTHERMAL WATERS

(Session 5, Part 2)

OXYGEN AND HYDROGEN ISOTOPE STUDIES OF THE LARDERELLO (ITALY) GEOTHERMAL SYSTEM

C. PANICHI, R. CELATI, P. NOTO,
P. SQUARCI, L. TAFFI, E. TONGIORGI
Istituto Internazionale per le Ricerche Geotermiche,
CNR-Pisa,
Pisa, Italy

Abstract

OXYGEN AND HYDROGEN ISOTOPE STUDIES OF THE LARDERELLO (ITALY) GEOTHERMAL SYSTEM.

Data collected on water and steam samples enabled a satisfactory picture of the geochemical and hydrogeological characteristics of the Larderello geothermal field to be obtained. The isotopic and chemical analyses of hot water from non-productive wells and thermal and cold springs enabled two different circulation patterns of fluids to be distinguished. The steam samples delivered from the wells show, as expected, the same deuterium content as local meteoric water, with ^{18}O enrichments ranging from 1.7 to 8‰. The geographical distribution of the $\delta^{18}O$ values of steam provides valid information about the preferential path of flow in the zone from which the geothermal fluids are derived. These flow lines are in agreement with the reconstruction of the regional hydrogeological scheme. The presence of tritium in the steam of some peripheric wells has indicated the existence of local influences of recent shallow waters on the deepest circulation. Repeated ^{18}O measurements in time of the steam samples have shown the usefulness of the isotopic survey in the control of the evolution of a geothermal field during its exploitation.

1. INTRODUCTION

The hydrogen and oxygen composition of the water has been analysed in samples from the most important geothermal fields in the world [1-3], including the Larderello area [1, 4].

In all cases the D/H ratio was shown to be the same in all the hot water or steam samples from a single area, and the same as the average value of the meteoric water of the region. The oxygen, on the contrary, was generally found to be enriched by different amounts of ^{18}O isotope compared with the meteoric water of the region, as a result of the isotopic exchanges at high temperature between the oxygen of the water and that of the rocks where deep circulation took place. When deep circulation occurs in carbonate rocks the isotopic exchange is often very evident. It is obvious that with increasing residence time the $^{18}O/^{16}O$ ratios in the water will approach more and more the equilibrium with the same ratio in the rocks.

As a wide range of ^{18}O enrichments was observed in the Larderello area, a systematic study of the whole Larderello geothermal area was considered useful to geohydrological research. It can, in fact, provide some suggestions regarding deep circulation patterns, and the interaction between the deep circulation waters and those infiltrating in permeable rocks outcropping in the neighbourhood of the field. Furthermore, the local waters appear to be a convenient target for the tritium content in respect to the deep waters. Variable tritium contents are reported by Banwell [5] for the hot water systems of New Zealand, by White and

co-workers [6] for the geothermal system of Steamboat Springs, Nevada, and by Koga [7] for the geothermal well waters at Otake, Japan. This was explained as a result of a certain mixing of young meteoric water with deep water systems.

White and co-workers [6] also reported some tritium contents for steam well samples at The Geysers, which is in agreement with a model which involves shallow condensation of steam, incorporation of some local precipitation and drainback.

With this aim, cold and thermal spring waters, waters sampled from non-productive wells, and steam samples will be examined in this report.

The $\delta^{18}O$ and δD values of water and steam samples are referred to SMOW [8], and the errors (1σ) are 0.1‰ and 1‰ respectively.

The tritium content is expressed in Tritium Units (TU) and the error (1σ) is quoted for each individual result.

2. HYDROGEOLOGICAL OUTLINES

The geological features of the Larderello geothermal area are shown schematically in Fig. 1. Details of the geology of the zone have been discussed elsewhere [9-12].

From the hydrogeological point of view, the various outcropping or buried terrains of the region, because of their geometric position and permeability, can be grouped as follows:

(a) Upper complex. This is on the whole impervious. It consists (from top to bottom) of neogenic deposits (U. Miocene-Pliocene) prevalently clay, of flysch facies formations, mostly consisting of shales and marls (Eocene-Cretaceous), with masses of ophiolites (Jurassic), and of sandstones alternated with siltstones and shales ("macigno", Oligocene) overlying a continuous level of impervious varicoloured shales ("scaglia", Eocene-Cretaceous).

In this complex some permeable levels exist which maintain locally shallow and frequently intense circulation, but usually do not contribute to deep circulation. This complex constitutes the cover of the geothermal field.

(b) Main pervious complex. This consists in the upper part predominantly of carbonatic formations (Upper Triassic-Jurassic), and, in the lower part, of a dolomitic-anhydritic formation (Upper Triassic). This complex constitutes the main reservoir in the region: when it outcrops, it represents absorption areas and, consequently, areas of hydrostatic pressure for the buried reservoir, Within, an active circulation develops, and from this practically all thermal springs of the region emerge.

(c) Basal complex. This consists mostly of phyllites and quartzites (crystalline regional basement, Paleozoic-U. Triassic). It includes a series of terrains which are generally low-permeable. A circulation of fluids is also possible in this complex, but not as actively as in the complex described above. At present steam drawn by new deeper wells in the Larderello geothermal field comes essentially from the more permeable horizons of this complex.

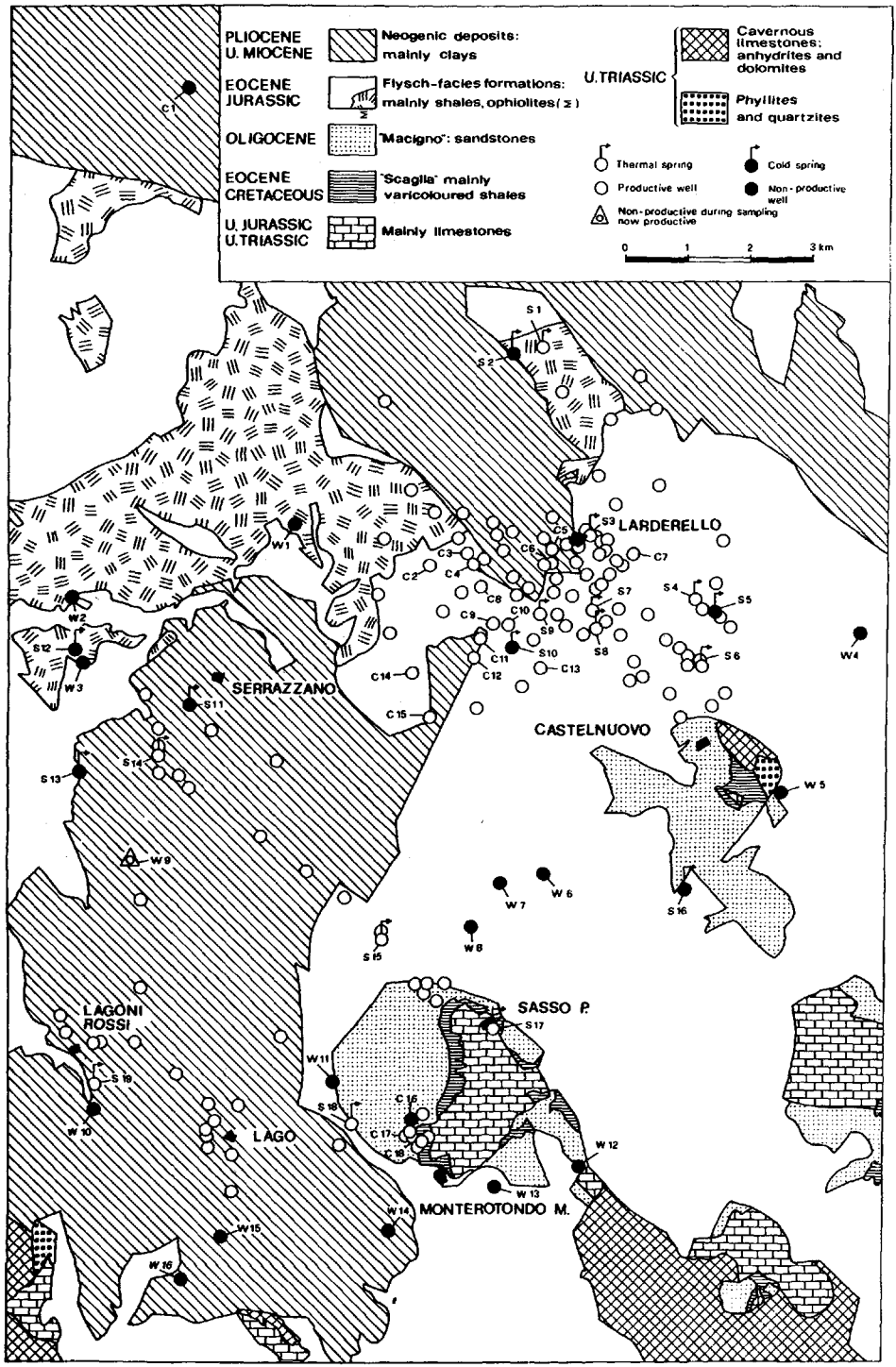

FIG.1. Location map of the samples studied (S = spring waters, W = well waters, C = carbonate from cores), and schematic representation of the geology of the area.

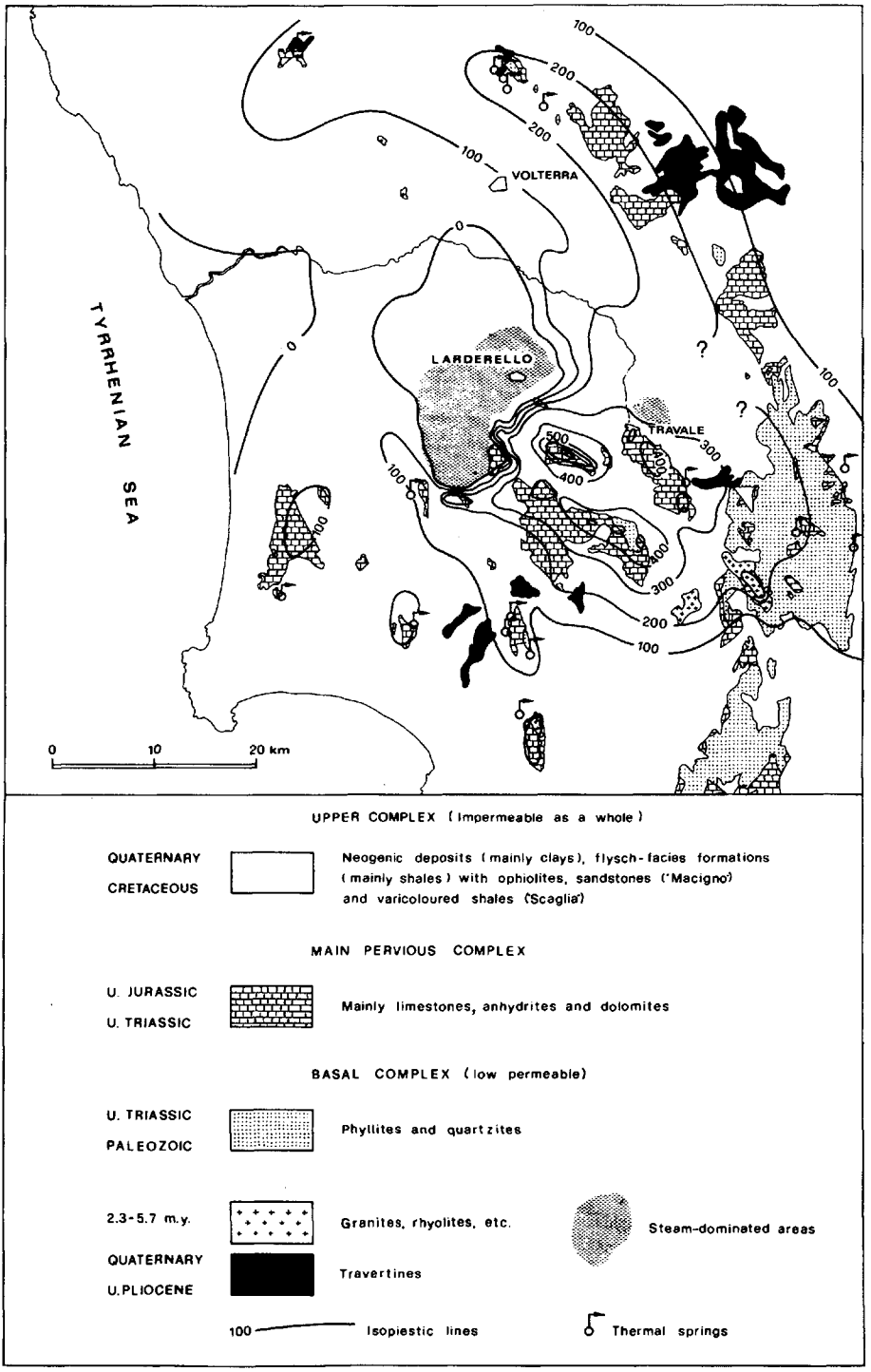

FIG. 2. Hydrogeological sketch map of the Larderello geothermal region.

Using this scheme, we have attempted to synthetize in Fig. 2 the hydrological situation of a large region surrounding the Larderello geothermal field. In this figure, the isopiestic lines have been drawn on the basis of the elevation of thermal springs directly connected with the main pervious complex, or on the piezometric levels measured in the wells which reached it.

On this map the steam-dominated areas (Larderello and Travale fields) were distinguished from those dominated by water, the piezometric surface showing a marked depression at the edges of the vapour-dominated areas. This phenomenon is well-defined at Larderello, where exploration and exploitation are at an advanced stage, and a lot of data are available.

3. SPRING WATERS

Thermal springs can be found in all the area studied, as shown in Fig. 1. We have assumed as "thermal" all the springs with surface temperature above 14°C, which corresponds to the yearly average value of the temperature in that region. Their chemical and isotopic composition is reported in Table I, along with analyses of some cold springs for comparison.

All the springs are HCO_3-type and HCO_3-SO_4-type waters, with the exception of S 1 spring which is Cl-type water. The latter also differs from the others in pH value. In fact, all the springs are nearly neutral or slightly acid, through an excess of free CO_2 in solution, whereas S 1 has a pH value of 10.0, probably from the presence of basic salts of magnesium.

The total salinity does not differ significantly in the cold and thermal springs, always showing values below 1 g/litre. The flow-rate is also always less than 1 litre/s.

The deuterium and oxygen composition of these waters indicates a common meteoric origin. The $\delta^{18}O$ values range from - 6.4 to - 8.1‰ for the cold springs and from - 6.6 to - 7.7‰ for the thermal springs. These variations are clearly connected with the elevation of the sampling point, and therefore with that of the absorption area (Fig. 3), confirming the hypothesis of a short and shallow circulation of the waters.

The thermality shown by several springs is due to heat conduction by the rocks as the underground path occurs in a zone with a very high geothermal gradient.

However, it must be noted that these springs could also be heated by steam escaping to the surface, because they emerge in vapour-dominated zones. In this case, the original isotopic composition of cold waters will be practically unchanged, as the amount of condensed steam ($\delta^{18}O \simeq 0$) required to heat the cold water from 14° to 50°C is less than 5% of the discharged water, and consequently the $\delta^{18}O$ variations would be less than 0.2‰. However, no volatile components usually accompanying steam, such as H_3BO_2, H_2S and NH_3, are present in appreciable amounts in the spring waters; therefore steam condensation at this level seems to be excluded. This confirms the efficacy of the separation due to the caprocks between the geothermal fluid reservoirs and the surface.

TABLE I. CHEMICAL AND ISOTOPIC CHARACTERISTICS OF SELECTED COLD AND THERMAL SPRINGS IN THE LARDERELLO GEOTHERMAL AREA[a]

No.	Name	Sampling date	pH	Ca	Mg	Na	K	Cl	SO_4	HCO_3[b]	T°C	δD (‰)	$\delta^{18}O$ SMOW	Sampling elevation (m)
Cold springs														
S 5	Podernuovo	19. 2.69	6.9	91	18	15	2	18	40	502	8	-52	-8.1	530
S16	M. Bruciano	30.11.65	7.0	42	5	15	2	23	18	247	12	-	-7.9	650
S10	Montelegaio	29.11.65	7.1	103	8	11	1	18	11	348	13	-	-7.7	620
S11	Arzilla	30.11.65	7.2	119	10	18	2	30	23	386	14	-	-7.3	425
S12	Serra	30.11.65	7.0	68	42	15	3	21	21	399	13	-40	-6.9	420
S13	S. Ottaviano	30.11.65	7.1	157	20	24	1	26	249	300	13	-	-6.9	334
S 2	Miniera rame	29.11.65	7.8	19	103	15	2	25	58	508	13	-	-6.7	400
S19	S. Edoardo	30.11.65	7.1	116	17	31	1	64	203	198	14	-38	-6.4	175
Thermal springs														
S 8	La Perla 1	29.11.65	6.2	142	22	110	11	15	18	1130	50	-	-7.7	500
S 9	Fontericci	29.11.65	6.9	36	21	18	3	19	59	210	17	-46	-7.7	560
S 6	S. Luigi	30.11.65	6.1	272	49	29	3	13	31	1509	22	-	-7.7	560
S 4	Podernuovo	29.11.65	6.7	109	6	19	2	15	40	387	27	-43	-7.4	575
S17	B. Lagoncino	28.11.69	6.3	128	19	14	3	20	138	554	45	-42	-7.2	475
S 7	B. Morbo	29.11.65	7.0	120	50	51	2	26	38	687	42	-	-7.1	450
S 3	La mensa	29.11.65	-	281	59	20	3	15	549	726	49	-	-7.0	425
S15	Lumiere	30.11.65	6.9	106	58	24	4	29	44	581	30	-	-7.0	370
S18	T. Bagnolo	3. 3.69	7.4	68	26	30	11	27	4	675	38	-42	-6.8	460
S14	Cioccaia	30.11.65	7.1	75	111	47	3	40	189	615	20	-	-6.7	350
S 1	B.S. Michele	21. 7.67	10.0	43	51	55	13	115	28	52	47	-	-6.6	325

[a] The geographical distribution of the samples studied is shown in Fig. 1.

[b] These figures consist of the CO_2 content expressed as HCO_3.

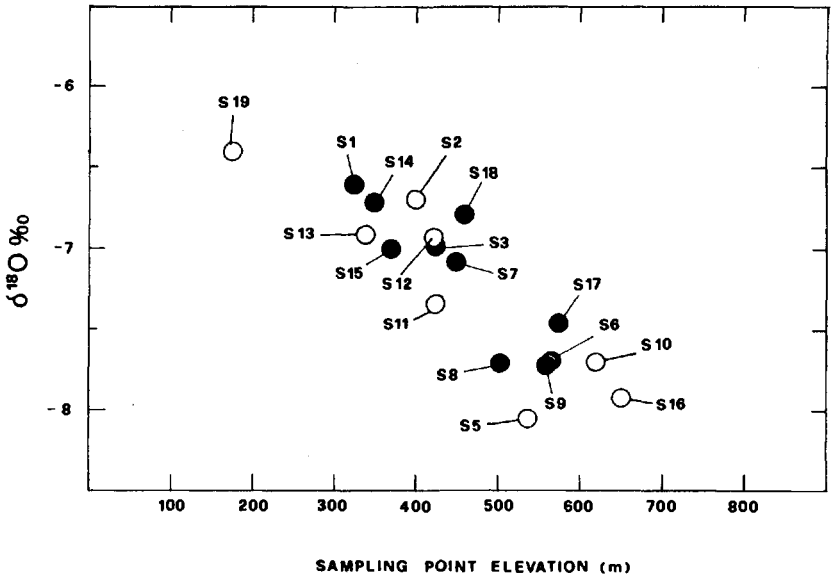

FIG.3. ^{18}O variations with the height of sampling point of the spring waters (thermal: filled circles; cold: open circles).

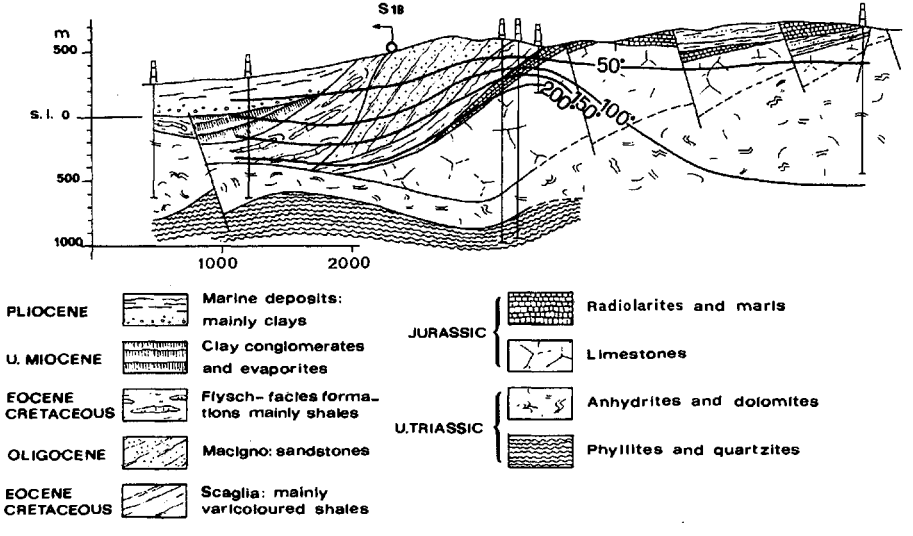

FIG.4. Cross-section and isotherms illustrating the circulation path of the S18 HCO_3-type water.

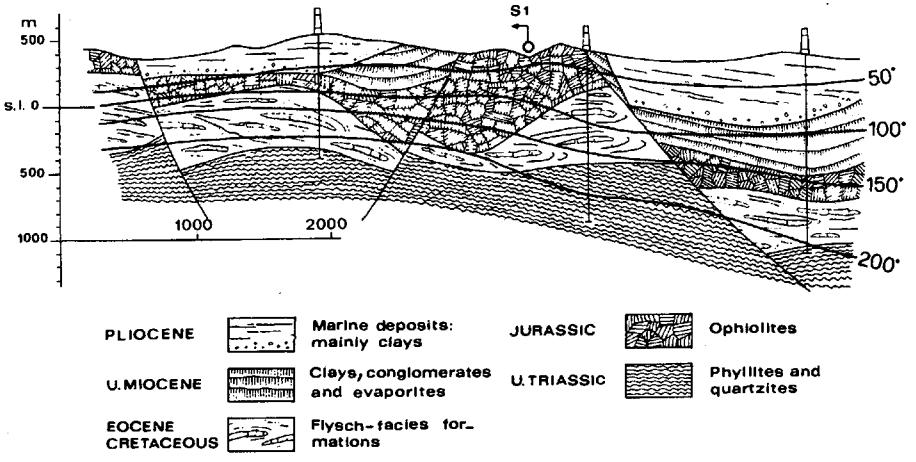

FIG. 5. Cross-section and isotherms illustrating the circulation path of the S1 Cl-type water.

Also from a geological point of view, it seems logical to consider the springs in the zone as connected to a shallow circulation in rocks which have no hydrogeological connections with the steam-dominated reservoir:

S18: HCO_3-type spring, temperature 38°C, represents the emergency point of a perched water which penetrates and circulates in a permeable horizon (quartzose-feldspatic-micaceous sandstone) interbedded between two mainly shaley formations (Fig. 4). Considering the isotherm distribution deriving from thermometric logs carried out in the wells nearby, a relatively shallow circulation (some hundreds of metres) is sufficient to justify the thermality of this water.

S1: Cl-type spring, temperature 47°C, is supplied by local meteoric waters penetrating and circulating in the permeable formation of the Upper Miocene, NaCl salt-rich, and in the Jurassic fracturated serpentines (Fig. 5). The underground temperatures permit the heating of the water at quite shallow depths, the 50°C isotherm in this area being 100 - 150 m from the surface. In this case too, between the permeable surface rocks and the steam-dominated reservoir there is a continuous impermeable horizon formed by shaley formations in flysch facies.

4. WATER FROM NON-PRODUCTIVE WELLS

Figure 1 shows the distribution over the geothermal area of the wells sampled for water analyses. From the chemical point of view the distribution into three main groups is quite significant, each group including wells having the main fracturation in the same geological complex, and practically the same ratios between the major chemical constituents dissolved in the water. These characteristics are summarized in Fig. 6 in which are separately shown wells having:

(A) Na-HCO_3-type waters which derive their salinity from circulation through sandstones;
(B) Ca, Na-SO_4-type waters from a dolomitic-anhydritic series;
(C) Na-Cl-type waters deriving from the schistose-quartzitic basement.

The waters that have circulated in sandstones (Group A) show $\delta^{18}O$ values and chemical composition which are very similar to those of the spring waters discussed above, though the total salinity is generally higher. This would also suggest that, in this case too, the water found in these wells had a short circulation in terrain where carbonate minerals are present in very small amounts. The waters, in fact, may reach several hundred metres depth, and can assume very high temperatures, but no significant isotopic exchange occurs with the oxygen of the rocks.

On the contrary, an isotopic exchange between CO_2 and water, resulting in a depletion of ^{18}O in water samples, is possible in these wells where there is an excess of CO_2. This behaviour has been observed in some waters of thermal springs and mofettes in Tuscany [4], where large amounts of CO_2 bubble through the water in small pools. This phenomenon is particularly evident in the W4 well, where we have found water with an ^{18}O content 2‰ lower than that of the local meteoric water.

In the water samples of the Groups (B) and (C) we have observed remarkable differences in the ^{18}O contents of different wells, and in some cases in waters sampled in the same well at different depths. This can be explained if we remember that several factors can contribute to determining the quality of the waters in the well, such as the permeability of the reservoir rocks, the isotopic exchange with the rocks, the evaporation in the well and the possibility of the condensation, on the inside or outside of the well, of steam coming from the surrounding zones.

In specific cases we can have water samples where some factors are prevalent over others.

The isotopic characteristics of the water of the wells located in the immediate vicinity of the calcareous outcrops suggest that the meteoric water which is absorbed in these formations reaches the southern limits of the field undergoing a small isotopic variation. In particular the W5, W12 and W13 wells show values ranging from - 5.6 to - 6.0‰, without any appreciable change in the deuterium content.

On the other hand, the water of the wells located at a remarkable distance from the calcareous outcrops appears to be mainly constituted by steam coming from deeper and hotter zones, and which condenses in the boundaries of the field where the temperature is relatively less. This is the case, for example, in the waters of the W1 and W2 wells, which are located in the north-western zones of the field near the Serrazzano area, in which the $\delta^{18}O$ values are equal to 0 and +2‰ respectively, and the H_3BO_3 concentration exceeds 1 g/litre. The exceptionally high ^{18}O content of the W2 well water is not surprising, because this well is located in a zone in which there is no intense circulation of either water or steam. Consequently, in this zone the steam condensation on the western edge, which is relatively colder, gives rise to a water phase that undergoes a very slow circulation for which the process of isotopic exchange between the oxygen of the water and that of the rocks crossed is made easier. This determines an ^{18}O enrichment of the circulating water, the same as results also from the steam samples discussed in Section 5.

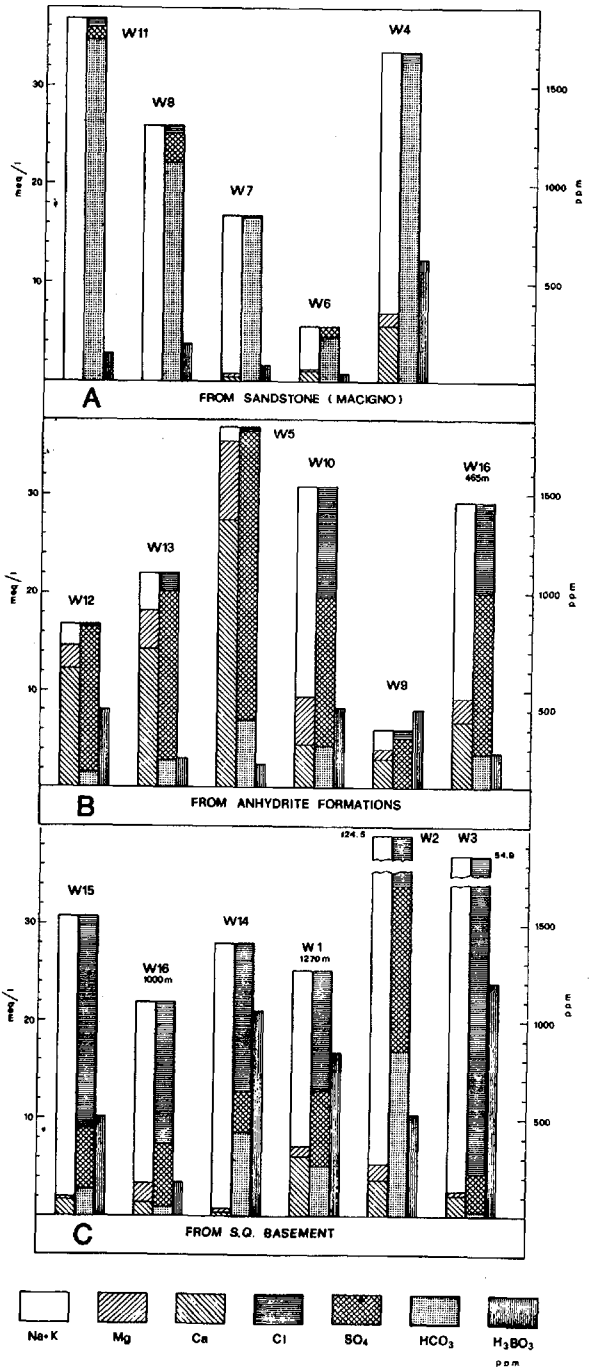

FIG.6. Chemical characteristics of hot waters from selected geological formations.

The wells situated very close to the steam-productive zones have a water which results from a certain mixing of locally infiltrating water, and some condensed steam. The former has undergone a progressive evaporation as it moves towards the vapour-dominated zones. In this case, we observe $\delta^{18}O$ values which range from - 5.0‰ in the W16 well to - 1.8‰ in the W9 well, reflecting the various amounts of the two components of the mixture.

It must be noted that the evaporation process can also play a particular role inside the wells, especially if they cross low permeability horizons. If the well is situated in a water-dominated zone, evaporation can cause notable increases in salt contents, together with D and ^{18}O enrichments.

5. STEAM AND CARBONATE SAMPLES

Steam samples from 125 productive wells were collected for ^{18}O, D and T analyses. The wells were widespread in the geothermal area to create a significant picture of the field. Measurements in single wells were repeated at different periods as a check on possible changes in the ^{18}O content with time. All these data are reported in Table II.

In Fig. 7 the isotopic composition of some steam samples is compared with that of the local meteoric waters.

The isotopic composition of hydrogen is constant within the measure errors, whereas the ^{18}O concentrations vary extensively, from - 5.5 to + 0.5‰.

The intersection of the straight line which fits all the steam samples with that of local meteoric waters gives values of $\delta D = -42$‰ and $\delta^{18}O = -7.2$‰ which can be considered a good yearly average value of the meteoric water composition supplying the steam field.

Isotopic exchange between water and oxygenated rocks (limestones and/or silicates) account for the ^{18}O enrichments. Considering, first, limestones, we have performed several analyses of oxygen and carbon isotopes of samples derived from the limestone intercalations of the cover, and the results are reported in Table III. From these data it appears that whereas the ^{13}C contents do not show significant variations with depth, the ^{18}O contents change to a large extent as a function of the distance of the sampling point from the reservoir rocks underlying the cover, as shown in Fig. 8. That is, a general tendency exists in which the greater the distance from the reservoir top the lesser the deviations from the $\delta^{18}O$ value of - 3.5‰, which can be assumed to be the representative value of this type of limestone, and corresponds well with the observed values for surface samples collected outside the geothermal area. Conversely, when the samples are nearer to the contact surfaces between the cover and reservoir, they show a lighter oxygen isotopic composition, reaching $\delta^{18}O$ values of - 16‰, as a consequence of a greater fracturation and higher temperatures in these zones.

It should also be noted that several samples collected at remarkable distances from the reservoir top have shown very negative $\delta^{18}O$ values. This fact can be explained by taking into account several emanations that in the past reached the surface, formed lagoons, fumaroles, etc., and the existence of faults, which cut through the cover. In fact, during the first drillings in the Larderello field, the productive wells never reached

TABLE II. HYDROGEN AND OXYGEN ISOTOPIC DATA OF GEOTHERMAL STEAM SAMPLES COLLECTED IN THE LARDERELLO AREA FROM 1964 TO 1973

No.	Well name or no.	Date	δD (‰)	$\delta^{18}O$ SMOW	Date	Tritium TU ± σ
1	144	Apr. 1968		-0.6		
2	Gabbro 9	Apr. 1968		-1.6		
		Jun. 1969		-1.7		
		Nov. 1971		-1.6		
3	Gabbro 7	Aug. 1965		-1.2		
		Jun. 1969		-0.3		
4	S. Dalmazio 4	Aug. 1965		-1.2		
5	Gabbro 6	Apr. 1968		-1.3		
		Jun. 1969		-1.2		
		Sep. 1971		-1.2		
6	122	Apr. 1968		-1.4		
7	155	Oct. 1971		-3.3		
8	161	Apr. 1965		-2.1		
		Jun. 1969		-2.6		
9	162	Apr. 1968		-2.7		
		Jun. 1969		-2.5		
10	107	Apr. 1968		-2.1		
11	114	Mar. 1965	-40	-4.2		
12	134	Mar. 1965		-1.8		
13	118	Aug. 1971		-2.2		
14	Miniera 1	Apr. 1968		-2.7		
		Nov. 1971		-1.1		
15	109	Apr. 1968	-41	-1.2		
16	135	Jul. 1971		-2.4		
17	102 bis	Apr. 1968		-2.5		
18	85	Aug. 1965	-40	-2.8		
19	C. Sportivo	Mar. 1965		-2.8		
		Jun. 1969		-2.4		
20	84	Apr. 1968		-2.2[5]		
		Jun. 1969		-2.2		
21	Pacciana 1	Apr. 1968		-3.0		
		Jun. 1969		-3.4		
22	Fabiani	Apr. 1968		-1.3	Oct. 1972	0.0 ± 0.6
		Jun. 1969		-1.2		

TABLE II. (cont.)

No.	Well name or no.	Date	δD (‰)	$\delta^{18}O$ SMOW	Date	Tritium TU ± σ
23	Pacciana 3	Aug. 1965	-42	-3.4	Oct. 1972	0.7 ± 0.6
24	Ciabattino	Aug. 1965	-41	-2.8		
25	54	Apr. 1968		-2.6		
		Sep. 1971		-2.6		
26	53	Nov. 1964		-3.1		
		Aug. 1971		-3.1		
27	89	Nov. 1964	-42	-1.9		
		Aug. 1965	-41	-2.3		
		Aug. 1971		-2.3		
28	129	Aug. 1971		-3.6		
29	137	Aug. 1971		-3.8		
30	138	Aug. 1971		-3.4		
31	101	Aug. 1969		-0.8		
32	5	Nov. 1964	-41	-3.1		
33	B. Prete	Apr. 1968		-3.3		
34	Pacciana 4	Apr. 1968		-2.4		
		Jun. 1969		-2.6		
35	120	Apr. 1968		-2.5		
36	Sperim. 2	Aug. 1971		-3.4		
37	65	Apr. 1968		-2.8		
		Jun. 1969		-2.2		
38	Alloro	Apr. 1968		-2.7		
		Jun. 1969		-2.8		
39	62	Nov. 1964		-4.8		
40	6	Aug. 1965	-43	-3.9		
41	71	Nov. 1971		-3.6		
42	82	Aug. 1969		-3.1		
43	119	Apr. 1968		-3.1		
		Jun. 1969		-3.0		
44	97	Apr. 1968		-2.9		
45	151	Mar. 1968		-0.3		
46	128	Apr. 1968		-3.4		
47	58	Mar. 1968		-3.3		
48	57	Apr. 1968		-3.1		
		Nov. 1971		-3.3		

TABLE II. (cont.)

No.	Well name or no.	Date	δD (‰)	$\delta^{18}O$ SMOW	Date	Tritium TU ± σ
49	80	Apr. 1968		-3.2		
		Aug. 1969		-3.2		
50	S.V. 9	Mar. 1965		-2.0[5]		
		Sep. 1969		-3.6		
51	S.V. 6	Apr. 1968		-3.9		
		Jun. 1969		-4.2		
52	S.V. 2	Apr. 1968		-3.4	Sep. 1973	0.9 ± 0.6
		Aug. 1969		-3.3		
53	Acquabona 2	Apr. 1968	-43	-4.0	Jan. 1973	0.5 ± 0.6
		Aug. 1969		-3.7[5]		
54	106	Mar. 1965		-3.8		
55	Pineta				Jan. 1973	2.1 ± 1.1
56	59	Aug. 1965	-40	-3.7	Sep. 1973	0.0 ± 0.5
57	110	Apr. 1968		-3.9		
		Dec. 1970		-3.3		
58	143	Mar. 1968		-3.7		
59	102	Mar. 1968		-2.9		
60	159	Nov. 1965		-2.1		
61	100	Nov. 1971		-3.6		
62	108	Apr. 1968		-4.0	Jan. 1973	8.6 ± 1.2
63	72	Apr. 1968		-3.4		
64	52	Apr. 1968		-3.5		
		Jun. 1969		-3.8		
65	44	Apr. 1968		-4.0		
66	S.V. 5	Mar. 1965		-3.6	Oct. 1972	0.5 ± 0.6
		Jun. 1969		-3.3		
67	S.V. 1	Aug. 1971		-5.5		
68	Colombaia 2				Jan. 1973	49.0 ± 1.5
69	73	Apr. 1968		-4.8		
70	112	Mar. 1968	-40	-3.4		
		Aug. 1971		-3.6		
71	145	Mar. 1968		-2.8		
		Jun. 1969		-2.1		
72	45	Apr. 1968		-4.8		
73	98	Apr. 1968		-3.8		

TABLE II. (cont.)

No.	Well name or no.	Date	δD (‰)	$\delta^{18}O$ SMOW	Date	Tritium TU ± σ
74	91	Apr. 1968		-4.5		
		Nov. 1971		-2.9[5]		
75	S. Luigi 3	Mar. 1965		-4.8	Sep. 1972	40.7 ± 1.6
		Jun. 1969	-42	-5.2		
		Jul. 1971		-5.9		
76	81				Sep. 1973	30.0 ± 1.3
77	38	Apr. 1968	-43	-4.7		
78	19	Jul. 1969		-3.6	Sep. 1972	27.0 ± 1.1
79	136	Mar. 1965		-4.8	Oct. 1972	0.9 ± 0.8
80	141	Mar. 1968	-41	-2.4		
		Jul. 1969		-1.5		
81	113	Apr. 1968		-4.2	Oct. 1972	1.0 ± 0.7
		Jun. 1969		-3.9		
82	26	Mar. 1965		-4.2	Oct. 1972	6.6 ± 1.2
		Jun. 1969		-4.2	Oct. 1973	41.3 ± 1.6
83	Caspeci					
84	Fornace	Sep. 1969	-43	-5.5	Oct. 1972	28.6 ± 1.5
85	66				Sep. 1972	38.0 ± 1.5
86	Serr. 8	Mar. 1968		-3.0	Dec. 1973	0.0 ± 0.5
		Jul. 1969		-2.0		
87	Pozzaie 2	Mar. 1968		-2.9	Dec. 1973	0.0 ± 0.6
88	Vignacce	Apr. 1968		-2.0	Dec. 1973	0.0 ± 0.6
		Jul. 1969		-1.8		
89	Cioccaie	Apr. 1968		-2.3		
		Jul. 1969		-2.0[5]		
90	Capanna	Mar. 1968		-2.5		
		Jul. 1969		-2.7		
91	Soffion. 1	Mar. 1968		-1.7		
92	Oliveta	Mar. 1968	-44	-1.7	Dec. 1973	0.0 ± 0.6
93	V.C. 10	Mar. 1968	-43	-0.7	Dec. 1973	0.0 ± 0.6
94	V.C. 2	Mar. 1968	-43	+0.1		
		Jun. 1969		0		
95	V.C. 5	Mar. 1968		-1.5		
96	Le Prata 4	Mar. 1968	-44	-2.4	Sep. 1973	0.8 ± 0.7
		Jun. 1969		-2.0		

TABLE II. (cont.)

No.	Well name or no.	Date	δD (‰)	$\delta^{18}O$ SMOW	Date	Tritium TU ± σ
97	Le Prata 2	Mar. 1968		-3.3	Sep. 1973	0.6 ± 0.7
		Jun. 1969		-3.2		
98	Le Prata 3	Mar. 1968		-2.9		
		Jun. 1969		-3.2		
99	S. Amicié 2	Mar. 1968		-3.3	Sep. 1973	1.2 ± 0.6
100	Sasso 9	Mar. 1968		-2.8	Sep. 1973	0.5 ± 0.7
101	Grotte 2	Mar. 1968	-42	-4.0		
		Jul. 1969		-3.5[5]		
102	Covo	Mar. 1968	-39	-3.5		
		Jul. 1969		-2.9		
103	Orto	Mar. 1968		-4.0	Sep. 1973	0.7 ± 0.7
		Jul. 1969		-3.4		
104	Querciola	Apr. 1968		-0.8	Dec. 1973	0.0 ± 0.5
105	LR-B	Mar. 1968		-2.3	Dec. 1973	0.5 ± 0.5
106	Bagnolo	Mar. 1968		-2.9	Dec. 1973	3.3 ± 0.6
107	Meli 2	Feb. 1968		-3.2		
108	Meli 1	Mar. 1968		-3.2	Dec. 1973	2.5 ± 0.7
		Jun. 1969		-1.6		
109	LR 1	Mar. 1968	-41	-0.5	Dec. 1973	0.0 ± 0.5
		Jun. 1969		-0.7		
110	VC 3	Mar. 1968		-1.4		
111	Lago 7	Mar. 1968		-2.7	Dec. 1973	0.0 ± 0.5
		Jul. 1969		-3.6		
112	Lago 6	Apr. 1968		-2.0		
		Jul. 1969		-2.0		
113	Lago 4	Mar. 1968		-1.4	Dec. 1973	0.7 ± 0.6
		Jul. 1969		-1.2		
114	Diga 2	Apr. 1968		-2.0		
115	Pescaie	Feb. 1968		-4.6		
116	Tassinaie	Feb. 1968		-3.4	Dec. 1973	6.5 ± 0.8
117	Capannone	Mar. 1968		-2.7	Dec. 1973	20.4 ± 1.0
118	S. Edoardo	Mar. 1968	-43	-2.1		
		Jul. 1969		-1.8		
119	S. Federico	Mar. 1968		-2.9	Dec. 1973	1.4 ± 0.8
120	V. Madama	Mar. 1968	-40	-2.4	Sep. 1973	3.2 ± 0.9

TABLE II. (cont.)

No.	Well name or no.	Date	δD (‰)	$\delta^{18}O$ SMOW	Date	Tritium TU ± σ
121	Pianacce 2	Mar. 1968		-3.1		
		Jul. 1969		-2.9		
122	M.R. 1	Mar. 1968		-3.5	Sep. 1973	5.9±0.8
		Jul. 1969		-3.3		
123	S. Adriana	Feb. 1968		-3.3		
124	H.N. 4	Feb. 1968		-3.3		
125	M.R. 11	Mar. 1968		-3.3	Sep. 1973	3.5±1.0
		Jul. 1969		-3.0		

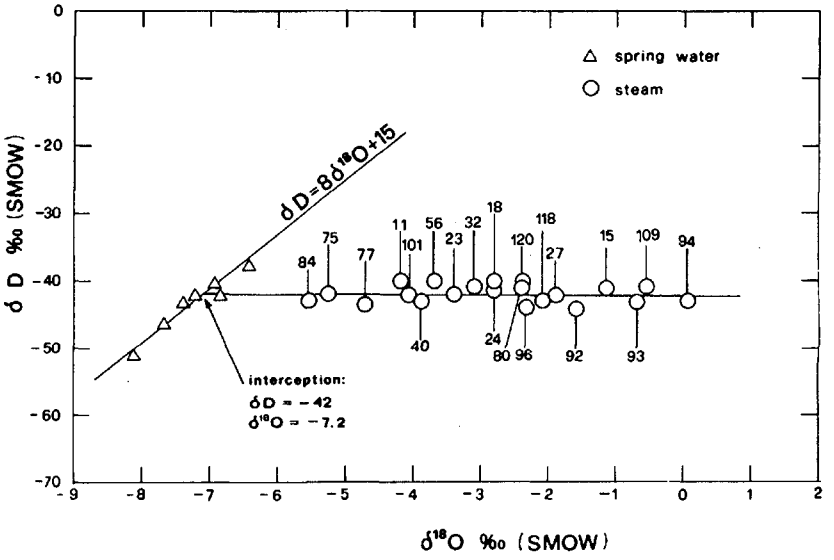

FIG.7. Deuterium and oxygen composition of some selected steam samples (circles; the numeration appears on Table II). The spring waters (triangles) represent local meteoric waters (see text).

the underlying Mesozoic formations, but drew the steam from the rocks of the cover.

In the carbonate formations which constitute the geothermal reservoir, one observes systematically more negative values from - 15 to - 23‰ (Fig. 8 and Table III) and a more regular distribution within the rock matrix. This indicates an active circulation over long periods of time, both in the fractures and in the pores of the non-fractured rocks. These facts are confirmed by the analyses of samples of outcropping rocks in Tuscany (unpublished data).

TABLE III. OXYGEN AND CARBON ISOTOPE COMPOSITION OF THE CARBONATE SAMPLES OBTAINED FROM SOME WELL CORES IN THE LARDERELLO FIELD

No.	Well name or no.	Sampling point depth (m)	Geologic formation[a]	$\delta^{18}O$ (‰)	$\delta^{13}C$ PDB	Distance from reservoir top (m)
C 1	Stratigrafico 1	280- 282	Ne	- 5.3	+1.6	774
		425- 426	AS	- 6.3	+0.2	630
		619- 621	AS	- 5.2	-0.1	435
		700- 701	AS	- 4.7	+0.3	355
		750- 751	AS	- 4.5	+0.6	305
		807- 810	AS	- 5.8	+0.4	246
		852- 854	AS	- 5.8	+0.2	202
		909- 911	AS	-13.3	+0.9	145
		1047-1048	D-An	-15.0	+1.1	8
		1151-1160	D-An	-15.1	+2.2	0
C 2	111	25- 52	AS	- 6.9	-0.1	540
		305- 436	AS	- 6.6	+0.9	200
C 3	138	81- 106	AS	- 7.6	+0.1	300
C 4	101	0- 66	AS	- 3.8	+0.9	310
C 5	89	23- 73	AS	- 5.3	+0.8	300
		212- 228	AS	-13.2	-2.3	170
C 6	88	185- 232	AS	-10.1	-2.4	200
C 7	120	0- 54	AS	- 9.7	+0.1	600
		208- 370	AS	- 5.8	+1.3	350
		506- 508	AS	-16.1	+1.2	125
C 8	119	28	AS	- 4.2	+1.5	490
C 9	143	40- 88	AS	- 7.5	+0.5	510
		316- 354	AS	- 8.2	+0.3	230
		566- 567	D-An	-19.7	-0.6	0
C 10	110	20- 90	AS	- 8.7	-1.3	480
C 11	100	0- 81	AS	- 6.2	-0.3	550
C 12	112	47- 121	AS	- 6.4	+0.4	580
C 13	116	0- 53	AS	- 5.6	+1.4	630
		89.5	AS	- 6.8	+1.2	570
		146.4	AS	- 6.8	+1.3	510
		189- 340	AS	- 7.9	+1.0	300

TABLE III. (cont.)

No.	Well name or no.	Sampling point depth (m)	Geologic formation[a]	$\delta^{18}O$ (‰)	$\delta^{13}C$ PDB	Distance from reservoir top (m)
C 14	145	0- 49	AS	- 3.9	+1.0	790
		213- 274	AS	- 4.4	+1.0	550
		433- 549	AS	- 7.9	-0.2	300
		732- 800	AS	- 9.5	-1.4	60
		1055-1056	D-An	-18.3	-2.6	0
C 15	141	0- 36	AS	- 4.7	+1.1	620
		221- 240	AS	- 7.7	+0.1	415
		521- 523	AS	-10.4	-0.8	120
		1172-1175	D-An	-15.2	-1.4	0
C 16	M. Rotondo 17	260- 266	L	-20.8	-0.3	0
		474- 476	L	-19.6	+0.8	0
C 17	M. Rotondo 15	312- 314	L	-23.0	+0.5	0
		524- 560	L	-18.5	+2.0	0
		645- 730	L	-16.1	+1.8	0
C 18	M. Rotondo 14	209- 210	L	-19.3	+1.1	0
		350- 383	L	-17.8	+3.0	0
		412- 454	L	-16.5	+2.3	0
		480- 488	L	-16.3	+1.9	0
		505- 506	L	-15.4	+2.2	0
		570- 603	L	-16.8	+1.8	0
		695- 720	L	-15.4	+1.8	0
		852- 855	L	-17.9	+1.9	0
		941- 943	L	-18.1	+2.0	0
		1017-1025	D-An	-20.8	+2.0	0
		1160-1162	D-An	-22.3	+4.5	0

[a] Ne = Neogenic deposits, mainly clays (U. Miocene - Pliocene); AS = flysch-facies formations: "argille scagliose" (U. Cretaceous - Eocene); D-An = dolomites, anhydrites and cavernous limestones (U. Triassic); L = massive limestones (U. Triassic - U. Jurassic).

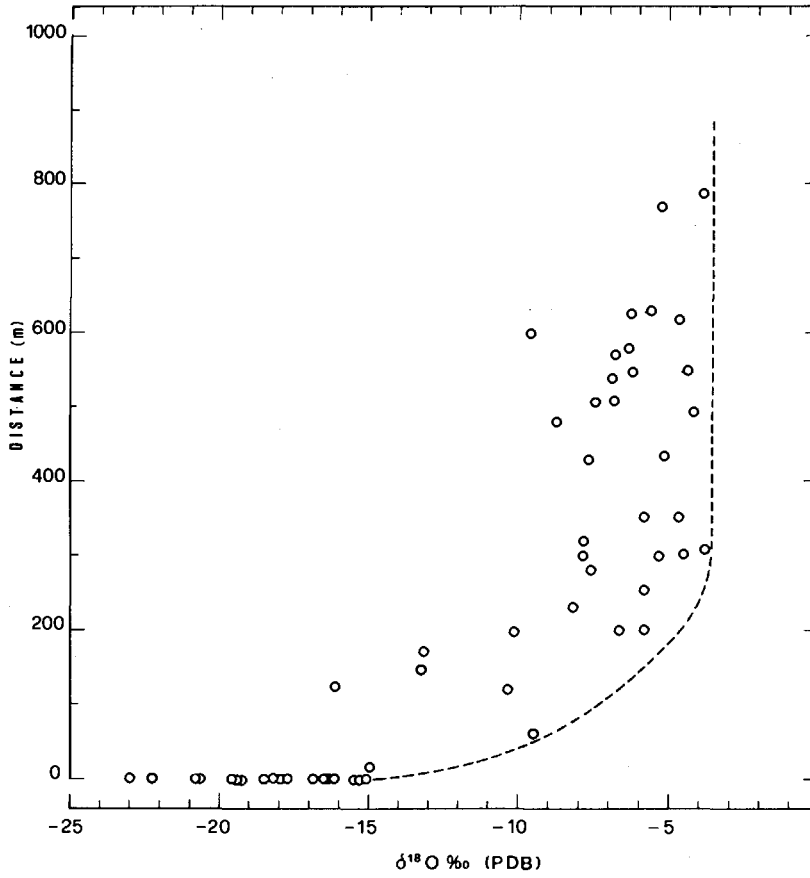

FIG. 8. Oxygen isotope variations of carbonates from core samples of several drillings, in relation to the distance of the sampling point from the top of the reservoir.

As regards the role of silicate rocks underlying the calcareous formations, there are, at present, no data related to the ^{18}O content of rock samples of the Larderello area. However, the steam samples produced by wells that extend across several hundred metres of such formation show an ^{18}O shifting caused by an interaction of water and rocks.

The possibility of isotopic exchange at high temperature in silicates was illustrated by Clayton and co-workers [13] who have shown a parallel depletion in ^{18}O contents in the calcareous and siliceous rocks in a well core in the Salton Sea geothermal field.

All these facts confirm that in geothermal areas by far the most simple explanation of the oxygen shift is that it is due to isotopic exchange with carbonates and silicates in the rock matrix through which the waters have moved. Different ^{18}O enrichments observed in steam samples produced in

a certain area reflect, in fact, the effects of complex deep circulation patterns as well as different thermal conditions that affect, in opposite directions, equilibrium fractionation and reaction kinetics, and different residence times.

In spite of this complicated situation, it can be foreseen that the isotopic exchange process remains dependent upon the distance of the zone of steam production from the zone of water infiltration. This factor can contribute to determining the distribution of ^{18}O content in the geothermal field.

However, this mechanism does not seem to be a single one, when the geological structures of a geothermal field can provide two or more different circulations of feeding waters. In other words, when absorption areas exist in the immediate vicinity of the field, and are hydrologically connected with the underlying steam-bearing formations, some waters tend to enter the field and can determine a mixing with deeper fluids.

Now, the shallow component of the mixture certainly represents a reservoir water derived directly from the local meteoric water, with little or no change in isotopic composition, as a consequence of a relative short and fast circulation in relation to that required for the isotopic exchange with rocks.

On the contrary, deeper waters can be submitted to a greater exchange because of greater temperature conditions and greater contact time with oxygenate rocks. This may result in a large water body of rather uniform isotopic composition that corresponds to a maximum isotopic exchange process which the waters have undergone during their history.

So, if the mixing occurs especially during exploitation conditions, different proportions of the two components in the mixture produce at surface steam samples with different ^{18}O contents, which progressively increase from the zones nearest to the local absorption areas to zones where the contribution of local water is less important.

6. GEOGRAPHICAL DISTRIBUTION OF ^{18}O VALUES

The data of Table II, referring to the variations in time of the ^{18}O contents, will be discussed below. Taking into account that the observed variations are generally less than 0.5‰, data relative to samples collected in different years can be used to draw the map of Fig. 9, showing the $\delta^{18}O$ distribution in the geothermal field, including all the sampling points.

This figure shows the following facts:

(a) The ^{18}O content increases progressively, from the borders of the field towards the centre, i.e. the ^{18}O enrichment occurs in the same direction as the flow lines of water into the productive layers.

(b) The ^{18}O enrichment gradient with distance differs from zone to zone: for instance, in Lago and Lagoni Rossi the isotopic gradient is much higher than in other fields.

(c) The peripheric wells in the Castelnuovo area have $\delta^{18}O$ values almost as negative as those observed in liquid water collected in wells in the non-productive area bordering the geothermal field in the east and in the south. In addition, in the Castelnuovo area a number of wells exhibit high tritium, up to a maximum of about 50 TU, indicating an inflow of recent water.

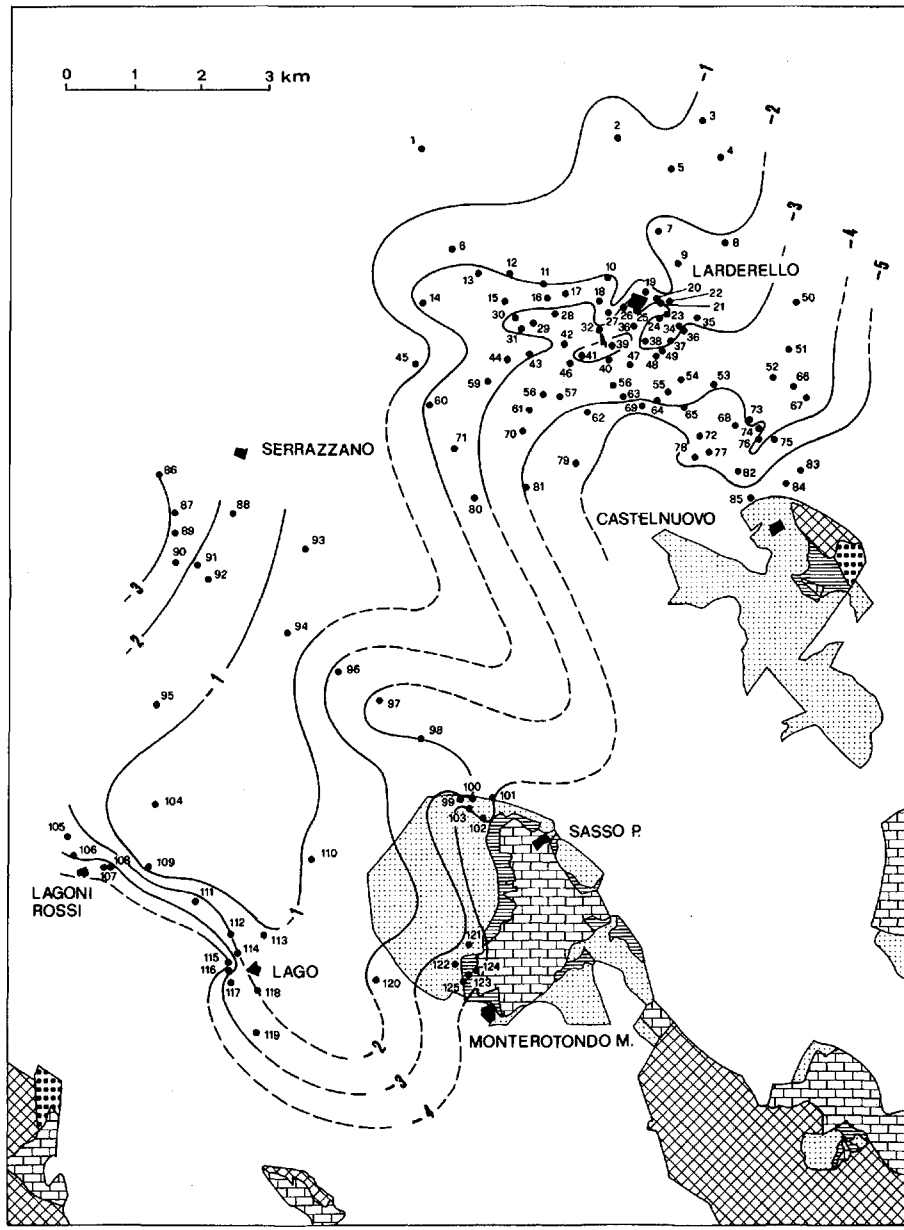

FIG. 9. Geographical distribution of the $\delta^{18}O$ values of the steam in the Larderello geothermal area. The numeration appears on Table II; the values used are those relative to the first sampling for a single well. The main outcropping formations are also shown (for details see Fig. 1).

(d) In the area of Monterotondo and Sasso, where $\delta^{18}O$ values are less negative than those observed in the Castelnuovo area, the tritium content is also lower, indicating that recent water is present in almost negligible amounts.

(e) The existence of an axis in a SW-NE direction, corresponding to the inner part of the field, is indicated. It is also deformed by some local situations which indicate some preferential ways of water infiltration in a direction orthogonal to the axis. In particular, this phenomenon is observed in the Castelnuovo area, but can also be seen along the Sasso-Monterotondo-Serrazzano directrix. The south-western edge of the field, on which lie the productive zones of Lago and Lagoni Rossi, repeats the same trend.

All these aspects may be explained by the hypothesis, described in Section 5, by which steam samples coming from the different zones of the geothermal field are the result of a superimposition by an exchange process and a mixing of steams, the first originated at depth and the second originated by a water circulating in a relatively superficial layer. In fact, taking into consideration the geohydrological characters outlined in Section 2, the following scheme of the Larderello geothermal field may be outlined.

The groundwater recharged in the limestone outcrops moves into the geothermal field. These waters follow two different paths in both the more permeable formations (anhydrites, limestones and the upper part of the basement, rather fracturated) and in the deeper and less permeable zone of the basement.

The deeper circulation waters, which experience higher temperatures and longer residence time, appear to be responsible for the higher ^{18}O content observed in steam which emerges in the inner zones of the field. On the other hand, the negative values of the southern zones of the field appear to be affected by a mixing with a relative shallow circulation, for which temperature and residence time are much less.

The mixing process is particularly evident in the Castelnuovo zone, where an inflow of recent water (tritium concentration up to 49 TU) can occur through the outcrop of the semi-permeable sandstone, the so-called "macigno", directly overlying the permeable anhydritic formations. In Monterotondo, the outcrop of sandstone and mainly limestone seems to be much less efficient for the infiltration of recent water, as indicated by the lower tritium and the higher ^{18}O compared with Castelnuovo. In fact, it is known that the limestone is made up, in its surficial part, of radiolarites having low to very low permeability, and which have undergone an intense silification.

On the other hand, the differences between Castelnuovo and Monterotondo can be due also to the different degree of exploitation of the two fields; in the Castelnuovo field the inflow of recent water may have been enhanced by the intense exploitation.

The high $\delta^{18}O$ gradients observed in the southern zones of the field (Lago and Lagoni Rossi), corresponding to the high hydraulic gradients shown in Fig. 2, may be due to the presence, at the field edges, of zones with low permeability which could prevent recent water infiltration in the field, so limiting at short distance mixing effects.

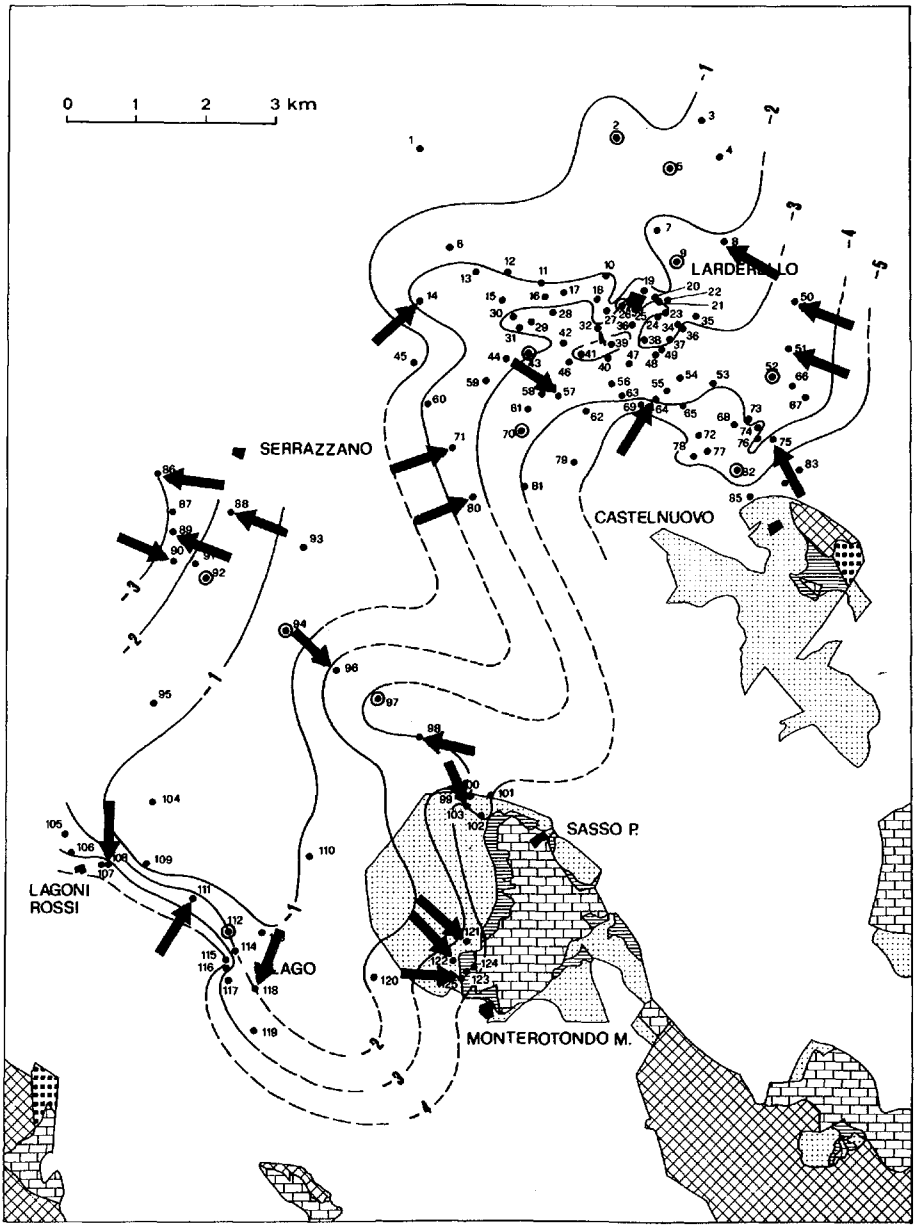

FIG.10. Sketch map of the $\delta^{18}O$ variations in time in several wells of the Larderello geothermal area. The ^{18}O contents tend to increase when the arrows indicate a direction from more positive to more negative values and vice versa. The circles indicate no detectable variations. The main outcropping formations are also shown (for details see Fig.1).

7. VARIATIONS IN TIME OF ^{18}O VALUES OF STEAM SAMPLES

Figure 10 shows, schematically, the ^{18}O variations observed in time in several steam samples. From this figure it appears that in the inner zones the wells have generally shown no variations, indicating that by now they are fed one single type of steam which is probably that produced by the deeper evaporation in the central zone.

On the other hand, in the peripheric area characterized by $\delta^{18}O$ values ranging from - 1 to - 3‰, there is a clear tendency to assume more positive values in time. This evidently signifies the widening of that zone in which the contribution of the deeper steam is prevalent.

On the contrary, in the most peripheric area, where the isotopic composition ranges from - 3 to - 5‰ in some parts of the boundary, there is a clear tendency towards the production of steam with more negative $\delta^{18}O$ values. This indicates that the relative contribution of the water, coming directly from the absorption area through the fast circulation, is increasing.

8. CONCLUSION

The isotopic tool is therefore an attractive one to use in determining the origin and mixing of groundwater sources.

Furthermore, in a geothermal field under exploitation, a detailed survey of the variation in the ^{18}O (and T) composition in time allows us to reveal the progressive modification that occurs in the field as a consequence of its exploitation.

Finally, we suggest that it is possible that this kind of investigation will also become a valuable tool to check the effects of re-injection of waste water in the field.

REFERENCES

[1] CRAIG, H., "The isotopic geochemistry of water and carbon in geothermal areas", Nuclear Geology on Geothermal Areas (TONGIORGI, E., Ed.), Spoleto (1963).

[2] WHITE, D.E., "Geochemistry applied to the discovery, evaluation and exploitation of geothermal energy resources", Sect.V, UN Symp. Development Utilization Geothermal Resources, Pisa (1970).

[3] GONFIANTINI, R., BORSI, S., FERRARA, G., PANICHI, C., Isotopic composition of waters from the Danakil depression (Ethiopia), Earth Planet. Sci. Lett. 18 (1973) 13.

[4] FERRARA, G.C., GONFIANTINI, R., PANICHI, C., La composizione isotopica del vapore di alcuni soffioni di Larderello e dell'acqua di alcune sorgenti e mofete della Toscana, Atti Soc. Toscana Sci. Nat. Pisa, P.V. Mem., Series A 72 (1965) 570.

[5] BANWELL, C.J., "Oxygen and hydrogen isotopes in New Zealand thermal areas", Nuclear Geology on Geothermal Areas (TONGIORGI, E., Ed.), Spoleto (1963).

[6] WHITE, D.E., CRAIG, H., BEGEMANN, F., "Summary of the geology and isotope geochemistry of Steamboat Springs, Nevada", Nuclear Geology on Geothermal Areas (TONGIORGI, E., Ed.), Spoleto (1963).

[7] KOGA, A., Geochemistry of the waters discharged from drillhole at Otake and Hatchobaru areas (Japan), Geothermics 2, Part 1 (1970) Special Issue 2.

[8] CRAIG, H., Standard for reporting concentrations of deuterium and oxygen-18 in natural waters, Science 133 (1961) 1833.

[9] CATALDI, R., STEFANI, G., TONGIORGI, M., Geology of Larderello region (Tuscany); contribution to the study of the geothermal basins, Nuclear Geology on Geothermal Areas (TONGIORGI, E., Ed.), Spoleto (1963).

[10] MAZZANTI, R., Geologia della zona di Pomarance – Larderello (Prov. di Pisa), Mem. Soc. Geologica Italiana 5 (1966).
[11] LAZZAROTTO, A., Geologia della zona compresa tra l'alta Valle del fiume Cornia ed il torrente Pavone (Prov. di Pisa e Grosseto), Mem. Soc. Geologica Italiana 6 (1967).
[12] CATALDI, R., ROSSI, A., SQUARCI, P., STEFANI, G., TAFFI, L., Contribution to the knowledge of the Larderello geothermal region: remarks on the Travale field, Geothermics 2 ,Part 1 (1970) Special Issue 2.
[13] CLAYTON, R.N., MUFFLER, L.J.P., WHITE, D.E., Oxygen isotope study of calcite and silicates of the River Ranch No.1 well, Salton Sea geothermal field, California, Am. J. Sci. 266 (1968) 968.

DISCUSSION

G. H. DAVIS: Have you found that the ^{18}O shift can be used effectively as a "geothermometer" in the Larderello area?

C. PANICHI: The reported ^{18}O values for carbonate samples collected during well drilling in this area confirm that temperature-dependent isotopic exchange between water and rocks occurs. Consequently, as the isotopic composition of the steam in the area is well known, isotopic exchange effects can in principle be used in estimating underground temperature. However, the temperatures obtained in this way do not exceed 150°C, whereas temperatures ranging from 200°C to 250°C are measured in the geothermal steam. I think the discrepancy can be attributed either to the fact that the isotopic exchanges do not reach equilibrium or to the fact that the isotopic composition of carbonate reflects previous hydrological conditions, when the temperatures of the investigated layers were probably lower than those now observed, that is, before the present vapour-dominated area developed as a consequence of exploitation.

HOT SPRINGS OF THE IGNEOUS TERRAIN OF SWAZILAND
Their noble gases, hydrogen, oxygen and carbon isotopes and dissolved ions

E. MAZOR*, B. T. VERHAGEN
Nuclear Physics Research Unit,
University of Witwatersrand,
Johannesburg, Republic of South Africa

E. NEGREANU
Isotope Department,
The Weizmann Institute of Science,
Rehovot, Israel

Abstract

HOT SPRINGS OF THE IGNEOUS TERRAIN OF SWAZILAND: THEIR NOBLE GASES, HYDROGEN, OXYGEN AND CARBON ISOTOPES AND DISSOLVED IONS.

The hot springs of Swaziland are of great interest as they occur in an area devoid of recent volcanism and issue in igneous, rather than in sedimentary rocks. An origin from directly infiltrating rain water is concluded from the Ne, Ar, Kr and Xe concentrations, and the δD and $\delta^{18}O$ values. The noble gases are shown to have been kept in closed system conditions, and their concentrations lead to the deduction of paleotemperatures at infiltration of 21°C to 31°C, which are similar to the present local summer temperatures. The ^{14}C age of the waters is calculated to be 4500 to 5400 years, and tritium concentrations are very low, indicating that the bulk of groundwater is indigenously deep seated. The chemical composition is unique, the total dissolved salts being 120 ppm, reflecting contact with igneous as opposed to sedimentary rocks.

1. INTRODUCTION

Hot springs are common all over the world, many of them being situated in regions of recent volcanic activity, to which their heat is often ascribed. In addition, many of the world's hot waters issue in sedimentary rocks and most, if not all, of their salt constituents are often attributed to dissolution from these rocks. Swaziland offers hot springs in a different geological setting, unassociated with any recent volcanism, and issuing in igneous rather than sedimentary rocks.

About ten hot springs are known in Swaziland (Fig. 1 and Table I), a few of them with several eyes. Seven of these have been sampled for detailed analysis of their dissolved noble gases, their stable hydrogen and oxygen isotopes, tritium and the composition of their dissolved ions. ^{14}C dating and stable carbon isotope analysis were carried out on three of the springs. In addition four adjacent rivers have been sampled for comparison.

The geology of Swaziland has been studied by Hunter [1] and a general description of the Swaziland hot springs has been given by the same investigator [2]. A number of chemical analyses are given by Rindl [3] and by

* On sabbatical leave from the Israel Atomic Energy Commission and the Weizmann Institute of Science, Rehovot, Israel, during 1972.

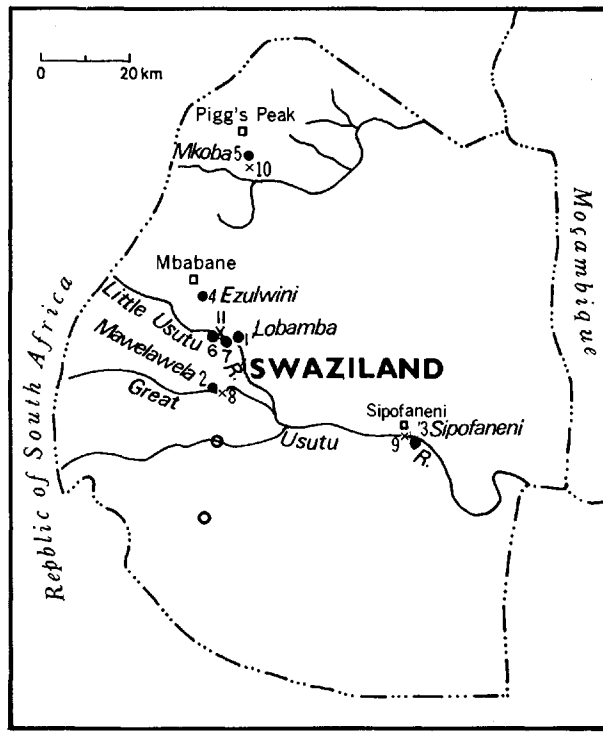

FIG. 1. Location map of sampled hot springs (●) and adjacent rivers (x). Known hot springs which were not included in the present study are marked by open circles.

the Geological Survey of Swaziland [4]. A physical description of the thermal Mkoba spring, in the Pigg's Peak region, is given by Spargo [5]. The springs are all situated in Precambrian granite or gneiss [2]. The springs, apart from Sipofaneni, are regarded by King [6] and Temperley [7] to lie on a line of crustal weakness, on whose South African extension four of the Natal hot springs are situated, namely Sulphur Springs (30.1°C), Warmbad (37.2°C), Frischgewaag (29.5°C) and Natal Spa (41.1°C). These springs are described also by Kent [8].

The Swaziland Springs are rather low yielding, with outputs varying from 3 to 19 m^3 hourly [2].

2. THE NOBLE GASES

The water samples for noble gas analysis were carefully collected in 1 cm^3 glass tubes with high vacuum stopcocks at both ends. These were sealed to an extraction system, the gas phase was separated and purified over a titanium getter and the noble gases were introduced into a Reynold's type 60°, 4.5" glass mass spectrometer (Nuclid Co.) and measured against

atmospheric standards. Details of the sampling technique, the mass spectrometric measurements and the analytical errors (± 5% or less for elemental concentrations in the present work) are given by Mazor [9].

The solubility of He and Ne in water is relatively independent of temperature, but the solubility of Ar, Kr and Xe is highly temperature-dependent (Fig. 2). Dissolved helium is often enriched by radiogenic helium, flushed out of the country rocks, but Ne enters groundwaters via contact with the air alone. As may be seen in Fig. 2, the maximum possible Ne content in air-equilibrated water at temperatures of 10°C to 60°C is 2.3×10^{-7} $cm^3 STP/cm^3$ water. Air bubbles trapped during sampling may increase this amount significantly, the contamination caused by free air being highest for Ne and progressively lower for the heavier noble gases. Samples with Ne contents significantly higher than the above-mentioned value of 2.3×10^{-7} cm^3 STP/cm^3 water may thus be rejected as contaminated, whereas samples with Ne at or below this value may be regarded as free from any significant contamination. Fifteen of the measured samples are uncontaminated by this criterion (Table II) and only one, run No. 239, is a borderline case. The accompanying Ar, Kr and Xe values are slightly lower than those of the twin sample, No. 236, however, and hence this case also appears to be uncontaminated (the Ne is probably high because of an analytical error somewhat above average). The air contamination problem is further discussed by Mazor [9].

The noble gas data are given in Table II. The following characteristics are seen.

2.1. Noble gas air-supersaturation at the time of sampling

In Fig. 3 the air-saturation percentages for the various samples are plotted for Kr and Xe. These values were obtained by multiplying the measured values by 100 and dividing by the amount expected in air-saturated water at the sampling temperature, the value being read for each case from the solubility curve (Fig. 2). It is seen that the samples (except for the Xe value of run No. 237) were air-supersaturated when sampled. The values are 100-150% for Ar, 115-152% for Kr and 96-158% for Xe. Hence, some losses could occur from the springs before sampling. For this reason each spring has been sampled two to three times, and in further discussions the sample of highest noble gas contents has been selected from each spring, assuming it to be closest to the indigenous state. The similar values obtained in this way for the various springs lead us to believe that the noble gas escape was indeed low for the selected samples.

2.2. Radiogenic helium enrichments

The ^4He contents are several orders of magnitude higher than the corresponding air-saturation value, i.e. up to $17\,000 \times 10^{-8}$ cm^3 STP/cm^3 water. These large excesses are attributed to flush-out of radiogenic helium from the decay of uranium and thorium, present in the ppm range in all common rocks. Such radiogenic He is often observed in hot waters and seems to be a useful indicator for slow moving, or static, water.

TABLE I. DESCRIPTION OF SPRINGS

Station	Spring	Location	Temperature (°C)	Geology
1	Lobamba 3	31°13'E; 26°27'S	44.0	Grey granodiorite
2	Mawelawele	31°09'E; 26°35'S	35.0	Porphyrite granite
3	Sipofaneni	31°41'E; 26°39'S	44.0	Alluvial valley in granodioritic terrain
4	Ezulwini ("Spa")	31°10'E; 26°24'S	45.0	Alluvial valley in granitic terrain
5	Mkoba	31°15'E; 26°01'S	51.5	Small acidic pink intrusion into grey coarse-grained granite
6	Lobamba 1	31°12'E; 26°26'S	44.0	Alluvial valley in granodioritic terrain
7	Lobamba 2	31°12'E; 26°26'S	45.5	Alluvial valley in granodioritic terrain

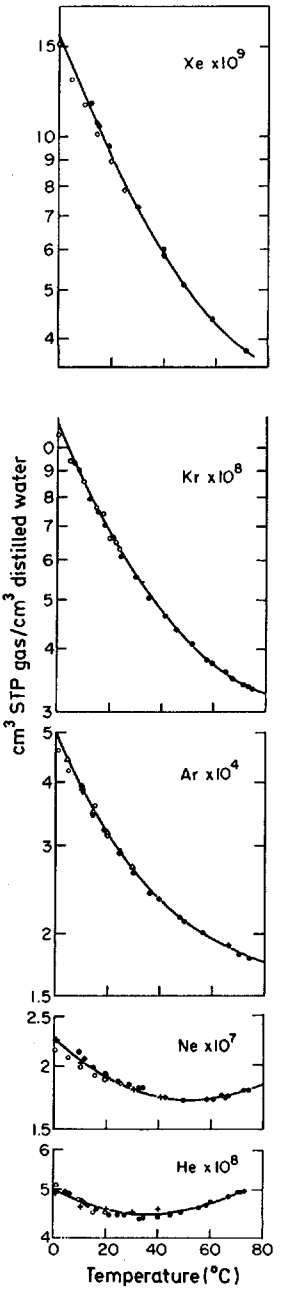

FIG. 2. Solubility of noble gases in fresh water. Source of data: ● - [10]: multiplying his sea-water data by his given ratios for solubility in distilled water to solubility in sea-water; + - [11]; ○ - [12]; and Δ - [13]: multiplying their data by the atmospheric abundances.

TABLE II. NOBLE GASES (cm^3 STP/cm^3 WATER)[a]

Station No.	Run No.	Spring	Temp. (°C)	He × 10^8	Ne × 10^8	Ar × 10^4	$^{40}Ar/^{36}Ar$ sample	$^{40}Ar/^{36}Ar$ standard	$(^{40}Ar/^{36}Ar)$ sample / $(^{40}Ar/^{36}Ar)$ standard	Atmospheric $^{40}Ar \times 10^4$	Radiogenic $^{40}Ar \times 10^4$	Kr × 10^9	Xe × 10^9
4	234	Ezulwini ("Spa")	45.0	12 266	19.5								
	235			9 519	19.8	3.17	312.5	296.8	1.053	3.01	0.16	58.0	7.20
	238			9 711	21.2	3.18	311.5	289.4	1.076	2.95	0.23	64.3	8.20
6	228	Lobamba 1	44.0	11 720	17.9	2.76	352.4	286.4	1.23	2.24	0.52	51.1	6.65
	237			10 068	18.8	3.00	323.7	292.5	1.11	2.70	0.30	52.7	5.30
7	226	Lobamba 2	45.5	8 198	14.0	2.93	312.1	288.9	1.080	2.71	0.22	53.8	7.23
	231			5 083	12.3	2.65	309.5	292.7	1.057	2.51	0.14	51.9	7.25
1	236	Lobamba 3	44.0	14 400	20.9	3.63	320.0	291.2	1.10	3.30	0.33	64.8	8.34
	239			17 545	25.8	3.65	325.3	289.6	1.12	3.26	0.43	61.6	8.20
2	229	Mawelawele	35.0	8 427	22.6	3.39	312.2	298.6	1.046	3.23	0.13	60.7	7.32
	233			6 422	17.1	3.33	313.3	282.1	1.110	3.00	0.33	61.7	7.84
3	224	Sipofaneni	44.0	8 759	18.2	3.22	326.4	290.0	1.12	2.88	0.34	60.1	8.70
	230			7 172	17.5	3.05	326.3	292.7	1.11	2.75	0.30	56.6	6.61
	240			8 560	20.3	3.38	323.7					55.7	6.20
5	227	Mkoba	51.5	14 478	13.5	3.37	352.9	296.7	1.19	2.83	0.54	47.1	5.54
	232			17 464	17.8	3.76	354.9	298.5	1.19	3.16	0.60	61.4	7.42
		Air-saturated water	25.0	4.5	18.5					2.85		60.5	8.0

[a] Elemental concentration errors are ±8% or less [9], and the $^{40}Ar/^{36}Ar$ ratio is assigned an error range of up to ±2%.

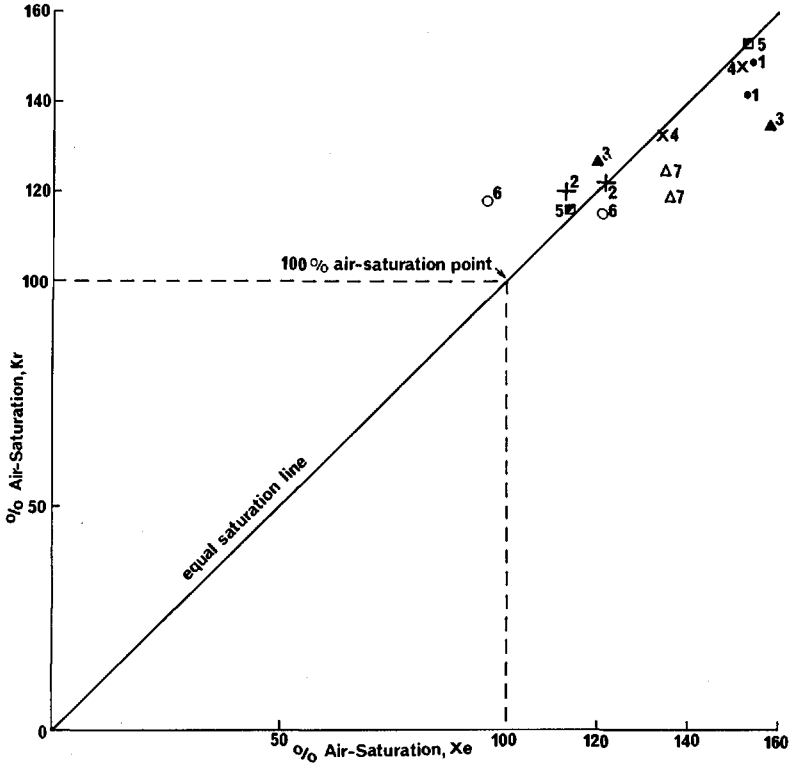

FIG. 3. Percentage air saturation of Kr and Xe. The values were obtained by multiplying the measured values (Table II) by 100 and dividing by the amounts expected for air-equilibrated water (Fig. 2) at the sampling temperature (Table I). All samples, apart from the Xe value of sample No. 6, are supersaturated. The corresponding values for Ar are similar to those of the Kr and Xe. This supersaturation at the time of sampling is taken as an indication that the waters were kept in the ground in closed system conditions with respect to their noble gases, but some gas could escape into the air before sampling. The highest values for each spring are therefore taken to be closest to the indigenous values.

2.3. Radiogenic argon

The $^{40}Ar/^{36}Ar$ ratio in the samples is significantly higher than in the atmospheric standards measured in the same runs. The ^{40}Ar enrichments are in the range of 5 to 23% (Table II). This ^{40}Ar excess is attributed to flush-out of radiogenic argon, formed by decay of ^{40}K, present in the ppm level in all common rocks.

A positive correlation is observed for the radiogenic He and Ar enrichment, as seen in Fig. 4. The range of radiogenic He/Ar ratio is 2.6 to 5. This is similar to ratios of 2-4 observed in New Zealand hot springs [14] and equal to a value of 4 found in Yellowstone hot waters [15]. This value is also in the range of the average He/Ar radiogenic production ratio of about 10, calculated by Zartman and co-workers [16] for common crustal rocks.

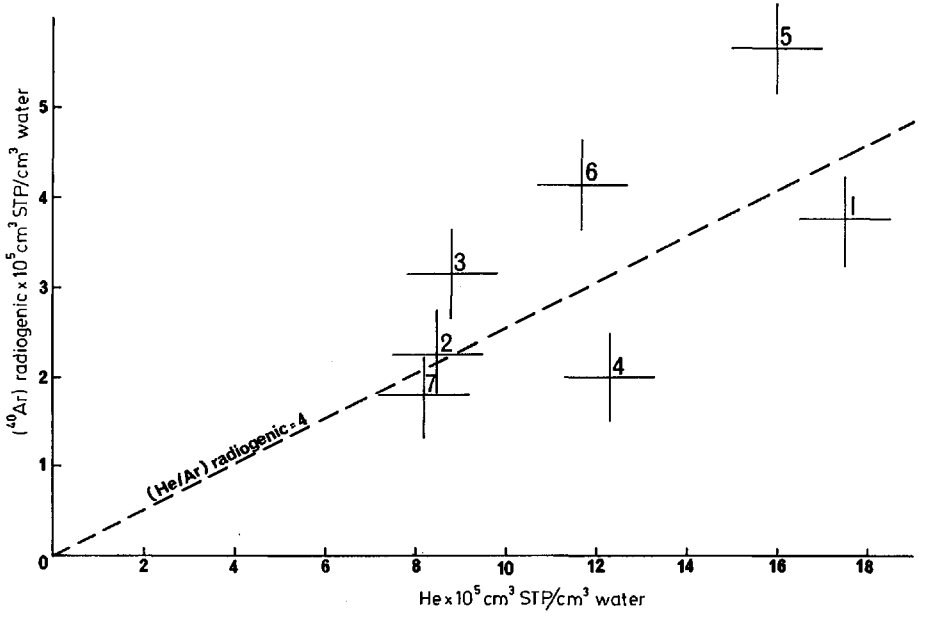

FIG. 4. Correlation of radiogenic ^{4}He and radiogenic ^{40}Ar. The average (He/Ar) radiogenic ratio is 4, similar to the values 2-4 found in New Zealand hot waters [14] and to the value 4 found in Yellowstone [15].

2.4. Atmospheric relative abundances indicating meteoric origin

The relative aboundance of Ne, atmospheric Ar (i.e. after correction for radiogenic additions (Table II) by use of the ^{40}Ar/^{36}Ar ratio in the accompanying standard measurement), Kr and Xe closely resemble those in air-saturated water. In Fig. 5 the selected samples (richest in noble gases for each spring) were plotted along with the abundance values of air-saturated water at 25°C, and the similarity of the lines is obvious.

This is taken as proof that we are dealing with meteoric water, which penetrated the ground after equilibration with air at the then prevailing ambient temperature. No other process is likely to exist in nature that can load these waters by noble gases in near atmospheric proportion. This meteoric nature is independently revealed by the stable isotopes, as discussed below.

2.5. Deduction of paleotemperatures

Thermal waters were air-supersaturated with respect to their noble gases when sampled. This is taken as an indication that once the meteoric water entered the ground it was kept in closed system conditions with respect to its atmospheric gas content, even though the water was subsequently heated.

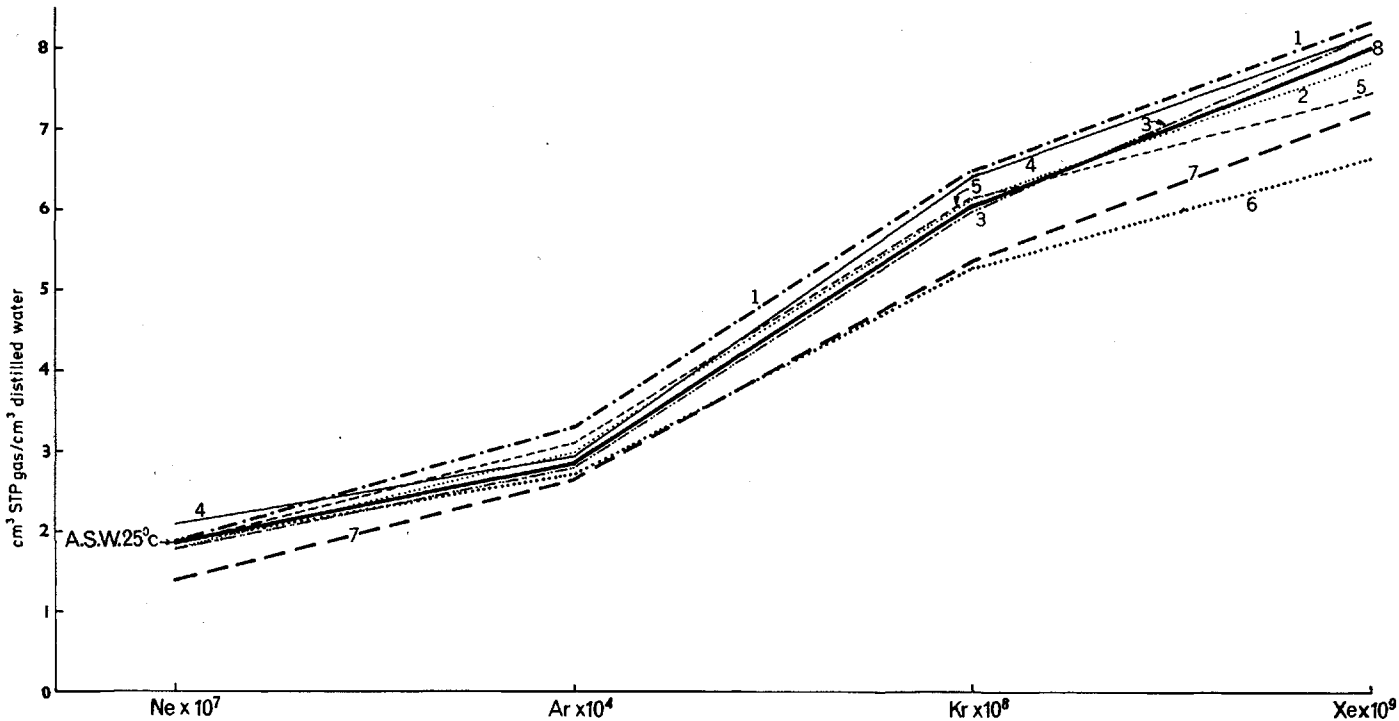

FIG. 5. The noble gas pattern (in the samples of highest noble gas contents in each spring, see text). The values are seen to group closely around the line of air-equilibrated water at 25°C (solid line). This is taken as a proof for the meteoric origin of the waters, as no other mechanism could load them with noble gases in atmospheric-like abundances.

TABLE III. PALEOTEMPERATURES

Run No.	Spring	Sampling temperature (°C)	Paleotemperatures (°C)			
			Ar	Kr	Xe	Mean [b]
238	Ezulwini ("Spa")	45.0	23	22	24	23 ± 1
237	Lobamba 1	44.0	28	32	33 [a]	31 ± 2
226	Lobamba 2	45.5	28	31	29	29 ± 1
236	Lobamba 3	44.0	17	22	23	21 ± 3
233	Mawelawele	35.0	22	23	26	24 ± 2
224	Sipofaneni	44.0	24	25	22	24 ± 1
232	Mkoba	51.5	19	24	28	24 ± 3

[a] The Xe value of run 237 is obviously too low, hence the value of run 228 was applied.

[b] The error cited is the mean deviation between the measurements of Ar, Kr and Xe. The estimated analytical error of ± 5% or better of these elements introduces an uncertainty of about ± 2°C. Thus the deviations observed between the Ar, Kr and Xe paleotemperatures are in the range of the analytical accuracy.

Hence, the atmospheric Ar and Kr and Xe concentrations may be used to calculate the "paleotemperatures" of the waters, i.e. the ambient temperatures that prevailed on the ground at the time of infiltration. These temperatures can be read from the solubility graph in Fig. 2. The paleotemperatures may be calculated for each spring independently from its Ar, Kr and Xe contents. Good agreement is seen (Table III) between the results of calculations for these three gases. The mean deviations of the three values for each spring vary from ± 1°C to ± 3°C. The mean paleotemperatures themselves vary from 21°C to 31°C.

The time, or age, to which these paleotemperatures are relevant can be deduced from ^{14}C measurements (see below). In any case it is interesting to note that the average "paleotemperatures" are close to the average summer temperatures of Swaziland (and it is the summer temperature that counts, as Swaziland is, and probably has been for some millenia, a summer rainfall area). In addition this origin from rain water is borne out by the stable isotope composition of the springs.

2.6. Average temperature in the aquifers feeding the hot springs

The noble gas contents enable us to make general deductions on the temperature of the water reservoirs that feed the springs.

Two basic types of atmospheric noble gas patterns have so far been found in hot springs. These are:

(a) Springs with temperatures below boiling point, in which the noble gases are kept in closed system conditions and hence issue with gas contents equivalent to those found in air-saturated waters at common surface temperatures (10°-30°C). The best examples of such cases so far studied occur in the Jordan Rift Valley in Israel [9] and a few hot springs in Rhodesia [17].

(b) Springs fed by superheated water from which separating steam can strip most of the noble gases, before or at the point of issue. Examples of this type were found in the Yellowstone National Park [15], in Sulfur Bank of the Pacific Tectonic Belt, United States of Ameria [18] and in the boiling Binga springs of Rhodesia [17]. In these cases as little as 10% of the original atmospheric noble gases may remain.

The Swaziland springs clearly belong to the first group, i.e. waters that retained their atmospheric noble gases. It seems, tentatively, that these springs are not fed by superheated water at depth, a conclusion independently supported by the stable isotopes as is shown below.

3. DEUTERIUM AND ^{18}O

The δD and $\delta^{18}O$ values have been measured mass-spectrometrically in the springs studied as well as in four adjacent rivers (Table IV and Fig. 6).

The four river values plot along a line which is typical for rain and derived surface water. The lightest of the samples is No. 10, collected from the short Mkoba tributary of the Komati River, in the mountainous area of Piggs Peak which might well have isotopically relatively light rains.

TABLE IV. CHEMICAL AND ISOTOPIC DATA

Station	Source	pH	K[a]	Na[a]	Mg[a]	Ca[a]	F[a]	Cl[a]	SO_4[a]	HCO_3[a]	Total ions	δD‰	$\delta^{18}O$‰	Tritium (TU)
4	Ezulwini ("Spa")	8.6	1[b]	35	2	4	6	11	11	53	123	-14.8 ± 1.6	-4.05 ± 0.09	0.5 ± 0.2
			0.026[c]	1.52	0.16	0.20	0.32	0.31	0.23	1.09	3.85			
6	Lobamba 1	7.9	1	48	1	4	6	14	8	81	163	-15.5 ± 1.6	-4.62 ± 0.09	1.3 ± 0.2
			0.026	2.09	0.082	0.20	0.32	0.40	0.17	1.44	4.70			
7	Lobamba 2	7.9	1	45	1	4	6	14	6	81	158	-18.1 ± 1.3	-4.11 ± 0.08	0.4 ± 0.2
			0.026	1.96	0.082	0.20	0.32	0.40	0.13	1.44	4.55			
1	Lobamba 3	8.0	1	45	1	4	7	14	6	74	152	-14.4 ± 1.6	-4.48 ± 0.09	0.6 ± 0.2
			0.026	1.96	0.082	0.20	0.37	0.40	0.13	1.33	4.48			
2	Mawelawele	7.9	1	45	2	9	7	14	6	87	171	-18.8 ± 1.6	-4.05 ± 0.09	0.2 ± 0.2
			0.026	1.96	0.16	0.45	0.37	0.40	0.13	1.54	5.03			
3	Sipofaneni	7.9	4	135	1	2	7	121	30	101	401	-14.7 ± 1.6	-4.09 ± 0.09	0.4 ± 0.2
			0.10	5.87	0.082	0.10	0.37	3.41	0.62	1.77	12.3			
5	Mkoba	8.3	1	58	1	4	6	21	6	93	190	-18.6 ± 1.6	-3.96 ± 0.09	1.1 ± 0.2
			0.026	2.52	0.082	0.20	0.32	0.59	0.13	1.74	5.61			
11	River at Lobamba Little Usutu R.	7.4	-	7	4	2	1	7	5	27	53	-12.1 ± 1.1	-3.27 ± 0.08	46.9 ± 1.8
				0.30	0.33	0.10	0.053	0.20	0.10	0.44	1.53			
8	River at Mawelawele Great Usutu R.	7.5	1	11	4	4	1	11	9	40	81	-10.5 ± 1.3	-2.60 ± 0.08	53.2 ± 3.5
			0.026	0.48	0.33	0.20	0.053	0.31	0.19	0.66	2.30			
9	River at Sipofaneni Great Usutu R.	7.6	1	9	7	4	1	11	8	47	88	- 4.5 ± 1.1	-2.16 ± 0.08	46.1 ± 2.5
			0.026	0.39	0.58	0.20	0.053	0.31	0.16	0.77	2.50			
10	River at Mkoba Mkoba R. (into the Komati)											-13.6 ± 1.1	3.40 ± 0.08	

[a] Geological Survey, Botswana. [b] mg/litre. [c] meq/litre.

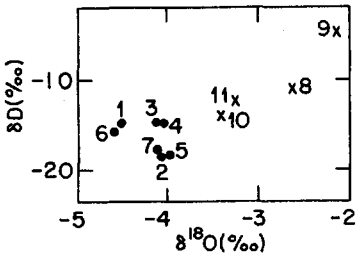

FIG. 6. Isotopic composition. The river samples (x) lie on a line which is common for rain. The sequence of the river samples along this trend is understood from their locations and reveals slight progressive evaporation (see text). The hot springs (●) may well originate from non-evaporated infiltrating rain water. The stable isotopes seem to reveal, independently, the meteoric origin of the hot springs studied.

TABLE V. CARBON ISOTOPES AND INFERRED AGES

Source	^{14}C (pmc) [a]	$\delta^{13}C$‰ [b]	Age I (years) [c]	Age II (years) [d]
Ezulwini ("Spa")	47.6 ± 2.1	-13.6 ± 0.07	4660	1080
Lobamba 2	43.5 ± 1.8	-14.48 ± 1.8	5400	2300
Sipofaneni	48.5 ± 2.5	-12.4 ± 0.07	4500	200

[a] In per cent modern carbon (pmc).
[b] Isotope Department, Weizmann Institute of Science.
[c] Assuming groundwater initially contains 85 pmc [19].
[d] ^{14}C value applied as initial content derived by dividing measured value by $\delta^{13}C/-25$. See text for evaluation of Ages I and II.

The next in the sequence is sample No. 11, collected at a tributary of the Little Usutu, and this is followed by samples 8 and 9, both from the Great Usutu, No. 9 being about 220 km downstream from No. 8. The four river samples thus reveal isotopic values resulting from slight progressive evaporation. The average rain composition seems to be close to, or very slightly lighter than, the values of sample No. 10.

The results of the hot springs are grouped around δD - 17‰ and $\delta^{18}O$ - 4.2‰, and are slightly lighter than the river waters, probably close to the composition of the local rain at the time of infiltration.

The stable isotope data therefore lead independently to the following conclusions:

(a) The hot springs are fed by rain water that did not undergo evaporation and, hence, infiltrated directly into the ground.

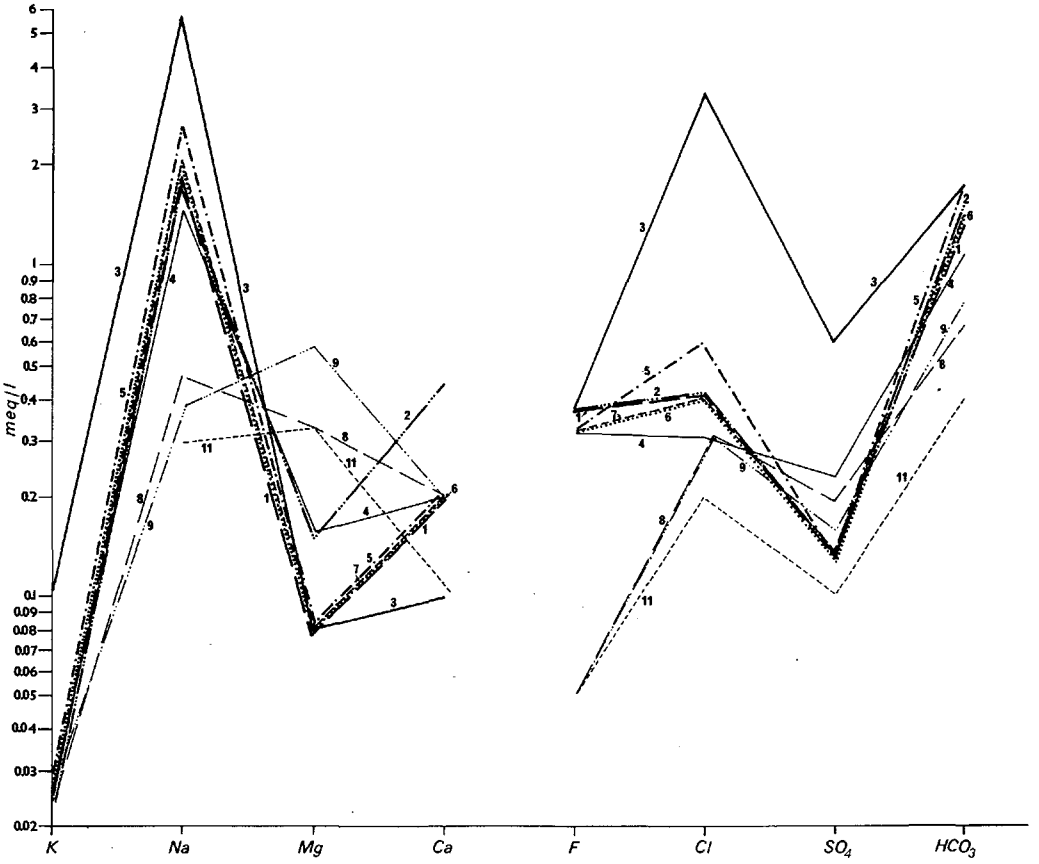

FIG. 7. The chemical composition. The hot spring waters (1 - 7) are higher in their salt contents than the adjacent river waters (8, 9, 11). If the rivers are taken to represent in their composition the original infiltrating meteoric water, then the hot springs must have picked up from the igneous and metamorphic country rocks, Na, F and HCO_3, and have lost Mg, perhaps by exchange reactions. The higher NaCl value of Sipofaneni (sample 3) might be caused by brief contact with Karroo sediments (see text).

(b) The hot springs did not suffer from partial losses of a steam phase, which would result in an isotopically heavier residual water phase. These waters are fed by reservoirs at temperatures that are significantly below boiling, a conclusion already reached on the basis of dissolved noble gas data.

4. TRITIUM CONCENTRATIONS

The tritium values for three measured rivers are 46-53 TU. The values found in the hot springs are, however, only 0.0-1.3 TU (Table IV). This suggests that the spring waters are virtually not mixed with river, or other very recent water met during their ascent. An upper limit for such additions may be reached if it is assumed that the indigenous hot waters are devoid of tritium. Even in such a case the additions from intermixing surface water will be limited to 0-2%. Hence, the spring waters may justifiably be regarded as indigenous, deep-seated when discussing their noble gas contents, stable isotope composition, ^{14}C values or composition of the dissolved ions.

5. CARBON ISOTOPES AND INFERRED AGES

Water from three springs has been extracted at the field for its carbon extraction. The measured $\delta^{13}C$ and ^{14}C values are given in Table V.

The measured springs issue in igneous terrain and in two of them $NaHCO_3$ is the dominant dissolved salt species. However, the observed $\delta^{13}C$ values of 12-14‰ are close to values known elsewhere from sedimentary terrain.

Two types of age calculations were applied in Table V. Age I was based on the assumption that the groundwaters had an initial ^{14}C content of 85 pmc [19, 20]. Age II was calculated by correcting for initial dilution by fossil carbon by dividing the observed ^{14}C value by $\delta^{13}C/-25$ [21]. The set of Ages I seems to reveal a better internal consistency than those of Ages II (Table V). There are, however, no criteria at hand with which to decide on the correct ^{14}C ages. These may perhaps be re-calculated in the future, once the art of ^{14}C age deduction reaches a more advanced state.

In conclusion, the ^{14}C content seems to indicate that the hot spring water studied in Swaziland is a few thousand years old, i.e. older than the water in the active cycle of shallow groundwater but not entirely fossil.

An age of a few thousand years would be in good agreement with the elevated contents of radiogenic He and Ar, which reached the observed level by prolonged contact with aquifer rocks.

6. THE CHEMICAL COMPOSITION

The chemical composition of the springs studied and the adjacent rivers is given in Table IV and Fig. 7. Comparison with a number of chemical analyses previously published [3, 4] reveal a general similarity;

a detailed comparison is not possible, as these sampling sites could not be accurately identified. The following features emerge from the chemical data:

(a) Remarkably low salt contents. The springs, though thermal, are surprisingly low in their salt contents, the total ions ranging from one case of 400 ppm. This is definitely to be attributed to the igneous rock environment composed mainly of granites (Table I), which contain very little soluble material. This is in remarkable contrast to most hot springs in the world, which are frequently loaded with salts, originating from sedimentary rocks.

In spite of the very low salinity, some of the waters are not palatable because of a sulphur taste and an occasional H_2S smell.

(b) Reactions with the igneous host rocks. The rivers have a total ion content of 53 to 88 ppm, whereas the hot springs have a content of 120 to 400 ppm. It has been shown from the noble gas and stable isotope data that the springs are of meteoric origin. It seems reasonable that the initial salt content of this meteoric water was, at most, as high as in the rivers. Hence, the additional ions result from the igneous rocks or their derived soils. The various springs, except Sipofaneni, have much in common in their dissolved salts (Fig. 7), their cations being $Na \gg Ca > Mg$, and their anions being $HCO_3 > Cl > F > SO_4$ and the dominant salt species being $NaHCO_3$.

The enrichments above river water are in Na, F, HCO_3 and very slightly in Cl. Magnesium has been depleted, possibly because of ion exchange, a process seen elsewhere, also in other water associations.

Sipofaneni has more than twice the T.D.S. of the other springs, the dominant addition being NaCl (Table IV and Fig. 7). This might well be explained by the location of this spring on a post-Karroo joint and adjacent Karroo outcrops. It seems likely that, although Sipofaneni issues in igneous rocks, its water comes into contact with Karroo sediments, which contribute additional salts [22].

ACKNOWLEDGEMENTS

We wish to warmly thank G. Sharig, Governmental youth adviser, for his generous help, and A. Mokatshwa for guidance to the Mkoba spring; also J.R. Abbott, Swaziland Senior Water Officer, for valuable information, and Mr. Ford, Superintendent of the Royal Swazi Spa, for his assistance.

Informative discussions with Professor J.P.F. Sellschop, Director of the Nuclear Physics Research Unit, University of the Witwaterstrand, and D.R. Hunter, the Department of Geology, University of the Witwatersrand, are gratefully acknowledged.

The stable hydrogen, oxygen and carbon isotope measurements were kindly done in the laboratories of Professor J.R. Gat, the Isotope Department of the Weizmann Institute of Science, Rehovot. The chemical analyses were carried out in the Chemical Laboratory of the Geological Survey of Botswana, headed by L. Hutton. The help of these colleagues and of the N.P.R.U. Environmental Isotope Group staff is much appreciated.

REFERENCES

[1] HUNTER, D.R., Geological map of Swaziland 1 : 250 000; Geological Survey and Mines Dept., Mbabane, Swaziland (1966).
[2] HUNTER, D.R., 23rd Int. Geol. Congr. 19 (1969) 165.
[3] RINDL, M., S. Afr. J. Sci. 29, Suppl. 4 (1932) 278.
[4] Swaziland Geological Survey, Bull. No. 6 (1966).
[5] SPARGO, P.E., S. Afr. J. Sci. 61 (1965) 179.
[6] KING, L.C., Trans. Geol. Soc. S. Afr. 64 (1961) 64.
[7] TEMPERLEY, B.N., Ann. Rep. Geol. Surv. S. Afr. 3 (1964) 139.
[8] KENT, L.E., 23rd Int. Geol. Congr. 19 (1969) 143.
[9] MAZOR, E., Geochim. Cosmochim. Acta 36 (1972) 1321.
[10] KONIG, von H., Z. Naturforsch. 18a (1963) 363.
[11] DOUGLAS, E.J., J. Phys. Chem. 68 (1964) 169.
[12] MORRISON, T.J., JOHNSTONE, N.B., J. Chem. Soc., Part III (1954) 3441.
[13] WEISS, R.F., J. Chem. Eng. Data 16 (1971) 235.
[14] WASSERBURG, G.J., MAZOR, E., ZARTMAN, R.E., "Isotopic and chemical composition of some terrestrial natural gases", Earth and Meteorics (GREISS, J., GOLDBERG, E.D., Eds), North-Holland Publishing, Amsterdam (1963).
[15] MAZOR, E., FOURNIER, R., Geochim. Cosmochim. Acta 37 (1973) 515.
[16] ZARTMAN, R.E., WASSERBURG, G.J., REYNOLDS, J.H., J. Geophys. Res. 66 (1961) 277.
[17] MAZOR, E., VERHAGEN, B.Th., Geochim. Cosmochim. Acta, in press.
[18] MAZOR, E., BARNES, I., unpublished data.
[19] MÜNNICH, K.O., Naturwissenschaften 44 (1957) 32.
[20] VOGEL, J.C., EHHALT, D., "The use of carbon isotopes in groundwater studies", Radioisotopes in Hydrology (Proc. Symp. Tokyo, 1963), IAEA, Vienna (1963) 383.
[21] INGERSON, E., PEARSON, F.J., Jr., "Estimation of age and rate of motion of ground water by the ^{14}C method", Recent Researches in the Fields of Hydrosphere, Atmosphere and Nuclear Geochemistry, Sugawara volume, Maruzen, Tokyo (1964) 263.
[22] HUNTER, D.R., private communication.

DISCUSSION

J.Ch. FONTES: To what extent was the rain water saturated in noble gases?

E. MAZOR: In the few rain-water analyses which we performed, we observed slight oversaturation, attributable to lower temperatures in the clouds. In that connection, I would mention that, when the rain water reached the ground surface, its temperature equilibrated rapidly with the ambient temperature.

P. FRITZ: The solubility of a gas depends not only on temperature but also on the ionic strength of the solution. Was the concentration of rare gases in your samples affected by the dissolving of salt underground?

E. MAZOR: No, for our samples contained a total of only 120 ppm T.D.S.

R.R. LETOLLE: With regard to Fig. 4, was the helium excess determined using the $^3He/^4He$ ratio?

E. MAZOR: No, we are not able to measure ^3He with our methods. We decided that the helium was radiogenic because its concentrations was four orders of magnitude higher than in air-equilibrated water.

H. OESCHGER (Chairman): Could you use the radiogenic helium and argon as a basis for dating?

E. MAZOR: I do not think so, for we do not know the volume ratio of water to flushed rock.

D. B. SMITH: Any loss of dissolved gas from the thermal water before obtaining the sample will apparently lead to an overestimate of the temperature of the recharge water. For two springs (Lobamba 1 and 2) Table III gives significantly higher recharge temperatures. Are there any geohydrological features associated with these particular springs which could cause a higher loss of gas than might occur in the other springs which were sampled?

E. MAZOR: Not as far as I am aware. In this connection I would stress, however, that our figures represent maximum temperatures and that additional data would be helpful.

F. J. PEARSON: Hydraulic models of hot spring systems in regions with no recent volcanism show that a source of heat greater than that supplied by a normal geothermal gradient is required for some of the systems to function. The source may be slightly higher than normal concentrations of such radioisotopes as ^{40}K or uranium in the aquifer material. If you have sufficient knowledge of the hydrology of your system, you may be able to make an order-of-magnitude estimate of aquifer radioisotope concentrations from your excess ^{4}He and ^{40}Ar concentrations. Such an estimate would be of great interest to those working with geothermal systems elsewhere.

E. MAZOR: I agree. However, the rise of hot water is often attributable to a head of fresh water, and we believe this may be the case in Swaziland.

V. T. DUBINCHUK: The reference data on gas solubility are for equilibrium states. Did you take into account the kinetics of gas dissolution in atmospheric water or did you assume that the saturation of the atmospheric moisture was complete and in equilibrium? In other words, was there sufficient time to establish equilibrium between atmospheric moisture and noble gases from the moment of condensation up to the moment of precipitation?

E. MAZOR: The saturation values were taken from the literature, where carefully conducted experiments have been reported. As regards the second part of your question, we found that the surface waters were generally in equilibrium.

M. LEVIN LIPSIN: In Section 6 of your paper you mention a sulphur taste and an occasional H_2S smell. If the waters are not magmatic, what in your opinion is the origin of the H_2S?

E. MAZOR: We assume that the H_2S derives from biogenic decomposition of the dissolved sulphate.

M. LEVIN LIPSIN: Is there any carbonate or sulphate mineralization in the fractured zone mentioned by you in your oral presentation?

E. MAZOR: I doubt it, judging by the very low salt contents of the spring waters.

T. FLORKOWSKI: In your oral presentation you mentioned gas bubbles escaping from the water of some of the hot springs. Did you attempt to collect the gas and determine its composition?

E. MAZOR: Not in this study. We did do so, however, in our study in the Yellowstone National Park and observed fractionation which can be explained in terms of a partial loss of dissolved gases.

W. G. MOOK: In your oral presentation you mentioned briefly the problem of correcting the conventional ^{14}C ages of groundwater. I should like to make a comment in this connection.

From a theoretical point of view the situation is quite clear. If you assume that the only source of inorganic carbon in the groundwater is soil limestone dissolved by the action of soil CO_2, that there is in the aquifer no isotopic exchange between the dissolved carbon and solid limestone and no addition of CO_2 (of magmatic origin or released from limestone by H^+ ions), and that there occurs no mixing of water masses of widely different ^{14}C ages, a straightforward calculation gives the original ^{14}C content of the groundwater. I presented this approach at the conference on radiocarbon dating held in New Zealand in 1972 (W.G. Mook, "On the reconstruction of the initial ^{14}C content of groundwater from the chemical and isotopic composition").

Two processes are taken into account: the dissolution of $CaCO_3$ by CO_2; isotopic exchange between the bicarbonate formed and the soil CO_2 in the unsaturated zone. It is irrelevant in what order these processes occur, whether they occur stepwise or even whether they occur continuously at the same time. The result is:

$$A_\Sigma = \frac{1}{a+b}\left[aA_{ao} + bA_{bo} + (A_{be} - A_{bo})\frac{(a+b)\delta_\Sigma - a\delta_{ao} - b\delta_{bo}}{\delta_{be} - \delta_{bo}}\right]$$

where

$A_{bo} = \frac{1}{2}(A_{ao} + A_{\ell o})$ and $\delta_{bo} = \frac{1}{2}(\delta_{ao} + \delta_{\ell o})$; $\delta_{be} = \delta_{go} - \epsilon_g$ and $A_{be} = A_{go} - 2\epsilon_g/10$;
ϵ_g is the carbon isotope fractionation (in per mille) between gaseous CO_2 and dissolved bicarbonate;
A is the ^{14}C content as a percentage of the modern standard;
δ is the ^{13}C value relative to PDB;
a and b refer to the concentrations of dissolved CO_2 and bicarbonate respectively, ℓ refers to the soil limestone and Σ refers to the total carbon content.

Of the nine variables, one is known (ϵ_g), and three can be determined (a and b — on the basis of pH, temperature and salinity — and δ_Σ). To calculate the original ^{14}C content of the sample, A_Σ, four values have to be assumed: A_{ao}, $A_{\ell o}$, δ_{ao} and $\delta_{\ell o}$. The conventional assumptions (100%, 0%, -25‰ and 0‰ respectively) are not necessarily correct.

Although the model is clear, this does not directly lead to a successful correction procedure. The advantage, however, is that one can play around with the figures and determine, for instance, age limits. Also, it often turns out that the assumption of A_Σ = 85% cannot be true. Conversely, assuming a value for A_Σ, one can calculate A_{ao}, as was done in a paper presented earlier in this Symposium.[1]

---

[1] MAZOR, E., VERHAGEN, B.T., SELLSCHOP, J.P.F., ROBINS, N.S., HUTTON, L.G., "Kalahari groundwaters: their hydrogen, carbon and oxygen isotopes and dissolved ions", these Proceedings 1, IAEA-SM-182/18.

PROBLEMS IN USING ENVIRONMENTAL ISOTOPES FOR GROUNDWATER STUDIES

(Session 6)

LOCAL VARIABILITY OF THE ISOTOPE COMPOSITION OF GROUNDWATER

J. R. GAT
Department of Isotope Research,
The Weizmann Institute of Science,
Rehovot, Israel

Abstract

LOCAL VARIABILITY OF THE ISOTOPE COMPOSITION OF GROUNDWATER.

The local variability of the isotope composition of groundwaters is used to obtain information on the recharge and flow regimes in the aquifer waters. The method is based on repeated samplings of groundwaters on an evenly spaced time and space grid. The spread of isotope compositions is then compared with the scatter resulting from the analysis itself and with the variability of composition of the precipitation. The systems investigated were in the phreatic coastal aquifer of Israel and a limestone mountain aquifer, which is largely confined. In the coastal aquifer 130 wells in a 100 km^2 test area showed a bimodal distribution of the ^{18}O isotope composition, which is displaced by a few tenths of a per mille relative to mean precipitation. Repeat sampling over eight years of wells in that aquifer also gave very reproducible results. By contrast, in the mountain aquifer both the spatial and temporal variability was greatly in excess of analytical scatter. Space and time inhomogeneity was also found in leakages into a limestone cavern which serves as a natural lysimeter for the recharge to such an aquifer.

INTRODUCTION

The stable isotope method attempts to relate the ^{18}O and deuterium content of groundwater bodies to the location and season of recharge and to the nature of the recharging waters. The method is based, on the one hand, on the geographic variability of the isotope composition of precipitation, primarily as a function of elevation, latitude and distance from the vapour source [1]. On the other hand, one uses characteristic differences between rainwater, snowmelt waters and surface waters which have been exposed to evaporation. Conservative behaviour of the isotope composition during the subsurface flow is one condition for the successful application of the method; this condition seems to be satisfied at moderate temperatures for limited time periods (up to 10^4 years). Changes in the isotope composition can occur as a result of mixing with other waters.

There is a large scatter in the isotope composition of individual rainfall events. These variations are damped in the transition to the aquifers, groundwaters representing an averaged sample of the precipitation. Shifts have, however, been observed between the amount of weighted composition of rain and that of groundwaters, due to either selection or fractionation processes [2]. Some residual noise remains in the isotope composition of groundwaters, and it can be asked to what extent aquifer units are characterized by a singular isotope composition and how constant in time and space this composition is. These questions have been posed in the context of the sharpness with which the origin of groundwaters can be defined, recognizing that any noise in the isotope data limits the quantitative application of the method [3].

The smoothing of the variations during recharge and the degree of homogeneity of waters in an aquifer are related to the recharge mechanism and to the flow and mixing patterns in the aquifer. In this report, time and space variations of the isotope composition in some selected groundwater bodies are presented. The aim is ultimately to relate this variability to the recharge and mixing pattern and thus use the scatter of isotope data as a tool for the study of hydrological processes.

ANALYTICAL REPRODUCIBILITY

The present study is based on the evaluation of small variations in the isotope composition, variations which are of the order of magnitude of the analytical errors. It then is imperative to define the analytical reproducibility exactly. The ^{18}O and deuterium content is measured by mass-spectrometer analysis of the isotopic species of CO_2 and hydrogen gas, respectively, carbon dioxide after isotopic equilibration with the water sample and hydrogen obtained by complete dissociation of water on a hot metal [4]. The analytical error, as quoted by most laboratories, is based on the repeated determination of some standard sample. However, analytical reproducibility depends among other factors on the chemical nature of the samples; volatile organic substances, sulphur compounds and other not yet identified materials affect the analytical process both in the determination of the deuterium abundance and in the mass spectrometry of carbon dioxide. Thus, Fleischer and co-workers [5] reported that the reproducibility of ^{18}O measurements of saline formation waters from oil-bearing strata was lower by a factor of 2 than that of clean (rainwater) samples. Obviously, the errors determined for some standard material may not be applicable to the set of samples which is being investigated.

The routine procedure of analysis of our Rehovot laboratory overcomes this problem in part. The measurements are done in batches, using an interpolation technique between two working standards whose δ-values are assigned [6]. Each batch consists of m_j aliquots of the j samples, usually m = 2 for the samples and m = 3 for the standards. If R is the instrument reading for the ratio of currents of the two isotope beams (or any other instrumental reading proportional to the isotope ratio) and assuming an equal statistical distribution of errors in all the samples, then the variance of the measurements is given [7]:

$$S^2 = \sum_{i,j} (R_{i,j} - \bar{R}_j)^2 \Big/ \sum_j (mj - 1)$$

where $\bar{R}_j$ is the average value of the m aliquots of sample j, S the standard error, characterizing the reproducibility within one batch. For the determination of $\delta^{18}O$ the normal range of values lies between s = 0.07‰ and s = 0.13‰. The probable error of the mean σ value of each sample is then $\sigma = S/\sqrt{mj}$, which usually is $\sigma = S/\sqrt{2}$. When comparing samples processed in different batches, this error has to be compounded with the error of measurement of the substandards. The detailed formulation has

been given by Tzur [8]. In actual practice the mean reproducibility of measurements of non-saline groundwater samples has been $\sigma(\delta^{18}O) = \pm 0.13‰$. This value, which seems consistent with the error analysis given above, will be taken as representative of the analytical reproducibility in this study. It should be realized, however, that the re-measurement of sample stored for extended periods may introduce additional errors due to changes in the samples caused, for example, by evaporation and exchange during storage.

THE ISOTOPIC COMPOSITION IN THE PHREATIC COASTAL AQUIFER

A total of 130 wells situated in the coastal plain of Israel, in a test area of about 10 × 10 km, were sampled in the summer of 1971 (Fig. 1). The aquifer is a free surface aquifer, mainly in sand and sandstone formations of Pleistocene age. Clay lenses separate it into locally confined sub-aquifers. The aquifer is wedge-shaped, narrowing towards the

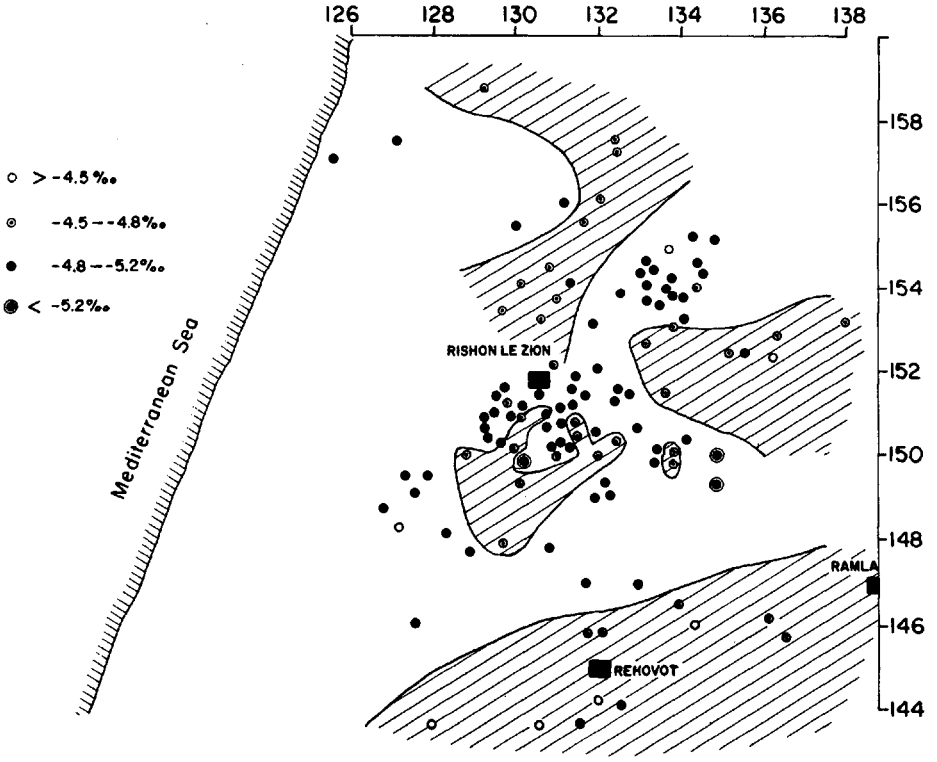

FIG. 1. Map of the test area, showing location of wells. Co-ordinates show local grid (in km). Symbols group the wells in terms of the $\delta^{18}O$ values. Shaded areas are those where groundwaters are predominantly enriched in heavy isotope species.

east. Possibly some saline waters leak into the aquifer from the mountain aquifers. Groundwater levels generally decrease westwards; however, the extensive pumping has resulted in severe local depressions of the water table in the Rehovot-Rishon area, whereas beneath the sand dune areas near the sea a ridge has established itself. The whole area is one of intensive irrigated agriculture. The water table varied in 1971 between -2 to +10 m (MSL), which in this area occurs at depths of 30-100 m. Wells are producing wells, most of which penetrate just a few metres into the aquifer.

Figure 2 is a frequency diagram which shows the ^{18}O composition data of these wells. The spread in data ($\sigma = 0.24‰$) is larger than the analytical error. The heavy isotope is somewhat enriched relative to the average composition of precipitation at Beit-Dagan, which is a meteorological station situated at the northern edge of the test area.

For the sake of analysis we can treat the data in terms of two superimposed Gaussian peaks, the width of which is that defined by the analytical errors (shown on the graph by a broken line). The major peak is situated around $\delta^{18}O = -5‰$ with a secondary one at $\delta^{18}O = -4.7‰$ (middle graph of Fig. 2). The data, however, show a tail of enriched samples (up to $\sigma = -4.3‰$), and there is one sample much more depleted in the ^{18}O composition ($\delta^{18}O = -6.2‰$). This latter sample is from a deep well, and its waters are obviously not recharged locally, but the isotope composition agrees very well with that of waters in the Judean mountain aquifers [9]. The composition of groundwaters of the whole coastal aquifer, as reported by Gat and Dansgaard [9], are shown in the lower graph of Fig. 2. It is interesting to see that the spread of values throughout the aquifer is very similar to that found in the small segment of the test area.

The geographic distribution of the wells belonging to each of the two groups (the $\delta^{18}O = -5‰$ and $\delta^{18}O = -4.7‰$ respectively) is shown in Fig. 1. There is no consistent overall gradient of isotopic composition in the test area, but the two groups are distinct geographically in a patchy manner. The distribution does not follow the water-level contours. There is also little or no correlation between the isotope composition and the salinity or age of the samples (as measured by tritium).

The information on the temporal variability of the isotopic composition in this aquifer is more meagre. From 10 wells, randomly situated throughout the coastal aquifer, there are analyses of repeat samples which were collected at intervals of at least one year. The mean scatter of these repeat measurements is $\sigma(\delta^{18}O) = 0.20‰$. At Migdal-1 in the Southern Coastal Plain there were six repeat samples available, taken during the period of 1960-68. Their isotopic compositions ($\delta^{18}O$) were found to be -4.65‰ (1960), -4.39‰ (1962), -4.62‰ (1963), -4.52‰ (1964), -4.42‰ (1966) and -4.46‰ (1968); the scatter of ^{18}O abundance measurements of these samples is $\sigma(\delta^{18}O) = 0.10‰$, i.e. equal to the expected analytical reproducibility.

ISOTOPIC VARIABILITY IN A CARBONATE AQUIFER

The carbonate aquifer of the Judean mountains consists of rocks of Cenomanian and Turonian age. Recharge occurs mainly in the outcrop area of the formation close to the groundwater divide, and eastwards and

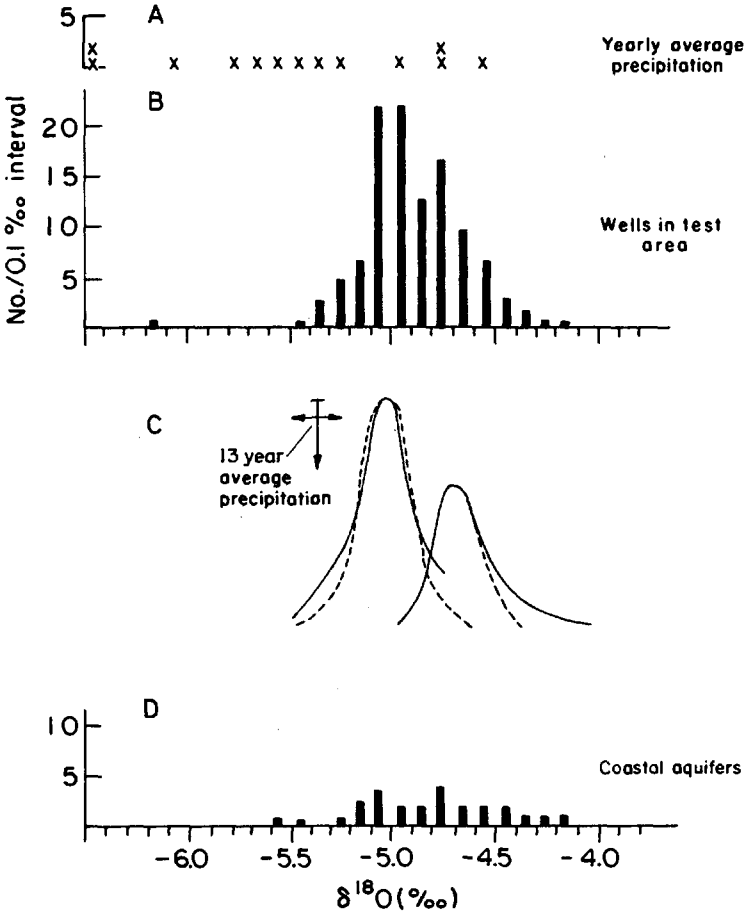

FIG. 2. Frequency diagrams of the ^{18}O content of groundwaters in the coastal aquifer and of the annual precipitation. A: Mean annual composition of precipitation at Beit-Dagan 1959-73. B: Isotope composition of 130 wells in the Rehovot-Rishon test area. C: Analysis of these data in terms of Gaussian distribution (13-year mean composition in precipitation is shown by an arrow for comparison). D: Isotope data reported by Gat and Dansgaard from the coastal plain.

westwards of the mountainous backbone aquifer is confined. The intake area extends over a considerable range of elevation; this is expected to contribute to some spread in the isotope composition in wells situated close to the replenishment area. Discharge from the aquifer occurs naturally through large springs in the foothill region.

There are far fewer wells in this aquifer, so that sampling is less meaningful from a statistical point of view. In the central section of the Cenomanian-Turonian aquifer, Gat and Dansgaard [9] have reported results from 18 wells and an additional 10 wells were sampled by Magaritz [10].

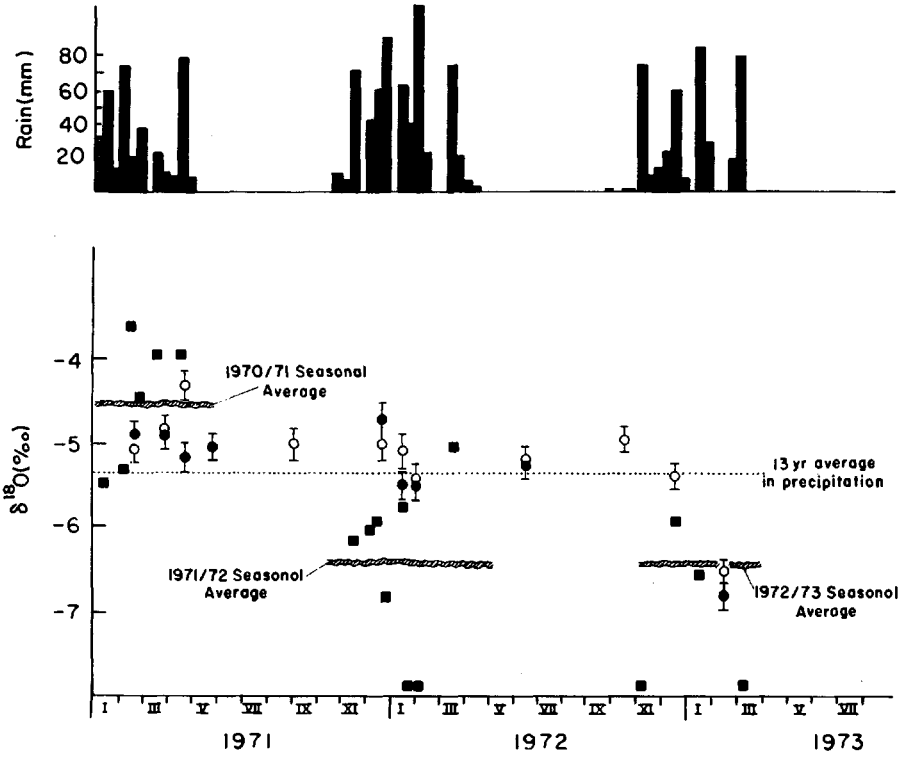

Fig. 3. Isotope composition of water seepages into the Hartuv (limestone) cave and of the local precipitation.
■ weighted mean monthly composition of precipitation
○ seepage No. 1
● seepage No. 2
Undulating and dotted lines denote the composition of seasonally averaged and long-term averaged precipitation.
Top diagram - monthly rainfall amounts.

However, eight of these are situated in the recharge area (the Ein-Karem well-field). The ^{18}O composition is spread out between $\delta^{18}O$ = -4.9‰ to -6.2‰, the range of -5.7‰ to -6.2‰ representing the Ein-Karem area. Mean temporal reproducibility in eight wells is $\sigma(\delta^{18}O) = \pm 0.41$‰. At Kfar-Uriya-4 and Lod-4, five repeat samples from a period of 10 years were analysed, the scatter being $\sigma(\delta^{18}O) = \pm 0.165$‰ and $\sigma(\delta^{18}O) = \pm 0.27$‰ respectively. A well near the recharge area (Ein-Karem-9) showed a scatter of σ = 0.225‰ over a four-year period, and the well Rosh Ayin-2, which is situated close to the major discharge spring, showed wider scatter.

There are indications in these data of a somewhat greater variability of the isotope composition in some of the wells of this aquifer compared with those in the coastal aquifer.

In this context, data of Magaritz [10] from a natural lysimeter are of interest. Water was collected from two adjacent seepages (2 m distant) in a limestone cavern in the Hartuv area. The three-year period during

which the sampling was carried out was exceptional in that the seasonally averaged isotope composition of precipitation was lower by about 1‰ than the long-term average of the preceding seasons. The data given in Fig. 3 show that the percolating waters respond rather rapidly to the change in composition of the precipitation. From the tritium data given by Magaritz [10], it can be seen that the response of the two seepages is somewhat different; such a difference is less noticeable in the stable isotope data. In evaluating this fact it must be realized that the soil cover above the cave roof is just a few centimetres deep and the bare rock is exposed at some spots. In the coastal plain, on the other hand, the soil cover usually extends to depths of several metres.

DISCUSSION

The isotopic composition of rain spans a wide range of $\delta^{18}O$ values. In rain samples collected daily at one site in the coastal plain of Israel we have measured values as low as $\delta^{18}O$ = -9‰ and up to slightly positive values. Even whole-season averaged data retain a scatter of $\sigma(\delta^{18}O) = \pm 0.45‰$. Evidently smoothing of fluctuations occurs in the transition to the aquifer. The simplest possible model is one of a well-mixed reservoir in which the remnant scatter in the isotope composition of the groundwater is the expression of the variations in the isotopic composition of the precipitation input. The standard error which describes the scatter of the composition of the same number of samples taken from such a reservoir at periodic intervals is then given by $\sigma \sim \sigma_i/n$, where n is the size of the reservoir in terms of periodic input volumes and σ_i measures the input scatter. This relation holds for a reservoir with yearly inputs that fluctuate randomly round the mean. For the actual data of precipitation in the coastal plain one would need a reservoir (mixing volume) of size $n \geq 4$ years, to reduce the variability in the precipitation to the observable limit defined by the analytical errors ($\sigma_{anal.} = 0.13‰$).

Actually, of course, recharge is not a simple process of addition of all the local precipitation to a mixed reservoir. Distortion of the isotope composition can occur as a result of water loss by surface evaporation, transpiration and run-off. In the coastal plain of Israel the net result of these processes is a slight enrichment of the heavy isotopes in the recharge waters by less than 1‰ ($\delta^{18}O$) on the average. The degree of enrichment depends on the local water balance and on parameters such as the intensity and duration of rainfall, the interval between successive showers and the moisture condition of the soil cover. The shift in the isotope composition has a time variable component; in most situations the overall effect is one of an increase in the variability of the isotope composition of the input to the groundwater system.

Another factor to be considered is the change in the composition of recharging waters from place to place. Systematic effects are the altitude effect on the composition of precipitation [1] and changes in the soil and vegetation cover. Random effects are caused, in addition, by inhomogeneity of rainfall in different areas and variable irrigation practices. These effects are responsible for the spatial variability of the composition of groundwater recharge; they may affect other geographic locations through lateral surface or subsurface transport. Obviously a steady transport

pattern cannot introduce a temporal variability based on the systematic effects. However, non-steady flow and mixing patterns, caused either by variations in the amounts of input water or by over-exploitation of aquifers by pumping, can transform steady spatial variations into changes with time of the isotope composition of groundwater. An extreme sample is found at Beer-Ora-1 in the Negev, where pumping has exhausted the local perched aquifer and started exploiting a large regional aquifer; the ^{18}O values of the pumped waters were as follows: in 1960, -4.99‰; 1962, -5.1‰; 1964, -7.0‰, and 1972, -6.73‰. The first two measurements correspond to the locally derived surface waters, whereas the last measurements identify contributions from a large paleowater reservoir of the area.

The data presented in this study from the coastal aquifer of Israel show that there is no measurable change in the isotope composition over the period of observation, but there is some spatial inhomogeneity. The aquifer does not constitute a well-mixed system in its lateral extent. A reasonable interpretation of these data is that the soil column acts as an efficient homogenizer of the recharge waters, but that mixing in the aquifer proper is a slow process. Tritium levels in this aquifer are very low [11], corresponding to ages of 30 years or more. This means that not much lateral movement can be expected during the rather short (in comparison) observation period. It would be of interest to observe drifts in the pattern shown in Fig. 1 over longer periods, commensurate with the ages of waters in this system.

In the more fractured mountain aquifer with its karstic developments, water movement is faster and the soil cover less efficient in homogenizing the input. As a result both temporal and spatial variations are somewhat greater.

REFERENCES

[1] DANSGAARD, W., Tellus 16 (1964) 436.
[2] GAT, J.R., TZUR, Y., "Modification of the isotopic composition of rainwater by processes which occur before groundwater recharge", Isotope Hydrology (Proc. Symp. Vienna, 1966), IAEA, Vienna (1967) 49.
[3] GAT, J.R., Water Resour. Res. 7 (1971) 980.
[4] GONFIANTINI, R., "Techniques of measuring stable isotope variations in natural waters", Hydrogen and Oxygen Stable Isotopes in Hydrology, IAEA, Vienna (in preparation).
[5] FLEISCHER, E., et al., Isotopic composition of formation waters from deep drillings in southern Israel (1974), preprint.
[6] DANSGAARD, W., Private communication, IAEA panel meeting, Vienna, 1966.
[7] BRANDT, S., Statistical and Computational Methods in Data Analysis, North-Holland, Amsterdam (1970).
[8] TZUR, Y., Isotope Effects in the Evaporation of Water into Air, PhD Thesis, Feinberg Graduate School, Weizmann Institute of Science, 1971.
[9] GAT, J.R., DANSGAARD, W., J. Hydrology 16 (1972) 177.
[10] MAGARITZ, M., Carbon and Oxygen Isotopic Composition of Some Carbonate Rocks from Israel, PhD Thesis, Feinberg Graduate School, Weizmann Institute of Science, 1973.
[11] CARMI, I., GAT, J.R., Israel J. Earth-Sci. 22 (1973) 71.

DISCUSSION

G. SAUZAY: In the Lebanon, to explain the isotope concentrations in a Quaternary aquifer we had to postulate the return to it of irrigation waters from a lower aquifer. In the Rehovot coastal region, where there

is intense irrigation, have you considered the influence of the return of irrigation waters as an explanation of the ^{18}O values?

J.R. GAT: Yes, we have, and I agree that the evaporation of irrigation waters is probably an important factor in the isotopic enrichment of recharge relative to precipitation. We have calculated from the isotopic enrichments that about 30% of the water is recycled, which seems also to agree with independent estimates based on water balances.

C.B. TAYLOR: I think we all agree that interpolation between two working standards is necessary for reliable ^{18}O determination; one obtains for each measurement batch a δ-value for working standard 2 relative to working standard 1 which should compare within the limits of the experimental error with the cumulative mean value from previous measurements. As a matter of experimental philosophy, if this value is only slightly in error, should one reject the whole batch or make a scale correction to the sample measurements?

J.R. GAT: I would at least re-measure some of the samples.

C.B. TAYLOR: In New Zealand we have encountered several systems where the ^{18}O distribution is unimodal in space within satisfactory experimental error limits (for example, in lakes and aquifers). In one case, however, we found an unexpected bimodal distribution where the $\delta^{18}O$ range was more than 0.5‰ and there was no apparent altitude correlation and no evidence (in terms of the ^{18}O-D correlation) of evaporation. The samples were from cold springs in the Rotorua volcanic region. The only difference we could find was that one set of waters emerged from ignimbrite and rhyolite below surface ash cover, whereas the other set related to volcanic breccia below ash. The precipitation is well distributed seasonally.

My own opinion is that the isotopic difference between the two sets must result from different rates of recharge through the surface cover, the time spent in the surface soil cover determining the balance of evaporation loss and recharge and hence possibly making for geologically induced selection of the seasonally varying isotopic composition of precipitation.

A. PLATA BEDMAR: I think that, in the case of wells, dispersion in space may often – and dispersion in time occasionally – be caused by faulty sampling. Frequently, due to local conditions, water from formations or aquifers other than the one of interest find their way into the wells. For proper sampling it is, in my opinion, essential to know about both the vertical and the horizontal flows so as to be sure of the origin of the water which is being sampled, This can be achieved very simply using artificial tracers. In Brazil, where we took samples from some 200 boreholes for deuterium, ^{18}O and tritium determinations, almost all discrepancies could be explained in terms of mixing of the water of the main aquifer with other waters.

B.T. VERHAGEN: I have a comment relating to Fig. 8 of paper IAEA-SM-182/18.[1]

The clustering of groundwater on the lower end of the rain line is due to a selection process which is very prevalent in environments like that of the Kalahari. The evaporation line characterizes groundwaters recharged from the surface drainage system in the north, forming a very distinct group.

---

[1] MAZOR, E., VERHAGEN, B.T., SELLSCHOP, J.P.F., ROBINS, N.S., HUTTON, L.G., "Kalahari groundwaters: their hydrogen, carbon and oxygen isotopes", these Proceedings 1, IAEA-SM-182/18.

When we plotted $\delta^{18}O$ values from our Kalahari survey against pmc ^{14}C and excluded values above -2‰ as containing recharge from known surface drainage, we found that there had been little or no change in average $\delta^{18}O$ values over the age range covered (about 30 000 years) and that there was greater consistency or clustering of the $\delta^{18}O$ values for the older (and deeper) waters.

The superficial aquifers, which show much greater scatter due to local conditions, feed the deeper waters, which tend to reflect a weighted mean from different superficial contributions.

SAMPLING OF LYSIMETERS FOR ENVIRONMENTAL ISOTOPES OF WATER

G. SAUZAY*
Department of Research and Isotopes,
International Atomic Energy Agency,
Vienna

Abstract

SAMPLING OF LYSIMETERS FOR ENVIRONMENTAL ISOTOPES OF WATER.

A summary is given of the environmental isotopic (^{18}O, deuterium and tritium) concentration of rain and of water which has percolated through lysimeters, with the object of establishing a relation between these two parameters. Although this has been possible for one lysimeter only, the data for other lysimeters are discussed in terms of the influence of vegetation cover and agricultural practice.

INTRODUCTION

In 1965, the International Atomic Energy Agency initiated a project, the aim of which was to establish the relation between the environmental isotopic (^{18}O, deuterium, tritium) concentration of rain and that of water infiltrating through the soil and reaching the water table. It was thought that lysimeters would represent a good tool for such a study.

After seven years, many data have become available and a summary of their interpretation is presented here. Only in the case of one lysimeter has it been possible to establish a relation between rain and groundwater. However, the other lysimeters included in the survey permit a discussion of some of the many factors involved in the relation, such as vegetation, time and the influence of man through the practice of irrigation and cutting.

THE THEORY OF THE RELATION BETWEEN RAIN AND GROUNDWATER ISOTOPE CONCENTRATION

A lysimeter can be considered as a system or a box model with inputs and outputs. During the time interval dt, an amount dR of water is deposited as rain, dE evaporates, dT is transpired and dP percolates. Condensation is neglected. The water balance equation is

$$dR = dE + dT + dP + dS$$

where dS is the change in the amount of water storage. Using monthly intervals and monthly values

$$R = E + T + P + \Delta S \qquad (1)$$

* Present address: CEN Saclay, Gif-sur-Yvette, France.

Any isotopic balance equation is

$$C_R dR = C_E dE + C_T dT + C_P dP + d(SC_S)$$

where C_R, C_E, C_T, C_P and C_S are the respective isotopic concentrations. Using monthly intervals,

$$RC_R = EC_E + TC_T + PC_P + C_s \Delta_s \tag{2}$$

where the capital letter indicates weighted mean monthly values. The weighted monthly values C_R and C_P have been measured systematically in several lysimeters.

The problem is to establish the relation between C_R and C_P.

Another equation can be established. The concentration in the percolate is obtained by the transformation in the system (the lysimeter) of the concentration function in the input. It may be represented by

$$C_P(t) = \frac{\int_\tau I(\tau)\, C_I(\tau)\, f(t-\tau)\, d\tau}{\int_\tau I(\tau)\, f(t-\tau)\, d\tau} \tag{3}$$

where I and C_I are the input and the concentration in the input. The input is defined as the resultant of the processes taking place at the top of the soil: rain and evapotranspiration.

$$I = R - E - T = P + \Delta S \tag{4}$$

$$IC_I = RC_R - EC_E - TC_T = PC_P + C_s \Delta S \tag{5}$$

The age distribution function $f(t-\tau)$ is characteristic of the system. C_s was measured in none of the lysimeters, hence Eqs (2) and (5) could not be applied. ΔS was measured in only one lysimeter which was, therefore, the only one where the input I could be computed accurately and Eq. (3) applied to discuss possible forms for the age distribution function of the lysimeter percolate. Since both Eqs (2) and (3) can be considered as representing the relation between the isotopic concentrations of the rain and the percolate, it is apparent that this relation was determined in only one out of seven lysimeters.

DETERMINATION OF THE AGE DISTRIBUTION FUNCTION IN THE GRASS-COVERED LYSIMETER AT PETZENKIRCHEN, AUSTRIA

In this station, two monolith lysimeters are available. One is covered with grass, and the other one is covered with bare soil. Both are filled with the same natural colluvial brown loam. The dimensions

are 1 × 1 × 1.3 m. Tritium, ^{18}O and deuterium analyses have been performed on weighted monthly samples of rain and percolates from both lysimeters. Both lysimeters are weighted at monthly intervals between March and October.

The grass-covered lysimeter has been in steady-state natural conditions since the 1950s. Using Eq. (4), monthly input values have been calculated. Positive values of the input represent a net vertical flow of water downward, equivalent to an increase in storage and/or percolate. Negative values of the input represent an upward net movement of water equivalent to a decrease in storage and/or percolate.

The frequency distribution of the months with positive inputs but weighted for the amount of input is found to be centred on November-December, with 80% of the input taking place between September and

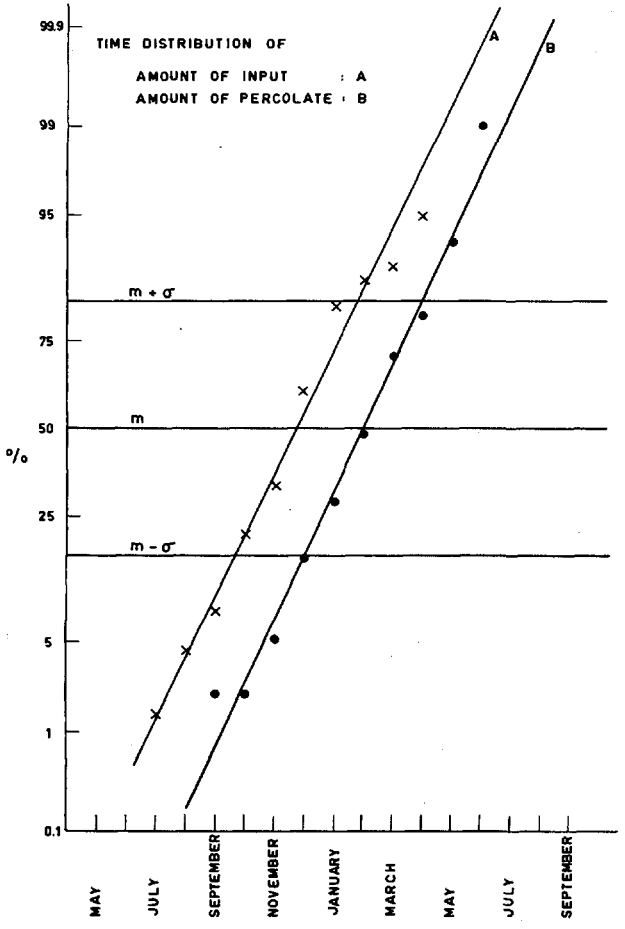

FIG. 1. Probability distribution of the time of water input and percolate in the Petzenkirchen lysimeter.

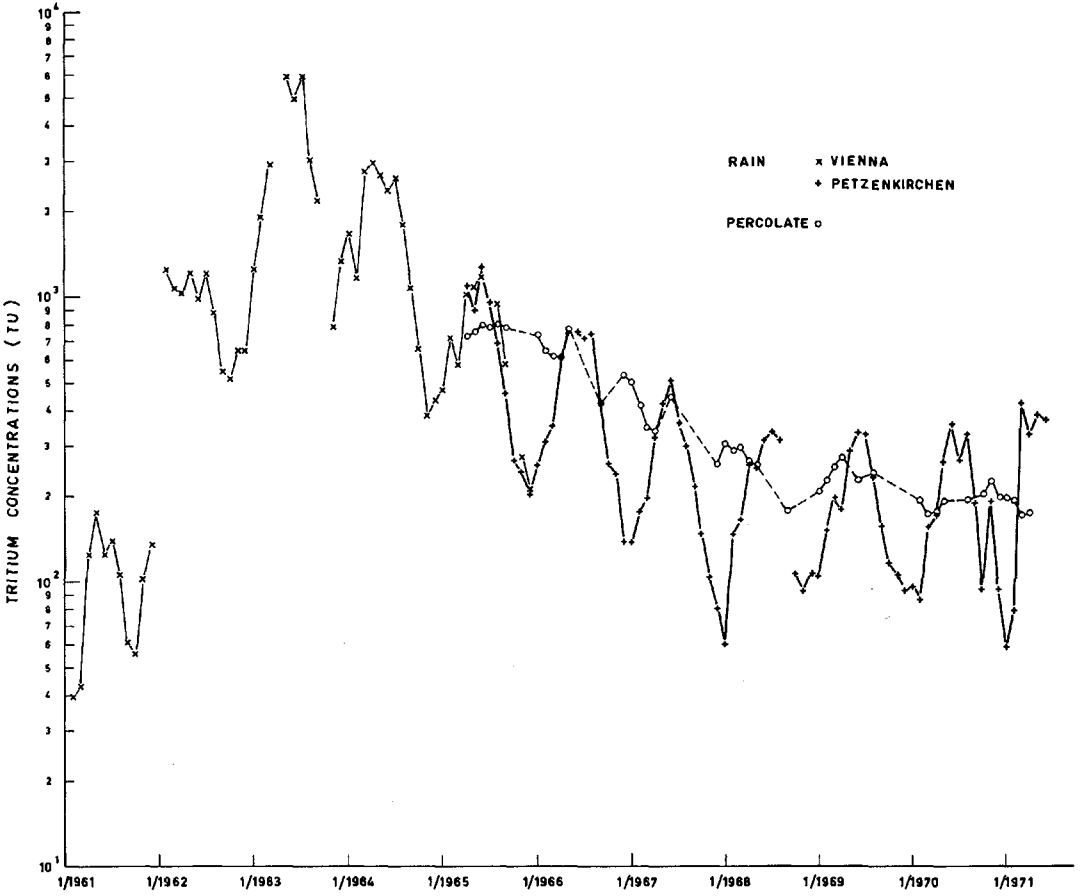

FIG. 2. Time concentration of tritium in rain and percolate in the Petzenkirchen lysimeter.

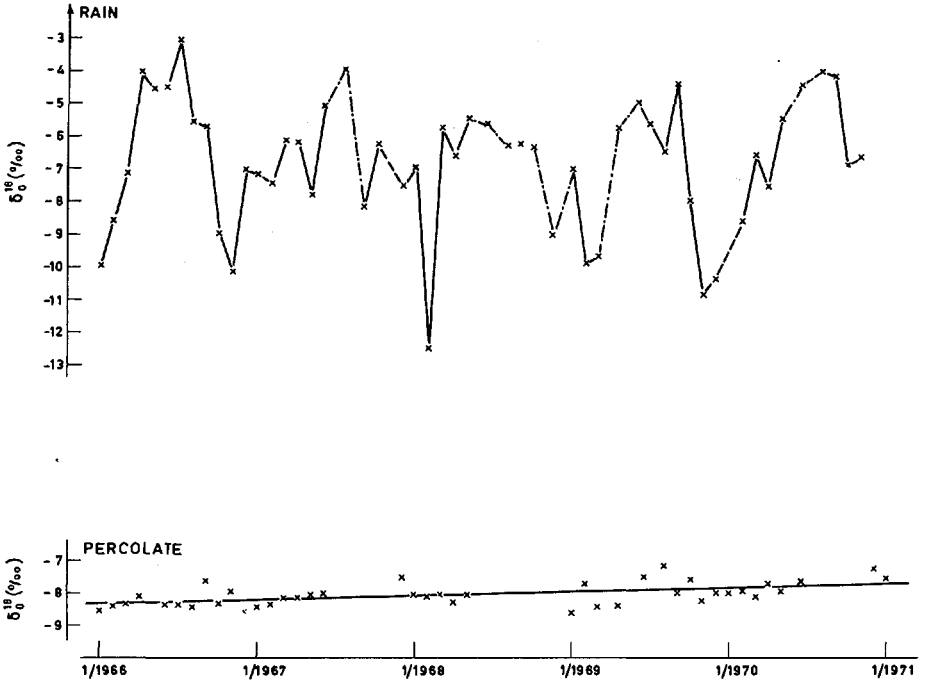

FIG. 3. Time concentration of ^{18}O in rain and percolate at Juprelle.

February, two months earlier than the frequency distribution of the amount of percolate (Fig. 1). This represents only the mean of a distribution which is very variable from one year to the next.

Equation (3) has been applied to the tritium data assuming several different models for the age distribution function. However, to simplify the calculations, the monthly inputs and amounts of percolate have been combined to provide annual rates to which Eq. (3) has been applied. The tritium data have been used since the concentrations of tritium are not significantly influenced by evaporation and transpiration. The tritium concentration of positive inputs is taken as that of rain during the same month.

The isotopic concentrations in rains are very variable for all three isotopes. The percolates always show smoothed concentrations (Figs 2 and 3).

An attempt has been made to fit the data using symmetric and asymmetric binomial distributions by analogy with the log normal distribution of pore spaces in the soil. The best result has been obtained with an age distribution function including the contributions (25/50/25%) of three years.

The mean residence time in the lysimeter is found to be one year. Therefore, the rain-percolate relation is governed by the seasonal input (Fig. 1) and the above age distribution function.

DISCUSSION OF SOME OF THE FACTORS INFLUENCING SUCH A RELATION

Influence of the vegetation cover

In the Petzenkirchen lysimeter station, there is a second lysimeter but without vegetation cover. It has been possible to compute some of the inputs since it is a weighable monolith lysimeter. Their distribution shows clearly the contribution of spring and summer rains to the input. It results in a percolate enriched by 1‰ in ^{18}O and 6‰ in deuterium. Thus growing vegetation uses spring and summer rains, leaving autumn and winter rains to percolate through the soil.

Influence of the type of vegetation

In Cedar River (Washington, United States of America), two lysimetric plates have been studied. One is under forest cover, the other is under grass cover (clear cut). There may be a difference between the isotopic concentrations in the percolates from the two plots:

Covered plot $\delta^{18}O = -10.7‰ \pm 0.3$

Uncovered plot $\delta^{18}O = -11.3‰ \pm 0.5$

Although these plates show seasonal variations in the percolate concentrations which are probably due to the lack of mixing and short residence time in the small thickness of soil, the forest may be interpreted as inducing a less depleted percolate than the grass. However, the difference is not really significant and not much weight can be given to the conclusion.

Influence of agricultural practice and vegetation cover

In Coshocton (Ohio, United States of America), two lysimeters have been studied. One lysimeter is covered with poverty grass and the farming operations are said to be of poor agricultural practice. The yearly mean isotope content of the percolate is

$$\delta^{18}O = -8.56‰$$

$$\delta D = -54.4‰$$

After cutting, such a lysimeter would slowly achieve a complete vegetation cover. Thus direct evaporation from the soil surface, infiltration and percolation of spring and summer rains would be more effective than in the second lysimeter, said to have a conservation practice of a cover consisting of blue grass. This lysimeter achieves a faster complete vegetation cover and suffers more losses by transpiration. The isotopic concentrations are

$$\delta^{18}O = -9.0‰$$

$$\delta D = -57.8‰$$

Both spring and summer rains and direct evaporation are known to be enriched or to enrich the water in heavy isotopes but transpiration is believed not to change the concentrations. Thus, the difference in isotopic content is in the expected direction.

Influence of irrigation

In a lysimeter in Taastrup (Denmark), after several years of natural regime, irrigation was applied to the lysimeter during some of the summer months. Under a natural regime yearly fluctuations of the stable isotope and tritium contents were observed. After irrigation was applied, the variations were smoothed out but there has been no significant change in the mean concentration.

Influence of time

A lysimeter in Juprelle (Belgium) shows a time variation of the percolate (Fig. 3). In five years it has increased by 0.65‰. This may be related to a variation in the autumn-winter rain values from year to year from 1966 to 1969 indicating a delay in the lysimeter of about one year.

DISCUSSION

G. B. ALLISON: You have used a binomial distribution for the flow of water in the soil because of the analogy with pore size distribution. However, it has been shown that diffusion will redistribute tritium and other environmental isotopes quite rapidly, so that perhaps one should not use information only about water movement in predicting the movement of isotopes. Would you care to comment on this point?

G. SAUZAY: The observed mixing, which may be quite apparent, can result from the combination in a single sample of waters which have flowed through pores characterized by different residence times. Calculation of the "input" values is based on piston flow in pores at different velocities. What is measured is only the result, it being impossible to discuss the process occurring within the soil.

G. B. ALLISON: Have you calculated the isotopic composition of water which would percolate through the lysimeter if one had layered input with diffusion?

G. SAUZAY: No, we have not, for this diffusion model contradicts the model which permits determination of the "input" values, and no solution has been found to the problem of incorporating diffusion into "input" calculations.

A. PLATA BEDMAR: One often encounters aquifers of differing permeability within a single region. In such cases, the isotopic composition of the water tends to indicate a higher concentration of deuterium and ^{18}O in the less permeable aquifers owing to fractionation during infiltration. In the more permeable aquifers, recharge is faster and the concentration of the stable isotopes is modified less by evaporation. It

would seem, therefore, that the isotopic composition under these circumstances is related to the recharge rate. In this connection I should like to know whether the isotopic composition of infiltrated water could be related to the rate of infiltration in a quantitative manner using the lysimetric techniques described by you.

G. SAUZAY: The problem was to relate the isotopic contents of rain and groundwater using lysimeters and their percolate. In a lysimeter, the rate of infiltration is given directly by the rate of percolation. The stable isotope content is quite constant in a lysimeter, whatever the yearly variations in the percolation rate.

J. DOWGIAŁŁO: The data for Juprelle, Belgium, in Fig. 3 indicate a slight tendency for the ^{18}O concentration to increase. What is the reason for this tendency?

G. SAUZAY: We do not know. We tried to relate it to weather patterns (polar front, Central Atlantic high, etc.), but without success.

J. DOWGIAŁŁO: Do you intend to continue carrying out measurements with a view to seeing whether the opposite tendency will set in?

G. SAUZAY: No, we do not. The project ended in 1971, and the data presented in the paper, covering a period of five years, are the only ones available.

W. G. MOOK: In my opinion, it is very difficult to draw conclusions about the correlation between the precipitation input and the lysimeter output of tritium and ^{18}O from the tritium concentrations and $\delta^{18}O$ values given by you. Would it therefore not have been better to give in Figs 2 and 3 the amounts of tritium and ^{18}O?

G. SAUZAY: The paper was too limited in size for the inclusion of all the data available and required. However, amounts, and not concentrations, were used in calculating the relationship between precipitation input and lysimeter output.

J. R. GAT: The change in the slope of the $\delta D/\delta^{18}O$ curve is not always a reliable criterion for distinguishing between evaporation losses of rainfall and rainfall selection through vegetation. While the "evaporation line" does usually have slopes $\Delta\delta D/\Delta\delta^{18}O \sim 4\text{-}5$, it has been shown that, at high humidity levels and when the deuterium excess of atmospheric moisture is appreciably greater than that of the evaporating waters, the evaporation slopes can be as high as 7 or 8.

G. SAUZAY: At the Petzenkirchen lysimeter station, there is a difference in apparent enrichment between recharge and percolate in the case of the grass-covered lysimeter and between the percolates of both lysimeters. In the case of the grass-covered lysimeter, the enrichment is associated with a slope of 5, while the difference in vegetation induces rainfall selection and a shift along the "slope-8" line.

U. SIEGENTHALER: In Fig. 1, the seasonal distributions of input and, to an even greater degree, percolate are Gaussian. Could you explain why this is so?

G. SAUZAY: The Gaussian distributions are simply the result of the superposition of several processes having different distributions ("central limit theorem") and bear no relation to any individual process, such as the recharge for a particular year, which can have a distribution of any shape. The Gaussian distributions represent long-term averaged distributions of the input function.

PROBLEMS IN ^{14}C DATING OF WATER FROM AQUIFERS OF DELTAIC ORIGIN
An example from the New Jersey coastal plain

I.J. WINOGRAD
US Geological Survey,
Reston, Va.

G.M. FARLEKAS
US Geological Survey,
Trenton, N.J.,
United States of America

Abstract

PROBLEMS IN ^{14}C DATING OF WATER FROM AQUIFERS OF DELTAIC ORIGIN: AN EXAMPLE FROM THE NEW JERSEY COASTAL PLAIN.

Major assumptions common to interpretive studies of ^{14}C in groundwater systems are: (a) no CO_2 is introduced after recharge; (b) $\delta^{13}C$ of carbonate phases in the aquifer is known and taken to be zero; and (c) inter-formational flow can be neglected. None of these assumptions are fulfilled in deltaic and marginal marine sediments comprising the Potomac-Raritan-Magothy aquifer system of New Jersey; and it is likely that the first two cannot be met in most aquifers of deltaic to marginal marine origin because: (1) variations of pH, H_2CO_3, HCO_3^-, and Ca+Mg in the groundwater show a significant amount of CO_2 being generated within the Potomac-Raritan-Magothy aquifer to distances of 45 kilometers down the hydraulic gradient. The hypothesis that coalification of ubiquitous lignitic detritus is the source of CO_2 described in other deltaic aquifers is tentatively accepted here; (2) the $\delta^{13}C$ of common carbonate mineral phases in deltaic and marginal marine sediments ranges from 0 to -20‰; (3) the aquifer is recharged both by infiltration on its outcrop areas and by leakage from overlying marine strata; the leakage is significantly more mineralized than the aquifer water; the ^{14}C content probably also differs. For these reasons, and despite regular variations of ^{14}C and $\delta^{13}C$ down the hydraulic gradient, meaningful interpretation of even relative ^{14}C ages and groundwater velociries cannot be made in the New Jersey aquifer. Similar difficulties should be expected in all aquifers of deltaic or marginal marine origin unless ^{14}C and $\delta^{13}C$ data are supplemented by detailed studies of subsurface stratigraphy, mineralogy, hydrodynamics, hydrochemistry and dissolved gas content.

INTRODUCTION

The need to adjust the measured ^{14}C content of groundwater for dilution by non-radiogenic carbonate of mineral origin has been recognized for nearly two decades [1]. Numerous adjustment methods were developed in the 1960s [2-4] and early 1970s [5, 6], and some have worked very well in the aquifer for which they were developed [7]. Although it was clearly recognized that the ^{14}C content of recharge may be diluted by oxidation of "dead" organic matter in some aquifers [7, 8], most of the studies cited above, and numerous others, have assumed, either explicitly or implicitly, that the diluting dead carbonate is of marine origin, that the principal source of CO_2 is the soil zone, and that cross-flow from strata overlying or underlying the aquifer can be neglected. Yet, in a major aquifer type, namely unconsolidated sands, silts, and clays of deltaic or marginal

marine origin, none of these assumptions appear valid, and interpretation of ^{14}C data for such aquifers is tenuous. These matters are well illustrated by the areal and vertical variations in $\delta^{13}C$, ^{14}C, P_{CO_2}, H_2CO_3 and HCO_3^- in water from the Potomac-Raritan-Magothy aquifer system of the New Jersey Coastal Plain.

HYDROGEOLOGIC SETTING

The Potomac Group, and the Raritan and Magothy Formations of late Early to Late Cretaceous age, comprise the principal artesian aquifer of New Jersey. The aquifer contains fresh water beneath an area of at least 6500 km^2. The average yield of over 100 wells tapping this aquifer in Camden County is about 70 litres/s, with an average specific capacity of about 6 litres/s per metre [9]. Transmissivities of wells in Camden County vary from about 200 to 2900 m^2/day (H. Meisler, written communication, 1973). The aquifer is composed of alternating beds of micaceous quartz sand and silt, and clay deposited in a non-marine to marginal marine deltaic environment [10]. Lignitic detritus is common in all size fractions, and siderite and pyrite are common accessory minerals. Glauconite and calcareous fossils, sparse in outcrop, become increasingly important constituents southeastward towards the coast [11,12]. The mineralogy and stratigraphy reflect cyclic deposition in river channel, floodplain, and in swamp and other deltaic environments. The aquifer system, about 75 to 140 m thick in outcrop (Fig. 1), dips southeastwards (Fig. 2), and thickens to almost 610 m along the central New Jersey coast [11], where its top is about 550 m below mean sea level.

The Potomac-Raritan-Magothy aquifer system, underlain primarily by pre-Cretaceous crystalline rocks [13], is capped by an extensive aquitard, the Merchantville Formation and Woodbury Clay of Late Cretaceous age (Fig. 2). The Merchantville Formation consists mainly of micaceous clayey silts and glauconitic sands, whereas the Woodbury Clay is principally a thick massive clayey silt with lenses of glauconitic sand [14]. The combined thickness of these formations is about 30 m in outcrop; downdip, towards the southeast, the thickness doubles (Fig. 2). The sediments comprising the regional aquitard, in contrast with those comprising the aquifer system, were deposited in a marine environment.

Late Cretaceous and younger sediments overlying the regional aquitard (Fig. 2) are principally glauconitic quartz sands or quartz sands, principally of marine origin. As in the underlying strata, fine- to coarse-grained lignitic matter is abundant, and pyrite and siderite, locally, are important accessory minerals. Invertebrate fossils are abundant in some of these younger strata, specifically in the Mount Laurel Sand, the Navesink Formation and the Red Bank Sand [14].

Recharge and regional movement of water through the Potomac-Raritan-Magothy aquifer system (hereafter referred to as the principal aquifer) under natural (pre-pumping) conditions was strongly influenced by topography. Recharge occurred both via infiltration on high-level outcrop areas northeast of Trenton, and via leakage (or cross-flow) from overlying strata beneath topographically high areas located as much as 13 km east-southeast of the outcrop areas (Figs 1 and 2). Regional movement of groundwater under natural conditions was towards the northeast, east, southeast and

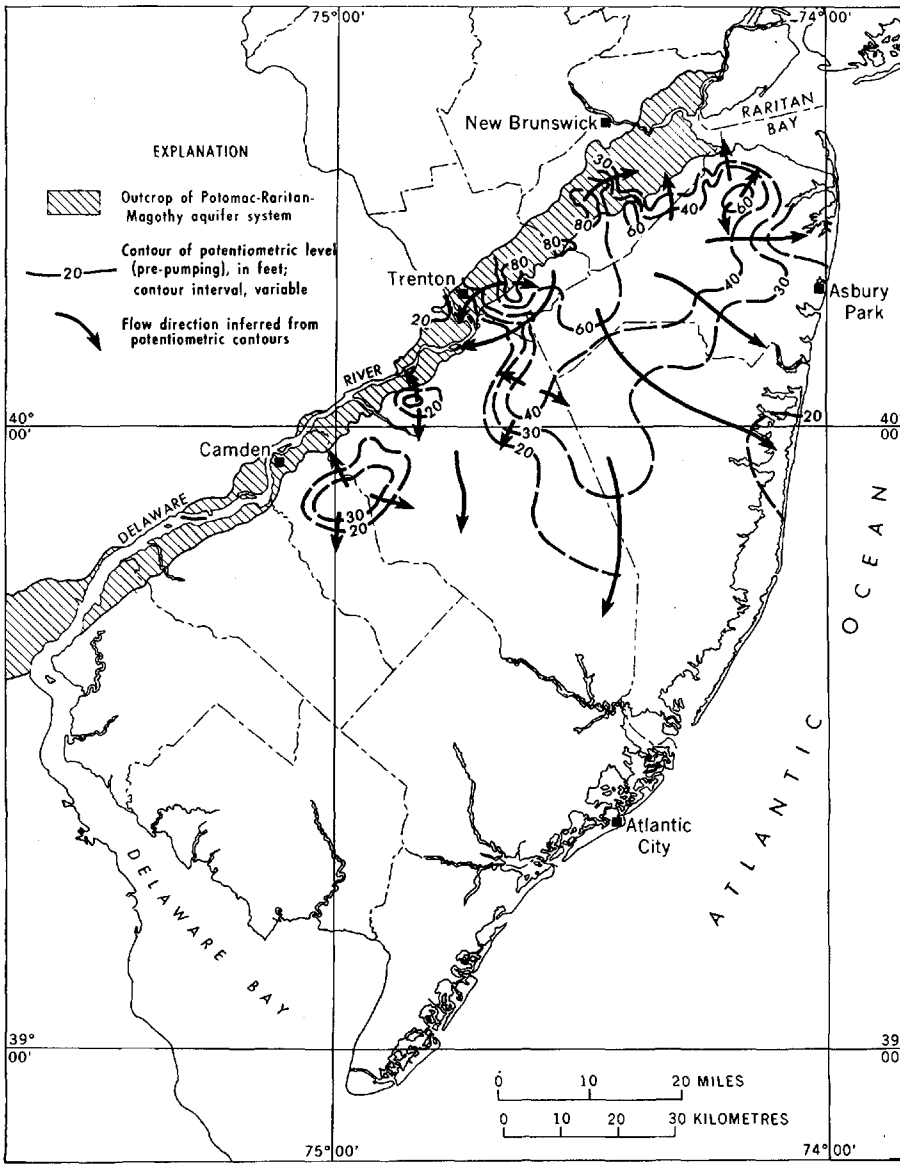

FIG. 1. Hydrogeologic map of the Potomac-Raritan-Magothy aquifer system, New Jersey (modified from H. E. Gill and G. M. Farlekas, written communication, 1969).

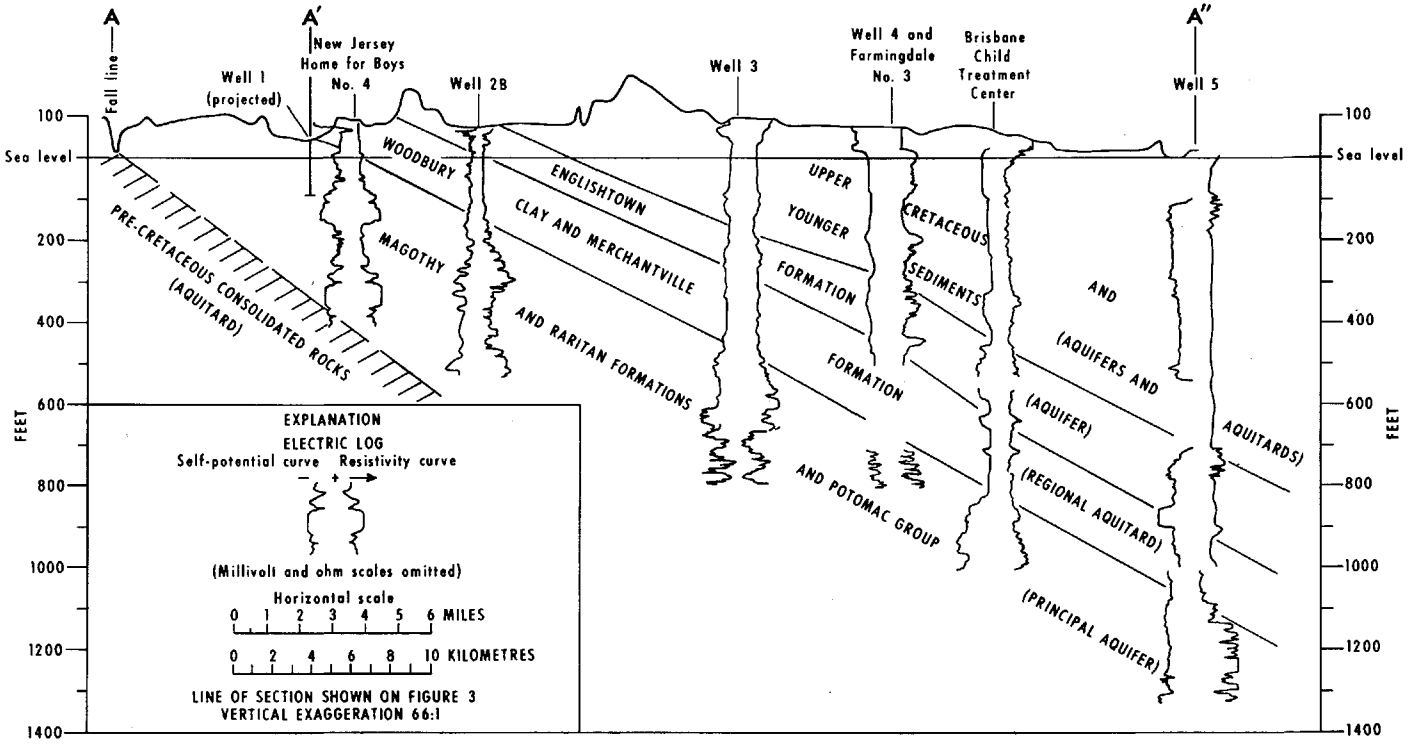

FIG. 2. Diagrammatic hydrogeologic section, A-A'-A".

south; also, beneath the recharge mounds east of the outcrop area, local flow was towards the northwest, west and southwest. The potentiometric contours shown on Fig 1 depict conditions in the aquifer before 1900 (H.E. Gill and G.M. Farlekas, written communication, 1969). Declines of the potentiometric surface in excess of 30 m have occurred since 1900 due to localized pumping. To obtain water samples representative of natural water chemistry, the wells sampled in this study were chosen, in part, on the basis of their remoteness from major centres of pumpage. The other major selection criterion was that the well sampled a restricted and accurately known segment of the thick principal aquifer. The map number and sampled interval for the wells is given in Table I, and the locations shown in Figs 3 and 4.

Water in the Potomac-Raritan-Magothy aquifer, where it has not been polluted, is extremely dilute within, and within a few miles of, the outcrop recharge area (Fig. 1). The dissolved-solids content in this region is commonly less than 25 mg/litre in the wells sampled, with SiO_2, SO_4^{2-}, HCO_3^-, and Fe^{+2} as major constituents; pH is normally less than 5.5. In intermediate portions of this regional flow system (namely the bulk of the contoured area on Fig. 1), dissolved solids increase gradually from 25 to 100 mg/litre, the pH from 5.5 to 7, and the waters acquire a calcium magnesium bicarbonate character. In the distal parts of the flow system, specifically in the vicinity of, and down the hydraulic gradient from wells 12, 18, 19 and 20A-C, dissolved solids increase from 100 to 170 mg/litre and pH from 7 to 8.5; these waters retain their calcium magnesium bicarbonate character but pick up significant amounts of sodium. Water from wells 23A (a sodium bicarbonate water) and 23B (a sodium chloride bicarbonate water) differ markedly from the other waters reflecting in part the probable exchange of calcium for sodium in coastal plain aquifers [15], and in part proximity to the fresh-salt water interface in the aquifer. Chemical and isotopic data are presented for these two wells solely to demonstrate the marked vertical variations of key constituents in the distal portions of this thick aquifer system.

The discussion of water and isotopic chemistry that follows is restricted to the recharge and intermediate portions of the groundwater flow system in the principal aquifer, that is, to areas up the hydraulic gradient from wells 12, 18, 19 and 20A-C.

DATA TRENDS

Contours of the ^{14}C and ^{13}C content of the aquifer water (Figs 3 and 4) roughly approximate the potentiometric contours (Fig. 1), and suggest groundwater flow eastwards, southeastwards and southwards from the high level outcrop areas northeast of Trenton, New Jersey. Other contour maps (not reproduced here) of pH, total dissolved carbonate, Ca+Mg, Fe^{+2} and P_{CO_2} show similar areal patterns. The correspondence between the hydrochemical and potentiometric contours, though approximate, is gratifying because the number of control points used in constructing Figs 3 and 4 was only a fraction of that used in preparation of the potentiometric map.

Variations of $\delta^{13}C$, ^{14}C, P_{CO_2}, total dissolved carbonate ($H_2CO_3 + HCO_3^- + CO_3^{2-}$ + various carbonate complexes, hereafter referred to as ΣCO_2 and expressed as millimoles per litre), pH, Ca+Mg, Fe^{+2} and temperature

TABLE I. ISOTOPIC, CHEMICAL AND WELL DATA FOR GROUNDWATER SAMPLED FROM THE POTOMAC-RARITAN-MAGOTHY AQUIFER SYSTEM, NEW JERSEY

Map No.	Depth interval (ft)	^{14}C (% modern)	$\delta^{13}C$ (‰ PDB)	pH	ΣCO_2 (mM/litre)[a]	H_2CO_3 (mM/litre)[a]	HCO_3^- (mM/litre)	Log P_{CO_2}[a]	Ca+Mg (mM/litre)	Fe^{+2} (mM/litre)
1	99-120	85.0 ± 3.5	-26.0	4.8	2.03	1.98	0.05	-1.37	0.09	0.00
2A	363-384	--	-22.0	5.7	0.41	0.35	0.06	-2.14	0.04	0.05
2B	641-671	--	-22.1	5.0	0.47	0.45	0.02	-2.02	0.02	0.03
3	679-760	44.7 ± 2	-19.6	6.2	1.19	0.70	0.49	-1.80	0.18	0.09
4	831-885	30.0 ± 3	-19.1	6.3	1.64	0.89	0.75	-1.66	0.30	0.15
5	1225-1342	6.1 ± 2	-16.1	7.1	1.42	0.21	1.20	-2.23	0.50	0.05
6	1183-1260	7.3 ± 3	-15.8	7.25	1.43	0.15	1.27	-2.36	0.55	0.05
7	205-215	--	-22.9	5.55	0.28	0.25	0.03	-2.29	0.05	0.05
8	520-560	--	--	6.03	0.40	0.28	0.11	-2.23	0.12	0.07
9	442-472	--	--	6.45	0.95	0.44	0.51	-1.99	0.27	0.16
10A	846-962	16.0 ± 2	-17.9	7.14	1.71	0.24	1.46	-2.20	0.59	0.05
10B	1345-1555	--	-19.3	6.5	0.84	0.34	0.49	-2.02	0.28	0.11
10C	1606-1728	23.9 ± 3	-21.5	7.05	1.49	0.24	1.24	-2.17	0.32	0.06
11	1397-1583	25.6 ± 3.5	-20.0	6.66	0.87	0.28	0.59	-2.10	0.32	0.11
12	1460-1480	4.4 ± 2	-7.6	8.17	2.54	0.04	2.45	-3.03	0.92	0.01
13	-230	--	-18.5	6.65	1.86	0.68	1.17	-1.85	0.56	0.14

TABLE I. (cont.)

Map No.	Depth interval (ft)	^{14}C (% modern)	$\delta^{13}C$ (‰ PDB)	pH	ΣCO_2 (mM/litre)[a]	H_2CO_3 (mM/litre)[a]	HCO_3^- (mM/litre)	Log P_{CO_2}[a]	Ca+Mg (mM/litre)	Fe^{+2} (mM/litre)
14	293-315	--	-18.9	6.98	1.99	0.42	1.56	-2.06	0.78	0.10
15	259-274	10.3 ± 3	-19.6	7.1	2.07	0.34	1.72	-2.13	0.84	0.03
16	603-613	13.8 ± 2	-19.0	7.03	1.61	0.30	1.30	-2.17	0.61	0.06
17A	490-521	--	--	7.1	1.68	0.24	1.43	-2.15	0.68	0.02
17B	739-815	3.8 ± 3.5	-18.0	7.3	1.41	0.14	1.25	-2.44	0.58	0.02
18	2102-2117	10.0 ± 2	-16.4	8.9	1.22	0.00	1.15	-4.08	0.42	0.02
19	237-248	6.8 ± 3	-17.0	7.6	2.06	0.10	1.92	-2.53	1.24	0.01
20A	400-410	3.1 ± 2	-16.3	7.9	1.79	0.05	1.72	-2.93	0.91	0.01
20B	740-750	12.3 ± 2	-18.4	7.6	1.67	0.10	1.56	-2.64	0.61	0.03
20C	1125-1145	10.5 ± 2	-17.7	8.35	1.62	0.02	1.57	-3.41	0.67	0.03
21	506-536	2.5 ± 3	-16.3	7.9	1.70	0.04	1.63	-2.90	0.79	0.00
22	645-713	5.4 ± 2	--	7.9	1.94	0.05	1.87	-2.87	0.58	0.00
23A	829-839	2.0 ± 2	-10.8	9.9	3.97	0.00	2.74	-4.72	0.11	--
23B	1485-1495	3.4 ± 2	-9.5	7.9	2.89	0.06	2.78	-2.79	0.35	0.01

[a] ΣCO_2 is the sum of dissolved carbonate species, namely $H_2CO_3 + HCO_3^- + CO_3^{2-}$ + various carbonate complexes, in millimoles per litre. ΣCO_2, H_2CO_3 and log P_{CO_2} calculated by computer program WATEQ [16] using field measurements of pH and HCO_3^-. Difference between ΣCO_2 and the sum of $H_2CO_3 + HCO_3^-$ equals CO_3^{2-} and other minor complexes.

Table I cont. on p. 76

TABLE I. (cont.)

Map No.	Well name	Map No.	Well name
1	N.J.W.C. - Jamesburg 6	13	N.J. National Guard 1
2A	Englishtown W.D. 2	14	Turnpike Junction Ind. Park 1
2B	Englishtown W.D. 1	15	Columbus W.C. 3
3	Adelphia W.C. 1	16	Rhodia Corp. Test Well 1
4	Rokeach and Sons 4	17A	Ionac Chem. Co. 2
5	Point Pleasant W.D. 5	17B	Ionac Chem. Co. 3
6	Point Pleasant W.D. 7	18	U.S.G.S. Butler Place 1
7	Kentile 1	19	Rancocas Woods W.C. 1
8	E. Windsor MUA - Twin Rivers 6	20A	U.S.G.S. Medford 1
9	Roosevelt W.D. 3	20B	U.S.G.S. Medford 5
10A	Glidden-Durkee 1	20C	U.S.G.S. Medford 4
10B	Glidden-Durkee 4	21	Medford W.C. 4
10C	Glidden-Durkee 3	22	Berlin W.D. 10
11	Lakehurst Naval Air Station 32	23A	U.S.G.S. New Brooklyn 2
12	Toms River Chem. Co. 84	23B	U.S.G.S. New Brooklyn 1

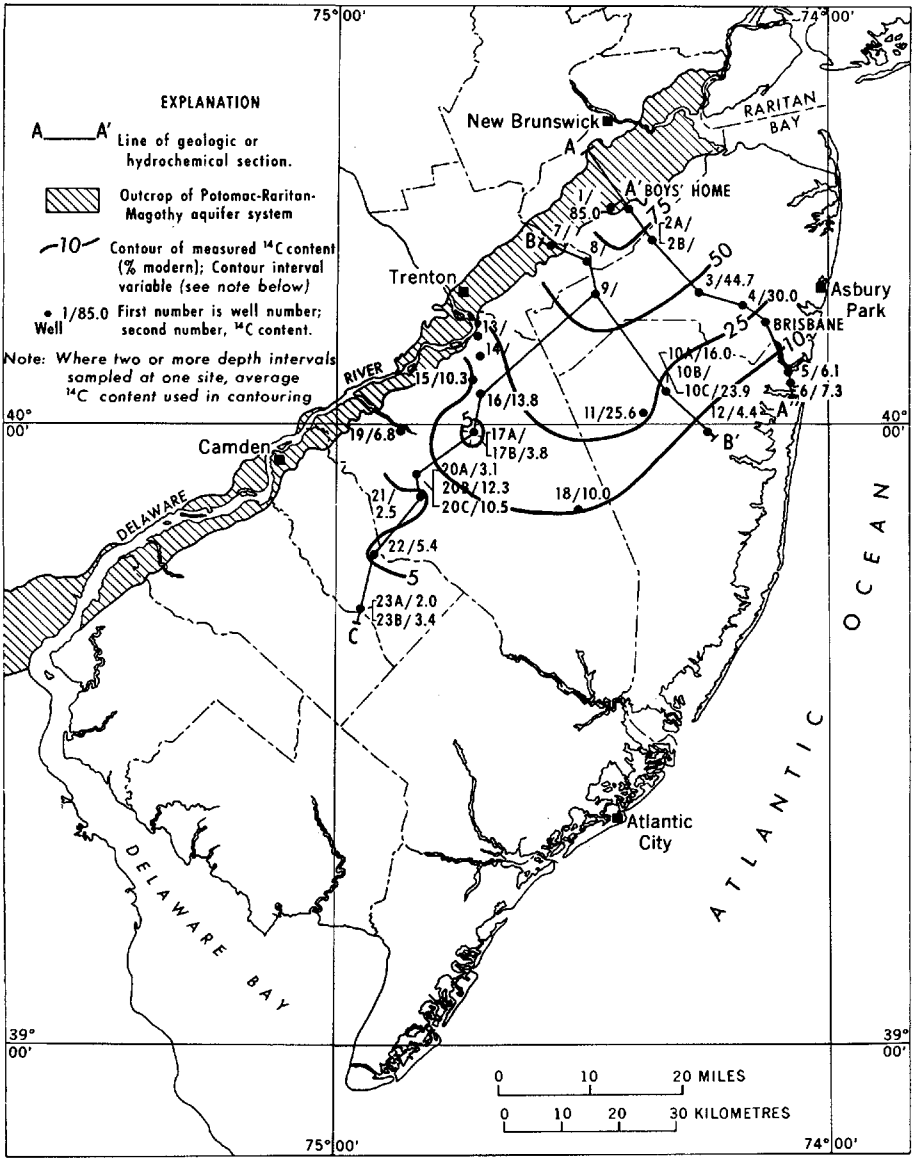

FIG. 3. Variation of ^{14}C in water from the Potomac-Raritan-Magothy aquifer system, New Jersey.

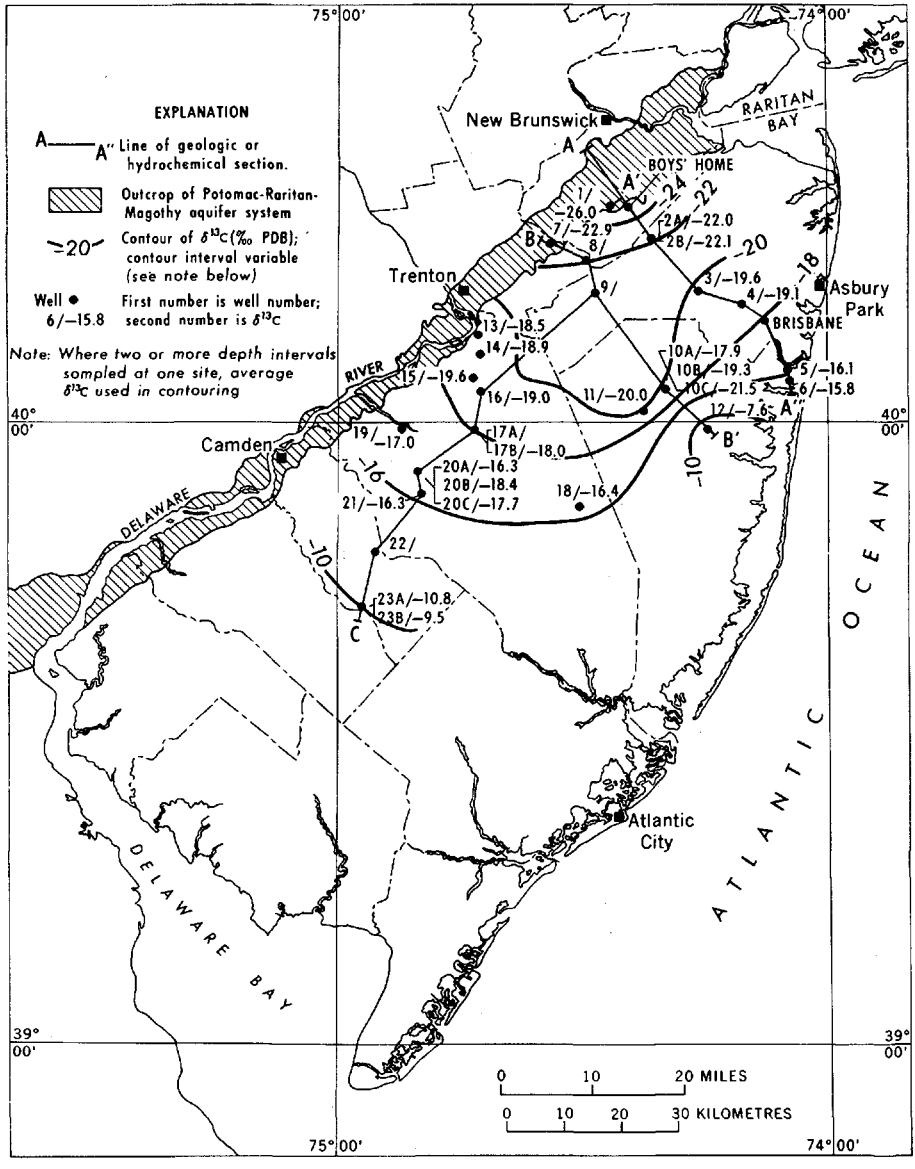

FIG. 4. Variation of $\delta^{13}C$ of water from the Potomac-Raritan-Magothy aquifer system, New Jersey.

along two southeast and one south-southwest trending cross-sections are given in Figs 5-7, and variation of the species H_2CO_3 and HCO_3^- is shown on Fig. 8. These graphs, like the contour maps, show regular changes of the cited parameters down the hydraulic gradient. These hydrochemical sections (Figs 5-8) also illustrate the magnitude of vertical as well as lateral changes in water and isotopic chemistry in the thick Potomac-Rariton-Magothy aquifer system. The vertical differences shown were determined by sampling of adjacent wells tapping different depth intervals, some as much as 240 m apart; multiple depth-zone sampling was possible at 5 out of 23 sampling locations. In general, the vertical variations of isotopic and chemical character, though significant, are not of a magnitude to mask or preclude contouring of the areal variations. However, to facilitate preparation of the contour maps (Figs 3 and 4), an average value was used for sites at which data were available for more than one depth interval. The isotopic and chemical data used in preparation of Figs 3-8 are given in Table I.

Within the intermediate parts of the flow system, that is, up the hydraulic gradient from wells 12, 18, 19 and 20A-20C, the following general down-gradient trends are evident: (a) the ^{14}C content drops from 85 to less than 10% of modern, suggesting maximum groundwater ages in the range of 1000 to more than 20 000 years; (b) $\delta^{13}C$ becomes more positive from -26 to -15‰ (relative to the PDB standard); (c) ΣCO_2 increases from 0.4 (average of wells 2A, 2B, 7 and 8) to 1.7 m$\underline{M}$/litre[1]; (d) P_{CO_2} remains relatively constant and may even increase somewhat, varying between values of 0.005 to 0.025 atm (log P_{CO_2} -1.6 to -2.3); (e) pH rises from 5 to 7.5; (f) Ca+Mg increases from 0.05 to about 0.6 m$\underline{M}$/litre; (g) iron (as Fe^{+2}) increases from nearly zero to a maximum of 0.15 m$\underline{M}$/litre and then decreases to nearly zero; and (h) temperature rises from about 13° to 25°C. No prominent patterns were observable in the variation of Na^+, K^+, Cl^-, or SO_4^{2-}, in the intermediate part of the flow system, and accordingly the concentrations of these ions, mostly less than 10 mg/litre, are neither tabulated nor discussed in this report.

The computer program WATEQ [16] was used to compute the P_{CO_2} and the ΣCO_2, Ca+Mg and Fe^{+2} molalities used on the hydrochemical maps and cross-sections. Field measurements of pH, alkalinity and temperature, made at each sampling site, and a complete chemical analysis of the well waters comprise the input to this program, which calculates the state of saturation of natural water with respect to 90 mineral phases.

Unadjusted ^{14}C data for wells 1, 3, 4 and 5 suggest apparent groundwater velocities of about 2 to 5 m yearly along section A'-A'' (Fig. 5). These values are similar to velocities computed using available hydraulic data for the principal aquifer. In making this computation it is assumed that downward leakage of groundwater from the regional aquitard (namely, the Merchantville Formation and Woodbury Clay) into the principal aquifer is only a fraction of the water in lateral transit through the aquifer from its high-level outcrop areas.

---

[1] The anomalous ΣCO_2 and P_{CO_2} of well 1 (Table I) is discussed below.

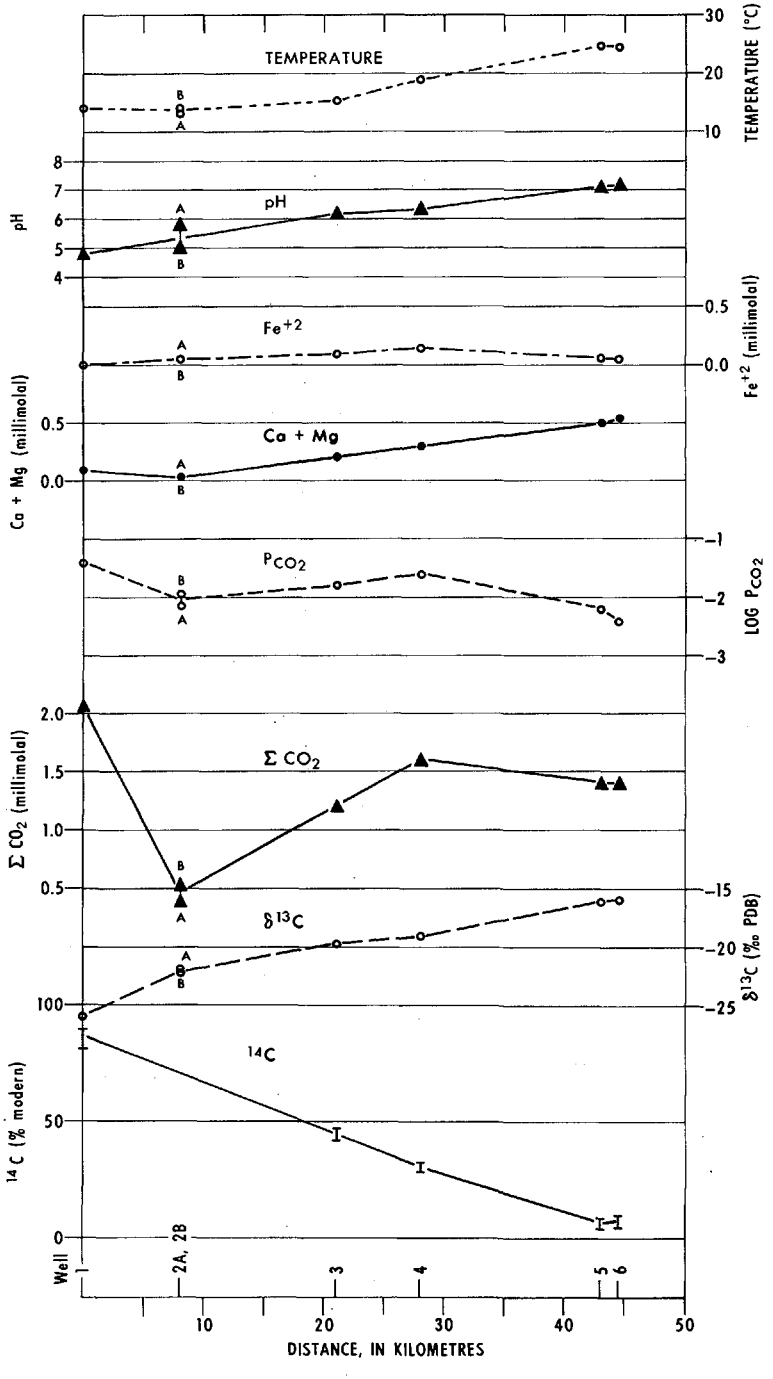

FIG. 5. Hydrochemical section A'-A" (line of section shown on Fig. 3).

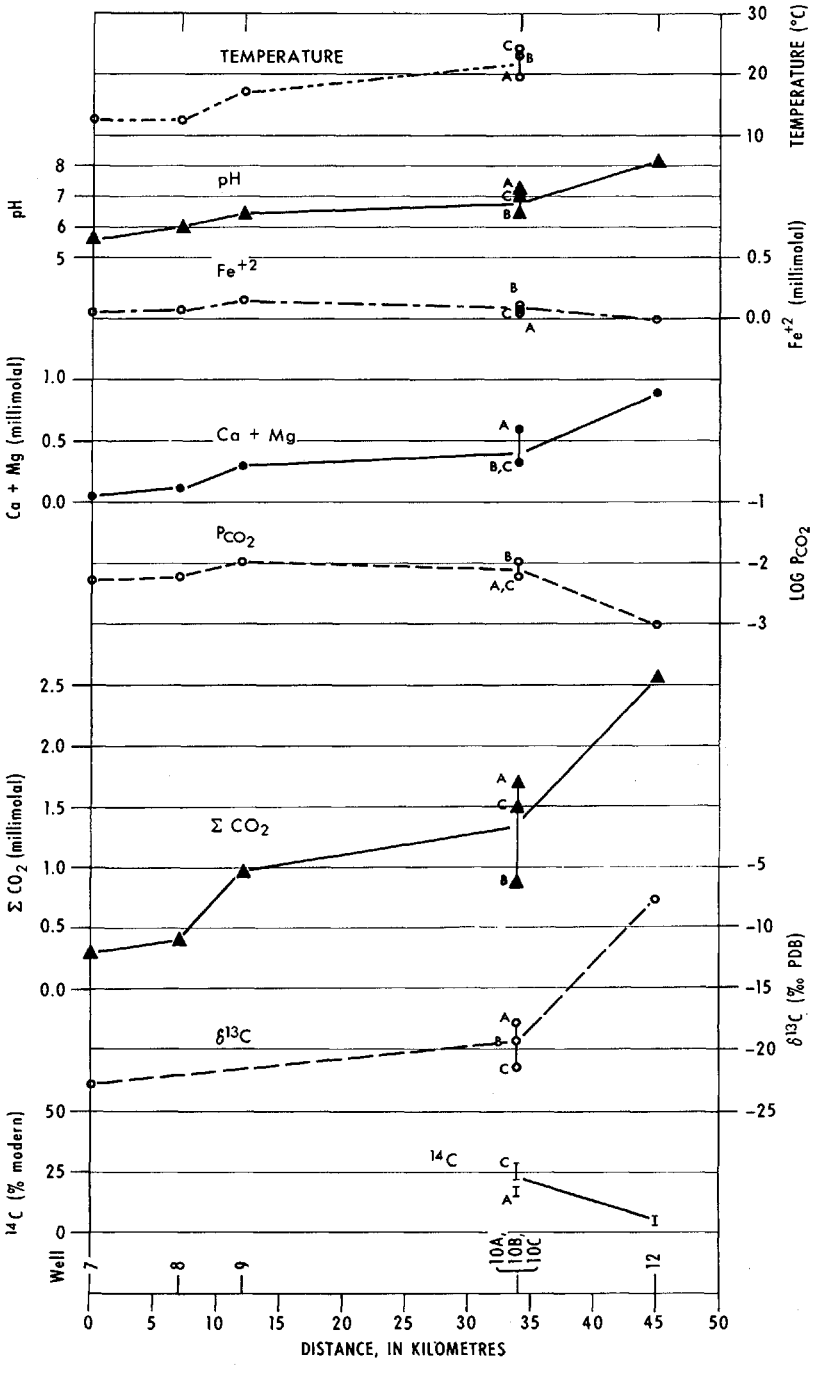

FIG. 6. Hydrochemical section B-B' (line of section shown on Fig. 3).

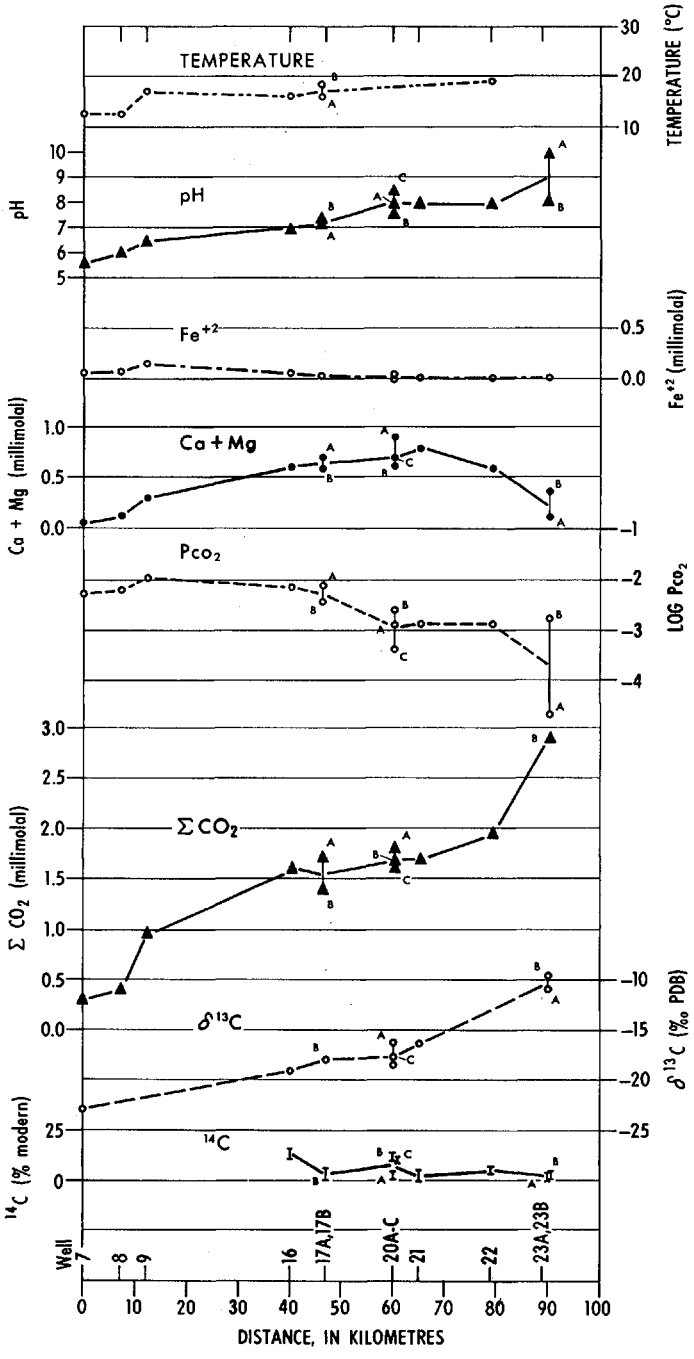

FIG. 7. Hydrochemical section B-C (line of section shown on Fig. 3).

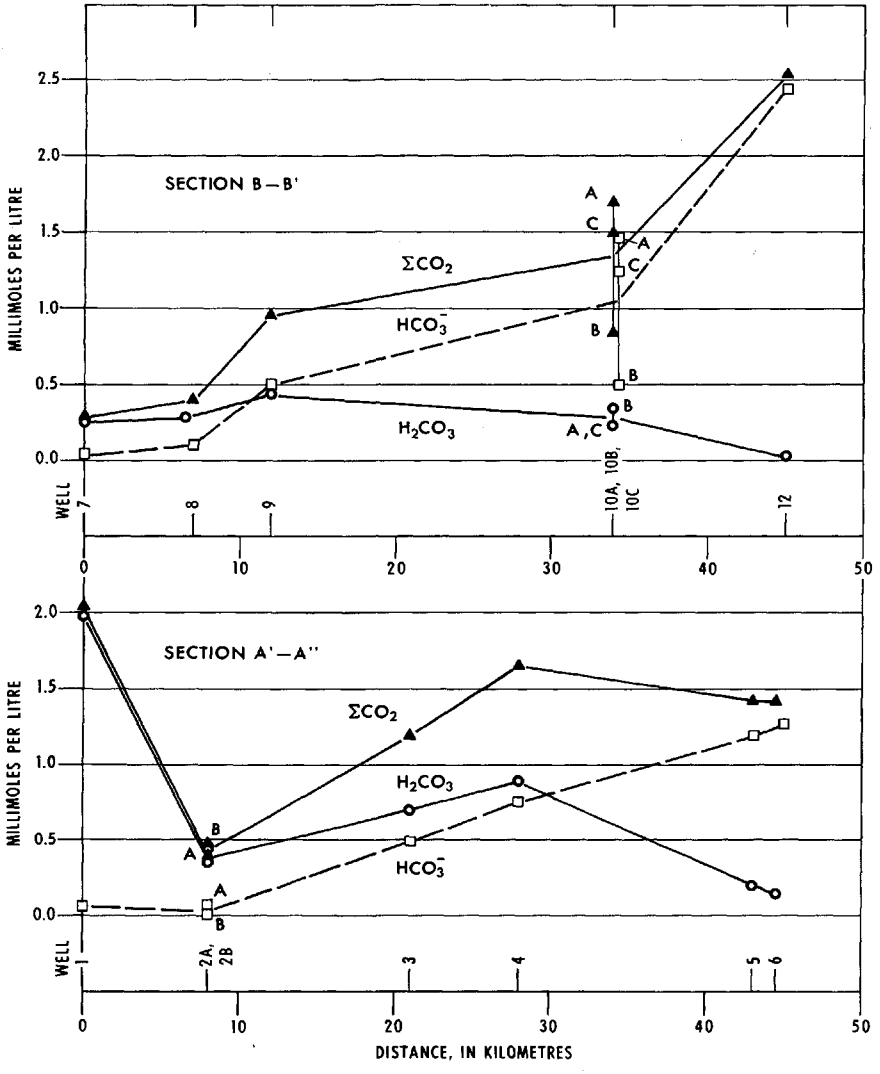

FIG. 8. Variation of total carbonate (ΣCO_2), bicarbonate and carbonic acid, along sections A'-A" and B-B'.

INTERPRETATION OF CHEMICAL DATA

A major source of dissolved carbonate other than that derived from soil zone CO_2 and from the dissolution of carbonate minerals appears to be present in the principal aquifer. According to the familiar reactions:

(1) $CO_2 + H_2O \rightleftharpoons H_2CO_3 \rightleftharpoons H^+ + HCO_3^-$

(2) $H^+ + HCO_3^- + CaCO_3 \rightleftharpoons Ca^{+2} + 2HCO_3^-$

and in a closed system, the initial P_{CO_2} (or H_2CO_3 content) should decrease, the pH rise, and the Ca+Mg and HCO_3^- contents increase away from the recharge area as carbonate mineral phases (calcite or siderite grains and cement, or calcareous fossils) are dissolved. However, over distances of 30-45 km down the hydraulic gradient, that is, within the intermediate parts of the groundwater flow system (as defined above), the P_{CO_2} (or the H_2CO_3 content) remains constant or increases (Figs 5-8) despite an increase in pH from 5 to 7, an increase in Ca+Mg of 0.05 to 0.55 m$\underline{M}$/litre and an increase in HCO_3^- from about 0.05 to 1.5 m$\underline{M}$/litre (at well 10A). This behaviour suggests the addition of significant quantities of CO_2 to the aquifer water miles from the principal recharge area. The data for wells 2A, 2B, 3 and 4 suggest, for example, a doubling of the H_2CO_3 content (Table I and Fig. 8).

Because of the acknowledged leakage of groundwater into the principal aquifer from overlying strata (see Hydrogeologic Setting section above), it may be argued that the aquifer system is open to the continued addition of CO_2 charged waters down the hydraulic gradient and that this process, in fact, accounts for the failure of P_{CO_2} (or H_2CO_3 content) to drop in the intermediate portions of the flow system. This argument appears untenable. First, before entering the principal aquifer, such leakage has to traverse up to 300 m of overlying strata including 30-60 m of the regional aquitard. The time needed for this traverse is certainly hundreds and possibly several thousand years. Moreover, most of the sediments traversed are of marine origin and some contain abundant fossil assemblages. Thus, it appears extremely unlikely that the P_{CO_2} (or H_2CO_3 content) of such leakage, as it enters the aquifer, could be as high as that in the recharge areas of the essentially non-fossiliferous (that is non-calcareous) sediments comprising the principal aquifer. (The ΣCO_2, particularly the HCO_3^- of the leakage may, on the other hand, be considerably higher than that in the principal aquifer; see below.) Second, computations [17] of the effects of mixing of leakage, of various assumed compositions (see below), with aquifer water, indicate a decrease in P_{CO_2} of the mixed waters.

The initial P_{CO_2} and ΣCO_2 in well 1 in the recharge area appears anomalously high when compared with other wells in and near the recharge area (see, for example, wells 7 and 8 in section B-B', Fig. 6, and wells 2A and 2B on section A'-A'', Fig. 5) and in recharge areas of the same aquifer on Long Island, New York [18]. The anomalously high value in well 1 may reflect the shallowness (less than 36 m) and proximity (about 60 m) of this well to a lake; the nitrate content of water from this well is also anomalous, 9 mg/litre versus less than 0.5 mg/litre at other well sites. In any event, even if the data from well 1 are accepted as accurately representing shallow recharge water, they do not detract from the preceding arguments because P_{CO_2} (or H_2CO_3 content) remains relatively constant, or increases southeastwards from well 2 (see wells 2A, 2B, 3, 4 along section A'-A'', Fig. 5).

The P_{CO_2} values must reflect a balance between that entering, or generated in, the aquifer and that utilized to dissolve carbonate mineral phases. Were the strata comprising the principal aquifer rich rather than poor in carbonate mineral phases (cement, shell fragments) it is likely that the P_{CO_2} would drop rather than remain relatively constant (within the intermediate part of the flow system) despite the addition of CO_2. It is the paucity of carbonate minerals in the principal aquifer that makes the

phenomena of CO_2 addition explicit even in simple diagrams such as Figs 5-8. The decrease in P_{CO_2} between wells 4 and 5 (Fig. 5) and 10A-C and 12 (Fig. 6) may reflect the shoreward increase in percentage of marine sediments comprising the aquifer.

In summary, the relatively constant or increasing value of P_{CO_2} (or H_2CO_3 content) over distances of 30-45 km in the intermediate parts of this flow system suggest, when coupled with marked increases in HCO_3^-, Ca+Mg and pH, that CO_2 is somehow entering, or being generated in, this aquifer system downdip from the recharge area.

The phenomena described above are not new. Pearson and Friedman [18] documented similar P_{CO_2} and ΣCO_2 conditions in the Magothy aquifer of Long Island, New York. Foster [15] has shown that the bicarbonate content of groundwaters from the distal portions of Atlantic and Gulf Coastal Plain aquifers of deltaic origin is commonly several times greater than can be attributed to the dissolution of calcite minerals by soil-derived CO_2.

Before discussing the effect of the non-soil zone CO_2 on interpretation of the ^{14}C content of water from the aquifer, some speculation on the origin of the CO_2 is in order.

Coalification processes operating in an anaerobic environment on the ubiquitous lignitic detritus in the principal aquifer appear plausible as the source of the CO_2. Foster [15] envisioned the coalification process as a dynamochemical one wherein temperature and pressure in an anaerobic environment progressively eliminate volatile matter, chiefly CO_2 and H_2O from peat and lignite. More recent work by Schumacher and co-workers [19], and by Teichmuller and Teichmuller [20] supports her contention as to the likely gaseous by-products of the coalification of lignite and its precursors.

Oxidation of the cellulose content of the lignite is a possible minor source of the CO_2 in the Potomac-Raritan-Magothy aquifer system. Pearson and Friedman [18] believed that the oxidation of lignite is principally responsible for the carbonate content of waters in the Magothy aquifer on Long Island, New York. There, as much as 10 mg/litre dissolved oxygen is available for lignite oxidation in the recharge area, and several mg/litre remain in solution a few kilometres down the hydraulic gradient [21]. In contrast, little dissolved oxygen occurs in water from the Potomac-Raritan-Magothy aquifer system. Oxygen was detected in only 5 out of 14 wells and only 3 of these had 1 or more mg/litre oxygen (0.2 mg/litre in well 5; 1.0 in well 10A; 2.2 in well 13; 3.0 in well 17A; and 0.8 mg/litre in well 17B). Surprisingly, only one of these wells (No. 13) is in or near a major recharge area. In any event, sufficient oxygen is not available in the principal aquifer to account for the observed H_2CO_3 content (Fig. 8). Moreover, part of the few mg/litre dissolved oxygen present in the principal aquifer may be utilized in other reactions, e.g. the oxidation of common iron accessory minerals, such as pyrite.

In summary, the undoubtedly complex processes called coalification may somehow be involved in the introduction of amounts of CO_2 in the principal aquifer comparable with that generated in the soil zone. The CO_2 by virtue of its mobility need not, of course, have originated in the immediate vicinity of the sampled wells. Some may have migrated many kilometres up-dip from areas where the aquifer is buried at depths of over 600 m; some may also have been formed in the lignitic and clayey swamp deposits interbedded with the permeable sands comprising the aquifer.

INTERPRETATION OF ^{14}C DATA

Two general methods have been developed [3] for handling the progressive dissolution of dead carbonate during movement of water through an aquifer. The first method involves a mass balance of the $\delta^{13}C$ content of water in the recharge area and in the aquifer. This method, introduced by Ingerson and Pearson [3] and modified by Mook [6], rests on the dual assumptions: (a) no input of originally derived CO_2 within the aquifer except in the recharge area, specifically CO_2 generated in the soil zone; and (b) a known and constant $\delta^{13}C$ of dissolved carbonate mineral phases. In practice this method relies on the large initial difference between the $\delta^{13}C$ of marine carbonate mineral phases (0 ± 3‰ PDB) and the $\delta^{13}C$ of soil-generated CO_2 (average value -25‰).[2] The $\delta^{13}C$ value of the admixture permits an estimation of the degree of dilution of soil zone-derived ^{14}C by dead carbonate dissolved from aquifer cement or shell materials. Neither assumption is fulfilled in the Potomac-Raritan-Magothy aquifer system, nor is it likely to be fulfilled in any aquifer of deltaic origin. First, there appears to be a major source of CO_2 within the aquifer itself, and this source is probably the ubiquitous lignitic detritus ($\delta^{13}C$ value 25 ± 5‰). Second, the aquifer is poor in carbonate mineral phases of marine origin, particularly within the intermediate parts of the groundwater flow system (as defined above). The carbonate mineral phases present are of marginal marine and deltaic origin, and they probably have $\delta^{13}C$ intermediate between 0 and -20‰. A summary of the potential sources of dissolved carbonate species and their expectable $\delta^{13}C$ content are listed in Table II. It is evident that a near continuum of $\delta^{13}C$ values is potentially present in marginal marine or deltaic sediments, and therefore in view of the cyclic alternation of deltaic, marginal-marine and marine sediments the described correction method is unlikely to be successful. That one or both of the listed assumptions are unwarranted for the principal aquifer is readily seen by comparing the graphs of $\delta^{13}C$ and ΣCO_2 (Figs 5-7) or the data in Table I. On the hydrochemical section B-B' (Fig. 6), for example, ΣCO_2 increases almost six times between wells 7 and 10A, but $\delta^{13}C$ varies by only 21%, from -22.9 to -17.9‰.

The second successfully applied adjustment method [3, 7] involves a comparison of the ratio of initial ΣCO_2 (namely that in the recharge area) to a final ΣCO_2 (namely that in water from any well-site of interest). The ratio indicates the magnitude of dilution of the initial carbonate by dissolution of dead carbonate in the aquifer. To adjust for this dilution, the measured ^{14}C is divided by the ratio yielding a higher ^{14}C value used to compute residence times. If the initial ΣCO_2 can be accurately determined, this method should work, in principle, regardless of the generation of CO_2, by whatever mechanism, within the aquifer. This method also fails for data from the principal aquifer yielding a future age or an age of modern recharge for water from depths of 200 to as great as 485 m beneath the surface. For example, using 0.39 m$\underline{M}$/litre (average ΣCO_2 of wells 2A, 2B, 7 and 8, Table I) as representative of ΣCO_2 in recharge water, that is, as $\Sigma CO_{2initial}$, and 1.64 m$\underline{M}$/litre (well 4, Table I) as a selected ΣCO_{2final}, the ratio $\Sigma CO_{2initial} / \Sigma CO_{2final} = 0.238$. Dividing the measured ^{14}C content of well 4 water (30.0 ± 3% modern; Table I) by this quotient

[2] Calvin (C_3) photosynthetic cycle assumed [22].

TABLE II. POTENTIAL SOURCES OF DISSOLVED CARBONATE SPECIES IN GROUNDWATERS FROM THE POTOMAC-RARITAN-MAGOTHY AQUIFER SYSTEM AND OTHER UNCONSOLIDATED AQUIFERS OF DELTAIC ORIGIN

Potential source	Expectable $\delta^{13}C$ (‰ PDB)
1. Soil CO_2[a]	-25 [22]
2. Cretaceous or Tertiary lignite	-25 ± 5 [23]
3. Cretaceous or Tertiary marine invertebrate shells	0 ± 3 [24, 25]
4. Cretaceous or Tertiary marginal-marine invertebrate shells	-4 ± 4 [26]
5. Cretaceous or Tertiary inorganic fresh-water carbonate, including siderite (swamp environment)	-15 ± 5 [27]

[a] Calvin (C_3) photosynthetic cycle assumed [22].

yields an adjusted ^{14}C content of 130% modern. The same procedure also leads to anomalous adjusted ages for wells 3 and 10C. Both the depth of the intervals sampled in these wells (Table I), and frequency of pumping of these industrial supply wells precludes contamination of this groundwater by H-bomb derived ^{14}C. The ΣCO_2 of water from well 7 (Table I) and that from wells in the recharge area of the Magothy aquifer on Long Island [18] suggest that $\Sigma CO_{2initial}$ may be closer to 0.3 than 0.39 m$\underline{M}$/litre. However, use of this lower $\Sigma CO_{2initial}$ value leads to still higher adjusted ^{14}C contents at the cited wells.

Failure of the second described adjustment method may be due to at least two factors. First, the value used for $\Sigma CO_{2initial}$ might be too low owing perhaps to the presence of dissolved organic species (in recharge water) not included in the dissolved carbonate inventory as determined by means of field pH and alkalinity measurement and use of equilibria for reactions (1) and (2) (F.J. Pearson, Jr., oral communication, Nov. 1973). Alternatively, the value ΣCO_{2final} may be too large due to cross-flow (or leakage) from the overlying aquifers. The first possibility appears unlikely in this aquifer system for two reasons: (a) there is little or no oxygen in the groundwater to oxidize the postulated dissolved organic carbon species; and (b) the non-volatile dissolved organic carbon (DOC) in New Jersey and in other unpolluted groundwaters is extremely low [28]. The DOC of groundwater from five wells in New Jersey tapping the principal aquifer ranged from 0.8 to 2.5 mg/litre with median and mean values of 1.5 mg/litre. In the United States of America as a whole, the median DOC of groundwater from 100 sites was 0.7 and the mean 1.2 mg/litre [28]. These values, it should be emphasized, do not include any dissolved but volatile organic carbon species.

The second reason cited for failure of the $\Sigma CO_{2initial}$ / ΣCO_{2final} ^{14}C adjustment method, namely that ΣCO_{2final} is too large due to cross-flow, appears plausible for the Potomac-Raritan-Magothy aquifer system.

As mentioned above, the aquifer is recharged both by infiltration entering high-level outcrop areas and by leakage from overlying strata, particularly beneath topographically high areas east of the outcrop area. This leakage is reflected by mounds in the potentiometric surface (Fig. 1) which are as much as 13 km east of the outcrop recharge area. Available hydrogeologic data do not permit estimation of the relative significance of each source of recharge. In contrast with water moving laterally through the aquifer from the outcrop recharge area, the leakage traverses marine sediments rich in carbonate mineral phases relative to the sediments comprising the principal aquifer. Calcareous fossils are particularly abundant in the Mount Laurel Sand, the Navesink Formation and the Red Bank Sand [14] of Late Cretaceous age; lignitic detritus is also common in the entire sedimentary column overlying the principal aquifer. Thus, granting the likelihood that the initial P_{CO_2} of recharge water beneath the topographic highs east of the outcrop area is not significantly different from that in the outcrop areas, the ΣCO_2 of water at the base of the regional aquitard should be considerably higher than water in the principal aquifer, simply because of the availability of abundant calcareous and lignitic detritus. It is this combination of constituents, namely calcareous and lignitic matter, that is believed to be responsible for the high bicarbonate content of the Coastal Plain aquifers studied by Foster [15]. It is not unlikely that the ΣCO_2 of leakage entering the principal aquifer may be about 1.5 to 2.5 m$\underline{M}$/litre; the P_{CO_2} of these waters, conversely, should be considerably less than waters derived from the outcrop area.

If the ΣCO_2 of leakage is indeed significantly greater than that of water in the aquifer, and some evidence for this is presented below, then it is readily understandable why the $\Sigma CO_{2initial}/\Sigma CO_{2final}$ adjustment method leads to impossible ^{14}C ages. Two systems, not one, are being compared. The $\Sigma CO_{2initial}$ is that for the principal aquifer, whereas ΣCO_{2final} is a mixture of water from two sources. Briefly the ΣCO_{2final} is far too high and not representative of dissolution of carbonate species in the principal aquifer. To complicate the story, the ^{14}C content of the leakage could be higher or lower than that in the aquifer.

Qualitative evidence that the ΣCO_2 of leakage may be significantly greater than water in the principal aquifer is provided by data from two shallow (less than 50 m) wells drilled into the marine strata overlying the aquifer. The Edward Marsh and Carousel Farms wells (not shown on Figs 3 or 4) tap the Merchantville Formation (Fig. 2), and the Mount Laurel Sand and Wenonah Formation respectively. The HCO_3^-, pH and Ca+Mg contents of water from these wells are respectively 1.7 and 2.5 m$\underline{M}$/litre, 8.3 and 8.1, and 0.8 and 1.2 m$\underline{M}$/litre (at these pH's, HCO_3^- is almost equivalent to ΣCO_3). It is stressed that these wells tap the top rather than the base of the sedimentary column through which leakage into the aquifer would have to pass, and that the water chemistry could change with depth, for example, exchange of alkaline earths for sodium. But removal of HCO_3^- is difficult to visualize. Additional qualitative evidence is provided by Figs 5-8 and Table I. On these figures, A, B and C denote respectively the shallowest, intermediate and deepest depth intervals sampled at a given site; actual depths are given in Table I. At wells 10A, 10B and 10C, for example, the $\delta^{13}C$, ΣCO_2, HCO_3^-, log P_{CO_2}, pH and Ca+Mg data all qualitatively support the notion that the downward leakage has moved through strata considerably more calcareous than

those comprising the aquifer. Note specifically that the ΣCO_2 and Ca+Mg content of the uppermost sampled zone (256-291 m) is twice that of the intermediate zone (408-471 m); the uppermost zone is only about 3 m below the base of the regional aquitard. Data for the intermediate and deepest intervals (487-524 m), however, are not entirely consistent with leakage (the Na+K content of water from the deepest interval nearly equals that for Ca+Mg, suggestive of some ion-exchange phenomena or other cation sources). The ΣCO_2, HCO_3^-, log P_{CO_2}, pH and Ca+Mg data for wells 2A and 2B, 17A and 17B, and 20A-20C also qualitatively support the notion of downward leakage.

In summary, downward leakage of groundwater with a ΣCO_2 considerably higher than that in the principal aquifer may account for the failure of the $\Sigma CO_{2initial}/CO_{2final}$ ^{14}C adjustment method in the Potomac-Raritan-Magothy aquifer system. Available data offer qualitative support for this notion, but it is stressed that groundwater from the base of the regional aquitard has yet to be sampled and analysed. Gathering of such samples must precede mass balance studies of the source and distribution of chemical or isotopic species in this aquifer system.

SUMMARY AND CONCLUSIONS

1. A major source of CO_2, in addition to that generated in the soil zone, significantly affects the dissolved carbonate content of water in the Potomac-Raritan-Magothy aquifer system. Decomposition of the ubiquitous lignitic detritus in the aquifer may be the source for the additional CO_2, as first proposed by Foster [15].
2. The $\delta^{13}C$ of carbonate mineral phases expectable in deltaic and marginal marine sediments ranges from 0 to -20‰.
3. Leakage of water from aquitards into aquifers is a common occurrence in regional groundwater flow systems, and significant variations of water and isotopic chemistry with depth are likely in thick aquifers. Accordingly, in an evaluation of areal changes of water and isotopic chemistry it is mandatory that water should also be sampled from wells tapping different and restricted depth intervals. Such vertical control is an essential prerequisite to mass balance studies of the distribution of isotopic and mineral species.
4. Regular variation of ^{14}C and $\delta^{13}C$ down the hydraulic gradient need not guarantee a meaningful interpretation of either absolute or relative groundwater velocities. Because of the factors listed above neither of two commonly used methods, for adjustment of ^{14}C data to account for dilution by non-radiogenic carbonate, work in the Potomac-Raritan-Magothy aquifer system. It is unlikely that either method will work in aquifers of deltaic or marginal marine origin unless the ^{14}C and $\delta^{13}C$ data are augmented by detailed studies of aquifer stratigraphy, mineralogy, hydrodynamics, hydrochemistry and dissolved gas content.

ACKNOWLEDGEMENTS

The authors are grateful to R. Hodges and E. Donsky for their assistance in collecting the water samples and in field determination of pH, Eh, alkalinity, temperature and dissolved oxygen. The ^{14}C analyses

were made in the laboratory of M. Rubin of the US Geological Survey, Washington, D.C., and the $\delta^{13}C$ analyses by Teledyne Isotopes, Inc., of Westwood, New Jersey. J. Chemerys analysed the water samples chemically. The co-operation of the New Jersey Division of Water Resources, Department of Environmental Protection, in expediting the study is appreciated. The manuscript benefited from review comments by D.W. Fisher, B.F. Jones, F.J. Pearson, Jr., and C.T. Rightmire. The work was funded by the Defense Advanced Research Projects Agency (DARPA) of the United States Department of Defense under Order No. 1813, Amendment no. 1.

REFERENCES

[1] MÜNNICH, K.O., Messungen des ^{14}C Gehaltes von hartem Grundwasser, Naturwissenschaften 44 (1957) 32.

[2] VOGEL, J.C., EHHALT, D., "The use of carbon isotopes in groundwater studies", Radioisotopes in Hydrology (Proc. Symp. Tokyo, 1963), IAEA, Vienna (1963) 383.

[3] INGERSON, E., PEARSON, F.J., Jr., "Estimation of age and rate of motion of ground water by the C^{14} method", Recent Researches in the Fields of Hydrosphere, Atmosphere, and Nuclear Geochemistry, Maruzen, Tokyo (1964) 263.

[4] WENDT, I., STAHL, W., GEYH, M., FAUTH, F., "Model experiments for ^{14}C water-age determinations", Isotopes in Hydrology (Proc. Symp. Vienna, 1966), IAEA, Vienna (1967) 321.

[5] GEYH, M.A., "On the determination of the initial ^{14}C content in groundwater", 8th Int. Conf. Radiocarbon Dating, Wellington, New Zealand (1972) D58.

[6] MOOK, W.G., "On the reconstruction of the initial ^{14}C content of groundwater from the chemical and isotopic composition", 8th Int. Conf. Radiocarbon Dating, Wellington, New Zealand (1972) D31.

[7] PEARSON, F.J., Jr., WHITE, D.E., Carbon-14 ages and flow rates of water in Carizzo Sand, Atascosa County, Texas, Water Resour. Res. 3 (1967) 251.

[8] PEARSON, F.J., Jr., HANSHAW, B.B., "Sources of dissolved carbonate species in groundwater and their effects on carbon-14 dating", Isotope Hydrology 1970 (Proc. Symp. Vienna, 1970), IAEA, Vienna (1970) 271.

[9] FARLEKAS, G.M., NEMICKAS, B., GILL, H.E., Geology and Ground-water Resources of Camden County, New Jersey, U.S. Geol. Survey open-file report (1973).

[10] OWENS, J.P., SOHL, N.F., "Shelf and deltaic paleoenvironments in the Cretaceous-Tertiary formations of the New Jersey Coastal Plain", Geology of Selected Areas in New Jersey and Eastern Pennsylvania (SUBITZKY, S., Ed.), Rutgers University Press, New Brunswick, N.J. (1969) 235.

[11] GILL, H.E., SEABER, P.R., VECCHIOLI, J., ANDERSON, H.R., Evaluation of Geologic and Hydrologic Data from the Test-drilling Program at Island Beach State Park, New Jersey; New Jersey Dept. Conserv. and Econ. Development, Water Resources Circular 12 (1963).

[12] BROWN, P.M., MILLER, J.A., SWAIN, F.M., Structural and stratigraphic framework, and spatial distribution of permeability of the Atlantic Coastal Plain, U.S. Geol. Surv., Prof. Pap. 796 (1972) 37.

[13] RICHARDS, H.G., OLMSTED, F.H., RUHLE, J.L., Generalized Structural Contour Maps of the New Jersey Coastal Plain, New Jersey Geol. Surv., Geol. Rep. Series 4 (1962).

[14] OWENS, J.P., MINARD, J.P., SOHL, N.F., MELLO, J.F., Stratigraphy of the outcropping post-Magothy Upper Cretaceous formations in southern New Jersey and northern Delmarva Peninsula, Delaware and Maryland, U.S. Geol. Surv., Prof. Pap. 764 (1970).

[15] FOSTER, M.D., The origin of high sodium bicarbonate waters in the Atlantic and Gulf Coastal Plains, Geochim. Cosmochim. Acta 1 (1950) 33.

[16] TRUESDELL, A.H., JONES, B.F., WATEQ, A Computer Program for Calculating Chemical Equilibria for Natural Waters, NTIS Publ. No. PB-220464 (1973).

[17] DEFFEYES, K.S., Carbonate equilibria: a graphic and algebraic approch, Limnol. Oceanogr. 10 (1965) 412.

[18] PEARSON, F.J., Jr., FRIEDMAN, I., Sources of dissolved carbonate in an aquifer free of carbonate minerals, Water Resour. Res. 6 (1970) 1775.

[19] SCHUHMACHER, J.P., HUNTJENS, F.J., von KREVELEN, D.W., Fuel 39 (1960) 223.

[20] TEICHMULLER, M., TEICHMULLER, R., "Diagenesis of coal (coalification)", Diagenesis in Sediments (LARSEN, G., CHILINGAR, G.V., Eds), Elsevier, Amsterdam (1967) 391.

[21] SMITH, S.O., Occurrence and Treatment of Iron in Groundwater of Long Island, Nassau County, Nassau County Dept. Health, Div. of Environmental Health, mimeographed rep. (1969).

[22] RIGHTMIRE, C. T., HANSHAW, B. B., Relationship between the carbon isotope composition of soil CO_2 and dissolved carbonate species in groundwater, Water Resour. Res. 9 (1973) 958.
[23] DEGENS, E. T., "Biogeochemistry of stable carbon isotopes", Organic Geochemistry, Methods and Results (EGLINTON, G., MURPHY, M. I. J., Eds), Springer, Berlin (1969) 304.
[24] LLOYD, R. M., Variations in the oxygen and carbon isotope ratios of Florida Bay mollusks and their environmental significance, J. Geol. 72 (1964) 84.
[25] KEITH, M. L., ANDERSON, G. M., EICHLER, R., Carbon and oxygen isotopic composition of mollusk shells from marine and fresh-water environments, Geochim. Cosmochim. Acta 28 (1964) 1757.
[26] KEITH, M. L., PARKER, R. H., Local variation of ^{13}C and ^{18}O content of mollusk shells and the relatively minor temperature effect in marginal marine environments, Mar. Geol. 3 (1965) 115.
[27] WHELAN, T., III, ROBERTS, H. H., Carbon isotope composition of diagenetic carbonate nodules from freshwater swamp sediments, J. Sediment Petrol. 43 (1973) 54.
[28] LEENHEER, J. A., MALCOLM, R. L., McKINLEY, P. W., ECCLES, L., Occurrence of dissolved organic carbon in selected ground water samples in the United States, J. Res. , U. S. Geol. Survey (in press).

DISCUSSION

P. FRITZ: Are $\delta^{13}C$ values affected by fractionation? To what extent, in your opinion, are the $\delta^{13}C$ variations a consequence of the groundwater pH variations?

I. J. WINOGRAD: In view of the widespread variation in the $\delta^{13}C$ values of the carbonate mineral phases I doubt whether such fractionation calculations would be worth performing.

H. OESCHGER (Chairman): From your results it looks to me as if we would be better off basing the ^{14}C ages of groundwaters on the $^{14}C/H_2O$ ratio rather than on the $^{14}C/C$ ratio. If the total carbon increases along an aquifer by up to a factor of four and if the additional carbon is dead, one may obtain "^{14}C-aging" by two half-lives as an artefact – an error one can avoid by using the $^{14}C/H_2O$ ratio.

I. J. WINOGRAD: The additional carbon, if derived from lignite, as postulated, certainly is dead. Your suggestion that one should use the $^{14}C/H_2O$ ratio is very interesting.

E. CUSTODIO GIMENA: Can SO_4^{2-} reduction to sulphides and the accompanying oxidation of organic matter produce the observed CO_2?

I. J. WINOGRAD: The mechanism which you propose certainly applies in some systems. In the aquifer system which I discussed and in others beneath the Atlantic Coastal Plain, SO_4^{2-} reduction does not appear to be important. First, there is too little sulphate (less than 10 mg/litre); second, the sulphate content does not appear to decrease down the hydraulic gradient.

E. CUSTODIO GIMENA: In a deep aquifer in the delta of the river Llobregat, near Barcelona, it is possible to date the water by chemical methods because at present recharge is mainly from the river and from canals carrying water which has been contaminated since 1925 by substantial saline effluent and whose composition over time is well known. Zones with water dating from before 1925 have been delimited by such chemical methods, the results agreeing with those of hydraulic calculations. In 1965, sampling for purposes of tritium determination was carried out, and water dating from later than 1953 was found. In an effort to resolve this inconsistency, it has been postulated that there may have been vertical infiltration of water from the surface aquifer through the thick semi-confining mud, for the hydraulic gradient favours such infiltration. This

water, being similar to that in the deep aquifer, hardly modifies the chemical composition; however, it can considerably alter the tritium concentration in cases of rapid circulation. On the other hand, the data derived from a hydrodynamic exploitation model contradict the existence of such rapid circulation. In this connection, samples of the mud have been collected for the purpose of determining its chemical composition and tritium content, and confirming beyond doubt that rapid vertical movement is not possible. The only explanation will then be that wells create a short-circuit through the mud. In areas where there are many wells, this mechanism can invalidate the results of dating, or at least one must interpret the results with care. Have you observed anything similar?

I. J. WINOGRAD: The question as to whether drawdown in a pumping well can cause a significant downward movement of water from shallower aquifers to the screen, via the annulus between the casing and the wall of the bore, is a very important one. The answer is that it can and does, the extent of the drawdown depending on factors such as well construction and bedrock type.

In the system which I described, I believe that such movement is negligible. First, the 30-60 m aquitard is composed of clay and silt which may seal the annulus above the aquifer; second, the regularity of chemical and isotopic changes down the hydraulic gradient suggests the absence of sampling problems; third, as can be seen from Table I, the ^{14}C content of shallower zones (well groups 10A-C, 20A-C and 23A-B) is less than that of deeper zones; fourth, the volume of flow along the annulus is probably just a small fraction of that coming from the aquifer, so that such flow in any event could only influence the tritium and ^{14}C contents, not the water chemistry or stable isotope content.

J.Ch. FONTES: In the first of your conclusions you suggest that organic matter is the source of additional CO_2 in the aquifer. This means oxidation. However, if the oxidation is due to dissolved oxygen, the oxygen balance imposes a maximum for the excess CO_2 of organic origin. If dissolved oxygen is not involved, what oxidation-reduction system would you postulate on the basis of the chemical composition of the water?

I. J. WINOGRAD: Dissolved oxygen is not involved; there is little or none in the water. Not being an organic chemist, I have no knowledge of the behaviour of the complex and heavy organic molecules comprising lignite. My guess is that the oxidation-reduction involved does not affect the water chemistry, for the change in valence of the carbon in CO_2 is balanced by changes in the remainder of the complex organic molecules from which the CO_2 was derived.

F. J. PEARSON: I should like to comment on the point raised by Mr. Fontes.

The oxidation of organic matter by dissolved oxygen or accompanying the reduction of sulphate to sulphide occurs frequently. As Mr. Winograd has pointed out, in the system which he described neither mechanism could have produced most of the additional CO_2 found. We know of other systems in which no reduction reaction balancing the CO_2 production within the aquifer can be demonstrated.

Lignite can be described crudely as a carbohydrate ($C_n(H_2O)_n$) in which the carbon has a formal charge of zero. If the carbohydrate reacts –

$$C_n(H_2O) \rightarrow \frac{n}{2} CO_2 + \tfrac{1}{2} C_n H_{2n+2}$$

– equal amounts of oxidized (+4) carbon and reduced (-4) carbon are produced, and CO_2 will appear in the water without a reducing reaction being evident in the water chemistry. Such a process may be occurring in the system described by Mr. Winograd and in other aquifers.

I. J. WINOGRAD: Thank you for what appears to be a plausible explanation for the production of CO_2 from lignite without a concomitant effect on the water chemistry.

^{14}C EVIDENCE FOR THE ORIGIN OF ARID REGION GROUNDWATER, NORTHEASTERN PROVINCE, KENYA*

F.J. PEARSON, Jr., W.V. SWARZENKI
US Geological Survey,
Reston, Va.,
United States of America

Abstract

^{14}C EVIDENCE FOR THE ORIGIN OF ARID REGION GROUNDWATER, NORTHEASTERN PROVINCE, KENYA.

A major natural resource of the arid Northeastern Province of Kenya is a body of fresh groundwater underlying the drainage-ways of the Ewaso Ngiro River and Lagh Dera for about 200 km southeast and east of Habaswein. Twenty samples of this fresh water and surrounding saline water have been analysed for their chemical and radio and stable carbon isotopic composition to investigate mechanisms of recharge of the fresh-water body. No samples contain detectable tritium, and measured ^{14}C contents range from 2.8 to 87.7% modern. The higher measured ^{14}C values are associated with the fresher water body, but there is no strict correlation between ^{14}C and salinity. The samples fall into several groups, the members of each of which show a striking correspondence between measured ^{14}C contents and $(C_{tot})^{-1}$ values. Our hypothesis to account for this correspondence is that each of the ^{14}C-C_{tot} groups represents a single recharge event. The different ^{14}C contents within each group are due to additions of varying amounts of ^{14}C free carbonate (by aquifer carbonate solution or mixing with older water) to water from a single recharge event. Because of lack of general knowledge about arid region carbonate chemistry and lack of samples to show chemical and isotopic variations with depth in the aquifer, we are unwilling to assign absolute ages to these waters. It is probable, though, that the recharge events recurred at intervals of a few millennia.

INTRODUCTION

As part of a range management and livestock development project, the Government of Kenya have constructed 70 large and small reservoirs and drilled 80 exploratory and production boreholes in the Northeastern Province of Kenya since 1969 [1]. Concurrently the US Geological Survey, under the auspices of the Agency for International Development, has been studying the groundwater resources. Twenty water samples for isotope measurements were collected by the authors in May 1973, as part of this study. The logistic support given by the Water Department, Ministry of Agriculture, under the direction of E.A. Ngunya and G.C. Classen, Deputy Director, is gratefully acknowledged. Moreover, the authors thank S. Wanyeki and J.O. Achieng for their assistance in the field and M. Bodden and J. Woodward for the isotopic analyses.

The Northeastern Province of Kenya extends from 2°S, near the Indian Ocean, northward to the Ethiopian border, and is bounded on the east by the Somali Republic. The province has a population of about a quarter of a million, predominantly nomadic Somali tribesmen, whose livelihood is based almost exclusively on raising livestock. There are no perennial streams within the province, and stock water is obtained from ephemeral natural ponds,

* Publication approved by the Director, US Geological Survey.

artificial pans and tanks filled during rainy seasons, and dug wells and bore holes. The ephemeral streams flow only for a few hours in seasons of adequate rainfall. The drainage-ways are generally broad and shallow, and, although many are ill defined, a few are fairly well integrated and extend entirely or nearly across the province. These major drainage channels, commonly from 3 to 15 m deep, interrupt the southeastward and southward sloping plains, generally less than 300 m above sea level, that constitute most of the Northeastern Province.

HYDROGEOLOGIC SETTING

The principal aquifer is contained in unconsolidated or semi-consolidated beds of late Tertiary age, which extend from south of Wajir to the Indian Ocean (Fig. 1). These beds are predominantly fine grained and consist of clayey and silty sand and pebbly or sandy clay. Groundwater is generally confined and found at depths of 100 m or more. Most of the sediments contain saline water, but a zone of fresh water from 20 to 80 km wide extends from Habaswein southeastward and eastward to the Somali Republic border near Liboi. This zone is about 200 km long, and is approximately in line with the drainage-ways of the Ewaso Ngiro River and Lagh Dera. The zone constitutes a major natural resource of the province. The extent to which it can be developed depends on the extractable volume of the fresh water, and ultimately on long-term recharge.

The Ewaso Ngiro River drains the well-watered central highlands of Kenya, including the northern and western slopes of Mount Kenya. It is perennial in the highlands, but, as it enters the arid Northeastern Province, it loses water, so that only in exceptional years does it flow as far east as Habaswein or the Lorian Swamp. It had been thought that the loss of normal flow from the Ewaso Ngiro River provides recharge to the fresh groundwater zone extending along its dry drainage-way southeast of Habaswein. However, recent drilling at Sericho, close to the Ewaso Ngiro River northwest of Habaswein, and also in areas north of the river, indicates that salty groundwater underlies the river bed. Thus, seepage from the river near Sericho, where it normally goes dry, is not a primary contributor to the fresh-water zone.

A second possible source of recharge is from intermittent major flooding, either of the Ewaso Ngiro River or other drainage-ways that enter the Lorian Swamp-Lagh Dera system from the southwest and northwest. This source is most in keeping with chemical and isotopic data.

Figure 1 shows the locations of the wells sampled, the chloride content of the well water and contours on the potentiometric surface in 1973. Unfortunately, data are too scant to suggest if or how fast this surface may be changing. The potentiometric surface slopes generally to the southeast towards the Indian Ocean; along the Lorian Swamp-Lagh Dera trend the contours are generally convex to the northwest. If the hydraulic conductivity of the system were isotropic, groundwater flow would be parallel to the steepest gradient of the potentiometric surface, and saline groundwater to the southwest and northeast would be moving towards the fresh water in the Lorian Swamp-Lagh Dera region. Information from test wells [1] shows that, although hydraulic conductivity in the region commonly does not exceed

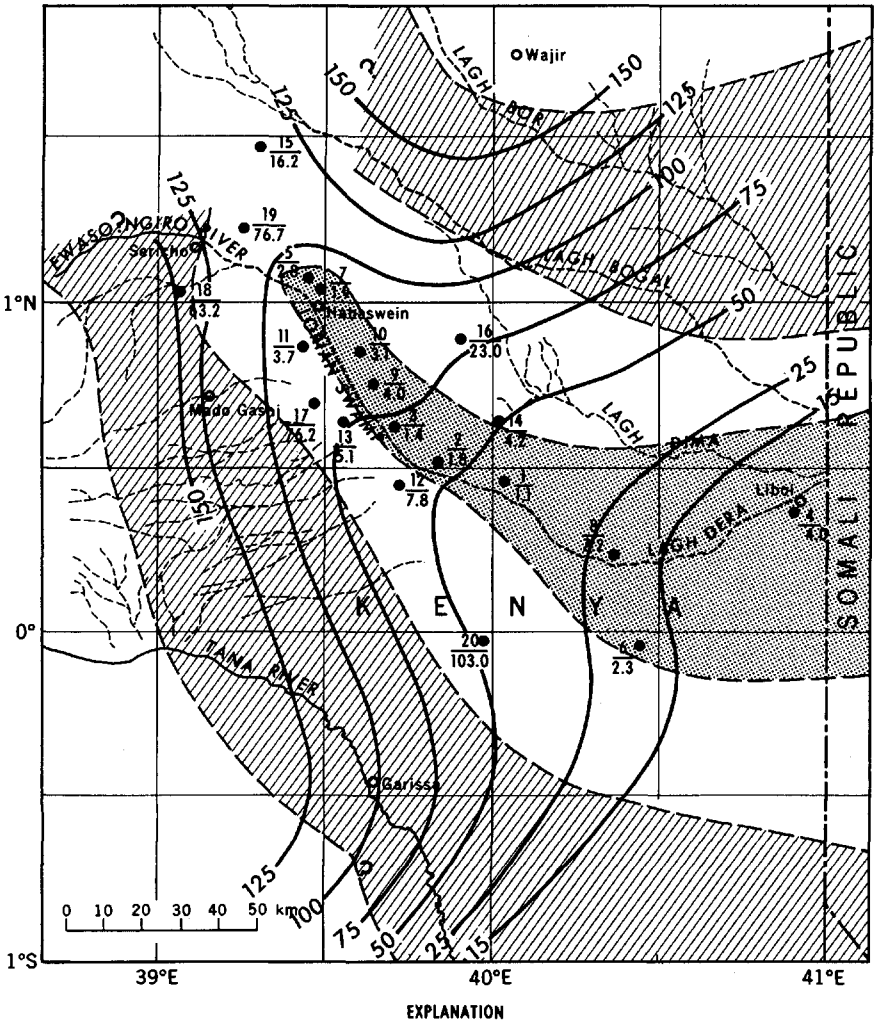

EXPLANATION

- ● 4/4.0 Well number / Chloride content (mM/litre)
- –50– Approximate contours on potentiometric surface of principal aquifer (1973), interval 10 and 25 m; datum is mean sea level.
- Approximate extent of groundwater with greater than 10000 mg/litre dissolved solids
- Approximate extent of groundwater with less than 1000 mg/litre dissolved solids

FIG. 1. Map of potentiometric surface and chloride contents of samples wells.

3 m daily, higher values are associated with the fresh-water zone, particularly in the Habaswein area and near Liboi, where hydraulic conductivity is as high as 10 m daily. The lower potentiometric surface in the fresh-water zone relative to its level in flanking areas, where salt water is present, may, therefore, reflect these differences in hydraulic conductivity.

Within the fresh-water zone itself, the potentiometric surface suggests flow from the Habaswein-Sericho area south and southeast toward Liboi. The chloride values on Fig. 1 show that such a simple flow system is not operating here. Although chloride increases away from the Lorian Swamp - Lagh Dera trend, along the trend chloride seems to be almost randomly distributed. The lowest chloride in well water, for example, is in wells 1, 2 and 3 at the south end of the Lorian Swamp, and chloride content is also small in the Habaswein region. Between these two groups of low-chloride wells, however, are wells 9 and 10, whose waters contain much more chloride. As chloride at these concentrations cannot be removed from flowing groundwater, a simple flow pattern, as suggested by the potentiometric surface from Habaswein through the Lorian Swamp towards Liboi, seems unlikely.

Average rainfall in this part of the province is not more than perhaps 25 cm yearly, whereas potential evapotranspiration may be more than 250 cm yearly. There are two maximum precipitations, in April and November. Rainfall is characterized by extreme variability, both seasonally and from year to year. Long-term records indicate wet and dry cycles of several years' duration. The concentration of rainfall and the intensity of storms in some seasons may cause considerable internal run-off and a small amount of groundwater recharge. In spite of the great excess of potential evapotranspiration over precipitation, there are good stands of grass and moderate-to-dense bush, which becomes verdant within a week of the rains.

The almost random chloride distribution within the fresh-water zone shown in Fig. 1 can be understood if the rainfall pattern is kept in mind. In an ordinary storm, rain will penetrate the upper part of the soil, and, in a more intense storm, some local run-off will develop, which itself will enter the soil beyond the immediate area of the storm. The moisture thus introduced into the soil will rapidly transpire or evaporate in this arid region. The salts in the rain will be left behind in the soil. The amount of soil salt will vary widely, depending upon the number and intensity of local storms. If an extraordinary storm leads to general flooding, water may be able to penetrate deeply enough to reach the deep water table, 100 m below the land surface, and recharge the groundwater body. Such recharge will have passed through and dissolved salts previously deposited in the soil, and thus will contribute varying amounts of salts to the groundwater body from place to place.

DATA COLLECTION AND ANALYSES

Samples for chemical, stable carbon, tritium and radiocarbon analyses were collected from 20 wells. pH and alkalinity were measured in the field, and the major dissolved cations and anions were determined in the laboratory of the Government Chemist, Nairobi. Samples for stable carbon isotope measurements were collected by adding a solution of ammonium hydroxide-strontium chloride to 1 litre of sample in the field. These samples were

TABLE I. CHEMICAL AND CARBON ISOTOPE CONTENTS OF GROUNDWATERS, NORTHEASTERN PROVINCE, KENYA

Sample number, this report	Well number	Chloride mM/litre	Total dissolved carbonate mM/litre	$\delta^{13}C_{HCO_3^-}$ (‰)	^{14}C content (% modern ± 1σ)
1	C-3788	1.13	7.11	-12.0	38.4 ± 0.5
2	C-3715	1.80	7.19	-13.1	39.4 - 0.5
3	C-3727	1.41	8.20	-11.3	37.9 ± 0.5
4	C-3667	3.95	6.05	-11.7	48.4 ± 0.5
	C-2685				
5	C-3655	2.82	9.85	-10.2	58.2 ± 0.6
6	C-3831	2.31	9.49	-11.4	12.8 ± 0.3
7	C-3218	1.89	10.89	-10.7	57.6 ± 0.5
8	C-3821	7.22	7.38	-12.0	42.1 ± 0.5
9	C-3792	3.95	10.23	-9.8	64.1 ± 1.4
10	C-3685	3.08	10.05	-	87.7 ± 0.7
11	C-3753	3.67	12.76	-9.5	52.4 ± 0.5
12	C-3751	7.84	9.88	-11.0	18.6 ± 0.3
13	C-3752	5.13	12.95	-9.5	21.0 ± 0.3
14	C-3726	4.23	18.21	-11.8	35.0 ± 0.4
15	C-3893	16.25	8.46	-9.4	2.8 ± 0.1
16	C-3769	23.02	11.09	-10.1	13.3 ± 0.4
17	C-3804	76.17	30.97	-10.4	7.3 ± 0.3
18	C-3822	63.19	55.15	-8.0	6.7 ± 0.2
19	C-3830	76.73	38.74	-8.8	28.9 ± 0.4
20	C-3770	102.97	22.40	-9.2	4.4 ± 0.3

filtered in the laboratory and the $\delta^{13}C$ measurements made on the strontium carbonate precipitate. Samples for ^{14}C were taken by direct precipitation of the total carbonate dissolved in about 100 litres of water. Isotopic analytical results and the chloride contents of the samples are given in Table I. No tritium could be detected at the 0.2 TU level in any sample.

The results of the chemical analyses were examined, using a theoretical equilibrium program [2], which, from a chemical analysis, first computes the distribution of solute species and then the state of saturation of the water with respect to several mineral species. The total dissolved carbonate contents given in Table I are from this program. In most samples more

TABLE II. DISTRIBUTION OF DISSOLVED CARBONATE SPECIES IN FRESH (No. 8) AND SALINE (No. 19) WATERS

Sample	Number 8	Number 19
Total dissolved carbonate (mM/litre)	7.38	38.74
Carbonate species (%)		
$H_2CO_3^0$	17.6	1.3
HCO_3^-	77.3	91.7
CO_3^{--}	0.0	1.5
$MgHCO_3^-$	1.6	0.0
$MgCO_3^0$	0.1	0.0
$CaHCO_3^-$	3.0	0.1
$CaCO_3^0$	0.1	0.0
$NaHCO_3^0$	0.2	3.5
$NaCO_3^-$	0.0	1.8
Other	0.1	0.1
Dissolved CO_2	17.6	1.3
Sum bicarbonate	82.1	95.3
Sum carbonate [a]	0.3	3.4
$\delta^{13}C_{total}$ (‰)	-13.4	-8.9
$\delta^{13}C_{bicarbonate}$ (‰)	-12.0	-8.9

[a] $\delta^{13}C_{bicarbonate}$ calculated from:

$$\delta^{13}C_{bicarbonate} = \delta^{13}C_{total} - \frac{\Sigma a}{100}\epsilon_{bg} - \frac{\Sigma c}{100}\epsilon_{cb}$$

where $\epsilon_{bg} = -7.8$‰ and $\epsilon_{cb} = +2.4$‰ at 36°C [3];

Σa = Dissolved CO_2 and Σc = sum carbonate, above.

than 90% of the total dissolved carbonate was present as bicarbonate (HCO_3^-), although in a few, less than 80% was bicarbonate. For consistency, the $\delta^{13}C$ values measured of the total dissolved carbonate were recalculated to arrive at the $\delta^{13}C$ values for the bicarbonate. The distribution of carbonate among various possible solution species required to make this calculation was derived from the computer program.

Table II shows carbonate speciation in two representative samples, one a fresh water of a relatively low pH, the other a more salty water of a higher pH. Complex species, such as $NaHCO_3^0$ and $CaHCO_3^-$, contain a significant quantity of the total dissolved carbonate. No carbon isotope fractionation factors for these species are available, and so it has been assumed that fractionation factors for equivalent uncomplexed carbonate species are also

applicable to their complexes; that is, fractionation factors for $MgHCO_3^-$, $CaHCO_3^-$ and $NaHCO_3^0$ were taken as equal to fractionation factors for bicarbonate, and factors for $MgCO_3^0$, $CaCO_3^0$, and $NaCO_3^-$ to those for carbonate. Fractionation factors used were taken from the work of Emrich and coworkers [3]. The $\delta^{13}C_{HCO_3^-}$ values are given in Table II.

CARBON ISOTOPE GEOCHEMISTRY

The measured ^{14}C content of a groundwater is a function of the age of the water, the ^{14}C content at time zero and the diluting effects of any carbonate added by solution of aquifer material or from mixing with other groundwater. To interpret the ^{14}C data, therefore, we must look closely at the implications of the carbonate and other chemical characteristics of the water in this system. The first consideration must be whether the ^{14}C content of the water has been changed by the addition of ^{14}C-free carbonate, either by mixing with older water or by solution of aquifer carbonate minerals within the saturated zone. Dilution or mixing effects can be displayed by plotting isotopic concentration, either of ^{14}C or ^{13}C, against the reciprocal of the total dissolved carbonate content. Let "r" and "d" represent the end members of a binary mixture "m", with total carbonate contents of C_r, C_d and C_m, and isotopic compositions, either ^{14}C or ^{13}C, of I_r, I_d and I_m respectively. The composition of any mixture will be

$$I_m = (I_r \times C_r + I_d \times C_d)/C_m$$

Because $C_m = C_r + C_d$,

$$I_m = \frac{C_r(I_r - I_d)}{C_m} + I_d \qquad (1)$$

This is a straight line in I_m, $(C_m)^{-1}$ space with intercept $I_d = I_m$ at $(C_m)^{-1} = 0$ and slope

$$\frac{I_m}{(C_m^{-1})} = I_m \times C_m = C_r(I_r - I_d)$$

The ^{14}C data plotted against reciprocal-carbonate-content are shown in Fig. 2. The points on this figure fall on several straight lines. Two of these lines, designated as II and III, are well defined, whereas the others, I and IV, are not as certain. Lines II, III and IV intercept zero reciprocal-total-carbonate at a ^{14}C content of zero, and line I at $^{14}C = 8\%$ of modern. Equation (1) means that for each line the product $C_r \times {}^{14}C_r$ is constant. Such water might come from a single recharge event and the several lines represent several separate such events. The ^{13}C data and carbonate chemistry of the waters support this hypothesis.

A scattered but recognizably linear relationship between $\delta^{13}C$ and reciprocal-total-carbonate content is evident in Fig. 3. Such a plot results from the solution, in a water of low total carbonate content and negative $\delta^{13}C$ value, of additional carbonate material of a more positive $\delta^{13}C$ value.

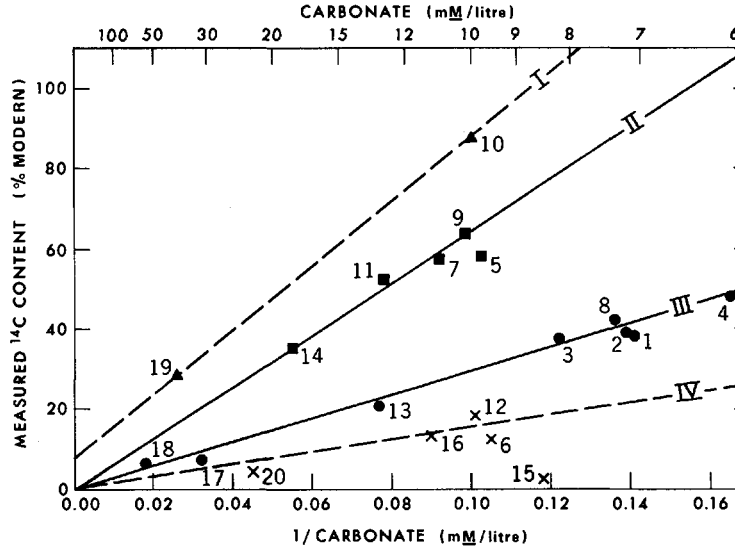

FIG. 2. Graph of measured ^{14}C content versus reciprocal total dissolved carbonate content (symbols correspond to linear groups; arabic numerals are well numbers).

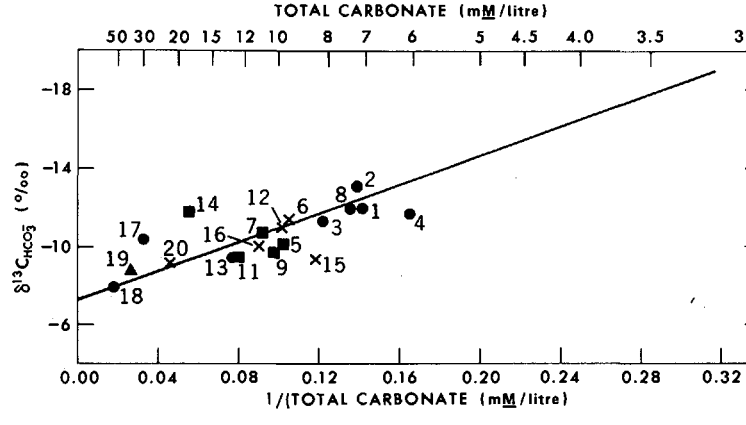

FIG. 3. Graph of δ^{13}C (bicarbonate) versus reciprocal total dissolved carbonate content (symbols correspond to linear groups, Fig. 2).

The intercept of the line on Fig. 3 at zero reciprocal-carbonate-content is -7.3‰, the composition of bicarbonate in isotopic equilibrium with a mineral carbonate of a $\delta^{13}C$ of about -5‰. No soil carbonate samples were taken as part of this study, but measurements of $\delta^{13}C$ of arid zone soil carbonate elsewhere are in the range of 0 to -10‰, and cluster around -5‰ [4-6].

Estimating the initial carbonate content and isotopic composition in the waters in this system cannot be done as simply as determining the isotopic composition of the diluting carbonate. There is a general lack of detailed information about soil and recharge processes in arid regions, and we have no samples of soil gas or soil carbonate from this region in Kenya. It is therefore necessary to deduce as best we can, from the carbonate chemistry and isotopic composition of the samples taken, what their initial composition was likely to have been.

General knowledge of plants and soils puts certain constraints on our speculations. First, the CO_2 pressure in the gas last in contact with the water must be within reasonable limits for a soil, say between 10^{-3} and 10^{-1} atm; second, the carbon isotope composition of the soil CO_2 must lie between approximately -27‰, if all the plants producing CO_2 in the soil metabolize through the Calvin photosynthetic cycle, and about -12‰, if all the plants in the area have a Hatch-Slack cycle [7]. A third constraint on our speculations is that the initial ^{14}C content ($^{14}C_r$) in these tritium-free waters cannot have greatly exceeded 100% of modern.

We first consider a closed-system model. In a closed system, the initial carbonate present in a water is derived only from solution of soil CO_2, the solution being complete before the water is exposed to any solid carbonate. If the soil CO_2 pressure were at its maximum, 10^{-1} atm, which in itself is unlikely in an arid zone, the carbonate content of a water in equilibrium with it would be about 2.5 m$\underline{M}$/litre. The slope of the line in Fig. 3, $C_r \times (\delta^{13}C_r + 7.3)$, is -36.7. At C_r = 2.5 m$\underline{M}$/litre, $\delta^{13}C_r \simeq -22$‰, not an unreasonable value for soil CO_2 in an area of Calvin plants [8]. However, the third constraint, that the initial ^{14}C content of the dissolved carbonate cannot have significantly exceeded 100% of modern, eliminates the closed-system model from further consideration. From Fig. 2, the slopes $C_r(^{14}C_r + {}^{14}C_d)$ of line II and I are 650 and 870 respectively. Thus, the minimum initial total carbonate contents of samples in these groups would have been 6.5 and 8.7 m$\underline{M}$/litre, much higher than reasonable soil CO_2 pressures in a closed-system model would permit.

We must then consider an open-system model, one in which gas, solid $CaCO_3$ and water are present together. If isotopic equilibrium occurs in the system, the bicarbonate present will be enriched in ^{13}C relative to the soil CO_2 by 7.8‰ [3], the fractionation factor between bicarbonate and CO_2 at 36°C, the temperature of this system. Again, choosing Calvin and Hatch-Slack plants as end members means that the $\delta^{13}C$ of the initial bicarbonate present in the water will be between -4 and -19‰. The ^{14}C content of the dissolved bicarbonate will be that of the soil CO_2 plus twice the $\delta^{13}C$ fractionation factor, about 102% of modern.

In an open system in equilibrium with calcite, at the highest permissible CO_2 pressure (10^{-1} atm), only 5 m$\underline{M}$/litre of total carbonate can be present in the solution. To account for the total carbonate present at 100% of modern on Fig. 2, 6.5 m$\underline{M}$/litre for line II and 8.7 m$\underline{M}$/litre for line I, we must consider the water chemistry more carefully. The theoretical equilibrium calculations made on all the samples show that they are saturated or nearly

so with respect to calcite. Inspection of the chemical analyses reveals that the major cation in most of these samples is sodium, rather than the calcium expected if calcite solution were the primary source of cations in the system. This suggests that not only is there equilibration between a calcium carbonate mineral, soil CO_2 and water, but also that there is a mechanism by which calcium is replaced in solution by sodium. Removal of calcium permits more carbonate to go into solution, thus increasing the total carbonate content of a water at a given partial pressure of CO_2, while maintaining equilibrium saturation conditions with respect to calcite.

The carbonate chemistry of these waters, when recharged and in their subsequent history, can be conveniently shown on a graph like that in Fig. 4, in which the total dissolved carbonate is plotted against Na/Ca ratios in the samples. The lines on the graph show the total dissolved carbonate concentration in waters with various Na/Ca ratios in equilibrium with calcite, at CO_2 pressures of 0.1 and 0.05 atm. As this figure shows, the most dilute waters and those which have the highest ^{14}C contents in their respective groups in Fig. 2 can be formed with CO_2 pressures of less than 0.1 atm. Thus sodium-for-calcium exchange in the soils permits total dissolved carbonate contents of the levels found in these waters to be formed at CO_2 pressures that are not unreasonably high for soils.

Figure 4 also illustrates the changes in the chemistry of the waters as they dissolve additional carbonate in the saturated part of the system. Once the water has entered the saturated zone, gas is no longer present, and solution of additional carbonate will lower the partial pressure of CO_2 in equilibrium with the system. It is likely also that further cation exchange will take place, increasing the Na/Ca ratio and permitting the total carbonate content to increase while maintaining saturation with calcite. On Fig. 4 a sample, such as 8 or 9 with an initially high CO_2 pressure will, in the saturated zone, attain higher dissolved carbonate contents and higher Na/Ca

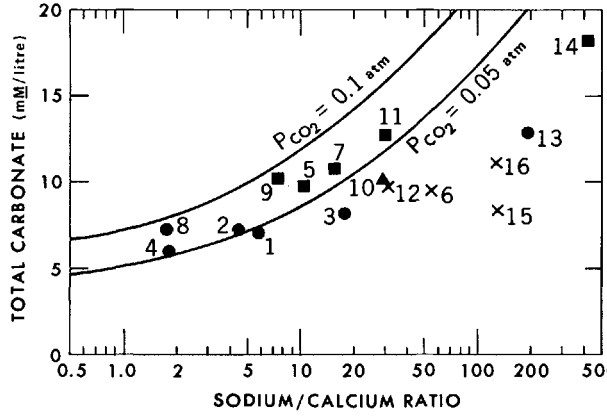

FIG. 4. Graph of total dissolved carbonate content versus sodium-to-calcium ratio (symbols correspond to linear groups, Fig. 2).

ratios and might follow such a progression as from samples 9 and 5 through 7, towards 11 and 14. Likewise, samples with an initially lower Na/Ca ratio, such as 4 and 8, would follow a progression through 1 and 2, towards 3 and 13. These two groups include the same samples in the same order as appear in Fig.2 on line II and line III. Although not as well defined, samples 12 and 6, towards sample 16, (line IV, Fig.2), also follow this progression.

INTERPRETATION

A hydrogeologic interpretation of these arguments is that the linear groups of samples on Fig. 2, which are also discernible on Fig. 4, represent separate recharge events. As water from each event enters the system, it displaces the groundwater beneath and to its sides. Recharge should occur primarily along the drainage-ways of the region, which receive the bulk of the run-off from extreme precipitation, when, we believe, recharge occurs. Associated with each event would be a change in the potentiometric surface in the region, but, because of the time elapsed since the last event, any potentiometric mound present at the time of recharge may have dissipated, and a surface responsive to regional groundwater flow and permeability differences been re-established.

The geographic distribution of these groups of wells, shown on Fig. 5, supports this hypothesis. Well waters in the group with the lowest ^{14}C content for a given total carbonate content, well numbers 6, 12, 16, 20 and 15, are in the distal parts of the system, although they are not necessarily the most salty. Samples of the next youngest group, line III on Fig. 2, cover the lower reaches of Lagh Dera and the region west of the Lorian Swamp and south of Sericho. Members of the next youngest group, II, are centred on the Lorian Swamp area itself. The southeastward convexity of the 75 m potentiometric surface contour on Fig. 1 near well number 3 is, we think, an expression of a local mound on the regional potentiometric surface produced by a recharge event. The high measured ^{14}C content of well number 10 and its inclusion in the youngest group (I) in Fig. 2, is consistent with its being at an anomalous high on the potentiometric surface. Water from well 19, although it has a very low ^{14}C content, is probably also about the same age as that from well 10. Well 19 is located near the Ewaso Ngiro River in an area where recharge from flood flow from the river may not be as infrequent as it is farther to the southeast.

It is tempting to try to deduce from the grouping of samples in Fig. 2 the length of time between the recharge events that we suggest cause the four lines. Although we realize that such deduction is tenuous at best, we are unable to resist temptation. Let us assume that the grouping of samples 10 and 19 on Fig. 2 is due to their having been recently recharged and, further, that other samples from the same general area were recharged under similar conditions of soil chemistry. Such similar samples would be those that on Fig. 2 have a total dissolved carbonate content of about 10 m$\underline{M}$/litre, that is, sample 10, sample 9, a hypothetical sample between 3 and 13, and sample 12. The chloride content of these samples ranges from 3.1 m$\underline{M}$/litre (number 10) to 7.8 m$\underline{M}$/litre (number 12) (Fig. 1), due, presumably, to rainfall variations from well to well between recharge events. The differences between the ^{14}C contents of the four sample groups at 10 m$\underline{M}$/litre total carbonate on Fig. 2 should reflect the time between

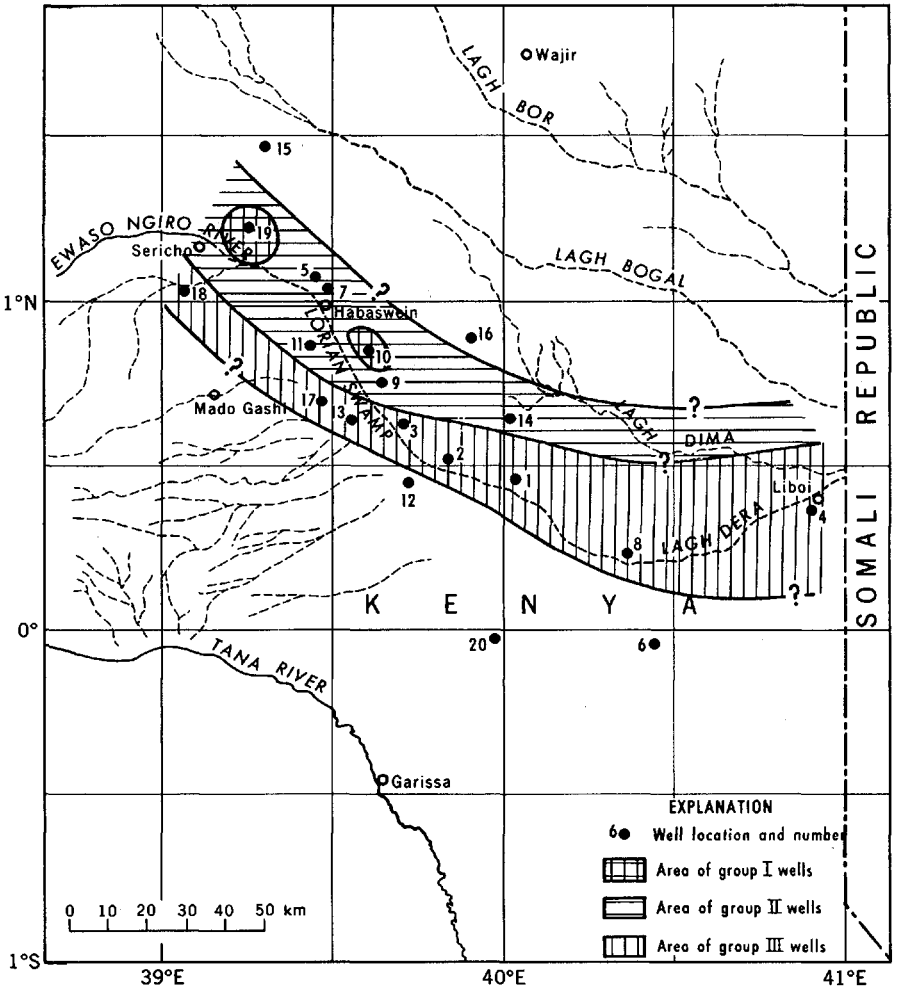

FIG. 5. Map showing areal distribution of linear groups, Fig. 2.

the recharge events they represent. On these assumptions, the time between events II and I is (8270(ln 0.64 - ln 0.88)) = 2600 years, between III and II is 6300 years and between IV and III is 5200 years. We would certainly be unwilling and unable to defend these age assignments, but they may be representative of the frequency of recharge events in this region, a frequency so low that historical records would be of little use in estimating it.

It is of interest to see whether the hydrologic data available, scant as they are, support the ^{14}C estimate that waters recharged from 10^3 to 10^4 years ago remain in the study area. This can be done using the equation

$$\text{velocity}\left(\frac{\text{km}}{10^3\ \text{yr}}\right) = \text{hydraulic conductivity}\left(\frac{\text{m}}{\text{d}}\right) \times 365\left(\frac{\text{d}}{\text{yr}}\right)$$

$$\times\ \text{potentiometric gradient}\left(\frac{\text{m}}{\text{m}}\right) \times \frac{1}{\text{porosity}}$$

Hydraulic conductivity, given above, may be from 3 to 10 m daily, and we assume a porosity of 0.3. The potentiometric gradient in the freshwater area (Fig. 1) ranges from 4×10^{-4} near well 8 and near Habaswein to 1×10^{-3} near well 3. Velocities near Habaswein would then be from 2 to 5 km/10^3 yearly and near well 3 from 4 to 12 km/10^3 yearly. These are not maximum flow rates because, except perhaps for the gradient chosen near well 3, they do not reflect the higher local gradients of the potentiometric surface caused by recharge-event mounding. However, they are still slow enough not to contradict our suggested ^{14}C interpretation.

FURTHER DATA NEEDS

Certain geologic processes and data specific to the area required for a more quantitative interpretation are not available. We think it worthwhile to summarize the data needs as a guide to future studies, and to show why we have not applied more detailed adjustment techniques, such as that recently proposed by Mook [9], to available data. A major lack is knowledge of soil physical and chemical processes in arid regions. Specific needs are data on soil gas composition and isotopic composition; soil mineralogy, including the amount, type and isotopic composition of soil carbonate minerals; and information on the cation exchange capacities and cation specificities of the minerals in the soil. Further, better knowledge of unsaturated flow phenomena at depths greater than those of interest to agronomists is required. Not only should such data be collected for present-day conditions, but every effort should be made to estimate what past conditions might have been, if reasonable assumptions about the isotopic composition of waters as they enter the saturated zone are to be made.

A second body of missing data relates to the chemical composition of rain in an area such as the Northeastern Province of Kenya. The composition of rain is known in, for example, parts of the northeastern United States of America and throughout much of Europe, but in these areas industrial fall-out affects the chemistry of rain, presumably not the case in East Africa. If, for example, the sodium, calcium and chloride contents of East African rain were known, it would be possible to estimate the amount of rain that fell and was evaporated between significant recharge events on the basis of the chloride content of groundwater. Furthermore, because the initial carbonate chemistry of the groundwater is apparently strongly affected by sodium-for-calcium exchange in the soil, it is possible that the sodium and calcium inputs to the soil from precipitation between recharge events may have an indirect effect on the carbonate chemistry of the recharge water.

A third type of useful information, we hope, may be forthcoming from continuing hydrologic exploratory work in the Northeastern Province. All wells described here were drilled only as deep as necessary to produce reasonable amounts of water, and so the groundwater body they tap has

been defined practically only in two dimensions. Deeper wells sampled at several depths would add a third dimension, knowledge of which would be helpful to test our interpretation that the ^{14}C pattern is a result of several recharge events, presumably thousands of years apart and of near catastrophic proportions.

REFERENCES

[1] SWARZENSKI, W.V., WANYEKI, S., "Groundwater exploration in northeastern Kenya", Proc. Seminar on Ground-Water in East Africa, Nov. 1972, E.A. Agric. and Forest. Res. Org., in press.

[2] TRUESDELL, A.H., JONES, B.F., WATEQ – A Computer Program for Calculating Chemical Equilibria in Natural Waters, National Technical Information Service, TB-220464 (1973).

[3] EMRICH, K., EHHALT, D.H., VOGEL, J.C., Carbon isotope fractionation during the precipitation of calcium carbonate, Earth Planet. Sci. Lett. 8 (1970) 363.

[4] BRINKMANN, R., MÜNNICH, K.O., VOGEL, J.C., Anwendung der C^{14}-Methode auf Bodenbildung und Grundwasserkreislauf, Geol. Rundsch. 49 (1960) 244.

[5] GALIMOV, E.M., GRINENKO, V.A., Effect of leaching under surface conditions on the isotopic composition of carbon in secondary calcite, Geochem. Int. 2 (1965) 79.

[6] RIGHTMIRE, C.T., A Radiocarbon Study of the Age and Origin of Caliche Deposits, Master's thesis, University of Texas at Austin (1967), unpublished.

[7] LERMAN, J.C., "Carbon-14 dating: Origin and correction of isotope fractionation errors in terrestrial living matter", Proc. 8th Int. Conf. Radiocarbon Dating, New Zealand, Royal Soc. N.Z. (1972) H16.

[8] RIGHTMIRE, C.T., HANSHAW, B.B., Relationship between carbon isotope composition of soil CO_2 and dissolved carbonate species in ground water, Water Resour. Res. 9 (1973) 958.

[9] MOOK, W.G., "On the reconstruction of the initial ^{14}C content of groundwater from the chemical and isotopic composition, Proc. 8th Int. Conf. Radiocarbon Dating, New Zealand, Royal Soc. N.Z. (1972) D31.

DISCUSSION

W.G. MOOK: With regard to Fig. 3, you deduce a $\delta^{13}C$ value for the soil carbonate from the interception of the straight line with the ordinate at $1/C_m = 0$. What is the significance of the value of the slope?

F.J. PEARSON: The slope of Eq. (1) includes two unknown parameters – the concentration and the isotopic composition of the ^{14}C-bearing carbonate in the recharge. If either parameter can be found independently, the other can be calculated from this slope.

R.E. ISAACSON: Have you considered the complexities in the ^{14}C results which would be introduced if one considered the ingression of catastrophic floodwaters through layers of caliche such as exist in the western United States of America.

F.J. PEARSON: The soils in the area investigated by us contain caliche-like carbonate, and it is probably such carbonate which gives some of the samples their high dissolved carbonate content, for soil carbonates commonly have $\delta^{13}C$ values of around -5‰. Unfortunately, the data on and knowledge of arid-region soil processes are insufficient to permit more detailed consideration of the effects of soil carbonate on the chemistry of the waters.

R.B. THOMAS: Your paper contains only very sparse hydrogeological data. Will you be making more detailed information available elsewhere?

F.J. PEARSON: Space and time does not permit a full discussion of the available hydrogeological information here. Needless to say, our hydrogeological generalizations and the potentiometric contours in Fig. 1

are based on many more wells than were sampled for isotopes. A detailed report on this region is in preparation and will be published (probably as a Water Supply Paper by the US Geological Survey).

I. SAINZ ORTIZ: Are you sure that the aquifer studied by you is a single flow system, or are there two or more confined or semi-confined aquifers of greater depth with different flow patterns? This could explain the differences mentioned by you.

F. J. PEARSON: The detailed information to which I referred in replying to Mr. Thomas indicates that we are dealing with a single flow system.

I. SAINZ ORTIZ: In connection with my question I should like to mention that in the Juárez valley, in the north of Mexico, there is an unconfined shallow aquifer running from northwest to southeast in which the waters become saline as they flow. Nevertheless, at a depth of 450 m there is a confined fresh-water aquifer whose recharge zone lies to the south, which runs from south to north and whose waters are older (according to ^{14}C data) than those in the shallow aquifer.

I have a second question. Would it not be worth carrying out deeper explorations in the aquifer and investigating the system piezometrically before attributing the fresh water to catastrophic flooding?

F. J. PEARSON: I agree that geological information obtained at greater depths would be most valuable.

G. SAUZAY: Your model resembles a mixture of perfect gases, whereas during the mixing of carbonates there may be precipitation. This does not show up in the mixing model.

F. J. PEARSON: The model is not intended to be chemically rigorous. Other calculations, however, show that precipitation probably does not take place in this system, so that no error is introduced if one neglects it.

G. SAUZAY: In Fig. 3 you have a correlation between independent measurements, so that you can derive a correlation coefficient mathematically. However, you have the possibility of two regression curves, depending on the quantity you choose as variable, either $\delta^{13}C$ or Σ_{carb}. The ordinate at the origin depends essentially on this choice, as does the interpretation which one arrives at.

F. J. PEARSON: Our knowledge of the process involved in this system does not warrant such a rigorous mathematical treatment. Mathematical overinterpretation of data on natural systems often leads to neglect of the physical problems involved, and we have tried to avoid this pitfall.

T. M. DINÇER: The annual precipitation of 250 mm mentioned by you is not very low; it does not preclude very heavy showers, which can cause "catastrophic" floods. Large floods occur not infrequently in arid countries. In Saudi Arabia, for example, floods (some of them very extensive) occur in regions with an annual precipitation of only 75 mm. It would therefore be misleading, in my opinion, to conclude from ^{14}C data (which is imprecise with regard to ages less than 5000 years) that "catastrophic" floods recurring at intervals of 5000 - 10 000 years constitute the origin of fresh waters.

F. J. PEARSON: Even in years of adequate rainfall, when floods are not uncommon, the conditions for groundwater recharge are not favourable, because of generally clayey soils and the soil-moisture deficiencies to be overcome. As I pointed out in my oral presentation, however, we are not adamant about our assignments of ages to these events.

RADIOCARBON, ^{13}C AND TRITIUM IN WATER SAMPLES FROM BASALTIC AQUIFERS AND CARBONATE AQUIFERS ON THE ISLAND OF OAHU, HAWAII

T.H. HUFEN, L.S. LAU
Water Resources Research Center,
University of Hawaii, Honolulu

R.W. BUDDEMEIER
Hawaii Institute of Geophysics,
University of Hawaii, Honolulu
Hawaii, United States of America

Abstract

RADIOCARBON, ^{13}C AND TRITIUM IN WATER SAMPLES FROM BASALTIC AQUIFERS AND CARBONATE AQUIFERS ON THE ISLAND OF OAHU, HAWAII.

Principal fresh water aquifers on the subtropical island of Oahu consist of basaltic rocks that are devoid of fossil carbonate minerals. In southern Oahu fresh water occurs as semi-independent basal lenses which float on salt water and are bounded by sedimentary formations along the coast and in valley bottoms. The latter formations contain carbonate aquifers. Fresh water also occurs in dike compartments located in the central parts of the mountains. The radiocarbon content of groundwater recharge on Oahu is between 96 and 100% modern. The ^{13}C concentration associated with fresh groundwater is between -17 and -19 δ‰ PDB and remains constant while such waters reside in, or travel through, basaltic rock aquifers. Radiocarbon and tritium data on basal waters withdrawn by major pumping stations show these waters to have ages between a few decades and several hundred years. Differences in these ages relate systematically to individual pumping rates of the stations, well depths and local lens thickness.

1. INTRODUCTION

The island of Oahu is one of the five major islands of the Hawaiian Islands chain. Its climate is subtropical, and perennial vegetation is lush. Temperatures are fairly constant; in the capital, Honolulu, mean monthly temperatures range between 22.2° and 25.8°C. Governmental, industrial and commercial activities are concentrated in the study areas 1 through 5 (pop. 320 000) of Honolulu and around Pearl Harbor, both located in southern Oahu. Agricultural lands and military bases are scattered over other parts of the island. Demand for fresh water is understandably high, and continues to increase because of ever-increasing population and per capita consumption. Close to 99% of domestic water used comes from groundwater sources. Accordingly, great concern exists regarding their extent and capacity to supply sufficient water to meet future demands.

For the past five years the Water Resources Research Center at the University of Hawaii has conducted isotopic studies of Oahu's natural waters, with the principal object of gathering hydrologic information on recharge and

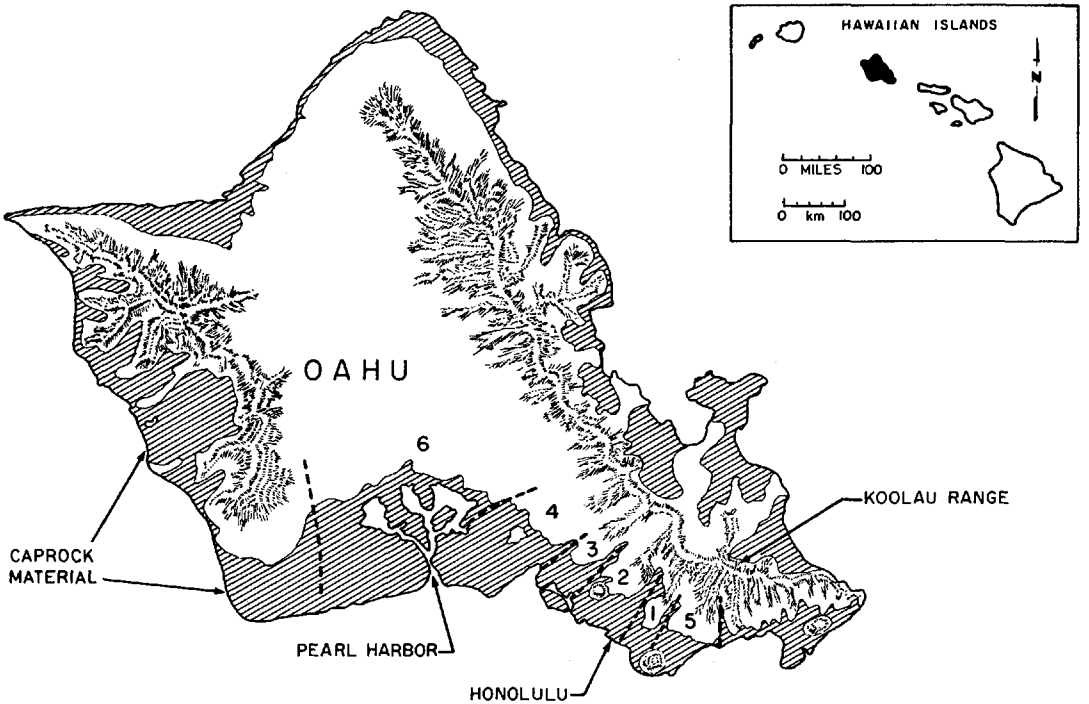

FIG. 1. The island of Oahu, Hawaii, showing mountain ranges, distribution of caprock material and southern isopiestic areas.

circulation patterns of high-level groundwaters and basal groundwaters. The present report contains a summary of isotopic data obtained for several different natural waters on the island, followed by results of a study, still in progress, on southern Oahu's basal groundwater systems.

2. GEOLOGY AND HYDROLOGY

Oahu consists primarily of two eroded volcanic domes covered by masses of sedimentary material in the coastal areas (Fig. 1). Volcanic material is largely composed of thinly layered lava flows of high permeability. Sedimentary material, locally called caprock, is of marine and terrestrial origin. The material includes layers of detritus, mud and clay interbedded with coral limestone. Caprock formations occur as valley fills, coastal plains and fringing reefs. The magnitude of these formations is quite variable; in places they are over 300 m thick. Overall permeability of this caprock material is quite low compared with that of basalt; hence, it acts as a barrier to the flow of water.

The occurrence and interaction of Oahu's natural waters exemplify a miniature hydrologic cycle. Northeasterly tradewinds normally bring moisture-laden air masses to the islands, where they give rise to orographic-type precipitation in the central parts of the mountain ranges. Tradewinds

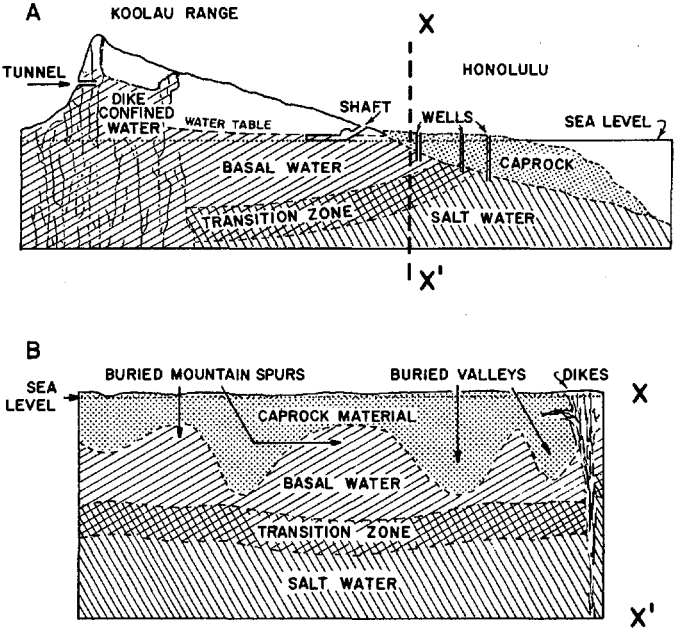

FIG.2. Schematic vertical cross-sections of southern Oahu illustrating basaltic rock aquifers. A: Lateral cross-section of the Koolau Range showing the occurrence of dike and basal waters. B: Cross-section normal to cross-section A, at X - X', showing compartmentalization of basal water underneath the Honolulu coastal plain.

are occasionally replaced by frontal-cyclonic systems which, especially between November and May, bring torrential rains to many parts of the island. Rainfall is highest over the Koolau Range, with maximum mean annual values of 760 to 890 cm near the crest. Overland run-off returns some of the water directly to the ocean, but a considerable fraction filters through the mountain soils into basaltic aquifers. Under natural conditions recharge must be balanced by an equivalent amount of discharge (i.e. outflow back into the ocean) completing the cycle.

Figure 2 illustrates two major types of basaltic aquifers as they occur in southern Oahu. The two are: dike compartments (located in the Koolau Range), and basal aquifers (Honolulu and Pearl Harbor coastal areas). Dike compartments consist of masses of permeable flow rock enclosed by vertical or near-vertical intrusive dikes of low permeability. Water trapped in these compartments can dam to levels reaching several hundred metres above sea level. Such water is usually called "high-level dike water" or "dike water". Dike compartments are recharged by rainwater that infiltrates their overlying surfaces. Amounts of recharge are potentially large because of the high rainfall on these surfaces.

Basal water is fresh water floating on salt water in the lower elevations (see Fig. 2B). Its basic configuration on Oahu is that of a Ghyben-Herzberg lens defined by the water table above sea level and the upper surface of a transition zone below sea level. Thick masses of caprock along the coast of southern Oahu somewhat modify this basic lens structure. The caprock considerably retards the escape of fresh water into the ocean and thickens the fresh water lens. In addition, the several valleys on the coastal plain are underlain to considerable depth, with the same sedimentary material as the caprock, hence creating compartments of basal water. Water communication between these compartments is possible below, but not through, the valley sediments. As a result, six different areas having this compartmentalized water exist in southern Oahu, each with a characteristic and quite uniform piezometric head, hence, in Hawaii, designated as isopiestic areas. There are five in the Honolulu area and one in the Pearl Harbor area (Fig. 1). On the basis of geologic and hydrologic data it is known that the high rain in the Koolau montains directly inland from Honolulu provides the major natural recharge water for isopiestic areas 1 through 5. The northern part of the Koolau mountains is the major intake area for groundwaters in Central Oahu and the down-gradient Pearl Harbor area. Agricultural activities in these two areas contribute irrigation return water to the top of the Pearl Harbor basal waters [1].

The mode of basal water recharge is complex, but a considerable amount must take place as direct recharge, i.e. infiltration and percolation of rainwater directly into the free basal water body. It is believed, however, that recharge is also derived from leakage of dike compartments.

In addition to dike water and basal water aquifers, a number of relatively small perched aquifers occur. These consist of pyroclastic cinderbeds and/or post-Koolau lava flows. Although of limited value for water supply, these waters are of interest because of their exceedingly short residence time. Groundwater occurs also within caprock material; however, it is generally brackish and high in calcium, magnesium and carbonate concentration.

Dike waters and basal waters generally are low in dissolved chemical species. Bicarbonate concentration is particularly low, due to the absence of carbonate minerals in basalts or basalt-derived soils. Some contact of

basal water with carbonate minerals cannot be ruled out in systems that are confined, bordered or interbedded with caprock material, as some of the results discussed in Subsection 4.3.1 will attest.

The sea water or transition-zone water underlying basal water poses a continuous threat to the fresh water salinity. In this report all samples designated as basal water samples have chloride concentrations of less than 300 mg/l. Most of these samples are well below 100 mg/l in chloride. Salt or brackish water contamination of their respective sources is thus minimal.

3. ISOTOPE ANALYSIS

Samples were collected from rain gauges, tunnels (dike waters), springs (perched waters), wells and shafts (basal gauges and other waters). The analyses consisted of the following: Radiocarbon (sample size was either 55, 80 or 160 gallons): (1) extraction of inorganic carbon, (2) conversion of generated CO_2 into benzene, (3) liquid scintillation counting of benzene samples. ^{13}C: mass spectrometric analyses on aliquots of CO_2 gas obtained in radiocarbon analysis step 1. Tritium ($1\frac{1}{2}$ litre water sample): (1) pre-distillation, (2) periodic addition electrolysis of 1000 ml samples down to ~8 ml, (3) vacuum distillation, (4) liquid scintillation counting of enriched samples. Further information on the procedures used can be found elsewhere [2, 3]. Chemical analyses were done using standard methods [4].

Tritium data are in tritium units: 1 TU = 0.0072 dpm/ml (disintegrations per minute/ml of water). Radiocarbon data are expressed as percentages of the activity of the Modern Standard (95% NBS oxalic acid). ^{13}C values are expressed as per mille deviations from the PDB standard. All analyses were performed in laboratories of the Water Resources Research Center at the University of Hawaii, except for the ^{13}C analyses which were done by Teledyne Isotypes Inc., Westwood, New Jersey, United States of America. Typical analytical error levels are: radiocarbon, ± 1.0% modern; ^{13}C, ±0.1 δ‰ PDB; tritium, ± 1.0 TU.

4. RESULTS AND DISCUSSION

4.1. Isotopic composition of various natural waters

Different natural waters on Oahu were investigated as to their isotopic characteristics. A specific object was to determine whether or not "bomb" tritium and "bomb" radiocarbon were present in sufficient quantities to be useful as tracers. Another specific object was to determine whether groundwaters in the study area might be old enough to qualify for the application of radiocarbon dating methods. Results are summarized in Table I. The entries are either typical ranges or averages where ranges are small or few data are available. A histogram of radiocarbon and tritium data on groundwaters alone is presented in Fig. 3.

From studies by Von Buttlar and Libby in 1953, it is known that tritium activity of pre-bomb Hawaiian precipitation was below 1.0 TU [5]. On the other hand post-bomb Hawaiian precipitation, as monitored by the International Atomic Energy Agency since 1962, has shown activities well in excess of 15 TU. More specifically, from 1962 through 1965, activities

TABLE I. ISOTOPIC AND CHEMICAL CHARACTERISTICS OF NATURAL WATERS FROM THE ISLAND OF OAHU, HAWAII (1970-73)

Type of water	Tritium (TU)	Radiocarbon (% modern)	^{13}C (δ ‰ PDB)	Cl^- (mg/litre)	HCO_3^- (mg/litre)
Precipitation	15 - 25	-	-	5	-
Surface waters	12 - 23	130 - 140	-	12	20 - 40
Perched waters	18 - 24	100 - 108	-16.9 [a]	21	125
Dike waters – Koolau Range	1 - 14	99 - 100	-18.8	15	45
Basal waters – Pearl Harbor area	0 - 3	94 - 102	-	40 - 90	60 - 90
Basal waters – Honolulu area	0 - 1	90 - 96	-18.0	45 - 100	60 - 80
Salt waters in basaltic rocks underneath basal lenses [b]	0	33	-	~ 18 000	100
Salt waters in confined carbonate aquifers	0	13	- 3.8	~ 10 000	108

[a] Single measurement.
[b] Average of two samples: one taken at 400 m below msl in area 3, and the other taken at 336 m below msl in area 6.

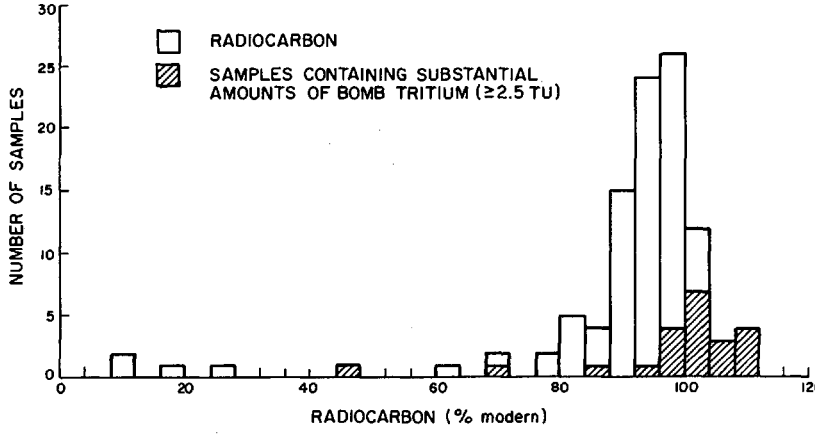

FIG.3. Histogram of radiocarbon and tritium data for groundwaters from the island of Oahu, Hawaii (1970-73).

were generally between 40 and 150 TU; from 1965 up to the present they were between 15 and 30 TU [6]. Clearly any groundwater sample collected today that contains tritium in excess of 1.0 TU can be said to contain bomb tritium. Consequently, its source contains waters that were recharged (at least partly) within the past 20 years. Similar conclusions can be reached when observing bomb radiocarbon activities, i.e. activities in excess of the "natural" activity level of 100% modern.

Examination of Table I indicates that bomb tritium is definitely present as expected in precipitation and in surface waters. It also is present in perched waters and in some dike waters. Marginal amounts are present in some basal waters. Bomb radiocarbon is obviously present in surface waters, but its presence in groundwaters is very limited. On the other hand, low to very low radiocarbon activities are associated with basal waters in the Honolulu area, deep salt waters and waters in confined carbonate aquifers. These data indicate that perched waters have the shortest residence times followed by the other waters in a sequence of increasing residence times approximately as given in the order of tabulation.

The magnitude of bomb tritium in perched and dike waters was high enough to make tracer studies possible as reported elsewhere [7]. Current tritium content of other groundwaters on Oahu is generally too low for such studies, although it proved to be useful in the qualitative identification of recent recharge [8]. The low radiocarbon activities associated with basal waters in the Honolulu area has prompted the more detailed studies of radiocarbon dating discussed in Subsection 4.3.

4.2. Isotopic composition of groundwater recharge

All radiocarbon measurements performed to date on Oahu's groundwaters are summarized into the frequency distribution shown in Figure 3. Most samples have activities between 80 and 112% modern which corresponds to an interval of apparent radiocarbon ages ranging from 1800 years to less

than 20 years respectively. Samples containing considerable amounts of bomb tritium (indicated with reference to an arbitrary value of 2.5 TU) are mainly associated with samples containing radiocarbon activities in excess of 100% modern, i.e. those containing bomb radiocarbon. This mutual endorsement of bomb tritium and bomb radiocarbon is very satisfying indeed, and lends support to the validity of using these bomb tracers for the identification of recent recharge (less than 20 years).

Another feature shown by this histogram is the modal ^{14}C value between 96 and 100% modern, ascribed to infiltrating waters uncontaminated by bomb radiocarbon. Vogel [9], who investigated groundwaters in temperate and arid regions of the world, reported such peaks between 80 and 90% modern. Some of the factors responsible for our higher values are undoubtedly the high turn-over rate of organic matter in sub-tropical soils and the absence of "dead" carbonate minerals in soils and basaltic aquifers.

The determination of the initial activity of regionally infiltrating waters is of great importance since it forms the zero time reference in calculating radiocarbon ages. In calculating such ages for southern Oahu's basal waters, discussed below in Subsection 4.3.1, the radiocarbon activity of dike waters is taken as reference. Dike waters are considered representative of waters recharging these basal waters on the basis of hydrologic and geochemical considerations. Detailed studies of dike waters [7] yielded 99 ± 1% modern

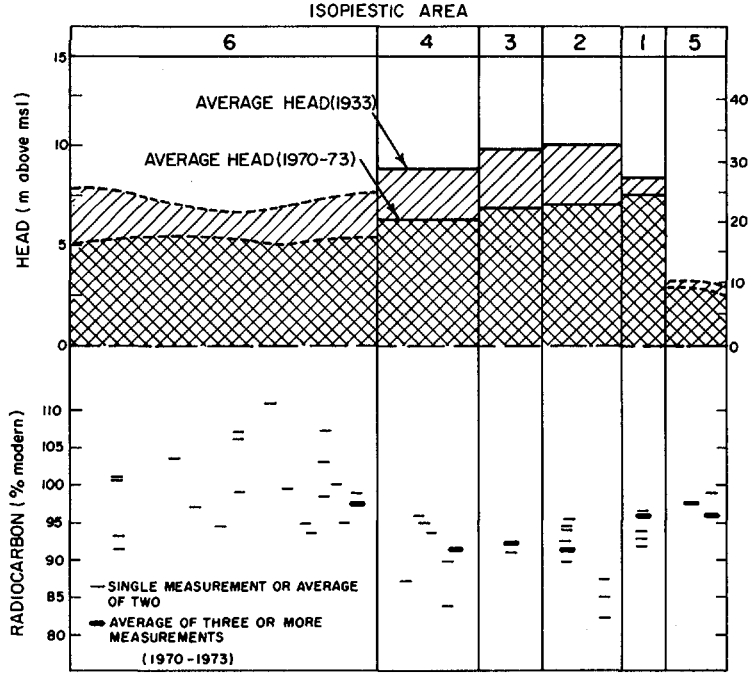

FIG.4. Average piezometric heads and radiocarbon activities of basal groundwater occurring in isopiestic areas 5, 1, 2, 3, 4 and 6 in southern Oahu.

as radiocarbon reference value. The same study indicated that 18 ± 1δ ‰ PDB could be used as a ^{13}C reference to adjust for possible limestone dilution effects.

4.3. Study of southern Oahu's basal waters

Basal water samples have been obtained from numerous wells, shafts and springs located in southern Oahu. Radiocarbon data for these samples are shown in Fig. 4, with their distribution along the horizontal axis reflecting the approximate location of the respective sources between the boundaries separating the isopiestic areas. Pumping station data which are identified as such by extra heavy bars are averages of three or more determinations made in the period 1970 through 1973. Piezometric heads are averages of measurements made during the same period.

Figure 4 clearly shows that basal waters in area 6 (area around Pearl Harbor) display predominantly higher radiocarbon values than do basal waters in areas 1 through 5 (all located in the Honolulu area). Several values are in the "bomb" radiocarbon range. The same samples showed small amounts of bomb tritium as well. None of the samples from areas 1 through 5 has radiocarbon activity greater than 100%, which would have indicated the presence of "bomb" radiocarbon. Tritium activities are generally too low to be significant in terms of our resolution capability of ± 1.0 TU.

A monitor well located in area 2 was sampled at eight different depths using specially designed equipment. Radiocarbon and chloride data are listed below:

	Basal lens					Transition zone		Salt water
Depth (m below msl):	140 [a]	210	230	240	260	320	360	400
Chloride (mg/litre):	52	59	59	95	83	8050	11700	18780
Radiocarbon (% modern):	92.3	91.8	92.2	94.0	91.4	87.5	84.8	41.6

[a] Just below casing and caprock contact.

No significant variation in radiocarbon activity is apparent in the basal water samples; on the other hand, the deeper brackish and salt waters are considerably lower in radiocarbon activity.

4.3.1. Pumping stations

Isotopic and chemical composition of basal waters pumped up by eight major pumping stations were studied as a function of time. Samples were collected and analysed for radiocarbon and tritium and several chemical species, once or twice a year over the period 1970 through 1973. None of the isotope records showed any significant trends, although some are smoother than others. Records for the chemical parameters on the whole show little or no variation with time. Average values for the time study data

TABLE II. AVERAGE HYDROLOGIC, CHEMICAL AND ISOTOPIC DATA FOR MAJOR BASAL WATER SOURCES IN SOUTHERN OAHU (1970-73)

Area	Pumping station	Draft (10^6 m^3/a)	Cl (mg/litre)	HCO_3^- (mg/litre)	Tritium (TU)	Radiocarbon (% modern)	^{13}C [a] (δ ‰ PDB)	^{14}C age (years)
5	Aina Koa Wells	0.57	134	82	1.0	96.1	-19.2	240
5	Waialae Shaft	0.47	135	102	0.8	97.5	-17.2	120
1	Kaimuki Wells	7.43	76	76	0.6	96.1	-18.5	240
2	Wilder Wells	10.79	43	107	2.9	85.0	-15.5	~ 0 [b]
2	Beretania Wells	12.76	56	73	0.3	91.4	-18.5	640
3	Kalihi Wells	10.88	73	74	0.3	92.2	-17.4	570
4	Kalihi Shaft	15.89	79	69	0.6	91.2	-18.3	660
6	Halawa Shaft	17.20	46	67	1.6	97.3	-19.2	140

[a] Single measurement.
[b] ^{13}C adjusted.

on radiocarbon, tritium and selected chemical parameters are summarized in Table II. Entries for draft are averages of measurements over the same time period. ^{13}C data are single determinations, however.

Previous studies on dike waters and perched waters had shown that water samples with greatly varying bicarbonate concentration have similar radiocarbon activities [7]. Comparison of stations (Aina Koa Wells and Waialae Shaft) in area 5 with the one (Halawa Shaft) in area 6 reveals a similar pattern of relatively high radiocarbon activities for samples that contain high as well as low bicarbonate concentrations. It is concluded therefore that high bicarbonate concentrations may be a consequence of geochemical conditions associated with soils in the recharge area, and do not, a priori, indicate dissolution of limestone deposits. The application of ^{13}C data [10, 11] appears more useful in this regard.

Basal water ^{13}C data listed in Table II are, with one exception, very similar to the dike water ^{13}C data [7], as is true of data (not presented here) for other wells in areas 1 through 5. This suggests that the carbon isotope composition of basal waters has not been altered by dilution or exchange processes involving limestone materials. Any loss of radiocarbon is thus to be ascribed to radioactive decay only, except in the case of Wilder Wells. In comparison, its radiocarbon value (85.0% modern) is quite low, bicarbonate (107 mg/litre) is high, and ^{13}C (-15.5 δ‰ PDB) is more positive. There is little doubt that in this case the low radiocarbon activity is not the result of radiocarbon decay but rather of limestone dilution effects. Further support for this conclusion is the fact that samples from this station consistently show bomb tritium, indicating the presence of recent recharge. Pearson and Hanshaw [11] have shown that ^{13}C data can be successfully used to separate out non-radiogenic effects, and hence to calculate adjusted ages. Application of their procedure to Wilder Wells data indeed yields approximately "zero age" in agreement with the tritium data.

Ages for basal waters discharged by the pumping stations are listed in column 7 of Table II. These ages were calculated using conventional procedures with 99% modern (dike waters) as the radiocarbon value for initial recharge, ^{13}C adjustment was applied only to Wilder Wells data, for reasons described above. Inspection of Table II reveals that only three pumping stations (Beretania Wells, Kalihi Wells and Kalihi Shaft) show significant radiocarbon ages. Ages for the other stations are all "recent". A further distinction in ages, other than between these two groups, is not justified considering both the uncertainties associated with the measurements and the variations of the averaged data as a function of time. Two sources (Halawa Shaft and Aina Koa Wells) show marginal but detectable amounts of bomb tritium (as do Wilder Wells), testifying to the presence of very recent recharge (< 20 years).

5. HYDROLOGIC INTERPRETATIONS

5.1. General

Tritium and radiocarbon data presented in Table I and Fig. 3 show that fresh groundwaters are primarily less than 1800 years old. Perched waters and dike waters have residence times of years or decades. Low radiocarbon values associated with transition-zone water and underlying salt

water probably reflect decay of radiocarbon due to long residence times of these waters. Further work on these waters involving ^{13}C analyses is needed and planned.

5.2. Basal waters

Representative data in Table I show that basal water in area 5 has a chemical and isotopic composition which is distinct from that of basal waters in other areas. As mentioned in Subsection 4.3.1, this composition is attributed primarily to geochemical conditions in the respective recharge area. If this is true then it follows that the recharge area of area 5 is distinct from the recharge area for areas 1 to 4. One might argue that waters from other areas flow into area 5 and on their way pick up additional chlorides and bicarbonates. However, such a mechanism would require the dissolution of limestone material, resulting in low radiocarbon and ^{13}C values, not what is observed here.

It was suspected from geologic and hydrologic information (not presented here) that areas 1 and 5 are separated not only by a valley fill but also by a nearby parallel rift zone. Hence the barrier between the two areas is considered very effective. Present data support this contention. Area 5 is to be regarded as an independent groundwater system. The distinctive chemistry of the water in this area is ascribed to the relatively low rainfall over its watershed. The latter is also responsible, at least in part, for the low head in the area.

Several samples collected in the Pearl Harbor area contained bomb radiocarbon and bomb tritium. These high values are associated with shallow wells and springs discharging water from relatively shallow depths. Chemical constituents in these waters were high relative to those in water from deeper wells. It is strongly suspected that these isotopic and chemical differences as a function of depth are caused by the presence of return irrigation water in the upper layers of the lens [12]. Very large amounts of water are used for the irrigation of sugar-cane fields located between Pearl Harbor and Central Oahu. A substantial part of this irrigation water after application percolates into the basal water which is tributary to the basal water in the Pearl Harbor area. Such irrigation return water, because of its exposure to the atmosphere, roots of growing plants and top soil, is believed to attain post-bomb radiocarbon activity levels, and as such can be identified. Current studies are in progress to verify this contention.

5.3. Age relationships

Samples from Wilder Wells have consistently shown bomb tritium, indicating that at least some of its discharge originated over the past 20 years. ^{13}C adjusted radiocarbon age is around zero. Further resolution is not justified considering the many variables involved in this calculation. It is clear though that water of recent origin provides a constant source of recharge supplying these wells.

Basal lenses that are recharged directly from overland must contain the youngest water in their upper layers. Shafts are constructed within the mountains at sea level elevations (Fig. 2A) so as to "skim" the top of basal lenses. Water developed by shafts should therefore be of recent origin also. On the other hand, wells penetrating several hundred metres into lenses and

located farther away from the mountain recharge areas should discharge water containing an undetermined fraction of water that is older than that from the shafts.

Two shafts (Table II) indeed have very young radiocarbon ages; one of them (Halawa Shaft) even shows small amounts of bomb tritium. However, a third shaft (Kalihi Shaft) shows a relatively old radiocarbon age, while intermediate ages are associated with some of the well stations. It is realized that the age of water from a particular source could be a function of local lens thickness, depth of well and pumping rate. To explore such dependence, a new parameter is introduced, Q/d, called draft-distance parameter[1], where Q = pumping rate and d = distance from the bottom of the well down to the fresh water-salt water interface. This parameter expresses the capability of a source to withdraw water from lesser or greater depth within a particular lens, and as such should relate to the water's radiocarbon age. Figure 5 shows this indeed to be the case with the exception of Halawa Shaft. No satisfactory reason can be given to explain this exception. It may be related to the fact that this shaft is in area 6; an area that on the whole shows higher radiocarbon values (i.e. younger ages) which in turn appears to relate to the magnitude of the groundwater flux which is known to be greater for this area than it is for those in the Honolulu area. Perhaps it should be pointed out that in the foregoing discussion distances between sources and recharge area(s) were considered the same for all stations involved. On the whole this agrees with reality, although shafts are somewhat farther inland than the other sources.

Based on the relationship shown between age and draft distance in Fig. 5, one could presume that individual lenses might show a vertical age stratification, but this is not borne out by the samples taken from five different depths in an observation well adjacent to Beretania Station. However, the data, presented in a previous section, did reveal that samples of brackish and salt waters taken from greater depths did show lower radiocarbon values. Interpretation of these data is in progress together with additional field sampling.

The old ages of water discharged by stations in areas 2, 3 and 4 raises the question whether water is being developed from the so-called bottom storage [13]. Interestingly enough these particular areas showed the highest head in 1933, but have since dropped drastically and are even below that of area 1. Additional data are needed before a valid answer can be given to the foregoing question.

---

[1] This parameter is adapted from a relationship expressing "ultimate rise" introduced by Dagan and Bear [14] in their study of upconing of the transition zone between fresh and salt water in coastal aquifers. Ultimate rise is defined as:

$$\frac{1}{2\pi \frac{\Delta\gamma}{\gamma} K_x} \frac{Q}{d}$$

where

Q = pumping rate of well

d = distance between the well's bottom and the interface at $t = 0$

$\frac{\Delta\gamma}{\gamma}$ = dimensionless density difference between fresh and salt water

K_x = horizontal permeability

For this paper in which a parameter is sought for preliminary assessment, the first is assumed constant and hydrodynamic dispersion is not yet considered, as was done in Schmorak and Mercado's work [15].

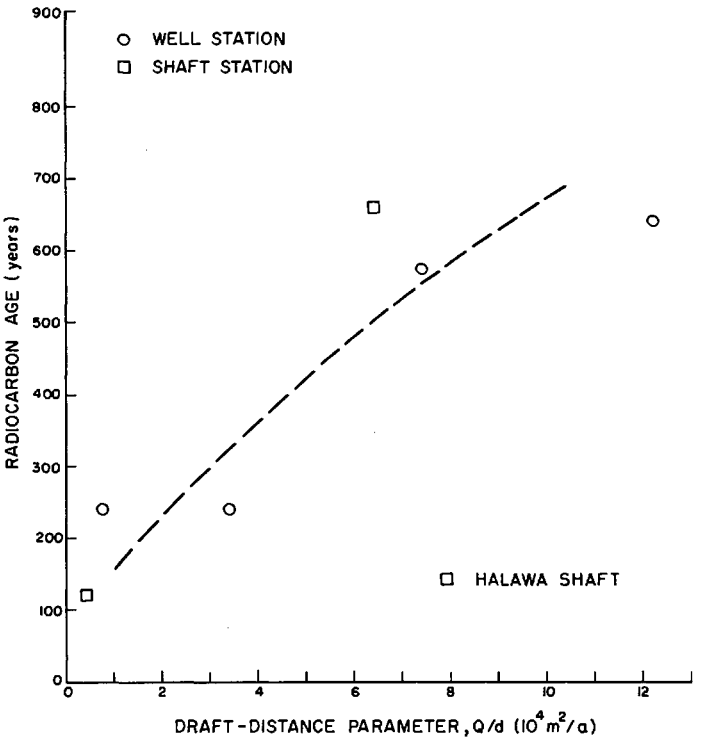

FIG.5. Radiocarbon age of basal water, discharged by major pumping stations in southern Oahu, as a function of the draft-distance parameter Q/d.

6. CONCLUSIONS

The geologic composition of Oahu together with its subtropical groundcover gives rise to groundwater systems which are hydrologically and geochemically unique. Oahu can be regarded as an ideal testing ground for groundwater carbon isotope studies because of the occurrence of carbonate-free basaltic aquifers which at lower elevations grade into carbonate-containing aquifers.

Data obtained to date indicate that the pre-bomb radiocarbon activity associated with waters recharging Oahu's aquifers is 99 + 1% modern. Bomb radiocarbon and bomb tritium are currently present in groundwater from some high-level sources and others.

Dike waters and basal waters both have ^{13}C values ranging between -17 and -19 δ‰ PDB. Since dike waters are representative of waters recharging basal aquifers it follows that groundwater ^{13}C concentrations remain unchanged as long as such waters reside or flow through basaltic aquifers. On the basis of data for groundwaters in carbonate aquifers (Table I) and certain basal waters (such as Wilder Wells), it is concluded that the effect of carbonate dissolution upon groundwater chemistry can be detected by the

simultaneous occurrence of high bicarbonate concentrations (> 100 mg/l), large ^{13}C values (> - 16 δ‰ PDB), and low radiocarbon activity (< 90% modern). ^{13}C data proved to be capable of adjusting "apparent radiocarbon ages" for such carbonate dilution effects. However, natural variations in the ^{13}C data increase age uncertainties and complicate the resolution of small age differences.

In general, Oahu's groundwaters are of recent origin as shown by radiocarbon and tritium data. Old ages are suspected for brackish and salt waters residing beneath basal-lenses. Basal waters from the six isopiestic areas in southern Oahu show radiocarbon activities which to some extent are characteristic for their area. Radiocarbon ages for waters withdrawn from these areas by major pumping stations range from a few decades to a maximum of 660 years. Apparently a relationship exists between these ages, pumping rate of the station, well depth and local thickness of the lens. One area (5) contains water that is isotopically and chemically distinct from that in the other areas and thus is considered an independent groundwater system.

This study has shown that the combination of multiple isotope and chemical analyses can yield valuable geochemical and hydrological information. Several of the observations or conclusions presented here serve to endorse or confirm existing hydrologic knowledge. However, some data such as the age relationships are unique and provide the tools for subsequent hydrodynamic studies of the basal lenses.

ACKNOWLEDGEMENTS

This research project was carried out with the active co-operation of the Board of Water Supply, City and County of Honolulu. Thanks are due to private well owners for their co-operation in sample collection and to all those who participated in the collection and processing of the samples. This work was financially supported by grants from the Office of Water Resources Research.

This paper constitutes Water Resources Research Center Contribution No. 55 and Hawaii Institute of Geophysics Contribution No. 589.

REFERENCES

[1] YOUNG, R.H.F., LAO, C., Return irrigation water in Hawaii, Water Resour. Bull., Am. Water Resour. Assoc. 9 (1973) 538.

[2] HUFEN, T.H., DUCE, R.A., LAU, L.S., Some Measurements of the Tritium Content in the Natural Water of Southern Oahu, Hawaii, Technical Rep. No.34, Water Resour. Res. Center, Univ. of Hawaii, Honolulu (1969).

[3] HUFEN, T.H., BUDDEMEIER, R.W., LAU, L.S., Tritium and Radiocarbon in Hawaiian Natural Waters, Technical Rep. No.53, Water Resour. Res. Center, Univ. of Hawaii, Honolulu (1972).

[4] AMERICAN PUBLIC HEALTH ASSOCIATION, Standard Methods for the Examination of Water and Wastewater, Washington, APHA (1971) 874.

[5] von BUTTLAR, H., LIBBY, W.F., Natural distribution of cosmic-ray produced tritium: II, J. Inorg. Nucl. Chem. 1 (1955) 75.

[6] INTERNATIONAL ATOMIC ENERGY AGENCY, Environmental Isotope Data No. 1: World Survey of Isotope Concentration in Precipitation (1953-1963), Technical Reports Series No. 96, Vienna (1969); Environmental Isotope Data No. 2: World Survey of Isotope Concentration in Precipitation (1964-1965), Technical Reports Series No. 117, Vienna (1970); Environmental Isotope Data No. 3: World Survey of Isotope Concentration in Precipitation (1966-1967), Technical Reports Series No. 129, Vienna (1971);

Environmental Isotope Data No.4: World Survey of Isotope Concentration in Precipitation (1968-1969), Technical Reports Series No. 147, Vienna (1973).
[7] HUFEN, T.H., BUDDEMEIER, R.W., LAU, L.S., Isotopic and chemical characteristics of high-level groundwaters on Oahu, Hawaii, Water Resour. Res., in press.
[8] LAU, L.S., HUFEN, T.H., Tritium Measurement of Natural Waters on Oahu, Hawaii: A Preliminary Interpretation, Technical Reports Series No.65, Water Resour. Res. Center, Univ. of Hawaii, Honolulu (1973).
[9] VOGEL, J.C., "Carbon-14 dating of groundwater", Isotope Hydrology 1970 (Proc. Symp. Vienna, 1970), IAEA, Vienna (1970) 225.
[10] RIGHTMIRE, C.T., HANSHAW, B.B., Relationship between the carbon isotope composition of soil CO_2 and dissolved carbonate species in groundwater, Water Resour. Res. 9 (1973) 958.
[11] PEARSON, F.J., Jr., HANSHAW, B.B., "Sources of dissolved carbonate species in groundwater and their effects on carbon-14 dating", Isotope Hydrology 1970 (Proc. Symp. Vienna, 1970), IAEA, Vienna (1970) 271.
[12] HUFEN, T.H., Isotopic and chemical characteristics of groundwater on the island of Oahu, Hawaii, Water Resources Seminar Series No.4, Water Resour. Res. Center, Univ. of Hawaii, Honolulu, in press.
[13] WENTWORTH, C.K., Geology and Groundwater Resources of the Honolulu-Pearl Harbor Area, Board of Water Supply, City and County of Honolulu, Hawaii (1951).
[14] DAGAN, G., BEAR, J., Solving the problem of local interface upconing in a coastal aquifer by the method of small perturbations, J. Hydraul. Res. 6 1 (1968).
[15] SCHMORAK, S., MERCADO, A., Upconing of fresh water-sea water interface below pumping wells - field study, Water Resour. Res. 5 6 (1969).

DISCUSSION

J. ŠILAR: How are the individual isopiestic zones determined?

T.H. HUFEN: Piezometric heads are measured at regular intervals at monitor wells and at a number of pumped wells where the pumps have been switched off temporarily.

J. ŠILAR: Is the surface morphology taken into account?

T.H. HUFEN: The surface morphology is not taken into account in this study of basal waters since, because of the high permeability of the basaltic flow rock, we do not think it an important factor with regard to water occurrence, flow or ages.

V.T. DUBINCHUK: Could you give more information about your draft-distance parameter?

T.H. HUFEN: The draft-distance parameter incorporates various hydrological parameters, such as discharge, thickness of lens and depth of well. In essence, it expresses the ability of a particular source to withdraw water from lesser or greater depths. If water in the lower parts of thick lenses is older than water in the upper parts or older than water in thin lenses, then a positive correlation should exist between the draft-distance and radiocarbon age. The results shown in Fig. 5 indicate that there is indeed such a correlation.

G.P. CONRAD: I should like to confirm what you said in your oral presentation about the close correlation between high ^{14}C activities and a clearly detectable tritium activity.

We have results relating to groundwater in the Saharan arid zone which agree with those for the Kalahari presented by Mr. Mazor in paper IAEA-SM-182/18.[1]

---

[1] MAZOR, E., VERHAGEN, B.T., SELLSCHOP, J.P.F., ROBINS, N.S., HUTTON, L.G., "Kalahari groundwaters: their hydrogen, carbon and oxygen isotopes", these Proceedings I, IAEA-SM-182/18.

^{14}C activities of 100% or more of modern carbon (Conrad, G. P., Fontes, J. C., C. R. Acad. Sci. 245 (1970) 165, and unpublished measurement results) correspond to 2-12 TU (Conrad, Olive, Marcé, Journal of Hydrology (in press)). These data, which are based on some 20 combined (^{14}C and tritium) measurements, lead me to think that the initial ^{14}C concentration in the arid zone was not 50% or 85% of modern carbon but close to 100%.

ENVIRONMENTAL ISOTOPES, OTHER THAN HYDROGEN, OXYGEN AND CARBON ISOTOPES, IN GROUNDWATER STUDIES

(Session 7, Part 1)

^{234}U AND ^{238}U IN THE CARRIZO SANDSTONE AQUIFER OF SOUTH TEXAS

J.B. COWART, J.K. OSMOND
Florida State University,
Tallahassee, Fla.,
United States of America

Abstract

^{234}U AND ^{238}U IN THE CARRIZO SANDSTONE AQUIFER OF SOUTH TEXAS.

The waters of the Carrizo Sand formation of South Texas, United States of America, exhibit a pattern of uranium isotopic disequilibrium, described in terms of $^{234}U/^{238}U$ activity ratio ("A.R.") and uranium concentration, which may be a function of geochemical factors and the hydrologic history of the area. In terms of uranium, two regimes seem to exist. The first, including outcrop and near outcrop sample locations, has waters with relatively high concentration and low A.R. Somewhat downdip, the uranium concentration decreases sharply at the downdip limit of the oxidation environment, a zone of uranium precipitation. Recoil of daughter products from the precipitated uranium causes an increase of A.R. of the water. Water of low uranium concentration and high A.R. is found throughout the downdip regime. If a constant input of ^{234}U through time is assumed, the downdip decrease in A.R. after the initial introduction of ^{234}U into the water may be ascribed to radioactive decay of ^{234}U. However, this assumption leads to the calculation of a water flow rate one twentieth that determined by other means. Alternatively, this pattern may be an artifact of a change of climate from 20 000 years to 10 000 years ago. In this case, the decrease in A.R. downdip is a function of a varying input of ^{234}U as well as decay.

INTRODUCTION

In a closed system, given sufficient time, the members of a radioactive decay series will achieve a state wherein the rate of production of each nuclide is equal to the radioactive decay of that nuclide. This state is called secular equilibrium; it follows then that the ratio of the activity of any two members of a decay series in equilibrium is equal to unity if the decay is in the same mode, for instance if the two nuclides both decay by emission of alpha particles.

That the ratio of abundances of ^{235}U and ^{238}U is essentially constant wherever uranium is found has been known for about 35 years. The unexpected abundance variation of ^{234}U relative to ^{235}U and ^{238}U was first reported in 1955. This abundance variation may be measured in terms of the variation of the activity ratio, $^{234}U/^{238}U$; if the value of this ratio is any value except unity, a state of "disequilibrium" exists. ^{234}U and ^{238}U are, of course, chemically alike and are separated only by the two short-lived nuclides, ^{234}Th and ^{234}Pa.

The variation in uranium isotopic abundances in natural waters has applications which have just begun to

be explored. These applications arise from several significant aspects of uranium geochemistry:

1. The isotopic variation is extreme; the activity ratio of ^{234}U to ^{238}U ("A.R.") varies by more than a factor of 20.

2. The determination of abundances of uranium isotopes at very low concentrations is relatively simple due to their alpha radioactivity.

3. Uranium has two common valence states, +4 and +6, which makes it sensitive to electrochemical variations in its environment.

4. The variable isotope, ^{234}U, is a daughter of ^{238}U and both the rate of disequilibrium development and its decay are governed by the half life of ^{234}U, approximately 250 000 years.

There are two principal types of natural water systems, in terms of their uranium isotope geochemistry, the near surface type and the deep ground water type. Many surface and shallow ground water systems, under oxidizing conditions, have relatively high uranium concentrations and moderate disequilibria. The waters of such systems have young ages and the ratio of their isotope abundances, due to the higher concentrations, is relatively stable and insensitive to change. Their uranium isotope ratios and abundances can be used as natural tracers to determine flow patterns and mixing proportions. In the other case, that of deep ground water systems which are normally reducing, the concentration of uranium is low and the age of the water greater. Here the isotopic ratio is more susceptible to change and the variation of isotope abundances can be interpreted in terms of evolutionary interaction of the uranium in the water with that of the solid through time.

This report is concerned with an aquifer system in which the direction and rate of water movement is well defined and the difference in age of water between the oxidizing zone of surface recharge and the deep confined aquifer is appreciable.

BACKGROUND

The fractionation of ^{234}U from ^{238}U in nature was first reported in 1955 [1]. Other studies not only substantiated the disequilibrium of the uranium isotopes but brought out the fact that the disequilibrium is to be found in profoundly different materials and environments.

The pertinent portion of the decay series of ^{238}U is shown in Figure 1. It should be emphasized that, at equilibrium, ^{238}U accounts for 99.28%, ^{235}U for 0.72% and ^{234}U for 0.0054% of the amount indicated by concentration figures. No $^{235}U/^{238}U$ disequilibrium has been found in natural uranium samples investigated [2].

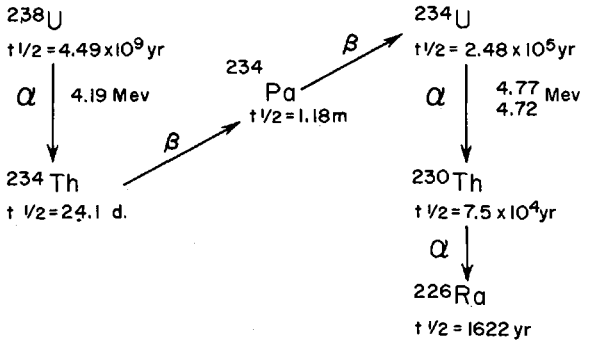

FIG. 1. The first several steps in the decay scheme for ^{238}U. At equilibrium every member of a non-branching chain has the same activity. Inasmuch as alpha particles are easily detected and their energy measured, the ratio of ^{234}U activity to ^{238}U activity is readily determined.

Uranium minerals and ores have been found to vary so that the ratio of the activity of ^{234}U to ^{238}U ("A.R.") might be somewhat deficient in ^{234}U (A.R. < 1) or might contain an excess of ^{234}U (A.R. > 1) [3-5]. Many soils and minerals containing uranium as a dispersed element have been found to have A.R.s different than unity [6-9].

Most waters are found to have $^{234}U/^{238}U$ activity disequilibrium. The ocean, the ultimate destination of most surface water, has an excess of ^{234}U of 15% [10-11]. Not surprisingly, the dissolved uranium in rivers usually has excess ^{234}U [12-14]; in small streams A.R.s as high as 6.4 have been found [15]. Conversely, the uranium in the sediments carried by rivers is often deficient in ^{234}U, the A.R. seemingly dependent upon the character and geologic history of the drainage basin and the amount of organic material associated with the sediment [13, 16].

In limestone terranes, dissolved uranium in springs and rivers may have A.R.s either greater or less than equilibrium. The infiltrating waters probably receive an input of uranium of given concentration and A.R. in a near surface zone. Because the input concentrations and/or A.R.s are different at different locations, natural isotope dilutions may occur where several sources contribute to a resultant water, such as a large spring, a river or a lake. The quantity of water contributed by each source can be calculated by mixing equations. Such determinations have been made and are consistent with independent studies, for ground water [17], for a ground water-spring system [18-20], and for a spring-river system [21].

Ground water shows a wide range of values. A.R.s as low as 0.50 have been reported [17] and high ratios have been found in deep ground waters, the values ranging from 4 to as high as 12 [19, 20, 22].

Changes in $^{234}U/^{238}U$ activity ratio have been noted in seismically active areas [23]. The activity ratios of water from boreholes taken after an earthquake were noted to be smaller by a factor varying from 2 to 5 than the A.R.s from the same wells taken before the earthquake. It is possible that dilatation effects may expedite the transfer of uranium at or near crystal boundaries into an aqueous phase.

The mechanism for the fractionation of the isotopes has frequently been attributed to a natural Szilard-Chalmers effect whereby the ^{234}U atoms are selectively extracted from the lattice because of lattice damage caused by recoil and/ or the higher oxidation state of ^{234}U as a result of electron stripping during recoil [24, 25]. Such extraction might be facilitated by the presence of an aqueous solution, slightly oxidizing, bathing the crystal grains [26].

That the recoil mechanism itself must be a primary cause of the ^{234}U fractionation was shown by Kigoshi [27], who noted the enrichment of ^{234}Th, the immediate daughter of ^{238}U, in the liquid phase surrounding powdered uraniferous zircon. Such a process could cause the buildup of ^{234}U in a liquid not capable of acquiring uranium by leaching.

The geochemistry of uranium is strongly influenced by its mobility in oxidizing environments, usually as a uranyl carbonate complex, and its low solubility in reducing environments [28, 29]. In sedimentary rocks, accumulations of uranium as films or encrustations on rock particles is often observed to have occurred at a well-defined "reducing barrier"; the updip rocks are oxidized with iron oxides present whereas the downdip rocks may still contain pyrite which shows no effect of oxidation [30]. The zone of uranium accumulation is usually quite distinct and compact.

AREA OF INVESTIGATION

The study area is located in central south Texas, USA (see Figure 2). The Carrizo sandstone is a member of the Claiborne group of Eocene age (Lutetian). It is thought that the sands were once part of a remarkably extensive and uniform dune field [31]. The Carrizo is a prolific source of irrigation water for this region.

The Carrizo consists almost entirely of quartz sand but there are small amounts of bentonitic clay, shale, lignite and isolated crystals of pyrite present. Also, a suite of heavy minerals, including uranium bearing zircon and xenotime, is ubiquitous [31]. The thickness of the sand varies from about 180m near the outcrop area to approximately 400m some 90 km downdip from outcrop (Figure 2). The Carrizo dips to the south or southeast at 20m to 25m per km for about the initial 60 km from the outcrop and thereon at a rate somewhat steeper [32,33].

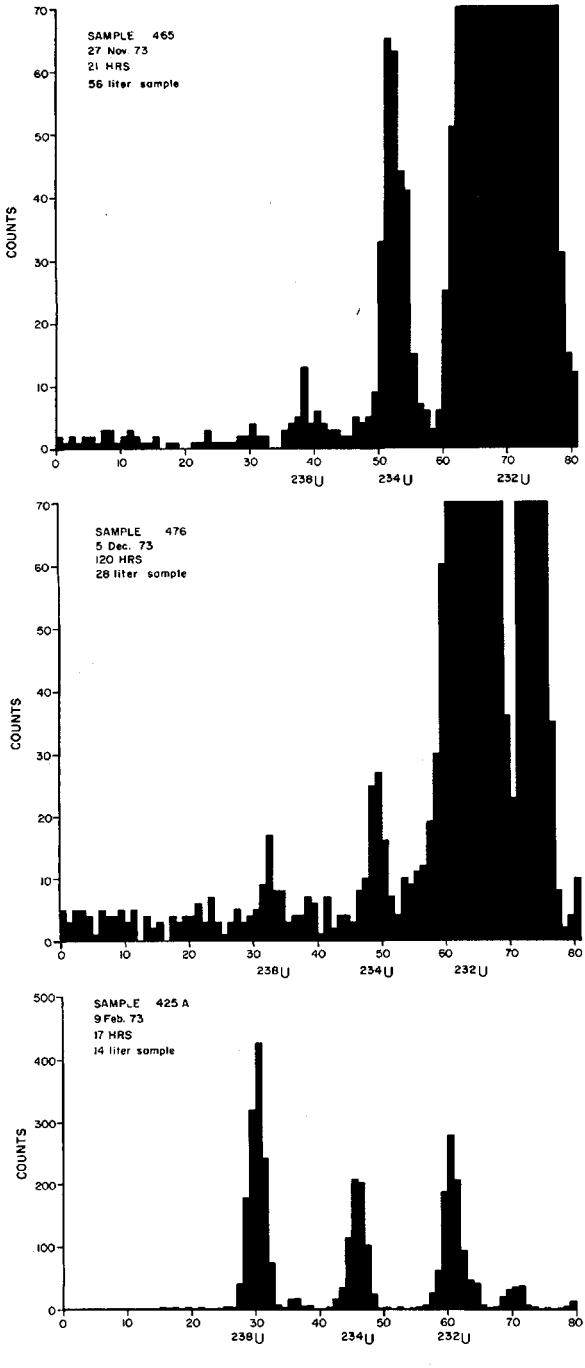

FIG. 2. Three alpha spectra, showing resolution of the three uranium isotope peaks. In low concentration samples (465, 476), development of the natural uranium peaks (^{234}U and ^{238}U) may require considerable time, with a resulting increase in background counts. In the two upper spectra, the ^{232}U spike peak has been truncated for the purposes of figure balance. In high concentration samples (425A), good counting statistics are achieved in a relatively short time. (Note vertical scale change.) The peak to the right of ^{232}U in some of these spectra is ^{224}Ra, a member of the ^{232}U decay series.

The Carrizo is of specific interest for several reasons:

1. It is a well confined aquifer with little leakage in or out of the sand.

2. It is well studied. The Texas Water Development Board (TWDB) has numerous observation wells in the area and some geochemical measurements have been made [32].

3. ^{14}C age determinations and determination of water flow rates have been made of water in the area [34].

4. Almost the entire amount of water in the Carrizo is meteoric water which has infiltrated the outcrop area. The uranium in the ground water must have its source in the Carrizo itself.

SAMPLING AND PROCESSING

The samples were obtained from wells which were identified as obtaining water from the Carrizo on maps compiled by the TWDB and the United States Geological Survey. The wells were either flowing or were allowed to pump for a time sufficient to permit the acquisition of a representative sample.

The volumes collected were 14, 28 or 56 liters, depending on the uranium concentration expected at that location. The samples were acidified to pH=1 in the field and transported to the laboratory for further processing. Each 3.5 liter bottle was prepared by adding 5 ml of an iron carrier solution and 1 ml "FSU Water Spike-2" (157 dph ^{232}U/ml). The samples were shaken vigorously daily for 10 days in order to effect spike equilibration. Each sample was brought to a temperature of 95°C for 10 minutes before the uranium was separated from interfering elements by coprecipitation. Organic extraction and anion exchange resin procedures followed. The separated uranium was electroplated onto a stainless-steel planchet. The alpha activities of the isotopes were measured by use of partially depleted surface barrier silicon detectors housed in a vacuum chamber. Each detector was linked to a 100-channel pulse-height analyzer.

Some of the samples from the downdip portion of the Carrizo have very low uranium concentrations, close to the detection limits of the methods employed. It was necessary to use counting intervals measured in days; background effects, which are usually insignificant in alpha counting, had to be carefully monitored. Among the background effects isolated were:

1. Clean planchet background.

2. "Spike tail," the encroachment of a ^{232}U counts into the ^{234}U envelope (9 channel window). This

is in part due to the presence of a thin film of iron on some planchets which tends to broaden all peaks; it is aggravated by the growth of short-lived ^{228}Th, which has approximately the same alpha energy as its parent, ^{232}U.

3. Adsorption of radioactive daughter products, including gases, on the planchet, detector and chamber walls.

4. Temperature effects. Since surface barrier detectors and associated electronic equipment are sensitive to temperature, stable background rates, usable for such low concentrations, cannot be maintained above about 22°C.

Each of these background factors was determined for each counting period and each planchet. In general, a net count rate above background of as little as 0.2 count per hour per peak envelope could be established as significant.

Each planchet was counted long enough to accumulate at least 10 000 counts per envelope or as long as was practicable. The errors estimated are at the 95 percent confidence level. Long counting times were not a serious problem since five counting systems were used simultaneously. However, for the achievement of lower detection limits in future work, the development of a practical field concentration procedure would seem to be advisable.

In Figure 3, sample 465 is an example of a downdip sample with high A.R. and low concentration. The amount of ^{232}U spike added to all samples was such as to produce a peak height which would be equivalent to a concentration of 1 pp10^9 ^{238}U.

Sample 476 is representative of downdip samples with relatively low A.R. Although the total number of counts accumulated in either the ^{238}U or ^{234}U envelope is not large, the fact that those samples which were counted numerous times each gave A.R.s and concentrations that are quite consistent lends strong support to the validity of the pattern of activity ratios.

Sample 425A shows the spectrum of a near outcrop sample with a low A.R. (less than unity) and a relatively high concentration. Note that the ordinate scale is ten times that of the other two samples shown. In this type sample, the background is quite small in comparison with the natural uranium peaks and presents little difficulty in the achievement of precise measurement.

RESULTS

The distribution of sample localities is shown on the map of Figure 2 and the uranium data is reported in Table I.

In general, the samples from the outcrop area and shallow aquifer are characterized by relatively high uranium

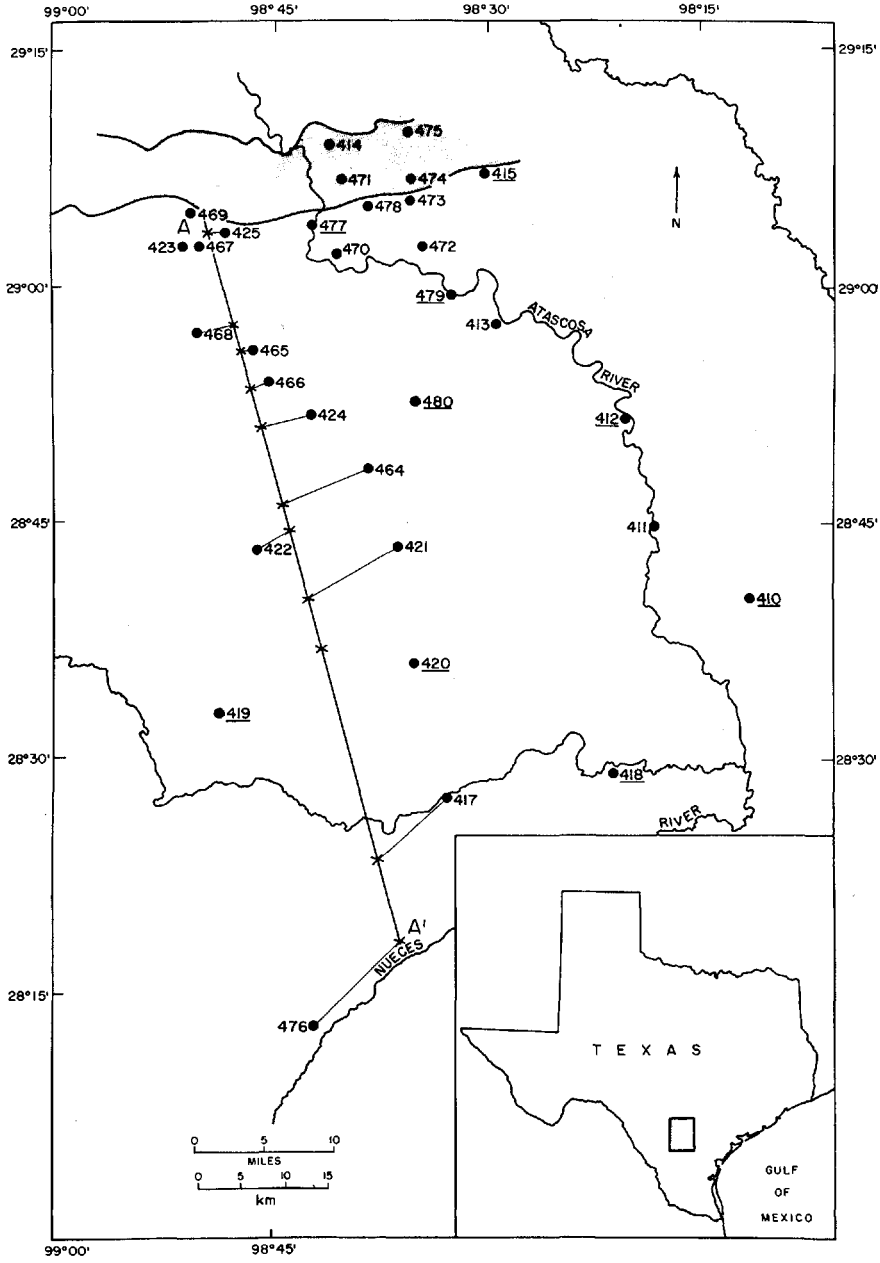

FIG.3. The study area in South Texas. Shading depicts the outcrop area of the Carrizo Sandstone which dips gently towards the South-Southeast. A - A' is the line of the cross-section of Fig.4. The projections of sample points on to this line are made parallel to the strike of the formation. An underlined sample number, e.g.410, indicates that no uranium data are available for that location.

concentrations and low activity ratios. Seven samples have activity ratios less than the equilibrium value of 1.00, and one sample, 425, has an A.R. of 0.52 which puts it among the group of lowest ratios reported [17]. Samples from downdip show much lower concentrations and higher A.R.s and the boundary between low and high A.R.s appears to be rather well defined.

Certain samples are transitional, in terms of geographic location, A.R., and/or uranium concentration, between the samples from the two larger regimes. Examples of this type along the profile are 423 and 467. Sample 423 has a rather low uranium concentration but an A.R. typical of outcrop samples. Sample 467, slightly further downdip, has a still lower concentration but has had enough ^{234}U introduced into the water so as to cause the A.R. to be slightly above unity. Possibly 478 and 472 are transitional, also.

The pattern of variation in concentration and A.R. along a downdip profile is shown in Figure 4. The line of this profile (A-A') is shown on the map in Figure 2. Along this profile, the highest A.R.s are somewhat downdip of the boundary between high and low concentrations. The A.R.s show a general decrease downdip in the direction of aging of the water (Figure 4, lower).

Further east, the pattern is less clear; the boundary between high and low concentrations is well defined but the existence of a maximum peak in A.R. is not as certain.

Samples 410, 412, 415, 416, 418, 419, 420, 477, 479 and 480 have uranium concentrations below the detection limits of the procedure; in most cases, the difficulty was compounded by a low yield.

DISCUSSION

The pattern exhibited by the concentration and isotope activity in the Carrizo aquifer is somewhat similar to that observed some 300 km to the northeast in the Trinity aquifer of Cretaceous age [22]. Infiltrating water picks up uranium deficient in ^{234}U but while moving downdip it gains an excess of ^{234}U while at the same time it loses most of its total uranium content. To explain this sequence of events the following model is proposed.

The sedimentary rock particles in a zone free from oxidizing effects may develop a surface zone or "rind" which is deficient in ^{234}U. Because the surrounding water is strongly reducing in character and uranium is not mobile in such an environment, selective leaching of ^{234}U is not thought to be effective. Recoil of ^{234}Th (a progenitor of ^{234}U) from a crystal lattice has been demonstrated by Kigoshi [27]. Such a process should cause the near surface volume of a grain to become deficient in ^{234}U even though the core of the grain (if the grain diameter is greater than 2 recoil distances) would remain in equilibrium. In zircon, Kigoshi calculated that the recoil distance is about 500 angstroms.

TABLE I. ACTIVITY RATIO, CONCENTRATION AND ^{234}U EXCESS OF SAMPLES

Sample number	Counting time (hours)	^{238}U	^{234}U	^{232}U	A.R.	Concentration (pp 10^9)	Excess ^{234}U (^{238}U equivalents)
411	583.0	87	342	21 923	3.93 ± 1.57	0.004 ± 0.002	0.012 ± 0.009
413 A	296.0	251	353	10 247	1.41 ± 0.27	0.025 ± 0.004	0.010 ± 0.006
413 B	258.0	202	372	12 128	1.84 ± 0.39	0.017 ± 0.003	0.014 ± 0.007
414 A	116.3	889	842	6 383	0.95 ± 0.09	0.139 ± 0.010	-
414 B	295.6	5344	4806	26 441	0.90 ± 0.04	0.202 ± 0.006	-
417	691.0	108	293	52 211	2.71 ± 1.00	0.002 ± 0.001	0.004 ± 0.002
421	387.0	130	447	104 903	3.44 ± 1.20	0.0012 ± 0.0004	0.003 ± 0.002
422	658.0	111	571	42 811	5.14 ± 1.87	0.003 ± 0.001	0.011 ± 0.006
423 A	243.0	4571	3154	22 366	0.69 ± 0.03	0.204 ± 0.007	-
423 B	182.9	2016	1374	10 075	0.68 ± 0.05	0.200 ± 0.010	-
424 A	473.1	74	536	13 185	7.24 ± 2.87	0.006 ± 0.002	0.035 ± 0.020
424 B	384.0	126	825	15 742	6.55 ± 1.73	0.006 ± 0.0015	0.034 ± 0.014
424 C	294.1	462	3087	83 821	6.68 ± 0.85	0.006 ± 0.001	0.031 ± 0.005
425 A	168.2	21 490	11 262	14 462	0.52 ± 0.01	1.486 ± 0.032	-
425 B	77.7	6079	3241	4007	0.53 ± 0.02	1.527 ± 0.063	-
464	712.5	247	1204	66 823	4.87 ± 0.95	0.004 ± 0.001	0.014 ± 0.004
465	498.8	628	5663	229 218	9.02 ± 1.03	0.003 ± 0.001	0.022 ± 0.004
466	265.0	128	814	36 253	6.36 ± 1.68	0.004 ± 0.001	0.019 ± 0.008
467	226.5	602	654	20 859	1.09 ± 0.16	0.029 ± 0.003	0.003 ± 0.005
468	359.6	96	526	21 895	5.48 ± 1.63	0.004 ± 0.001	0.020 ± 0.009
469	175.0	9372	9784	14 901	1.03 ± 0.03	0.629 ± 0.016	-
470	187.5	11 661	12 978	41 342	1.11 ± 0.03	0.282 ± 0.006	0.031 ± 0.008
471	103.7	30 865	23 676	12 046	0.77 ± 0.03	2.562 ± 0.055	-

TABLE I. (cont.)

472	575.8	360	639	42 666	1.77 ± 0.29	0.088 ± 0.001	0.006 ± 0.003
473	113.4	26 325	21 405	15 488	0.81 ± 0.04	1.700 ± 0.034	-
474	121.5	2458	2140	11 799	0.87 ± 0.05	0.209 ± 0.009	-
475	124.0	11 601	6732	9655	0.58 ± 0.02	1.202 ± 0.033	-
476	852.0	234	487	117 731	2.08 ± 0.51	0.002 ± 0.0004	0.002 ± 0.001
478	365.1	487	852	23 151	1.75 ± 0.23	0.021 ± 0.002	0.016 ± 0.005

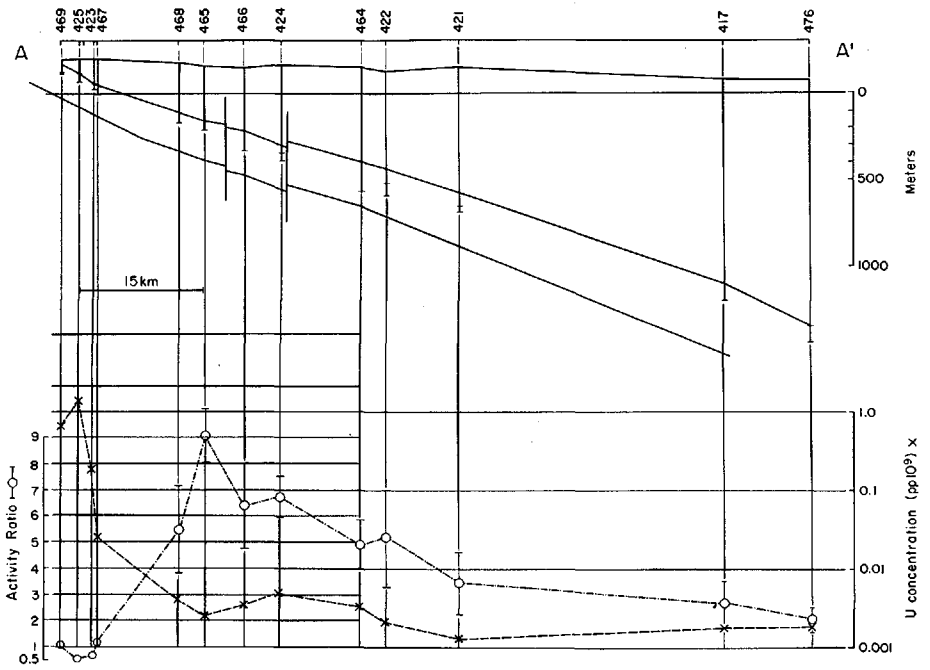

FIG.4. (Upper) Cross-section along A- A' of Fig.3, showing the sample well locations relative to the dipping Carrizo aquifer. (Lower) The $^{234}U/^{238}U$ activity ratios (linear scale on left) and the U concentration values (logarithmic scale on right) as a function of the corresponding well positions.

Although the outermost part of the grain might be as much as 50% deficient in ^{234}U, a relatively large grain, as a whole, would show only a slight deficiency, the actual value depending on the grain size and the ratio of surface area to volume.

When such a grain is introduced into an oxidizing, slightly acid environment, it is then possible for leaching to occur. The leaching may be selective in the sense that ^{234}U is preferentially extracted because of its greater vulnerability to leaching as has been proposed by various investigators [24-26]. On the other hand, in the near surface zone of the earth, corrosion of the grain may occur, resulting in an isotopically non-selective input of uranium into the ground water. This non-selective input would have a low A.R. (A.R. $<$ 1) because the corrosion would be localized in the depleted outer zone or rind. This latter case seems consistent with the observational data with regards to the Carrizo.

Regardless of the source of dissolved uranium in the outcrop regime, as it is carried downdip a zone of reduction is encountered where almost complete precipitation of

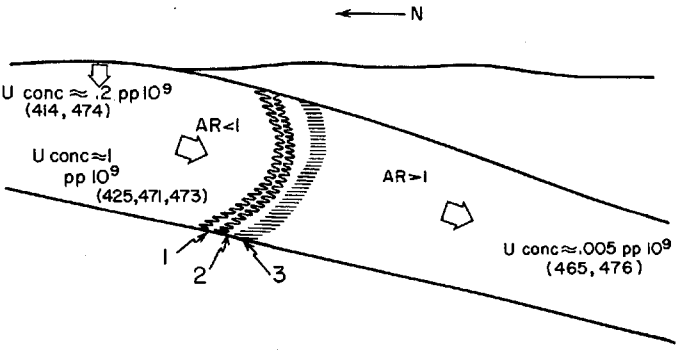

FIG.5. A diagrammatic model of uranium isotopic geochemistry in an aquifer like the Carrizo. Updip, the uranium concentration is relatively high and the A.R. is low. Downdip, the uranium concentration is low and the A.R. high. Zone 1 is the site of the reducing barrier where uranium solubility decreases and precipitation occurs today. Zone 3 is the location of a previous barrier. Low concentration water passing through the uraniferous zone 3 tends to collect an excess of ^{234}U. Zone 2 is transitional, where uranium concentration has decreased but the excess has not yet increased greatly.

uranium occurs, forming an encrustation or film on the sand grains (see Figure 5). Such a process has been shown to result in uranium accumulations under similar conditions [26, 35-37]. Further downdip, of course, the water would have only a very small concentration of uranium.

Because the precipitation of uranium is an isotopically non-selective process, this process cannot account for the excess of ^{234}U found in the water further downdip. However, if the now low uranium concentration water flows through a "fossil" uranium accumulation zone, it will receive the daughter products recoiling from the radioactive decay of ^{238}U. Because of the low electrochemical potential of the water, the uranium coating the sand grains will not be leached. In effect, the water is only a passive recipient of the recoiling ^{234}Th.

According to the recoil model of Kigoshi [38] and others [20], a steady state of disequilibrium should be established in very old ground water systems in which the addition of excess ^{234}U into the water by recoil processes would be balanced by decay of the excess with time. Since the concentration of uranium in the solid phase is several orders of magnitude greater than in the liquid phase, such a steady state would result in a net deficiency, though relatively small, in the solid phase, and a corresponding net excess, often very large relative to the dissolved ^{238}U, in the liquid phase.

As water percolates through a zone of uranium enrichment, for example at the hypothesized fossil reducing barrier, this steady state excess would be large, and an increase in A.R. would be expected, the amount being a function of the effective uranium concentration in the solid

phase relative to that in the liquid phase, and the time over which the water is exposed to the enriched zone. By "effective" is meant that uranium within recoil range of the liquid phase.

After leaving this zone, the ^{234}U enriched water finds itself in an environment where the amount of uranium in the solid phase is much less; therefore the initial large ^{234}U excess in the water is unsupported by the solid phase. The "extra excess" now decays toward a new steady state level which is a function of concentration of the dispersed uranium in the rocks and certain aquifer properties such as surface to volume ratio, porosity and permeability. In the case of most aquifers, it is likely that the uranium is widely dispersed in the region below the reducing barrier so that a steady state can be assumed for the downdip aquifer as a whole.

(1) $X = (A.R. - 1.00) \quad (C)$

where X is the excess ^{234}U, in units of ^{238}U equivalents, $ppl0^9$,

A.R. is the alpha activity ratio of ^{234}U to ^{238}U,

1.00 is the equilibrium alpha activity ratio,

C is the concentration of uranium (essentially ^{238}U) in $ppl0^9$; and

(2) $X_p = X_s + (X_o - X_s) \exp(-0.69\ t/T)$

where X_p is the observed excess ^{234}U at any point,

X_s is the steady state excess,

X_o is the initial excess,

t is the time elapsed between the initial condition of X_o and the time of measurement of X_p,

T is the half life of ^{234}U, approximately 250 000 years.

Figure 6 is a graph of the excess ^{234}U relative to the position of the water samples down the flow direction of the aquifer. The large excess of ^{234}U from sample 467 to sample 421 is due to the presence of the fossil uranium accumulation zone in the aquifer. At this accumulation zone, the value of X_s is unknown but must be large inasmuch as the time elapsed during percolation is far short of the time needed to achieve the steady state.

The decrease in this excess downdip is such as to suggest an approach to an equilibrium excess value less than about .002 $ppl0^9$ ^{238}U equivalent. If this were the case, a flow rate of less than 8 cm per year for the water would be indicated, this being the best fit line ("Apparent decay") drawn through the data of Figure 6. The two assumptions of this line are that the steady state excess downdip

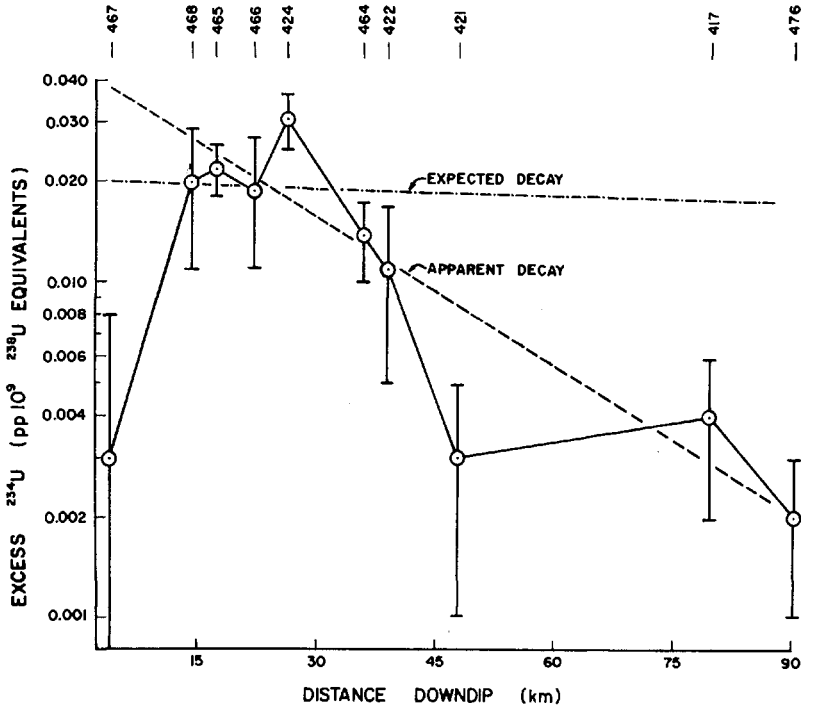

FIG.6. Plot of ^{234}U excess (pp 10^9 U equivalent) as a function of distance down the flow direction and in the direction of increasing age of water. The excess decays with a half-life of 250 000 years. If the downdip samples, e.g. 476, had an original excess like those of 468 through 424, and the flow rate is 150 cm per year, then very little decrease in excess would be expected downdip. That the decrease is considerable is probably due to a change in position of the reducing barrier rather than to a very slow flow rate.

is small and that the decrease is due to decay only. However, hydrologic estimates (Alexander and White, 1966) and radiocarbon determinations (Pearson and White, 1967) indicate a flow rate for the Carrizo water which is a minimum of 150 cm/yr. For this flow rate the "Expected decay" curve is the upper line of the figure.

The disparity between expected and observed decay lines probably means that the older downdip water was never as high in ^{234}U excess as the water presently updip. Whether or not a high ^{234}U/^{238}U ratio is produced depends on the position of the reducing barrier relative to previous positions of the reducing barrier, and this relationship can change.

A fossil accumulation must be located on the reducing side of the barrier in order to cause striking high activity ratios. If the reducing barrier has moved downdip from the fossil accumulation zone, the input of recoil products will be into water containing a relatively large amount of uranium.

Although this input might radically change the A.R. of a water containing .005 ppl0^9, it would be barely noticeable in water containing 1 ppl0^9. The coincidence of the reducing barrier with a fossil accumulation would produce a water with an activity ratio greater than the A.R. of the oxidized water but probably not as great as those observed in the Carrizo (9) or the Trinity (12) [22].

In the uranium deposits found in Eocene sandstones in Wyoming, which seem to have many similarities to the system under discussion, the uranium ore usually has a ^{234}U deficiency, the deficiency ranging from a few percent to as much as 60 percent [5, 26]. This is consistent with the low A.R. of oxidizing water being precipitated at the reducing barrier and a continued loss of ^{238}U daughter products. Furthermore, multiple parallel "roll fronts" or zones of accumulation are often found [30]. Interphase isotopic exchange can be a factor in changing uranium activity ratios [39]. In the Powder River Basin, Wyoming, Rosholt et al., [40] concluded, after investigation, that equilibration was not a predominant process at that location. According to the recoil model, such equilibration must be effected through several hundred angstroms of solid crystalline material; therefore isotopic equilibration is not believed to be a factor in the downdip decrease in A.R. exhibited by the Carrizo.

The presence of a fossil accumulation zone at a location different from the present reducing barrier may be useful as a paleoclimate indicator. In addition, it has the potential of indicating the flow rate of water in certain aquifers.

The updip migration of the reducing barrier may be a function of a slower rate of flow which resulted from decreased rainfall on the outcrop area. In the Carrizo, as the reducing barrier moved updip, it left its accumulated uranium (the incipient fossil zone) which became increasingly effective as the source of ^{234}U as the surrounding water became increasingly depleted in uranium. In Figure 6, a segment of the curve shows that the water from sample 421 to sample 424 has an increasing excess of ^{234}U. Radiocarbon indicates that the water at sample 421 has an age of about 20 000 years and sample 424 an age of about 10 000 years. These ages are consistent with the evidence of decreasing volume of lakes in the Great Basin region of North America which occurred at about this time [41, 42]. The almost constant excess since that time may indicate that the rainfall has not changed significantly although the wide spacing of control points makes any such conclusion highly tentative.

Assuming the validity of the ^{234}U pulse, the location of such pulses in other confined aquifers could provide flow rate information not otherwise known or could provide an estimate independent of radiocarbon or classical hydrologic methods.

ACKNOWLEDGMENTS

This research was supported by grant no. 14-31-001-3710 of the Water Resources Research Office of the Department of Interior. Dr. F. J. Pearson of the U. S. Geological Survey suggested the system to be studied and assisted in the sample collection. M. I. Kaufman made constructive suggestions regarding the manuscript; and Rosemary Raymond and Dennis Cassidy assisted in preparation of the figures.

This paper is based on a dissertation [43] submitted in partial fulfillment of the Ph.D. requirements at Florida State University, Tallahassee.

REFERENCES

[1] CHERDYNTSEV, V.V., CHALOV, P.I., KHAIDAROV, G.Z., Transactions of the 3rd Session of the Committee for Determination of Absolute Ages of Geological Formations, Izv. Akad. Nauk SSSR (1955) 175.

[2] ROSHOLT, J.N., GARNER, E.L., SHIELDS, W.R., Fractionation of Uranium Isotopes and Daughter Products in Weathered Granite and Uranium-Bearing Sandstone, Wind River Basin Region, Wyoming, US Geol. Survey, Prof. Paper 501-B (1964) B-84.

[3] BARANOV, V.I., SIRKOV, Y.A., VILENSKII, V.D., Isotopic shifts in natural uranium compounds, Geochem. Int. (1958) 591.

[4] ISABAEV, E.A., USATOV, E.P., CHERDYNTSEV, V.V., Isotopic composition of uranium in natural samples, Sov. Radiochem. 2 (1960) 97.

[5] ROSHOLT, J.N., HARSHMAN, E.M., SHIELDS, W.R., GARNER, E.L., Isotopic fractionation of uranium related to roll features in sandstone, Shirley Basin, Wyoming, Econ. Geol. 59 (1964) 570.

[6] CHERDYNTSEV, V.V., KAZACHEVSKII, I.V., KUZ'MINA, E.A., Isotopic composition of uranium and thorium in the supergene zone, Geochem. Int. (1963) 271.

[7] SYROMYATNIKOV, N.G., TOLMACHEV, I.I., Study of the isotopic ratio $^{234}U/^{238}U$ in aqueous extracts from uranium-phosphate-zirconium ores with consideration of their formation, Soviet At. Energy 13 (1962) 1333.

[8] DOE, B.R., NEWELL, M.F., Isotopic composition of uranium in zircon, Am. Mineral. 50 (1965) 613.

[9] ROSHOLT, J.N., DOE, B.R., TATSUMOTO, M., Evolution of the isotopic composition of uranium and thorium in soil profiles, Geol. Soc. Am., Bull. 77 (1966) 987.

[10] THURBER, D.L., Anomalous $^{234}U/^{238}U$ in nature, J. Geophys. Res. 67 (1962) 4518.

[11] KOIDE, M., GOLDBERG, E.D., "$^{234}U/^{238}U$ ratios in sea water", Progress in Oceanography 3 (SEARS, M., Ed.), Pergamon, Oxford (1965).

[12] KAZACHEVSKII, I.V., CHERDYNTSEV, V.V., KUZ'MINA, E.A., SULERZHITSKII, L.D., MOCHALOVA, V.F., KYUREGYAN, T.N., Isotopic composition of uranium and thorium in the supergene zone and in volcanic products (Natural waters and volcanic deposits), Geochem. Int. (1964) 1068.

[13] MOORE, W.S., Amazon and Mississippi River concentrations of uranium, thorium, and radium isotopes, Earth Planet. Sci. Lett. 2 (1967) 231.

[14] BHAT, S.G., KRISHNASWAMY, S., Isotopes of uranium and radium in Indian rivers, Proc. Indian Acad. Sci., Sect. A. LXIX I (1969) 1.

[15] THURBER, D.L., The concentrations of some natural radioelements in the waters of the Great Basin, Bull. Volcanol. 28 (1965) 195.

[16] SCOTT, M.R., Thorium and uranium concentrations and isotope ratios in river sediments, Earth Planet. Sci. Lett. 4 (1968) 245.

[17] KAUFMAN, M.I., RYDELL, H.S., OSMOND, J.K., $^{234}U/^{238}U$ disequilibrium as an aid to hydrologic study of the Floridan aquifer, J. Hydrol. 9 (1969) 374.

[18] OSMOND, J.K., RYDELL, H.S., KAUFMAN, M.I., Uranium disequilibrium in ground water: an isotope dilution approach in hydrologic investigations, Science 162 (1968) 997.

[19] RYDELL, H.S., Implications of Uranium Isotope Distributions associated with the Floridan Aquifer of North Florida, unpubl. PhD dissertation, 1969, Florida State University, Tallahassee, Florida, United States of America.

[20] OSMOND, J.K., KAUFMAN, M.I., COWART, J.B., Mixing volume calculations, sources and aging trends of the Floridan aquifer water by uranium isotope methods, Geochim. Cosmochim. Acta (1974) in press.

[21] BRIEL, L.I., An Application of the $^{234}U/^{238}U$ Disequilibrium in the Analysis of the Sources and Mixing Patterns of the Santa Fe River System of North Central Florida, unpubl. PhD dissertation, 1974, Florida State University, Tallahassee, Florida, United States of America.
[22] KRONFELD, J., Hydrologic Investigations and the Significance of $^{234}U/^{238}U$ Disequilibrium in the Ground Waters of Central Texas, unpubl. PhD dissertation, 1971, Rice University, Houston, Texas, United States of America.
[23] GORBUSHINA, L.V., TYMINSKI, V.G., SPIRIDONOV, A.I., Significance of radiohydrogeological anomalies in a seismically active area for predicting earthquakes, Int. Geol. Rev. 15 (1973) 380.
[24] CHERDYNTSEV, V.V., Uranium-234, Israel Program for Scientific Translations, Jerusalem (1971), a translation of Uran-234, Atomizdat, Moskva (1969).
[25] CHALOV, P.I., MERKULOVA, K.I., Comparative oxidation rates of U-234 and U-238 atoms in certain minerals, Dokl. Akad. Nauk SSSR 167 (1966) 146.
[26] ROSHOLT, J.N., BUTLER, A.P., GARNER, E.L., SHIELDS, W.R., Isotopic fractionation of uranium in sandstone, Powder River Basin, Wyoming and Slick Rock District, Colorado, Econ. Geol. 60 (1965) 199.
[27] KIGOSHI, K., Alpha recoil Th-234: dissolution in water and the U-234/U-238 disequilibrium in nature, Science 173 (1971) 47.
[28] LISITSIN, A.K., Form of occurrence of uranium in ground waters and conditions of its precipitation as UO_2, Geochem. Int. (1962) 876.
[29] HOSTETLER, P.B., GARRELS, R.M., Transportation and precipitation of uranium and vanadium at low temperatures, with special reference to sandstone-type uranium deposits, Econ. Geol. 57 (1962) 137.
[30] SHAWE, D.R., GRANGER, H.C., Uranium ore rolls – an analysis, Econ. Geol. 60 (1965) 240.
[31] LONSDALE, J.T., Geology and Ground-Water of Atascosa and Frio Counties, Texas, US Geol. Survey, Water Supply Paper 676 (1935).
[32] ALEXANDER, W.H., WHITE, D.E., Ground-Water Resources of Atascosa and Frio Counties, Texas, Texas Water Development Board, Rep. 32 (1966).
[33] HARRIS, H.B., Ground-Water Resources of LaSalle and McMullen Counties, Texas, Texas Water Commission, Bulletin 6520 (1965).
[34] PEARSON, F.J., WHITE, D.E., Carbon 14 ages and flow rates of water in Carrizo sand, Atascosa County, Texas, Water Resour. Res. 3 (1967) 251.
[35] VICKERS, R.C., Alteration of sandstone as a guide to uranium deposits and their origin, northern Black Hills, South Dakota, Econ. Geol. 52 (1957) 599.
[36] EVSEEVA, L.S., IVANOV, K.E., KOCHETKOV, V.I., Some laws of the formation of epigenetic uranium ores in sandstones, derived from experimental and radiochemical data, Soviet At. Energy 14 (1963) 492.
[37] KASHIRTSEVA, M.F., Mineral and geochemical zonation of infiltration uranium ores, Int. Geol. Rev. 9 (1967) 100.
[38] KIGOSHI, K., "Uranium 238/234 disequilibrium and age of underground water", Interpretation of Uranium Isotope Disequilibrium as a Natural Hydrological Tracer, IAEA Panel Meeting, Vienna, 5-9 March 1973 (unpublished).
[39] SYROMYATNIKOV, N.G., Interphase isotopic exchange of ^{234}U and ^{238}U, Geochem. Int. (1960) 320.
[40] ROSHOLT, J.N., TATSUMOTO, M., DOOLEY, J.R., Radioactive disequilibrium studies in sandstone, Powder River Basin, Wyoming, and Slick Rock District, Colorado, Econ. Geol. 60 (1965) 477.
[41] FLINT, R.F., Glacial and Quaternary Geology, Wiley, New York (1971).
[42] BROECKER, W.S., "Isotope Geochemistry and the Pleistocene Climatic Record", The Quaternary of the United States (WRIGHT, H.E., Jr., FREY, D.G., Eds), Princeton University Press, Princeton, N.J. (1965).
[43] COWART, J.B., ^{234}U and ^{238}U in the Carrizo Sandstone Aquifer of South Texas, unpubl. PhD dissertation, 1974, Florida State University, Tallahassee, Florida, United States of America.

DISCUSSION

K. PRZEWŁOCKI: The assumption that there must exist within an aquifer a location with a higher uranium concentration is, in my opinion, an oversimplification. For his model of ^{234}U leaching from rocks, Kigoshi assumed that the ^{234}U excess was proportional to the concentration of uranium in the rocks, the contact surface and the contact time. I therefore think it is more appropriate to assume a low but uniform uranium concentration rather than local enrichment. Would you care to comment on this point?

J. B. COWART: The model presented in our paper, in which the input of ^{234}Th is mostly localized, applies to areas such as those in Texas and Wyoming where distinct uranium accumulations in sandstone are known to occur. In a carbonate aquifer in Florida, locations have been found which have overlying water with an activity ratio of less than one and water from a lower zone, perhaps 75 m below the surface, with an activity ratio of about five. In such a system, a well-defined zone of uranium accumulation probably does not occur.

R. COPPENS: May the transition from ^{238}U to ^{234}U via ^{234}Th not automatically cause $^{234}U/^{238}U$ disequilibrium, because of the low solubility of ^{234}Th and in spite of its short half-life?

J. B. COWART: Disequilibrium occurs only if the ^{234}Th or the ^{234}U is separated from the parent system. If the $^{234}U/^{238}U$ disequilibrium does occur, as it does, then it occurs despite the low solubility of thorium rather than because of it in cases where the ^{238}U was originally in a solid.

J. A. P. SARROT-REYNAULD: In what form is the uranium present in the water of the sandstone aquifer and what anions are present?

J. B. COWART: The uranium is most likely present in the form of uranyl-dicarbonate and -tricarbonate. In the outcrop region, HCO_3^- and SO_4^{2-} are present to a few tens of ppm. The chloride concentration is low. In the downdip region, the concentration of these anions increases to 500 ppm or more.

J. A. P. SARROT-REYNAULD: Do bacteria participate in reduction reactions and cause isotopic fractionation?

J. B. COWART: Bacteria may play a role in the development of the reducing zone, but no direct role in the fractionation of the ^{234}U and ^{238}U (otherwise the ^{235}U would also be fractionated).

$^{234}U/^{238}U$ DISEQUILIBRIUM IN WATERS OF THE JUDEA GROUP (CENOMANIAN-TURONIAN) AQUIFER IN GALILEE, NORTHERN ISRAEL

E. WAKSHAL
Groundwater Research Center,
School of Applied Science and Technology,
The Hebrew University of Jerusalem,
Jerusalem

F. YARON
Israel Atomic Energy Commission,
Nuclear Research Center, Negev,
Israel

Abstract

$^{234}U/^{238}U$ DISEQUILIBRIUM IN WATERS OF THE JUDEA GROUP (CENOMANIAN-TURONIAN) AQUIFER IN GALILEE, NORTHERN ISRAEL.

Analysis of $^{234}U/^{238}U$ activity ratios and uranium concentrations were carried out on samples from 60 water sources of the Judea Group (Cenomanian -Turonian) carbonate aquifer of Galilee, northern Israel. The $^{234}U/^{238}U$ activity ratios were found to vary from 1.04 to 2.81, and successive analyses of selected water sources showed that values from the same sampling sites remained consistent over a three-year period (1970-73). The recorded values of the $^{234}U/^{238}U$ activity ratio may be grouped into three main clusters clearly related to the paleohydrological evolution of the area under consideration: (a) Low $^{234}U/^{238}U$ activity ratios ranging from 1.04 to 1.72 (the majority not exceeding 1.55) were reported from the water sources of western Upper Galilee. This area is drained into the Mediterranean, and its meteoric groundwater circulation regime is as old as the Neogene. (b) Intermediate $^{234}U/^{238}U$ activity ratios (1.65 - 1.93) are common among the water sources of the Pleistocene Jordan Rift Valley catchment area. (c) Higher $^{234}U/^{238}U$ activity ratios, ranging in general from 1.9 to 2.8, were found in the water sources of the Lower Galilee, where there has been renewed active groundwater circulation both eastward and westward caused by the latest subsidence of the Jordan Rift Valley and the Mediterranean Young Pleistocene Sea Regression. These results point to the possibility that the mechanism of uranium isotope fractionation within this type of aquifer is basically governed by the solid rock-freshwater flow contact history. Further information gained by such studies might be useful in developing a better hydrogeological model for the groundwater flow regime within carbonate aquifers.

1. INTRODUCTION

Because of their world-wide distribution and good reservoir qualities, carbonate aquifers play an important role in hydrological cycles. Lithologically they consist of limestone, dolomite and chalk, all of which may contain varying percentages of insoluble residue.

The water-bearing properties of carbonate aquifers are determined by different genetic factors: mineralogy and sedimentary textures, solution and diagenesis, tectonic structure and degree of fissuring. A general classification of such features is given by Choquette and Pray [1], relating them to time criteria as follows: Primary porosity (pre-depositional and depositional porosity) and secondary porosity (post-depositional porosity). Using a

descriptive approach, carbonate reservoirs may be described in terms of three broad categories of porosity systems: intercrystalline-intergranular, fracture and vugular-solution.

In studying the evolution of the hydrological regime within a given carbonate aquifer, any source of direct information on the system is of great value. Despite the important paleohydrological applications of techniques utilizing stable and radioactive isotopes (such as ^{18}O, D, ^{34}S, ^{14}C, ^{3}H) within the water, difficulties arise in the common situation where the age of the liquid-solid contact in the aquifer is much greater than the age of the water itself. In such cases, the most useful information would be in the form of measurable changes in the chemical composition of the water resulting from known processes occurring during contact with the conduit rock. That is, the sign of the liquid-conduit memory must be transmitted to and by the water in a manner which can be quantitatively analysed. Such investigations in circulating carbonate aquiferous systems could be carried out by analysing the $^{234}U/^{238}U$ radioactive disequilibrium [2-4].

The aim of the present research is to study the karst evolution of carbonate aquifers using the $^{234}U/^{238}U$ disequilibrium as the memory carrier for the history of groundwater flow within existing hydrological basins.

As a case history for this approach, the Judea Group Cenomanian-Turonian aquifer of Galilee, northern Israel, was selected. A detailed comparison was carried out between the radiochemical results obtained and the regional geological evolution, which has been intensively investigated. These data were recently reviewed by Freund [5, 6], Horowitz [7], Picard [8], Schulman [9] and Schulman and Weiler [10].

2. HYDROLOGICAL FRAMEWORK OF GALILEE

2.1. Geological background

The Galilee is a mountainous terrain bounded by the Mediterranean coastal plain on the west, inland structural depressions to the south (Kishon, Esdraelon, Harod and Beit Shean), and the Hula-Jordan Rift Valley on the east. Northwards Galilee merges with the Lebanon Mountains (Fig. 1).

Physiographically, Galilee is divided into two sub-units along a transversal fault line facing southwards: Upper Galilee, reaching a maximum elevation of 1208 m above mean sea level (Mt. Meron), and Lower Galilee, ranging in elevation from 600 m above mean sea level down to -260 m south of Lake Kinneret. The area is considered as varying from rainy to semi-arid, with the highest annual precipitation of 1000 mm in central Upper Galilee. In Lower Galilee the precipitation values decrease to an average of 400 mm yearly (Fig. 1).

The exposed rock sequence [11] ranges in age from Early Cretaceous up to Recent (Fig. 2). Most of the section, excepting its basal and uppermost parts, is dominated by marine carbonate accumulations, as indicated in Table I. The oldest outcrops are Lower Cretaceous sandstone, shale, marl and shaley limestone, reaching a total thickness of 450 m. The Cenomanian-Turonian strata overlying it (700 m thick) form the Judea Group, consisting of the following formations [12]:

Mount Scopus Group (Senonian-Paleocene)

Judea Group:
- Sakhnin Dolomite and Bina Formation: 300 m of hard dolomite and limestone
- Deir Hana Formation: 200 m of soft chalk and chert with some dolomite and limestone
- Kamon Dolomite: 200 m of well-bedded hard dolomite

Kurnub Group (Lower Cretaceous)

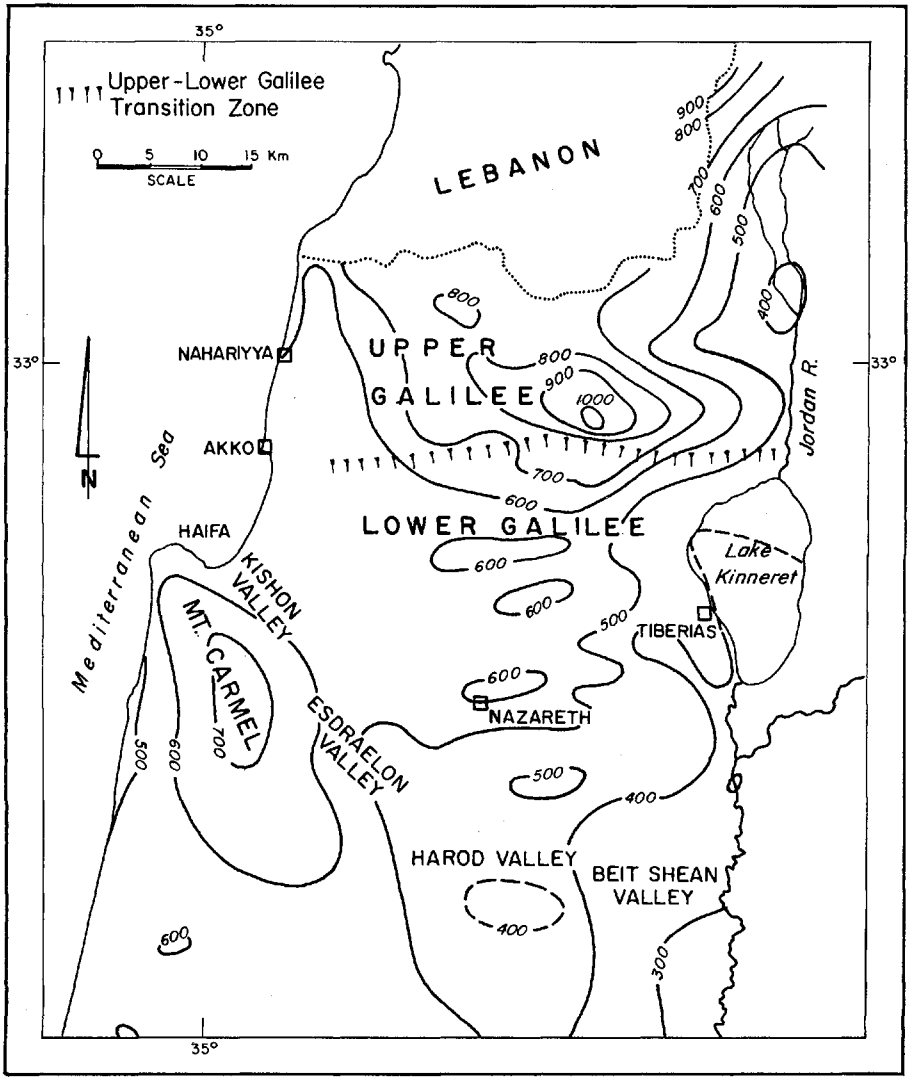

FIG.1. Average annual rainfall (mm), 1931-60, in the area studied.

TABLE I. LITHO-HYDROSTRATIGRAPHIC UNITS

Time unit	Time-rock unit		Lithology	Average thickness (m)	Hydrostratigraphic units	Transmissibility ranges[a] (m^2/day)
	Group	Formation				
Neogene-Pleistocene			Sand, conglomerates, marl, clay and limestone; basalts	0 - 800	Basalts and coastal sands — aquifers	
Eocene	Avedat		Chalk and limestone	600	Aquitard or aquiclude. In eastern Galilee — aquifer	
Senonian - Paleocene	Mount Scopus		Chalk and soft limestone	400	Aquiclude	
Turonian	Judea	Bina Formation	Bedded limestone and dolomite	100	Aquifer (JG - UAU)	15 900 - 94 000 (western Lower Galilee)
Cenomanian		Sakhnin Dolomite	Hard dolomite	200		
		Deir Hana Formation	Soft chalk with some dolomite and limestone	200	Aquiclude Rarely aquitard	
		Kamon Dolomite	Hard dolomite	200	Aquifer (JG-LAU)	126 - 3220 (western Upper Galilee)
Lower Cretaceous	Kurnub		Shaley sand and marley limestone	450	Aquiclude	

[a] Values are presented according to interference tests only.

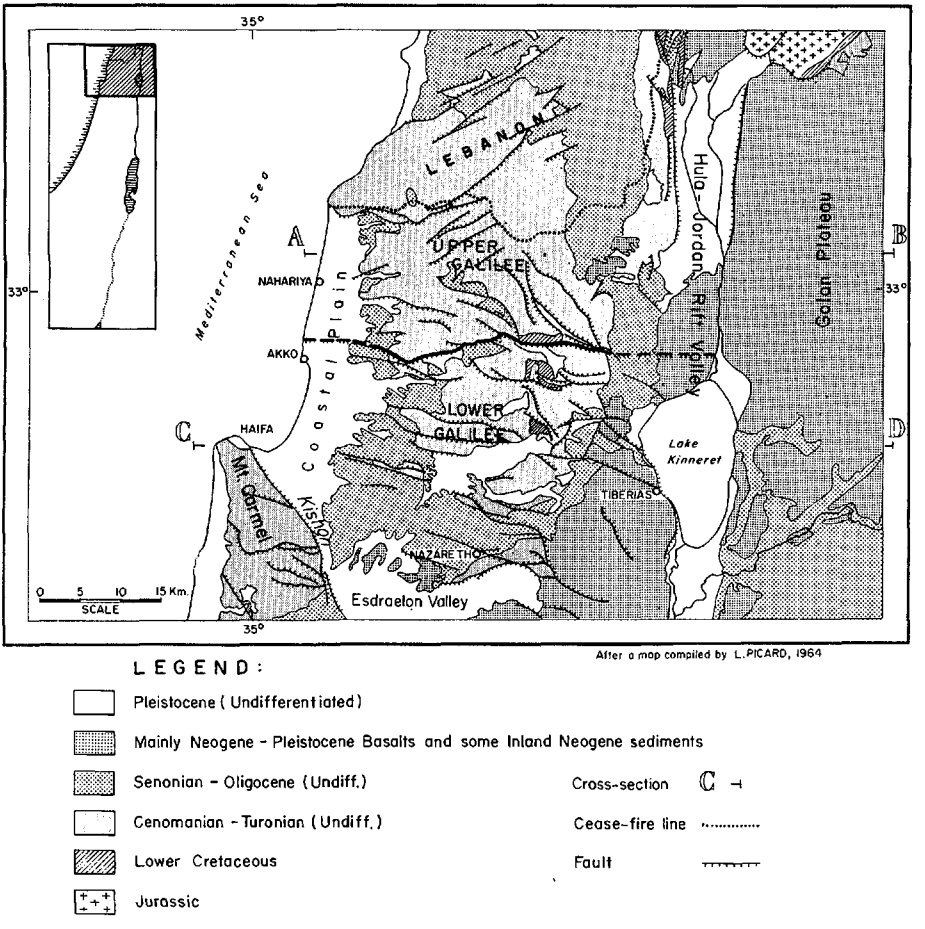

FIG. 2. Geological map of northern Israel.

The Senonian-Eocene-Oligocene sequence above the Judea Group — about 1000 m thick — is mostly a continuous sedimentation of soft chalk and limestone. Towards the Upper Eocene, and in places even during the Middle Eocene, the present mountainous area had already emerged above sea level, starting a new regional erosion (peneplanation) as well as accumulation cycle.

Because of this emergence, the Neogene strata are almost completely restricted in their distribution to the Coastal Plain, and to inland depressions and basins where intermittent shallow marine connection took place. These strata are composed of clastics, marls and detrital limestone of marine to fresh-water facies. Volcanic flows of alkaline olivine basalt, ranging in age from Miocene to Lower Pleistocene, and reaching a thickness of up to several hundreds of metres, cover an appreciable area within eastern Galilee and the Golan Plateau.

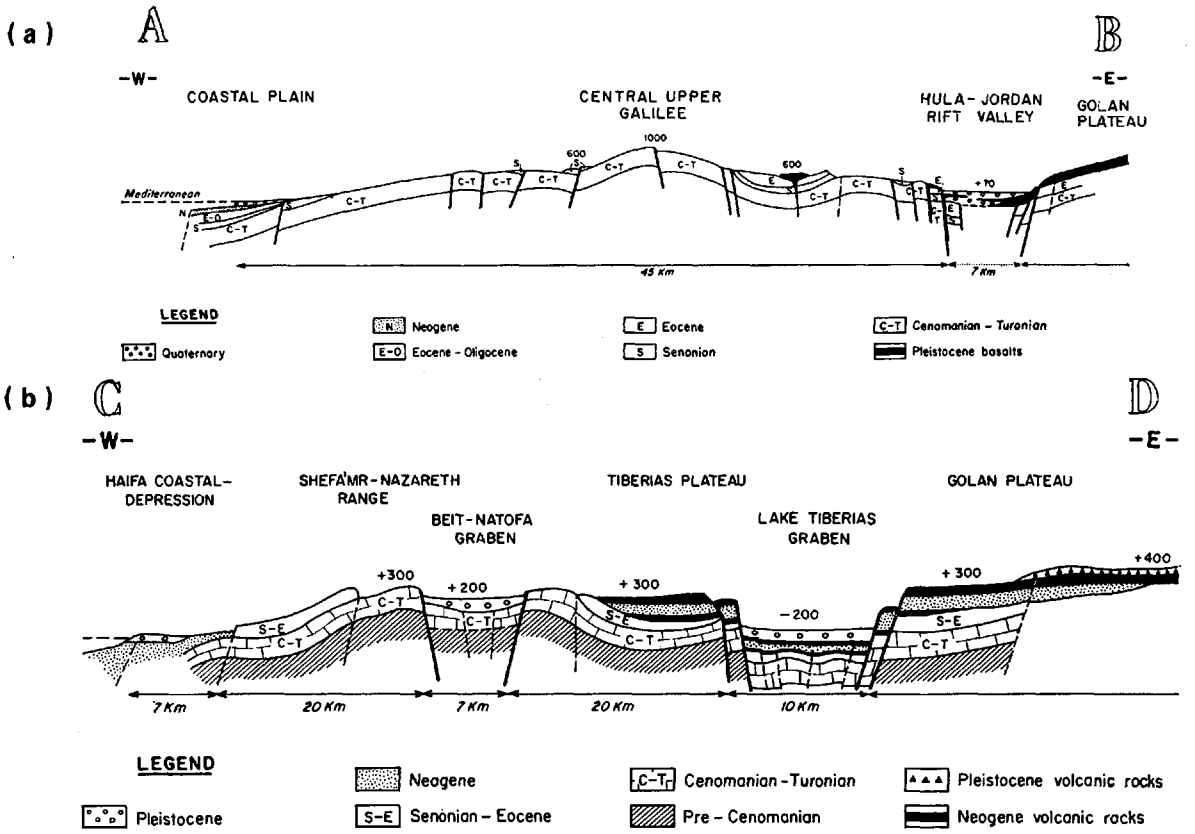

FIG. 3. (a) Cross-section through northern Galilee, the Hula depression and the Hauran plateau, showing stratigraphy and structure.
(b) Cross-section through southern Galilee, the Lake Tiberias depression and the Golan plateau, showing stratigraphy and structure.

The Quaternary deposits of the Coastal Plain average 90 m in thickness, and consist of gravel and sandstone with interbedded alluvial terra rossa. Along the Jordan Rift Valley the Quaternary is characterized by continuous subsidence and accumulation of fluviatile-limnic sediments as well as renewed small-scale volcanic activity yielding a fill more than 1.7 km thick.

The tectonic pattern of Galilee is presented in the geological cross-sections of Fig. 3. Anticlinal and synclinal axes generally trend in the NE-SW direction. The major folding phase took place during the Post-Middle Eocene — Pre-Neogene period, although earlier slight movements can also be recognized in the Late Cretaceous and Early Tertiary.

The original folding structure of Galilee is now largely masked by the intensive faulting activity which dominates the present structure of the area. Such faulting phases can be traced during the Neogene (Miocene), Neogene (Pliocene)-Pleistocene transition and the Middle Pleistocene [9].

These faults may be grouped schematically according to the following orientations:

(a) East-west faults and diagonal faults of NW-SE and NE-SW trends. Many of these faults were active and rejuvenated during the various successive taphrogenic phases.

(b) The north-south Jordan Rift Valley (= Graben) trend of Pleistocene age.

This lithological and structural description of Galilee might be summarized by the following generalized evolutional sequence (Fig. 4):

(a) Continuous marine cover (Tethys) from the Lower Cretaceous transgression until the Pre-Neogene (Late Eocene — Oligocene) land emergence and sea regression (approximately 30 million years ago).

(b) Continental erosion and peneplanation of the mountainous backbone, with the Mediterranean constituting the sole base level.

(c) Taphrogenic activity yielding the intermittent Inland Neogene Basins.

(d) Taphrogenic activity of Middle Pleistocene (about 0.9-0.5 million years ago) forming two independent erosional base levels as well as the catchment areas of the Mediterranean and the Jordan-Dead Sea Rift Valley.

2.2. The hydrological regime

The Judea Group aquifer is a well-developed karstic system forming the major source of water within the replenishment area of Galilee [13-19]. The aquifer is bordered at its base and top by impermeable strata of Lower Cretaceous and Senonian ages respectively. Because of the poor water-bearing properties of the Deir Hana Formation, the Judea Group is divided into two sub-aquifers: The lower aquiferous unit (JG-LAU) of the Kamon Dolomite, and the upper aquiferous unit (JG-UAU) of the Sakhnin Dolomite and the Bina Formation.

The flow regime at the replenishment area is phreatic, whereas downstream either confined flow (with confining pressure up to 50 atm) or phreatic conditions may prevail.

Springs form the natural outlets of the system, and yield a total of about 150×10^6 m^3 yearly [20]. In addition, the aquifer is exploited by wells, with an annual pumpage of 130×10^6 m^3. Several studies indicate that further flow takes place at the subsurface towards the two base levels, reaching the Mediterranean and Lake Kinneret as submarine springs. The groundwater divide between these basins follows in general the upward and folding axis where the impervious Lower Cretaceous strata are at their highest structural elevation.

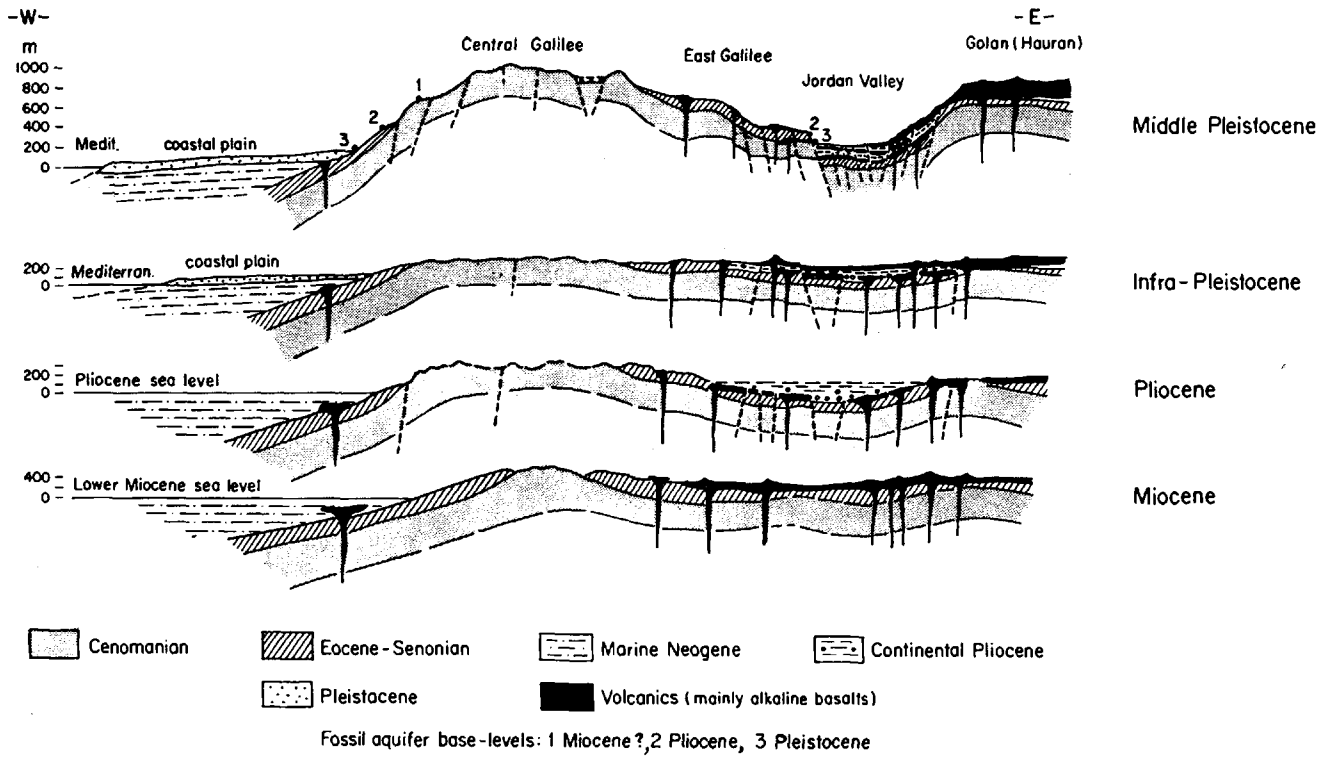

FIG.4. Diagram illustrating the evolutionary stages from Miocene to Pleistocene in the Levant sector between the Mediterranean, Galilee and the Hauran.

A water level map of the various Cenomanian-Turonian water sources is presented in Fig. 5. It shows two different hydrodynamic regions in accordance with the structural-morphological subdivision between Lower and Upper Galilee. Whereas gradients of about 2° prevail within the uplifted Upper Galilee in both the eastern and western drainage directions, Lower Galilee is dominated by flat potentiometric surfaces.

In regard to the chemical quality of the sampled sources (Table III), the chlorinity varies from 18 to 274 mg/litre Cl^-, with prominent enrichment (580 mg/litre Cl^-) observed in sources Nos 211 and 213.

3. URANIUM DISEQUILIBRIUM IN NATURAL WATERS AND MODE OF FRACTIONATION

The geochemistry of uranium has been intensively investigated and most of these data have been recently reviewed by Adams, Osmond and Cowart [21], Cherdyntsev [22], Kolodny [23], and Rogers and Adams [24]. Only a few basic considerations concerning its occurrence and isotopic distribution will be discussed briefly here.

The flow of meteoric water in carbonate aquifers is characterized by the solution and leaching of the rock. The hydrochemical process of the solution models in carbonate aquifers may be presented schematically according to the following reactions governed by both environmental and kinetic factors [25, 26]:

$$CO_2(\text{gas in air}) + H_2O \rightleftharpoons \underset{\text{(dissolved in water)}}{H_2CO_3} \rightleftharpoons H_2O + CO_2$$

$$CaCO_3 + H_2CO_3 \rightleftharpoons Ca^{+2} + 2HCO_3^-$$

$$CaMg(CO_3)_2 + 2H_2CO_3 \rightleftharpoons Ca^{+2} + Mg^{+2} + 4HCO_3^-$$

Groundwater flow is accompanied by removal of uranium from the surface layer of the crystals at the conduits of the carbonate aquifer. In carbonate rocks, uranium concentrations average 2 ppm [24], with most of the uranium substituting for Ca^{+2} ions within the carbonate mineral crystallographic lattice. To a lesser extent (about 20%), the uranium might follow thorium in the insoluble residue content. Of the two stable oxidation states of uranium in nature, U(IV) (uranous) and U(VI) (uranyl), the latter is much more soluble, forming in the presence of CO_3^{2-} and a pH range between 6 and 9, the uranyl non-polymeric complexes $UO_2(CO_3)_2(H_2O)_2^{-2}$ and $UO_2(CO_3)_3^{-4}$. Since the transition from U(IV) to U(VI) has an oxidation potential within the normal range of the common geological environment, one expects to find naturally occurring compounds of these valences [27].

Because of the appreciable difference in the life of the parent and daughter within the ^{234}U- ^{238}U pair, secular equilibrium ($A^{234}U/A^{238}U = 1$,

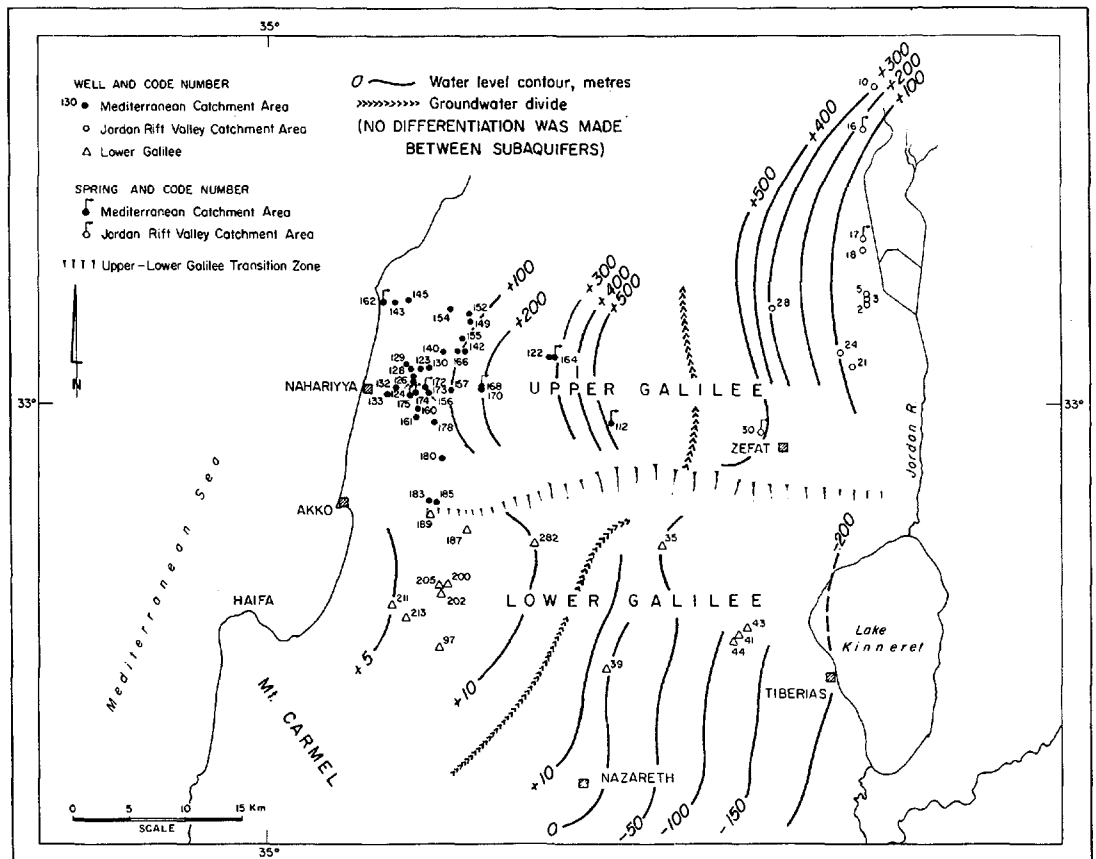

FIG.5. Generalized map of water levels in the Judea Group aquifer, Galilee.

where A = alpha activity) should exist between the two isotopes in closed systems older than 1 million years, according to the radioactive decay series:

$$^{238}U \xrightarrow[\alpha]{4.51 \times 10^9 \text{ year}} {}^{234}Th \xrightarrow[\beta]{24.1 \text{ day}} {}^{234}Pa \xrightarrow[\beta]{1.175 \text{ min}}$$

$$^{234}U \xrightarrow[\alpha]{2.48 \times 10^5 \text{ year}}$$

Cherdyntsev and co-workers [2] were the first to detect an excess of $A^{234}U$ over $A^{238}U$ in some systems of uranium minerals, pointing to selective migration of these two isotopes under certain geological environments. Such disequilibrium was later confirmed by several others [22] as taking place in various lithological and mineralogical associations where ^{234}U is preferentially leached by the circulating aquatic phase, yielding, finally, in ocean water, the activity ratio of $^{234}U/^{238}U = 1.15$.

Several models have been proposed for the mode of $^{234}U/^{238}U$ fractionation. Whereas there exists a general agreement among the various hypotheses that during the $^{238}U \rightarrow {}^{234}U$ transition, in the tetravalent U phase, ^{234}U is more favourably oxidized into the highly soluble uranyl ion than the parent ^{238}U, the exact mechanism is still controversial.

Cherdyntsev and co-workers [2] relate the fractionation to ^{234}U re-location by recoil and radiation damage resulting in crystal defects and micro-fractures. At these sites the daughter ^{234}U is more exposed to the oxidizing agents than the parent ^{238}U. Thus, the higher $^{234}U/^{238}U$ activity ratio should be expected in association with the more oxidizing environment [28].

Rosholt and co-workers [29, 30] and Dooley and co-workers [31] assume that the recoil energy of alpha decay is sufficient to break the chemical bonds of uranium and to strip it of two electrons. Following such a transformation, the ^{234}U preferentially attains the soluble VI valence compared with the tetravalent ^{238}U. According to this electron-stripping mechanism, fractionation of ^{234}U takes place due to the more oxidized state from the time of transition, and no oxidizing agent is essential.

Kolodny and Kaplan [32] indicate the possibility that the increasing oxidation of U(IV) to U(VI) during the radioactive transformation $^{238}U \rightarrow {}^{234}U$ may be the result of an increase in positive charge of the ions caused by beta decay.

Kigoshi [33] proposed that the main source of ^{234}U excess in groundwater is alpha recoil ^{234}Th ($T_{\frac{1}{2}} = 24.1$ d) originating from the solid surface of sand or clay. Thus, the excess ^{234}U in groundwater should be directly related to both the surface area of the rock (porosity) and the age of the water.

The general scheme relating ^{234}U enrichment to the decay and oxidation process [4, 28, 32] indicates the enhanced solubility of the ^{234}U (IV) from the solid rock in open systems where weathering activity and water circulation prevail. Good agreement was found in the few studies estimating the fraction R of radiogenic ^{234}U which is oxidized during radioactive decay. Rydell [4], investigating the Floridan carbonate aquifer, recorded a value of 0.35. Analysis of marine phosphorites by Kolodny and Kaplan [32] yielded a value of 0.3, and the same researchers later similarly interpreted analytical observations on pelagic sediment by Ku [34].

TABLE II. $^{234}U/^{238}U$ ACTIVITY RATIO, URANIUM CONCENTRATION AND INSOLUBLE RESIDUE PERCENTAGE IN ROCK SAMPLES OF THE JUDEA GROUP

No. of rock sample	$^{234}U/^{238}U$ activity ratio	U concentration (ppm)		Insoluble residue (%)	Remarks
		Delayed neutron activation analysis[a]	Alpha spectrometry		
W.R. 50	-	3.00 ± 0.10	-	0.4	Core, 670 m depth
W.R. 52	-	0.70 ± 0.10	-	0.8	Core, 624 m depth
W.R. 57	-	1.39 ± 0.21	-	1.7	Core, 243 m depth
W.R. 60	1.02 ± 0.04	4.77 ± 0.36	4.13 ± 0.30	1.3	Core, 737 m depth
W.R. 61	0.96 ± 0.03	2.51 ± 0.13	2.62 ± 0.15	2.7	Core, 911 m depth
W.R. 62	-	1.28 ± 0.06	-	0.8	Core, 484 m depth
W.R. 63	0.91 ± 0.03	2.14 ± 0.11	1.77 ± 0.15	9.0	Core, 546 m depth
W.R. 65	-	1.26 ± 0.04	-	0.5	Core, 392 m depth
W.R. 66	0.97 ± 0.04	4.44 ± 0.13	4.52 ± 0.40	0.9	Core, 782 m depth
W.R. 69	-	1.51 ± 0.08	-	0.3	Core, 269 m depth
W.R. 70	-	1.56 ± 0.16	-	0.2	Core, 171 m depth
W.R. 71	-	3.18 ± 0.10	-	0.4	Core, 734 m depth
W.R. 72	-	3.03 ± 0.12	-	12.0	Core, 546 m depth
W.R. 77	-	1.80 ± 0.09	-	1.5	Core, 392 m depth
W.R. 81	-	1.79 ± 0.09	-	0.9	Outcrop
W.R. 82	-	1.71 ± 0.17	-	0.3	Outcrop
W.R. 84	-	0.74 ± 0.13	-	17.9	Outcrop
W.R. 86	-	2.50 ± 0.08	-	0.3	Outcrop
W.R. 87	-	0.79 ± 0.10	-	3.3	Outcrop

[a] Analyses carried out at the Soreq Nuclear Research Center, Yavne, Israel.

4. URANIUM ISOTOPE DISTRIBUTION IN THE JUDEA GROUP AQUIFER OF GALILEE

4.1. Rock analyses

Uranium concentration in the rocks of the aquifer were analysed in 19 samples collected from outcrops and drill cores located over the entire area under investigation (Table II). The analytical method used was the delayed neutron activation technique [35]. The observed range of uranium concentration is 0.7 - 4.8 ppm; most of the results are between 1.5 and 3.0 ppm. This is in accordance with the values reported for other carbonate terrains [24], but is definitely lower than the values recorded in some of the aquifers of Florida, United States of America [4]. No correlation could be established between the concentration of uranium and the percentage of insoluble residue (0.1 - 18%) of the specimens, thus indicating that the major distribution of the uranium in this lithology is in the carbonate mineral lattice phase of the rock.

The $^{234}U/^{238}U$ activity ratio of the rock has been analysed in four samples only, although further analyses are currently being prepared. In three of the four analyses available, the activity ratio approaches 1 (samples W. R. 60, 61 and 66), whereas in the fourth sample (W. R. 63) it is 0.91 ± 0.03.

4.2. Water samples

A systematic study and analysis of the various water sources in the area being researched was begun in the summer of 1970 and is still going on. During this period analyses of 60 springs and wells were performed to determine the uranium concentration and $^{234}U/^{238}U$ activity ratios using the alpha-spectrometry method (Appendix).

The results obtained, including the relevant hydrogeological data, are presented in Table III. A location map of the sampling sites is given in Fig. 6.

In five of the water sources (Code Nos 2, 5, 10, 28 and 130) repeated analyses were carried out (Table IV). They indicated a fair consistency regarding the $^{234}U/^{238}U$ activity ratio of the successive results, with the exception of a small discrepancy in water source No. 130.

The uranium concentration in some of these determinations showed variations (such as source Code No. 10), while in the case of Enan 5 well (source Code No. 5) uniform values were obtained.

The constant activity ratios along these sampled intervals indicate that the $^{234}U/^{238}U$ activity ratio constitutes a typical radioisotopic parameter for a hydrologically defined water source, in agreement with previous findings of Chalov and co-workers [36] in Soviet Asia and Rydell [4] in Florida, United States of America. However, as will be discussed below, such periodic reproducibility of the $^{234}U/^{238}U$ activity ratio of a particular water source is restricted to those cases in which no sudden change occurs in the structure of the aquifer, e. g. earthquake fractures [37]. As to the changes in the concentration of uranium dissolved in water which could also be observed in the two studies mentioned above [4, 36], additional research is essential for clarifying the phenomena.

TABLE III. $^{234}U/^{238}U$ ACTIVITY RATIO AND URANIUM CONCENTRATION IN THE JUDEA GROUP (CENOMANIAN-TURONIAN) WATER SOURCES IN GALILEE, NORTHERN ISRAEL

Source Code No.	Source name	Date of sampling	$^{234}U/^{238}U$ activity ratio	U (mg/litre)	Ca (mg/litre)	Cl (mg/litre)	Hydrogeological remarks	
	UPPER GALILEE, MEDITERRANEAN CATCHMENT AREA							
112	En Tiriyya spring	19. 7.1973	1.14 ± 0.05	0.75 ± 0.04	-	-	JG-UAU	Approximate yield: 10 m^3/h
122	Rosh Hamabbua No.2 well	14.10.1971	1.72 ± 0.07	0.85 ± 0.05	88	24	JG-LAU	Phreatic
123	Kabri: well No. 1	6.10.1970	1.04 ± 0.05	2.12 ± 0.15	97	49	JG-UAU	Phreatic
124	Kabri: well No. 2	6.10.1970	1.40 ± 0.05	-	93	31	JG-UAU	Phreatic
126	Kabri: well No. 4	6.10.1970	1.27 ± 0.07[a]	0.58 ± 0.05	100	51	JG-UAU	Phreatic
128	Kabri: well No. 6	6.10.1970	1.23 ± 0.10	0.65 ± 0.06	100	68	JG-UAU	
129	Kabri: well No. 7	6.10.1970	1.30 ± 0.10[a]	0.55 ± 0.05	106	90	JG-UAU	Confined
130	Kabri: well No. 8	17. 8.1971	1.30 ± 0.04	1.68 ± 0.05	-	23	JG-LAU	Confined
132	Kabri: well No.15	19. 8.1971	1.56 ± 0.03	1.81 ± 0.11	93	22	JG-LAU	Confined
133	Kabri: well No.16	23. 8.1971	1.12 ± 0.03	2.14 ± 0.07	92	26	JG-LAU	Confined
140	Nahal Qeren well No. 3	22.10.1971	1.45 ± 0.05	1.37 ± 0.05	90	23	JG-LAU	Confined
142	well No. 5	21.10.1971	1.34 ± 0.03	1.71 ± 0.08	87	23	JG-LAU	Confined
143	Rosh Haniqra well	23. 8.1971	1.57 ± 0.03	1.22 ± 0.05	98	109	JG-LAU	Phreatic
145	Shelomi well No.1	7.10.1971	1.61 ± 0.04	1.19 ± 0.05	87	49	JG-LAU	Confined
149	Yaara: well No.1	26. 8.1971	1.44 ± 0.03	1.37 ± 0.06	91	23	JG-LAU	Confined
152	well No.4	7.10.1971	1.48 ± 0.04	1.13 ± 0.05	91	24	JG-LAU	Confined
154	well No.6	7.10.1971	1.43 ± 0.03	1.46 ± 0.05	92	23	JG-LAU	Confined
155	Avdon: well No.1	31. 8.1971	1.37 ± 0.04	1.33 ± 0.06	92	23	JG-LAU	Confined
156	Gaaton well No.1	12.10.1970	1.40 ± 0.09[a]	0.46 ± 0.03	80	27	JG-UAU	
157	Gaaton well No.2	23. 8.1971	1.67 ± 0.02	1.51 ± 0.05	-	-	JG-LAU	Confined
160	Dove well No.1	12.10.1970	1.53 ± 0.14	0.85 ± 0.10	101	36	JG-UAU	Confined
161	Dove well No.2	12.10.1970	1.31 ± 0.07	0.82 ± 0.06	111	41	JG-UAU	Confined

TABLE III. (cont.)

	UPPER GALILEE, MEDITERRANEAN CATCHMENT AREA							
								Average annual yield = AAY[b]
162	En Misrafot spr.	25. 8.1971	1.52 ± 0.03	1.35 ± 0.05	91	43	JG-LAU	AAY 926 × 10^3 m^3
164	En Ziv spr.	16.10.1971	1.37 ± 0.04	1.00 ± 0.05	102	23	JG-UAU	AAY 3750 × 10^3 m^3
166	En Hardalit spr.	22.10.1971	1.35 ± 0.04	0.79 ± 0.05	72	28	JG-UAU	AAY 3270 × 10^3 m^3
168	Gaaton (Anqalit) spr.	21.10.1971	1.36 ± 0.03	1.00 ± 0.05	87	22	JG-UAU	AAY 3190 × 10^3 m^3
170	Gaaton (Tina) spr.	21.10.1971	1.26 ± 0.03	1.01 ± 0.05	88	22	JG-UAU	
172	En Zuf spr.	26. 8.1971	1.24 ± 0.05	1.00 ± 0.05	-	24	JG-UAU	AAY 1540 × 10^3 m^3
173	En Hashayara spr.	25. 8.1971	1.28 ± 0.10	1.09 ± 0.06	88	25	JG-UAU	AAY 1540 × 10^3 m^3
174	En Giah spr.	19.10.1971	1.33 ± 0.05	0.93 ± 0.05	90	23	JG-UAU	AAY 891 × 10^3 m^3
175	En Shefa spr.	19.10.1971	1.34 ± 0.03	0.98 ± 0.05	90	22	JG-UAU	AAY 4550 × 10^3 m^3
178	Amqa No.3 well	30. 9.1971	1.53 ± 0.03	1.66 ± 0.06	-	24	JG-LAU	Confined
180	Kfar Yasif No.1 well	17. 8.1971	1.35 ± 0.03	1.05 ± 0.03	89	33	JG-UAU	Confined
183	Akko No.2 well	4.10.1970	1.44 ± 0.7[a]	0.55 ± 0.03	84	56	JG-UAU	Confined
185	Akko No.4 well	4.10.1970	1.40 ± 0.08	0.57 ± 0.05	80	38	JG-UAU	Confined
	UPPER GALILEE, JORDAN RIFT VALLEY CATCHMENT AREA							
2	Enan No.2 well	12. 7.1973	1.76 ± 0.05	1.14 ± 0.06	-	-	JG-UAU	Phreatic
3	Enan No.3 well	14. 8.1970	1.80 ± 0.10	0.92 ± 0.06	61	24	JG-UAU	Phreatic
5	Enan No.5 well	14. 8.1970	1.72 ± 0.11	1.04 ± 0.08	64	23	JG-UAU	Phreatic
10	Hula No.3 well	19. 8.1970	1.91 ± 0.16	0.82 ± 0.08	-	18	JG-UAU	Phreatic
16	En Zahav spr.	19. 8.1970	1.93 ± 0.15	0.45 ± 0.03	69	20	Probably Judea Group aquifer	AAY 4060 × 10^3 m^3
17	En Teo spr.	9. 8.1971	1.73 ± 0.04	1.18 ± 0.05	69	27	JG-LAU	AAY 4490 × 10^3 m^3
18	Jahula well	10. 8.1971	1.71 ± 0.03	1.07 ± 0.05	71	27	JG-LAU	Phreatic
21	Tel Hazor well No.1	10. 8.1971	1.65 ± 0.04	1.48 ± 0.05	68	26	JG-UAU	Phreatic
24	Hindaj well No.2	24. 8.1970	1.85 ± 0.12[a]	1.13 ± 0.09	74	24	JG-UAU	Phreatic
28	Bir Ubba well No.1	27. 8.1970	1.77 ± 0.11[a]	1.05 ± 0.10	76	28	JG-UAU	Confined
30	En Poem spr.	30. 8.1970	1.20 ± 0.10[a]	0.75 ± 0.06	-	23	JG-UAU	AAY 1430 × 10^3 m^3

TABLE III. (cont.)

Source Code No.	Source name	Date of sampling	$^{234}U/^{238}U$ activity ratio	U (mg/litre)	Ca (mg/litre)	Cl (mg/litre)	Hydrogeological remarks	
	LOWER GALILEE							
35	Hazon well No.2	25. 8.1970	2.05 ± 0.09	1.55 ± 0.10	-	35	JG-LAU	Phreatic
39	Netofa well No.1	1. 9.1970	2.69 ± 0.12	1.48 ± 0.28	83	88	JG-LAU	
41	Hittin well No.1	22. 9.1970	2.65 ± 0.11	0.19 ± 0.02	75	66	JG-UAU	Confined
43	Hittin well No.3	22. 9.1970	2.81 ± 0.09	0.45 ± 0.03	76	69	JG-UAU	Confined
44	Hittin well No.4	22. 9.1970	2.71 ± 0.14[a]	0.48 ± 0.04	76	55	JG-UAU	Phreatic
97	Shefaram well No.2	28. 9.1970	2.47 ± 0.08	-	105	195	JG-UAU	Confined
187	Havat Hazera No.2	13. 9.1971	1.71 ± 0.04	1.12 ± 0.05	90	49	JG-UAU	Confined
189	Birwa well No.3	4.10.1970	1.85 ± 0.13	-	93	-	JG-UAU	Confined
200	Damun well No.1	27. 9.1970	2.10 ± 0.12[a]	0.92 ± 0.07	98	205	JG-UAU	Confined
202	Damun well No.3	27. 9.1970	2.08 ± 0.08[a]	1.47 ± 0.08	99	184	JG-UAU	Confined
205	Damun well No.6	28. 9.1970	1.86 ± 0.17	1.10 ± 0.14	99	274	JG-UAU	Confined
211	Kurdani well No.1	28. 9.1970	1.93 ± 0.04	-	118	584	JG-UAU	
213	Afeq well No.2	28. 9.1970	2.00 ± 0.10	1.02 ± 0.07	131	582	JG-UAU	Confined
282	Meged Kramin No.1	9. 9.1970	1.53 ± 0.07	-	83	28	JG-UAU	Phreatic

[a] Indicate an average result of two simultaneous samples.
[b] Average annual yield of the springs according to Ref. [20].

An investigation of the $^{234}U/^{238}U$ activity ratio of the water sources in Galilee compared with the direction of the flow regime (Figs 7 and 8) yields three clusters of values:

(a) Low $^{234}U/^{238}U$ activity ratios [1.04 - 1.72] are characteristic of the western (i.e. Mediterranean) catchment area of Upper Galilee. Activity ratio values somewhat higher than 1.55 were found in only three out of thirty-five samples (Code Nos 122, 145 and 157) belonging to this basin. Two water sources located outside the accepted limits of the hydrographical area of western Upper Galilee should also be included in this cluster of low $^{234}U/^{238}U$ activity ratios. One is the Ein Po'em spring (source Code No. 30, $A^{234}U/A^{238}U = 1.20$), which drains eastward towards the Rift, and emerges at the fringe of a Neogene karstic plain undisturbed by Young Pleistocene tectonics. The other is the Meged Kramim No. 1 well (Code No. 282), which is situated in Lower Galilee close to the transition zone with western Upper Galilee ($A^{234}U/^{238}U = 1.53$).

(b) $^{234}U/^{238}U$ activity ratios ranging from 1.65 to 1.91 are common in the eastern catchment area of Upper Galilee, which drains into the Jordan Rift Valley. Twelve water sources of this hydrogeologic basin were analysed, eleven of which were found to lie in this range of activity ratio, the only exception being the Ein Po'em spring.

(c) A somewhat wider range of $A^{234}U/A^{238}U$ values could be identified in fourteen wells along the width of Lower Galilee from the Jordan Rift Valley to the Mediterranean Sea. These data may be subgrouped as follows:

(i) High $^{234}U/^{238}U$ activity ratios (2.47 - 2.81) characterize the central Lower Galilee (as in Source Code Nos 39, 41, 43, 44 and 97).

(ii) $^{234}U/^{238}U$ activity ratios of about 2.0 ± 0.1 have been found in most of the water sources within Lower Galilee (Code Nos 35, 189, 200, 202, 205, 211 and 213).

(iii) Lower $A^{234}U/A^{238}U$ values, of 1.53 and 1.71, were found in water sources located along the transition zone between Upper and Lower Galilee (Code Nos 187 and 282). Such a tendency to lower activity ratios in this area could also be inferred from the general trend of slight decreases in $A^{234}U/A^{238}U$ in a northwesterly direction over the whole of Lower Galilee, as can be seen in Fig. 7.

A discussion of the physico-chemical significance of these clusters in relation to hydrogeological patterns is given in Section 5.

5. THE URANIUM-WATER SYSTEM IN CARBONATE AQUIFERS

The present model for the interpretation of the $^{234}U/^{238}U$ activity ratio distribution pattern in the Judea Group aquifer of Galilee is based primarily on the correlation which could be established between the analytical data and the paleohydrological evolution of the region.

The Uranium-Water system in carbonate aquifers, where the uranium occupies scattered positions in inactive minerals within the rock, reflects the freshwater-crystal surface flow providing other physical conditions remain unchanged.

Preferential leaching and extraction of ^{234}U by water results in $A^{234}U/A^{238}U \geq 1$ within the aquatic phase whereas the surface of the solid minerals becomes impoverished of ^{234}U to a smaller extent due to the law of mass action [22]. Nevertheless, continued and prolonged leaching of the

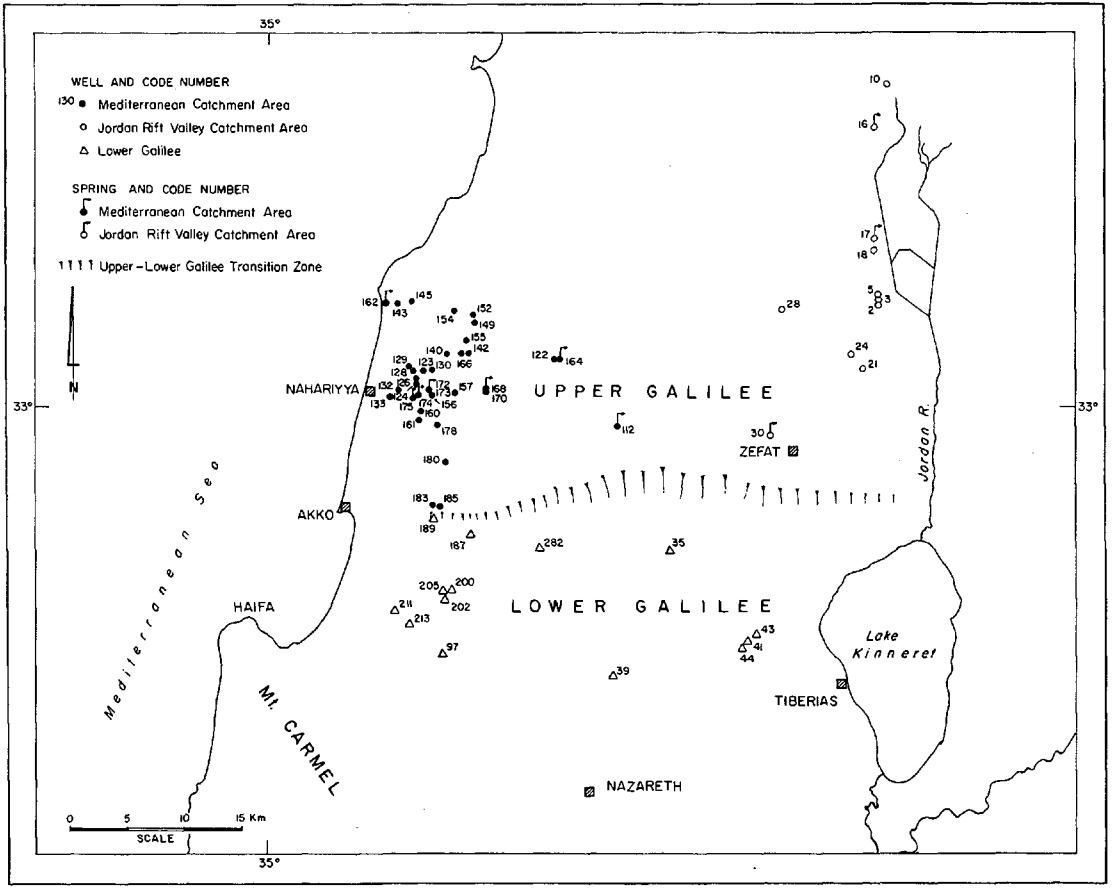

FIG.6. Location map of sampling sites.

TABLE IV. SUCCESSIVE ANALYSES OF $^{234}U/^{238}U$ ACTIVITY RATIO AND URANIUM CONCENTRATION IN SELECTED WATER SOURCES OF THE JUDEA GROUP (CENOMANIAN-TURONIAN) AQUIFER

Source Code No.	Source name	Date of sampling	Yield (m^3/h)	$^{234}U/^{238}U$ activity ratio	U (mg/litre)
2	Enan No. 2 well	13. 8.1970	1200	1.73 ± 0.12	1.47 ± 0.13
		12. 7.1973	1200	1.76 ± 0.05	1.14 ± 0.06
5	Enan No. 5 well	20. 5.1970	1300	1.75 ± 0.06	1.00 ± 0.09
		14. 8.1970	1300	1.72 ± 0.11	1.04 ± 0.08
		21. 5.1973	1300	1.68 ± 0.03	1.06 ± 0.04
10	Hula No. 3 well	20. 5.1970	240	1.90 ± 0.08	0.90 ± 0.06
		19. 8.1970	240	1.91 ± 0.16	0.82 ± 0.08
		18. 9.1973	350	1.87 ± 0.06	1.17 ± 0.05
28	Bir Ubba well	27. 8.1970	70	1.77 ± 0.11	1.05 ± 0.10
		18. 9.1973	70	1.74 ± 0.06	1.27 ± 0.05
130	Kabri No. 8 well	6.10.1970	260	1.18 ± 0.06	-
		17. 8.1971	260	1.30 ± 0.04	1.68 ± 0.05

water will cause more depletion of the ^{234}U content, thus lowering with time the $A^{234}U/A^{238}U$ of the water flowing through. However, analysis for the activity ratio within a whole rock sample might not reflect these changes, since they are restricted mainly to the boundary layer of the conduits and pores of the aquifer. The quantitative model for time variations of $A^{234}U/A^{238}U$ in regard both to carbonate and basaltic aquifers will be discussed elsewhere [38].

The meteoric cycle of groundwater in carbonate aquifers is initiated with flow via primary porosity passages, to which may be later added new conduits of a structural origin. Chemical solution of the rock is governed by the amount and rate of CO_2 supply, whether from the root zone, as is usual, or by oxidation of organic matter within the carbonate rock. This implies that the corrosive activity of the water is limited mainly to the first stages of the subsurface flow cycle, attacking chiefly and congruently the vadose zone of the aquifer [39]. Thus, during this early hydrochemical stage the water obtains the $A^{234}U/A^{238}U$ of the rock itself, i.e. 1, since the rate of solution is high enough to avoid any fractionation between ^{238}U and ^{234}U in the solid conduit crust. As the water continues to flow downstream, and active corrosion ceases, the ^{234}U leaching effect dominates in accordance with factors discussed above. The possibility cannot be excluded that, because of the accumulative ^{234}U leaching from the solid surface, the probability of additional ^{234}U nuclide migrating to the water phase may decrease. In this case, towards infinite time of subsurface flow in a given conduit, the $A^{234}U/A^{238}U$ of the water may approach that of the solid aquifer in the vadose zone of the replenishment area.

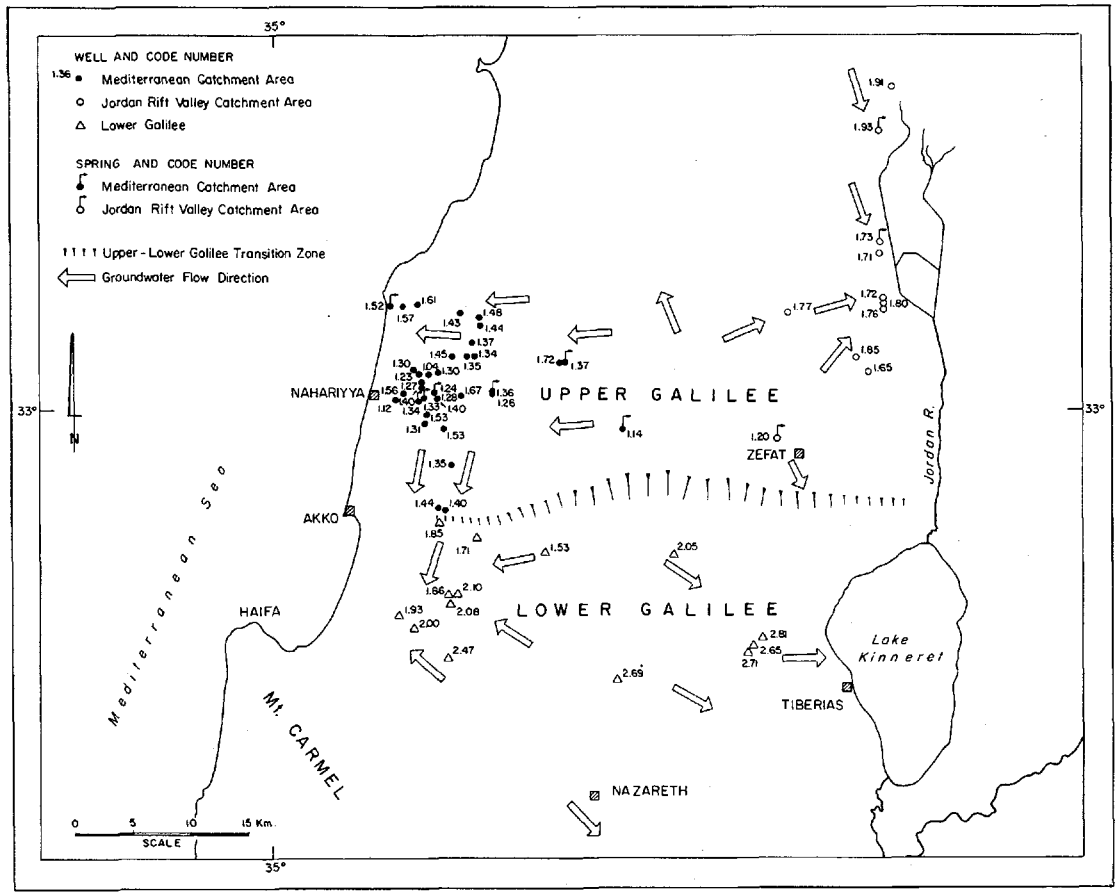

FIG. 7. $^{234}U/^{238}U$ activity ratio and groundwater flow direction within the Judea Group aquifer in Galilee, northern Israel.

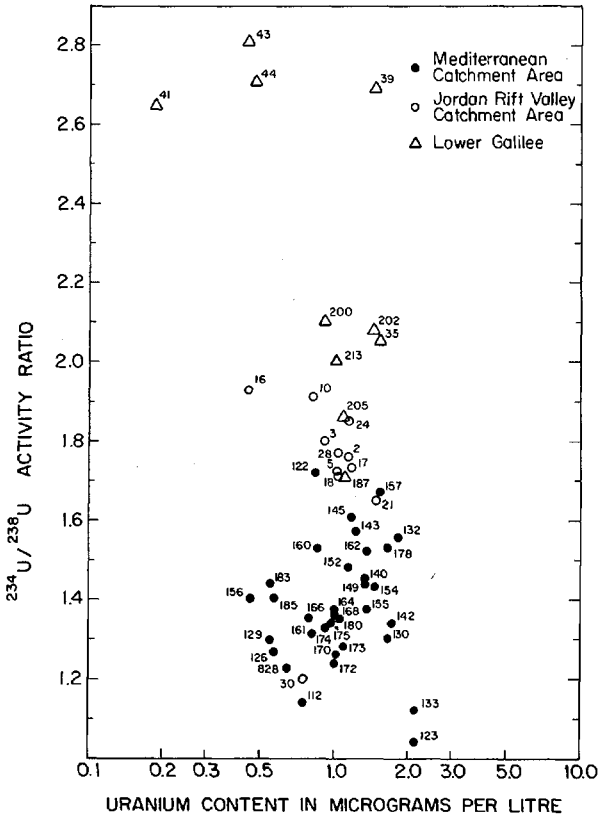

FIG.8. Distribution of $^{234}U/^{238}U$ activity ratio within natural waters of the Judea Group aquifer, Galilee.

A typical example of the changes which developed in the $A^{234}U/A^{238}U$ within two hydrogeological basins similar in climate, lithology and Eh-pH ranges of the water, but differing in the duration of the flow regime, is found in the two flanks of the Upper Galilee uplift (Figs 3, 7, 8). The 46 water sources that were sampled in the area are clearly grouped into two clusters representing the structural-paleohydrological evolution of Galilee. Whereas the continental western drainage system can be traced back at least twenty million years, the eastern drainage, towards the Jordan Rift Valley, is much younger, in the age magnitude of only about one million years.

A detailed comparison between the $A^{234}U/A^{238}U$ and the hydrological regime within Lower Galilee is more difficult, and further research is essential for a completely satisfactory explanation. According to our present understanding of the system, it is proposed to relate the high $A^{234}U/A^{238}U$ to the inferred structural lowering of Lower Galilee which took place during the Pliocene – Pleistocene transition. This regional downthrown movement, which followed the filling of the Neogene basins eastwards and southwards, and the Mediterranean Lower Pleistocene ingressions, considerably reduced

TABLE V. COMPARISON OF $^{234}U/^{238}U$ ACTIVITY RATIO, TRITIUM AND RADIOCARBON IN WATER SAMPLES FROM THE JUDEA GROUP AQUIFER, GALILEE

Source name and Code No.	Date of sampling	$^{234}U/^{238}U$ activity ratio	^{3}H content (TU)	^{14}C (% modern)	Radiocarbon age[c] (years)	Remarks
UPPER GALILEE JORDAN RIFT VALLEY CATCHMENT AREA						
Enan No. 2 well 2	13. 8.1970	1.73	< 0.5[b]	41.4[a]	5 790	
Hula No. 3 well 10	19. 8.1970	1.91	< 2.8[b]	22.3[a]	10 770	
En Zahav spring 16	19. 8.1970	1.93	-	59.1[a]	2 940	
Jahula well 18	10. 8.1971	1.71	3.6[b]	39.5[b]	6 150	
UPPER GALILEE MEDITERRANEAN CATCHMENT AREA						
En Gaaton (Anqalit)spr. 168	21.10.1971	1.36	20.0[b]	81.8[b]	310	Recent water
Kabri No. 8 well 122	17. 8.1971	1.30	< 1.4[b]	53.8[b]	3 690	
En Ziv spring 164	16.10.1971	1.37	27.5[b]	81.1[b]	390	Recent water
Amqa No. 3 well 178	30. 9.1971	1.53	< 3.4[b]	48.9[b]	4 460	
LOWER GALILEE						
Hazon No. 2 well 35	25. 8.1970	2.05	< 2.5[b]	77.8[a]	720	
Hittin No. 3 well 43	22. 9.1970	2.81	0[a]	50.5[a]	4 200	

[a] Analysed by A. Kaufman, Weizmann Institute of Science, Rehovot, Israel.
[b] Analysed by M. A. Geyh, Niedersächsisches Landesamt für Bodenforschung, Hanover, Fed. Rep. of Germany.
[c] Assuming 85% as initial ^{14}C concentration.

the fresh-water circulation. Whereas Upper Galilee northwards was structurally sufficiently high to retain the hydraulic gradient towards the base levels, no similar hydraulic driving head could have prevailed in Lower Galilee. The flat gradient prevented ^{234}U leaching, and thus the $A^{234}U/A^{238}U$ at the conduit surface could have been re-established towards unity at that time. Following the Mediterranean sea regression in the west [40], and the deepening of the Rift Valley in the east, the groundwater flow has again become more intensive, resulting in higher $^{234}U/^{238}U$ activity ratios in the first stages of the current drainage system.

The lowering of the $^{234}U/^{238}U$ activity ratio towards the northwestern part of the area (in the vicinity of the transition zone between Upper and Lower Galilee) is related to a mixing effect with ^{234}U-depleted water flowing southwards from western Upper Galilee [41].

A relation such as that mentioned above between the $^{234}U/^{238}U$ ratio and the paleohydrological evolution of an area is little influenced by the age of the water itself, which in all the cases discussed here is in the upper order of thousands of years. Table V summarizes the results of some contemporaneous water analyses carried out for $A^{234}U/A^{238}U$, ^{3}H and ^{14}C. The low $^{234}U/^{238}U$ activity ratios of the western drainage pattern of Upper Galilee thus includes water ranging in age from Recent to 4500 years B. P. (source Code Nos 164 and 178), whereas the cluster of higher $A^{234}U/A^{238}U$ values belonging to the Jordan Rift Valley catchment area contains sources having the age of 3000 years to 11 000 years B. P. (source Code Nos 16 and 10). The same disagreement between radiocarbon content and $^{234}U/^{238}U$ activity ratio is also observed in the analyses of samples from Lower Galilee (source Code Nos 35 and 43).

6. CONCLUSIONS

Variations in the $^{234}U/^{238}U$ activity ratio were found to represent changes in the paleohydrological evolution of karstic carbonate basins. The magnitude of the ^{234}U excess in the water could be related to the duration of groundwater circulation and leaching along a given direction of base level.

Thus, the drainage patterns prevailing in western Upper Galilee since the Neogene are responsible for the low activity ratios characterizing the basin. Intermediate activity ratios in the waters of the Jordan Rift Valley catchment area represent groundwater flow within both newer conduits opened by the more recent Rift tectonic activity and older rock planes already leached by the flow since the Neogene. The high values of the Lower Galilee can be attributed to intermittent groundwater flow due to structural evolution; this flow has recently been rejuvenated by the Middle — Young Pleistocene Sea Regression and the latest downward movement of the Rift Valley.

No direct correlation could be established between the activity ratios of the water samples and radiocarbon or tritium ages. This points to the possibility that the mechanism of uranium isotope fractionation within this type of aquifer is governed basically by the solid rock-freshwater flow contact history. Additional information gained by such studies might be useful in developing a better hydrogeological model for the groundwater flow regime within carbonate aquifers. It is essential to investigate the distribution of $^{234}U/^{238}U$ activity ratios in differing lithologies and hydrological regimes in order to obtain sufficient comparative data [42, 43].

ACKNOWLEDGEMENTS

Grateful acknowledgement is made to A. Kaufman, of the Weizmann Institute, Rehovot, M. A. Geyh, of the Niedersächsiches Landesamt für Bodenforschung, Hanover, and Mrs. S. Sheinberg, of the Soreq Nuclear Research Center, for invaluable discussion of theoretical aspects, as well as various analytical determinations.

The collection of samples was carried out with the help of H. Levi, of the Groundwater Research Center, The Hebrew University, Jerusalem, and various chemical analyses were performed by Mrs. Z. Schochat. Considerable help in the radiochemical analyses was given by R. Levin, of the Nuclear Research Center, the Negev, and the staff of the NRCN-IAEC Analytical Laboratories.

Sampling arrangements were worked out in close co-operation with the Mekorot Water Company, Israel.

Fruitful discussions concerning the $^{234}U/^{238}U$ activity ratio took place during the IAEA Panel in Vienna in March 1973.

The research was supported by Grant No. 37-691 donated to the Groundwater Research Center through the Swiss Friends in Geneva of The Hebrew University.

Part of the paper is based on a PhD dissertation submitted to The Hebrew University by E. Wakshal.

APPENDIX

ANALYTICAL PROCEDURE

The samples were collected in two 25-litre plastic containers previously washed and rinsed with distilled water and finally with the sampled water. Since in most cases several weeks passed between the time of sampling and analysis the samples were brought to pH 1 by addition of nitric acid of analytic purity, in the course of sampling time. In all cases, the water samples were filtrated using two 37 μm stainless-steel sieves in order to remove any dirt present. Wells were sampled only during routine operation. When necessary, a portable electric pump was used during the sampling of springs.

A measured volume of the sample was spiked with calibrated ^{232}U and equilibrated by boiling for a few hours. The volume of the sample was reduced, and after separating the silica, hydroxides were precipitated at pH 8 by the addition of ammonia. The precipitate was centrifuged, the supernate was decanted and the hydroxides were dissolved in HCl, re-precipitated and separated again. This procedure was repeated once more to get rid of the remaining nitrate. Finally, the solution was brought to 8 N (HCl) and loaded on a Dowex 1 × 8, 100 - 200 resin, conditioned in 8 N HCl. The column used was 10 mm in diameter and packing height was about 20 cm; this ensured a percolation rate of not more than 8 drops per minute. After loading, the resin bed was washed with 50 ml of 8 N HCl and then the uranium was eluted with 50 ml water. The eluate was evaporated to dryness and the residue was dissolved in 8 N HCl. Iron was extracted with iso-propyl ether, and the uranium-containing eluate was evaporated to dryness. In some cases the residue was then suitable for the direct TTA extraction but mostly more purification was required. In these cases the residue was dissolved in 1 N HNO_3 saturated with aluminium nitrate, and from this solution uranium was extracted into ethyl acetate, leaving behind the impurities. The uranium was back-extracted with water and the solution was evaporated to dryness in a 10 ml beaker.

The residue was dissolved in 0.1 N HCl and the solution was contacted with an equal volume of a 0.4 molar solution of TTA (Trifluoro-tienyl-acetone) in benzene. This extraction, like all the others, was done in a test-tube with the help of a "shpitzer" pipette (a drawn-out eye-dropper). The first extract which may contain – among other things – residual quantities of thorium, was rejected. The solution was then brought to pH 3 and extracted twice with about 20 drops of the TTA solution in benzene. The extracts were combined, and a source

was prepared by dropping the extract on to a stainless-steel planchet kept hot enough to evaporate the benzene. The planchet was then flamed in a Bunsen burner flame to destroy all organic matter and to transform the uranium into a strongly adhering oxide. Alpha-spectrometry was carried out, and the $^{234}U/^{238}U$ and $^{238}U/^{232}U$ ratios were calculated. Counting of each planchet was performed at least twice, and only results significantly similar were considered and combined. From the latter ratio and from the quantity of ^{232}U spike added to the sample, the uranium content was computed. The error given in the summary of the results is based on statistics only (1σ).

REFERENCES

[1] CHOQUETTE, P.W., PRAY, L.C., Geologic nomenclature and classification of porosity in sedimentary carbonates, Am.Assoc.Pet.Geol.Bull. 54 (1970) 207.

[2] CHERDYNTSEV, V.V., CHALOV, P.I., KHAIDAROV, G.Z., Transactions of the Third Session of the Committee for the Determination of Absolute Ages of Geological Formations, Izv.Akad.Nauk SSR, Ser.Geol. (1955) 175.

[3] KAUFMAN, M.I., RYDELL, H.S., OSMOND, J.K., $^{234}U/^{238}U$ disequilibrium as an aid to hydrologic study of the Floridan aquifer, J.Hydrol. 9 (1969) 374.

[4] RYDELL, H.S., The Implications of Uranium Isotope Distributions associated with the Floridan Aquifer of North Florida, PhD Thesis, Florida State University (1969).

[5] FREUND, R., et al., The shear along the Dead Sea Rift, Philos.Trans.R.Soc. London, Ser.A 267 (1970) 107.

[6] FREUND, R., The geometry of faulting in the Galilee, Israel J.Earth-Sci. 19 (1970) 117.

[7] HOROWITZ, A., Development of the Hula Basin, Israel, Isr.J.Earth-Sci. 22 (1973) 107.

[8] PICARD, L., On Afro-Arabian graben tectonics, Geol.Rundsch. 59 (1970) 337.

[9] SCHULMAN, N., The Geology of the Central Jordan Valley, PhD Thesis, The Hebrew University, Jerusalem (1962), in Hebrew.

[10] SCHULMAN, N., WEILER, Y., The geometry of faulting in the Galilee (Freund, 1970); Reply and remarks, Isr.J.Earth-Sci. 21 (1972).

[11] PICARD, L., Geology and oil exploration of Israel, Bull.Research Council Israel, Section G, Geo-Sciences 8 (May 1959).

[12] GOLANI, U., On the Cenomanian-Turonian lithostratigraphy of Central Galilee, Bull.Research Council Israel, Section G, 10 (1961) 116.

[13] BLAKE, G.S., GOLDSCHMIDT, M.J., Geology and Water Resources of Palestine, Government Printer, Jerusalem (1947).

[14] KAFRI, U., The Cenomanian-Turonian calcareous aquifer of Central and Western Galilee, Israel, IASH Bull. 15 4 (1970) 77.

[15] MANDEL, S., ARAD, A., First Report on the Geohydrology of the Western Galilee, Tahal, Tel Aviv (1958), in Hebrew.

[16] SERRUYA, C., La basse Galilée Occidentale: étude hydrogiologique du Bassin de Kurdani, Thèse de Doctorat de 3° Cycle, Université Paris, Laboratoire de Géologie Dynamique (1958).

[17] SHIFTAN, Z., ROSENTHAL, E., Water Sources Development in the Hula Valley, Geological Survey of Israel, Jerusalem (1963), in Hebrew.

[18] BEIN, A., The hydrogeology of the Cenomanian-Turonian aquifer in the Central-Eastern Galilee, Geological Survey of Israel, Jerusalem (1967), in Hebrew.

[19] MERO, F., Hydrological Investigation of the Na'aman Spring Region, Tahal, Tel Aviv (1958).

[20] ISRAEL HYDROLOGICAL SERVICE, Hydrological Year-book of Israel, Summary of Records prior to October 1967, Jerusalem (1971).

[21] ADAMS, J.A.S., OSMOND, J.K., COWART, J.B., "Interpretation of uranium isotope disequilibria as a hydrological tracer", Working Paper, IAEA Panel Meeting, 1973, unpublished.

[22] CHERDYNTSEV, V.V., Uranium-234, Israel Program for Scientific Translations, Jerusalem (1971). English Translation of the Russian edition (1969).

[23] KOLODNY, Y., Studies in Geochemistry of Uranium and Phosphorites, PhD Thesis, University of California, Los Angeles (1969).

[24] ROGERS, J.J.W., ADAMS, J.A.S., "Uranium", Ch.92, Handbook of Geochemistry (WEDEPOHL, K.H., Ed.), Springer, Berlin (1969).

[25] GARRELS, R.M., CHRIST, C.L., Solutions, Minerals, and Equilibria, Harper & Row, New York (1965).

[26] LANGMUIR, D., The geochemistry of some carbonate ground waters in central Pennsylvania, Geochim. Cosmochim. Acta 35 (1971) 1023.

[27] KRAUSKOPF, K.B., Introduction to Geochemistry, McGraw-Hill, New York (1967).
[28] CHALOV, P.I., MERKULOVA, K.I., Influence of oxidation processes of fractionation of uranium isotopes during their leaching from minerals, Geokhimiya (1968) 872, in Russian.
[29] ROSHOLT, J.N., SHIELDS, W.R., GARNER, E.L., Isotopic fractionation of uranium in sandstone, Science 139 (1963) 224.
[30] ROSHOLT, J.N., DOE, B.R., TATSUMOTO, M., Evolution of the isotopic composition of uranium and thorium in soil profiles, Geol.Soc.Am., Bull. 77 (1966) 987.
[31] DOOLEY, J.R., Jr., GRANGER, H.C., ROSHOLT, J.N., Uranium-234 fractionation in the sandstone-type uranium deposits of the Ambrosia Lake District, New Mexico, Econ.Geol. 61 (1966) 1362.
[32] KOLODNY, Y., KAPLAN, I.R., Uranium isotopes in sea-floor phosphorites, Geochim.Cosmochim. Acta 34 (1970) 3.
[33] KIGOSHI, K., Recoil Th-234 dissolution into water and the U-234/U-238 disequilibrium in nature, Science 173 (1971) 47.
[34] KU, T.L., An evaluation of the $^{234}U/^{238}U$ method as a tool for dating pelagic sediments, J.Geophys. Res. 70 (1965) 3457.
[35] AMIEL, S., Analytical application of delayed neutron emission in fissionable elements, Anal.Chem. 34 (1962) 1683.
[36] CHALOV, P.I., TUZOVA, T.V., MUSIN, Ye.A., The U-234/U-238 ratio in natural waters and its use in nuclear geochronology, Geochem.Int. No.3 (1964) 402.
[37] SPIRIDONOV, A.I., TYMINSKII, V.G., Change of the U-234/U-238 isotope ratio in ground waters in 1966-67 after the 1966 Tashkent earthquake, Izv.Akad.Nauk, SSSR, Fiz.Zemli 3 (1971) 91.
[38] WAKSHAL, E., et al., in preparation.
[39] THRAILKILL, J., Chemical and hydrologic factors in the excavation of limestone caves, Geol.Soc.Am., Bull. 79 (1968) 19.
[40] ISSAR, A., KAFRI, U., Neogene and Pleistocene geology of the Western Galilee coastal plain, Isr.Geol. Survey Bull. No.53 (1972).
[41] MICHAELI, A., SHAHRABANI, M., BLANK, D., Development and Calibration of Groundwater Flow Digital Model in Naaman Basin, Tahal, Tel Aviv (1973),in Hebrew.
[42] KRONFELD, J., Hydrologic Investigations and the Significance of U-234/U-238 Disequilibrium in the Ground Waters of Central Texas, PhD Thesis, Rice University, Houston, Texas, 1971, unpublished.
[43] KIGOSHI, K., "Uranium 238/234 disequilibrium and age of underground water", IAEA Panel Meeting, Vienna, 1973, unpublished.

DISCUSSION

K. PRZEWŁOCKI: Did you use delayed-neutron activation analysis because it was more accurate in some cases than alpha spectrometry?

E. WAKSHAL: No, we used it in addition to alpha spectrometry mainly because it is a rapid analytical technique.

P.Ch. LEVEQUE: We regularly use the concentrations of total uranium in the same way as those of calcium, magnesium, SO_4^{2-} and so on as a means of obtaining additional information about the origin of waters. In what forms and concentrations do you expect to find dissolved uranium?

E. WAKSHAL: In normal fresh groundwater, dissolved uranium should be in the form of complexes with CO_3^{2-} and SO_4^{2-}. Theoretical considerations suggest that the total concentration of dissolved uranium will depend on the pH-Eh.

So far we have analytical data only on carbonate aquifers.

R.B. THOMAS: From your oral presentation I understood your argument to be that, during the period of higher Pleistocene Sea levels, outflow and circulation stopped. In such circumstances, however, recharge would also have stopped, and I know of no cases where recharge stopped when the sea level was higher. It is unlikely, therefore, that the system was static. Would you care to comment on this point?

E. WAKSHAL: The rate of ^{234}U leaching from solid rock seems to be influenced by the intensity of groundwater circulation. We assume that this was reduced in the Lower Galilee area by the higher Pleistocene Sea levels. However, more data are needed before our hypothesis explaining the high $^{234}U/^{238}U$ activity ratios can be proved or disproved.

J. R. GAT: With regard to Mr. Thomas's comment, I imagine that the whole drainage pattern experienced an upward shift when the sea level rose, leaving the area which is now leached in a stagnant layer. Then, as the sea level fell, the area which had been continuously leached was left in what is today not part of the Lower Galilee aquifer but a zone located above it.

R. B. THOMAS: Currently available data indicate that the aquifer is active below the present sea level, so it may have been active when the sea level was higher.

^{39}Ar DATING OF GROUNDWATER

H. OESCHGER, A. GUGELMANN, H. LOOSLI,
U. SCHOTTERER, U. SIEGENTHALER, W. WIEST
Physikalisches Institut,
Universität Bern,
Berne, Switzerland

Abstract

^{39}Ar DATING OF GROUNDWATER.

The basic information for demonstrating the feasibility of an ^{39}Ar dating method is given. The present cosmic-ray-produced specific activity of ^{39}Ar in atmospheric argon is 0.112 ± 0.012 dpm/litre Ar. It can be assumed that this activity has been constant within a few per cents for the last thousand years. For possible man-made contributions from nuclear explosions and reactors in the period 1940 to 1973, an upper limit of 12% can be given. The ^{39}Ar dating method was successfully checked first by measuring argon extracted from polar ice samples of known age. The application of this method, together with ^{85}Kr, ^{3}H and ^{14}C measurements, on groundwater has great value in isotope hydrology. A system which allows the extraction of the gases from 20 tonnes of water in about one day has been developed, and preliminary details of experiences with it are given. A procedure for the separation of argon and krypton from the extracted gases is described. The ^{39}Ar specific activity in the argon sample is measured in a low level counting system. Its background for a 1.8 litre argon (STP) gas sample is 0.27 counts/min and the modern net effect is 0.14 counts/min. Up to now only one ^{39}Ar age of water of a thermal spring in Zurzach, Switzerland, is available. From the ^{3}H result it can be concluded that the water is older than 50 years. The preliminary age information from ^{39}Ar (younger than 70 years) is in contradiction to the low specific ^{14}C activity of 12.4 pmc. Possible reasons for this discrepancy are discussed.

1. INTRODUCTION

Environmental isotope hydrology has mainly been based on the analysis of either D/H- and ^{18}O/^{16}O-ratios on the one hand or on T/H- and ^{14}C/C-ratios on the other. The possibility of applying a new technique to hydrological problems has been given by the detection of the noble gas isotope ^{39}Ar in atmospheric argon. Although the specific activity of cosmic-ray-produced ^{39}Ar, ~0.1 dpm/litre Ar, is very low compared, for example, with ^{14}C (~ 7 dpm/litre CO_2), examination of its possible use in isotope hydrology seemed justified because of the following reasons:

(a) The ^{39}Ar half-life of 269 years allows dating of samples in the range of 50 to 1000 years, thus filling in the gap between times accessible with ^{3}H (12.3 years) and with ^{14}C (5730 years).

(b) As a noble gas isotope ^{39}Ar shows a simple geochemical behaviour. Within its mean life of 390 years there exists only one, well-mixed reservoir, the atmosphere. The behaviour of dissolved Ar (and ^{39}Ar) in water is also simple, since no chemical interaction with the aquifer can take place.

In addition to use in isotope hydrology, ^{39}Ar has great potential value in isotope glaciology and in isotope oceanography.

For several years the Physics Institute of the University of Berne has been developing the applications of ^{39}Ar in the above-mentioned fields. A review is given here of the present state of ^{39}Ar dating in glaciology and hydrology, and prospects for its future importance in these fields.

2. THE BASIS OF THE ^{39}Ar-DATING METHOD

^{39}Ar is produced by cosmic radiation in the atmosphere in a similar fashion to ^{14}C and ^{3}H. The most important production reaction is ^{40}Ar(n, 2n) ^{39}Ar. Because its half-life of 269 years is long compared with atmospheric mixing times, the ^{39}Ar activity is uniformly mixed with atmospheric argon.

The present ^{39}Ar activity of atmospheric argon was measured for the first time in 1968 [1], and was re-measured again in 1973 [2]. Values of 0.10 ± 0.02 and 0.112 ± 0.012 dpm ^{39}Ar/litre Ar were obtained. For the second measurement the proportional counter used was calibrated with an ^{39}Ar standard provided by Stoenner and Davis, Brookhaven National Laboratory. It is important to know whether, similarly to ^{3}H and ^{14}C, ^{39}Ar is produced in nuclear bomb tests or in nuclear reactors in amounts comparable with the naturally occurring atmospheric level. To examine this problem, argon extracted from the atmosphere in the years 1940, 1959, 1961, 1963, 1965, 1967 and 1973 was analysed. No significant increase in ^{39}Ar activity was observed. An upper limit for a possible bomb contribution for the whole period is 12%. The small value of the artificial production means that in model calculations used for determining ages we can assume a constant input concentration. This holds for the whole time span that is of interest for ^{39}Ar dating.

The amount of argon dissolved in the oceans, in ground- and surface water, or trapped in ice is small compared with that in the atmospheric reservoir. The geochemical behaviour therefore is simple, since we deal essentially with one well-mixed atmospheric reservoir only. From ^{14}C measurements in tree rings we know that the ^{14}C/C ratio in atmospheric CO_2 shows variations which are partly due to changes in the production rate of this isotope. In Ref. [3] we assumed the ^{14}C variations during the last 1000 years to be due entirely to production rate changes, and calculated how much the production rate would need to have varied in order to cause the observed variations. In a second step we have then here assumed these ^{14}C production rate variations to be valid for the ^{39}Ar production also, and calculated the resulting variations of the ^{39}Ar/Ar ratio. The result is given in Fig. 1. It can be seen that ^{39}Ar/Ar variations up to about 7% may have occurred, corresponding to a maximum error in the age of ~30 years, which certainly is unimportant compared with the general uncertainties involved in dating of natural water in the range of 50 to 1000 years.

To demonstrate that a dating method based on ^{39}Ar activity measurements gives useful results, we first applied the technique to ice dating.

During the transition from firn to ice, air is trapped in bubbles which then move with the surrounding ice along the flow lines of the glacier. If enough air trapped in a certain ice layer can be extracted to allow the measurement of the specific ^{39}Ar activity of the argon component, we can then determine the time elapsed since the occlusion of the air. Air samples were collected from ice at Dye 3 (Greenland) in 1971 and at Byrd Station (Antarctica) in 1969-70 and 1971-72. The ^{39}Ar ages obtained correspond well with those determined by ^{18}O/^{16}O-, ^{14}C- and ^{32}Si-analyses [2, 4].

In principle, ^{39}Ar measurements allow age determinations of groundwater in a similar way. Water percolating through the ground down to groundwater reservoirs contains dissolved atmospheric argon with "modern" specific ^{39}Ar activity. In the groundwater an exchange with the atmosphere is negligible, and the ^{39}Ar activity decays according to the law of radioactive

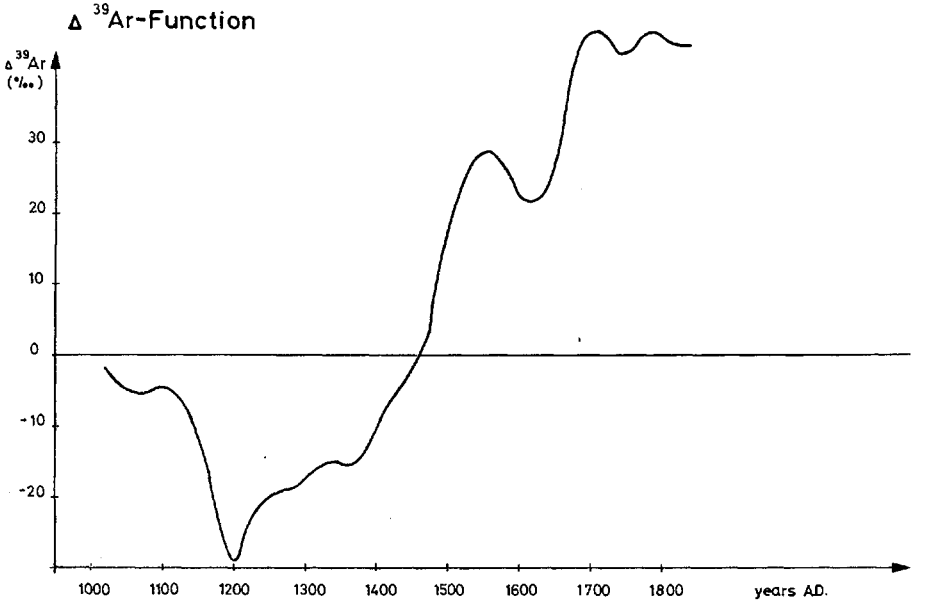

FIG. 1. Calculated deviations of the atmospheric ^{39}Ar activity. The relative deviation of the ^{39}Ar activity from the average ^{39}Ar level in atmospheric argon is plotted as function of time. It is assumed that the observed $^{14}C/C$ variations are entirely due to production rate changes. By assuming that these production rate changes are also valid for the ^{39}Ar production, the plotted $\Delta\,^{39}Ar$ values were calculated.

decay. If we succeed in extracting the necessary amount of argon from a groundwater well, the ^{39}Ar measurement allows an age determination. In Table I we give the equilibrium amounts of argon and krypton dissolved at different temperatures in water. From this it can be estimated that a minimum amount of about 20 tonnes of water is necessary to obtain an argon sample of 3 litres, which is the amount required for the radioactivity measurement.

For the application of the ^{39}Ar-dating method one has to know if ^{39}Ar is produced in significant amounts underground. A possibility is the $^{39}K(n, p)^{39}Ar$ reaction, the neutrons coming from the spontaneous fission of ^{238}U in the aquifer. Although we cannot at present exclude this possibility completely we consider this interference to be improbable, at least for aquifers with average U contents. A possible dilution of the dissolved Ar in the water by ^{40}Ar originating from ^{40}K decay can be corrected based on $^{36}Ar/^{40}Ar$ ratios measured by mass spectrometry.

For ^{39}Ar age determinations the following technical procedures are necessary:

(a) Extraction of the gases contained in about 20 tonnes of water.
(b) Separation of the argon from the collected gases, with special attention given to the separation of krypton because of the relatively high ^{85}Kr activity of recent atmospheric krypton.
(c) Measurement of the ^{39}Ar activity of the argon component.

All these steps required the development of new technical procedures. These procedures are described below.

TABLE I. DISSOLVED ARGON AND KRYPTON IN WATER

Temperature (°C)	Ar cm^3/tonne	Kr cm^3/tonne
10°C	382	0.078
20°C	302	0.057
40°C	230	0.040

TABLE II. EXTRACTION OF AIR SAMPLES FROM WATER

Location	Extraction time for one sample	Amount of gas extracted	Amount of water used	Average temperature of heated water	Heater used	Extraction date
Zurzach	68 h	366 lt	24.5 m^3	85 °C	Electric 12 kW (self-made)	May 73
Marzili	19 h	340 lt	17.3 m^3	100 °C	Loos. Strahlfix SF 1100	Aug. 73
Hilpoltstein III	25 h	350 lt	28.5 m^3	90 °C	Kärchner HDS 1200	Mar. 74
Jahrsdorf I	15 h	340 lt	16.5 m^3	98 °C	Kärchner HDS 1200	Mar. 74

3. EXPERIMENTAL PROCEDURE

3.1. The extraction of air from water

As mentioned in Section 2, it is necessary to outgas up to 20 tonnes of water to obtain an argon sample of a few litres as required for the radioactivity measurement. Outgassing could be done by different methods, e.g. vacuum extraction, extraction at high temperatures or degassing by ultrasonic means. For our purpose we heated the water to ~95°C to outgas, and pumped off the escaping gas at about atmospheric pressure. The advantages of this method are high extraction yield (~90%), and low probability of contamination by modern atmospheric air since the outgassing takes place at a pressure of about 1.05 atm.

On the other hand, for one sample $2 \cdot 10^6$ kcal of heat are required, which may be a disadvantage in fieldwork done in remote areas. The extraction line is schematically given in Fig. 2. Up to now four air gases samples of about 350 litres each have been collected. Two sources in Switzerland (thermal spring in Zurzach and a groundwater source, "Marzili", near Berne) were selected because their low ^3H content indicated that most of the water originates from before 1954. We have extended these first extractions of air from water to two groundwater sources in the Federal Republic of Germany (Hilpoltstein III and Jahrsdorf I), near Nuremberg, which have been extensively studied by ^3H-, ^{14}C- and other hydrological methods [5, 6]. The data for the extractions are given in Table II. By using commercially available heaters of higher power, and by raising the extraction temperature, the extraction yield was increased and the collection time reduced from 68 h (first sample) to 15 h. It is planned to use in future heaters with a power allowing a complete extraction in about 8 h. Thus it will be possible to collect an ^{39}Ar sample (and in the same procedure a ^{85}Kr and a ^{14}C sample) in one day, which certainly is not an unreasonable time considering the special value of the ^{39}Ar and ^{85}Kr information.

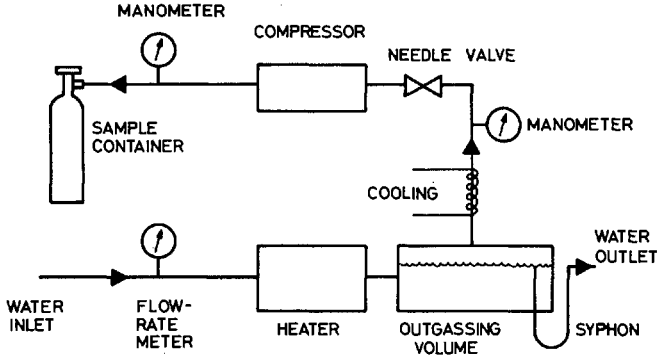

FIG.2. Field extraction of air from water. The bubbles in the heated water are allowed to reach the water surface in the outgassing volume. A small over-pressure in the space above the water level is maintained by adjusting the needle valve opening. The dry gas is compressed into containers of known volume to a pressure of up to 100 atm.

TABLE III. CHARACTERISTICS OF THE COUNTING SYSTEMS

	System A	System B
Shield and anti-coincidence arrangements	15 m rock 10 cm of Pb Anti-coincidence ring counter 2 cm of Pb Counter	20 cm Pb Anti-coincidence ring-counter 2 cm Pb Counter
Counter volume Gas pressure Gas composition	100 cm^3 20 atm Ar + 10% CH_4	1 litre 3 - 5 atm Ar + 5% CH_4
Background (≥ 14.4 keV)	0.26 counts/min	1.20 counts/min
Net counting rate of modern Ar (≥ 14.4 keV)	0.14 counts/min (~ 1.8 litres Ar STP)	0.24 counts/min (~ 3 litres Ar STP)
Examples of possible results (10 000 min): 2 litres Ar	300 ± 40 years	300 ± 85 years
Examples of possible results (10 000 min): 5 litres Ar	800^{+175}_{-120} years	800^{+130}_{-100} years

Accurate extraction yields for the four samples cannot be given since the gas contents in the water were not measured. They can, however, be estimated by assuming that the water is saturated with air at a temperature of 10°C. For the Marzili sample we then obtain a yield of ~ 90%.

3.2. The separation of argon and krypton

The separation of argon and krypton (after adding pre-bomb krypton carrier) from the extracted total gas is carried out in essentially three steps. In a first step the gas (approx. 300 litres) is passed through a Cu-furnace at a temperature of about 600°C. The oxygen is fixed as CuO. In the second step most of the nitrogen is removed by fractional distillation. The remainder of the gas, consisting of the noble gases and the remaining nitrogen, is then further separated by preparative gas chromatography. Argon and krypton are frozen out as they come off one column. After the hydrogen, which serves as carrier gas, is removed by using CuO, very pure argon and krypton are obtained. The krypton content of the argon fraction is smaller than 0.1 ppm, corresponding to a ^{85}Kr activity of < 0.003 dpm/litre Ar. For proportional counting no further purification is necessary. The complete preparation of an argon sample takes about three days. About 40 hours are needed for the fractional distillation. A detailed description of the procedure is given in Refs [2] and [4]. Probably less laborious than our procedure is the removal of the nitrogen and the oxygen with hot CaC_2 as carried out by Currie and co-workers [7] in their procedure for the preparation of atmospheric argon samples for ^{37}Ar measurements.

3.3. Radioactivity measurement

The radioactivity measurements were carried out in two counting systems, A and B. Some characteristics are given in Table III and more details can be found in Refs [1], [2] and [4]. System A shows an extremely low background mainly because the counter is very small, being filled with high gas pressure of up to 20 atm. The cosmic-ray-produced equilibrium activity in the atmosphere is measured to be 0.112 ± 0.012 dpm/litre Ar. The error contains counting statistic (5%). and estimated calibration uncertainties. With special care it is possible to keep the uncertainties from one filling to the next below the statistical ones. Table III shows for two samples of different age the accuracy (statistical errors only) which can be obtained at present with a counting time of 10 000 min. During this period no changes in the performance of the counters, for example, from outgassing of electronegative inpurities from the plastic walls, can be observed. An increase in sensitivity of the counting system is difficult to obtain, since the background is already extremely low. However, it may be feasible to work with a smaller counter at even higher pressure and to increase considerably the counting time. The latter strategy requires the construction of a counting system with a series of counters in order to have a reasonable counting capacity.

The measurement of the extremely low specific beta-activities is very delicate. Sources of error can be:

(a) Small contributions by ^{222}Rn (3.8 d half-life), probably originating from a molecular sieve in some of the cold traps used after the gas chromatographic separation.

TABLE IV. GAS COMPOSITION, STABLE AND RADIOACTIVE ISOTOPE CONTENT

		Zurzach	Marzili	Hiltpoltstein III	Jahrsdorf I
Composition of extracted gas	N_2	96.7%	83.0%	Not yet measured	Not yet measured
	O_2	0.26%	0.68%		
	Ar	1.76%	1.39%		
	CO_2	1.25%	15%		
$\delta^{18}O/^{16}O$		-10.20‰	-10.27‰	-9.61‰	-9.63‰
^{3}H		≤ 0.3 TU	4.9 ± 0.3 TU	35.4 ± 1.4 TU	< 2 TU [5] 7.3 ± 0.5 TU
^{14}C age		> 1000 years (12.4 pmc)	Not yet measured	870 years [6]	1810 ± 310 years [5]
^{39}Ar age		Younger than 70 years	Not yet measured	Not yet measured	Not yet measured

(b) Insufficient purity of the samples for porportional counting which leads to irreproducibility. The purity can be tested by the very sensitive method of external calibration of the counter with gamma- and X-ray sources.

4. MEASUREMENTS AND FIRST RESULTS

The results available up to now on gas composition and on stable and radioactive isotope content are given in Table IV. With respect to the composition of the gases extracted from Zurzach and Marzili the low O_2 content is striking. From this low O_2 content an upper limit of 1.3% and 3.3% respectively for the contamination of the samples with modern atmospheric air can be estimated. This means that, in terms of ^{39}Ar dating, the samples are uncontaminated, in spite of the long extraction time. The CO_2 content of the gas samples must be considered as only preliminary. This also does not have much meaning since the CO_2 amount extracted depends very much on temperature and pressure during the extraction. The Ar content, which is higher by a factor of 1.4 - 1.9 than in the atmosphere, is in agreement with values obtained from solubility estimates in water.

From the fact that the ^{3}H activity of the water from the thermal spring in Zurzach is below the detection limit it can be concluded that this source does not contain a significant amount of fresh water younger than about 20 years. The same was true a few years ago for the Hilpoltstein and Jahrsdorf wells [5, 8]. Now, however, in 1974, a measurable amount of ^{3}H has been observed, indicating that these German sources are beginning to contain some young water components. Based on average values in the last few years, an amount of 3 to 20% of rain-water admixed would be necessary to account for the increased ^{3}H activity. If in recent years the extraction of water from the ground exceeds the flow rate of the groundwater streams, then a change of the water components seems possible. The planned ^{85}Kr measurements will help to clarify the situation. The ^{3}H value of about 5 TU in the Marzili water can possibly be explained by contamination of the water by fresh water since the well is situated in a construction area. For the last two years about 1 - 2 m^3/min of water have been released from this well, which is in an old moraine near the Aare river. No pressure change and therefore no significant reduction of the reservoir size has been observed during this time.

Up to the present time only one ^{39}Ar result has been obtained, for the thermal spring of Zurzach. It indicates that the age of the water is younger than 70 years. This is in disagreement with the ^{14}C result (12.4 pmc). The reasons for this could be:

(a) The ^{39}Ar age is incorrect because of contamination in the separation procedure, or because there is a significant contribution of ^{39}Ar from the reaction $^{39}K(n, p)^{39}Ar$.
(b) The ^{14}C age is incorrect because of continuous dissolution of aquifer material resulting in a dilution by dead carbon.

5. CONCLUSIONS

To solve water supply problems it has become more and more important to increase our knowledge of the behaviour of natural water systems. One

important problem is dating of groundwater. There is a great need for the development of new techniques in isotope hydrology for the following reasons:

(a) In the currently available dating range by radioisotopes there is a gap between 50 years and 1000 years.
(b) There are uncertainties in ^{14}C dating of groundwater regarding the initial $^{14}C/C$ ratio and possible dilution by dead carbon.
(c) Because the ^{3}H concentration in precipitation is levelling off, dating of groundwater with ages of a few years is becoming difficult.
(d) Simple mixing models for a groundwater reservoir sometimes do not work well enough, and more sophisticated models would be preferred if enough parameters could be measured.

The application of noble gas isotope analyses to hydrology in addition to already known methods would help to overcome these difficulties for the following reasons:

(a) ^{39}Ar is produced in measurable amounts by cosmic radiation and, because of its half-life of 269 years, it allows water dating in the missing range of 50 years to 1000 years.
(b) ^{85}Kr is produced mainly in nuclear reactors and released into the atmosphere during fuel reprocessing. During the last decade the ^{85}Kr concentration in atmospheric krypton has shown a nearly linear increase with time, and it is therefore ideal for dating of groundwater which has an age of a few years.

The functioning of the ^{39}Ar dating method was demonstrated by the measurement of air samples of known age, extracted from polar ice. Up to now four gas samples have been extracted from groundwater for ^{39}Ar and ^{85}Kr determinations. Time and counting capacity allowed only for the ^{39}Ar measurement of one of them so far. The hot spring from Zurzach shows an ^{39}Ar age of younger than 70 years. This value is only preliminary since the sample showed at the beginning a contamination with ^{222}Rn.

On the basis of the present results we are optimistic that the ^{39}Ar method will yield as satisfactory results in isotope hydrology as it already has in isotope glaciology. One important application of ^{39}Ar will be the comparison with ^{14}C results which will help to provide more information on the initial ^{14}C concentration of the hydrocarbon in natural waters.

The amount of work in extracting the gas and separating the components for a ^{39}Ar analysis is several times that of a ^{14}C analysis, but during the extraction CO_2 and krypton for ^{14}C- and ^{85}Kr-measurements are simultaneously collected. In addition, the determination of the low specific ^{39}Ar activity requires the best low level counting facilities available at present. But the ^{3}H-, ^{85}Kr-, ^{39}Ar- and ^{14}C-measurements altogether applied on the same water source will allow its age distributions to be determined in the now fully covered range of a few years to a few 10 000 years. There are certainly cases where such detailed information is desired in spite of the costs involved.

ACKNOWLEDGEMENTS

The gas-chromatographic measurements of the gas composition were carried out by P. Bucher and W. Berner. Technical support was given by P. Wittwer and K. Hänni.

We are thankful to many people who helped during the field work in the extraction of the gas from water at the four wells. We would particularly like to thank the Electric Co., Zurich, and Kärcher Co., Nuremberg, who supplied the heaters.

This work has been supported by the Schweizerischer Nationalfonds zur Förderung der wissenschaftlichen Forschung.

REFERENCES

[1] LOOSLI, H.H., OESCHGER, H., Detection of ^{39}Ar in atmospheric argon, Earth Planet. Sci. Lett. 5 (1968) 191.

[2] WIEST, W., Messung von Argon-Isotopen in Luftproben und Vergleich mit Modellrechnungen, Dissertation der Universität Bern, 1973.

[3] OESCHGER, H., STAUFFER, B., BUCHER, P., FROMMER, H., MOELL, M., LANGWAY, C.C., HANSEN, B.L., "^{14}C and other isotope studies on natural ice", Proc. 8th Int. Conf. Radiocarbon Dating, Lower Hutt, New Zealand, 1972, 1, Roy. Soc. N. Z. (1972) D 70.

[4] LOOSLI, H.H., WIEST, W., OESCHGER, H., STAUFFER, B., BUCHER, P., An ^{39}Ar dating method for earth sciences, in preparation.

[5] ANDRES, G., GEYH, M.A., Untersuchungen über den Grundwasserhaushalt im überdeckten Sandsteinkeuper mit Hilfe von ^{14}C- und ^{3}H-Wasseranalysen, Wasserwirtschaft 60 8 (1970).

[6] ANDRES, G., GEYH, M.A., Paläohydrogeologische Studien mit Hilfe von ^{14}C über den pleistozänen Grundwasserhaushalt in Mitteleuropa (südliche Frankenalb), Naturwissenschaften 59 (1972) 418.

[7] CURRIE, L.A., LINDSTROM, R.M., "The NBS measurement system for natural ^{37}Ar", Proc. Noble Gases Symposium, 22-28 Sep. 1973, Las Vegas, Nevada, in press.

[8] GEYH, M.A., personal communication.

DISCUSSION

T. FLORKOWSKI: In your oral presentation you said that ^{85}Kr measurements are much easier to perform than ^{39}Ar measurements. Why, then, did you not start with ^{85}Kr?

H. OESCHGER: Because we already had a routine, with calibrated counters, for ^{39}Ar measurements. A counting system for ^{85}Kr is being set up at present.

B.T. VERHAGEN: Why did you choose to take samples from a thermal spring?

H. OESCHGER: We chose the Zurzach thermal spring because of its low tritium content (≤ 0.3 TU), hoping to obtain samples with an age in the ^{39}Ar dating range. Moreover, for carrying out the first extraction, which lasted several days and nights, we could use the local facilities. In other words, practical rather than hydrological considerations prompted our choice.

J.C. LERMAN: Groundwater dating on the basis of radioactive noble gases will, in my opinion, shed light on the problem of the initial ^{14}C activity of groundwater. For this reason I regret the large age discrepancy observed in your first result. Have you a purely hydrological estimate of the age of your groundwater? I ask this because we were encouraged to date water on the basis of radiocarbon when good agreement between isotopic and hydrological age was obtained by Hanshaw, Back and Rubin[1] in the case of the Florida aquifer.

---

[1] HANSHAW, B.B., et al., Radiocarbon determination for estimating groundwater flow velocities in central Florida, Science 148 (1965) 494.

H. OESCHGER: Perhaps Mr. Schotterer, one of my co-authors, would answer this question.

U. SCHOTTERER: No, we only have dates based on chemical findings, and we have no idea where the water comes from (if it comes from the north, the possibility of a contribution of radiogenic ^{39}Ar cannot be ignored).

E. MAZOR: I feel intuitively that the spring waters are older than a few tens of years, especially if they come from the mountains some distance away.

As regards the ^{14}C age and the possibility of dilution by magmatic CO_2, I would recall the suggestion made by you in the discussion of paper IAEA-SM-182/31 that the $^{14}C/H_2O$ ratio be used.

H. OESCHGER: We could make the necessary correction only if we knew the initial $^{14}C/H_2O$ ratio, but, as Mr. Schotterer said, we do not know where the water comes from.

B. R. PAYNE: Would you like to give your views on the potential use of ^{39}Ar as a dating tool in hydrology compared with ^{32}Si?

H. OESCHGER: The dating ranges are similar, but ^{39}Ar is simpler from a geochemical point of view (except in so far as the possible production of ^{39}Ar underground is concerned). We plan to obtain samples of ^{32}Si, ^{85}Kr, ^{14}C, ^{39}Ar and other isotopes so as to exploit the full spectrum of dating methods.

J. P. A. MOLINARI: Could you give us some information about the time involved in and the costs of carrying out ^{39}Ar and ^{85}Kr measurements?

H. OESCHGER: Extraction takes about one day and noble gas separation about three days with the present technique; sample counting takes 1-3 weeks. In conclusion, I think that the cost of an ^{39}Ar analysis is 3-5 times that of a ^{14}C analysis. The separation of ^{85}Kr is simpler and counting much easier because of the higher specific activity.

J. P. A. MOLINARI: What improvements do you think are possible?

H. OESCHGER: I expect the main improvements to relate to the noble gas separation process; it will be very difficult to achieve improvements with regard to the background of the ^{39}Ar counter.

J. P. A. MOLINARI: Do you think other laboratories should start using these new dating methods?

H. OESCHGER: I think other laboratories should start ^{85}Kr work, but I have hesitations regarding the ^{39}Ar method because it is very delicate from the analytical point of view.

DISTRIBUTION OF SULPHUR ISOTOPES OF SULPHATES IN GROUNDWATERS FROM THE PRINCIPAL ARTESIAN AQUIFER OF FLORIDA AND THE EDWARDS AQUIFER OF TEXAS, UNITED STATES OF AMERICA

C.T. RIGHTMIRE, F.J. PEARSON, Jr., W. BACK
US Geological Survey,
National Center,
Reston, Va.

R.O. RYE, B.B. HANSHAW
US Geological Survey,
Denver, Colo.,
United States of America

Abstract

DISTRIBUTION OF SULPHUR ISOTOPES OF SULPHATES IN GROUNDWATERS FROM THE PRINCIPAL ARTESIAN AQUIFER OF FLORIDA AND THE EDWARDS AQUIFER OF TEXAS, UNITED STATES OF AMERICA.

New information on the sources of sulphate dissolved in groundwater is obtainable from the measurement of the sulphur isotope composition of sulphates. Field studies in the Floridan aquifer, Florida, and the Edwards aquifer, Texas, show that the use of sulphur isotope data in conjunction with hydrologic and geochemical techniques permits refinements of interpretation. In the Floridan the interpretation of the chemical data, particularly the SO_4^{2-} concentration and the SO_4^{2-}/Cl^- ratio, leads to the conclusion that recharging maritime rainfall, solution of intraformational gypsum, and mixing with ocean-like saline waters are the sources of sulphate in the groundwater. Sulphur isotope data substantiate this interpretation. The Edwards in the area studied can be separated into two hydrologic units on the basis of water chemistry and aquifer characteristics. The sulphide-free waters in the part of the aquifer upgradient from a distinct sulphide boundary are low in sulphate (less than 100 mg/l) and contain no sulphide. The waters downgradient from that boundary contain greater than 150 mg/l sulphate and all contain measurable quantities of sulphide. Interpretation of the SO_4^{2-} concentration and SO_4^{2-}/Cl ratio on the basis of the Florida study leads to the erroneous conclusion that the solution of intraformational gypsum is again a major source of sulphate in the sulphide-free part of the aquifer. Isotope analyses, however, show that the gypsum is likely to be Permian in age and introduced into the aquifer by the recharge water. The absence of evidence for enrichment in ^{34}S in the sulphate in the sulphide-bearing portion of the aquifer leads to the possibility of H_2S migration upgradient from downdip oil fields.

INTRODUCTION

The sulfur-bearing chemical species most commonly found dissolved in low temperature natural waters are: $SO_4^=$, HS^- and H_2S. Which species dominates depends on the oxidation potential and pH of the system. The major contributions of these species to a system of interest include solution of evaporite minerals, mixing with encroaching ocean waters, decomposition of organic material, solution and oxidation of sulfide minerals, the inward migration of H_2S and recharge of sulfate-bearing precipitation. Such sources tend to have differing ranges of stable sulfur isotope contents. Most previous sulfur isotope studies have been in the fields of ore genesis, hydrothermal solutions and the atmosphere.

The purpose of this paper is to show how sulfur isotope data can be combined with hydrologic and geochemical techniques to determine the sources of sulfate dissolved in ground water. Parts of the Floridan aquifer in central and south Florida and the Edwards aquifer in the vicinity of San Antonio, Texas, were selected for preliminary studies. In the Florida system geochemical and sulfur isotope techniques independently lead to the same conclusions regarding the sources of the sulfate. In the Edwards system consideration of the geochemistry alone leads to an erroneous interpretation of the source of dissolved sulfate, and the sources of dissolved sulfate cannot be determined without sulfur isotope data.

SULFUR GEOCHEMISTRY

Sulfur has four stable isotopes, the most common of which are ^{32}S and ^{34}S with relative abundances of 95% and 4.2% respectively. The other two isotopes, ^{33}S and ^{36}S, constitute the remaining 0.8%. The sulfates analyzed in this study were derived from water samples freed of sulfide in the field by precipitation as zinc sulfide. For samples containing greater than 100 mg/l sulfate, sulfate was precipitated as barium sulfate. For waters containing less than 100 mg/l sulfate, sulfate was extracted by exchange on chromatographic alumina [1]. The sulfates so collected were reduced to silver sulfide (Ag_2S) by techniques described by Rafter [2] and Thode and others [3]. The Ag_2S was oxidized to SO_2, which was analyzed for sulfur isotopic composition on a Nuclide RMS-60 double-collecting isotope ratio mass spectrometer.

Table I shows the distribution of $\delta^{34}S$ values[1] in various natural sulfur-containing substances. The range of $\delta^{34}S$ values in sulfate from present-day sea water is small and has a mean value of +20.3‰ [4]. Although the $\delta^{34}S$ of marine evaporite sulfate of various ages range from +8 to +32‰, Holser and Kaplan [5, Figure 2] have shown that, for samples of a given geologic age, the range is generally less than 5‰. The range shown in Table I is the result of combining samples of all geologic ages. Because of the narrow range of $\delta^{34}S$ ($SO_4^{=}$) values of samples of a single age, however, the range of $\delta^{34}S$ ($SO_4^{=}$) values of sulfate dissolved from a given formation is likely to be quite narrow.

Sulfate in precipitation is derived mainly from solution of gaseous SO_2 and inclusion of sulfate in sea spray aerosols. The gaseous SO_2 is derived from oxidation of natural H_2S, volcanic emmanations, burning of fossil fuels, and other sources. Sulfate concentrations in precipitation over continental areas usually range from 1 to 10 mg/l, with an average of 3 mg/l. Over the oceans the values usually range from 1 to 2 mg/l [6]. Low sulfate rainfall most prevalent in nonindustrial rural areas contains sulfate derived mostly from sea spray and the oxidation of natural H_2S. The $\delta^{34}S$ ($SO_4^{=}$) is generally within the range of +3.2 to 15.6‰ [7], [8]. Higher sulfate rainfall largely in industrial

[1] Sulfur isotope variations are reported in the standard δ notation:

$$\delta^{34}S = \left[\frac{R_{sample}}{R_{standard}} - 1\right] \times 1000, \text{ where } R = {}^{34}S/{}^{32}S.$$

The analyses here are reported relative to the Canon Diablo meteorite standard.

TABLE I. SULFUR ISOTOPIC COMPOSITION OF THE PRINCIPAL SOURCES OF GROUND WATER SULFATE[a]

	Mean $\delta^{34}S$ (‰)	Range of $\delta^{34}S$ (‰)
Sea water $SO_4^=$	+20.3	+18.9 to +20.7
Marine evaporite sulfate minerals	-- [b]	+8 to +32
Precipitation $SO_4^=$	+8.1	-1.5 to +19.4
Biogenic H_2S	-15	-35 to +4
Sedimentary rock sulfide minerals	-15	-35 to +42

[a] Means and ranges after Refs [5] and [4] and others.
[b] Since the range of $\delta^{34}S$ for marine evaporite sulfate minerals differs with geologic age, the calculation of an overall mean is not meaningful.

areas is depleted in ^{34}S because of the SO_2 from fossil fuels. Rafter [9], Rafter and Muzutani [10] and Muzutani and Rafter [11], using sulfur and oxygen isotopes, determined that both sea spray and industrial SO_2 were significant contributors to $SO_4^=$ in rainfall in New Zealand. Cortecci and Longinelli [12] determined that industrial SO_2 was the primary contributor in the vicinity of Pisa, Italy.

H_2S is mobile, and, where a downgradient source for its migration into an oxidizing environment exists, it is a potential source of sulfate. As with the oxidation of sulfide minerals, the presence of a minor amount of H_2S-derived sulfur could alter the isotopic composition of dissolved sulfate significantly, especially where sulfate concentrations are low. The $\delta^{34}S$ values of reduced sulfur can vary widely, depending on the ultimate source of the reduced sulfur. (See Table I.)

FIELD STUDIES

The Floridan aquifer in central and southern Florida and the Edwards aquifer in the vicinity of San Antonio, Texas, were selected for field studies because of the great variation in $SO_4^=$ concentration in each of them and the availability of good hydrologic and geochemical control within each system.

Hydrology of the Floridan Aquifer

The area of study in Florida, shown on Figure 1 [13] extends from about latitude 25° N to slightly north of 29° N. The area is tropical to sub-tropical, and the primary climatic controls are its relatively low latitude, proximity to the Atlantic Ocean and Gulf of Mexico, and numerous inland lakes. Mean annual rainfall ranges from about 1300 to 1500 millimeters.

Descriptions of the Florida peninsula pertinent to geochemical studies have been given in previous papers [14], [15], [16]. The principal artesian (Floridan) aquifer is one of the most extensive limestone aquifers in the United States. In central Florida the maximum thickness of the fresh water lens in the aquifer is approximately 650 meters [17].

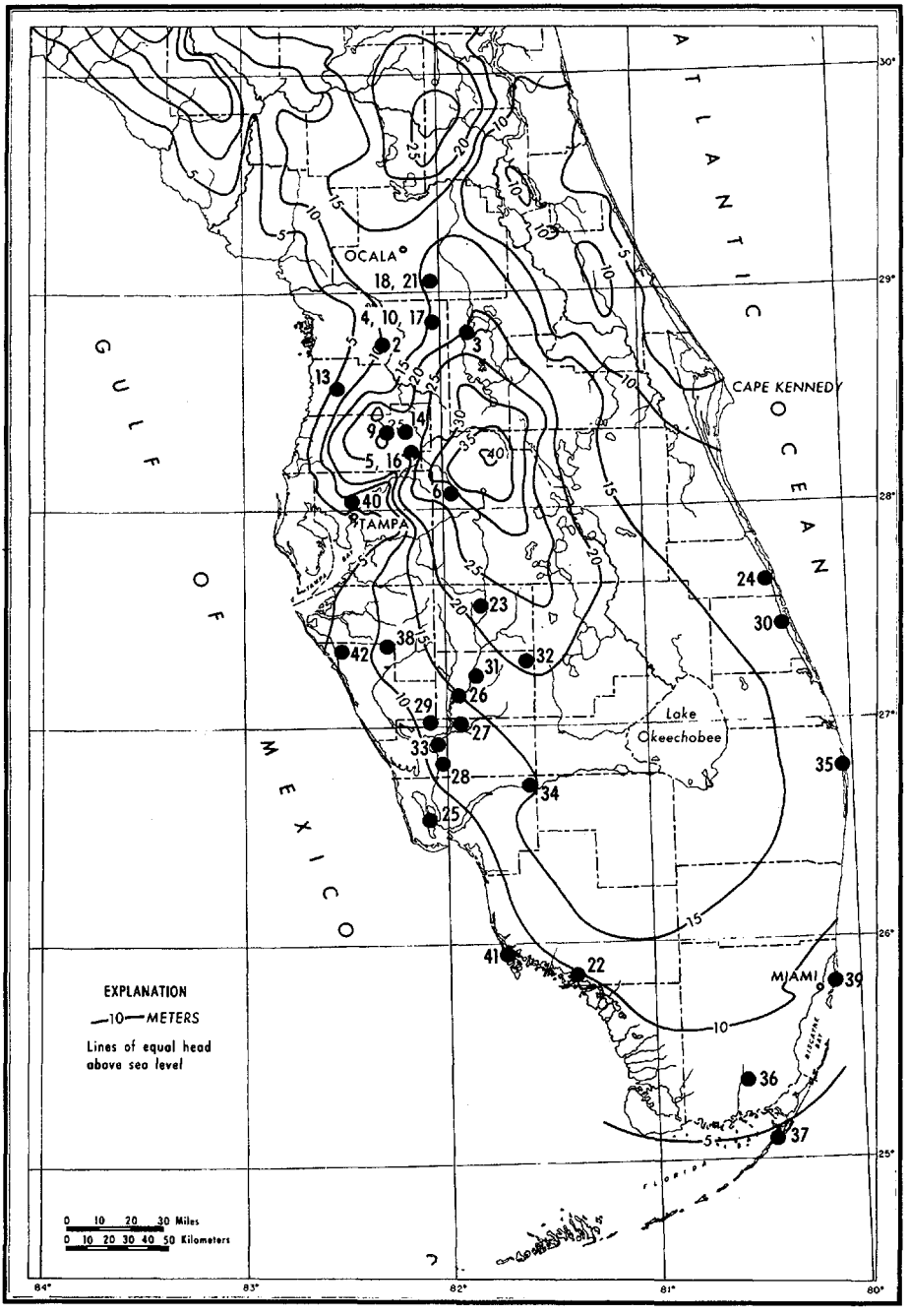

FIG. 1. Potentiometric map of the principal artesian aquifer of Florida and location of sampling sites (after Ref. [13]).

The potentiometric map of the Floridan aquifer south of Ocala is dominated by two ground-water mounds (Figure 1). Areas in which these potentiometric highs occur, however, are covered by the rather impermeable Hawthorne Formation. Water from the central potentiometric high moves outward in all directions and discharges near the coast to the east. In the general vicinity of Ocala, overlying sediments that form the confining bed are thin or lacking. Because the limestone is exposed in this area, a great deal of recharge occurs there, but the potentiometric gradient is low due to the rapid discharge of the water. This discharge is through the many springs in the area of the ground-water saddle near Ocala. Because of the lack of an effective confining bed, much rainfall infiltrates to the water table, resulting in small quantities of direct runoff to streams.

Although the potentiometric surface has essentially the same gradient and shape both to the north and south of the central high, less recharge occurs in the southern portion of the elongated dome owing to a thicker confining bed and lower transmissivity of the aquifer. Water that flows southward discharges either upward through the confining beds or to the ocean and the gulf.

Although no chemical analyses of the deep salt water underlying central Florida are available, it probably has (1) sodium, chloride, and sulfate concentrations similar to ocean water; (2) a significantly lower concentration of magnesium because of dolomitization of limestone; and (3) a higher concentration of calcium resulting from both replacement by magnesium in the dolomitization process and solution of limestone. These conclusions are based in part by interpretation of analyses of brines in southern Florida [15].

In the principal artesian aquifer of central and southern Florida ground water moves at about 7 meters per year [18] in the areas where it is effectively confined. In areas of greatest recharge and discharge the movement is far more rapid and can be as high as a meter per day.

Geochemistry and Sulfur Composition of Sulfate in the Floridan Aquifer

The concentrations and $\delta^{34}S$ ($SO_4^=$) values in 32 samples from central and southern Florida are given in Table II. The distribution of sulfate in the Floridan aquifer is essentially the same as that of other constituents in the water. The lowest concentrations are in the recharge area and in the area of the highest potentiometric surface [14], and the sulfate increases gradually downgradient to values greater than 500 mg/l. The highest concentration (868 mg/l) is in the area of Well 42, south of Tampa Bay. It has been recognized that the high sulfate concentrations in the waters here and elsewhere in southern Florida result from solution of sedimentary gypsum that is present in the Floridan aquifer system. Even the waters of highest sulfate content, though, are not saturated with respect to gypsum. Sulfide is absent in the recharge area, but is present in concentrations of less than 3.5 mg/l throughout the remainder of the system.

In Figure 2, $SO_4^=/Cl^-$ ratios are plotted against sulfate concentration as an aid to determining the origin of the sulfate dissolved in the Floridan ground water. Samples 2, 3, 4 and 5 have a $SO_4^=/Cl^-$ ratio of 0.2 to 0.3 and contain less than 5 mg/l of sulfate in solution. These samples were all taken from the area of high recharge south of Ocala and are characteristic of the recharge to the system as a whole. Although no analyses of rainfall in Florida were readily available, studies of coastal rainfall in North Carolina [19], and of rainfall on the island of St. Thomas [20], show that the sulfate concentration in maritime rainfall is generally less than 2 mg/l and that the $SO_4^=$ concentration of

TABLE II. CHEMICAL DATA FOR WATER SAMPLES FROM FLORIDAN AQUIFER

Sample number	Location	Sulfate concentration (mg/l)	δS^{34}_{CD} (SO_4) (‰)	Sulfide concentration as H_2S (mg/l)	Chloride concentration (mg/l)
2	Floral City	2.4	+12.5	0	10
3	Leesburg	2.8	+8.1	0	9
4	Wildwood 2	3.2	+14.1	0	11
5	Zephyrhills	3.6	+14.3	0	9
9	San Antonio	6.2	+9.8	0	8
10	Weekiwachee	6.2	+15.5	0	6
13	Brooksville 2	12	+23.1	0	11
14	Dade City	13	+17.7	0	8
16	Zephyrhills 2	31	+23.2	0	8
17	Wildwood 1	34	+10.5	0	14
18	Belleview 1	36	+20.4	0	8
21	Belleview 2	112	+20.7	0	8
22	Everglades City	120	+21.4	0.53	380
23	Wauchula	155	+24.9	1.2	11
24	Vero Beach	158	+29.6	3.3	705
25	Big Pine Island	219	+24.3	1.3	808
26	Hull Cemetery	257	+25.3	2.4	117
28	Burnt Store	267	+24.1	2.0	1160
29	Port Charlotte	277	+24.4	1.3	700
30	Fort Pierce	286	+27.4	1.99	350
31	Arcadia	344	+24.5	1.5	28
32	Tropical R. Groves	358	+23.8	1.7	29
33	Punta Gorda	380	+23.8	1.3	1360
34	Alva	389	+23.3	1.5	1340
35	Peanut Island	400	+25.7	1.2	1520
36	Royal Palm	500	+26.1	0	3040
37	Pennecamp	500	+23.1	1.8	2300
38	Verna	505	+23.7	1.5	19
39	La Gorce	516	+22.3	0.89	3290
40	Sulfur Springs	636	+22.3	0.90	3680
41	Marco Island	674	+22.2	2.2	4040
42	Sarasota	868	+22.8	1.5	236

the recharge samples here may be due to evaporative concentration of the water prior to recharge. Samples 36, 39, 40 and 41 are all near the coast or salt water embayments and have sulfate concentrations of 500 mg/l or more, and $SO_4^{=}/Cl^-$ ratios approaching 0.1. They fall on a line defining a mixing trend between recharge water and ocean water. Another group of waters (samples 9, 10, 14, 16, 18 and 21) show increasing $SO_4^{=}/Cl^-$ ratios with increasing sulfate concentration. Solution of sedimentary gypsum in waters of the recharge type would produce waters such as are found in these wells. The remainder of the waters plotted on Figure 2

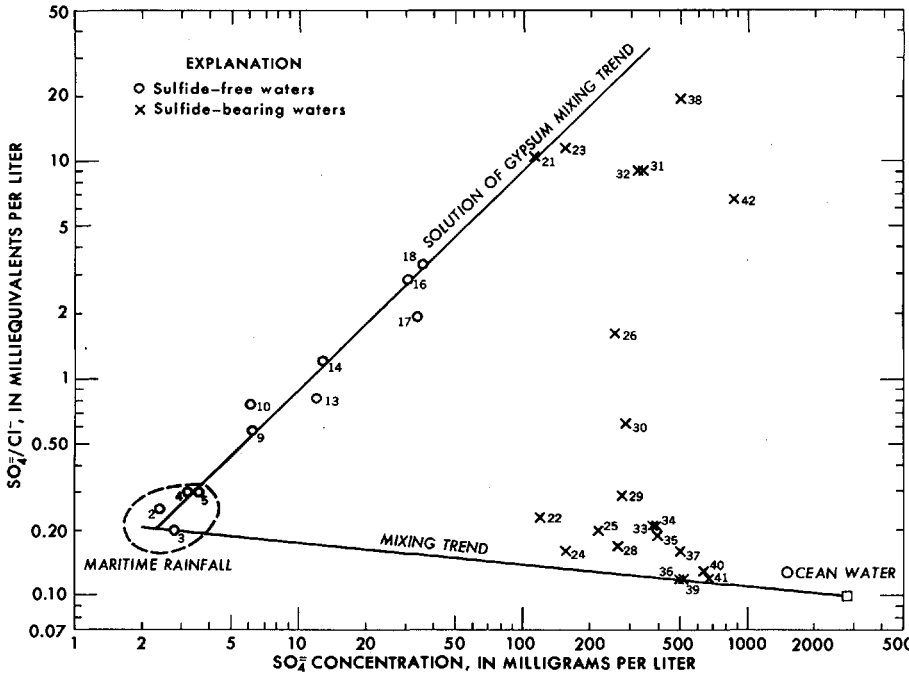

FIG.2. Relationship between $SO_4^=/Cl^-$ ratio and $SO_4^=$ concentration in water from the Floridan aquifer.

are apparently mixtures in recharge water of sulfate derived both from the solution of gypsum and from mixing with water chemically similar to ocean water.

These conclusions about the source of sulfate in the water tend to be substantiated in Figure 3, which is a plot of $\delta^{34}S$ ($SO_4^=$) versus sulfate concentration. The water containing low sulfate concentrations and identified as being derived predominantly from atmospheric precipitation has $\delta^{34}S$ ($SO_4^=$) values of from +8 to +15‰. Samples with higher sulfate concentrations (those exceeding 100 mg/l) have $\delta^{34}S(SO_4^=)$ values more positive than +20.7, with the majority being around +24‰. The curve A-B on Figure 3 represents mixing of sulfate derived from maritime rainfall, here assumed to have an average $\delta^{34}S$ ($SO_4^=$) value of +10, and a sulfate concentration of 3 mg/l, with sulfate derived from marine $SO_4^=$ (ocean water or evaporite minerals) with a $\delta^{34}S$ ($SO_4^=$) of +22‰. Samples 10, 14, and 18 follow this line reasonably well. However, samples 9 and 17 contained additional amounts of sulfate, which, from their isotopic composition, would be expected to be rainfall-derived. However, the higher $SO_4^=$ concentrations of these samples (Figure 2) are not accompanied by higher chloride concentration and thus they are not simply concentrated rainfall. Samples 13 and 16 seem to contain excess sulfate derived from the solution of marine evaporite gypsum.

Although the $\delta^{34}S$ ($SO_4^=$) values of the Floridan waters containing sulfate concentrations of greater than 100 mg/l are consistent with a sulfate source either in present-day ocean water or from ancient oceanic

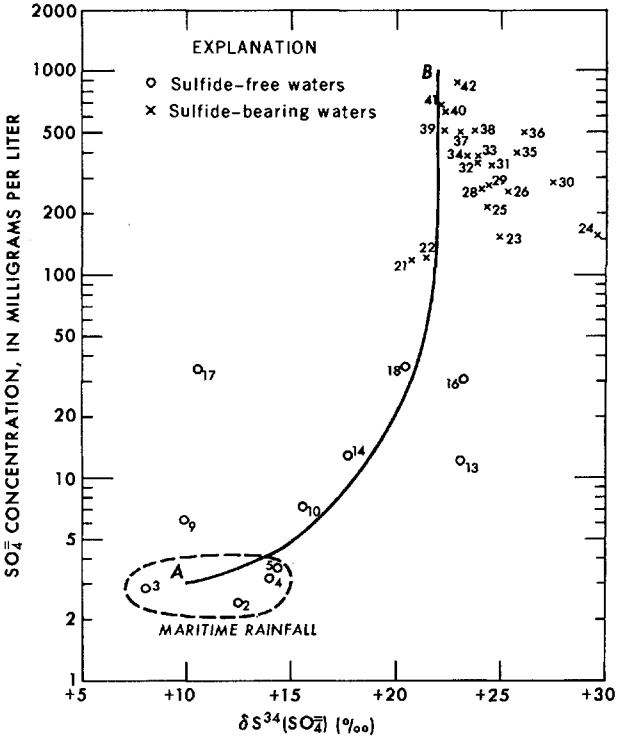

FIG. 3. Relationship between $\delta^{34}S$ ($SO_4^=$) and $SO_4^=$ concentration in water from the Floridan aquifer. Curve A-B represents mixing of sulphate derived from various sources.

evaporite minerals, approximately +22‰ , some of the δS ($SO_4^=$) values are somewhat more positive than present-day oceanic sulfate. Sulfur isotope fractionation during reduction of sulfate will result in the enrichment of ^{34}S in the sulfate. Production of sulfide by reduction of sulfate dissolved in these waters could, therefore, result in a higher $\delta^{34}S$ ($SO_4^=$) value in the residual sulfate in solution and may cause the measured $\delta^{34}S$ ($SO_4^=$) values in these samples to be more positive than +20 to +22‰ [21].

Hydrogeochemistry of the Edwards Aquifer, Central Texas

The Edwards and associated limestones form the aquifer that is the chief source of water to the city of San Antonio, Texas, and vicinity (Figure 4). The north and northwest parts of the San Antonio area are in the Edwards Plateau region, while the south and southeast parts are on the Gulf Coastal Plain. These two physiographic areas are separated by the Balcones fault zone. The base flow of the streams that drain the Edwards Plateau is spring flow from the water table aquifer in the Plateau. This base flow and part of the flood flow are lost by seepage into the outcrop of the Edwards aquifer at the Balcones fault

zone. Recharge to the aquifer is partly by this seepage and partly by direct infiltration of precipitation on the outcrop. Water supply from the Edwards is from that section lying just to the south of the Balcones fault zone. The general flow path in the part of the Edwards aquifer used for water supply is to the east and northeast, with natural discharge at large springs at New Braunfels and San Marcos. The western boundary is at a ground-water divide near the western boundary of Uvalde County. This sulfide-free water supply is an oxidizing calcium bicarbonate type with a total dissolved-solids content of 250 to 300 mg/l. The lower limit of sulfide-free water is shown on Figure 4 as the sulfide boundary. Downdip, the character of the water changes abruptly. It becomes strongly reducing, has a high sulfate content, and contains considerable quantities of hydrogen sulfide. The geology and hydrology of the Edwards have been described by Garza [22] and by Pettit and George [23]; its petrology and depositional environment by Fisher and Rodda [24].

There are differences in the aquifer material as well as the water on the two sides of the sulfide boundary shown on Figure 4. Studies in progress [25] indicate that calcite is dominant in the sulfide-free zone and that most of the sulfate minerals have been removed by solution in zones of fresh water circulation. The dominant mineralogy in the sulfide-bearing part of the Edwards is dolomite, and both celestite and gypsum are preserved there, at least in part. In both the sulfide-free and the sulfide-bearing zones, collapse breccias have been formed by solution of sulfate minerals.

Geochemistry and Sulfur Isotope Composition of Sulfate in the Edwards Aquifer

The concentrations and isotopic composition of sulfate and the concentration of sulfide dissolved in samples from 29 Edwards wells and two recharging streams are given in Table III. In the sulfide-free-water part of the aquifer the sulfate concentration ranges from 7.8 to 83 mg/l, while in the sulfide-bearing part, the sulfate concentration is as high as 2 000 mg/l. Mineral equilibrium calculations [26] show that waters of highest sulfate concentration (samples 24, 25, 26, 31 and 32) are saturated with gypsum.

Figure 5 shows the variation in the sulfate concentration with $SO_4^{=}/Cl^-$ ratio in the Edwards water and Figure 6 the variation of $\delta^{34}S$ $(SO_4^{=})$ with sulfate concentration. On Figure 5, the sulfide-free waters (samples 1 through 17) fall on a line apparently representing the addition of sulfate to a water of low $SO_4^{=}/Cl^-$ ratio and relatively low sulfate concentration. By analogy with the Florida system, these could be interpreted as waters to which sulfate from the solution of intraformational gypsum was being added. However, the isotopic data, Figure 6, shows that this is an erroneous interpretation of the chemical data.

A sample of playa water collected northwest of the recharge area immediately after a rainstorm yielded a sulfate concentration of 4.1 mg/l and a $\delta^{34}S$ $(SO_4^{=})$ of +3.6‰. The sulfate concentration of two recharging streams are 13 and 16 mg/l, and their $\delta^{34}S$ $(SO_4^{=})$ values are +11.3 and +10.9‰ respectively. The sulfate concentration of the rainfall could easily be increased to that of the streams by evaporation, but this cannot account for ^{34}S enrichment to 11‰.

If the sulfate in the sulfide-free water were a mixture of atmospheric sulfate ($\delta^{34}S$ $(SO_4^{=})$ ≈ +4‰) and formation evaporite sulfate ($\delta^{34}S$ $(SO_4^{=})$ ≈ +22‰), the sulfate in the samples should have isotopic compositions between those limits, but approaching +22‰ for the higher

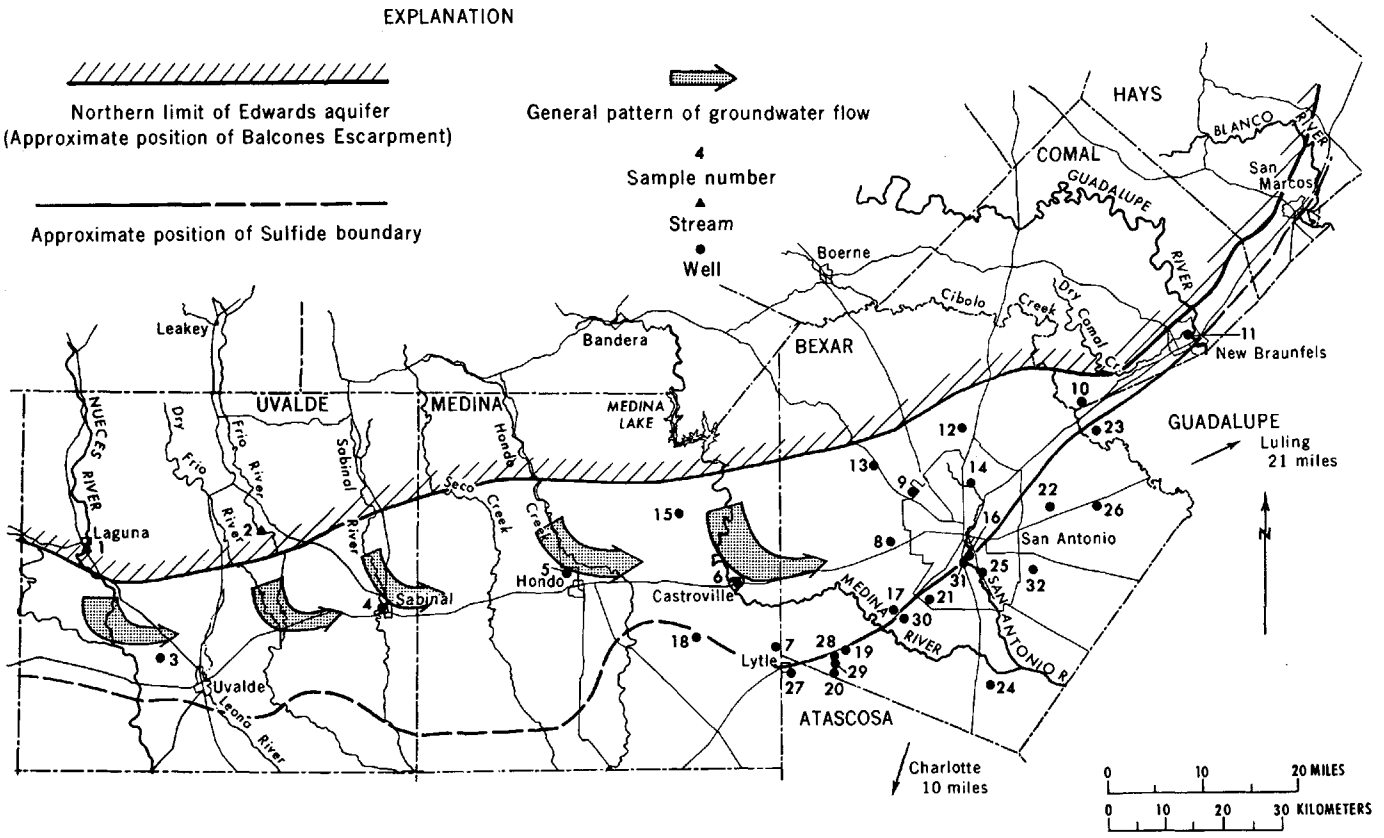

FIG. 4. Index map showing area of Edwards aquifer and sampling sites.

TABLE III. CHEMICAL DATA FOR WATER FROM EDWARDS AQUIFER

Sample number	Sulfate concentration (mg/l)	δS^{34}_{CD} (SO_4) (‰)	Sulfide concentration as H_2S (mg/l)	Chloride concentration (mg/l)
		RECHARGING STREAMS		
1	13	+11.3	0	14
2	16*	+10.9	0	14
		SULFIDE-FREE GROUND WATER		
3	10	+11.5	0	17
4	83	+19.1	0	18
5	16	+13.3	0	12
6	14	+10.5	0	14
7	15	+14.9	0	14
8	15	+10.6	0	11
9	29	+13.3	0	14
10	29	+8.3	0	13
11	23	+12.8	0	12
12	7.8	+15.2	0	14
13	21	+8.6	0	14
14	31	+11.5	0	12
15	22	+14.0	0	10
16	25	+13.4	0	15
17	25	-	0	15
		SULFIDE-BEARING GROUND WATER		
19	220	+19.1	3.2	86
20	490	+20.1	10	204
21	211	+18.3	1.2	97
22	195	+26.7	0.04	147
23	619	+22.0	6.7	552
24	1880	+21.5	63	870
25	2000	+20.6	50	871
26	1880	+21.3	18	1560
27	169	+21.8	0.5	44
28	187	+20.0	3.7	85
29	466	+21.1	12	244
30	730	+22.5	22	376
31	1440	+22.2	55	1050
32	1850	+22.0	46	934

sulfate waters. In fact, as Figure 6 shows, all the sulfide-free samples, except number 4, have $\delta^{34}S$ ($SO_4^{=}$) values of less than +15‰.

We interpret the relatively constant $\delta^{34}S$ ($SO_4^{=}$) values of the sulfide-free water in the Edwards as follows: Atmospheric precipitation in the region of Texas from which recharge to the Edwards is derived often occurs in brief, but rather violent, storms, which are accompanied by high winds and dust. When the winds in the area of study are from the west, they have had the opportunity to gather evaporite dust as they crossed the exposed reaches of Permian Delaware Basin evaporite deposits $\delta^{34}S$ value of approximately +11‰ [27], [5].

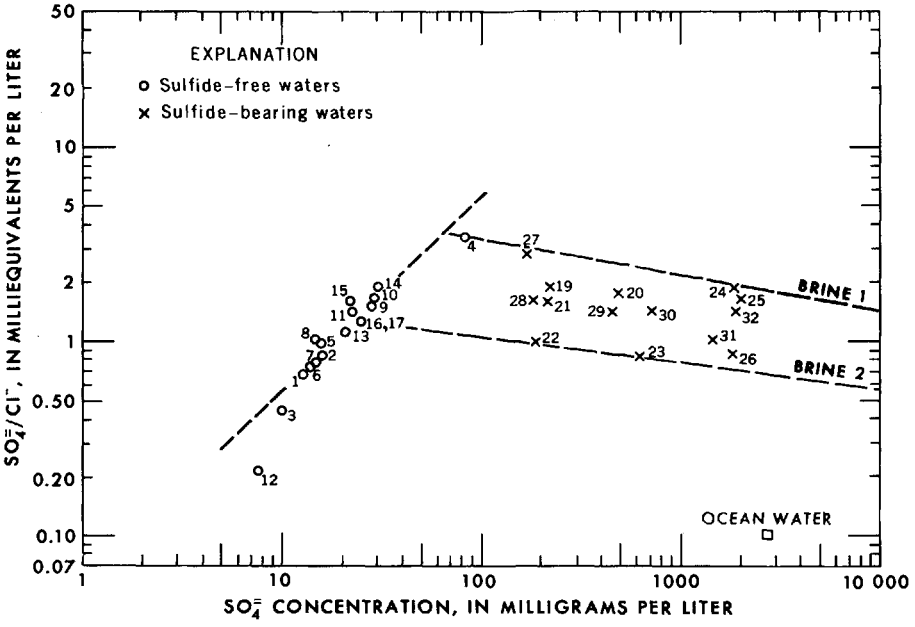

FIG.5. Relationship between $SO_4^{=}/Cl^-$ ratio and $SO_4^{=}$ concentration in water from the Edwards aquifer.

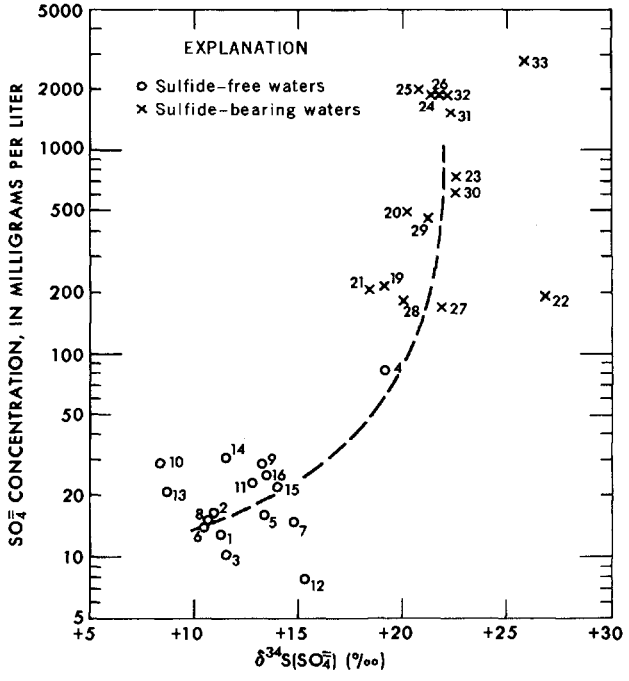

FIG.6. Relationship between $\delta^{34}S$ ($SO_4^{=}$) and $SO_4^{=}$ concentration in water from the Edwards aquifer.

This dust settling or washed to the ground could then be a source of sulfate in the recharging water. Surface runoff would quickly dissolve sulfate-dust fallout and thereby greatly increase the dissolved sulfate concentration in the waters of the recharging regional streams.

The chloride in the rainfall is likely to be fairly constant as a result of oceanic aerosols in the precipitation, but, because of blowing dust, the sulfate concentration may vary greatly from storm to storm, depending on the amount of dust associated with the storm. Thus, it is possible that waters entering the Edwards could have a widely varying $SO_4^{=}/Cl^-$ ratio coupled with a relatively constant $\delta^{34}S\,(SO_4^{=})$ (Permian evaporites).

This hypothesis would explain the relatively constant chloride concentrations of the waters in the sulfide-free water from the Edwards. It would also account for the lack of apparent systematics of sulfate concentration within the aquifer, such lack resulting from the aquifer's many recharge points, each point deriving its water from a region with varying local climatic, dust and precipitation conditions. It is also known from mineralogic studies presently in progress that the aquifer generally contains no gypsum in the sulfide-free part of the aquifer. Well Number 4, which contains sulfide-free water with the highest $SO_4^{=}/Cl^-$ ratio and with a $\delta^{34}S\,(SO_4^{=})$ value of about +19‰, however, is located in a region in the Edwards where water circulation is not as rapid as elsewhere in the sulfide-free zone and which may still contain some residual sedimentary gypsum. It is, therefore, probably the only one of the sulfide-free waters that, on the basis of sulfur isotopes, contains significant sulfate derived from the formation itself.

Water circulation in the sulfide-bearing part of the Edwards is much more restricted than in the sulfide-free section, and it is known that sedimentary gypsum remains in this part of the aquifer. Thus, the more positive $\delta^{34}S(SO_4^{=})$ values from samples in the sulfide-bearing portion of the formation are not surprising; and, as shown on Figure 6, there is a reasonable agreement between their sulfate contents and sulfur isotope compositions based on a model of mixing sulfate of +22‰, such as would be typical of the formation, with water typical of the sulfide-free Edwards with a $\delta^{34}S\,(SO_4^{=})$ of 10‰ and 12 mg/l SO_4. However, Figure 5 shows that, while there is an enormous increase in the sulfate content of the sulfide-bearing water in the Edwards, there is a slight decrease in the $SO_4^{=}/Cl^-$ ratio.

A summary of the chemical character of the Edwards aquifer (Figure 7) shows a very tight grouping of the samples from the sulfide-free zone in the calcium bicarbonate region of the diagram. This is the type of water expected in a carbonate aquifer system.

Figures 5 and 7 show the development of approximately parallel trends away from low sulfate, sulfide-free waters to sulfide-bearing waters with much higher sulfate concentrations. Generally speaking, waters with the highest sulfate concentrations also yield the highest sulfide concentrations (Table III), indicating the possibility that both the sulfide and the sulfate in the sulfide-bearing waters have been derived, at least in part, from a downdip source. The high sulfate samples, with the exception of number 22, however, show no evidence of significant ^{34}S enrichment in the sulfate that might accompany reduction of sulfate (Figure 6)[20]. This suggests that the sulfate is a result less of the solution of sedimentary gypsum than it is of the presence deeper in the formation of residual brines of marine origin. Such brines are known to exist in parts of the Edwards farther downdip from the part studied here, where they are associated with producing oil fields in the Edwards, located at Luling and Charlotte (Figure 4).

As total dissolved solids (Figure 7) increase downgradient, away from the sulfide-free water, trends develop, as on Figure 5, pointing

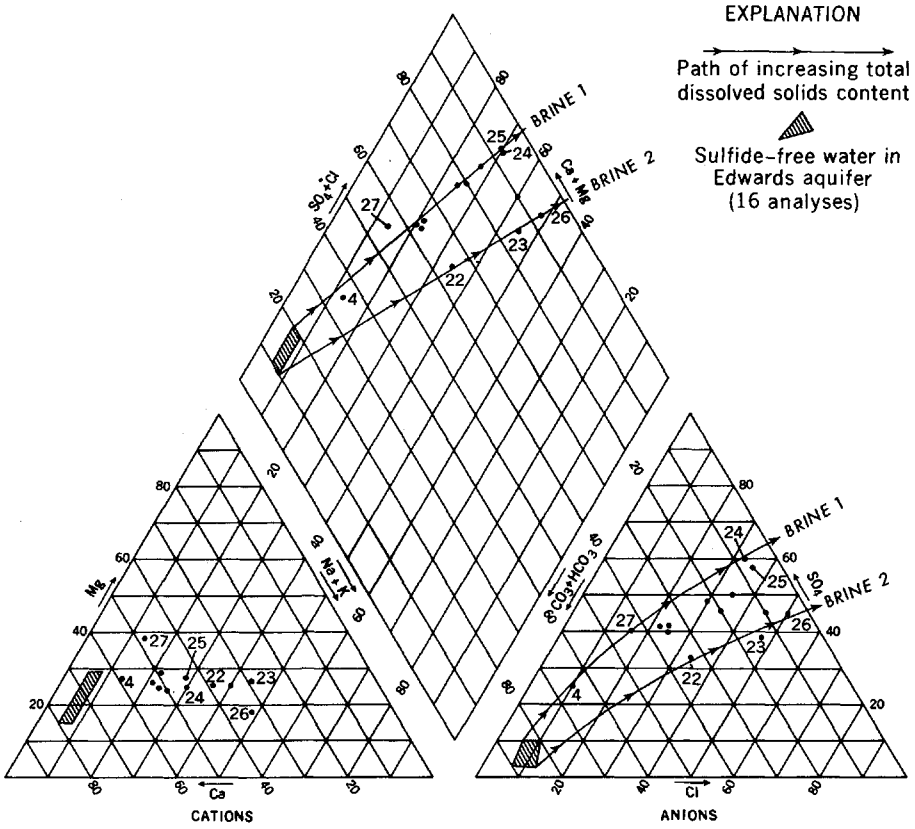

FIG. 7. *Chemical character of water from the Edwards aquifer.*

in the direction of a hypothetical residual brine of marine origin of some composition intermediate between Brine 1 and Brine 2 (Figures 5 and 7), a brine that could be associated with the oil fields at Luling and Charlotte.

SUMMARY

We have shown, using chemical and hydrologic data, that, although a small part of the sulfate in the water of the Floridan aquifer is derived from maritime rainfall, most results from either solution of gypsum by recharging rainfall, mixing of maritime rainfall with sea water within the aquifer, or both. The use of the $\delta^{34}S$ ($SO_4^{=}$) versus $SO_4^{=}$ concentration (Figure 3) confirms the interpretation. In the recharge area, both the concentration and the $\delta^{34}S$ of the dissolved sulfate are in the range of maritime rainfall. Using only Figure 3, $\delta^{34}S$ ($SO_4^{=}$) and the sulfate concentration, it would be impossible to distinguish between marine evaporite sulfate and ocean water sulfate. The $SO_4^{=}/Cl^{-}$ ratio versus $SO_4^{=}$ concentration plot (Figure 2) permits the distinction to be made.

In the Edwards there are, in effect, two separate hydrologic units within the same aquifer. By studying the hydrology of the sulfide-free water zone and interpreting the stable isotope data, one can see that the dashed line plotted on the $SO_4^{=}/Cl^-$ versus $SO_4^{=}$ concentration plot for the Edwards (Figure 5) resembles the solution of gypsum trend shown in the same plot for the Floridan (Figure 2), although the relative differences in $SO_4^{=}/Cl^-$ ratio are smaller. Solution of gypsum can be a source of sulfate in low sulfate waters, but the isotopes show that the gypsum is not predominantly sedimentary Cretaceous gypsum that occurs in parts of the aquifer. The major source seems to be sulfate dust derived from Permian evaporite deposits and dissolved by precipitation prior to recharge. The decrease in the $SO_4^{=}/Cl^-$ ratio accompanying the large increase in $SO_4^{=}$ concentration above 100 mg/l (Figure 5), as well as the trends developed with increasing total dissolved solids (Figure 7), suggest a mixing of waters of the composition of those in the sulfide-free water zone with waters with the composition of hypothetical brines 1 and 2. The isotope data (Figure 6), which show no indication of ^{34}S enrichment in the sulfates of the samples that contained sulfide, suggest that, unlike the Florida data, the H_2S is not derived from the reduction of sulfate. Instead, this raises the possibility of H_2S migration into the system.

It has been shown that, on the basis of chemistry and hydrology alone, it is not always possible to determine precisely the sources of dissolved sulfate in ground waters. While the interpretation based on chemical and hydrologic evidence that the source of sulfate in sulfide-free waters is solution of gypsum is accurate, it takes the isotope data to show whether this sulfate is derived from intraformational gypsum within the aquifer.

ACKNOWLEDGEMENTS

We would like to thank Messrs. G. H. Davis, D. W. Fisher, and I. J. Winograd for stimulating discussions and reviews of the manuscript. This study was supported in part by U. S. Army Research Office - Durham, Grant 10790-EN.

REFERENCES

[1] BODDEN, M.D., FISHER, D.W., RIGHTMIRE, C.T., Extraction of sulfate ion from low sulfate natural waters for isotopic analysis (in preparation).

[2] RAFTER, T.A., Sulphur isotopic variations in nature, 2: A quantitative study of the reduction of barium sulphate by graphite for recovery of sulphide-sulphur for isotopic measurements, N.Z. J. Sci. Technol. 38 (1957) 955.

[3] THODE, H.D., MONSTER, J., DUNFORD, H.B., Sulphur isotope geochemistry, Geochim. Cosmochim. Acta 25 (1961) 159.

[4] AULT, W.U., KULP, J.L., Isotopic geochemistry of sulphur, Geochim. Cosmochim. Acta 16 (1959) 201.

[5] HOLSER, W.T., KAPLAN, I.R., Isotope geochemistry of sedimentary sulfates, Chem. Geol. 1 (1966) 92.

[6] JUNGE, C.E., "Air chemistry and radioactivity", International Geophysics Series 4, Academic Press, New York (1963) 365.

[7] OSTLUND, G., Isotopic composition of sulfur in precipitation and sea water, Tellus 11 (1959) 478.

[8] JENSEN, M.L., NAKAI, N., Sources and isotopic composition of atmospheric sulfur, Science 134 (1961) 2102.

[9] RAFTER, T.A., Recent sulfur isotope measurements on a variety of specimens examined in New Zealand, Bull. Volcanol. 28 (1965) 3.

[10] RAFTER, T.A., MIZUTANI, Y., Oxygen isotope composition of sulfates, 2: Preliminary results on oxygen isotopic variation in sulfates and the relationship of their environment and to their $\delta^{34}S$ values, N.Z. J. Sci. 10 (1967) 816.

[11] MIZUTANI, Y., RAFTER, T.A., Isotopic composition of sulfate in rain water, Gracefield, New Zealand, N. Z. J. Sci. 12 (1969) 69.
[12] CORTECCI, G., LONGINELLI, A., Isotopic composition of sulfate in rain water, Pisa, Italy, Earth Planet. Sci. Lett. 8 (1970) 36.
[13] STRINGFIELD, V.T., Artesian water in the Florida Peninsula, US Geol. Survey Water Supply Paper 773-C (1936) 115.
[14] BACK, W., HANSHAW, B.B., Comparison of chemical hydrogeology of the carbonate peninsulas of Florida and Yucatan, J. Hydrol. 10 4 (1970) 330.
[15] BACK, W., HANSHAW, B.B., "Rates of physical and chemical processes in a carbonate aquifer", Advances in Chemistry Series, No. 106, Nonequilibrium Systems in Natural Water Chemistry (HEM, J.D., Ed.) (1971) 77.
[16] HANSHAW, B.B., BACK, W., DEIKE, R.G., A geochemical hypothesis for dolomitization by groundwater, Econ. Geol. 66 (1971) 710.
[17] PRIDE, R.W., MEYERS, F.W., CHERRY, R.N., Hydrology of the Green Swamp Area in Central Florida, Fla. Geol Surv., Rep. of Investigation No.42 (1966).
[18] HANSHAW, B.B., BACK, W., RUBIN, M., Radiocarbon determinations for estimating groundwater flow velocities in Central Florida, Science 148 3669 (1965) 494.
[19] FISHER, D.W., Annual variations in chemical composition of atmospheric precipitation, Eastern North Carolina and Southeastern Virginia, US Geol. Survey Water Supply Paper 1535-M (1968) M1-M21.
[20] JORDAN, D.B., FISHER, D.W., Contribution of bulk precipitation to water quality of St. Thomas, Virgin Islands (in press).
[21] PEARSON, F.J., RIGHTMIRE, C.T., RYE, R.O., BACK, W., HANSHAW, B.B., Fractionation of sulfur isotopes in ground-water systems (in preparation).
[22] GARZA, S., Groundwater Resources of the San Antonio Area, Texas: A Progress Report on Studies, 1960-1964, Texas Water Development Board Report 34 (1966).
[23] PETTIT, B.M., Jr., GEORGE, W.O., Groundwater Resources of the San Antonio Area, Texas: Texas Board Water Engineers Bull. 5608 (1956).
[24] FISHER, W.L., RODDA, P.U., Edwards formation (Lower Cretaceous), Texas: Dolomitization in a carbonate platform system, Bureau of Econ. Geol. Circular 69-1, The Univ. of Texas (1969) 55.
[25] DEIKE, R.G., written communication (1973).
[26] TRUESDELL, A.H., JONES, B.F., WATEQ, A computer program for calculating chemical equilibria for natural waters, NTIS Pub. No. PB-220464 (1973).
[27] THODE, H.G., Stable isotopes: a key to our understanding of natural processes, Bull. Con. Petrol. Geologists 12 (1964) 242.

DISCUSSION

J. DOWGIAŁŁO: Could you tell us something about the age of the aquifers you were dealing with and the $\delta^{34}S$ values of the gypsum?

C.T. RIGHTMIRE: The Floridan aquifer system is of Eocene age and the $\delta^{34}S$ value of the sulphate minerals present is approximately +21‰. The sulphate minerals are largely missing from the recharge zone, owing to dissolution, and their abundance increases downgradient. The Edwards aquifer is of Cretaceous age and the $\delta^{34}S$ value of the sulphate minerals is approximately +22‰. Sulphate minerals are missing almost totally from the sulphate-free part of the aquifer and are present in the sulphide-bearing part as gypsum and celestite.

E. MAZOR: In Fig. 6 we see that the high-$SO_4^=$ waters contain sulphides and the low-$SO_4^=$ waters do not. This is what one would expect if the H_2S is a product of biological decomposition; the same pattern has been observed in the Jordan Rift Valley. Perhaps the biological activity is encouraged by a higher $SO_4^=$ content and one has waters which enter into limited but intense contact with gypsum strata, only the latter undergoing H_2S-forming biological processes.

C.T. RIGHTMIRE: The isotopic composition of the dissolved sulphate in the high-sulphate waters of the Edwards aquifer does not point to ^{34}S enrichment, which would be indicative of sulphate reduction, thereby suggesting the possibility of H_2S migration into the system.

F.J. PEARSON: As a co-author of this paper I should like to make a comment.

I am sure that Mr. Mazor did not mean to imply that the bacterial reduction of sulphate occurs only in high-sulphate waters. We know of at least one aquifer in which H_2S is forming in water containing less than 10 mg of $SO_4^{=}$ per litre.

J.A.P. SARROT-REYNAULD: Are both the Floridan and the Edwards aquifers confined systems?

C.T. RIGHTMIRE: Yes, they are.

The Edwards aquifer is in effect composed of two hydrological units, the flow in the up-dip sulphide-free unit being from west to east along the strike. There is no isotopic evidence of ^{34}S enrichment in the sulphate of the sulphide-bearing unit and hence no indication of sulphate reduction.

P. FRITZ: I should like to mention data we have obtained in a very similar study. In the study area (south-west Ontario), the typical $\delta^{34}S$ values of the rain-water are between 0 and +5‰, but the shallow aquifers in the recharge area have typical values between - 2‰ and - 10‰. Thus, unlike you, we are not able to start with a mixing line for the mixing of precipitation and water with marine sulphate; in our case, mixing begins after the water has passed the upper soil horizons. As in your case, the positive component is water with marine sulphate having $\delta^{34}S$ values of up to +25‰.

Both studies clearly show that ^{34}S in groundwater sulphate can be successfully employed to obtain information about the origin of the dissolved sulphur species and the flow paths of groundwaters.

UTILISATION DES VARIATIONS NATURELLES D'ABONDANCE DE L'AZOTE-15 COMME TRACEUR EN HYDROGEOLOGIE
Premiers résultats

R. LETOLLE, A. MARIOTTI
Département des Sciences de la Terre,
Université de Paris VI,
Paris, France

Abstract

UTILIZATION OF NATURAL VARIATIONS IN THE ABUNDANCE OF NITROGEN-15 AS A TRACER IN HYDROGEOLOGY – INITIAL RESULTS.

Nitrogen compounds dissolved in natural waters exhibit considerable variations in nitrogen-15 content (more than 10‰). The authors describe briefly the analytical techniques used in measuring $\delta^{15}N$, the main features of the isotopic cycle of nitrogen and the results obtained so far. A simplified model of the nitrogen cycle and its isotopic implications is presented; with this model one can deduce from a number of observed variations the physical or biological mechanism (or mechanisms) involved. Isotopic studies of nitrogen may be a useful additional tool for detecting and interpreting certain forms of pollution.

UTILISATION DES VARIATIONS NATURELLES D'ABONDANCE DE L'AZOTE-15 COMME TRACEUR EN HYDROGEOLOGIE – PREMIERS RESULTATS.

Les composés azotés dissous dans les eaux naturelles montrent des variations notables de leur teneur en ^{15}N (plus de 10‰). On expose brièvement les techniques analytiques utilisées pour la mesure de $\delta^{15}N$ et les grandes lignes du cycle isotopique de l'azote, ainsi que les résultats obtenus jusqu'à présent. Un modèle simplifié du cycle de l'azote et de ses implications isotopiques est présenté. Il peut permettre de déduire d'un certain nombre de variations observées, le ou les mécanismes physiques ou biologiques en jeu. L'étude isotopique de l'azote peut représenter un bon outil complémentaire pour la détection et l'interprétation de certaines pollutions.

INTRODUCTION

L'hydrologie isotopique tire ses informations, outre de l'eau elle-même, des teneurs en isotopes stables d'un certain nombre de substances dissoutes. Ainsi, les bicarbonates ont déjà fait l'objet de nombreuses publications, tandis que plus récemment on a pu tirer profit de la composition isotopique du soufre, des sulfures et sulfates dissous, ainsi que de celle de l'oxygène des derniers.

Parmi les autres substances dissoutes dont l'étude isotopique peut être abordée, on peut citer:

– Les phosphates et la silice, par leur teneur en oxygène-18, mais dont l'approche technologique est très onéreuse et non sans difficultés.

– Les chlorures, par les variations de leur rapport $^{35}Cl/^{37}Cl$. Il semble cependent, au vu de très rares travaux sur cet élément [1], que les variations détectées soient trop faibles pour être utilisées au traçage naturel.

– Les composés azotés, par leur teneur en azote-15. Dans les eaux, ils sont représentés par un peu d'ion ammonium, en général présent à des teneurs inférieures à 5 mg/l, des nitrites, qui proviennent de l'oxydation du précédent et sont eux aussi généralement peu abondants, et des nitrates.

Les formes organiques dissoutes seront pour l'instant ignorées. Pour les nitrates, on peut aussi envisager le dosage de l'oxygène-18, possible selon les techniques utilisées classiquement pour les phosphates et les silicates (Longinelli, communication personnelle).

L'intérêt de l'étude isotopique de l'azote est multiple: à côté d'enseignements purement géochimiques et biochimiques, elle permet d'apporter des informations nouvelles sur le mouvement des substances azotées, en rapport par exemple avec la protection des eaux. Des normes de protection ont été établies dans divers pays, visant à limiter le rejet des nitrates qui, au-dessus du niveau moyen d'environ 50 mg/l de nitrate, sont susceptibles de provoquer des troubles du métabolisme sanguin (méthémoglobinurie). D'autre part, l'excès de nitrate dans les eaux libres accélère la prolifération du plancton avec des conséquences néfastes sur l'équilibre biologique.

L'augmentation constante de l'emploi d'engrais azotés dans les régions agricoles a modifié considérablement l'équilibre naturel de l'azote. Alors que dans les contrées encore peu « colonisées », les teneurs en azote nitrique de l'eau atteignent rarement 1 mg/l, elles peuvent dépasser 10 mg/l dans les zones de culture industrialisées. Là où de surcroît on utilise les eaux usées urbaines comme fertilisant, la teneur en azote (nitrate) peut atteindre 100 mg/l.

Les divers mécanismes naturels qui interviennent dans les transformations pédologiques de l'azote provoquent un fractionnement isotopique dont les grandes lignes sont connues, au moins pour certains d'entre eux. On peut ainsi établir des modèles d'évolution isotopique de l'azote dans les sols et dans les eaux, grâce auxquels, dès à présent, il est possible d'interpréter les variations naturelles du rapport $^{15}N/^{14}N$.

Notre contribution à cette étude générale est encore modeste. Dans le cadre d'un travail sur le cycle de l'azote – y compris les problèmes biochimiques – entrepris voici dix-huit mois, nous avons tout d'abord testé les différentes techniques analytiques possibles, avant d'aborder l'étude d'échantillons naturels. Nous avons eu connaissance récemment du résultat des travaux du Center for the Biology of Natural Systems de Saint-Louis (USA), et il y sera fait fréquemment référence [2-6].

1. LES VARIATIONS ISOTOPIQUES NATURELLES DE L'AZOTE

L'azote-15 a été très largement utilisé comme traceur artificiel en agronomie et en biologie [7] et de multiples publications ont permis d'apporter de nombreuses précisions sur le devenir de l'azote dans les sols. Cependant l'étude des variations naturelles de $^{15}N/^{14}N$ n'a fait l'objet que de quelques articles épars, revus par Létolle [8], et ce n'est que récemment que le cycle isotopique de l'azote commence à se dessiner.

Les variations isotopiques sont exprimées dans la formulation classique en delta par rapport à l'azote atmosphérique dont la composition est supposée constante, par suite de la grande masse de l'atmosphère et de son brassage constant par le vent.

$$\delta^{15}N = \left[\frac{(^{15}N/^{14}N)_{éch.}}{(^{15}N/^{14}N)_{std.}} - 1 \right] \times 1000$$

Les variations naturelles actuellement répertoriées dépassent 80‰; la majorité des valeurs mesurées ont des deltas positifs par rapport à l'air, quoiqu'un certain nombre d'échantillons d'origine végétale aient des deltas négatifs, par suite sans doute de fractionnements favorisant l'isotope léger au cours de l'assimilation, comme cela est bien connu par ailleurs pour le carbone.

C'est dans le domaine pédologique que les variations les plus importantes ont été observées, atteignant 30‰ [9-11]; elles sont en grande partie expliquées par le modèle qui sera décrit ci-dessous et qui rend également compte des variations de teneur en ^{15}N relevées dans l'azote dissous.

2. TECHNIQUES ANALYTIQUES

La préparation des échantillons a largement bénéficié des travaux relatifs aux traceurs enrichis en azote-15. Cependant, la précision requise pour la détection des faibles variations naturelles est sans commune mesure avec celle qui est demandée pour le dosage de ^{15}N dans les traceurs enrichis, même faiblement: Bremner et al. [12] ont fait remarquer à ce sujet l'importance des petites variations naturelles dans l'interprétation des petites différences observées lors du dosage de traceurs enrichis.

La qualité des mesures pour le but recherché ici implique l'utilisation de mesures par double collection, avec système d'introduction visqueuse. Ceci exige des quantités de matériel importantes, de l'ordre de 4 à 5 mg d'azote, et des techniques de préparation non fractionnantes.

Après divers essais, nous avons choisi les méthodes décrites par Keeney et Bremner [13] après quelques modifications, en particulier d'après Ross et Martin [14]. Ces techniques seront décrites en détail ailleurs.

Les substances azotées sont tout d'abord concentrées, soit par échange sur résines, soit par simple évaporation. Les nitrates sont réduits par l'alliage de Arndt ou de Devarda, l'ammoniaque étant distillé sur milieu sulfurique. Le sulfate d'ammonium est ensuite attaqué par l'hypobromite de lithium, qui libère l'azote moléculaire sans donner d'oxygène libre. L'azote est concentré sur du charbon actif, procédure utilisée par Hoering [15] et qui n'introduit pas de fractionnement notable, avant d'être transféré sur le spectromètre de masse. Celui-ci est soit un appareil Varian CH7, soit un VG Micromass 602C, de plus grande sensibilité. Un spectre de masse complémentaire permet de mesurer l'oxygène à la masse 32, et l'argon à la masse 40. Ce dernier permet de vérifier, d'une matière quelque peu arbitraire, l'existence d'une pollution du gaz analysé par de l'air et d'opérer une correction sur le delta mesuré.

La reproductibilité est de l'ordre de 0,3‰ sur les sels d'ammonium et de 1‰ sur les nitrates. Nous ne disposons pas de méthode permettant de séparer les nitrites, quand ils existent. Ces résultats confirment les données analytiques de Shearer et al. [4]. Il est vraisemblable que ces reproductibilités seront améliorées dans l'avenir, soit en perfectionnant les techniques de préparation par voie humide utilisées, soit en travaillant à sec dans le vide par des méthodes de Dumas; nos essais en ce sens ne sont pour l'instant guère concluants.

Nous donnons (tableau I) nos résultats, obtenus sur un certain nombre de substances (produits synthétiques ou naturels); ces valeurs, à quelques exceptions près, correspondent bien à celles de Shearer et al. [4] (fig.1).

TABLEAU I. RESULTATS OBTENUS PAR NOS SOINS SUR DIVERS ECHANTILLONS
δ en ‰ par rapport à l'azote de l'air

KNO_3	+ 1,2	Triméthylamine	+28
KNO_3	+ 4,0	Diméthylamine	+11,6
KNO_3	- 6,3	NH_4OH	+ 1,3
KNO_3	+ 3,2	NH_4OH	+ 0,5
KNO_3	+ 2,6		
$NaNO_3$	+11	Engrais	
$NaNO_3$	+ 4,2	Urée (naturelle)	+ 4,3
NH_4NO_3	+ 2,5 (NO_3)	Urée (naturelle)	+ 6,1
NH_4NO_3	- 1,5 (NH_4)	Urée (naturelle)	+ 2,8
NH_4NO_3	+ 1,3 (NO_3)	Urée (synthétique)	0,0
NH_4NO_3	- 4,4 (NH_4)	Salpêtre terreux $(CaNO_3)_2$	+ 5,3
NH_4Cl	-15	Compost (N total)	+13
NH_4Cl	- 2,2	Purin (N total)	+23
NH_4Cl	- 1,0	Nitrate du Chili	- 3,3

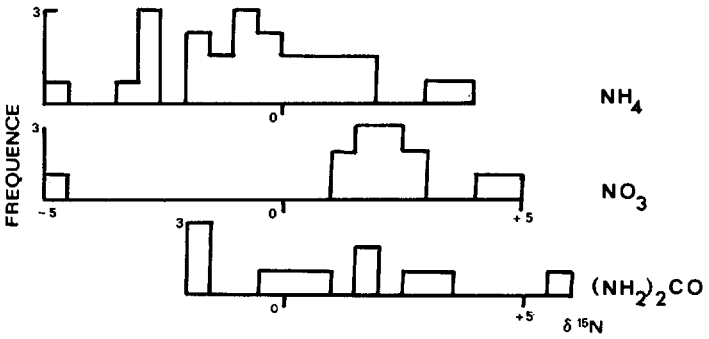

FIG. 1. Histogramme des compositions isotopiques déterminées par Shearer et al. [4], à comparer avec les résultats donnés ici.

3. LE CYCLE DE L'AZOTE DANS LE SOL ET DANS LES EAUX

Les grandes étapes en sont rappelées d'une manière synthétique sur la figure 2.

Les apports externes dans un milieu naturel sont représentés d'une part par l'azote atmosphérique ($\delta^{15}N$ = 0‰) fixé par certaines bactéries, qui l'incorporent au stock organique avec un fractionnement connu dans le cas de Azotobacter vinelandii (-3‰) [10], et d'autre part par celui des pluies,

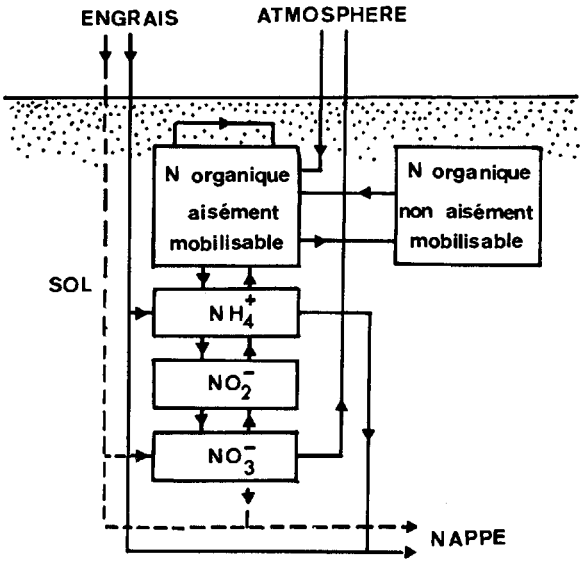

FIG. 2. Schéma simplifié du cycle de l'azote dans les sols.

qui constitue un apport non négligeable. On dispose de quelques résultats isotopiques obtenus sur la pluie et donnés par Hoering [16], montrant une différence d'environ 5‰ entre ammonium (+5 à 0‰) et nitrate (0 à -5‰).

Indirectement, les plantes qui ont fixé l'azote de diverses sources constituent après leur mort et la dégradation de leur matériel organique une source complémentaire (la boucle fermée sur le bloc « azote aisément mobilisable» de la figure 2). La composition isotopique du matériel végétal frais est très variable; nous disposons de valeurs sur du matériel varié, allant de -5‰ à +28‰ mais généralement comprises entre +2‰ et +5‰. Après fermentation toutefois et départ préférentiel de l'azote léger, l'azote intégré au réservoir du sol acquiert une composition isotopique supérieure à + 7‰ (au moins pour la majorité des sols étudiés jusqu'à présent).

La troisième source est représentée par les engrais artificiels (les fumures naturelles étant analogues sur le plan isotopique aux sources précédentes), déversés volontairement, mais aussi apportés par le ruissellement.

Les engrais artificiels ont des deltas voisins de zéro, tandis que les amendements naturels atteignent des teneurs en ^{15}N très élevées (tableau I, voir aussi [11]).

Les agronomes ont démontré que les diverses sources, quoique indépendantes, semblent interrégulées: ainsi il semble que la fixation d'azote atmosphérique soit freinée, sinon arrêtée, par l'arrivée d'azote directement assimilable provenant d'une autre source.

L'ion ammonium représente l'étape intermédiaire constante, tant dans le processus d'assimilation biochimique (« immobilisation») que dans celui de « dénitrification ».

La dénitrification présente selon les sols une importance variable et aboutit soit à des oxydes d'azotes, soit à l'azote moléculaire lui-même. Ce processus est fondamental dans l'interprétation des valeurs isotopiques obtenues sur les eaux.

Les diverses étapes du cycle introduisent un fractionnement isotopique dont l'importance est connue dans certains cas: la nitrification appauvrit le nitrate d'environ 25‰ par rapport à l'ammonium de départ (ceci pour l'équation ammoniun-nitrite [10]); mais le passage nitrite-nitrate, en régime permanent, n'introduit pas de fractionnement [3]; la dénitrification par réduction bactérienne appauvrit les composés formés aux dépens des nitrates, d'environ 17‰ [10, 17], en régime permanent, mais le processus global est très complexe [17].

La fixation d' ammonium dans la matière organique semble aussi appauvrir celui-ci de quelques ‰ [10].

Les autres fractionnements n'ont pas encore été étudiés.

Shearer et al. [3] ont déjà proposé un modèle pour l'évolution isotopique de l'azote des sols, basé sur un schéma similaire à celui des figures 2 et 3. Ils dénomment respectivement A, B, C et D les réservoirs d'azote correspondant au stock organique général, à l'ammonium libre, dont la concentration, comme pour A, est supposée constante, au nitrate (l'étape nitrite étant omise car le fractionnement $NH_4 \rightarrow NO_3$ est le même que pour $NH_4 \rightarrow NO_2$, ainsi qu'ils le démontrent), et enfin à la matière organique synthétisée à partir de NH_4. R est la vitesse de réaction de la transformation matière organique $\rightarrow NH_4^+$ (ordre zéro), K_1, K_3, K_2, K_4, les constantes de réaction du premier ordre pour la nitrification, la dénitrification et la

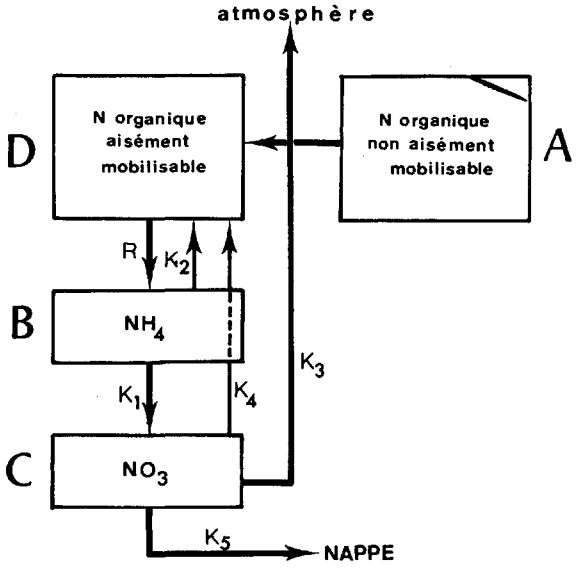

FIG. 3. Partie du cycle analysé au point de vue isotopique; pour les notations voir le texte.

synthèse organique à partir de NH_4^+ et NO_3^-, respectivement. Leurs observations de terrain les amènent à simplifier leur modèle en prenant K_3 et $K_4 = 0$. Les constantes sont évidemment légèrement différentes selon qu'on considère ^{14}N ou ^{15}N.

Nous ajouterons une constante supplémentaire, K_5, relative au drainage par la nappe du nitrate formé dans le sol. Elle peut être considérée comme équivalente à une constante chimique du premier ordre, et est identique pour les deux isotopes. On peut écrire pour le nitrate et l'ammonium:

$$\frac{d(C)}{dt} = K_1 \cdot (B) - (K_3 + K_5) \cdot (C) \qquad \text{et} \qquad \frac{d(B)}{dt} = R - (K_1 + K_2) \cdot (B)$$

Shearer et al. déduisent de ces équations relatives à chaque isotope que lorsque l'état de régime est atteint $(^{15}N/^{14}N)_{(B)}$ ne dépend plus que des diverses constantes et devient lui-même constant:

$$\left(\frac{^{15}N}{^{14}N}\right)_{(B)} = \frac{R_{(^{15}N)}}{R_{(^{14}N)}} \left(\frac{K_{1\,(^{14}N)} + K_{2\,(^{14}N)}}{K_{1\,(^{15}N)} + K_{2\,(^{15}N)}}\right)$$

L'équation générale donne après intégration:

$$(C) = \left\{K_1 \cdot (B)\left[1 - \exp\left\{-\left(K_3 + K_5\right)t\right\}\right] + \left(K_3 + K_5\right) C_0 \exp\left[-\left(K_3 + K_5\right)t\right]\right\} \cdot \frac{1}{K_3 + K_5}$$

Après l'établissement du régime permanent, ceci se simplie en:

$$(C) = \frac{K_1}{K_3 + K_5} \cdot (B)$$

Shearer et al. désignent par β le coefficient de fractionnement isotopique $K_{i\,(^{15}N)}/K_{i\,(^{14}N)} = \beta_i$.

$$\left(\frac{^{15}N}{^{14}N}\right)_{(C)} = \left(\frac{^{15}N}{^{14}N}\right)_{(B)} \cdot \beta_1 \cdot \frac{1/\beta_3 + K_5/K_{3\,(^{15}N)}}{1 + K_5/K_{3\,(^{15}N)}}$$

Dans le cadre des hypothèses simplificatrices exposées plus haut, Shearer et al. démontrent que la composition isotopique des divers réservoirs d'azote mobile est fonction inverse du rapport $K_2/(K_1 + K_2)$, donc de l'importance relative des processus de nitrification et d'immobilisation sous forme organique de l'ammonium: la diminution relative du processus de nitrification s'accompagne d'une diminution du delta de ces réservoirs, donc en particulier des nitrates.

Si, par contre, cas non encore étudié par Shearer et al., la dénitrification devient notable, avec un fractionnement isotopique de l'ordre de celui trouvé par Cook et al. [17], la quantité de nitrate disponible diminue alors que son delta augmente; à la limite, comme les deux processus de nitrification et dénitrification sont antagonistes, on peut prédire au moins qualitativement le processus prédominant. Comme ils sont fonction de manière complexe de divers paramètres des sols (humidité, oxygène dissous, teneur en matière organique ...) eux-mêmes liés entre autres aux variations saisonnières, la composition isotopique des nitrates doit donc montrer, avant amortissement, une fluctuation périodique annuelle. Shearer et al. l'ont peut être détectée dans leur étude des eaux de la rivière Sangamon.

Ce modèle simple sera évidemment complété et perfectionné. En tout état de cause, il montre que la variation saisonnière du delta des nitrates et de leur concentration peut être un paramètre auxiliaire très utile en hydrologie, permettant le traçage de masses d'eaux spécifiques qui peuvent ne pas être distinguées par d'autres indications isotopiques. Une étude plus détaillée des modèles peut être faite en adaptant la méthodologie présentée par Przewłocki et Yurtsever [18].

Le nitrate drainé par l'eau des nappes a donc une origine complexe:

a) Une partie peut provenir directement des engrais, par simple percolation, si celle-ci est assez rapide. Il faut cependant noter que, sans modification chimique, une partie peut en être stockée par adsorption sur les argiles et restituée ultérieurement, peut-être avec un fractionnement isotopique, lequel a été démontré en laboratoire [10].

b) Dans le cas d'apports ammoniaqués, à delta voisin de zéro, l'azote apparaît généralement dans la nappe sous forme de nitrate à la suite de divers phénomènes, d'abord par nitrification directe de cet ammonium qui aboutit à la production de nitrate à delta négatif par rapport à celui observé en régime permanent sans apport ammoniaqué (deltas < 0 observés par Feigin et al. [2]. Mais on observe aussi la mobilisation et mise en solution par une sorte d'effet catalytique de l'azote de la matière organique du sol: dans ce cas, l'augmentation de la concentration en nitrate dans le drainage ne s'accompagnera pas d'un abaissement du delta par rapport au régime permanent. Cet effet, dit « priming effect », est bien connu des pédologues et son importance relative par rapport à la nitrification directe de l'ammoniaque doit pouvoir être établie par le traçage isotopique.

Dans ces deux cas, l'intervention d'un apport massif d'azote en un temps court équivaut à l'imposition d'un signal « impulsion » à l'entrée du système, modifiant simultanément (B) et $(^{15}N/^{14}N)_{(B)}$. L'évolution du système peut être étudiée à partir de l'équation générale.

On peut montrer que, en fonction de la nature physico-chimique du sol et de l'importance relative des divers processus utilisant l'azote, le signal sera « étouffé », ou transféré vers la nappe de façon variée et avec un déphasage également différent. La réponse isotopique, comme on l'a vu, n'est pas nécessairement parallèle à la réponse chimique.

c) Le « bruit de fond » correspond au nitrate produit dans la filière matière organique/ammonium/nitrate tel qu'on peut le voir dans le modèle de Shearer et al. en équilibre dynamique (steady state) et dont la réalimentation naturelle en dernière analyse se fait à partir de N_2 atmosphérique pour les sols livrés à eux-mêmes.

Les résultats du groupe de St-Louis (Feigin et al. [2]) et ceux obtenus par nous-mêmes sur des eaux de régions n'ayant pas subi l'influence d'amendements artificiels (forêts, par exemple), nous amènent à postuler une valeur moyenne pour le delta du nitrate rejeté voisine de + 8‰. Ceci, évidemment, ne tient pas compte de la fluctuation saisonnière que nous avons évoquée ci-dessus, mais qu'au stade actuel de nos investigations nous n'avons pas encore prouvée.

d) Les sols alimentés depuis longtemps et de manière régulière avec des engrais synthétiques (ammonium ou urée), à $\delta^{15}N$ voisin de zéro, appellent le commentaire suivant: dans un sol naturel, il y a « équilibre isotopique » dynamique entre la matière organique et NH_4^+, chacun ayant, comme on l'a vu, un delta assez élevé.

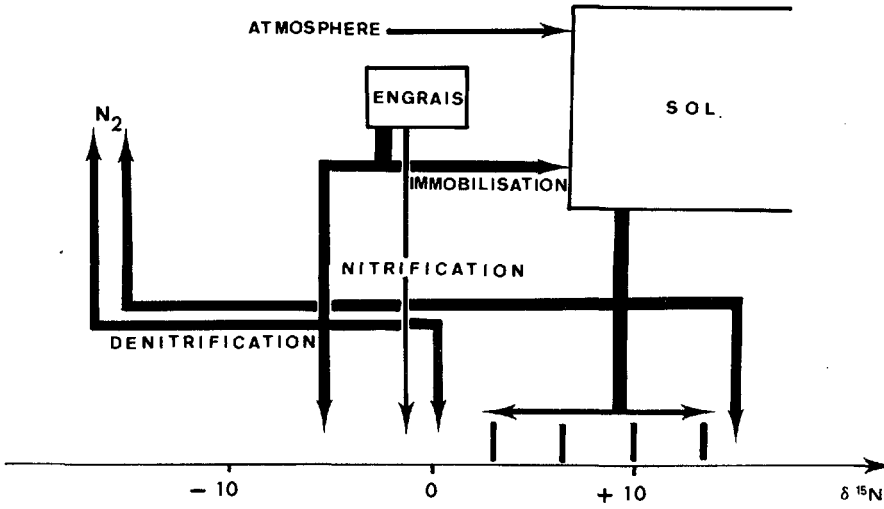

FIG. 4. Essai de diagnostic des valeurs isotopiques relevées sur les nitrates des eaux.

Donc, si on maintient artificiellement NH_4^+ à un delta inférieur à sa valeur naturelle, la matière organique du sol prendra peu à peu elle aussi une valeur isotopique plus basse que celle observée pour les sols n'ayant pas subi d'alimentation artificielle. Comme, toutes choses égales par ailleurs, le nitrate passant dans la nappe en régime permanent a une composition isotopique liée à celle de la matière organique, il en ressort qu'en moyenne, le nitrate sécrété par des sols amendés depuis longtemps avec des engrais de synthèse à delta peu élevé aura un delta inférieur à celui de ceux qui ne l'auront pas été.

La figure 4 est une tentative de diagnostic sur l'origine de l'azote à partir de sa composition isotopique. Une sorte de grille analytique – très provisoire – est proposée, qui tient compte à la fois du delta et de la concentration des nitrates:

- deltas négatifs et concentrations élevées: apport récent dans le bassin versant d' engrais ammoniacaux (cf. [6] et alinéa b) ci-dessus);
- deltas voisins de zéro, ou légèrement supérieurs: influence nette et continue d'une longue pratique d'amendements azotés artificiels (conséquence des conclusions de l'alinéa d) ci-dessus);
- deltas compris entre environ +5 et +15: la surveillance simultanée des deltas et des concentrations peut permettre, à la faveur des éléments de discussion donnés plus haut, de préciser la nature du processus biochimique en cause;
- deltas élevés (plus grands que 15 environ) et concentrations basses correspondent au « régime permanent naturel» et à ses fluctuations;
- deltas élevés et concentrations fortes peuvent (nous soulignons) correspondre à une abondance d'apports azotés extérieurs mais d'origine organique.

Ces diagnostics ne tiennent pas compte de l'apport possible d'effluents d'origine purement industrielle; dans tous les cas, une étude hydrologique de terrain s'impose pour orienter le diagnostic basé sur l'analyse de l'azote.

Les résultats actuellement en notre possession couvrent pour les nitrates un domaine de deltas allant de 0 à + 15 environ. Obtenus sur des échantillons variés dans un rayon d'une centaine de kilomètres de Paris, ils n'ont malheureusement pas été choisis en fonction de critères pédologiques précis, ni suivis dans le temps. Nous avons entrepris sous cet aspect une surveillance plus rigoureuse sur des parcelles étudiées régulièrement sur le plan hydrologique (bassin de l'Orgeval, à 60 km à l'est de Paris).

Les diverses publications citées provenant du groupe de St-Louis illustrent cette méthodologie. Il convient de s'y reporter. Nous donnerons deux exemples personnels montrant l'intérêt du traçage naturel par l'azote:

a) L'eau des égouts parisiens contient NH_4^+ et pas de nitrate ni de nitrite (3 à 5 milliéquivalents de N [19]), dont le delta est de l'ordre de + 3; ceci conduit à conclure qu'une part importante de l'azote n'est pas d'origine biologique, mais correspond à de l'ammonium industriel (détergents) à delta voisin de zéro. Ces eaux sont épandues sur des sols couverts de cultures, à Achères, à l'ouest de Paris. L'eau des drains de ces terrains d'épandage a un delta compris entre + 7 et + 13 pour l'ensemble nitrates + nitrites (≃ 6 milliéquivalents environ; l'ammonium, trop peu abondant, n'a pas été dosé isotopiquement). Le bilan azoté global n'est pas équilibré sur le plan isotopique; il y a donc élimination, soit dans la matière organique prélevée (cultures vivrières), soit par rejet dans l'atmosphère d'azote isotopiquement plus léger.

b) En amont de Compiègne (France), la rivière Oise, non canalisée, traverse une zone essentiellement agricole et forestière. Nous y avons trouvé en automne 10 ppm de NO_3^- pour un delta de + 6 à + 7‰. Immédiatement à l'aval de Compiègne, où existent des industries chimiques, nous avons relevé le même jour environ 50 ppm de NO_3^-, pour un delta de + 2‰.

Le stock de nitrate a complètement changé de nature.

CONCLUSION

Notre ambition a été pour l'essentiel d'attirer l'attention sur une méthode nouvelle de traçage isotopique, venant s'ajouter à celles portant sur d'autres ions dissous. De nombreux progrès analytiques doivent être faits afin d'améliorer la finesse des mesures. De nombreuses informations relatives aux fractionnements isotopiques sont à acquérir. Le plus gros handicap est la nécessité de disposer d'échantillons de taille suffisante (1 à 50 litres) et de concentrer l'azote. On a ici volontairement négligé de parler de l'ammonium dissous, dont l'étude paraît irréalisable en routine, des nitrites que nous ne savons pas isoler des nitrates, non plus que de l'azote organique dissous, qui peut représenter une part très importante de l'azote éliminé dans les nappes. Nous estimons que les résultats obtenus par deux laboratoires indépendants sont suffisamment démonstratifs pour encourager l'extension des recherches dans la même voie.

REFERENCES

[1] MORTON, R.D., CATANZARO, E.J., Stable chlorine isotope abundances in apatites from O Degardens Verk, Norway, Norsk Geologisk Tidsskrift 44 (1964) 307-13.

[2] FEIGIN, A., SHEARER, G., KOHL, D.H., COMMONER, B., The amount and $^{15}N/^{14}N$ ratio of nitrate in soil profiles in two Central Illinois fields in a corn-soybean rotation, Soil Sci. Soc. Am., Proc. (à paraître).

[3] SHEARER, G., DUFFY, J., KOHL, D.H., COMMONER, B., A steady state model of isotopic fractionation accompanying nitrogen transformations in soil, Soil Sci. Soc. Am., Proc. (à paraître).

[4] SHEARER, G.B., KOHL, D.H., COMMONER, B., $^{15}N/^{14}N$ ratios in soils, fertilizers and shelf chemicals, Soil Sci. (à paraître).

[5] KOHL, D.H., SHEARER, G.B., COMMONER, B., Fertilizer nitrogen: Contribution to nitrate in surface water in a corn belt watershed, Science 174 (1971) 1331-33.

[6] KOHL, D.H., SHEARER, G.B., COMMONER, B., Variations of ^{15}N in corn and soil following application of fertilizer nitrogen, Soil Sci. Soc. Am., Proc. (à paraître).

[7] HAUCK, R.A., BYSTROM, M., ^{15}N, A Selected Bibliography for Agricultural Scientists, Iowa State Univ. Press (1970).

[8] LETOLLE, R., Etat actuel des connaissances relatives à la géochimie des isotopes de l'azote, Rev. Géogr. Phys. Géol. Dyn. (sous presse).

[9] CHENG, H.H., BREMNER, J.M., EDWARDS, A.P., Variations of nitrogen 15 abundances in soils, Science 146 (1964) 1574-75.

[10] DELWICHE, C.C., STEYN, P.L., Nitrogen isotope fractionation in soils and microbial reactions, Environ. Sci. Technol. 4 (1970) 929-35.

[11] RIGA, A., VAN PRAAG, H.J., BRIGODE, N., Rapport isotopique naturel de l'azote dans quelques sols forestiers et agricoles de Belgique soumis à des traitements culturaux, Geoderma 6 (1971) 213-22.

[12] BREMNER, J.M., CHENG, H.H., EDWARDS, A.P., Assumptions and Errors in Nitrogen 15 Tracer Research, Report of the FAO/IAEA Technical Meeting, Brunswick, sept. 1963, Pergamon Press (1963) 429-42.

[13] KEENEY, D.R., BREMNER, J.M., Determination and isotope ratio analysis of different forms of nitrogen in soils, Part. 4, Soil Sci. Soc. Am., Proc. 30 (1966) 583-87.

[14] ROSS, P.J., MARTIN, A.E., Rapid procedure for preparing gas samples for nitrogen 15 determination, Analyst 95 (1970) 817-22.

[15] HOERING, T., Variations of nitrogen 15 abundance in naturally occuring substances, Science 122 (1955) 1233-34.

[16] HOERING, T., The isotopic composition of the ammonia and the nitrate ion in rain, Geochim. Cosmochim. Acta 12 (1957) 97-102.

[17] COOK, F.D., WELLMAN, R.P., KROUSE, H.R., «Nitrogen isotope fractionation in the nitrogen cycle», Int. Symp. on Hydrochemistry and Biochemistry, Tokyo, août 1970, mémoire BI.6.

[18] PRZEWŁOCKI, K., YURTSEVER, Y., «Some conceptual mathematical problems for evaluation of the tracer input-output relations in hydrological systems», ces comptes rendus, IAEA-SM-182/49.

[19] BENOIT, P., Bilan de l'efficacité des champs d'épandage de la ville de Paris, Thèse, Paris (1973).

DISCUSSION

W.G. MOOK: In Groningen, we too have started isotopic studies of nitrogen, for $^{15}N/^{14}N$ variations in molecular nitrogen are also interesting from a hydrological point of view.

From your data on nitrates and ammonium one would expect measurable deviations of the $\delta^{15}N$ value of soil nitrogen gas from the atmospheric value. Have you looked into this?

R.R. LETOLLE: No, we have not yet investigated the mixing of atmospheric nitrogen with the nitrogen resulting from soil activity. However, I agree that one would expect measurable deviations of the $\delta^{15}N$ value of soil nitrogen gas from the atmospheric value.

E. MAZOR: With regard to Mr. Mook's question and the importance of elemental nitrogen dissolved in groundwater, I would recall that ^{36}Ar is a good monitor for nitrogen entering water by dissolution from air. One quite frequently encounters significant nitrogen excesses (relative to ^{36}Ar), both in sedimentary and in igneous terrains.

R.R. LETOLLE: Thank you for your comment. In this connection I would mention a paper by Richards and Benson (Deep Sea Research 7 (1961) 254) where an attempt was made, using the total argon/nitrogen ratio, to determine the extent of nitrogen production in anaerobic fjord conditions. The authors also demonstrated that there was slight fractionation in the dissolution of nitrogen, and their balance gave very low delta values for biogenic nitrogen.

G.P. CONRAD: The nitrates found in aquifers can have origins other than those indicated in Fig. 3 of your paper.

I might mention as an example the unconfined aquifer in the "Grand erg occidental" (Algerian Sahara), where one finds nitrate concentrations of 20-80 mg/litre in waters sampled at the natural outlets. As there is clearly no substantial biological activity at the surface of the "erg", the nitrates may derive, via precipitation, from direct synthesis in the atmosphere or from the leaching of nitrate-bearing soil.

R.R. LETOLLE: I would think that the nitrates derive from rainwater (up to 10 ppm NO_3^-), in which case their origin is either industrial activity or direct synthesis in the atmosphere. However, they could also have an origin similar to that of the nitrates of the Atacama caliches, about which little is known (they may derive from leaching of paleosols, the $\delta^{15}N$ value of Chilean nitrates being about -2‰).

P. FRITZ: Your discussion of analytical data was essentially limited to an evaluation of ^{15}N variations in surface waters. Could you comment briefly on the possible application of such analyses to the evaluation of subsurface systems taking into account the extreme complexity of the nitrogen system?

R.R. LETOLLE: I think use could be made of the mean isotopic composition of nitrogen in different aquifers; in this connection I would mention the work being done by investigators of the Centre for the Biology of Natural Systems, St. Louis, United States of America.

By way of example I might refer to the results of studies carried out by us in France. Near Compiègne, we took samples from two ponds which were not connected with any creeks or ditches. For the first pond, which is about 1 km from the river Aisne, we obtained a delta value of +7‰, which is close to the delta value obtained for the river; this suggests that the pond receives water from an aquifer connected with the river. For the second pond, which is in a forest south-east of Compiègne about 15 km from any significant river, we obtained a delta value of +11‰. As all samples were collected on the same day, the difference between the delta values may reflect different nitrogen systems.

G. CREMA: Could ammonium form complex salts with heavy metals present in the soil?

R.R. LETOLLE: Yes, but I have no information on whether ammonium complexes fractionate isotopically, for it is generally not possible to obtain sufficient ammonia from soils to perform isotope analyses.

AQUIFER CHARACTERISTICS STUDIES

(Session 7, Part 2; Session 8)

UTILISATION DES TECHNIQUES ISOTOPIQUES POUR LA RESOLUTION DE PROBLEMES HYDROLOGIQUES EN GENIE CIVIL
Etude de trois cas précis

P. Ch. LEVEQUE, J. Cl. GROS, Catherine MAURIN,
J. SEVERAC, Cl. VIGUIER
Laboratoire de radiogéologie
et de mécanique des roches,
Université de Bordeaux I,
Talence, France

Abstract–Résumé

THE USE OF ISOTOPE TECHNIQUES TO SOLVE HYDROLOGICAL PROBLEMS IN CIVIL ENGINEERING; A STUDY OF THREE SPECIFIC CASES.

Three examples of the use of natural and artificial radioisotopes are presented. The first relates to a study for a project involving civil engineering work beneath a built-up area. Investigations with tritium showed that the age of the water was variable and irregularly distributed within the acquifer; using natural ^{222}Rn and ^{82}Br, it was possible to determine with a high degree of precision the location of permeable zones. The second example relates to investigations with tritium and ^{82}Br which showed that the confined aquifer beneath an area where the construction of a large industrial complex is planned also consisted of units of different ages and that there was no substantial movement of water in the aquifer. The third example relates to an earth dam in which natural tritium and ^{222}Rn, and subsequently ^{82}Br and ^{131}I were used to study certain anomalies due to differences in the extent to which the earth had been packed. It was found that the permeability of the main body of the dam and its structural elements varied. A counter check based on the potential adsorption of ^{131}Cs + ^{131}Ba demonstrated the presence of granulometric heterogeneities, especially with regard to the fine argillaceous particles.

UTILISATION DES TECHNIQUES ISOTOPIQUES POUR LA RESOLUTION DE PROBLEMES HYDROLOGIQUES EN GENIE CIVIL – ETUDE DE TROIS CAS PRECIS.

Le mémoire présente trois exemples d'utilisation d'isotopes radioactifs naturels et artificiels. Le premier exemple a trait à l'étude d'un projet de souterrain sous une grande agglomération. L'étude de l'activité en tritium a montré la présence de nappes sous-multiples d'âges différents. L'utilisation du ^{222}Rn naturel et du ^{82}Br a permis de préciser la localisation des passages perméables. Le second exemple est celui de l'étude d'un site industriel, lors de laquelle on a pu montrer, grâce au tritium et au ^{82}Br, que la nappe captive située sous une zone où l'on projette la construction d'un vaste complexe est également formée d'unités d'âges variés et qu'elle n'est pas animée de mouvements notables. Le dernier exemple est constitué par les résultats de travaux de contrôle d'un barrage en terre compactée. Certaines anomalies dues à des tassements différentiels ont été étudiées grâce au tritium naturel, au ^{222}Rn, puis par ^{82}Br et ^{131}I, qui ont mis en évidence les perméabilités différentielles du corps du barrage et de ses formations. L'utilisation en contre-épreuve de ^{131}Cs + ^{131}Ba et de leur adsorption potentielle a donné la preuve de certaines hétérogénéités granulométriques concernant notamment les particules fines et argileuses.

Depuis plusieurs années, l'utilisation des techniques isotopiques pour la résolution de problèmes hydrodynamiques posés par l'exécution et le contrôle des grands travaux de Génie civil, a atteint le stade de la routine. Le Laboratoire de Radiogéologie et de Mécanique des Roches de l'Université de Bordeaux a été sollicité pour participer à de nombreuses études préliminaires et aux différents stades de l'évolution des projets, soit pendant la réalisation ou la surveillance et le contrôle d'ouvrages hydrauliques et d'installations industrielles, soit lors de travaux de protection de l'environnement naturel.

La note qui suit donne trois exemples d'utilisation des radioéléments, le premier lors de l'étude préliminaire d'installations en site urbain, le second pour un projet de constructions industrielles et le troisième dans le cas particulier de contrôle d'un barrage. Dans ces trois types d'application, l'utilisation de traceurs radioactifs artificiels et celle, conjointe, de marqueurs naturels, ont fourni des solutions directement utilisables aux problèmes posés et ont constitué le moyen de recherche spécifique et unique.

1 - ETUDE DE SITE URBAIN

1-1 - Caractéristiques du projet

Le projet prévoit l'installation et la construction d'un réseau de transport en grande partie souterrain, dans une agglomération de cinq cent mille habitants, ce chiffre devant s'accroître notablement au cours des dix prochaines années.

Les terrains sont constitués, de bas en haut, par une série marno-calcaire, surmontée de calcaires hétérogènes altérés par dissolution et, de ce fait, particulièrement perméables dans certaines zones très localisées. Au-dessus des calcaires, des formations plus récentes comprennent des sables et des argiles hétérogènes, puis des alluvions anciennes d'une terrasse quaternaire 12-15 m, enfin, par endroits, des conglomérats à cimentation irrégulière provenant également de terrasses plus anciennes que la précédente.

La définition des axes principaux du futur réseau a été établie à partir de données économiques et d'une étude prospective de l'aménagement ultérieur de la ville. Les reconnaissances des conditions géologiques générales et, surtout, celles relevant de l'hydrogéologie, de la mécanique des sols et de la mécanique des roches, ont suivi obligatoirement les axes précédemment définis.

Le problème principal réside dans la présence de nappes libres et captives, contenues dans les calcaires et les marno-calcaires hétérogènes et dans les formations superficielles.

1-2 - Travaux réalisés

Les travaux ont consisté en une série de mesures préliminaires et systématiques de la transmissivité et des activités en Radon-222, dans les sondages de reconnaissance, par une méthode déjà décrite précédemment (1,2). En ce qui concerne le ^{222}Rn, les mesures ont été effectuées sur des échantillons d'eau prélevés tous les 25 centimètres, dans les zones les plus perméables ou supposées telles. Par la suite, des mesures de diffusivité et de perméabilité relative ont été effectuées avec du Brome-82, suivant les méthodes largement utilisées en routine depuis plusieurs années (3,4,5,6).

Les modalités d'injection du ^{82}Br sont classiques et conformes à celles effectuées antérieurement. Rappelons que le procédé consiste à injecter quelques m^3 d'eau marquée par 1 à 3 mCi de traceur, dans des sondages crépinés, de 20 et 30 m de longueur moyenne dans le cas présent. La répartition de la radioactivité induite est mesurée sur la verticale du sondage par une ou plusieurs sondes à scintillation,

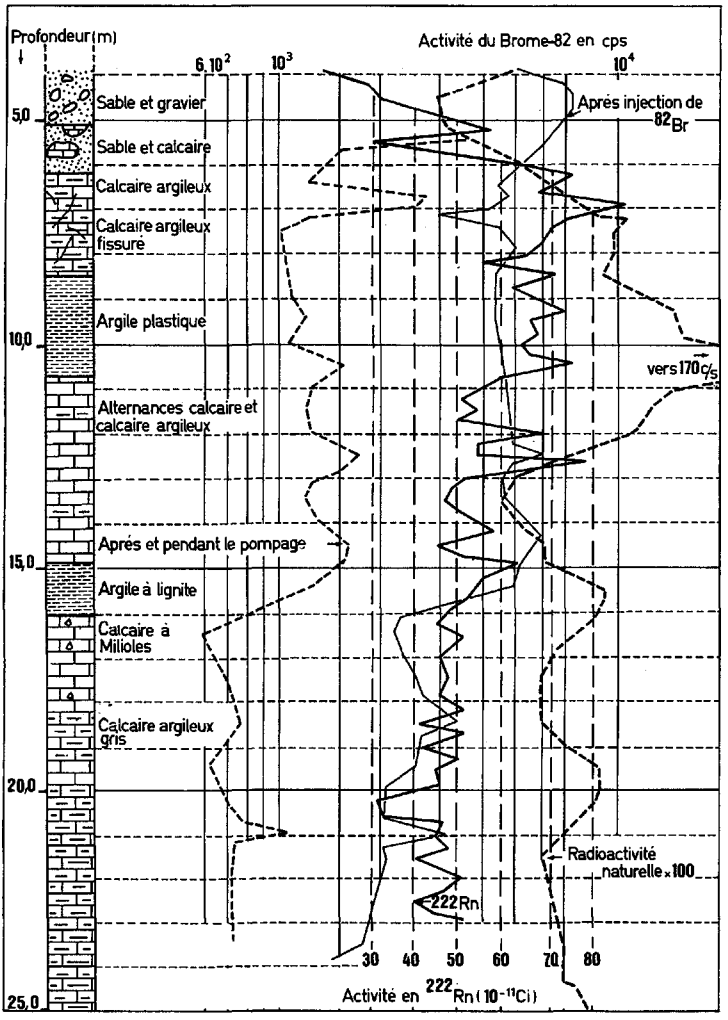

FIG.1. Exemple n° 1: site urbain (sondage S2).

après injection du traceur puis au cours d'un pompage, en retour, de l'eau injectée. L'ensemble des observations est rassemblé dans les figures 1 et 2 qui montrent les corrélations entre les résultats obtenus avec la radioactivité naturelle des terrains traversés et ceux obtenus avec le ^{82}Br.

Les activités relativement fortes mesurées sur le radon sont à rapprocher de la teneur en uranium des eaux de ces nappes, de l'ordre de 6 à 7 $\mu g.l^{-1}$, teneur exceptionnellement élevée pour la région étudiée. Les pics de radioactivité naturelle mesurée dans les terrains traversés par les sondages confirment cette teneur en uranium, très localisée dans quelques minces couches.

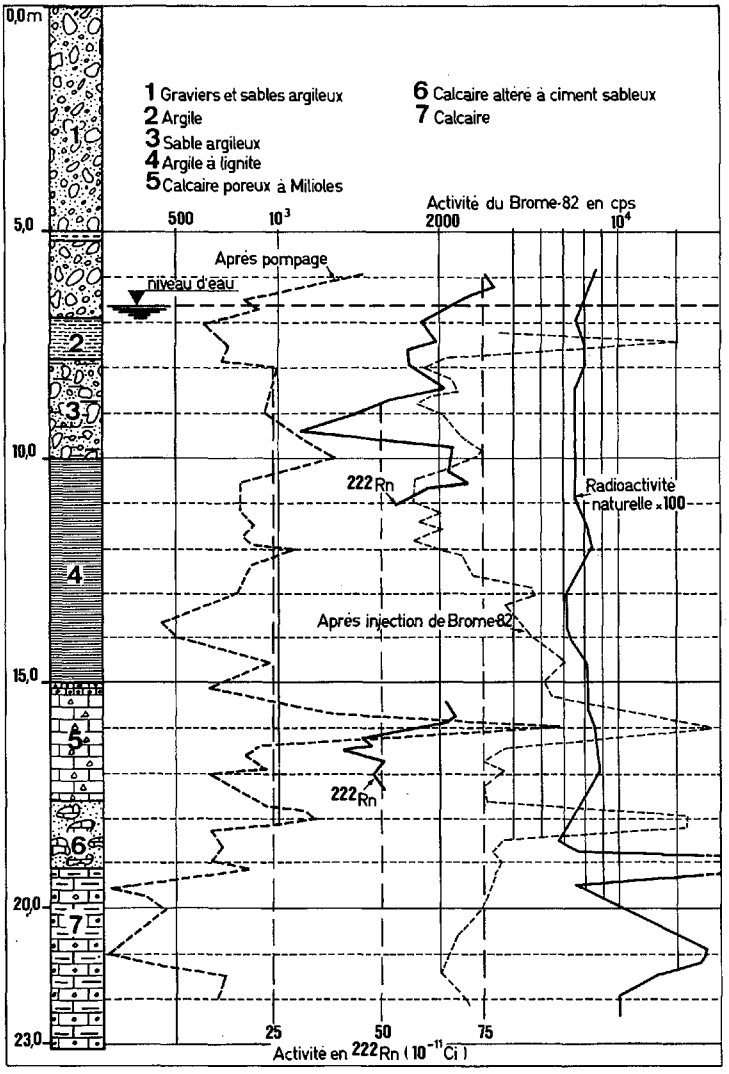

FIG. 2. Exemple n° 1: site urbain (sondage S4).

Par ailleurs, des mesures d'activité en tritium, ont donné des valeurs variées, comprises entre 4 et 50 UT, qui ont été comparées à des résultats antérieurs (7, 8).

On note une bonne corrélation d'ensemble entre les activités en radon et les zones perméables, bien mises en évidence par les pics de ^{82}Br. La courbe correspondant aux activités à la fin du pompage qui a suivi l'injection confirme les données précédentes.

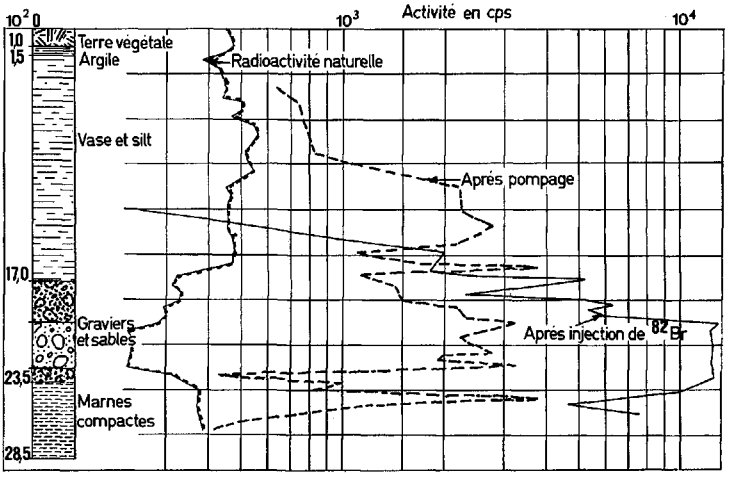

FIG.3. Exemple n° 2: site industriel (sondage S7).

On devra donc compter sur une distribution hétérogène des sous-ensembles des nappes. L'"âge" relatif de ces sous-ensembles indique soit une répartition très variable des vitesses, en supposant une alimentation homogène par les précipitations, soit des alimentations artificielles localisées, provenant d'eaux usées issues des forages profonds de la ville, donc sans tritium.

Les terrassements en tranchées ou en souterrain auront donc à affronter des venues d'eau importantes et difficilement prévisibles. Ces terrassements devront être précédés par des travaux préliminaires d'étanchement par injections, dont les caractéristiques et les modalités devront être étroitement adaptées à ce type de terrain. On doit écarter la solution de pompages énergiques et localisés qui épuiseraient rapidement les aquifères hétérogènes, ce qui risquerait d'augmenter dangereusement la contrainte principale réelle des bâtiments construits, sur leurs fondations.

2 - ETUDE D'UN SITE INDUSTRIEL

2-1 - Problèmes posés et caractéristiques des terrains

Le deuxième exemple présenté s'applique au projet de construction d'un important complexe de pétrochimie sur la presqu'île du Bec d'Ambès dans le Sud-Ouest de la France. La Garonne et la Dordogne qui longent l'isthme sont soumises à des marées qui peuvent atteindre 5,50 m d'amplitude.

Les terrains rencontrés sont constitués, de bas en haut, par une série de marnes compactes, imperméables, surmontée par des alluvions perméables de puissance très variable, formées de sables et de graviers à la base et de silts vaseux jusqu'à la surface. La puissance des formations supérieures -alluvions et vases- est

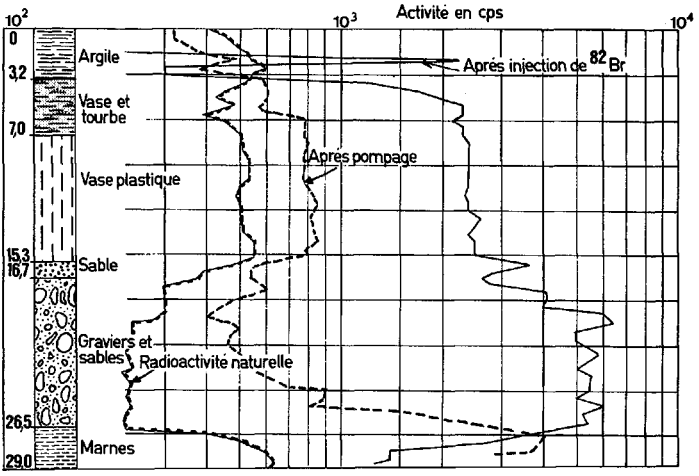

FIG. 4. Exemple n° 2: site industriel (sondage S19).

comprise entre 20 et 25 mètres. L'utilisation éventuelle de la nappe captive des alluvions pour des usages industriels a été envisagée, malgré la mauvaise qualité des eaux et notamment sa teneur en chlore. Par ailleurs, les dispositions légales concernant la défense contre la pollution ont conduit à poser le problème du potentiel de transport de cette nappe.

2 - 2 - Travaux effectués

Comme précédemment, l'étude de la transmissivité a été abordée par des méthodes traditionnelles. Ces résultats ont été complétés par des mesures d'activité en tritium et par des localisations de zones perméables sur les cinq premiers sondages crépinés, destinés à des travaux préliminaires.

Les figures 3 et 4 donnent l'ensemble des résultats obtenus sur deux sondages-types.

Des analyses d'activité en tritium ont été effectuées par ailleurs sur des échantillons prélevés aussitôt après la confection du piézomètre et, par la suite, suivant un rythme normalisé, à intervalles réguliers au cours des pompages. Le tableau I donne les principaux résultats obtenus sur trois des cinq sondages soumis aux tests.

Dans les trois cas, on constate une diminution nette de l'activité en tritium, en fonction de la durée des pompages qui ont été effectués à des débits assez faibles, de $1,6\ l.s^{-1}$ au maximum et avec des rabattements compris entre 0,28 et 2,80 m. La transmissivité était de l'ordre de $1,75.10^{-4}\ m^2.s^{-1}$, avec une valeur maximale de $1,5.10^{-3}\ m^2.s^{-1}$ au sondage S7(7,8).

La décroissance de l'activité parallèle à l'augmentation du volume pompé, c'est-à-dire l'augmentation corrélative de l'"âge", dans les trois sondages cités, évoque une mobilisation systématique d'eaux plus anciennes et relativement voisines en plan,

TABLEAU I. ACTIVITES EN TRITIUM AU COURS DES MESURES DE PERMEABILITE

	Dates	Profondeur de prélèvement	Activité du tritium en U.T.	Volume total pompé	Transmissivité	Rabattement en fin de pompage
S2	22-05-73 avant pompage	5 m	23	1,7 m^3	$1,75.10^{-4}$ $m^2.\ s^{-1}$	2,70 m
	22-05-73 avant pompage	18 m	14			
	fin du pompage	4 m env.	8			
	05-06-73 avant pompage	5 m	BdF	Prélèvements en état statique		
	05-06-73 avant pompage	18 m	BdF			
S7	30-05-73 avant pompage	5 m	2	19,5 m^3	$1,5.10^{-3}$ $m^2.\ s^{-1}$	0,88 m
	30-05-73 avant pompage	18 m	6			
	30-05-73 fin du pompage	3 m env.	BdF			
S19	06-06-73 avant pompage	5 m	20	3,42 m^3	-	0,28 m
	06-06-73 avant pompage	18 m	6			
	fin du pompage	3 m env.	2			

puisque le volume d'eau pompé n'intéresse, en définitive, qu'un volume total de terrain assez faible qui interdit d'envisager une alimentation par les deux rivières. D'ailleurs, la teneur en chlore ne permet pas de retenir cette hypothèse.

La répartition des zones perméables déterminées et précisées par le ^{82}Br montre des résultats en général attendus. Les zones les plus absorbantes sont situées dans les sables et graviers de la base de la série alluviale. On observe toutefois une répartition bien plus localisée que celle qui est théoriquement admise, des passages perméables de la formation des alluvions sablo-graveleuses, réputée perméable en totalité.

Bien que l'examen détaillé des mesures de radioactivité naturelle du terrain ait fourni des résultats préliminaires dans le même sens, seule, l'utilisation d'un traceur radioactif pouvait permettre de préciser les limites et les valeurs de la perméabilité relative et de localiser, par exemple, les passages perméables sur 3,50 m environ au sondage S2 -au lieu des 8 m théoriquement admis et correspondant à l'épaisseur des sables et graviers- sur 3 m au lieu de 5 au sondage S7, sur 1,5 m, soit sur toute la puissance trouvée au sondage S12, sur 5 à 6 m au lieu de 10 au sondage S19, sur 2,5 m au lieu de 5 au sondage T62. Toutefois à ce dernier sondage, deux passages perméables de quelques décimètres ont été mis en évidence dans des formations dites "vases plus ou moins sableuses".

Les pourcentages de récupération du traceur ont été de 50 à 60%. Les effets de la marée sur les transferts de pression et sur ceux des mouvements des masses d'eau dans les formations perméables, sont responsables de ces valeurs de récupération relativement faibles.

Il est évident que dans l'évaluation de la vitesse réelle de transport des pollutions éventuelles par la nappe, les vitesses théoriques calculées à partir de la transmissivité, elle-même évaluée par une appréciation arbitraire de l'épaisseur des couches perméables, conduisent à des valeurs qui s'écartent notablement de la réalité. Dans le cas présent, cette surévaluation va dans le sens contraire à la sécurité, puisque les vitesses réelles sont, ici, 2 à 3 fois supérieures aux valeurs théoriques traditionnelles généralements admises.

2-3 - Conclusions recueillies

L'ensemble des données recueillies permet d'énoncer les conclusions suivantes :

-La nappe est constituée d'unités secondaires, d'"âge" variable. La circulation y est donc très anisotrope, sous l'action conjuguée des alimentations, à fréquence aléatoire, dues aux précipitations, ainsi que sous l'action des gradients sinusoïdaux et réguliers, dus aux marées. L'existence d'eaux dont l'"âge" est plus ancien que 20 ou 25 ans, donc sans tritium mesurable, implique soit la présence de volumes d'eau captifs, dans des formations perméables lenticulaires fermées, au sein des vases, soit une alimentation par les calcaires gréseux inférieurs.

-La présence d'une assez forte teneur en chlore dans la plupart des prélèvements semblerait faire pencher vers l'hypothèse des volumes d'eau captifs. En effet, les nappes plus profondes ne contiennent que de faibles quantités de chlore et les eaux des deux rivières n'atteignent pas davantage les concentrations maximales de la nappe.

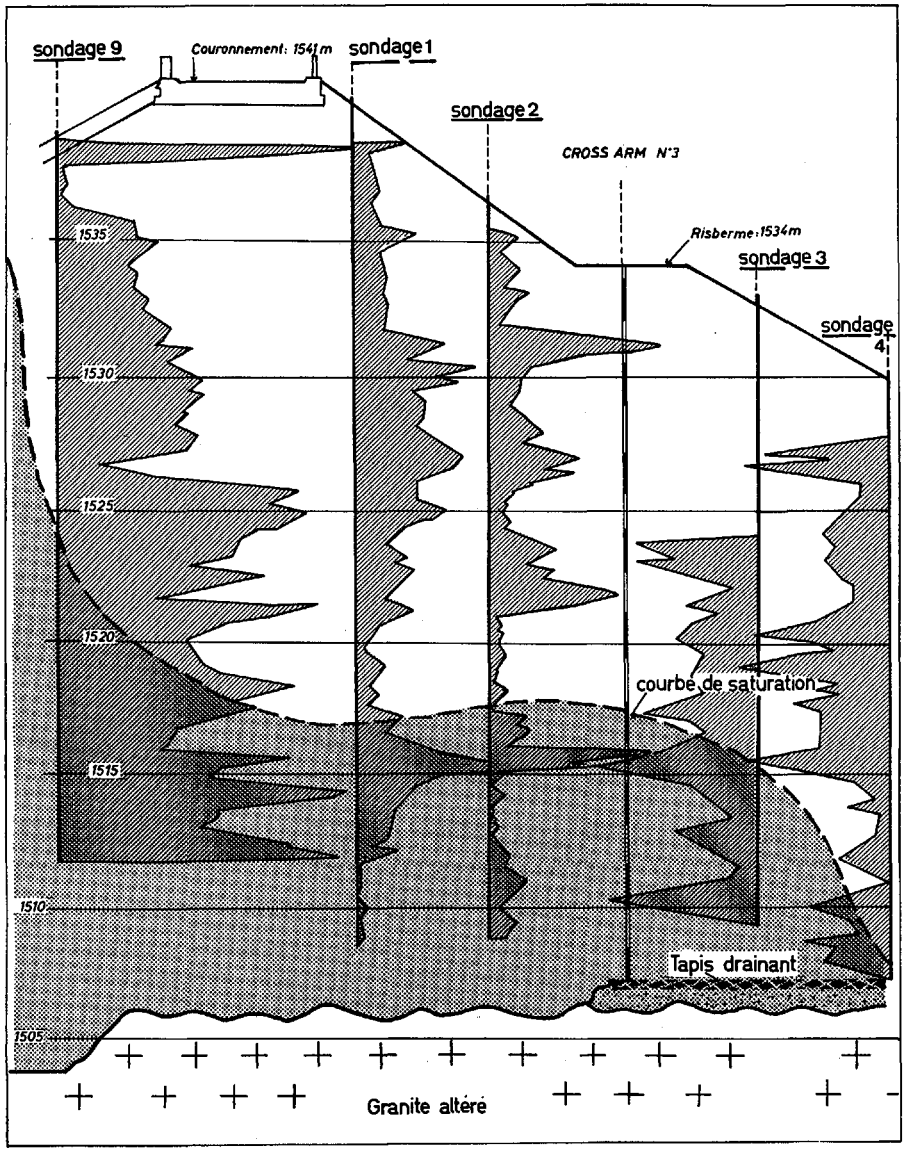

FIG. 5. Exemple n° 3: barrage en terre. Coupe partielle perpendiculaire au couronnement.

- Bien qu'il y ait des mouvements de va-et-vient de la nappe -les pourcentages de récupération du ^{82}Br le suggèrent, ainsi que les variations piézomètriques cycliques- la résultante de ces mouvements au centre de la presqu'île est à peu près nulle, comme l'indique la faible activité en tritium. Le danger de dissémination de la pollution est donc assez faible et, en tous cas, les mouvements d'ensemble de la nappe paraissent assez lents pour qu'il soit possible de procèder à un blocage de la zone polluée par des moyens classiques, en un temps suffisant.

3 - CONTROLE D'UN BARRAGE

3-1 - Problème posé

Le troisième cas a trait aux contrôles qui ont dû être effectués sur un barrage en terre compactée, composé de matériaux homogènes, à la suite de la découverte de tassements différentiels localisés autour d'un appareillage de mesures et, d'autre part, de tenter de délimiter en plan l'étendue de la zone intéressée par le phénomène.

Toutefois, après l'étude des documents permettant de localiser et de préciser cette zone, il est apparu que la cote des anomalies était située à une profondeur relativement basse de l'ouvrage. La figure 5 donne une idée approximative de la zone intéressée.

3-2 - Caractéristiques de l'ouvrage, des fondations et méthodes utilisées

La partie centrale du barrage correspond sensiblement à l'axe de la vallée majeure de la rivière c'est-à-dire, approximativement à la zone de hauteur maximum de l'ouvrage.

La constatation de tassements différentiels verticaux, avec création probable de zones de tension, conduisait à l'hypothèse de zones à perméabilité préférentielle facilement déterminables par le procédé d'injection déjà utilisé à de nombreuses occasions en France et à l'étranger par notre Laboratoire (5,6,9).

Les sondages ont été effectués soit à partir du couronnement du barrage, soit à partir de la zone supérieure du parement amont, soit enfin sur le parement aval. Au total, 19 sondages ont été traités par des traceurs.

Par ailleurs, une batterie de drains dont les sorties sont particulièrement bien visibles et facilement exploitables à l'aval de l'ouvrage, a également fait l'objet de prélèvements d'échantillons d'eau destinés à des analyses de tritium, d'uranium et de radon. Quelques éléments chimiques majeurs ont également été dosés, pour compléter l'ensemble des informations sur les caractéristiques des eaux.

La chronologie des travaux a été établie de manière à n'envisager les deuxième et troisième phases que dans le cas du plein succès de la première.

La phase initiale a consisté en mesures de radon et en mesures d'activité en tritium.

A l'aval de tout barrage en terre construit, comme c'était le cas ici, sur un terrain de fondation plus ou moins fissuré et passablement altéré, il est normal de

constater des venues d'eau parasites qui peuvent provenir soit directement de percolations à travers la fondation de l'ouvrage, soit indirectement par les rives, après un circuit assez long. Toutefois, ainsi que nous avons pu le constater sur d'autres ouvrages analogues, des fuites à l'aval peuvent provenir simplement de sources dont le trajet de résurgences a été perturbé par la construction de l'ouvrage ou qui proviennent des rives immédiatement à l'aval du barrage. En d'autres termes, ces eaux ne doivent pas avoir d'analogie étroite avec celles de la retenue.

Le barrage étudié est, comme nous l'avons mentionné, fondé sur des granites de l'axe cristallin pyrénéen, dans l'une de ses zones les plus tectonisées. Le granite des fondations est particulièrement diaclasé, fracturé et altéré chimiquement, avec, dans la majorité de la surface des fondations, une dissociation des minéraux. Le résultat de cette altération est un matériau ayant davantage les caractéristiques géotechniques d'un sable faiblement cimenté que celles d'une roche cristalline.

La perméabilité moyenne de cet ensemble est très variable. En effet, dans les zones peu altérées chimiquement, des diaclases de quelques millimètres à quelques centimètres d'épaisseur au maximum, permettent un débit de fuite relativement important, du moins si ce réseau de diaclases se prolonge sans interruption de l'amont vers l'aval.

Toutefois, la répartition des masses de granite altéré ne permet guère à ces diaclases de se prolonger sur de longues distances et elles se referment en général dans le matériau sableux qui contient également quelques éléments argileux. Il en résulte une perméabilité d'autant plus élevée que le granite est lui-même moins altéré.

Tout d'abord, il a été effectué des mesures d'activité en radon et en tritium sur les échantillons d'eau prélevés à l'aval du barrage, à la sortie des tubes de drainage du tapis filtrant aval. Les premières, celles de l'activité en radon, ont été effectuées sur place, avec le matériel de terrain prévu à cet effet. La seconde série de mesures, concernant l'activité en tritium, a été réalisée en Laboratoire, par le procédé classique d'enrichissement électrolytique et comptage en scintillation liquide.

3-3 - Première phase. Utilisation des traceurs naturels

Trois séries d'analyses de ces radioéléments naturels ont été effectuées en Mars, en Juillet et en Septembre 1971. Dans l'ensemble, toutes les valeurs de radon correspondent bien à un terrain granitique. En effet, certains échantillons ont atteint $580.10^{-11} Ci.l^{-1}$. Les variations sont particulièrement importantes, puisque la valeur minimum rencontrée a été de 13.10^{-11} $Ci.l.^{-1}$. On compte 10 valeurs au-dessus de 300.10^{-11} $Ci.l.^{-1}$.

En ce qui concerne les activités en tritium, nous n'avons enregistré que trois valeurs inférieures à 100 UT, sur 70 analyses au total. L'ensemble des autres valeurs est situé en moyenne autour de 130 à 140 UT, ce qui est un chiffre normal, étant donné l'altitude et la latitude de l'emplacement de l'ouvrage.

Nous verrons par la suite les valeurs des corrélations entre les différents éléments. On peut observer tout d'abord que, comme il est de règle, les valeurs de radon les plus élevées correspondent précisément aux circuits les plus rapides des eaux de la retenue à travers le corps du barrage.

Ces vitesses ont pu être mesurées lors de l'injection de brome et d'autres traceurs artificiels dans les différents forages crépinés, le traceur étant sorti à l'aval, par les tubes de drainage. Par ailleurs, on trouve également des valeurs relativement élevées de tritium, notamment des chiffres de 199 et 170 UT, évoquant des pluies antérieures de 1 à 2 ans.

Les différents groupes de valeurs correspondent à des familles de chiffres assez bien délimitées.

L'eau de la retenue a été analysée au cours de trois périodes antérieures. On constate que l'activité en tritium est comprise entre 116 et 171 UT. La valeur maximum correspond au résultat de la fonte des neiges, c'est-à-dire, aux prélèvements de Juillet. A part quelques rares valeurs extrêmes, l'ensemble de l'activité en tritium mesurée sur les débits de drains et aux résurgences aval correspond bien à la moyenne des eaux de la retenue.

Par ailleurs, les mesures de résistivité effectuées systématiquement sur l'ensemble des tubes du drain aval varient assez largement. Elles sont comprises entre 6950 et 32300 ohms·cm.

Au total, nous avons pu disposer de 72 mesures de tritium sur des prélèvements effectués pendant les trois périodes, de 22 points de mesures d'activité en radon, de 55 mesures de résistivité, ainsi que de nombreuses prises de température des eaux de prélèvements.

Cet ensemble de résultats d'analyses a été traité en corrélation linéaire. Les coefficients sont donnés dans ce qui suit, avec les remarques qui suggèrent.

Résistivité/^{3}H : coefficient voisin de 0. L'"âge" des eaux est indépendant de la minéralisation.

$^{222}Rn/^{3}H$: coefficient 0,31, pour 11 couples de valeurs. Sur l'ensemble des drains de l'ouvrage situés au droit du voile, sur la rive gauche, la dispersion de l'activité du ^{222}Rn ne permet pas de distinguer de corrélation nette entre le tritium et le ^{222}Rn. Toutefois, il y a une certaine probabilité de corrélation.

$^{222}Rn/^{3}H$: coefficient 0,85, pour 17 couples sur les résurgences et les drains de la rive gauche. Dans cette zone où les circulations sont moins faussées par la présence du voile d'étanchéité, la corrélation est bonne.

Résistivité/^{222}Rn : coefficient 0,89, pour 19 couples, sur toute la zone de l'ouvrage. La corrélation est excellente et les valeurs des deux nuages de points sont bien alignées. Ceci confirme d'une part le drainage efficace qui s'effectue sur la rive gauche, d'autre part l'augmentation de la vitesse de percolation par l'accroissement considérable de l'activité en radon dans la zone relativement peu affectée par le voile d'étanchéité.

Débit des drains/^{222}Rn : coefficient voisin de 0,58, pour 11 couples dans la zone du voile. A première vue, on aurait pu espérer une meilleure corrélation. Ce résultat rappelle l'indépendance relative entre vitesse de percolation et débit à l'extérieur du drain. Cette notion a été maintes fois confirmée ailleurs et sur le terrain et son existence est une évidence en théorie des écoulements.

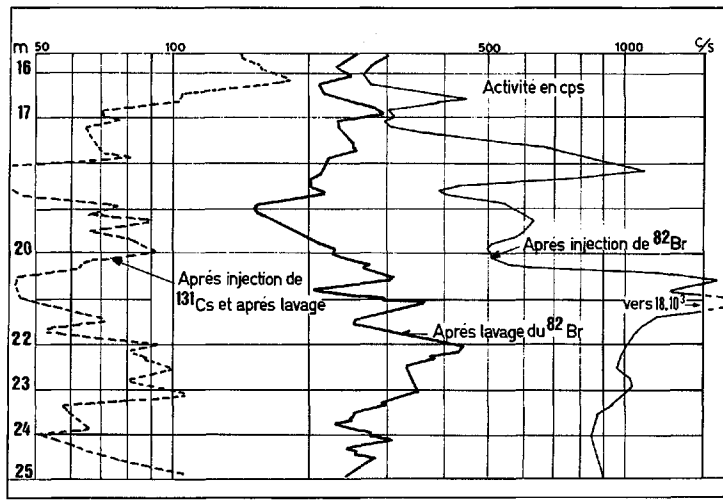

FIG. 6. Exemple n° 3: barrage en terre (sondage 6).

Tritium de Juillet/tritium de Septembre : coefficient 0,31, pour l'ensemble des 24 couples de valeurs disponibles. Le coefficient montre une certaine probabilité de corrélation sur ces 24 couples. On constate donc des réactions différentes d'écoulement sur l'ensemble des drains et des résurgence de l'ouvrage. Or, les valeurs de Juillet/Septembre devraient varier comme les deux résultats d'activité mesurée sur l'eau de la retenue, soit respectivement 171/116.

Tritium de Juillet/tritium de Septembre : coefficient 0,68, pour 16 couples de valeurs choisies dans la zone du barrage et du voile. En choisissant des valeurs plus logiques, on obtient donc un coefficient plus élevé, avec une probabilité de corrélation supérieure à 95%. Les 16 couples de valeurs sélectionnées varient comme les activités en tritium de la retenue, c'est-à-dire avec un faible retard, donc avec une vitesse de percolation importante.

Certains points de prélèvements montrent toutefois un retard sensible, apparemment de quelques mois, sur l'écoulement des premiers échantillons cités ci-dessus.

D'une manière générale, après examen des seuls traceurs naturels, on constate que la majorité des fuites à l'aval provient de la retenue ainsi que les percolations recueillies par le filtre aval et rejetées par les drains.

3-4 - Deuxième phase de mesures. Utilisation des traceurs artificiels anioniques

Cette phase a consisté en l'exécution d'un premier ensemble de sondages crépinés qui ont été effectués sur le couronnement, dans l'axe central des appareils de surveillance de tassement et perpendiculairement à cet axe. A partir de ces sondages, il a été possible d'obtenir la courbe dite de saturation de l'ouvrage qui a montré

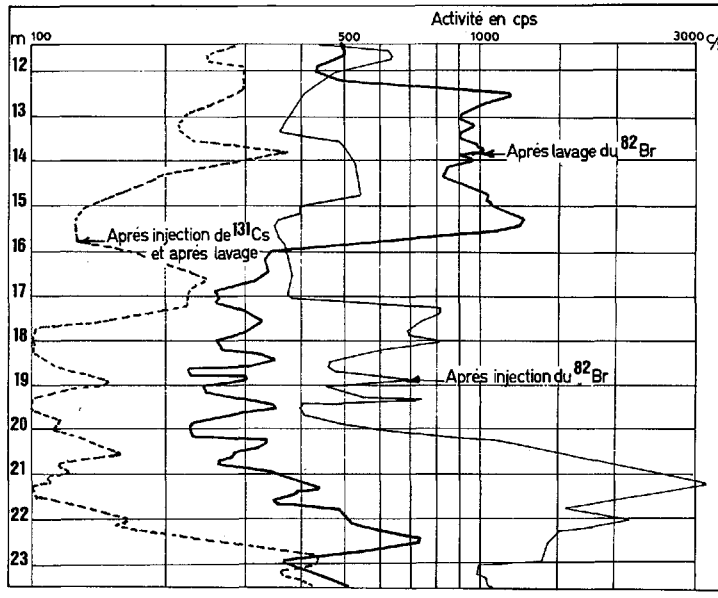

FIG. 7. Exemple n° 3: barrage en terre (sondage 7).

une pente très raide vers la partie amont du filtre, ce qui dénote des réactions hydrodynamiques particulièrement saines de l'ouvrage (fig 5).

Les premiers sondages ont fait l'objet d'injections à l'aide d'eau marquée par du brome-82 et par de l'iode-131. Il est apparu rapidement que le débit d'absorption de ces piézomètres était très variable. Dans certains cas, avec un débit de pompe supérieur à 1,5 l/s, le niveau de l'eau dans les piézomètres n'est monté que de quelques mètres au-dessus du niveau statique initial.

Dans d'autres cas, le piézomètre a manifesté une perméabilité relativement faible, puisque le niveau de l'eau est monté jusqu'au sommet du tube du piézomètre, ceci pour des débits de l'ordre de 0,5 l/s ou même légèrement inférieurs.

Les résultats ont été identiques lorsque les deux traceurs ont été utilisés dans le même sondage-piézomètre, pour la localisation des absorptions, c'est-à-dire des couches perméables. La hauteur relative des pics observés est la même. D'autre part, la distribution de ces pics, aussi bien au-dessus qu'au-dessous de la courbe de saturation, présente une certaine répétitivité.

Dans la zone saturée, lorsque le traceur était laissé sans autre action dans le sondage, on observait, au droit de certaines zones, la disparition rapide de ces pics qui étaient remplacés par des zones à valeurs anormalement basses de la radioactivité. Le phénomène s'établissait sur des durées assez courtes, de l'ordre de 10 à 15 minutes, indiquant l'entraînement du traceur par l'eau.

Enfin, au droit de la zone où s'étaient manifestés les signes de tassement, des pics très importants ont confirmé l'existence de passages à haute perméabilité.

En général, les résultats de cette deuxième phase suggéraient donc soit une action d'entraînement de particules fines et une augmentation de la perméabilité dans les plans de compactage du matériau soit, comme dans le cas particulier du tassement, une zone confirmant cet effet par ouverture localisée du terrain.

La contre-épreuve a été réalisée au cours de la phase suivante.

3-5 - Troisième phase. Utilisation de traceurs cationiques

Pour tenter de localiser des passages plus argileux traversés par les sondages, nous avons pensé utiliser un traceur cationique, le ^{131}Cs, malgré la faiblesse de son émission γ. En fait, après essais et spectrométrie en laboratoire, une impureté constituée de ^{131}Ba, contenue dans la livraison, a fortement contribué au succés de l'opération, grâce à des émissions γ nettement plus énergiques que celles du ^{131}Cs.

La contre-épreuve a étéententéesur 9 sondages. Les figures 6 et 7 montrent quelques exemples de résultats obtenus.

Aux pics de ^{82}Br correspondent également des pics de ^{131}Cs + ^{131}Ba puis, après lavage à l'eau sans traceur, des déficits très marqués des deux traceurs cationiques. Par contre, aux zones faiblement marquées par ^{82}Br ou ^{131}I, correspondaient des pics très marqués de ^{131}Cs + ^{131}Ba.

La mesure de l'activité du ^{131}Ba a été effectuée à l'aide d'un ensemble de spectrométrie de sondage qui fut utilisé avec succés lors d'opérations analogues en Italie (9).

L'hétérogénéité du matériau mise en évidence grâce à l'adsorption de traceurs cationiques par les minéraux argileux a été observée en détail sur des radiographies des carottes obtenues au cours des sondages. Il est d'ailleurs fort probable que la même série d'expériences aboutirait à des constatations analogues sur d'autres barrages en matériaux compactés. En effet, les réactions mécaniques des matériaux aux différents types de compactage sont en général rarement isotropes sur la totalité de l'épaisseur de la couche traitée.

4 - CONCLUSIONS

Ces trois exemples montrent quelques-unes des nombreuses possibilités d'utilisation des radioisotopes dans le domaine du Génie civil.

Les avantages les plus évidents présentés par les radioisotopes résident surtout dans leur souplesse d'emploi.

Ainsi, le tritium et le carbone-14 fournissent une notion de durée de transfert des nappes et des masses d'eau en général, qui place les données du problème posé dans un cadre chronologique réel. Les traceurs artificiels de leur côté permettent, outre l'obtention classique de notions sur des temps de transfert relativement courts, des informations sur la localisation précise de couches perméables.

Les études citées dans cette note ne peuvent donner qu'un aperçu des nombreuses possibilités d'utilisation des traceurs radioactifs dans le domaine du Génie civil, surtout si l'on tient compte des variations possibles de combinaison de traceurs, en fonction des exigences des problèmes posés.

Si cette utilisation pouvait être assez largement étendue, les ingénieurs responsables de grands travaux de Génie civil, en général sceptiques sur les études de caractère académique, pourtant indispensables, pourraient être sensibilisés par l'apport d'informations nouvelles qui leur permettraient de résoudre leurs problèmes pratiques et de serrer la réalité de plus près.

REFERENCES

[1] LEVEQUE, P.Ch., MAURIN, C., SEVERAC, J., Le ^{222}Rn, traceur naturel complémentaire en hydrologie souterraine, C.R. Acad. Sci. 272 (mai 1971) 2293.

[2] MAURIN, C., Contribution à l'étude du ^{222}Rn et à son utilisation en géologie de l'environnement, Thèse de spécialité, Bordeaux (sept. 1971).

[3] SZYMANSKI, J., Détermination des zones perméables dans les puits d'injection à l'aide de traceurs radioactifs, Icofiz. Jadrowa, Prace Zjezdzie Geofizkow Jadrow, Krakov, Warzawa Osrodek Infor. Techn. Ekon (1962) 942.

[4] DEGOT, B., LEVEQUE, P.Ch., COURTOIS, G., GASNIER, M., GODAR, S., «Deux utilisations du brome-82 en hydrodynamique souterraine», Radioisotopes in Hydrology (Compt. Rend. Coll. Tokyo, 1963), AIEA, Vienne (1963) 321.

[5] LEVEQUE, P.Ch., Emploi des traceurs radioactifs naturels et artificiels en hydrologie souterraine, Houille Blanche, Société hydrotechnique de France (12 juin 1969) 833.

[6] FRIED, J.J., Etudes théoriques et méthodologiques de la dispersion en milieu poreux naturel, Thèse de Doctorat, Bordeaux (1972).

[7] LEVEQUE, P., VIGNEAUX, M., ALVINERIE, J., «Evolution de l'activité en tritium dans le Sud-Ouest de la France», Isotopes in Hydrology (Compt. Rend. Coll. Vienne, 1966), AIEA, Vienne (1967) 417.

[8] PAYNE, B.R., Isotope hydrology, Adv. Hydroscience 8 (1972) 95.

[9] LEVEQUE, P.Ch., GIANNOTTI, G.P., GRISON, G., MITTENPERGHER, M., SIDOTI, G., «Critères hydrodynamiques de garantie de perennité pour le stockage géologique superficiel des déchets radioactifs», Réunion de Tokyo, 1972, Association internationale des hydrogéologues (1973) 145.

DISCUSSION

G.S. TAZIOLI: I was particularly interested in the evidence of a relationship between radon concentration and groundwater flow velocity (see in this connection Isotope Hydrology 1970, IAEA, Vienna (1970) 835).

For some years we have been determining groundwater CO_2 in addition to radon, and our results have contributed considerably to solving various hydrogeological problems – especially in relation to aquifers with an irregular natural radioactivity distribution.

I should like to take this opportunity to stress the importance of the relationship between CO_2 enrichment and groundwater flow velocity as regards the hydrogeology of carbonate rocks and the behaviour of carbon isotopes.

Have you made CO_2 determinations in addition to radon?

P.Ch. LEVEQUE: In reply to your question, we have not used your method of parallel determinations as, in the first two examples given in

our paper, the aquifers were too heterogeneous and the risk of contamination from industrial or natural (lignite) sources was too great. However, we intend to make CO_2 determinations in the study we are to carry out of a large homogeneous aquifer in fissured carbonate rocks.

We have been following closely your work on the waters of the karstic system of southern Italy, which is of more than just local interest.

APPLICATION OF SINGLE BOREHOLE METHODS IN GROUNDWATER RESEARCH

W. DROST, F. NEUMAIER
Gesellschaft für Strahlen- und Umweltforschung mbH,
Institut für Radiohydrometrie,
Munich,
Federal Republic of Germany

Abstract

APPLICATION OF SINGLE BOREHOLE METHODS IN GROUNDWATER RESEARCH.

Single borehole methods with improved field instrumentation have been extensively and reliably used in the Federal Republic of Germany for various groundwater investigations. Useful experiences from measurements for about hundred projects in more than a thousand boreholes in alluvial and karst aquifers during the last decade were obtained. While establishing the usefulness of single borehole methods, this reports offers practical examples of investigations of groundwater exploitation, bank filtration, groundwater pollution as well as foundation and hydraulic engineering.

1. INTRODUCTION

Many problems of groundwater investigations require an exact insight into the phenomena of movement of water in the subsurface layers. For every groundwater exploration project, the amount of water that can be tapped, the spread of the catchment area and the residence time of groundwater in the subsoil have to be evaluated. For special problems of waste water disposal information must be available on the waste volume the soil can accommodate, the degree of dilution by natural groundwater and the direction of movement of the pollutants. In projects of foundation and hydraulic engineering data are required on the behaviour of groundwater in the vicinity of the structure whether planned or existing. All these investigations essentially require determination of groundwater flow and direction of its movement.

To measure these hydrological parameters, single borehole methods employing the use of radioisotopes have been developed in the Federal Republic of Germany. Reviewing the present status of single borehole measuring techniques this survey offers practical examples of the investigations of groundwater exploitation, bank filtration, waste water disposal as well as foundation and hydraulic engineering with due regard to the limitation of the methods.

2. MEASURING TECHNIQUES

Single borehole techniques are used for determining filtration velocity, direction of flow and the vertical currents of groundwater in a boring. The requirements for the successful application of these methods have

been carefully worked out during the last 15 years. The establishment of experimental and theoretical assumptions was possible following extensive trial experiments both in the laboratory and in the field [1-8].

The extensive measurements necessitate continuous improvement upon the methods and development of a more versatile instrumentation for more rational field work. Based on the experiences of the trial runs it was possible to design and use a special borehole probe for measuring filtration velocity, as shown in Fig.1. Inside the sealed measuring volume of the probe are the detector, the injector and the mixing coil. Above and below this measuring volume are rubber packers in which detectors are placed to monitor vertical flow. To avoid flow outside in the gravel pack, vertical groundwater currents when present are forced through the pressure equalizing tube of the probe. When this is provided the influence of vertical currents on the measured filtration rates is negligible.

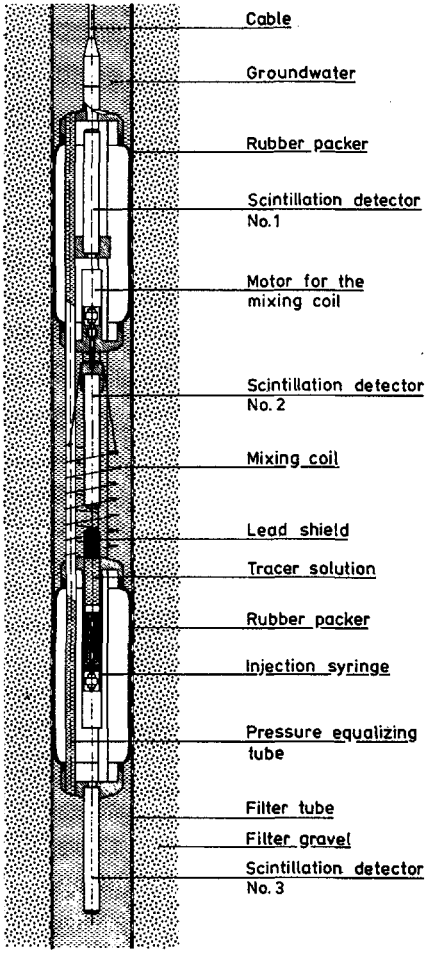

FIG. 1. Borehole probe for determination of filtration velocity of groundwater.

The probe can be lowered into the borehole ($\phi \geq 2$ in) by means of a cable whose diameter is only 10 mm. The cable consists of a pressure air line in addition to wires for power supply to the detectors, injecting and mixing devices. Using this probe, measurements of filtration velocity can be carried out by one person with professional experience of hydrological problems, measuring techniques and the basic principles of radiation protection.

Vertical currents of groundwater in a boring are a function of the filtration velocity and the pressure distribution in the surrounding aquifer. To ascertain such vertical flows, tracer logging methods have been developed [4, 9]. For performing these logs the probe shown in Fig.2 was constructed. This probe consists of an injector for the radioactive tracer solution and two detector units. The injector, which is remotely controlled, has a syringe with 10-ml capacity. Each detector unit has two GM counters (Type LND 732) which are fitted 50 cm apart. The detector units can be connected with the injector by bayonet sockets above and below. Because of its small diameter, the probe can be used for logging in borings with a diameter down to ϕ = 1.5 in. Using a power-driven cable drum, tracer logging with this probe can likewise be performed by one person.

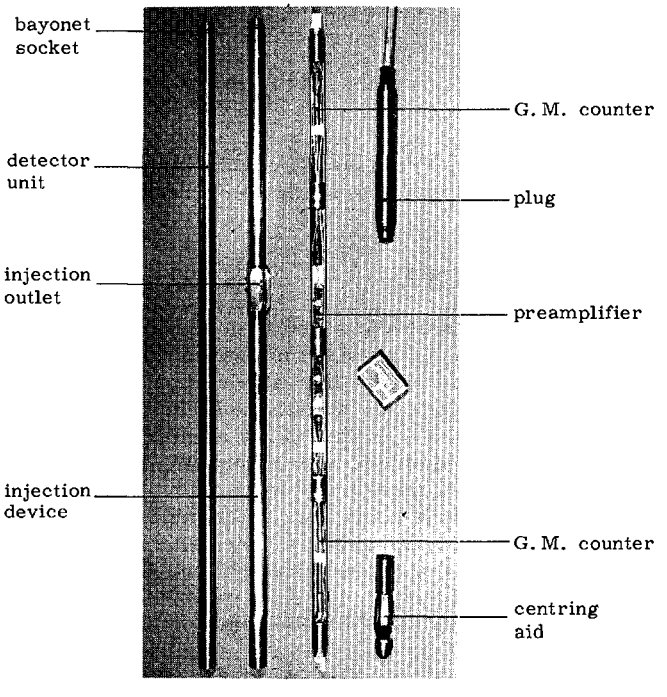

FIG. 2. Tracer logging device for determining vertical throughflows in a groundwater boring.

3. FIELD INVESTIGATIONS

Single borehole techniques have proved to be quite reliable in hydrological field investigations. For the last decade these techniques have been used increasingly for successful investigations of various groundwater problems. We have carried out field measurements for about 100 projects in about 1000 boreholes with more than 20 000 m filter casing. It has been possible to obtain the required data from many boreholes in a short time. The field experiments were simplified through the use of our improved instrumentation.

Single borehole methods have been successfully applied in many hydrological studies relating to the opening of groundwater fields. Besides evaluating the productivity of fields, data have been obtained on the protection zone. In many cases the amount of bank filtrate from rivers into the aquifer was determined. In addition it was possible to locate better permeable zones in the subsoil so that construction of the wells could be carried out optimally with regard to depth and type of filter casing. Measurements were carried out in areas surrounding city refuse deposits, nuclear power plants, traffic systems and other industrial installations to determine the extent of groundwater pollution and the degree to which drinking water galleries were adversely influenced. In engineering geology, the single borehole methods were applied to ascertain the nature and the volume of required pumping in certain practical projects of subways construction and design of foundations. It was possible to determine to what extent existing structures affect the groundwater movement, and also in which direction groundwater moved after the consolidation of the subsoil [4-6, 8, 10].

The investigations were carried out mainly in areas of alluvial gravel and sands but many measurements in fractured and karstic rock have also been performed. Water movement in fractured and karstic rock is generally anisotropic and inhomogeneous, consequently the movement of the groundwater cannot be described by universally valid laws. On the other hand, in gravel and sands, the laws of groundwater have been investigated in detail.

3.1. Investigations in alluvials

Using the single borehole technique in alluvials the filtration velocity can be determined and, if the gradient is known, the k_f-value of a groundwater field. Thus two parameters that play a decisive role in problems of groundwater investigations can be obtained. In some of the field experiments performed by us, the k_f-value of the aquifer was determined by conventional hydrological methods. By comparing the results of the single borehole method with these measurements we could ascertain the extent to which the various methods confirmed and complemented each other. The traditional method of determining the k_f-value in situ is pump experiments. If we are to compare the results obtained from them with those of the single borehole techniques, the first question that arises is whether they are genuinely comparable. In the single borehole methods we measure the stream line density of the groundwater in the horizontal plane, whereas in pumping experiments both the horizontal and vertical planes are involved. But the horizontal permeability can be up to 20 times as great as the

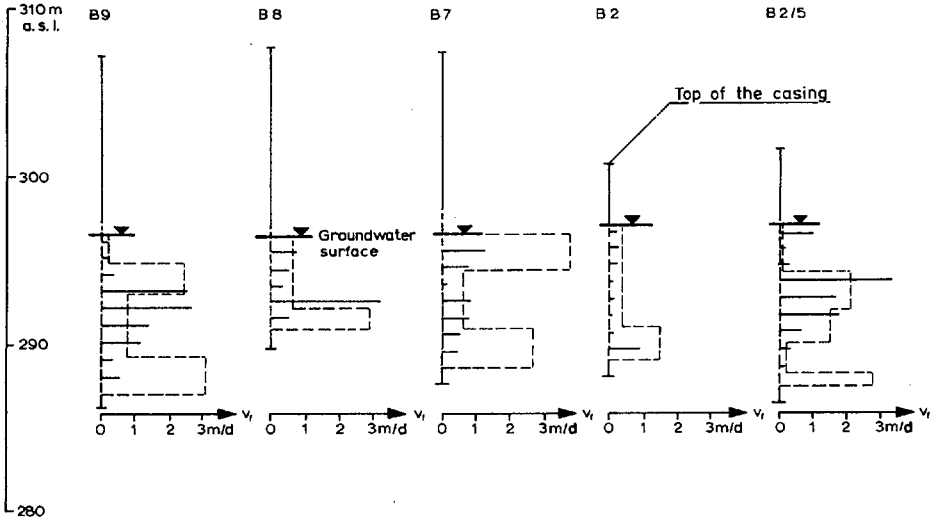

FIG. 3. Results of single borehole measurements in Nuremberg city in an alluvial-filled valley. Solid line: Filtration velocity measured by the borehole probe shown in Fig. 1. Dashed line: Filtration velocity calculated from vertical flows.

vertical. In addition, it should be noted that the various methods cover a larger or smaller region of the aquifer. For these reasons, in comparing these independent measuring techniques, there can be said to be agreement as long as the k_f-values obtained are of the same order of magnitude [6, 11].

Systematic determination of the k_f-value, first by pump tests and then by single borehole techniques, has been carried out in the Bavarian Lower Alps by the Munich Waterworks and by our Institute. The Munich Waterworks obtained k_f-values by site tests during drilling, using a perforated cylinder introduced into the drill hole, after withdrawing the pipes. The k_f-value was ascertained by pumping or infiltration experiments. Altogether, 53 comparative measurements in the cylinder were carried out in the alluvial coarse gravels of the area. The agreement between the pair of measured values was up to 85%. In 15% of the cases the difference was less than ± 10%, in 30% it was ± (10-25)%, and in 35% it was ± (25-50)%. In the light of this comparison and in accordance with the results from other pumping tests in alluvial gravel and sands in the southern part of Germany, it can be said that the single borehole methods can produce substantially the same results as the usually very onerous pumping experiments. In addition to supplementing the pumping technique, the single borehole methods yield the stratification of the k_f-values in the vertical profile of a borehole [2, 6, 12, 13].

An important prerequisite for such a comparison test is the exact knowledge of the groundwater slope. Determination of the slope, though apparently simple, is often erroneous if the pressure distribution in the aquifer is not uniform. Thus, even an exactly measured filtration velocity is liable to be misinterpreted as is shown in the following example. In

Nuremberg city the course of a planned subway lies through an alluvial-filled valley. Pumping tests revealed that the base of the valley consists of highly permeable layers. In contrast to this, the single borehole measurements carried out at five gauges showed that the lowest filtration velocities were at the bottom of the valley (Fig.3). This apparent disagreement is due to the fact that the borings near the bottom are situated in a hydrological system where there is hardly any flow because the hydraulic gradient near the base is small. Because of unequal pressure distribution in the aquifer and consequent short circuiting, it was found that groundwater was flowing vertically downwards in the borehole. The vertical currents were in accordance with the permeabilities of the different layers in the aquifer indicating high permeability at the base of the valley.

In investigating a groundwater field it is often required to estimate the amount of groundwater flow. The city of Munich has installed a well gallery in the Loisach valley. Using single borehole methods the groundwater discharge during two measurements series was found to be approximately 5 m^3/s which corresponded with the value derived from soil mechanical investigations, pump tests and water balances [6, 10, 13].

In many cases, water winning is based on the bank filtration of surface water. In the construction of a well gallery in the Hockenheim Rhine Bend (Badenia), the problem arose of determining the proportion of infiltrating Rhine bank filtrate in addition to the amount of water that could be exploited from two groundwater storeys in approximately 50-m-thick sands and gravels. The investigations of Rhine bank filtrate are of special priority because of the increasing trend in the pollution of Rhine water from organic and inorganic materials. Measurements of filtration velocity were performed during a yield pump test. The results obtained from the upper storey at the site of well K 5, closest to the Rhine, are presented in Fig.4. From a mean velocity $\bar{v}_f \sim 15$ m/d within 5 m distance from pumped well K 5 on the upper storey, there results a discharge rate of approximately 4000 m^3/d. After ascertaining the total pumping rate of well K 5 (about 11 000 m^3/d) and the results of simultaneous tritium measurements[1] (Rhine ~ 350 TU, second storey ~ 10 TU, pumped water ~ 130 TU), we could determine the tritium value of the upper storey to be about 340 TU. Thus it became clear that well K 5 was receiving in the upper storey only the Rhine bank filtrate.

Another well gallery for water supply has been constructed in the Weisser Bogen section of the Rhine near Cologne. Using isotope methods in this Rhine bend we have begun a series of measurements for investigating groundwater movement as a function of the Rhine water level. The results of the first series during the lower level of the Rhine indicate that the gallery taps bank filtrate only from the southern part of the catchment area ensuring that the residence time of water in the underground is more than the 50 days required for reasons of hygiene.[2]

---

[1] The tritium measurements were performed by W. Rauert, Institut für Radiohydrometrie, Munich.

[2] The investigations of bank filtrations within the Weisser Bogen section of the Rhine were performed in co-operation with U. Chandra, at present at the Institut für Radiohydrometrie, Munich, and H. Kussmaul, Bundesgesundheitsamt, Düsseldorf.

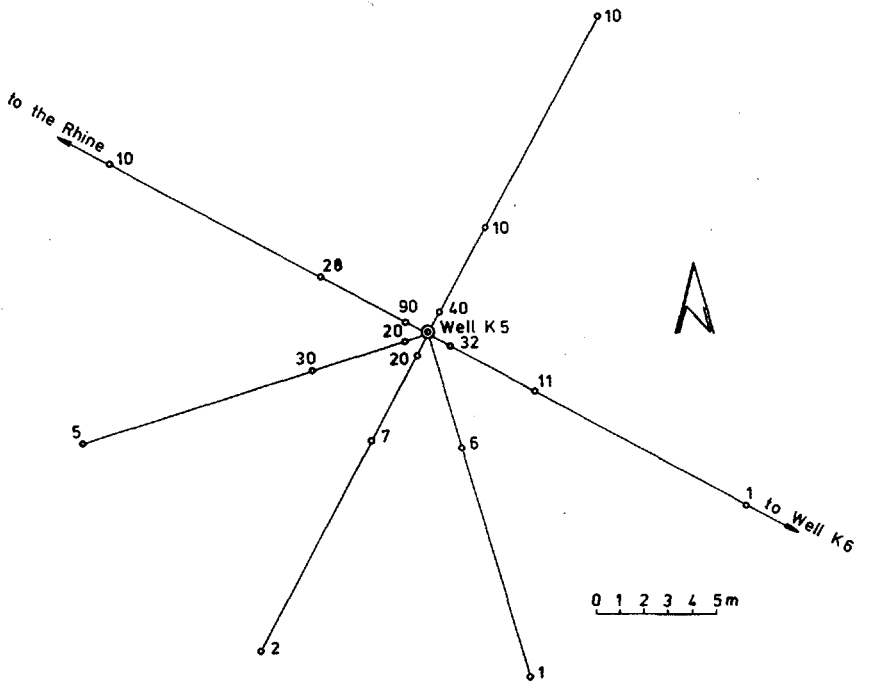

FIG. 4. Bank filtration field at Hockenheim Rhine bend. Results of single borehole measurements in the upper storey (thickness about 8 m) of the aquifer at the site of Well K5. The points are gauges, the numbers being the measured filtration velocities (in m/d).

At the site of the refuse dump of the city of Munich numerous temperature and conductivity measurements, chemical analyses and bacteriological tests have proved unmistakably that the groundwater is detrimentally affected with respect to its chemistry and temperature as it passes through the detritus under the refuse dump. It has been possible so far to follow the polluted groundwater up to a distance of 3000 m from the dump, discovering that it spreads tonguelike in the general direction of flow. Additional tracer measurements to determine filtration velocity and flow direction indicated that beyond this 3000-m zone the groundwater flows uniformly in the general direction of run-off. Within the polluted zone, on the other hand, most of the flow directions ascertained vary from the main run-off direction and are also inconsistent in relation to each other. This effect is due to the fact that in part the aquifer has been compacted by the pollutants so that the groundwater deviates within local limits from the general flow direction [10, 14]. Measurements of this kind are also conducted before new waste disposal facilities are established so that an assessment can be made of the filtration velocities and flow directions as well as the pressure distribution in the aquifer to find out the possible

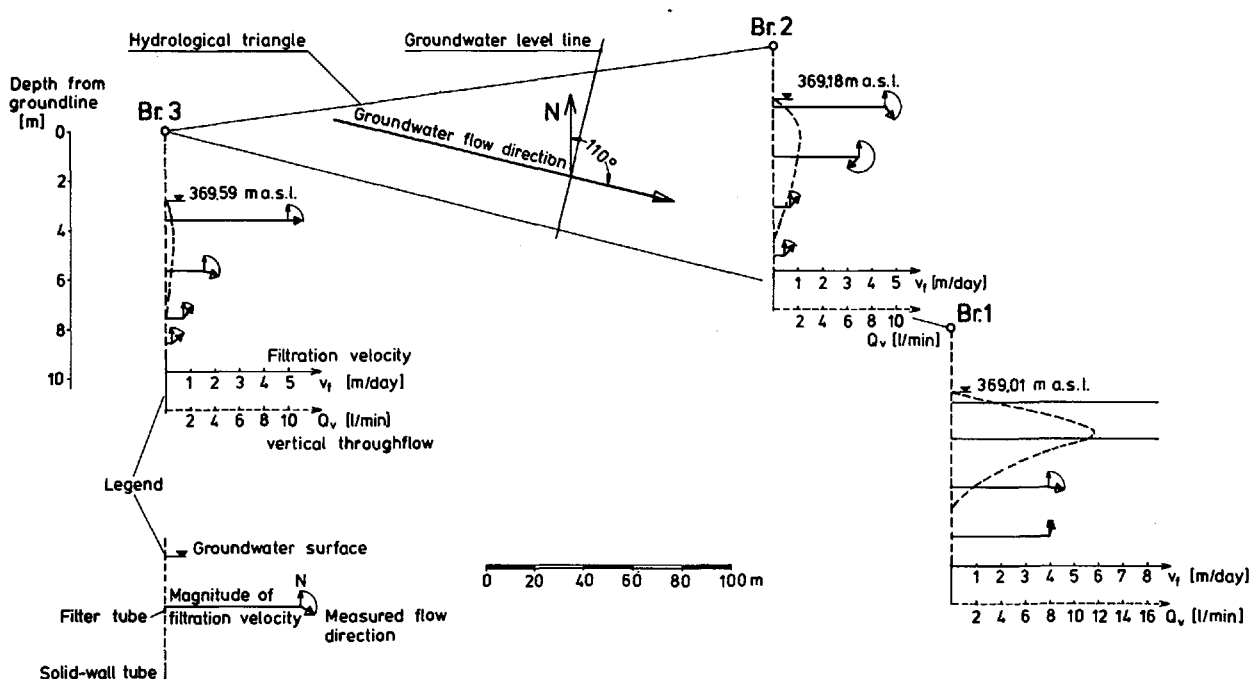

FIG. 5. Plan of the groundwater borings Br. 1, Br. 2 and Br. 3, at the Isar nuclear power plant; profiles of the borings with the filtration velocity v_f are shown, the flow direction and the vertical throughflow Q_V as results of single borehole measurements, as well as the flow direction obtained from the hydrological triangle.

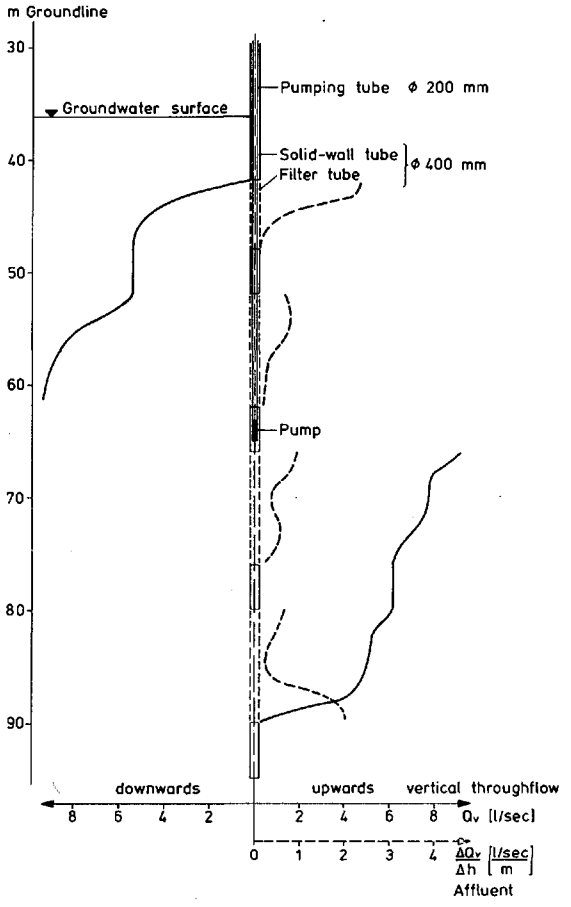

FIG. 6. Design of a well in the town of Vogt, and the results of a tracer-log for determining vertical throughflows at a withdrawal rate of 20 litres/s.

extent of groundwater pollutions of varying concentration should water-soluble pollutants enter the groundwater despite all safeguards. At the site of a nuclear power plant near the Isar River in Bavaria single bore-hole measurements were carried out, before construction began, to determine the k_f-value. Contrary to the findings of the drilling, the results shown in Fig.5 prove that two groundwater storeys exist in the approximately 8-m-thick gravels. In the upper storey the filtration velocities fall within the range of a few metres daily, and the flow direction agrees with that determined by the hydrological triangle. For the lower storey the filtration velocity values are smaller by one magnitude than those encountered in the upper storey and the flow direction values deviate by about 100° from those obtained in the upper storey. In the borings

there exists a downward vertical exchange of water between the two storeys, i.e piezometric pressure is higher in the upper storey than in the lower. From these findings it is possible to make an assessment of the spread of a possible pollution of the groundwater by reactor wastes. It could be expected that possible pollutants will be contained only by the upper storey.

In the exploitation of groundwater the determination of the protection zones plays a predominant part. In the case of a well in the town of Vogt (Württemberg), the drilling indicated water-bearing stratum only near the bottom of the boring, but additional measurements of the vertical groundwater flow in the tertiary sands of the borehole during a pumping test revealed that a subsurface storey was contributing about 50% of the withdrawal (Fig.6). These findings called for a reconsideration of the protection zone estimated by means of the drilling results.

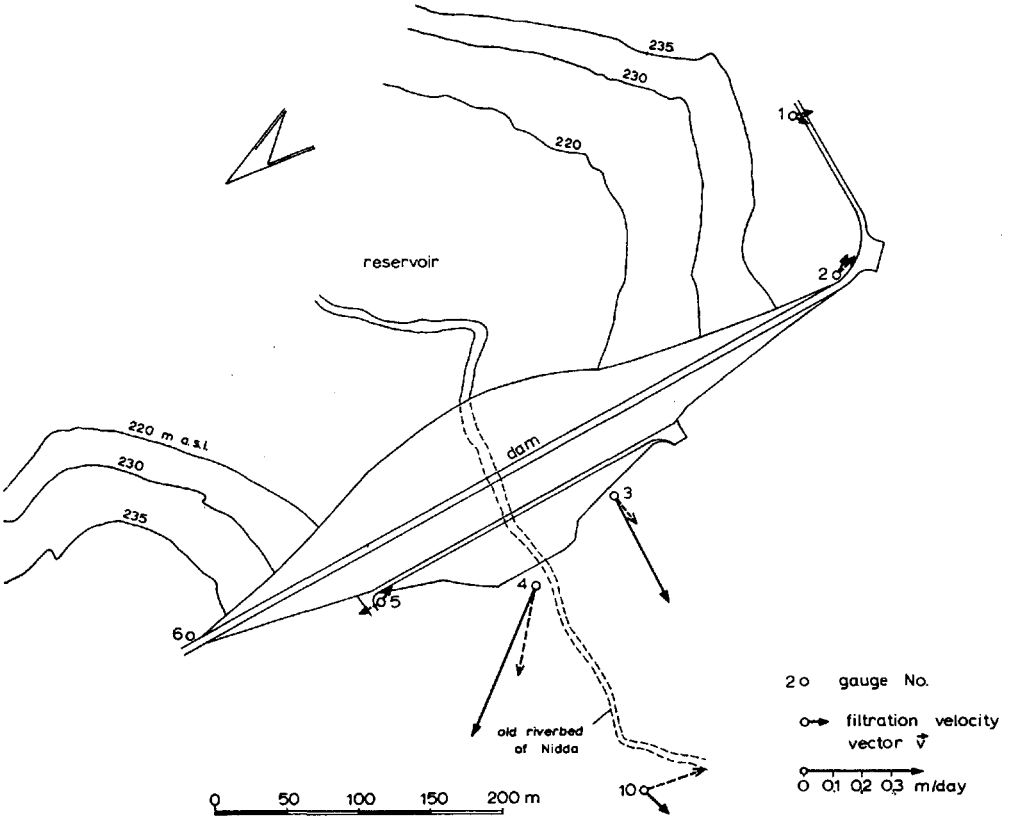

FIG. 7. Results of two series of measurements at the site of the Nidda dam. Solid arrows: Filtration velocity vector before cement injection at the base of the dam, storage level ~210 metres above sea level. Dashed arrows: Filtration velocity vector after cementation, storage level ~226 metres above sea level.

3.2. Investigations in fractured and karstic aquifers

In the light of the foregoing groundwater investigations, the single borehole techniques can be considered as reliable methods to determine quantitatively hydrological parameters in alluvial gravel and sands. On the other hand, in fractured and karstic rock the results of single borehole methods are utilizable normally only quantitatively because of the absence of a relation between the water movement in the boring and the aquifer. But even relative values prove to be useful for correct interpretation. This can be shown by the following examples.

The Nidda barrage at the Vogelsberg site in Hesse, with a capacity of approximately 10 million m^3, has been constructed for water management purposes, flood control and low-water improvement. The foundation of the Nidda dam lies on a basaltic aquifer which is in part highly permeable due to the presence of fissures and caverns. Surrounding the dam and the reservoir there are several groundwater gauges with casing in the basaltic aquifer. Using single borehole techniques a first series of measurements were performed in the network of the gauges at low storage (~ 210 m above sea level). The results shown in Fig.7 (continuous arrows) indicate high seepage rates near the old bed of the Nidda river. But this finding can be misleading considering the anisotropy of the basaltic aquifer. A second series of measurements were continued at a higher storage level (~ 226 m above sea level) after the base of the dam was stabilized by injection of cement. The efficiency of this measure was confirmed by the results of the second series. At a higher level of the storage lower seepage rates were observed downstream of the dam. Comparing the results of the two series at the site of gauge 10, it can be seen that the velocity vector has turned southwards indicating an inflow to the aquifer at the downstream side after the injection.

Whether the well receives an inflow of subsurface groundwater was another problem to be solved during a pump test in a karstic well in the town of Gammertingen (Württemberg), situated under 10-m-thick gravels in cavernous and fissured rock of the white Jurassic. The vertical flow movements in the well were measured by the tracer logging method. The measurement results shown in Fig.8 reveal that no groundwater is being drawn from the subsurface gravels. Consequently, the protection zone for this well will be more confined than had the inflow from the gravels been present. In addition the measurement results indicate that the well has two inflow horizons that exchange water when the well is not pumped. These results are demonstrating the possibilities of measuring vertical groundwater movement in borings in fractured or karstic aquifers. Under pumping conditions it is possible to determine the discharge rate of an inflow horizon quantitatively. Vertical water movement without pumping gives only some information about the pressure distribution in the aquifer and the site of water-bearing horizons. Below a depth of 50 m no water motion towards the well was detected. This result has been confirmed by two gamma logs in the boring: the gamma log recorded after the first tracer logging (Fig.8d) has a higher radiation level below a depth of 50 m in comparison with the gamma log registered before the tracer measurements. This was due to the fact that the radioactive tracer solution added during tracer logging was incapable of flowing away. It is advisable, as done on many occasions, to perform such measurements before the

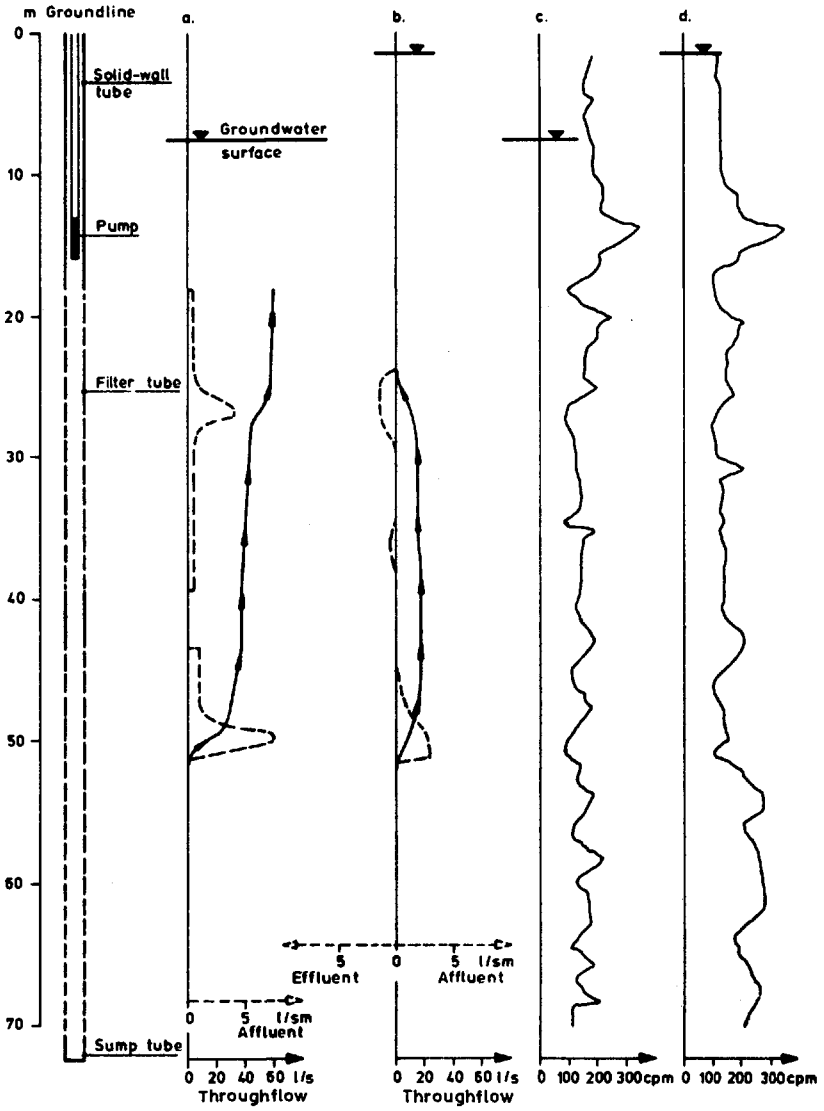

FIG. 8. Gammertingen karstic well: well design and results of single borehole measurements.
(a) Results of a tracer log at a withdrawal rate of 60 litres/s.
(b) Results of a tracer log without withdrawal.
(c) Results of a gamma log before the tracer log.
(d) Results of a gamma log after tracer log (a).

boring is developed so that the results can be turned to advantage in equipping the boring, and avoiding, as was the case with the Gammertingen well, an unnecessary filter length for the lowest 20 m of the boring.

ACKNOWLEDGEMENTS

These investigations were possible only through close co-operation with many government and communal water-management agencies. The authors are grateful to the members of these offices for their assistance in arranging field experiments.

REFERENCES

[1] HALEVY, E., MOSER, H., ZELLHOFER, O., ZUBER, A., "Borehole dilution techniques: a critical review", Isotopes in Hydrology (Proc. Symp. Vienna, 1966), IAEA, Vienna (1967) 531.
[2] DROST, W., KLOTZ, D., KOCH, A., MOSER, H., NEUMAIER, F., RAUERT, W., The Borehole Dilution Method of Measuring Groundwater Filtration Velocity, GsF-Bericht R 16, Munich (1968).
[3] DROST, W., KLOTZ, D., KOCH, A., MOSER, H., NEUMAIER, F., RAUERT, W., Point dilution methods of investigating groundwater flow by means of radioisotopes, Water Resour. Res. 4 (1968) 125.
[4] DROST, W., "Groundwater measurements at the site of the Sylvenstein dam in the Bavarian Alps", Isotope Hydrology 1970 (Proc. Symp. Vienna, 1970), IAEA, Vienna (1970) 421.
[5] DROST, W., Grundwassermessungen im Bereich eines Mooreinsprengdammes im Degenseemoos bei Penzberg (Oberbayern), Geol. Jb. C2 (1972) 339.
[6] DROST, W., Grundwassermessungen mit radioaktiven Isotopen, Geologica Bav. 64 (1971) 167.
[7] KLOTZ, D., Untersuchungen von Grundwasserströmungen durch Modellversuche im Massstab 1:1, Geologica Bav. 64 (1971) 75.
[8] DROST, W., MOSER, H., NEUMAIER, F., RAUERT, W., Isotopenmethoden in der Grundwasserkunde, Inf. 61, Büro Eurisotop, Brussels (1972).
[9] DROST, W., Der Tracerlog, ein neues Bohrlochverfahren zu Grundwassermessungen mit radioaktiven Isotopen, Informationsheft 55, Büro Eurisotop, Brussels (1972) 379.
[10] DROST, W., Application of groundwater measurements by means of radioisotopes on groundwater exploration, First World Congress on Water Resources, Chicago (1973).
[11] WEEKS, E., Determining the ratio of horizontal to vertical permeability by aquifer test analysis, Water Resour. Res. 5 (1969) 196.
[12] LOHR, A., Beitrag zur Ermittlung des k_h-Wertes durch hydraulische Feldversuche, Gas- u. WassFach 110 14 (1969) 369.
[13] LOHR, A., Different methods of estimating discharge of subterranean waters, International Water Supply Congress and Exhibition, Special Subject No. 2, Vienna (1969) E 3.
[14] EXLER, H.J., Ausbreitung und Reichweite von Grundwasserverunreinigungen im Unterstrom einer Mülldeponie, Gas- u. WassFach 113 3 (1972) 101.

DISCUSSION

A. PLATA BEDMAR: What are the maximum depths at which you have used the equipment for measuring horizontal flows? I ask this because we have found that there is a considerable risk of such equipment becoming stuck in the piezometers.

W. DROST: We have used it down to depths of 300 m without any problems, and it can be used at even greater depths.

S. GAONA VIZCAYNO: During your oral presentation you showed a slide illustrating groundwater flow directions in the vicinity of a Munich

refuse dump. At some points the flow directions were opposite to the general pattern. Could this be due to blocking of the aquifer pores around the boreholes as a result of the drilling operations?

W. DROST: I do not think so. The deviations from the general flow direction pattern are confined to the polluted zone and related to the degree of pollution.

S. GAONA VIZCAYNO: Were the boreholes drilled purely for your study?

W. DROST: No, they were drilled for monitoring pollution by various conventional methods, including pumping tests. No pumping was carried out during our measurements.

R.E. ISAACSON: How is your method used to determine anisotropy in hydraulic conductivity in a radial direction?

W. DROST: In the absence of a dense radial network of boreholes at the investigation site, the single borehole data need to be supplemented by geophysical information.

R.E. ISAACSON: It is not quite clear how variations in permeability along the entire length of a borehole can be determined: is it possible, or must one predetermine which zones are to be tested?

W. DROST: Our measurements were performed in wells, which are provided with screens in the water-bearing horizons. The vertical permeability profile was obtained by measurements at different depths using the probe mentioned in the paper.

U. CHANDRA: As a member of the Munich field team, I should like to stress that borehole dilution techniques were useful in detecting stratification of groundwater flow lines even in the absence of a geological stratification at the site, which consisted of Quaternary gravels and sand. In the lower Bavarian Alps we observed filtration rates near the water table two to three times higher than in the bottom layers in a borehole penetrating only 10 m of the aquifer. The flow directions were also characteristically different in the upper and lower layers. This led us to take samples of water from different depths in the borehole and determine their deuterium contents. The deuterium values for the upper layers corresponded to the mean value of the surface waters. The deuterium values for the deeper layers were lower and indicated that the water in the deeper layers was seepage water from the hills. This further confirmed the stratification of groundwater flow. The borehole logging data, however, did not indicate any geological stratification at the site.

MODELOS MATEMATICOS SIMPLIFICADOS PARA INTERPRETACION DE RESULTADOS POR EL METODO DE MARCACION DE TODA LA COLUMNA PIEZOMETRICA

H.A. MUNERA
Instituto de Asuntos Nucleares,
Bogotá, Colombia

Abstract–Resumen

SIMPLIFIED MATHEMATICAL MODELS FOR INTERPRETING THE RESULTS OF TESTS CARRIED OUT BY LABELLING THE WHOLE PIEZOMETRIC COLUMN IN WATER WELLS.

Approximate methods used to interpret the results of tests based on radioactive tracer dilution in a single water well by labelling the whole piezometric column are described; these simple mathematical models have been used to obtain semi-quantitative data on the apparent velocity (horizontal) in non-homogeneous aquifers with flow rates of metres daily. Measurements have also been made in a homogeneous aquifer with velocities of centimetres daily. Interpretation is based on determination of the average concentration for the various well zones; this involves recognition of a mean velocity for each region. All the tracer dilution effects that are not due to horizontal or vertical flow between two zones, i.e. convection, artificial mixing, diffusion and so on, are grouped together as a single term, which is taken arbitrarily to be proportional to the difference in concentration between the regions under consideration; its value is obtained from the experimental dilution curve.

The model was applied to the solution of the three cases encountered most frequently during our measurements in Colombia: (a) when the well penetrates a permeable zone and adjacent impermeable zone; (b) when the well penetrates a permeable zone contained between impermeable regions; and (c) when the well traverses an aquifer with two adjacent zones of different permeability contained between impermeable zones. The shape of the dilution curve (logarithm of concentration versus time, usually with two or more slopes) is predicted by the model, the approximate nature of which is consistent with the fact that the method of labelling the whole piezometric column is semi-quantitative. The results obtained for measurements made when there are considerable vertical flows are apparently correct, but there is no other experimental measurement available to confirm them.

MODELOS MATEMATICOS SIMPLIFICADOS PARA INTERPRETACION DE RESULTADOS DE ENSAYOS POR EL METODO DE MARCACION DE TODA LA COLUMNA PIEZOMETRICA.

Se describen en esta memoria los métodos aproximados utilizados para interpretar los resultados de los ensayos por dilución de trazador rediactivo en pozo único por el método de marcación de toda la columna piezométrica; estos modelos matemáticos simples han sido usados para obtener información semicuantitativa sobre la velocidad horizontal de filtración en acufferos no homogéneos, con flujos del orden de metros por día. También se han realizado mediciones en un acuffero homogéneo con velocidades del orden de centímetros por día. La interpretación se basa en la definición de concentraciones promedias para las distintas zonas del pozo, lo que implica aceptar una velocidad promedia para cada región. Todos los efectos de dilución del trazador no debidos a corrientes horizontales o verticales entre dos zonas, por ejemplo convección, mezclado artificial, difusión, etc., se agrupan en un solo término que se toma arbitrariamente como proporcional a la diferencia de concentración entre las regiones en consideración; su valot se obtiene de la curva experimental de dilución.

El modelo se aplicó a la solución de los tres casos más frecuentemente encontrados en nuestras mediciones en Colombia: a) el pozo penetra una zona permeable y una zona impermeable adyacente; b) el pozo penetra una zona permeable comprendida entre regiones impermeables, y c) el pozo atraviesa un acuffero con dos zonas adyacentes de distinta permeabilidad, comprendidas entre zonas impermeables. La forma de las curvas de dilución (logaritmo de concentración en función de tiempo, generalmente con dos o más pendientes) es predicha por el modelo, cuyo carácter aproximado es consistente con la naturaleza semicuantitativa del método de marcación total de la columna piezométrica. Los resultados obtenidos para mediciones ejecutadas en presencia de flujos verticales apreciables son correctos aparentemente; sin embargo, no existe ninguna otra medida experimental para confirmarlos.

1. INTRODUCCION

El método de dilución puntual en pozo único para obtener información sobre la velocidad de filtración en el acuífero está ya muy bien establecido; las técnicas disponibles se resumen en [1 y 2]. El desarrollo de las técnicas de dilución se inició en algunos lugares con el método de marcación de toda la columna piezométrica [3], que fue más tarde desechado en favor de la marcación puntual que permite un mayor control experimental, una más fácil interpretación y una mejor cuantificación de los resultados.

En los últimos años se ha vuelto a ensayar en la India [4] y en España [5,6] la marcación de toda la columna como un método conveniente para obtener rápidamente información semicuantitativa a lo largo de todo el perfil de interés. En particular, el sistema empleado por Plata [5,6] es bastante simple, de buena portabilidad y bajo costo, siendo por lo tanto adecuado para ser utilizado en sitios de difícil acceso y por países o instituciones que no dispongan de abundantes recursos.

Durante la estadía del mencionado autor en Colombia como experto del OIEA (1972), la técnica en cuestión empezó a usarse para medir el orden de magnitud de la velocidad de filtración en el acuífero de la Isla de San Andrés, aprovechando pozos que ya habían estado en explotación por varios años; por tratarse de una isla de origen coralino el agua viaja por grietas y fisuras con alta velocidad (m/d). Posteriormente, se han realizado mediciones en un acuífero homogéneo de baja velocidad (cm/d) y en varios pozos localizados en un depósito aluvial (m/d). El trazador utilizado ha sido siempre ^{82}Br, en la forma de bromuro de amonio, con abundante portador. Desde la iniciación de los trabajos se aprecia que es difícil obtener un valor adecuado de la pendiente de la curva de dilución (logaritmo de concentración vs. tiempo) para tiempo cero; igualmente, en algunos casos se nota que dicha curva presenta más de dos pendientes características, en contraste con los resultados indicados por Plata [5,6]. Entonces, tal como lo habían sugerido Smith y Moser durante la discusión de la memoria [5], se hizo necesario elaborar un poco más el proceso de interpretación de los datos experimentales, para así tener en cuenta efectos de convección, de flujo vertical y de incremento en el fondo radiactivo, entre otros.

Si se considera que el método de marcación de toda la columna piezométrica es esencialmente semicuantitativo, especialmente cuando se trata de flujo por fisuras, no se justifica recurrir a un tratamiento riguroso del movimiento del trazador, similar, por ejemplo, al usado en [7,8]. Se optó, en consecuencia, por un modelo simplificado que definiera implícitamente una velocidad aparente promedia sobre la zona de flujos.

A continuación se indican las suposiciones básicas del modelo y se ilustra su aplicación a los distintos casos que se presentaron en el estudio de la Isla de San Andrés; los resultados fueron consistentes internamente, en el sentido de que las curvas teóricas se ajustan a las experimentalmente halladas.

2. SUPOSICIONES BASICAS DEL MODELO

Las suposiciones básicas del modelo se refieren principalmente al comportamiento del trazador, a su forma de inyección y a su distribución posterior en el sistema pozo-acuífero. Las suposiciones referentes a la interrelación entre el flujo en el acuífero y el flujo a través del pozo de observación son comunes con otros métodos y modelos y se dejan implícitas. Explícitamente se supone lo siguiente:

a) El trazador es un material ideal que no se fija en el sistema. Su concentración fuera del pozo de observación es cero, tanto antes como después de la inyección.
b) La marcación inicial de toda la columna es instantánea y perfecta, tanto longitudinal como radialmente; esto es, la concentración inicial de trazador es $\bar{C}_o$ en cualquier punto del pozo.
c) La columna piezométrica del pozo puede dividirse en varias zonas de concentración uniforme, sendas representantes de regiones del acuífero con permeabilidad constante y flujo horizontal uniforme.
d) Todos los efectos de transferencia de trazador que no sean debidos a flujo horizontal o vertical de agua se agrupan en un término de difusión y convección. La corriente J (actividad/área•tiempo) de radio-trazador desde la zona i de concentración $\bar{C}_i$ hacia la zona j de concentración $\bar{C}_j$ se define como proporcional a la diferencia de concentraciones[1], por ejemplo

$$J = - v_c(\bar{C}_j - \bar{C}_i) \qquad (1)$$

donde v_c es una velocidad de difusión y convección que se espera sea constante.

Las dos últimas condiciones permiten eliminar del modelo todas las variables de espacio (por ejemplo z, r y θ en coordenadas cilíndricas) dejando como única variable independiente el tiempo t.

A continuación se ilustra la aplicación del modelo al caso ideal de un acuífero homogéneo; el pozo de observación penetra solamente en este acuífero. Luego se tratan los casos en que el pozo atraviesa varias zonas de diferente permeabilidad.

---

[1] Nótese que ésta es una versión numérica de la ecuación de difusión en una sola dimensión z : $J_z = - D_z \partial C/\partial z$. En el caso particular de que el único efecto importante sea la difusión, la suposición equivale a aceptar a lo largo de z una distribución exponencial de C en cualquier instante.

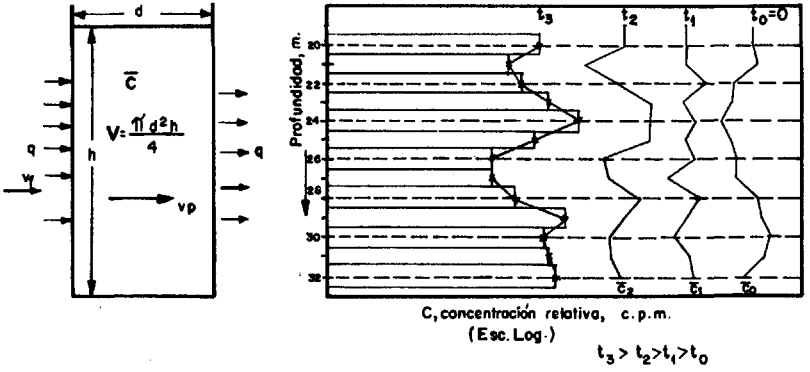

a) Flujos existentes y perfiles de concentración.

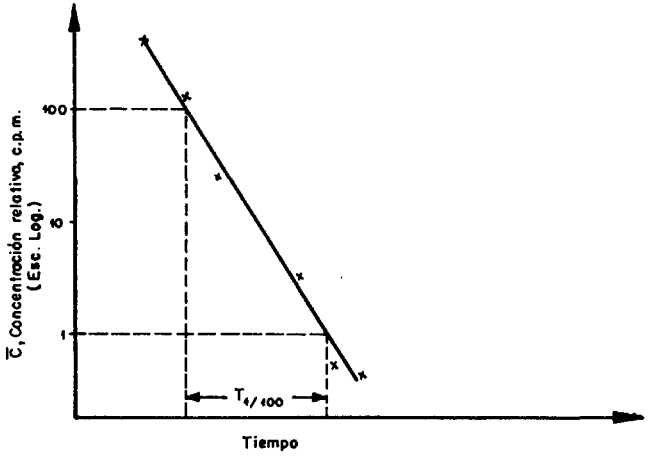

b) Curva Concentración – Tiempo para la zona de flujos.

FIG. 1. Acuífero homogéneo; pozo completamente contenido en el acuífero.

3. CASO No. 1. EL POZO ATRAVIESA SOLAMENTE UN ACUIFERO HOMOGENEO

3.1. Aplicación del modelo

Sea un pozo de observación de diámetro d ranurado en toda su extensión h; la velocidad de filtración en el acuífero v_f está relacionada con el caudal horizontal q que fluye a través del pozo por medio de la ecuación

$$q = hd\alpha v_f \tag{2}$$

donde α es el bien conocido factor que correlaciona los caudales que fluyen a través de secciones iguales en el pozo y el acuífero [1].

Para determinar q experimentalmente, se inyecta uniformemente el pozo con una actividad A_o de trazador en el tiempo t = 0, con lo que se establece una concentración promedia $\bar{C}_o$ [figura 1a)]. La actividad A remanente dentro del pozo en cualquier instante t > 0, será proporcional a $V\bar{C}$, donde V es el volumen del pozo y $\bar{C}$ la concentración promedia medida en unidades convenientes (mCi/cm^3 o cuentas por minuto -cpm-).

La variación de la actividad según el tiempo solamente tiene dos componentes:

a) Salida del trazador en el caudal q : $q\bar{C}$
b) Salida del trazador por convección y difusión JS, donde S es el área de transferencia de masa entre el pozo y el acuífero (πdh).

La ecuación diferencial para la velocidad de dilución es entonces

$$\frac{d(V\bar{C})}{dt} = -(q+Q)\bar{C} \tag{3}$$

en la que $Q = Sv_c$ es el caudal de convección y difusión (L^3T^{-1}).

Resolviendo la ecuación anterior para $\bar{C}$,

$$\bar{C} = \bar{C}_o \exp(-(q+Q)t/V) \tag{4}$$

que es una recta en escala semilogarítmica; su pendiente m es

$$m = -\frac{(q+Q)\log(e)}{V} \tag{5}$$

De las Ecs.(2) y (5) se llega directamente a

$$v_f = -\frac{\pi dm}{4\alpha\log(e)} - \frac{\pi v_c}{\alpha} \tag{6}$$

la velocidad de filtración puede entonces calcularse a partir de m, siempre y cuando se disponga de algún estimativo adecuado para v_c.[2]

3.2. Tratamiento de la información experimental

Para cada uno de los n perfiles experimentales medidos en t_o, t_1,.., t_j,.., t_{n-1}, se obtiene $C^*(t_j)$ definido por

$$C^*(t_j) = \sum_{i=1}^{p} C_i(t_j) = p\bar{C}(t_j) \tag{7}$$

donde p es el número de puntos con espaciamiento uniforme Δh (por ejemplo, de un metro) que se ha usado para construir el perfil de concentraciones sobre la altura h de la columna piezométrica del pozo [figura 1a)].

Con estos valores de $C^*(t_j)$ se construye la curva de dilución [figura 1b)] de la cual se calcula inmediatamente m como

$$m = \frac{\log(C^*(t_a)) - \log(C^*(t_b))}{t_a - t_b} \tag{8}$$

donde las unidades de m son T^{-1}.

4. CASO No. 2. EL POZO ATRAVIESA UNA ZONA PERMEABLE Y UNA IMPERMEABLE

4.1. Aplicación del modelo general

4.1.1. Ecuaciones de $\bar{C}$ y $\bar{C}_1$

Sea un pozo de observación completamente perforado que atraviesa un acuífero homogéneo y un estrato adyacente impermeable, tal como se indica en la figura 2a)[3]. El subscrito 1 se refiere a la zona impermeable, los distintos símbolos tienen el significado indicado en el caso No. 1, excepto q_1 que representa flujo vertical hacia la región permeable.

---

[2] Los criterios aproximados indicados por Halevy [1] son bastante útiles; así, si la difusión es el único efecto importante, expresiones similares a la de Matveev $v_c = 2\pi D/d$ pueden ser usadas para estimar el orden de magnitud de este término.

[3] Para efectos del modelo las condiciones son iguales si el pozo está ranurado solamente en una porción h de la altura total de la columna piezométrica $h + h_1$, aunque el estrato externo no sea realmente impermeable.

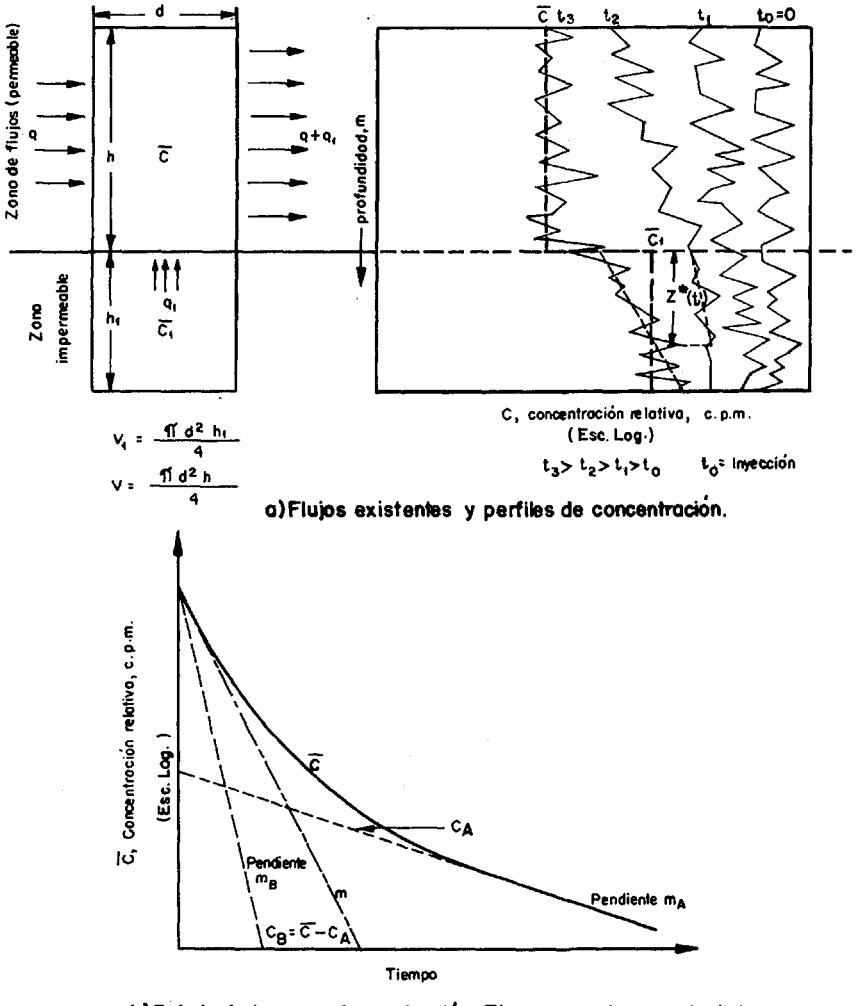

FIG.2. Pozo en acuífero homogéneo con zona impermeable.

El balance de trazador en la zona permeable puede escribirse como

$$\frac{d(\bar{C}V)}{dt} = Q_1(\bar{C}_1 - \bar{C}) + q_1\bar{C}_1 - Q(\bar{C} - \bar{C}_{ext}) - (q + q_1)\bar{C} \qquad (9)$$

en que $Q_1 = \pi d^2 v_{c1}/4$ es el flujo de convección y difusión proveniente de la zona impermeable, y $C_{ext} = 0$. La concentración promedia de trazador en la zona impermeable puede obtenerse de un balance local

$$\frac{d(\bar{C}_1 V_1)}{dt} = - q_1\bar{C}_1 - Q_1(\bar{C}_1 - \bar{C}) \qquad (10)$$

El sistema de ecuaciones (9) y (10) puede convertirse en una ecuación homogénea de segundo grado,

$$(D^2 + bD + c)\bar{C} = 0 \qquad (11)$$

donde $D \equiv d/dt$,

$$b = \frac{q + Q + q_1 + Q_1}{V} + \frac{q_1 + Q_1}{V_1} \qquad (12)$$

$$c = \frac{(q + Q + q_1)(q_1 + Q_1)}{VV_1} \qquad (13)$$

Resolviendo la ecuación (11) con la condición de contorno $\bar{C} = \bar{C}_1 = \bar{C}_o$ para $t = 0$ se obtiene

$$\bar{C} = A.\exp(r_1 t) + B.\exp(r_2 t) \qquad (14)$$

y

$$\bar{C}_1 = A_1\exp(r_1 t) + B_1\exp(r_2 t) \qquad (15)$$

donde r_1 y r_2 son las raíces de la ecuación característica $x^2 + bx + c = 0$,

$$r_1 = \frac{1}{2}(-b + \sqrt{b^2 - 4c}) \qquad (16)$$

$$r_2 = \frac{1}{2}(-b - \sqrt{b^2 - 4c}) \qquad (17)$$

Los coeficientes no se han utilizado hasta ahora en la interpretación de resultados en el modelo; también pueden expresarse en términos de r_1 y r_2:

$$A = - \bar{C}_o(r_2 + \frac{q + Q}{V})/(r_1 - r_2) \qquad (18)$$

$$B = -\bar{C}_o(r_1 + \frac{q + Q}{V})/(r_2 - r_1) \tag{19}$$

$$A_1 = -\bar{C}_o\ (r_2 + q_1/V_1)/(r_1 - r_2) \tag{20}$$

$$B_1 = -\bar{C}_o\ (r_1 + q_1/V_1)/(r_2 - r_1) \tag{21}$$

4.1.2. Pendientes de las curvas de dilución

La ecuación (14) en papel semilogarítmico tiene la forma de las curvas de dilución encontradas experimentalmente, tanto por nosotros como por otros autores [5,6], [figura 2b)]. La pendiente m para t = 0 está dada por la misma Ec.(5) del caso simple.

Como $|r_2|>|r_1|$ es fácil ver que cuando $t\to\infty$ la pendiente de la curva de dilución tiende a m_A,

$$m_A = r_1 \log(e) \tag{22}$$

y que $\bar{C}$ tiende a C_A, donde

$$C_A = A.\exp(r_1 t) \tag{23}$$

La pendiente de la curva de la ecuación (15) también se aproxima asintóticamente a m_A (escala semilogarítmica), cuando $t\to\infty$. Para t = 0 su pendiente m_1 esta controlada por el flujo vertical,

$$m_1 = -(q_1/V_1).\log(e) \tag{24}$$

4.2. Interpretación de los resultados experimentales

Para cada uno de los perfiles experimentalmente obtenidos en el tiempo t_j se calcula $C^*(t_j)$ definido de manera análoga a la Ec.(7), el número de puntos p que corresponden a la zona permeable se obtiene por inspección de los perfiles [figura 2a)][4].

La curva de dilución tiene forma similar a la figura 2b); por extrapolación de la parte final se obtiene C_A y de aquí C_B definida como

$$C_B = \bar{C} - C_A = B.\exp(r_2 t) \tag{25}$$

---

[4] Cuando se usa escala semilogarítmica (con la profundidad en la escala lineal), las concentraciones en la región de transición entre las zonas permeable e impermeable forman una línea recta cuando no hay flujos verticales, lo cual, recordando la nota 1, provee cierta justificación experimental para la suposición d) del modelo. Ver también 4.4.1.

su pendiente es m_B

$$m_B = r_2 \log(e) \tag{26}$$

La pendiente m puede calcularse de los valores de m_A y m_B obtenidos del "pelado" de la curva de dilución que se acaba de describir. En efecto, reemplazando las Ecs.(16) y (17) en (22) y (26) se tiene

$$m = \frac{1}{2}\{m_A + m_B + (q_1/V)\log(e) \pm \sqrt{[(q_1/V)\log(e) - m_A - m_B]^2 - 4(1+f)m_A m_B}\} \tag{27}$$

donde $f = V_1/V$. La solución con signo positivo se selecciona cuando $q_1/V_1 + Q_1(1+f)/V_1 > (q+Q)/V$ y la de signo negativo en caso contrario; la primera condición es la normalmente existente cuando hay flujo vertical apreciable, mientras que la segunda es la dominante en su ausencia.

Las pendientes m_A y m_B también pueden obtenerse de la curva de dilución para la zona impermeable, o de la curva de dilución para toda la columna del pozo, como es obvio por consideración de las Ecs.(14) y (15). Este hecho es muy interesante pues permite obtener dos estimativos independientes de la pendiente m, con una sola medición experimental.

4.3. Modelo simplificado

Una solución más simple del sistema de Ecs.(9) y (10) puede obtenerse si en un período corto después de la inyección se alcanza el estado $\bar{C}_1 \gg \bar{C}$. Bajo estas condiciones $\bar{C}_1$ está dado aproximadamente por

$$\bar{C}_1 = \bar{C}_o \exp(-d_1 t) \tag{28}$$

donde

$$d_1 = (q_1 + Q_1)/V_1 \tag{29}$$

La concentración en la zona permeable sigue siendo una expresión similar a la Ec.(14):

$$\bar{C} = \frac{d_1 f \bar{C}_o}{b' - d_1} \exp(-d_1 t) + \bar{C}_o\left(1 - \frac{d_1 f \bar{C}_o}{b' - d_1}\right) \exp(-b' t) \tag{30}$$

en que $b' = b - d_1$.

La interpretación de los datos experimentales procede de acuerdo con los lineamientos de 4.2. para llegar a

$$m = m_B - f m_A \quad \text{para } (q+Q)/V > d_1(1-f) \tag{31}$$

y

$$m = m_A - f m_B \quad \text{para } (q+Q)/V < d_1(1-f) \tag{31a}$$

Las Ecs.(31) y (31a) son, en efecto, un caso especial de la Ec.(27), a utilizar con un cierto error que depende del menor ε que cumpla

$$\frac{m_A\{fm_B + q_1\log(e)/V\}}{\{m_A - m_B+q_1\log(e)/V\}^2} < \varepsilon \qquad (32)$$

4.4. Distribución del trazador en la zona impermeable

El valor de $\bar{C}_1$ que se ha utilizado en la Ec.(9) representa en forma aproximada el comportamiento total de la zona impermeable, en la que existe una cierta distribución de concentración $C_1(t,z)$ para cada tiempo t, cuya forma depende del proceso dominante de transferencia de trazador hacia la región permeable del pozo. Experimentalmente se ha observado que los perfiles de concentración en la zona impermeable ocurren dentro de dos grupos, el primero corresponde a transferencia dominada por procesos similares a la difusión, el segundo a transferencia controlada por flujos verticales. A continuación se indican brevemente las distribuciones correspondientes a los casos límites de difusión pura y flujo vertical puro.

4.4.1. Distribución generada por transferencia por difusión

Aplicando la suposición d) de la sección 2 al trazador que abandona en el instante t un diferencial de volumen localizado a una distancia $\hat{z}$ de la interfase entre las zonas permeable e impermeable se tiene

$$J = - D \frac{\partial C_{1t}}{\partial z} = v_c(C_{1t} - \bar{C}(t)) \qquad (33)^5$$

donde $C_{1t}(z)$ es la concentración en z en el instante t y D es el coeficiente de difusión de trazador; se elige como origen del sistema de coordenadas Z el primer punto a partir de la interfase -hacia abajo en la figura 2a)- en que C_{1t} sea un máximo $C_1^*(t)$, la posición de la interfase en este sistema de coordenadas varía con el tiempo y se define como $z^*(t)$ tal que $z^*(0) = 0$ y $z^*(t\to\infty) = h_1$; también se cumple que $C_1^*(0) = \bar{C}_o$. Resolviendo la Ec.(33) con las condiciones anteriores para el instante t,

$$C_{1t}(\hat{z}) - \bar{C}(t) = \{C_1^*(t) - \bar{C}(t)\}.\exp\{-v_c(z^*(t)-\hat{z})/D\}=\Delta C_1 \qquad (34)$$

que predice para cualquier momento t una distribución lineal de log ΔC_1 vs. $\hat{z}$, lo que ha sido observado experimentalmente por nosotros en varios casos.

---

[5] Nótese que esta ecuación no es un balance de trazador, i.e. una ecuación de continuidad, sino una definición de v_c.

4.4.2. Distribución generada por un flujo vertical puro

Sea un flujo vertical q_1 que entra a la zona impermeable por el extremo opuesto a la interfase con la región permeable, el punto de entrada se elige como origen del sistema de coordenadas Z; la interfase estará entonces en $z = h_1$. Despreciando el efecto de difusión, la ecuación de continuidad puede escribirse como [9],

$$\frac{\partial C_1}{\partial t} = - v_1 \frac{\partial C_1}{\partial z} \tag{36}$$

donde $v_1 = 4q_1/(\pi d^2)$ es la velocidad vertical del agua que viaja hacia la zona permeable.

Para la condición de contorno $t = 0$, $C_1 = \bar{C}_o$ para todo z, es difícil obtener una expresión explícita de $C_1(t,z)$; sin embargo, utilizando técnicas numéricas es fácil obtener la variación temporal y espacial de C_1. Para ello se subdivide la zona impermeable en p_1 intervalos de altura Δh_1, y se numeran a partir del origen; el balance de trazador para el diferencial de volumen i con concentración $C_{1,i}$ lleva a

$$\frac{dC_{1,i}}{dt} = \frac{v_1(C_{1,i-1} - C_{1,i})}{\Delta h_1} \quad \text{para } 1 = 1,2,\ldots,p_1 \tag{37}$$

en que $C_{1,o} = 0$. Resolviendo con la condición límite indicada arriba,

$$C_{1,i} = \bar{C}_o \exp(-\tau) \sum_{j=0}^{i-1} \frac{\tau^j}{j!} \tag{38}$$

donde el tiempo adimensional τ está definido por

$$\tau = \frac{v_1 t}{\Delta h_1} \tag{39}$$

La Ec.(38) predice que la concentración de trazador disminuye más rápidamente en la zona alejada de la interfase, mientras que en ésta tiende a mantenerse en valores cercanos a $\bar{C}_o$; este comportamiento ha sido confirmado experimentalmente por nuestras observaciones.

Los resultados anteriores sugieren que el uso del término $q_1\bar{C}_1$ en la Ec.(9) equivale a una subvaloración de la contribución del flujo vertical, conduciendo, entonces, a estimativos de q por exceso; la substitución de dicho término por $q_1\bar{C}_o$ llevaría por el contrario, a obtener un valor de q por defecto. La expresión que se aplicaría para calcular m en este último caso sería

$$m = \frac{1}{2}\{m_A + m_B \pm \sqrt{(m_A + m_B)^2 - 4(1+f)m_A m_B}\} + q_1 \log(e)/V \tag{40}$$

en que la solución con signo negativo es válida cuando $(q + Q + q_1)/V > Q_1(1 + f)/V_1$ (ésta es la condición normalmente existente, sea en presencia de flujo vertical o no); la solución con signo positivo rige en caso contrario[6]. Resumiendo, las Ecs.(27) y (40) permiten obtener un rango de valores para v_f -Ec.(6)- cuando el flujo vertical es apreciable.

5. CASO No. 3. EL POZO ATRAVIESA UNA ZONA PERMEABLE LIMITADA POR DOS REGIONES IMPERMEABLES

5.1. Aplicación del modelo general

La ecuación de continuidad del trazador en la zona permeable [figura 3a)], puede escribirse en forma similar a la Ec. (9),

$$D(\bar{C}V) = \sum_{i=1}^{2} (Q_i(\bar{C}_i - \bar{C}) + q_i\bar{C}_i) - Q\bar{C} - (q + q_1 + q_2)\bar{C} \quad (41)$$

donde el subíndice 2 se refiere a esa zona impermeable. El balance local de la región 1 es la misma ecuación (10); el de la zona 2 es idéntico, usando el subscrito apropiado. Resolviendo este sistema de ecuaciones se llega a una ecuación homogénea de tercer grado,

$$(D^3 + pD^2 + sD + r)\bar{C} = 0 \quad (42)$$

donde

$$p = (q + Q)/V + d_1(1 + f_1) + d_2(1 + f_2) \quad (43)$$

$$s = (d_1+d_2)x(q+Q)/V + d_1d_2(1+f_1+f_2) + (q_1d_1 + q_2d_2)/V \quad (44)$$

$$r = d_1d_2(q+Q+q_1+q_2)/V \quad (45)$$

en que d_2 está dada por la Ec.(29) usando subíndice 2. Como antes,

$$f_i = V_i/V \quad \text{para } i = 1,2 \quad (46)$$

La ecuación característica $x^3 + px^2 + sx + r = 0$ de la Ec. (42), tiene cuando más dos raíces negativas, lo que implica un máximo de dos pendientes en la curva de dilución. De esta información no es posible despejar m.

---

[6] Como es de esperarse, las Ecs.(40) y (27) son idénticas en ausencia de flujo vertical.

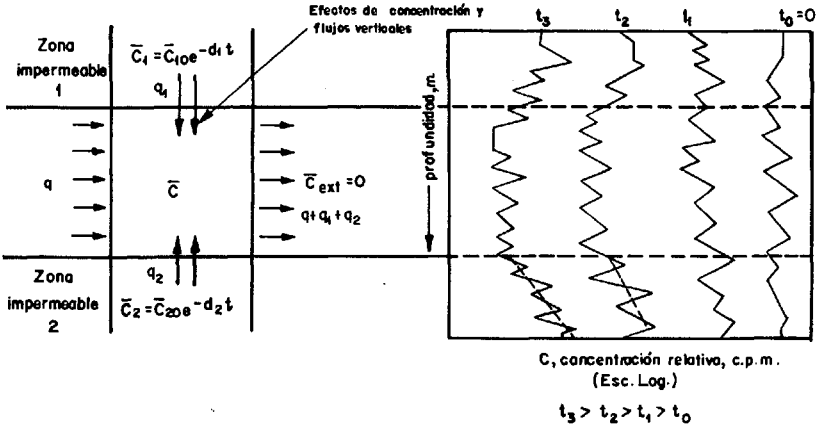

a) Flujos existentes y perfiles de concentración.

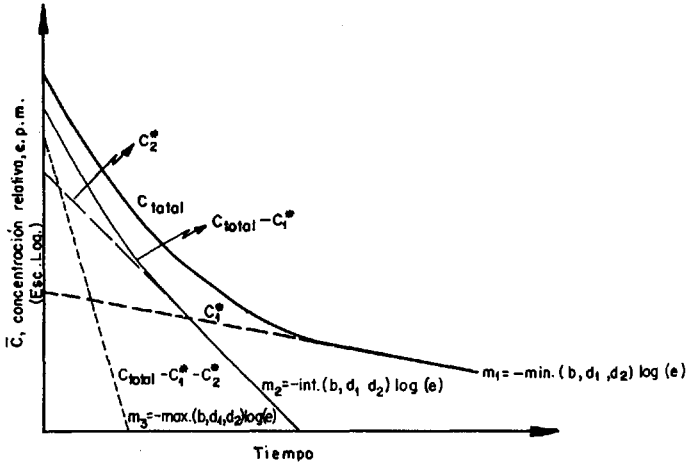

b) Pelado de la curva concentración-tiempo para la zona de flujos.

FIG. 3. Pozo en acuífero homogéneo con dos zonas impermeables.

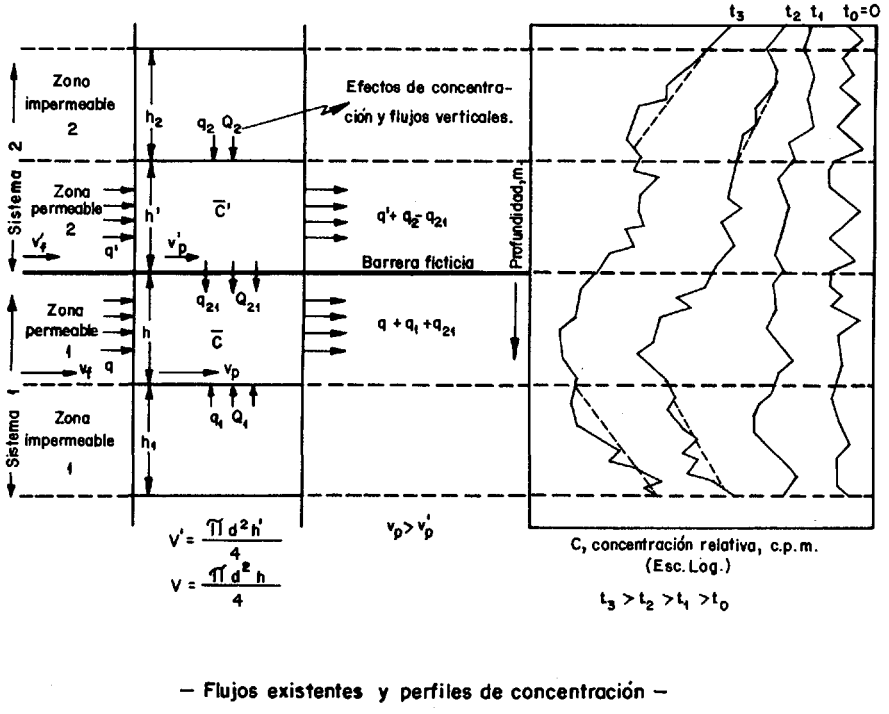

FIG.4. Pozo en acuífero con dos zonas de diferente permeabilidad limitadas por zonas impermeables.

5.2. Reducción al caso No. 2

5.2.1. División del pozo en dos sistemas

Cuando existe dentro de la zona permeable un plano a través del cual no hay flujos verticales, y si en ese punto el gradiente de concentración es cero[7], se tiene entonces una barrera impermeable que divide el pozo en dos sistemas aislados, similares a los mostrados en la figura 4. Cada uno de ellos puede tratarse como un pozo con una zona permeable adyacente a una impermeable (Caso No. 2), obteniendo así dos valores m_1 y m_2 de la pendiente en t = 0. Por tratarse de flujo homogéneo es fácil ver que

$$m_i = (q'_i + Q'_i)/V'_i = m = (q + Q)/V \quad i = 1,2 \qquad (47)$$

[7] Como se trata de flujo homogéneo esta condición debe cumplirse en principio. El subscrito i en la Ec.(47) se refiere a flujos horizontales en cada uno de los sistemas 1 y 2.

5.2.2. Fusión de las dos zonas impermeables

Si el procedimiento anterior no es factible por no haberse identificado un plano de flujos verticales inexistentes, se procede a construir la curva de dilución para toda la zona permeable. Si se observan tres pendientes se utiliza el modelo aproximado 5.3.; si únicamente aparecen dos se procede a definir una zona impermeable equivalente pues, como se dijo en 5.1., el método general no es aplicable.

Sea una zona impermeable con los parámetros

$$q_1^* = q_1 + q_2 \tag{48}$$

$$Q_1^* = Q_1 + Q_2 \tag{49}$$

$$V_1^* = V_1 + V_2 \tag{50}$$

que se define adyacente a la región permeable y como equivalente a las dos zonas impermeables 1 y 2, con lo que se genera de nuevo el caso No. 2. A las dos pendientes experimentales se aplica, entonces, el tratamiento indicado en 4.2.

El procedimiento acabado de describir es especialmente válido cuando las dos secciones impermeables son aproximadamente iguales en volumen y flujos. De hecho, en caso de que sean idénticas se puede probar que la Ec.(42) se reduce a la (11), con q_1, Q_1 y V_1 reemplazados por q_1^*, Q_1^* y V_1^*.

5.3. Modelo simplificado

Una solución rápida de la Ec.(41) se obtiene admitiendo que la concentración promedia en las dos zonas impermeables decrece en forma exponencial según expresiones análogas a la Ec. (28), en que se usa d_1 ó d_2 de acuerdo con la zona en consideración [figura 3a)].

Resolviendo para $\bar{C}$ se tiene,

$$\bar{C} = \bar{C}_o \left\{\frac{d_1 f_1}{b^*-d_1}.\exp(-d_1 t) + \frac{d_2 f_2}{b^*-d_2}.\exp(-d_2 t) + \left(1- \frac{d_1 f_1}{b^*-d_1} - \frac{d_2 f_2}{b^*-d_2}\right)\exp(-b^* t)\right\} \tag{51}$$

donde

$$b^* = (q + Q)/V + d_1 f_1 + d_2 f_2 \tag{52}$$

Las tres pendientes m_1, m_2 y m_3 [figura 3b)] de la curva de dilución (log $\bar{C}$ vs t) están relacionadas con la Ec.(51) por[8]

$$m_1 = - \min(b^*, d_1, d_2).\log(e) \tag{53}$$

$$m_2 = - \text{int}(b^*, d_1, d_2).\log(e) \tag{53a}$$

$$m_3 = - \max(b^*, d_1, d_2).\log(e) \tag{53b}$$

El valor de m se calcula de las Ecs.(5) y (52), aplicando las condiciones (53) para seleccionar cada uno de los parámetros. Por ejemplo, si $f_1 \geq 1$ y $f_2 \geq 1$, b^* es siempre el mayor, pudiendo usar entonces,

$$m = m_3 - m_2 f_1 - m_1 f_2 \quad \text{para} \quad q_1/V_1 > q_2/V_2 \tag{54}$$

y

$$m = m_3 - m_2 f_2 - m_1 f_1 \quad \text{para} \quad q_1/V_1 < q_2/V_2 \tag{54a}$$

pues Q_1 y Q_2 son del mismo orden.

6. CASO No. 4. EL POZO ATRAVIESA UN ACUIFERO CON DOS REGIONES DE DIFERENTE PERMEABILIDAD COMPRENDIDAS ENTRE ZONAS IMPERMEABLES

6.1. Aplicación del modelo general

Este caso se ilustra esquemáticamente en la figura 4; el uso del modelo general lleva a un sistema de cuatro ecuaciones diferenciales que pueden convertirse en ecuaciones homogéneas de cuarto grado. Las ecuaciones resultantes después de eliminar las concentraciones de las zonas impermeables son

$$(D^2 + b_e D + c_e)\,\bar{C} = (q_{21} + Q_{21})(D + d_1)\bar{C}'/V \tag{55}$$

$$(D^2 + b'_e D + c'_e)\bar{C}' = Q_{21}(D + d_2)\bar{C}/V' \tag{56}$$

donde b_e y b'_e están dadas por la Ec.(12) reemplazando q y Q por valores equivalentes:

$$q_e = q + q_{21} \quad \text{y} \quad Q_e = Q + Q_{21} \quad \text{para } b_e \tag{57}$$

y

$$q'_e = q' \quad \text{y} \quad Q'_e = Q' + Q_{21} \quad \text{para } b'_e \tag{58}$$

---

[8] min ≡ valor menor, int ≡ valor intermedio, max ≡ valor máximo. El caso descrito por este modelo hasta ahora sólo ha sido observado por nosotros en ausencia de flujos verticales.

igualmente c_e y c'_e están dados por la Ec.(13). El subscrito 21 se refiere a flujos del sistema de menor permeabilidad (el 2) al de mayor (el 1).

La ecuación de cuarto grado resultante de las Ecs.(55) y (56) puede tener hasta cuatro raíces reales distintas, pero es difícil obtener una expresión explícita para calcular m, por lo que a continuación se recurre a soluciones aproximadas.

6.2. Solución aproximada

Si el término de la derecha en la Ec.(56) se considera despreciable[9], se obtiene directamente

$$\bar{C}' = A'\exp(r'_1 t) + B'\exp(r'_2 t) \tag{59}$$

que es la misma Ec.(14) con valores apropiados de cada uno de los términos -Ecs.(16) a (19), usando los caudales equivalentes de la Ec.(58)-. La pendiente m'_e que se obtiene de la curva de dilución usando el método de 4.2., Ec.(27) es

$$m'_e = -\ (q'_e + Q'_e)\log(e)/V' \tag{60}$$

de las Ecs.(2) y (60) se despeja v'_f.

Para la zona permeable del sistema 1 se reemplaza $\bar{C}'$ de la Ec.(59) en (55); la solución correspondiente a $\bar{C}$ es

$$\bar{C} = A.\exp(r_1 t) + B.\exp(r_2 t) + A''\exp(r'_1 t) + B''\exp(r'_2 t) \tag{61}$$

donde los primeros dos términos de la derecha corresponden a la solución de la parte homogénea (Ec.(14) y siguientes) y

$$A'' = \frac{A'(q_{21} + Q_{21})(d_1 + r'_1)}{V(r'^2_1 + b_e r'_1 + c_e)} \tag{61}$$

$$B'' = \frac{B'(q_{21} + Q_{21})(d_1 + r'_2)}{V(r'^2_2 + b_e r'_2 + c_e)} \tag{62}$$

Cuando las regiones permeables de los sistemas 1 y 2 tienen características aproximadamente iguales, se cumple que $q_{21} \simeq 0$ y $Q_{21} \simeq 0$, la curva de dilución solamente tiene dos pendientes y los dos sistemas se comportan como pozos independientes (este es el mismo caso 5.2.1.); si por el contrario, una de ellas es mucho más permeable se tienen las condiciones apropiadas para utilizar la simplificación aquí indicada. En este caso la cur

[9] Este caso ocurre si: i) $Q_{21} \simeq 0$, o sea cuando las dos regiones tienen permeabilidades casi iguales, o ii) $\bar{C} << \bar{C}'$ lo que ocurre cuando el sistema 1 es mucho más permeable que el 2.

va de dilución tiene cuatro pendientes, dos de ellas idénticas a las del sistema 2; con las restantes se calcula m_e usando la Ec.(27). El valor de m es, entonces,

$$m = m_e + (q_{21} + Q_{21})\log(e)/V \qquad (63)$$

el cual se lleva a la Ec.(6) para obtener v_f.

7. CONCLUSION

Se ha propuesto en esta memoria un modelo simplificado que permite obtener información semicuantitativa sobre los flujos horizontales a través de un pozo, cuando se usa el método de dilución por marcación de toda la columna piezométrica con un trazador radiactivo. El modelo ha sido utilizado para obtener flujos en el rango de cm/d a m/d, a veces en presencia de flujos verticales considerables, aunque en estos últimos casos no existen mediciones experimentales alternativas directas para confirmar los resultados.

Se indicaron los varios casos más frecuentemente encontrados en Colombia, y se mostró que casi siempre pueden reducirse a un pozo con una zona permeable adyacente a una impermeable.

AGRADECIMIENTOS

Los métodos aquí propuestos empezaron a desarrollarse durante la estadía en el IAN del Dr. Antonio Plata B. como experto del OIEA en 1972; se agradecen las provechosas discusiones que se sostuvieron en aquella ocasión.

REFERENCIAS

[1] HALEVY, E., MOSER, H., ZELLHOFER, O., ZUBER, A., "Borehole dilution techniques: a critical review", Isotopes in Hydrology (Proceedings of a Symposium, Vienna, 1966), IAEA, Vienna (1967) 531-64.

[2] DROST, W., MOSER, H., NEUMAIER, F., RAUERT, W., "Utilisation des traceurs radioactifs artificiels", Capítulo 3, Methodes Isotopiques en Hydrogeologie, EUROISOTOP, Bruxelles (1973) 17-39.

[3] MOSER, H., Comunicación privada (1973) y Discusión de la memoria [5] 710.

[4] KRISHNAMURTHY, K., RAO, S. M., "Tracer logging", Sección II.D., Nuclear Well Logging in Hydrology, Technical Reports Series No. 126, IAEA, Vienna (1971) 44.

[5] BAONZA, E., PLATA, A., PILES, E., "Aplicación de la técnica del pozo único mediante el marcado de toda la columna piezométrica", Isotope Hydrology 1970 (Proceedings of Symposium, Vienna, 1970), IAEA, Vienna (1970) 695-711.

[6] PLATA, A., "Hidrología subterránea, zona saturada", Capítulo 7, Isótopos en Hidrología, Editorial Alhambra, S.A., Madrid (1972) 276-80.

[7] LENDA, A., ZUBER, A., "Tracer dispersion in groundwater experiments", Isotope Hydrology 1970 (Proceedings of a Symposium, Vienna, 1970), IAEA, Vienna (1970) 619-41.

[8] BAESTLE, L.H., SOUFFRIAU, J., "Fundamentals of the dispersion of radionuclides in sandy aquifers", Isotopes in Hydrology (Proceedings of a Symposium, Vienna, 1966), IAEA, Vienna (1967) 617-28.

[9] BIRD, R.B., STEWART, W.E., LIGHTFOOT, E.N., "The equations of change for multicomponent systems", Capítulo 18, Transport Phenomena, John Wiley & Sons, Inc., New York (1960) 559.

DISCUSSION

H. MOSER: In the initial stage of our investigations of the borehole dilution method we tried to use the method described by you. However, because various physical processes (such as vertical convection due to density or pressure differences, horizontal displacement of the tracer due to the groundwater flow, and molecular diffusion) were occurring during the decrease in tracer concentration (with different concentration decrease functions) in the borehole, we were unable to derive appropriate correction formulas. As a result, we now think that, for success in using dilution methods, it is necessary to stir the dilution volume throughout the measurement period so as to maintain a homogeneous distribution of the tracer and to seal off the dilution volume so as to prevent the intrusion of vertical streams.

H.A. MUNERA: Thank you for your comment.

It is precisely because of the difficulties inherent in a rigorous treatment of the processes mentioned by you that we resorted to an approximate, linear correction, using measured values. We do not claim that our correction method takes detailed account of the processes in question, but it is a heuristic method of obtaining semi-quantitative horizontal velocity values which may be of significance in engineering (civil, hydraulic or sanitary).

Our ideas have been confirmed in principle by the internal consistency of the results and by the fact that the velocities are of the order expected for karstic and alluvial soils.

A. PLATA BEDMAR: We recently used the method described in your paper to measure flows in aquifers which had already been studied intensively with conventional methods and for which isotransmissibility curves had been obtained. With a margin of error not exceeding 40-50% our results agreed with those obtained with conventional methods.

Using the method described by you in conjunction with several thousand piezometers, we have found over a period of eight years that:

(a) The exponential attenuation law applies satisfactorily in piezometers with a diameter greater than about 10 cm when the detector is moved along the piezometer axis.

(b) With piezometers of smaller diameter we obtain non-exponential curves like those in your paper, for we are detecting tracer material which is outside the piezometer.

(c) One should therefore use as tracer a gamma-emitter of low energy (^{131}I is better than ^{82}Br, but a gamma-emitter of even lower energy would be still better).

(d) We have no difficulty in maintaining a homogeneous distribution of the tracer in the water column, for the detector creates sufficient turbulence as it is lowered and raised within the piezometer.

(e) The influence of tracer diffusion depends on a number of factors, but mainly on flow velocity and permeable layer thickness. (If the radioactive tracer is used without a carrier, the coefficients of molecular and osmotic diffusion are extraordinarily low, and diffusion then occurs only in the case of very localized flows or very thin permeable layers; if the permeable layer is more than 2-3 m thick and the flow velocity is greater than about 4 cm daily, diffusion occurs only near the surface of the permeable layer – not near its centre.)

(f) In the presence of vertical flows it is very difficult to obtain quantitative or semi-quantitative information about the horizontal flow velocity, and one has to use the method described by Mr. Drost. [1]

H.A. MUNERA: Thank you for your comments on the work done by you in Spain, which served as a basis for our work.

I should like to take this opportunity to clarify certain points regarding our measurements. First, the boreholes used by us had a diameter of 15 cm or more, and were generally drilled in heterogeneous aquifers with apparent mean velocities of some metres daily or more, so that the influence of tracer material outside the borehole was reduced (we were unable to detect ^{82}Br outside the borehole and therefore assumed the tracer concentration – C – to be zero outside the borehole). Second, the diffusion-like behaviour of the tracer was due not only to molecular diffusion (which was relatively high in our case as we used a considerable amount of carrier) but also to the other processes mentioned by Mr. Moser. Third, the effect of vertical flows has to be eliminated, by point dilution, but in some cases of low vertical flow velocity the proposed model yields semi-quantitative information about the horizontal flows.

---

[1] DROST, W., NEUMAIER, F., "Application of single borehole methods in groundwater research", these Proceedings II, IAEA-SM-182/12.

THEORETICAL POSSIBILITIES OF THE TWO-WELL PULSE METHOD

A. ZUBER
Institute of Nuclear Physics,
Cracow,
Poland

Abstract

THEORETICAL POSSIBILITIES OF THE TWO-WELL PULSE METHOD.

The problems of the determination of aquifer parameters by the two-well pulse method are described. This method involves an instantaneous injection of tracer in one well and the observation of its transit time to a pumping well. A recent solution of the dispersion equation is used for the theoretical description of the concentration curve measured in the pumping well. Characteristics of this solution are discussed as opposed to those of the commonly known solution. It is pointed out that only this new solution has its first moment, i.e. the mean arithmetic time, also called the centre of gravity, equal to the mean transit time of water. The conditions under which the first moment for a layered system represents the mean transit time of water are also discussed. This time can be found from experimental data either by calculating the first moment or by matching a theoretical curve. Other methods often applied such as time of the maximum concentration, and time of the half-width, can be accepted in approximations applicable only for slightly dispersed concentration curves. Interpretational methods for determining the parameters of particular layers in layered systems are reviewed in detail. These methods are based both on individual transit times and on relative recoveries. Under favourable conditions it is possible to find the mean effective porosity, hydraulic conductivities and thicknesses of all the layers, and the mean thickness or diameter of fissures in fissured rocks. However, under unfavourable conditions it may be difficult to learn anything from a tracer experiment.

1. INTRODUCTION

The two-well pulse method was first used for determination of effective porosity in the Soviet Union [1], and later with the aid of radioisotopes by Halevy and Nir [2]. Mercado and Halevy [3] have shown the possibility of finding the permeability coefficients of a layered system. Laguna [4] used the method for finding partial pumping rates, which in turn served for improved interpretation by the Jacob method.

The principle of the method consists in an instantaneous injection of a tracer in a well situated within the symmetry of the drawdown cone caused by pumping in another well. The tracer concentration is measured in the pumped-out water supplying information on the transit time of the tracer between the wells. For a homogeneous aquifer the following relation holds:

$$Qt_0 = \pi x^2 hn - V_d \tag{1}$$

where Q is the pumping rate, x is the distance between the wells, t_0 is the mean transit time of plug flow between the wells, h is the thickness of the water-bearing formation, n is the effective porosity defined as that fraction of the total volume in which the water movement takes place, and V_d is the volume of the involved part of the depression cone in a phreatic aquifer, or in a confined aquifer if it reaches the formation. Very often V_d can be

neglected as being much smaller than the second term in Eq. (1). The definition of the effective porosity quoted above means that it gives values lying between those of the total porosity and the specific yield for phreatic aquifers, the coarser the aquifer material, the closer the values of these three parameters.

The following sections deal with the dispersion of tracer, and problems related to the interpretation of experiments in layered systems.

2. DISPERSION OF TRACER

The differential equation of dispersion is the most commonly applied mathematical model for the description of bulk effects of dissolved matter in flow through porous media. In unidimensional flow of conservative and non-adsorptive matter, called the tracer, this equation reads

$$\frac{\partial c}{\partial t} = D \frac{\partial^2 c}{\partial x^2} - v \frac{\partial c}{\partial x} \tag{2}$$

where c is the concentration of the tracer, D is the dispersion coefficient, v is the mean interstitial velocity, and x and t are the space and time variables respectively. There are a number of solutions of Eq. (2) for different initial and boundary conditions, e.g. Himmelblau [5]. Sometimes it may be difficult to decide which initial and boundary conditions are best for a given experimental situation. An example is a comparison of several solutions of Eq. (2) with another model published by Coats and Smith [6]. In the quoted paper different values of the effective porosity, related to mean transit time, had to be assumed to obtain a good matching of different theoretical solutions with the experimental concentration curves measured at the output of the experimental column. In extreme cases the differences in the effective porosities approaching 10% were observed. This means that the mean transit time found from a tracer experiment, performed even with an ideal tracer, may depend on the chosen theoretical approach. The choice of a proper model is neither free from ambiguities nor absolutely physically clear.

This is especially true in field experiments where many parameters, not necessarily involved in the model, are neither known nor controlled, and the initial and boundary conditions difficult to satisfy.

Lenda and Zuber [7] derived a new solution of Eq. (2) for the following initial and boundary conditions discussed in detail by Hubert and co-workers [8]:

$$c(0, t) = \frac{m}{nvS} \delta(t) \tag{3a}$$

$$c(x, 0) = 0 \tag{3b}$$

$$c(\infty, t) = 0 \tag{3c}$$

where m is the mass or activity injected, S is the cross-section area of flow, $\delta(t)$ is the Dirac delta-function, and n appears here if the flow takes place in a

porous medium and if c is defined as the concentration in water, i.e. mass or activity per unit volume of water. In this report this definition of c will be used. This new solution given in a normalized form reads

$$\frac{ncSx}{m} = \frac{1}{\sqrt{4\pi \frac{D}{vx}\left(\frac{t}{t_0}\right)^3}} \exp\left[-\frac{\left(1-\frac{t}{t_0}\right)^2}{4\frac{D}{vx}\frac{t}{t_0}}\right] \tag{4}$$

where t_0 is the mean transit time of water defined as x/v. It appears that almost an identical solution is quoted and used by Niemi [9], and also given in unnormalized form by Bansal [10], but in the latter case with an erroneous physical interpretation. If Eq. (4) is denoted by E, and by F the well known solution for a continuous tracer injection with the concentration of c_0 at $x = 0$ [11]

$$\frac{c}{c_0} = F = 1/2 \operatorname{erfc}\left(\frac{1-\frac{t}{t_0}}{\sqrt{4\frac{D}{vx}\frac{t}{t_0}}}\right) + 1/2 \exp\left(\frac{vx}{D}\right)\operatorname{erfc}\left(\frac{1+\frac{t}{t_0}}{\sqrt{4\frac{D}{vx}\frac{t}{t_0}}}\right) \tag{5}$$

then the following relations hold [7]

$$\frac{\partial F}{\partial\left(\frac{t}{t_0}\right)} = E \quad \text{and} \quad \int_0^{\frac{t}{t_0}} E \, d\left(\frac{t'}{t_0}\right) = F \tag{6}$$

It has also been shown [7] that the first moment of Eq. (4) calculated in dimensionless time is equal to unity, which implies that the mean real transit time of tracer is equal to the mean transit time of water, i.e.

$$\bar{t} \overset{\text{def}}{=} \frac{\int_0^\infty tc(t)dt}{\int_0^\infty c(t)dt} = t_0 \tag{7}$$

Relations (6) and (7) are not obeyed if the following well-known solution is applied:

$$\frac{ncSx}{m} = \frac{1}{\sqrt{4\pi \frac{D}{vx}\frac{t}{t_0}}} \exp\left[-\frac{\left(1-\frac{t}{t_0}\right)^2}{4\frac{D}{vx}\frac{t}{t_0}}\right] \tag{8}$$

The first moment of Eq. (8) is [5]

$$\frac{\bar{t}}{t_0} = 1 + 2\frac{D}{vx} \tag{9}$$

Unfortunately Eq. (4) also has its drawbacks as it is neither valid for $v = 0$, nor normalized in space, i.e. its integral over the space co-ordinate does not yield the injected quantity of tracer. However, Eq. (4) gives a better fitting to experimental data than Eq. (8) when the tracer distribution in time is measured, and its use is more logical because it satisfies Eq. (6) and Eq. (7).

It is well established that in radial flow the dispersion phenomena may often be treated unidimensionally. In the method discussed in this report it is especially true as all the water lines converge in the pumping well, so that the effects of the lateral dispersion disappear in the pumped water. Lenda and Zuber [7] have shown that Eq. (4) describes quite satisfactorily the concentration observed in the pumping well, if the volume given by Eq. (1) is inserted into it instead of Sx. Further discussion related to the problems of obtaining the concentration curve parameters is given in the following section.

The dispersion coefficient, D, appearing in the dispersion equation may be thought of as being defined by that equation. The dependence of this coefficient on the aquifer parameters is discussed in several excellent papers [12-15]. Lenda and Zuber [7], and in more detail Zuber [16], gave a compilation of theoretical, laboratory and some field data. However, it has to be kept in mind that the value of the dispersion coefficient obtained from a given experiment depends, sometimes to a high degree, on the chosen solution or more generally on the mathematical model [6], and/or on the scale of the experiment, as will be discussed below. In spite of these limitations the importance of D or D/v as one of the aquifer parameters becomes better understood with the development of both environmental and artificial tracer methods, and a growing danger to groundwater resources from pollutants and saline water intrusions. For unconsolidated media the following relation is reported [12, 13]

$$\frac{D}{D_m} = \frac{1}{\tau} + \delta \left(\frac{vd}{D_m}\right)^n \tag{10}$$

where D_m is the coefficient of molecular diffusion, d is the mean grain size diameter, τ is the tortuosity factor defined as the tortuous length along which fluid or electric current must flow through the medium divided by the length of the medium, n is here a constant slightly larger than unity, and δ is here a constant which depends on grain shape, packing, and on that if longitudinal or lateral dispersion is considered [12]. The tortuosity factor is easily measurable in the laboratory as it is equal to the product of the formation resistivity factor and porosity. Its values range from 1.3 to 1.5 for unconsolidated media, and from 1.5 to 2.5 for consolidated media [13]. If $v \neq 0$, Eq. (10) can roughly be approximated by

$$\frac{D}{v} \cong \frac{D_m}{v\tau} + \delta d \tag{11}$$

which shows that for large velocities the value of D/v is constant and may be considered as a parameter of the porous medium. Usually it is called the hydrodynamic dispersion coefficient [17] or the dispersion constant [18]. Equation (10) and in approximation Eq. (11) are valid for laboratory experiments and probably for homogeneous formations of the deep sea. Field

experiments, compiled by Lenda and Zuber [7], show that for granular media of fluvial or fluvio-glacial origin the dispersion constant may range from a few centimetres to a few metres, whereas for fissured rocks the quoted values range from 2 to 100 metres or even more [7, 16, 18-20]. It is evident that under field conditions differences in hydraulic conductivity of particular zones are responsible for macroscopic dispersion effects.

In experiments on a small scale, involving a particular zone of a given permeability, values of the dispersion constant consistent with Eq. (11) may be expected under favourable conditions. In intermediate scale experiments layering may be observed [3, 20, 21]. Interpretation of the dispersion may be then performed for each layer separately, or the joint effect may be estimated, as shown in the following section. Finally, in experiments on a large scale, for instance, much larger than the extent of particular zones, the dispersion effects may be described again by one term, as postulated by Skibitzke [22]. For example, in recent studies of the movement of pollutants in a fluvio-glacial formation, a value of 8 m was obtained as the dispersion constant from measurements performed in piezometers at distances from a few tens of metres to 600 m [23]. The hydraulic conductivity was about 12 m/d, the mean grain diameter d = 0.02 cm, the thickness about 10 m, and v about 110 m/year = 3.5×10^{-4} cm/s. It is evident that the dispersion constant measured in that case exceeds by several orders of magnitude the value estimated from Eq. (11) or more exactly from Eq. (10). For instance, putting $\delta = 8.8$, $n = 1.17$, $\tau = 1.5$ (line 1 in Fig. 7 in Ref. [7]), and $D_m = 1.2 \times 10^{-5}$ cm^2/s, the following result is obtained:

$$\frac{D}{v} = \frac{D}{D_m} \times \frac{D_m}{v} = 5 \times \frac{1.2 \times 10^{-5}}{3.5 \times 10^{-4}} = 0.17 \text{ cm}$$

which is 4700 times less than the measured field value of 8 m.

The theoretical works of Saffman [24] and De Jong [25], as well as Eq. (11), show that the dispersion constant is of the order of the length of an elementary capillary, obviously related to d in unconsolidated media. It seems that for heterogeneous media, instead of Eq. (10) the following relation may be postulated:

$$\frac{D}{D_m} = \frac{1}{\tau} + \delta\left(\frac{vd}{D_m}\right)^n + \kappa\frac{v}{D_m}, \qquad (12)$$

where κ is a constant, which for a given medium is related to the dimensions and the permeability distribution of particular zones. In other words, the dispersion constant can be thought of as a measure of the aquifer heterogeneity, if the first two terms on the right hand side of Eq. (12) are negligible.

3. DETERMINATION OF THE MEAN TRANSIT TIME AND THE DISPERSION CONSTANT

It was shown in the previous section that for a homogeneous medium the mean transit time can be found either by fitting the function E to the experimental data or by calculation of the first moment. The latter requires that the measurement be completed, or that the tail be extrapolated with a sufficient degree of accuracy.

However, extrapolation is always a dubious procedure and may lead to serious errors. The fitting procedure described in several papers [7, 16, 20] consists in matching at a guess and in assuming that the areas under the experimental and theoretical curves should be equal. The working formula for the theoretical concentration curve is then [16]

$$c(t)_{th} = \frac{E\left(\frac{t}{t_0}, \frac{D}{vx}\right) \int_0^{t_e} c(t)\,dt}{t_0 F\left(\frac{t_e}{t_0}, \frac{D}{vx}\right)} \tag{13}$$

where t_e is the end time of the experimental curve. Fitting is done by choosing t_0 and D/vx for successive approximations. A slide rule and graphs of the E and F functions given in [7] or [16] are sufficient. An improved procedure was developed by Kreft and Lenda [26] in which fitting is based on the chi-square test and executed by a computer. A nice example of the manual interpretation was given in Ref. [7] and its computer re-interpretation in [20]. One of the worst examples encountered so far is given in Fig. 1. The measurement was not continued until the background count-rate. Matching by Eq. (13) gave a poor agreement in the initial part of the curve, and the mean transit of 45 h. The next step was to extrapolate the curve by an exponential function, which could be done quite well. The mean time calculated by Eq. (7) was $\bar{t}$ = 39.6 h. The third method of interpretation consisted of separating the experimental curve into partial curves, and in this particular case three curves were obtained.

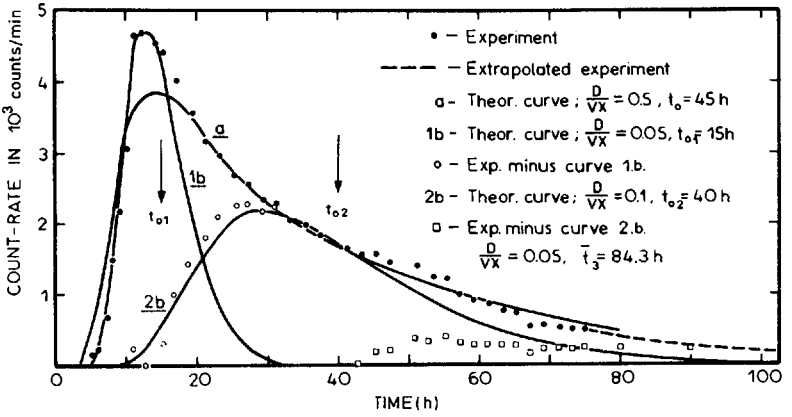

FIG. 1. Experimental data interpreted by a single theoretical curve or by three sub-curves.

The mean time was then calculated as

$$t_0 = \bar{t} = R_1 t_{01} + R_2 t_{02} + R_3 \bar{t}_3 = 38.3 \text{ h} \tag{14}$$

where R_i is the partial relative recovery defined by

$$\int_0^\infty c_i(t)dt = R_i \int_0^\infty c(t)dt \tag{15}$$

The increased number of parameters implies the presence of three layers or zones, which can be neither rejected nor supported by the geological evidence. Applying the general principles for choosing the best model [5] it may be safer to adhere to the model of the lowest number of parameters, i.e. the single layer model. This example is also discussed in Ref. [20] where the re-interpretation by a computer is quoted. Analysis of the theoretical curves, as well as this example, show that in cases of very high dispersion, i.e. low Peclet numbers, $P_e = vx/D$, the interpretation has a limited accuracy as the tail is usually not completely measured, or even is not measurable at all.

In many papers other intuitive methods of the interpretation were applied, e.g. time of the maximum concentration, time of the half width, and time of the half relative recovery. These methods are not physically justified, as can be seen by inspection of the E function. However, it is also evident that for slightly dispersed, nearly symmetrical, curves, i.e. for large P_e, these methods can be applied as an approximation.

It may be of interest to know the total value of the dispersion constant for an experiment that yields several peaks on the concentration curve. Using the definition of variance as the departure formula

$$\sigma^2 = \frac{\int_0^\infty c(t)\ (t - t_0)^2\ dt}{\int_0^\infty c(t)dt} \tag{16}$$

and applying the concepts of the partial relative recovery, R_i, and the partial mean transit time, t_{0i}, one can easily obtain

$$\sigma^2 = \sum R_i \left[\sigma_i^2 + (t_0 - t_{0i})^2 \right] \tag{17}$$

Variance of the E function given by Eq. (4) is [16]

$$\sigma^2 = \frac{2D}{vx}\ t_0^2 \tag{18}$$

which applied to Eq. (17) gives

$$\frac{D}{vx} = \sum R_i \left[\left(\frac{D}{vx}\right)_i \left(\frac{t_{0i}}{t_0}\right)^2 + \tfrac{1}{2}\left(1 - \frac{t_{0i}}{t_0}\right)^2 \right] \tag{19}$$

There is still one crucial question, namely, if the definition (7), or its equivalent form (14), can be used for irregular curves which result from the presence of several layers, and under what conditions $t_0 = \bar{t}$ in such a case.

In a layered system the mean transit time of water is given as

$$t_0 = \frac{\sum Q_i\, t_i}{\sum Q_i} = \frac{\sum h_i\, k_i\, t_i}{\sum h_i\, k_i} \tag{20}$$

Eq. (7) is equivalent to

$$\bar{t} = \frac{\sum m_i\, t_i}{m} \tag{21}$$

If the injection is performed under some pressure then

$$\frac{\sum m_i\, t_i}{m} = \frac{t^{in}\, c^{in} \sum q_i\, t_i}{t^{in}\, c^{in} \sum q_i} = \frac{\sum h_i\, k_i\, t_i}{\sum h_i\, k_i} = \frac{\sum h_i\, k_i\, t_i}{h\bar{k}} \tag{22}$$

where t^{in}, c^{in} and q are the time, concentration and volumetric flow rate of the injection respectively. Equations (20), (21) and (22) show that for an ideal, non-adsorptive tracer, $\bar{t} = t_0$. It still holds if the relative losses of tracer are the same in each layer. Then Eqs (7), (14) and (19) are physically justified.

As was mentioned above, the tailing effect makes the interpretation difficult. The following sources of this effect can be listed:

(a) High dispersion effects discussed earlier.
(b) Heterogeneous medium with more or less continuous stratification of permeability. An example is given in Ref. [20].
(c) Double porosity as shown by Nielsen and Biggar [27].
(d) Presence of pores with stagnant water or coat films to which the tracer diffuses during the rising part of its passage and afterwards diffuses back to the mobile water after the passage of the maximum concentration. Coats and Smith [6] developed this model though their formulation of the departure equations is not free of mistakes, as will be shown elsewhere. For field experiments in highly permeable formations this effect can be neglected.
(e) Reversible adsorption of tracer. This can be neglected for radioisotope compounds and other substances known as good tracers for groundwater experiments.
(f) Adsorption of a radioisotope tracer near the detection equipment. This is easy to avoid and should be controlled, and if necessary allowed for, by making use of a control source [3].
(g) Trapping effects. A part of the injected volume can be trapped in the dead zones of the injection well, or perched in its vicinity. These effects probably contribute strongly to the low recoveries observed in the pulse-injection experiments.

The first three effects listed above produce necessary information though they may be indistinguishable. The next four are unwanted, but only

the last three of these can be controlled to some extent at least. On the other hand, irreversible losses of tracer are still not well understood. All the theoretical models suggest that in cases of low recovery the shape of the concentration curve should be affected. Field experiments [7, 16, 20] seem to show that the shape is not influenced, and the only correction is as if a smaller quantity of tracer were injected. Thus, the concept of the recovery defined as the ratio of the measured to injected quantity of tracer comes into the picture in comparing theoretical curves with the experiment [7, 16]. An interesting laboratory experiment which seems to support this hypothesis is described by Corey and Nielsen [28]. Needless to say when a radioisotope tracer is used, the experimental concentrations have to be corrected for the radioactive decay before comparing them with the theoretical ones.

4. MEAN POROSITY

In a homogeneous layer it is irrelevant how and at what depth the injection is performed. The effective porosity is then found from Eq. (1).

An identical expression is obtainable for a layered system of p layers:

$$\frac{Q \sum_{i}^{p} Q_i t_i}{Q} = Q\bar{t} = \pi x^2 \frac{\sum_{i}^{p} n_i h_i}{h} h = \pi x^2 h \bar{n} \tag{23}$$

where $\bar{t} = t_0$ is determined in one of the ways described in the previous section. The product $h\bar{n}$ is obtained when the thickness is unknown.

5. INDIVIDUAL PUMPING RATES IN A LAYERED SYSTEM

Laguna [4] used the method with the aid of a chemical tracer for determining the pumping rates from individual layers in a semi-confined aquifer. In that case each n_i has to be assumed as a known quantity

$$Q_i t_i = \pi x_i^2 h_i n_i \tag{24}$$

Pumping rates found in this way served for a considerable improved interpretation of pumping tests by the Theis-Jacob method for each layer.

6. SYSTEM OF p LAYERS WITH KNOWN h_i, UNKNOWN k_i AND $n_i = \bar{n}$

This case was described by Mercado and Halevy [3] for a two-layered system and extended in an approximation for a four-layered one. In the paper quoted the principles of proper weighting given by Eqs (7) and (14) were not applied, though incidentally this did not lead to serious errors. Here a more general approach is proposed. However, it has to be stressed that starting from here all the interpretational possibilities require that the hydraulic gradient be the same in each layer. In other words, the particular layers cannot be separated by impermeable or semi-permeable interbeddings.

The following set of p + 1 equations is easily obtainable

$$Q\ t_i = \pi x_i^2\ n\ \frac{h\,\bar{k}}{k_i} \tag{25}$$

$$\sum h_i\ k_i = h\,\bar{k} \tag{26}$$

where $\bar{k}$ is the mean hydraulic conductivity known from the pumping test. The solution of Eqs (25) and (26) reads [29]

$$k_i = \frac{\bar{k}\ h\ x_i^2}{t_i \sum_{j=i}^{p} h_j \frac{x_j^2}{t_j}} \tag{27}$$

and

$$\bar{n} = \frac{Q}{\pi \sum_{j=i}^{p} \frac{h_j\ x_j^2}{t_j}} \tag{28}$$

In this case the injection can be performed in each layer separately and even at different distances x_i. If each $\bar{t}_i$ is interpreted separately, the condition of the injection proportional to the $h_i k_i$ product discussed earlier does not need to be satisfied. However, if it is satisfied, and the injection is performed in a single well, then

$$k_i = \bar{k}\ \frac{\bar{t}}{t_i} \tag{29}$$

and $\bar{n}$ is to be found from Eq. (23).

7. SYSTEM OF p LAYERS WITH UNKNOWN h_i, k_i AND $n_i = \bar{n}$

In this case there are 2p + 1 unknowns, so the same number of independent equations is needed. Equations (23) and (29) serve for finding $\bar{n}$ and k_i respectively, whereas h_i is found from the ratio of recoveries

$$\frac{R_i}{R} = \frac{h_i\ k_i}{h\,\bar{k}} \tag{30}$$

where $R = \sum R_i$ and is equal to one if the relative recoveries, defined above, are used. An interpretational example is given in Ref. [20]. Equation (30) can also serve for checking k_i values found from Eq. (29) when h_i is known.

8. SYSTEM OF p LAYERS WITH KNOWN h_i, BUT UNKNOWN k_i AND n_i

Applying Eqs (25) and (30), after simple rearrangements, one obtains

$$k_i = \frac{h\,\bar{k}\,R_i}{h_i\,R} \tag{31}$$

$$n_i = \frac{Q\,t_i\,R_i}{\pi x^2\,h_i\,R} \tag{32}$$

9. COMPARISON WITH OTHER TRACER METHODS

Schwartz [19], and Sternau and co-workers [30] described a method consisting in prolonged injection and pumping operations. It seems that, because of economic reasons, their method can be applied only when there are other justified needs for prolonged pumping operations, e.g. testing of artificial aquifer recharge. The author has no knowledge whether this method is currently being applied, and if so to what extent.

Another method, in which the recharging-discharging well-pair is used, was described by Grove and Beetem [18], and in other related papers [31, 32]. They applied a continuous injection, which is rather a matter of choice. The main differences result from the different flow fields. The advantages of the well-pair method over the two-well method discussed here lie in a much shorter measuring time and larger volume of the aquifer for the same pumping rate and distance between the wells.

In other words the well-pair method enables larger distances to be applied, involving larger investigation areas, or the total measurement time to be shortened for large distances between the wells. However, this advantage may sometimes turn into a disadvantage. For instance, in the experiments No. 1, 2 and 3 performed in the geological situation shown in Fig. 1 in Ref. [20], it would not be possible to apply a larger distance because of the diversion of flow lines into the quaternary sands, which would undoubtedly take place in the unconfined area. On the other hand, the use of the method in the existing wells would be difficult because of strong recirculation effects, which can be accounted for only when their influence is of minor importance [18].

In the well-pair method the tracer travels along different flow lines with different transit times. This causes additional flattening effects which in consequence may overshadow the differentiation caused by the aquifer layering. Depending on the situation all these characteristics of both methods may be treated either as advantageous or disadvantageous. The well-pair method is more mathematically complicated, and a computer interpretation is unavoidable. For some users this may be a deciding factor.

10. PLANNING OF EXPERIMENTS

In planning an experiment the problems considered in the previous section have to be taken into account. For the two-well pulse method the injection well has to be situated within the cylindrical symmetry of the depression cone.

Roughly speaking this distance should be not larger than half the distance to the downstream water divide, x_0, created during the pumping.

$$x \leq \frac{1}{2} x_0 = \frac{0.5\,Q}{2\pi h \bar{k} i} \tag{33}$$

where i is here the areal hydraulic gradient.

For existing wells the measuring time has to be estimated from Eq. (1). If the wells are to be drilled, their distance has to be chosen depending on the hydrogeological situation (h, and estimated range of $\bar{n}$), and on the available technical means in obtaining a given pumping rate (a pump, well-diameter) for a given transmissivity, $h\bar{k}$. For deep boreholes it is necessary to measure their deviation by downhole surveying for a proper calculation of x at depth [18, 20]. Graphs of the E function (for the radial flow Sx in Eq. (4) is changed to $\pi x^2 h$) given by Lenda and Zuber [7] serve for estimating proper quantities of tracer. The dispersion constant can be chosen from the values given in Section 3 above, whereas the recovery has to be assumed in order to increase m to a safe margin. Usually, the recovery is not worse than 0.2. Needless to say, the detection efficiency of the measuring equipment has to be known [7, 16].

11. LIMITATIONS AND APPLICABILITY OF THE METHOD

It is self-evident that the accuracy or reliability of the method depends on how well the condition of the cylindrical symmetry of the depression cone is satisfied. Some experimental evidence on the range of results for a highly heterogeneous formation is given in Ref. [20]. In general, caution is necessary in this respect. For a layered formation geological evidence should be available to help in attributing particular peaks, or components, of the concentration curve to the particular layers. When differences in hydraulic conductivities are small, the dispersion effects may overshadow the splitting of the mean transit times. On the other hand, if the hydraulic conductivities differ by a factor of 5 or 10, it may be difficult to measure the parameters of the less permeable layer. The quantity of the tracer entering this layer may be so low, and the transit time so long, that they will be hardly measurable.

In addition to these physical limitations there are a number of technical difficulties. In the first place, there is the above-mentioned deviation of the wells from the vertical. Secondly, there is difficulty in realizing an instantaneous injection that ensures the proportionality of the tracer quantities to the transmissivities, and at the same time involves negligible disturbances of the depression cone. The two-pair method does not have this difficulty. Thirdly, a long pumping is necessary in comparison with pumping periods usually applied in conventional pumping tests. Fourthly, organizational difficulties arise in applying radioisotopes, e.g. the need for a licence, high qualifications of the field team and proper planning of the delivery of the radioisotopes.

Experience gained so far in applying the method shows that it is useful for determining the effective porosities of fissured rocks. It may also be helpful in determining permeability stratifications. The method should be applied when some indicative figures for a given aquifer are required or

when local information is needed. These remarks become clearer when one realizes that a general application of the method is not advised when two closely situated wells are involved. However, whenever such wells are obtainable the use of the method should be considered as it supplies information unobtainable in other ways.

The use of the method for determining the effective porosities of granular formations does not seem to be justified. In such media very irregular concentration curves are observed [20, 33] which bring in an error additional to the errors mentioned earlier resulting from deviations from the cylindrical symmetry. A limited accuracy combined with a limited range of the values encountered make the method questionable in that case. However, as discussed above, Laguna [4] has produced a nice example of the applicability in a layered granular formation.

It is hoped that further development of dye tracers and portable fluometers may lead to cheaper and easier execution of field experiments, and consequently to a more frequent application of artificial tracer methods in general, and this method in particular.

TABLE I. DIFFERENT MODELS OF FISSURES

Eq. No.	Formula	Ref.	Model	Ratio of d_f to that given by Eq. (34)
34	$K = \frac{1}{96} n d_f^2$	[24]	Network of capillaries	1
35	$K = \frac{1}{32 \tau^2} n d_f^2$	[34]	Tortuous capillaries	0.87 for $\tau = 1.5$ 1.45 for $\tau = 2.5$
36	$K = \frac{1}{12 \tau^2} n d_f^2$	This work	Tortuous slits	0.55 for $\tau = 1.5$ 0.89 for $\tau = 2.5$

12. EFFECTIVE THICKNESS OF FISSURES

It will be shown here that any method supplying in situ values of the effective porosity can be used to estimate the effective fissure thickness if the hydraulic conductivity is known for the same area.

In Table I different formulae for the permeability coefficient, K, are compared. In Eqs (34) and (35) (Table I), d_f is the mean or effective diameter of capillaries, whereas in Eq. (36) it denotes the mean or effective thickness of fissures. The effective diameter or thickness has to be understood here as that which would give the same hydraulic conductivity if all the fissures had the same dimensions for a given porosity. In other words, it is the mean value weighted by flow rates in particular fissures. Equation (36) was derived similarly to Eq. (35), but in that case the departure formula was that for a flow through a slit rather than through a capillary. The approach applied here is somewhat different from that considered by Louis [35]. Equation (34) rearranged to the hydraulic conductivity, k_{10}, at 10°C, expressed in m/d reads

$$k_{10} = 6800\ n\ d_f^2 \tag{37}$$

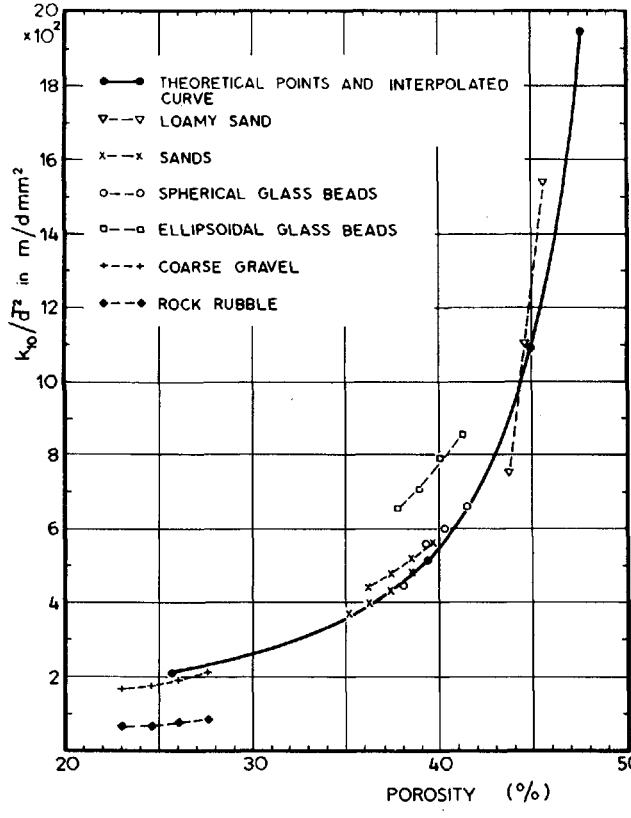

FIG.2. Theoretical ratio of hydraulic conductivity to mean grain diameter versus porosity compared with experimental values.

where d_f is in mm's. This formula was checked experimentally for granular media, after finding the relationship between the mean pore diameter and the mean grain size diameter defined as

$$\bar{d} = \frac{100}{\sum \frac{w_i}{d_i}} \tag{38}$$

where w_i is the weight percentage of the i-th fraction with diameter d_i. Figure 2 gives theoretical values of the k_{10} to $\bar{d}^2$ ratio versus porosity compared with experimental values obtained for different media having k_{10} from 0.34 to 211 m/d, $\bar{d}$ from 0.022 to 1.02 mm (d_{min} < 0.001 mm and d_{max} = 40 mm) and U (ratio of d_{60} to d_{10}) from 1.02 to 47.

A significant deviation from the theoretical values is observed in Fig. 2 only for materials having a grain shape markedly different from spherical.

TABLE II. EXAMPLES OF d_f VALUES

k_{10} m/d	Porosity	d_f (mm)	Ref.	Remarks
9.7 9.7	0.12 0.04	0.1 0.2	[20] [20]	Grzybów region, limestone
41	0.06	0.3	[7,20]	Olkusz region, fault zone in diplopora and ore-bearing dolomites
50	0.025	0.6	[20]	Klucze region, ore-bearing dolomite, diplopora dolomite assumed as impermeable k = 0.1 m/d
560	0.01	3	[36,37]	

In spite of that, the theoretical values of k_{10} calculated from Fig. 2 are in much better agreement with the experimental values than those calculated from the known formulae of Hazen, Slichter, Krüger and others. Details of this study will be given elsewhere. Here it has to be noted that Fig. 2 may serve both for finding k_{10} from the grain size curve and as an experimental check of the theoretical approach. This experimental evidence plus the closeness of the theoretical values given in Table I show that Eqs (34), (35) and/or (36) may serve for estimating the effective diameter or thickness of fissures.

Errors of k and n caused by any possible wrong estimation of h cancel in the formulae for d_f as long as the same h is used for calculating both k and n.

Table II gives some examples of d_f values calculated from Eq. (37). Estimation of these data for the Reynolds number shows that an assumption of a laminar flow holds with an exception for the well vicinity.

The values of the effective porosities for the regions of Olkusz and Klucze agree with the range of 0.03 to 0.08 found from observations in existing mines and by the Theis-Jacob method [38, 39]. The evaluation of the found d_f values is more difficult. Usually, the hydraulic conductivities do not exceed 120 m/d, which means that d_f does not exceed 1 mm. It is known from observations in the mines that fissures of about 1 cm, and more, as well as large caverns of about 1 m, are encountered [39-41]. However, there were also about 20 wells in which no depression was obtained during the pumping tests. For the applied pumping rates and the obtainable accuracy of the depression measurement it can be estimated that the hydraulic conductivity exceeded 12000 m/d, which in turn gives $d_f > 6$ mm. It seems that these highly cavernous and fissured zones are of limited extent, are only occasionally encountered in drillings, and contribute only slightly to the average hydraulic conductivity of the region. When encountered by mining works they are, however, highly troublesome [40]. Further investigations in that region and in the Grzybów region are planned.

13. CONCLUSIONS

Detailed observations show the applicability of the method for determining the mean porosity, hydraulic conductivities and thicknesses of layered systems, the dispersion constant and the effective thickness of fissures. The latter cannot be treated as a hydrological parameter, but it may be useful for some technical purposes. The method is limited mainly by possible deviations of the depression cone from a cylindrical symmetry, and by difficulties in determining the mean transit time of water from tracer experiments in heterogeneous media. Experiments performed under unfavourable conditions may fail, as they will produce no additional information, or they will be ambiguous because of low accuracy. It seems that whenever two wells close together are available or planned, the use of the method should be considered as its cost is usually a small percentage of the drilling. It is hoped that further development of the tracer techniques, particularly dye tracers, may lead to a wider use of the method.

ACKNOWLEDGEMENTS

The author is indebted to J.A. Czubek, Z. Wilk, J. Motyka, A. Kreft and A. Lenda for valuable discussions at different stages of this study. Special thanks are due to J. Tyrała, Hydrological Enterprise, HYDROKOP, Cracow, in whose laboratory the measurements described in Section 12 were performed.

REFERENCES

[1] GRINBAUM, I.I., Geofizićeskie metody izućenija dviženija podzemnych vod. Gosgeoltehnizdat, Moscow (1965).

[2] HALEVY, E., NIR, A., The determination of aquifer parameters with the aid of radioactive tracers, J. Geophys. Res. 67 (1966) 2403.

[3] MERCADO, A., HALEVY, E., Determining the average porosity and permeability of a stratified aquifer with the aid of radioactive tracers, Water Resour. Res. 2 (1966) 525.

[4] DE LAGUNA, W., Tracer aids interpretation of pumping test, Water Resour. Res. 6 (1970) 172.

[5] HIMMELBLAU, D.M., Process Analysis by Statistical Methods, Wiley, New York (1970).

[6] COATS, K.H., SMITH, B.D., Dead-end pore volume and dispersion in porous media, SPE Soc. Pet. Eng. 4 (1964) 73; 282.

[7] LENDA, A., ZUBER, A., "Tracer dispersion in groundwater experiments", Isotope Hydrology 1970 (Proc. Symp. Vienna, 1970), IAEA, Vienna (1970) 619.

[8] HUBERT, J., LENDA, A., ZUBER, A., A solution of the dispersion-adsorption equation with linear adsorption isotherm, Nukleonika 16 (1971) 271.

[9] NIEMI, A., On the dynamic of a pneumatic flotation cell, Acta Polytech. Scand., Chem. Metall. Ser., No.49 (1966).

[10] BANSAL, M.K., Dispersion in natural streams, J. Hydr. Div. ASCE 97, No. HY 11 (1971) 1867.

[11] BANKS, R.B., OGATA, A., A Solution of the Differential Equation of Longitudinal Dispersion in Porous Media, US Geol. Surv. Prof. Paper 411-A, Washington (1961).

[12] PERKINS, R.K., JOHNSTONE, O.C., A review of diffusion and dispersion in porous media, Trans. Metall. Soc. AIME. 3 (1963) 70.

[13] RICHARDSON, J.G., "Flow through porous media", Handbook of Fluid Dynamics (STREETER, V.L., Ed.), McGraw-Hill, New York (1961) 16-1.

[14] BLACKWELL, R.J., RAYNE, J.R., TERRY, W.M., Factors influencing the efficiency of miscible displacement, Trans. Am. Inst. Min. Metall. Petrol. Engrs 217 (1959) 1.

[15] FRIED, J.J., COMBARNOUS, M.A., Dispersion in porous media, Adv. Hydrosciences 7 224 (1971) 169.

[16] ZUBER, A., Dispersion of tracer in flow through porous media and its aspects in applications to hydrology, Sci. Bull. Acad. Mining and Metall., No.302 (1971) (in Polish).
[17] NIR, A., On the interpretation of tritium age measurements of groundwater, J. Geophys. Res. 69 (1964) 2589.
[18] GROVE, D.B., BEETEM, W.A., Porosity and dispersion constant calculations for a fractured carbonate aquifer using the two well tracer method, Water Resour. Res. 7 (1971) 128.
[19] SCHWARZ, J., Underground Water Storage Study, Rep. No.5, Tahal – Water Planning for Israel Ltd.(1963).
[20] KREFT, A., LENDA, A., TUREK, B., ZUBER, A., CZAUDERNA, K., "The determination of effective porosity by the two-well pulse method", these Proceedings I, IAEA-SM-182/46.
[21] MERCADO, A., The Spreading Pattern of Injected Water in a Permeability Stratified Aquifer, Int. Ass. Sci. Hydr. Symp., Haifa Publ., No.72 (1967).
[22] SKIBITZKE, H.E., Fluid Movement in Earth Materials, US Geol. Survey Paper 411-F, US Govt Printing Office, Washington D.C. (1964).
[23] WITCZAK, S., ZUBER, A., HUBERT, J., ADAMCZYK, A., International Report, Institute of Hydrogeology, Academy of Mining and Metallurgy, Cracow (1973).
[24] SAFFMAN, P.G., Dispersion in flow through a network of capillaries, Chem. Eng. Sci. 11 (1959) 125.
[25] DE JONG, G. de J., Longitudinal and transverse diffusion in granular deposits, Trans. Am. Geophys. Un. 39 (1958) 67.
[26] KREFT, A., LENDA, A., A Fortran Program for the Interpretation of Porosity Measurements by the Two-Well Pulse Technique, Rep. No.46/I, Institute of Nuclear Techniques, Academy of Mining and Metallurgy, Cracow (1974).
[27] NIELSEN, D.R., BIGGAR, J.W., "Radioisotopes and labelled salts in soil-water movement", Soil-Moisture and Irrigation Studies (Proc. Panel, Vienna, 1966), IAEA, Vienna (1967) 61.
[28] COREY, J.C., NIELSEN, D.R., "Some factors influencing the interpretation of soil-solute-water interactions", Soil-Moisture and Irrigation Studies II (Proc. Panel, Vienna, 1970), IAEA, Vienna (1973) 87.
[29] MAJERCZYK, J., ZUBER, A., Application of Radioisotopes to Groundwater Investigations, Internal Report, Institute of Nuclear Techniques, Cracow (1966) (in Polish).
[30] STERNAU, R., SCHWARZ, J., MERCADO, A., HARPAZ, Y., NIR, A., HALEVY, E., "Radioisotope tracers in large-scale recharge studies of groundwater", Isotopes in Hydrology (Proc. Symp. Vienna, 1966), IAEA, Vienna (1967) 489.
[31] GROVE, D.B., An Analysis of the Flow Field of a Discharging-Recharging Pair of Wells, Rep. USGS-474-99, USGS, Denver (1971).
[32] GROVE, D.B., BEETEM, W.A., SOWER, F.B., Fluid travel time between a recharging and discharging well pair in an aquifer having a uniform regional flow field, Water Resour. Res. 6 (1970) 1404.
[33] WIEBENGA, W.A., ELLIS, W.R., SEATONBERRY, W., ANDREW, J.T.G., Radioisotopes as groundwater tracers, J. Geophys. Res. 72 16 (1967) 4081.
[34] PIRSON, S.J., Handbook of Well Log Analysis, Prentice-Hall, Englewood Cliffs, N.J. (1963).
[35] LOUIS, C., Strömungsvorgänge in klüftigen Medien und ihre Wirkung auf die Standsicherheit von Bauwerken und Böschungen im Fels (PhD thesis), Technische Hochschule Karlsruhe, Karlsruhe (1967).
[36] HALEVY, E., NIR, A., Use of Radioisotopes in Studies of Groundwater Flow, Tahal – Water Planning for Israel Ltd. (1960).
[37] NIR, A., HALEVY, E., MANDEL, S., HARPAZ, Y., Research on the Use of Radioactive Isotopes in Hydrology, Tahal – Water Planning for Israel Ltd. (1959).
[38] ZUBER, K., Hydrogeology of the Olkusz Region, Internal Report, Geological Enterprise, Cracow (1964) (in Polish).
[39] WILK, Z., et al., Internal Report, Institute of Hydrogeology, Academy of Mining and Metallurgy, Cracow (1973) (to be published).
[40] WILK, Z., MOTYKA, J., NIEWDANA, J., Characteristics and classification of waters in mine works of cavernous-fissured formation, Trans. No. 292, Academy of Mining and Metallurgy, Geology No.14, Cracow (1971) (in Polish).
[41] BOGACZ, K., DZULYŃSKI, S., HARAŃCZYK, Cz., SOBCZYŃSKI, P., Contact relations of the ore-bearing dolomite in the Triassic of the Cracow-Silesian region, Rocznik Polskiego Towarzystwa Geologicznego 42 (1972) 347.

DISCUSSION

D. B. SMITH: Do you pump the abstraction well for a period before the injection of the tracer, so as to establish equilibrium hydraulic conditions?

A. ZUBER: Yes, we do.

D. B. SMITH: Is the method equally applicable to an unconfined aquifer, where there would be a change in the cross-section of the saturated zone due to the drawdown near the abstraction well?

A. ZUBER: In the case of an unconfined aquifer, the volume has to be corrected for the depression cone. The accuracy is then undoubtedly lower.

S. S. H. KASI: What is the accuracy of porosity determination by your method?

A. ZUBER: It is impossible to answer this question on the basis of one experiment because deviations from cylindrical symmetry contribute most to the error. Several measurements in a given region should, however, give some idea of the range of values and/or of the accuracy of the experiments.

G. SAUZAY: In 1970[1] we suggested that, when measuring concentrations over time, one should use the weighted mean of the reciprocals of the residence times rather than the weighted mean of the residence times. You reject the usual solution of the diffusion-dispersion equation on the grounds that it is not in accordance with your Eq. (7), which we do not accept. Have you tried using the weighted mean of the reciprocals? If so, what do you think of this approach? Incidentally, I am surprised that you are satisfied with a law which does not obey completely the fundamental law of mass conservation.

A. ZUBER: I do not agree with you as regards the weighted means of the reciprocals of the residence times (the so-called harmonic mean). Whenever the amounts of tracer in particular flow lines are proportional to their velocities, and hence to the flow rates (even in a single pipe or capillary), the arithmetic mean of the tracer distribution gives the mean transit time of the water.

If I recall correctly, in your paper published in Isotope Hydrology 1970 you claim that the tracer cloud moves with a velocity different from that of the medium (the factor was 1.2). I cannot agree with that either. There are many solutions of the dispersion equation, depending on the boundary and initial conditions. It is an open question which conditions best describe a given experimental situation. Our solution obeys the law of mass conservation over time, for we measure the distribution over time. I would draw your attention to the fact that the "conventional" solution is not without ambiguities either, for it gives the tracer distribution from minus infinity to plus infinity. In other words, part of the tracer moves against the flow lines.

---

[1] ALQUIER, M., GRUAT, J., COURTOIS, G., SAUZAY, G., « La notion de « bon mélange» dans l'emploi de traceurs – vitesse débitante et vitesse du centre de gravité d'un nuage de traceurs dans l'étude d'un écoulement», Isotope Hydrology 1970 (Proc. Symp. Vienna, 1970), IAEA, Vienna (1970) 441.

DETERMINATION OF EFFECTIVE POROSITIES BY THE TWO-WELL PULSE METHOD

A. KREFT, A. LENDA, B. TUREK,
Institute of Nuclear Physics and Techniques,
Academy of Mining and Metallurgy,
Cracow

A. ZUBER
Institute of Nuclear Physics,
Cracow

K. CZAUDERNA
Hydrological Enterprise HYDROKOP,
Cracow,
Poland

Abstract

DETERMINATION OF EFFECTIVE POROSITIES BY THE TWO-WELL PULSE METHOD.

Results obtained in the use of the two-well pulse method in fissured and granular media are presented. The measurements in the former were aimed mainly at obtaining the effective porosity of Zn-Pb and sulphur deposits in limestone and dolomite formations. Breakthrough curves obtained in these fissured and cavernous formations appeared to be rather regular though highly asymmetrical, due to a high dispersion. Both manual and computer interpretations have been developed on the basis of a new, analytical solution of the dispersion equation. This solution is exact in a unidimensional flow, and approximate in a radial flow. The manual interpretation is based on an assumption of equal surfaces under both theoretical and experimental curves and fitting at a guess, whereas the computer interpretation is based on minimizing the chi-squared value. Some experiments could be interpreted only under an assumption of a breakthrough curve consisting of two or more component breakthrough curves. However, the interpretation is not always unambiguous because in cases of a high dispersion the tail part of the breakthrough curve is seldom measurable. In granular media of fluvial and fluvio-glacial origin usually irregular, though less dispersed, curves were observed. Their interpretation was performed either by a rough approximation or by calculating the mean arithmetic time as the ratio of the first to zero moments.

1. INTRODUCTION

An account is given of the field experience with the two-well pulse method, used for determining the effective porosities of aquifers. The outline of the method has been given by Halevy and Nir [1], and Mercado and Halevy [2], who extended the use of the method for the case of a multi-layered aquifer. The recent work of Zuber [3] presents a thorough review of the possibilities of the method, following, in addition to the present work, the new interpretational approach to the dispersion phenomena proposed by Lenda and Zuber [4]. This new approach, consisting in applying an approximate formula for description of the tracer dispersion in a radial flow in porous media, seems to improve considerably the interpretation of both the aquifer dispersivity and the mean transit time of tracer.

A number of field tests are presented. The aim of these tests was to determine effective porosities of fissured dolomites and/or limestones, mineralized either by lead and zinc ores or by sulphur deposits. A series of measurements was also performed in granular media. In this case the mean transit time of tracer was measured between two rows of boreholes, before and after the installation of a sealing mud screen between them. The measurements of the transit times were intended as estimates of the screen efficiency.

All the measurements have been interpreted manually. Recently, however, a number of measurements has been re-interpreted with the aid of a computer program developed by Kreft and Lenda [5]. The results of the computer interpretation are presented in Subsection 3.4.

According to Lenda and Zuber [4], the tracer concentration in the pumping well, resulting from an instantaneous injection in another well, is given by the formula

$$c(x,t) = \frac{m}{V} \frac{1}{\sqrt{4\pi \frac{D}{vx}\left(\frac{t}{t_0}\right)^3}} \exp\left[-\frac{1-\left(\frac{t}{t_0}\right)^2}{4\frac{D}{vx}\frac{t}{t_0}}\right] \tag{1}$$

where m is the mass (activity) of the injected tracer; t_0 is the mean transit time of water, $t_0 = x/v$, x being the distance between the two wells and v being the mean interstitial velocity of the flow, and D is the dispersion coefficient. In the radial flow v is not constant, but the ratio of D/v remains constant, i.e. Eq. (1) applies for the case of a pure hydrodynamic dispersion [3,4]. The volume V appearing in Eq. (1) is the total volume of water-saturated pores in which the water movement takes place. For the case of a cylindrical aquifer of the thickness h and the mean effective porosity n this volume is

$$V = n\pi x^2 h \tag{2}$$

The above formula applies for the case when the involved volume of the depression cone is negligible or it does not reach a confined aquifer. If this is not so a more general formula has to be used:

$$V = \pi n \int_0^x 2x'h(x')dx' = \pi x^2 hn - V_d \tag{3}$$

where V_d represents the volume of the involved part of the depression cone. It may also happen that the shape of the water-bearing layer cannot be approximated by a simple cylinder minus the depression cone. In such cases the volume V has to be calculated as the volume of a corresponding geometrical body.

The volume V is, on the other hand, equal to the volume of water pumped out during the time t_0, i.e.

$$V = Qt_0 \tag{4}$$

where Q is the pumping discharge. Thus combining Eq. (4) with Eq. (2) or (3), one can calculate the effective porosity. The mean transit time is

determined from a tracer experiment and usually it can be taken as the parameter t_0 of a theoretical curve of best fit. It may happen, however, that an experimental curve cannot be fitted by a single curve given by Eq.(1). In such a case the mean transit time can sometimes be calculated directly from its definition formula [3,4]:

$$t_0 = \bar{t} \stackrel{\text{def}}{=} \frac{\int_0^\infty tc(t)dt}{\int_0^\infty c(t)dt} \qquad (5)$$

This requires however the registration of the complete breakthrough curve, which, especially for highly asymmetric curves, is not easy. For an incomplete curve Eq.(5) can still be used, provided the curve could be extrapolated. Such an extrapolation, however, can be a somewhat tricky business, especially for asymmetric curves characterized by a long tail.

Another way of interpreting a breakthrough curve which cannot be fitted by a single theoretical curve consists in assuming a multi-layered system. In such a case the experimental concentration curve is fitted by a sum of several theoretical curves and the mean transit time $\overline{t_0}$ is calculated as a weighted mean of the transit times $t_{0,i}$ characterizing each sub-curve. Such a procedure can unfortunately lead to severe ambiguities, due to the increase in the number of parameters. Unless the introduction of a larger number of parameters is justified from the knowledge of geological profiles such an interpretation should be treated with caution (see Section 3).

2. EXPERIMENTAL SET-UP

The general idea of the experimental set-up used in the measurements described was similar to that of Halevy and Nir [1]. The measuring tank of 1 m^3 volume contained a horizontal pipe half way up its height, so that the probes could be introduced and/or replaced into this pipe at the time of measurement. Standard scintillation probes of 2 in. × 2 in. and 1 in. × 1 in. NaI(Tl) crystals, connected with standard electronic equipment, were used. Their sensitivities for ^{131}I were 2500 counts/min·$m^3/\mu Ci$ and 580 counts/min·$m^3/\mu Ci$, and the background rates were about 2300 counts/min and 600 counts/min respectively. The minimal detectable concentrations (MDC) of ^{131}I, calculated under the assumption that a single read-out takes 5 min [4], were about 0.1 $\mu Ci/m^3$ and 0.2 $\mu Ci/m^3$ respectively.

The injection tank with the solution of tracer and carrier was situated above a steel pipe connecting both wells. Before the injection, part of the water pumped out of the pumping well was diverted through this pipe into the injection well. It was assumed that such an injection performed under sufficient pressure also ensures that quantities of tracer enter particular layers proportional to their transmissivities [3].

3. THE MEASUREMENTS

3.1. Zn-Pb deposits

The two-well pulse technique was applied in Poland for the first time in 1969 [4] for measuring effective porosities in the region of zinc and lead

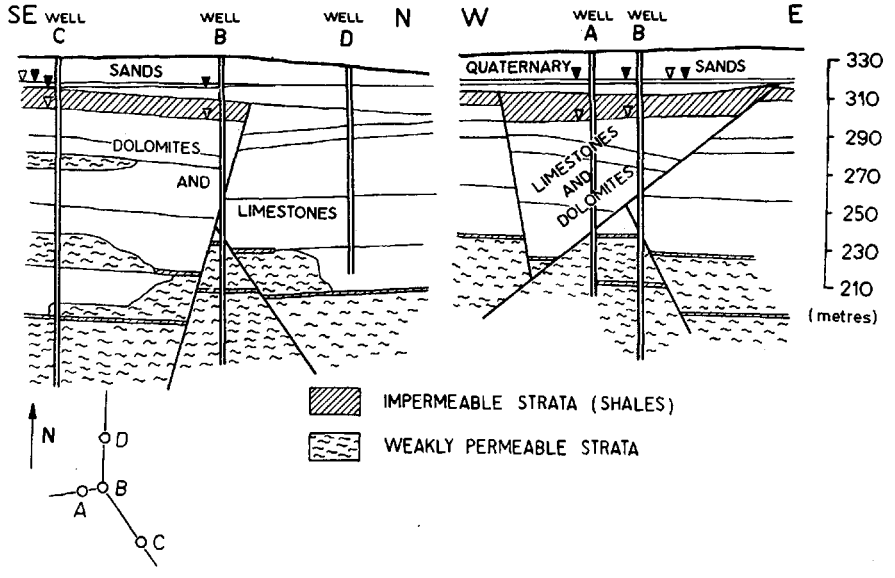

FIG. 1. Geological profiles in the effective porosity measurement of a zinc-lead deposit, Subsection 3.1 (after S. Kurek).

deposits. A rather complicated geological situation at the measuring site is shown in Fig. 1. The injection and the pumping were carried out at wells A and B respectively, 22 m apart. The locally confined aquifer consisted of two layers: diplopora dolomite (upper layer) and ore-bearing dolomite (lower layer). The pumping tests in the upper layer enabled its hydraulic conductivity be determined as equal to 21.6 m/d. The hydraulic conductivity of the second layer, calculated from the pumping tests performed in the whole aquifer, was 40.6 m/d. Nevertheless the tracer experiment did not result in a double-layer concentration curve, so for the calculations of the effective porosity a single layer of 57-m thickness has been assumed.

The measurement was repeated three times with three different pumping rates (1.7 m^3/min; 0.66 m^3/min and 1.4 m^3/min). The concentration curves obtained showed a high asymmetry which could not be explained on the basis of known solutions of the dispersion equation. This experimental evidence has become a decisive incentive in the search for a new solution, which would have been more adequate for the interpretation of the experimental data. The solution found by Lenda and Zuber [4] has appeared to agree well with the experimental data, and the asymmetry could have been explained as due to high values of the dimensionless parameter D/vx. For the three measurements the value of D/vx ranged from 2 to 5, which corresponded to the variation of the dispersion constant D/v from 44 to 110 m. Such values of D/v agree well with other values reported for fissured rocks [3].

The manual interpretation, assuming a single-layer aquifer, gave three very close values of the effective porosity (see Table I for detailed results). One of the breakthrough curves can be seen in Fig. 2 (for Q = 1.4 m^3/min), another one was quoted earlier [4]. All three measurements were recently re-interpreted with the aid of the computer program, and the detailed results of the computer and manual interpretation can be found in Table I.

Another measurement of effective porosity in similar formations was carried out in 1972. The pumping rate was about 2 m^3/min. The confined aquifer consisted again of two layers, diplopora and ore-bearing dolomites. The upper layer has been assumed to be practically impermeable as its hydraulic conductivity was about 500 times lower than that of the lower layer. Thus, in the interpretation only the ore-bearing dolomite layer, with a thickness of 48 m, was considered. Some difficulties arose in determining the pumping-to-injection well distance. The downhole surveying showed that the wells were declining seriously from the vertical, the distance x being 29 m at the surface, 24 m at the top of the investigated layer and 18.5 m at the bottom of the layer. In the final calculations a mean value $\bar{x}$ = 21.3 m was used. An attempt was also made to carry out the interpretation assuming the existence of three hypothetical sub-layers characterized by the same values of n, D/v and different values of x, and replacing the theoretical curve of Eq.(1) (for n, D/v, h and $\bar{x}$) by the sum of three theoretical sub-curves (for n, D/v and h_i, x_i; $\sum_i x_i = 3\bar{x}$ and $\sum_i h_i = h$, i = 1,2,3). However, it has appeared that both ways were practically equivalent.

During the interpretation it became evident that the breakthrough curve obtained (Fig. 3) could not be fitted, in spite of its regular shape, by the single theoretical curve given by Eq.(1). Therefore the interpretation was carried out assuming a double-layer system, and the mean transit time has been finally calculated as a weighted mean of the two transit times for assumed sub-layers (the weights were the partial recoveries of the tracer) [3]. The interpreted mean effective porosity was 2.4% (for the other parameters see Table II). It is to be emphasized that in this particular case the assumption of a two-layer system was not supported by any geological evidence, and that the sum of the two theoretical curves matches rather poorly the tail of the experimental curve. However, the computer interpretation (Subsection 3.4) resulted also in a double-layer system.

3.2. Sulphur deposits

A series of five measurements was performed in one of the Polish sulphur deposits in limestone formations. The measurements were carried out in a series of four boreholes situated in a straight line (Fig. 4). The geological profiles showed the existence of three layers in the investigated aquifer: shales, limestones and marls. However, in calculations of both the hydraulic conductivity and the effective porosity only the limestone layer was taken as the permeable one. Its thickness was determined as varying from 6 to 8 m and the coefficient of the hydraulic conductivity was calculated as equal to 9.7 m/d. The pumping tests performed in wells B and C also, as in some other wells situated in the vicinity of the measuring site, showed a high variability of the hydraulic conductivity with declining values in the direction of wells C and D. In consequence of this fact the second and the fifth

TABLE I. RESULTS OF THE EFFECTIVE POROSITY MEASUREMENTS DESCRIBED IN SUBSECTION 3.1

Measurement	Interpretation[a]	Number of curves	R_i (relative)	R_{t0t} (%)	$\left(\frac{D}{v}\right)_i$ (m)	$\left\langle \frac{D}{v} \right\rangle$ (m)	$\tau_{0,i}$ (min)	$\bar{\tau}_0$ and $\bar{\tau}$ (min)[b]	Effective porosity (%)
I	M	1	-	32.0	110.0	110.0	3150	3150 / -	6.3
	C	2	0.32 0.68	27.7	4.8 11.2	21.4	166 1270	922 / 817	1.85 1.64
	C	1[d]	-	29.5	122.0	122.0	3330	3330 / -	6.6
II[c]	M	1	-	4.0	110.0	110.0	8100	8100 / -	6.2
	C	4	0.14 0.14 0.37 0.35	3.0	1.82 1.29 2.20 1.27	13.1	164 358 1030 2418	1295 1735	1.00 1.33
	C	1[d]	-	3.1	142.0	142.0	7206	7206 / -	5.5
III	M	1	-	38.0	44.0	44.0	4200	4200 / -	6.8
	C	3	0.13 0.50 0.37	32.8	92.0 15.7 9.35	20.3	859 1324 3049	1909 1589	3.1 2.6
	C	1[d]	-	31.2	69.6	69.6	5057	5057 / -	8.1

a M = manual; C = computer.
b The lower value in this column, where given, represents $\bar{\tau}$ calculated by extrapolation from Eq. (5).
c The results of this measurement may be doubtful because of the low recovery.
d Imposed by the interpreter.

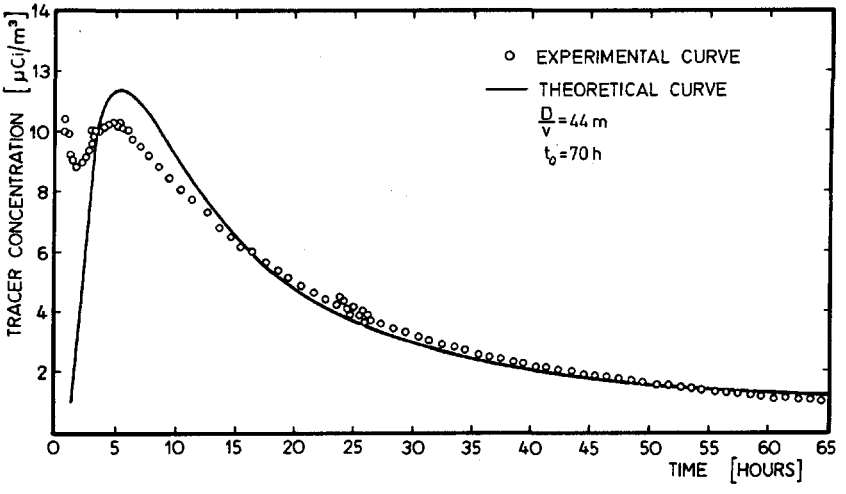

FIG. 2. Experimental and theoretical concentration curves for an effective porosity measurement in a zinc-lead deposit (third measurement of Subsection 3.1).

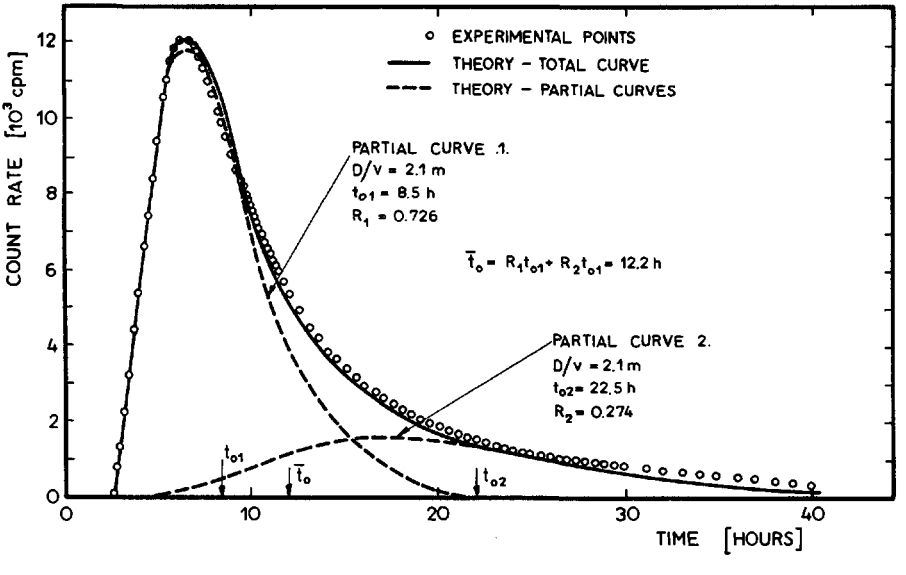

FIG. 3. Fitting with two theoretical curves a breakthrough curve from a dolomite formation (fourth measurement of Subsection 3.1).

TABLE II. RESULTS OF THE MANUAL AND COMPUTER INTERPRETATION OF THE MEASUREMENT OF Fig. 3

Measurement	Interpretation[a]	Number of curves	R_i (relative)	R_{t0t} (%)	$\left(\frac{D}{v}\right)_i$ (m)	$\left\langle \frac{D}{v} \right\rangle$ (m)	$t_{0,i}$ (min)	$\bar{t}_0$ and $\bar{t}$ (min)[b]	Effective porosity (%)
Fig. 3	M	2	0.73 0.27	38.2	2.1 2.1	8.1	510 1350	732 -	2.4
Fig. 3	C	2	0.82 0.18	39.5	2.47 1.42	7.96	566 1564	745 809	2.44 2.65

[a] M = manual; C = computer.
[b] The lower value in this column, where given, represents $\bar{t}$ calculated by extrapolation from Eq. (5).

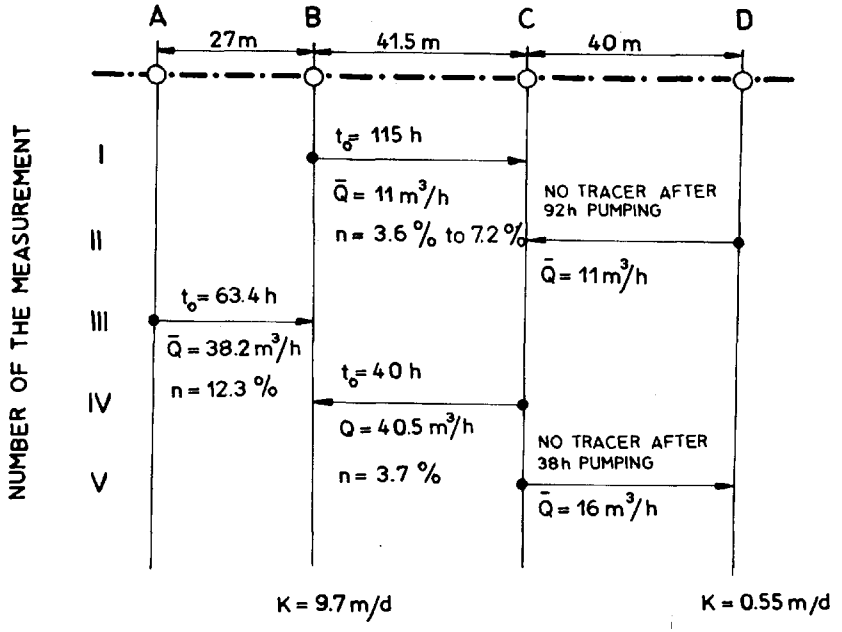

FIG.4. Schematic diagram of the series of measurements described in Subsection 3.2.

measurement (injection at well D, pumping at well C and vice versa) gave negative results, i.e. no tracer has been observed in spite of a relatively long pumping. The third measurement (injection at well A, pumping at well B) was a clear two-layer case, the breakthrough curve having two well-defined peaks (Fig. 5). The values of the D/v parameter for the two separated sub-curves differed seriously, though the corresponding two values of the transit time were very close. The mean transit time of tracer was calculated according to the formula

$$\overline{t_0} = R_1 t_{01} + R_2 t_{02} \qquad (6)$$

where R_1 and R_2 were the relative recoveries for the two partial curves. As the values of t_{01}, t_{02} and $\overline{t_0}$ were very close (Table III) it has been finally assumed that a single layer was involved and its porosity has been calculated according to Eq.(2) giving a value of 12.3%.

The first and the fourth measurements were of particular interest as they represented two measurements in the same layer with the injection well replaced by the pumping well and vice versa (wells B and C). The breakthrough curve for the first measurement was fitted by a single theoretical curve, giving t_0 = 115 hours. However, the negative results of the measurements between the C and D wells show that the effective porosity in this measurement cannot be calculated univocally. Two extreme values can be estimated: the first one (n = 3.6%) corresponding to the assumption that the pumping in well C has been radially symmetric and the

TABLE III. RESULTS OF THE EFFECTIVE POROSITY MEASUREMENTS IN A SULPHUR DEPOSIT, MANUAL INTERPRETATION (Subsection 3.2 and Fig. 4)

Measurement	Interpretation[a]	Number of curves	R_i (relative)	R_{r0t} (%)	$\left(\frac{D}{v}\right)_i$ (m)	$\left\langle \frac{D}{v} \right\rangle$ (m)	$t_{0,i}$ (min)	$\bar{t}_0$ and $\bar{t}$ (min)[b]	Effective porosity (%)
I[c]	M	1	-	23.7	20.8	20.8	6900	6900 / -	3.6 to 7.2
III	M	2	0.69 0.31	13.2	27.0 2.7	20.4	3900 3600	3800 / -	12.3
IV[c]	M	1	-	20.0[d]	20.8	20.8	2700	2700 / -	4.2
		3	0.34 0.51 0.15	20.0[d]	2.1 4.2 2.1	11.2	900 2400 5060	2300 2380	3.6 3.7

[a] M = manual.
[b] The lower value in this column, where given, represents $\bar{t}$ calculated by extrapolation from Eq. (5).
[c] Computer re-interpreted (see Table IV).
[d] Roughly estimated, as the probe sensitivity was not measured for the radioisotope used (^{58}Co-EDTA).

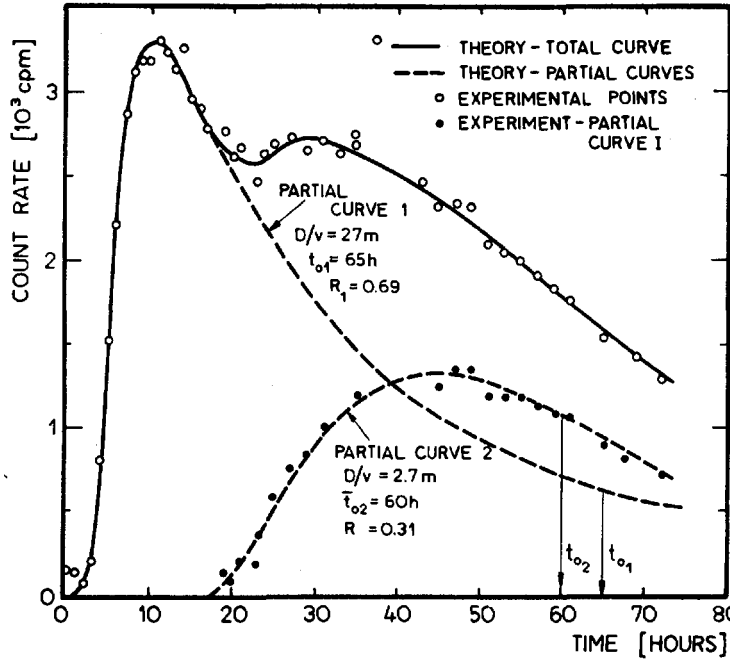

FIG.5. An example of a two-peak breakthrough curve (third measurement of Subsection 3.2).

volume involved in the measurement was that of a cylinder; the second (n = 7.2%) corresponding to the assumption that only the volume of a half-cylinder was "active" in the measurement.

The breakthrough curve for the fourth measurement presented an even more complex case. From the detailed analysis of the curve reported in Zuber's paper [3], it has appeared that a single theoretical curve could not be well fitted to the experimental values. Thus, three theoretical curves were finally used in fitting, and the mean transit time was calculated as the weighted mean of the partial t_0's. In that case the calculated value of $\bar{t}_0$ agrees well with the value of $\bar{t}$ found from Eq.(5). In the latter case the experimental values were extrapolated by an exponential curve.

Table III gives a detailed account of the results obtained. It is evident that the observed heterogeneities of the aquifer undoubtedly affected the radial symmetries of the depression cones in the vicinity of the pumping wells. Therefore the calculated values of effective porosities can hardly be treated as univocally representative for different parts of the aquifer. They should be rather considered as constituting a range of the variations of the effective porosity.

3.3. Granular media

A series of measurements was performed in a shallow sandy formation underlaid by impermeable clays. The tracer was injected at shallow

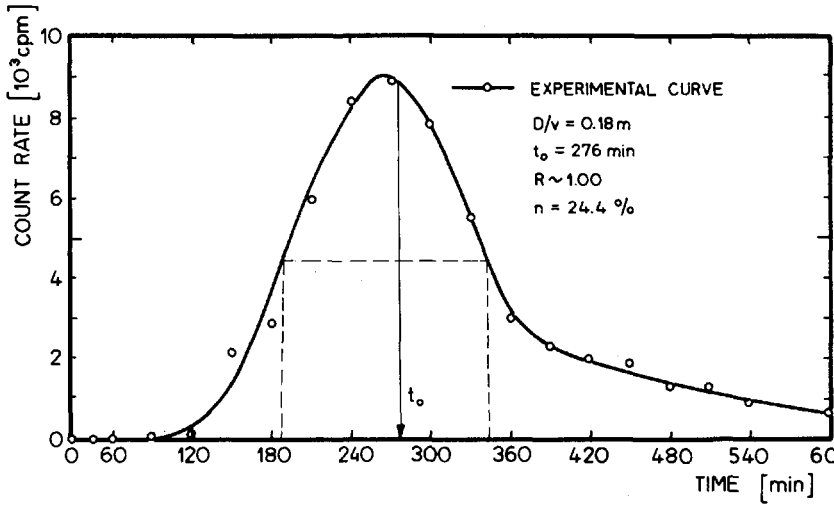

FIG. 6. A typical breakthrough curve from the measurements in sandy aquifers (Subsection 3.3).

piezometers, situated close to the pumping wells (x = 5 to 6 m). The calculation of the effective porosities of the investigated layers was hindered by the varying thickness of the aquifer.

The measured concentration curves did not show a strong asymmetry similar to that observed for fissured rocks. In most of the experiments the interpretation of the transit time was carried out according to the simplified procedure of Lenda and Zuber ([4], Subsection 2.2.3). An example of a typical breakthrough curve is shown in Fig. 6. Another example shown in Fig. 7 is of particular interest. In this case the existence of a two-layer system was known from geological profiles, a fine-sand layer gradually transgressing into a silty-sand layer. This information has been confirmed in the tracer experiment by a long tail. In this case the concentration curve was divided into two sub-curves. For the first sub-curve the value of the transit time was found by the simplified procedure [4]; for the second, by the use of Eq. (5) ($\overline{t_2}$). Together with the values of t_{01} and $\overline{t_2}$ the corresponding recoveries R_1 and R_2 were calculated. Assuming now that both layers have the same effective porosity (an assumption which can be accepted for granular media), one can calculate the corresponding values of the hydraulic conductivities k_1 and k_2 and the thicknesses h_1 and h_2 of the two sub-layers from the system of equations [3]:

$$h_1k_1 + h_2k_2 = h\overline{k}$$

$$\frac{k_1}{k_2} = \frac{t_{02}}{t_{01}} \qquad (7)$$

$$\frac{h_1k_1}{h_2k_2} = \frac{R_1}{R_2}$$

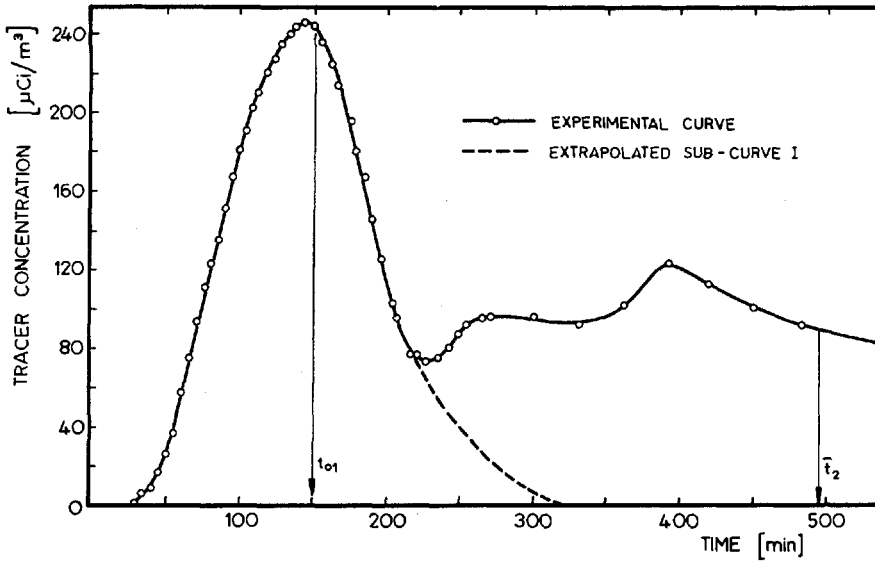

FIG.7. A breakthrough curve for a two-layered sandy aquifer (Subsection 3.3).

where $\bar{k}$ is the mean value of the hydraulic conductivity for the whole layer, as determined from a pumping test. The values in this experiment were as follows: $\bar{k}$ = 4.08 m/d, h = 2.49 m, t_{01} = 149 min, $\bar{t_2}$ = 492 min, R_1 = 0.58, and R_2 = 0.42. From these data (using Eq.(7)) it has been found that the aquifer consisted of two sub-layers of 0.33 m and 2.16 m in thickness, and characterized by hydraulic conductivities of 12.9 and 2.72 m/d respectively.

3.4. Computer interpretation of the tracer experiments

The manual interpretation of the experimental curves, especially for multi-layered aquifers, is a tiresome and time-consuming procedure. Moreover, its results can be affected by the subjectivism of an interpreter. Therefore a Fortran program has been recently developed [5], to determine the mean transit time of tracer from experimental curves.

The program possibilities, its algorithms, flow diagram and full listing are presented in Ref.[5]. The input data for the program are experimental concentrations of the tracer, plus some additional parameters of the measurement (background intensity, pumping discharge, probe sensitivity for a given type of tracer, dead time of the electronic equipment, etc.). The program introduces all the corrections allowing for the radioactive decay of the tracer, variation of the pumping discharge, dead time of the electronic set-up, etc. The fitting of the experimental data by a single theoretical curve of Eq.(1) or by a sum of such curves is then carried out. The program itself determines the number of sub-curves, which are to be used in fitting, though there is an option of imposing a number of theoretical curves, together with approximate values of their

TABLE IV. COMPUTER INTERPRETATION OF THE FIRST AND FOURTH MEASUREMENTS OF THE SERIES OF SUBSECTION 3.2

Measurement	Interpretation[a]	Number of curves	R_i (relative)	R_{t0t} (%)	$\left(\frac{D}{v}\right)_i$ (m)	$\left\langle \frac{D}{v} \right\rangle$ (m)	$t_{0,i}$ (min)	$\bar{t}_0$ and $\bar{t}$ (min)[b]	Effective porosity (%)
I	C	1	-	26.3	28.9	28.9	9439	9439 7702	4.9 4.0
	C	2[c]	0.74 0.26	24.1	13.2 4.40	17.0	4828 12281	6762 7702	3.5 4.0
IV	C	3	0.47 0.27 0.26	18.4	27.5 12.8 12.0	28.3	999 1950 3329	1865 1930	2.9 3.0
	C	1[c]	-	19.3	11.0	11.0	2049	2049 1930	3.2 3.0

[a] C = computer.
[b] The lower value in this column represents $\bar{t}$ calculated by extrapolation from Eq. (5).
[c] Imposed by the interpreter.

parameters t_0 and D/vx. In either case the number of sub-curves cannot be greater than five. The fitting procedure, starting at the values of t_0 and D/xv imposed by an interpreter, or at the values estimated roughly by one of the program's subroutines, is a trial-and-error technique, using the Monte-Carlo random sampling of the values of the parameters. It must be pointed out, however, that the criteria used in the computer fitting are different from those used in the case of the manual interpretation. The manual interpretation uses two criteria: first, equal surfaces under both experimental and theoretical curves; second "good" fitting of the declining part of the curve. The program minimizes the chi-squared value giving the best fitting for the time interval in which experimental data were collected. The lack of the tail again causes uncertainties in the extrapolated part of the measurement. It is assumed that the curve(s) of the best fitting gives the best extrapolation, but a caution is necessary as an unfinished measurement is always of a limited accuracy.

The measurements which have been re-interpreted with the help of the program are all the measurements reported in Subsection 3.1 and two of the tracer experiments reported in Subsection 3.2.

All the three concentration curves for the first tracer experiment of Subsection 3.1 were initially recognized by the program as corresponding to a multi-layered medium (see Table I), the number of layers being different for every curve (2, 4 and 3). Because of this inconsistency these results were rejected, and the interpretation was repeated imposing a single-layer aquifer. The results of this stage of interpretation are confronted in Table I with those of the manual fitting. The agreement seems to be reasonably good, though the scatter of the computer-interpreted results is somewhat greater than that of the manually calculated ones. One notices the great difference between the values of the transit times determined via fitting and those calculated by the program according to Eq. (5). (Incidentally, the values of $\bar{t}$'s are similar to those obtained via the multi-layer fitting.) This seems to be due to the high asymmetry of the breakthrough curves, characterized by strong tailing effects. In such a case the exponential extrapolation, used by the program in calculations of $\bar{t}$, may lead to serious errors.

Table II contains a comparison of the computer and manual interpretation of the breakthrough curve presented in Fig. 3. It is interesting that the breakthrough curve has been recognized by the program as a sum of two theoretical curves, similarly to the manual interpretation. Both ways of interpretation led to very similar results, especially for the values of the mean transit times of tracer.

Table IV contains the results of the computer interpretation of the first and fourth measurements of the Subsection 3.2 series. For the first the breakthrough curve has been recognized by the program as a single-layer curve, but the value of the transit time differed seriously from that calculated manually (Table III). This difference results from a low accuracy of the manual fitting and limited accuracy of both fittings, caused by a high dispersion and the experiment finishing too early. As the quality of the computer fitting with a single curve was still far from perfect the interpretation has been repeated for a two-curves fitting. The results of this step of the interpretation are given in the second line of Table IV. The quality of the fit was much better (the chi-squared value has gone down by an order of magnitude) but, and this is quite interesting, the essential parameter, the

mean transit time of tracer has not changed much. The following lines of Table IV contain the results of the computer interpretation of the fourth measurement of Subsection 3.2. The program claimed the existence of a three-layered system, but it was re-run, after imposing a single-curve fitting. In this case the differences between the computer and manual interpretation (Table III) were about 30%. This may be due to the difference mentioned in the criteria of the fitting quality employed by the program and that by an interpreter performing the manual interpretation. Having no other independent information about the hydrological parameters of the investigated aquifers, it is practically impossible to state a preference for either way of interpretation. However, when there is no geological evidence for accepting a model of several layers, the single-layer model has to be assumed as that of the lowest number of parameters, in accordance with the general rules for choosing a model. Thus, for the cases given in Table I in which big differences have been obtained between multi-layer models and a single-layer model, the former were rejected whenever the single-layer model was acceptable. Obviously this approach is somewhat subjective. To minimize the subjectivism as much as possible judgement must be based on the available geological evidence. The computer interpretation is undoubtedly faster, more efficient and probably more objective, though, as stated above it is the authors' feeling that the results obtained by a computer can never be accepted without the critical judgement of the interpreter.

The first version of the program was worked out for a continuous measurement given in a digital form or for any set of readings having the same measuring time. This version was used for the interpretation of the measurements given in Table I and IV. However, the actual measurements were taken from a scaler in short intervals, and with short measuring times at the beginning, and with longer measuring times at the tailing part of the breakthrough curve. A new version of the program allows for this kind of measurement, and it was used for the interpretation of the measurement of Fig. 3 (Table II). It is possible that the first version attributed, for the described measurements, a larger error to the tailing part than the actual one, thus increasing discrepancies between the manual and computer interpretation (Tables I and IV).

4. CONCLUSIONS

The experimental evidence presented in the previous sections seems to indicate that the formula given by Lenda and Zuber [4] describes well the shape of the breakthrough curves in fissured rocks. Its adequacy is less pronounced for the case of granular media of fluvial and fluvio-glacial origin, for which irregular curves are observed. However, even in fissured rocks, for the cases of a high dispersivity, an ambiguity exists regarding the determination of the mean transit time. This ambiguity results first of all from the difficulty or even impossibility in determining the tail part of the breakthrough curve. Different fitting criteria can be used, but when a single theoretical curve is used, the accuracy of the fitting is limited, but resulting effective porosities do not differ more than 20% with an exception for measurement No. IV of Tables III and IV, where the difference was 30%.

In some cases fitting with a single curve was practically impossible as a long part of the breakthrough curve remained unaccounted for (Fig. 3, Table II). In such cases fitting with two or more theoretical curves, or calculations by Eq. (5), are imperative. However, if there is no geological evidence for a higher number of parameters such a procedure has to be accepted with caution.

Measurement No. IV (Tables III and IV and Fig. 1 in Ref. [3]) gave close results when interpreted both by a single-layer and by a three-layer model. However, in that case the manual and computer interpretations gave differences of about 20%, which resulted from different fitting criteria.

The most unexpected results are contained in Table I, where the same measurement was repeated three times with different pumping rates. In spite of a very high dispersivity, both manual and computer interpretation with a single-layer model gave a reasonable scatter of the effective porosity values, though fitting was far from excellent (except for measurement No. I in which fitting was quite good). Fitting by a multi-layered model was much better but yielded surprisingly low values of the effective porosity. These values were rejected under the assumption that, in choosing a mathematical model, the best one is that of the lowest number of parameters.

It is evident that in unfinished measurements with a high dispersivity, the accuracy of interpretation is limited as it is not possible to interpret objectively the non-existing part of the measurement. In spite of that the approximate formula used for the theoretical curves seems to be very useful for the interpretation of such measurements. However, when different methods of interpretation (single-layer, multi-layer model or definition) yield different results, extreme caution is necessary in accepting or rejecting a given model. It is the authors' feeling that a proper choice of the interpretation criteria is still an open question which needs further work.

REFERENCES

[1] HALEVY, E., NIR, A., The determination of aquifer parameters with the aid of radioactive tracers, J. Geophys. Res. 67 (1962) 2403.

[2] MERCADO, A., HALEVY, E., Determining the average porosity and permeability of a stratified aquifer with the aid of radioactive tracers, Water Resour. Res. 2 (1966) 525.

[3] ZUBER, A., "Theoretical possibilities of the two-well pulse method", these Proceedings II, IAEA-SM-182/45.

[4] LENDA, A., ZUBER, A., "Tracer dispersion in groundwater experiments", Isotope Hydrology 1970 (Proc. Symp. Vienna, 1970), IAEA, Vienna (1970) 619.

[5] KREFT, A., LENDA, A., A Fortran Program for the Interpretation of Porosity Measurements by the Two-Well Pulse Technique, Rep. No. 46/I, Institute of Nuclear Physics and Techniques, Academy of Mining and Metallurgy, Cracow (1974).

DISCUSSION

E. CUSTODIO GIMENA: Have you any experience of fractured media? If so, is it easy to interpret the curves obtained and do the permeability values coincide with those for other media?

A. LENDA: Many of our measurements were performed in fissured rocks, and the resulting breakthrough curves could be fitted fairly easily

using the theoretical solution which we had proposed previously.[1] They could not be fitted, however, using conventional solutions of the dispersion equation. As for the effective porosity values obtained by interpreting the curves, they were in all cases reasonable and in some cases confirmed by geological evidence.

A. ZUBER: I would add in this connection that our initial results were lower than had been expected by some hydrologists. There is now a mine in the region, however, and the interpretation of Z. Wilk and J. Motyka on the basis of the drainage effects attributable to the mine has confirmed our estimate.

I. SAINZ ORTIZ: Is the water velocity in porous media as calculated by your method the real velocity of the water in the pores of the soil, or is it the Darcy velocity? If it is the latter, you calculated the flow rate; if it is the former, you would have to take into account the effective porosity, which is not known with the precision necessary for it to be of practical use.

A. LENDA: We measure the mean transit times, from which particular parameters (such as effective porosity and transmissivity) are calculated. The Darcy velocity does not appear in explicit form in the formulas.

J. P. GAUDET: You attribute regular deformations of the tracer concentration curve to the superposition of two response curves each due to a different permeability layer. One could also attribute it, however, to the existence of different water flow velocities within a single layer with tracer exchange between the different flow lines. If there are different flow velocities, the apparent propagation velocity of the tracer is not the same as that of the water. Serious thought should be given to this phenomenon, which is particularly important when the effective porosity differs from the porosity of the porous medium.

I. J. WINOGRAD: Are any of the breakthrough curves for fissured rocks jagged?

A. LENDA: No, they are all smooth.

---

[1] LENDA, A., ZUBER, A., "Tracer dispersion in groundwater experiments", Isotope Hydrology 1970 (Proc. Symp. Vienna 1970), IAEA, Vienna (1970) 619.

INVESTIGATIONS OF EFFECTIVE POROSITY OF TILL BY MEANS OF A COMBINED SOIL-MOISTURE/DENSITY GAUGE

L. NORDBERG, S. MODIG,
Geological Survey of Sweden,
Stockholm,
Sweden

Abstract

INVESTIGATIONS OF EFFECTIVE POROSITY OF TILL BY MEANS OF A COMBINED SOIL MOISTURE/DENSITY GAUGE.

Effective porosity and processes of saturation and dewatering in till have been investigated. The study was performed in undisturbed till columns, surrounded by ring-shaped excavations filled with sand. The procedure allowed for a raising and lowering of an artificial groundwater level in the till under controlled conditions, which in turn made possible controlled processes of saturation and dewatering. A combined gamma-neutron soil moisture/density gauge was used. The water content was recorded during a period in which water was added to a specially prepared, undisturbed in-situ soil column until a state of saturation was reached. This was followed by a period of induced dewatering by gravity drainage. The drainage was recorded until a steady state, approximately equalling field capacity, was approached (5-16 d). Water contents at saturation are assumed approximately to equal total porosity, having a range of 17.9 - 32.0% in the investigated till. The intensity of drainage was highest on the first day of dewatering and then diminished with time. A perfectly steady state was never reached. Therefore field capacity is used with indices, indicating the length of time of drainage. Consequently, effective porosity is qualified by the corresponding indices. After 15 - 16 days of gravity drainage, effective porosity was calculated to be on the average 7.4% at one test plot and 3.4% at another. The difference has been attributed to a corresponding difference in depth to the natural groundwater level; because of the method used a higher groundwater level and capillary fringe may have hampered the complete drainage, resulting in a relatively low value of effective porosity. The investigation is most likely to be applicable in water balance studies, groundwater discharge predictions and various construction and waste-water projects in moraine terrain.

INTRODUCTION

Water balance projects within the framework of the International Hydrological Decade (IHD) in Sweden have focused an important part of their interest upon the problem of the effective porosity of till. To enable observed changes of groundwater level in an aquifer to be transformed into changes of water volumes, knowledge of the effective porosity is necessary. The characteristic, heterogeneous texture and structure of till complicates the determination of effective porosity, as it is very difficult to insert tubes into the ground without disturbing the soil considerably.

ABBREVIATIONS AND SYMBOLS USED IN THIS PAPER

n = porosity
n' = effective porosity
V_w = water content, volume of water
$V_{w\,max}$ = maximum water content, saturation
$V_{w\,D=15\,d}$ = water content after 15 days of drainage
gwl = groundwater level

DEFINITIONS

Total porosity (= porosity), n, stands for the total volume of all voids in a body of material, including closed pores.

Effective porosity (= specific yield) is "the ratio expressed as a percentage of the volume of water which, after being saturated, can be drained by gravity to its own volume" [1]. Because of the difficulties of determining in the field when a state of no further drainage is at hand, the effective porosity, in this paper, is referred to with an index, indicating the period of drainage, e.g. $n'_{D=15\,d}$.

Water content, in geotechnical literature, commonly stands for the ratio of volume of water to the dry weight of the material. In this paper, however, the hydrological definition is used, i.e. water content equals the ratio of water volume to total volume of a body. It is expressed as a volume percentage (V_w). The methods of this investigation, i.e. the neutron scattering technique, give the water content calculated from calibration functions produced by the instrument manufacturer (see below).

Saturation is the water content in a body of material when all interstices are filled with water. In this paper saturation, designated $V_{w\,max}$, is assumed approximately to equal total porosity.

Field capacity is defined as "the amount of water held in the soil after the excess gravitational water has drained away and after the rate of downward movement of water has materially decreased" [1]. Field capacity is expressed as a volume percentage. As for effective porosity, difficulties arise when determining the length of time necessary for drainage. Therefore field capacity, in this paper, is designated by indices indicating the time of drainage, e.g. $V_{w\,D=15\,d}$.

GEOLOGY OF THE AREA INVESTIGATED

During the latest glaciation the region investigated obtained its main geological surface features; they have been only very moderately altered through post-glacial activities. At least 75% of the area of Sweden is covered by till, i.e. a heterogeneous mixture of different grain sizes (boulders, stones, gravel, sand, silt, clay), deposited by the melting ice. The composition of the till reflects mainly the type of underlying bedrock at the point of sampling and at some distance in the direction from where the ice was moving. The most common type of bedrock in Sweden is Archaean granites and gneisses; therefore, most of the till is characterized by fragments of these rocks. The thickness of the till cover is relatively thin, exceeding 10 m in a few places only.

After a small-scale, introductory investigation in the IHD representative basin of Lappträsket in northern Sweden, the main investigation was performed in the IHD representative basin of Velen in southwestern Sweden (see map, Fig.1). These two representative basins are established and administered by the Swedish Meteorological and Hydrological Institute (SMHI).

The representative basin of Velen, an area of 45 km^2, is underlain by granites and gneisses. Minor outcrops of basic rocks are also found. The glacial overburden is dominated by sandy till, having a very varying boulder frequency. The composition of the till at the point of investigation is shown

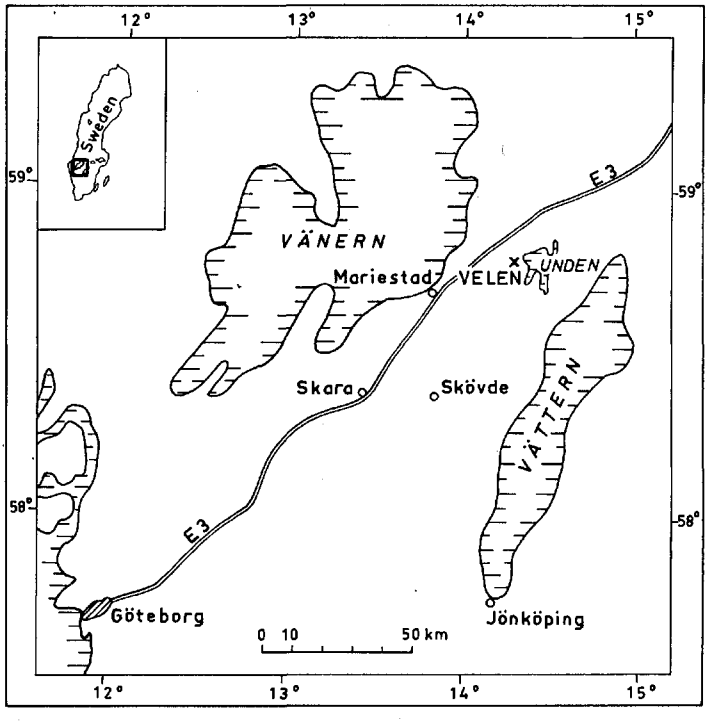

FIG. 1. Map showing the position (x) of the investigated area Velen.

in Fig. 15. The range of values refers to samples taken from the whole profile of investigation. In many parts of the area the till has a surface morphology of its own. Drumlin-shaped ridges in roughly a north-south direction are found as well as irregularly hilly terrain. Elsewhere the till forms an even cover conformable with the basement morphology.

The thickness of the till has been investigated within a centrally located part of the area [2]. The thickness was determined by seismic and electric resistivity measurements along five lines, having lengths of 350 m, 400 m, 450 m, 250 m and 90 m respectively. The mean thickness was found to be 4.6 m, 3.0 m, 3.4 m, 4.4 m and 4.8 m respectively. As the investigation covered different types of moraine terrain, the values obtained are regarded as representative for a larger area.

Some insignificant glaciofluvial deposits are also found within the basin. Some of them were formed supra-aquatically, and others were formed sub-aquatically. The maximum sea level reached 130 - 140 m above the present sea-level, which implies that the exposed parts of the lower portion of the basin were subject to wave-washing after the deglaciation. The intensity of the wave-washing is assumed to have been very moderate, and to have had little significant influence on the composition of the till.

After the retreat of the sea, the formation of peat began in many low-lying parts of the area. Nowadays 23% of the basin is covered by peat.

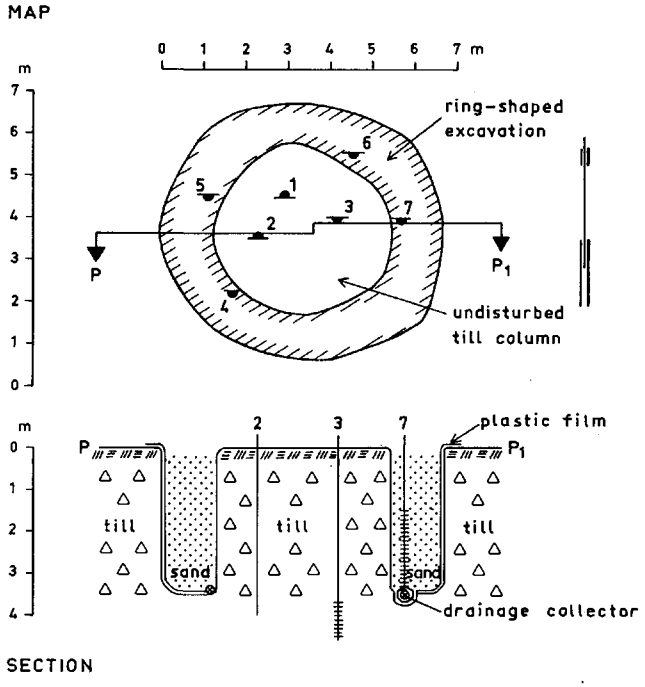

FIG. 2. Schematic map and section of a plot. Tubes 1 - 2 for gamma-neutron measurement, tubes 3 - 7 for observation of groundwater level.

PREPARATORY FIELD ARRANGEMENTS (Fig. 2)

After the preliminary seismic and geo-electrical investigations and percussion soundings had been completed, two test plots (A and B) were selected at a distance of 700 m from each other in the representative basin of Velen. The thickness of the soil at plot A was determined by soundings to be 4.6 m. Three iron tubes about 1.2 m equidistant in a triangle were hammered down to the bedrock. The tubes, with an inner diameter of 50 mm, were designated A 1, A 2 and A 3. Tubes A 1 and A 2 were equipped with a closed lower end; i.e. they were completely waterproof under the ground surface. They were installed as access tubes for gamma-neutron measurements, and were calibrated beforehand for these measurements. Tube A 3 was equipped with a perforated lower end allowing for free movement of water into and out of the tube. It was supposed to function as a regular groundwater level observation tube.

At plot B the sounded soil thickness exceeded 6 m. In conformity with the procedure at plot A, three similar tubes were installed, B 1, B 2 and B 3. However, the latter tubes did not penetrate the whole soil thickness, which, from the seismic investigation, was calculated to be 8 - 8.5 m.

In order to facilitate the work with artificial watering and dewatering of the undisturbed soil sequence at the test plots, a ring-shaped excavation

was made around each tube triangle, at a distance of 1.0 - 1.5 m from the tubes. In this way a free-standing column of undisturbed till was left, surrounded by the excavation. The diameter of the columns containing the tubes was 3.0 - 3.5 m, whereas the width of the circular trench excavations was 1 - 2 m. The depth of the excavation at plot A was a maximum of 2.8 m. The existing high groundwater level made further deepening impossible because of the risk of the soil column collapsing.

At plot B the excavation reached 3.5 m below the ground surface. No groundwater was encountered.

Immediately following the process of excavating, a sturdy plastic film was placed in position to cover the bottom and the outer walls of the excavations, in order to obtain a partially closed space defining the test areas. At the bottom of the excavation, encircling the till columns, drainage collectors with a diameter of 90 mm were positioned. From the collectors two perforated plastic tubes led to above ground. Another two plastic tubes were installed in each excavation for the control of water levels. After the installation of plastic film, drainage collectors and tubes, the ring-shaped excavations were filled with permeable coarse sand, which gave a support to the column and facilitated the raising and lowering of the artificial groundwater. Finally, the test areas were protected from precipitation and wind by shelters of tarpaulin and boards erected over the plots.

PROCESSES OF WATERING AND DEWATERING

In order to saturate the till columns, water was added to the sand-filled excavations after the preparatory field arrangements. In this way the water penetrated into the till from below and from the sides. This procedure allows for an effective removal of air during the process of saturation, as air can escape upwards relatively freely. The volume of trapped air after saturation is assumed to be negligible with this mode of action.

Initially 12 000 litres of pure water were added within a few hours to each plot. After that the water supply was continued by pumping from a nearby lake (plot A) and from a brook (plot B). A practically continuous water supply was in action for 6 and 12 days respectively. The supply was adjusted to maintain uninterruptedly a free water surface above the sand in the excavations.

When full saturation was assumed to be present in the till columns (the assumptions being verified by minor diggings in the till) the supply of water was terminated. The watering process was followed by a process of dewatering, enforced by continuous pumping from the plastic tubes in the excavations. The water level was kept close to the bottom of the excavations. The pumped water was run into the lake and brook respectively. The process of dewatering was studied intensively for 15 and 16 days respectively.

METHOD FOR MEASUREMENTS OF WATER CONTENT

A combined soil moisture/density gauge, type BASC, was used. The instrument, manufactured by Nordisk Elektrisk Apparatfabrik, Copenhagen,

Denmark, utilizes gamma-ray absorption for the determination of wet soil density and neutron scattering for the determination of soil moisture. The BASC instrument has been described by Somer [3]. As this report deals with the hydrogeological application of the instrument no further discussion of it is made; reference is made to Jensen and Somer [4] and Somer [3]. Calibration functions for the tubes used in the investigation were supplied by the manufacturer.

MEASURING PROGRAMME

At the two test plots, reference measurements were made before the beginning of excavation and water supply processes to obtain values of natural water content. Readings were taken on every 10th cm from the depth level of 100 cm to the bottom of the tubes. From the day after the beginning of the addition of water, readings were made at an interval of about 24 hours throughout the periods of watering and dewatering. A total of 2687 readings of water content were made during the period of observation, i.e. from 18 September to 19 October 1972.

In order to trace the changing, artificial groundwater level during watering and dewatering, the level was gauged in tubes A 3 and B 3 several times daily during the investigation.

RESULTS

The main results of the measurements are presented in Figs 3-10 and 12-13. All measuring levels, referred to below, indicate the depth in centimetres below the ground surface.

The dry density of the till was measured with the gamma probe. At tube A 1 (levels 100 - 445 cm) the range was found to be from 1.59 to 2.10 g/cm^3, with a mean value of 1.79. At tube A 2 (levels 100 - 420 cm), corresponding values were 1.65 - 2.08 and 1.85. At tubes B 1 (levels 100 - 336 cm) and B 2 (levels 100 - 370 cm), the values were 1.49 - 1.84 (1.65) and 1.57 - 1.89 (1.74) respectively.

PLOT A, TUBE A 1 (Figs 3 - 4)

The initial, natural water content in the investigated soil column (100 - 445 cm) ranges from 18.3 - 30.8%. The range within the depth interval 100 - 170 cm was 21.7 - 26.8%. The corresponding groundwater surface was located at 122 cm, which is assumed to be in the middle of the zone of groundwater variation.

Water was added to the till column for six consecutive days. In this way the groundwater level was raised by 74 cm and after the six days of watering the column was assumed to be saturated from 60 cm downwards. Water content at saturation ranges from 17.9 - 30.8% through the investigated profile, with a mean value of 24.6%. These values express the total porosity of the till. It is noteworthy that the highest values refer to the deep levels in the profile, whereas the upper levels consistently have smaller values of porosity. Contrary conditions were expected as the influence of frost and

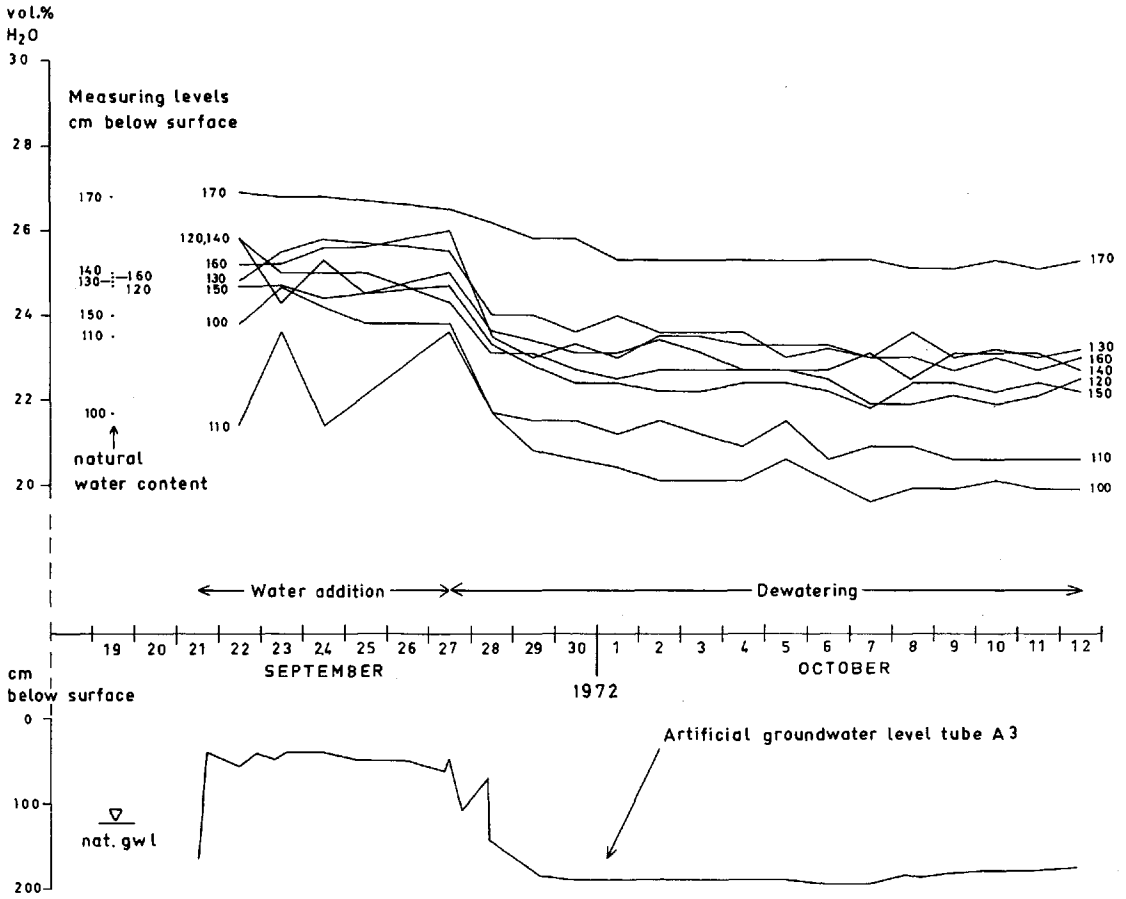

FIG. 3. Tube A 1: water content during water addition and dewatering; measuring levels 100 - 170 cm below surface.

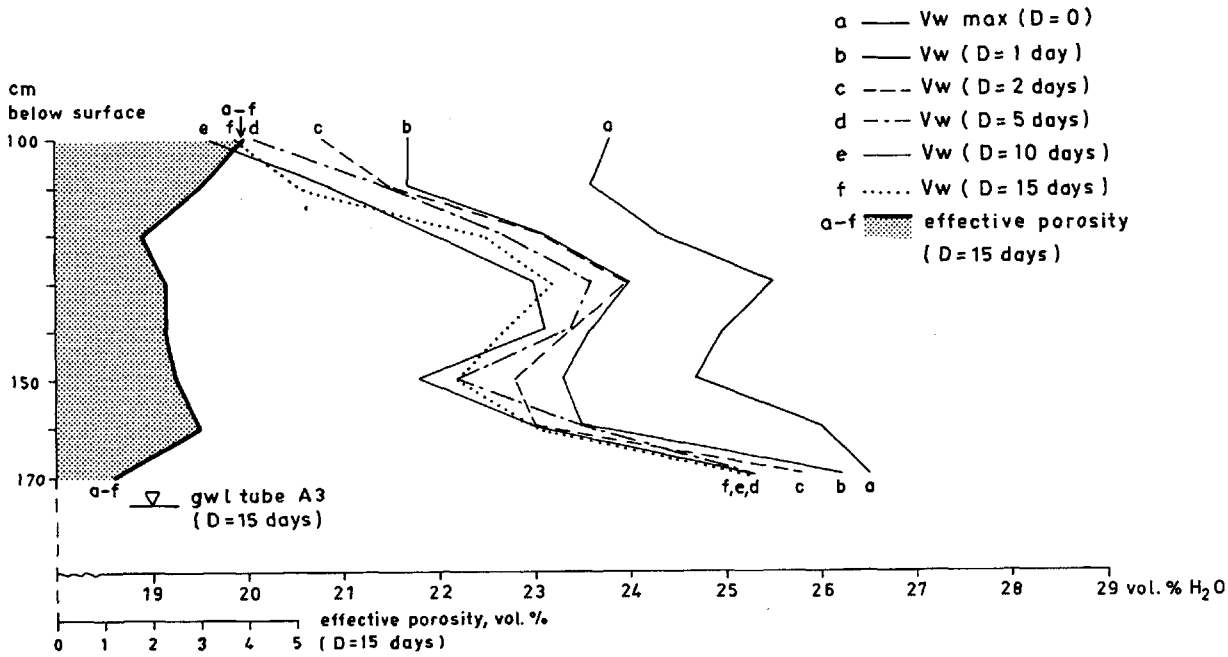

FIG. 4. Tube A 1: water content after different periods of dewatering and effective porosity after 15 days of drainage; note the difference in scale.

root wedging on the soil decreases with increasing depth. No indications of soil processes were seen below 70 cm when inspecting the trench walls at the time of excavation. After six days of watering, the process of dewatering began. The withdrawal of water, which is wholly attributed to drainage by gravitation, was most intensive during the first day of drainage. Approximately 50% of the totally withdrawn water was drained during the first day. The process of dewatering was studied for 15 days. Daily observations of the artificial groundwater level in the till column were made in tube A 3. Almost steady water content conditions were obtained after 5 - 10 days (Fig. 3).

The values of effective porosity after 15 days of drainage (D - 15 d) range from 1.2 - 3.9% with a mean value of 2.5%. Because of incomplete dewatering below 180 cm, no calculations of effective porosity are presented from a greater depth.

PLOT A, TUBE A 2 (Figs 5 - 6)

The initial, natural water content in the investigated profile (100 - 420 cm) ranges from 19.7 - 32.3%. In the depth interval of 100 - 170 cm the corresponding values are 25.8 - 30.4%. Because of the high-lying groundwater level at plot A, these values correspond approximately to full saturation. After six days of watering the investigated till column was assumed to be saturated. The total porosity of the soil profile ranges from 19.3 - 31.9% with a mean value of 24.2%. The highest values are found within the depth interval 100 - 280 cm, whereas smaller values are obtained at greater depth.

The watering process was terminated after six days, and an initially rapid water withdrawal was noted. After 5 - 10 days of drainage almost steady water content conditions were obtained. Effective porosity, calculated after 15 days of drainage, in the depth interval 100 - 170 cm, ranges from 1.1 - 8.0% with a mean value of 4.3%. The values of effective porosity for the levels presented decrease with increasing depth, which corresponds to an analogous distribution of values of total porosity.

PLOT B, TUBE B 1 (Figs 7 - 8)

The natural groundwater level at plot B is permanently located considerably deeper than at plot A. Both in April and September 1972 the depth to the water at plot B was sounded to exceed 4.4 m. Therefore, the natural water content in the till column at plot B is lower than at plot A. The range of natural water content at tube B 1 was measured as 20.7 - 27.7%. After 12 days of watering a state of saturation was present in the column. The values of water content obtained at saturation correspond to total porosity at various levels in the till column. The range is 20.7 - 32.0% with a mean value of 26.4%. The highest values refer to the levels 230 - 260 cm and 110 - 120 cm.

Because of technical difficulties with the pump equipment the water supply was temporarily interrupted during the process of watering. An insufficient supply of water to the upper levels on 25 - 27 September caused a considerable decrease in water content at the levels 100 - 130 cm (Figs 7 - 8). On the twelfth day of watering, minor diggings in the till column confirmed saturation from 20 cm downwards.

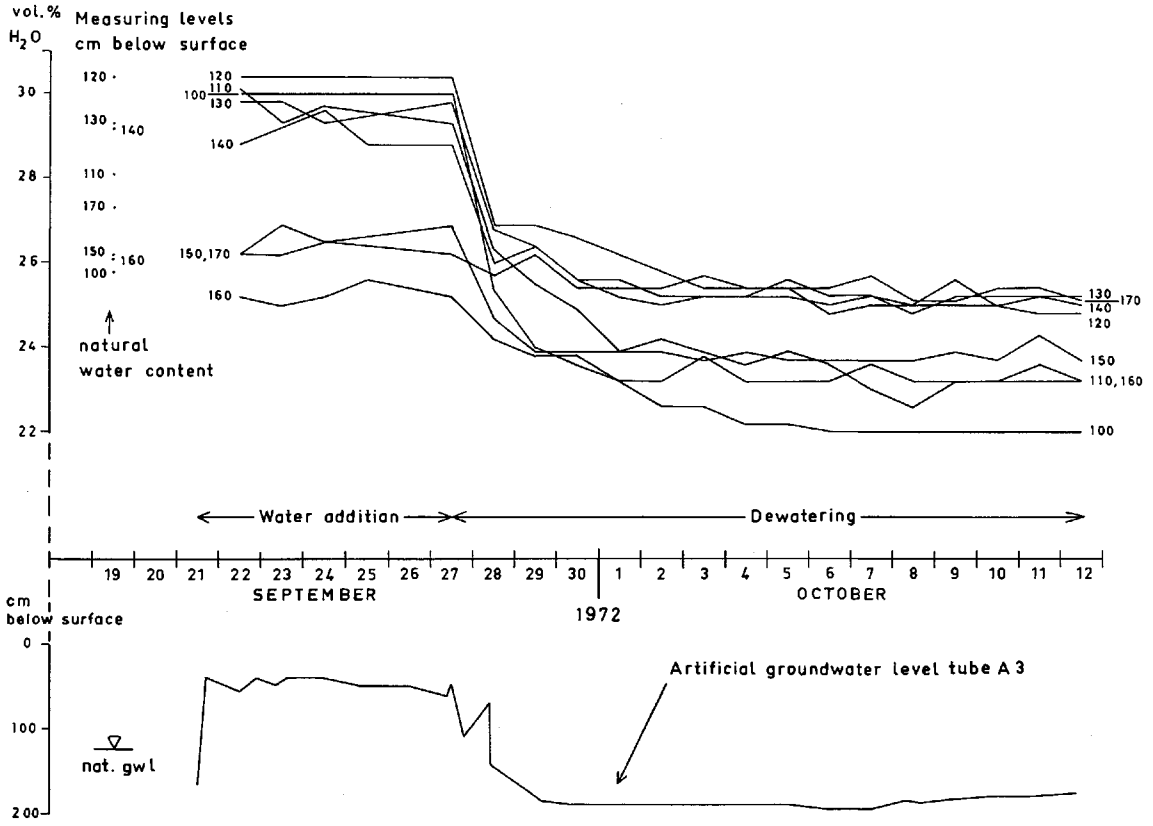

FIG. 5. Tube A 2: water content during water addition and dewatering; measuring levels 100 - 170 cm below surface.

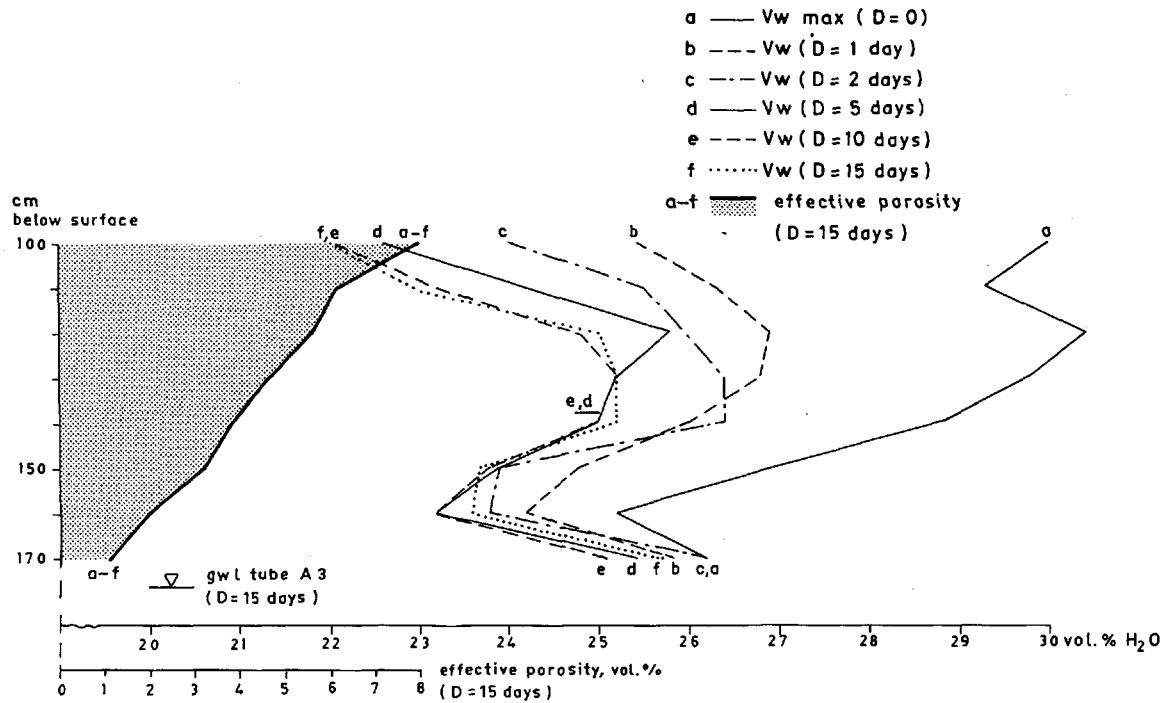

FIG. 6. Tube A 2: water content after different periods of dewatering and effective porosity after 15 days of drainage; note the difference in scale.

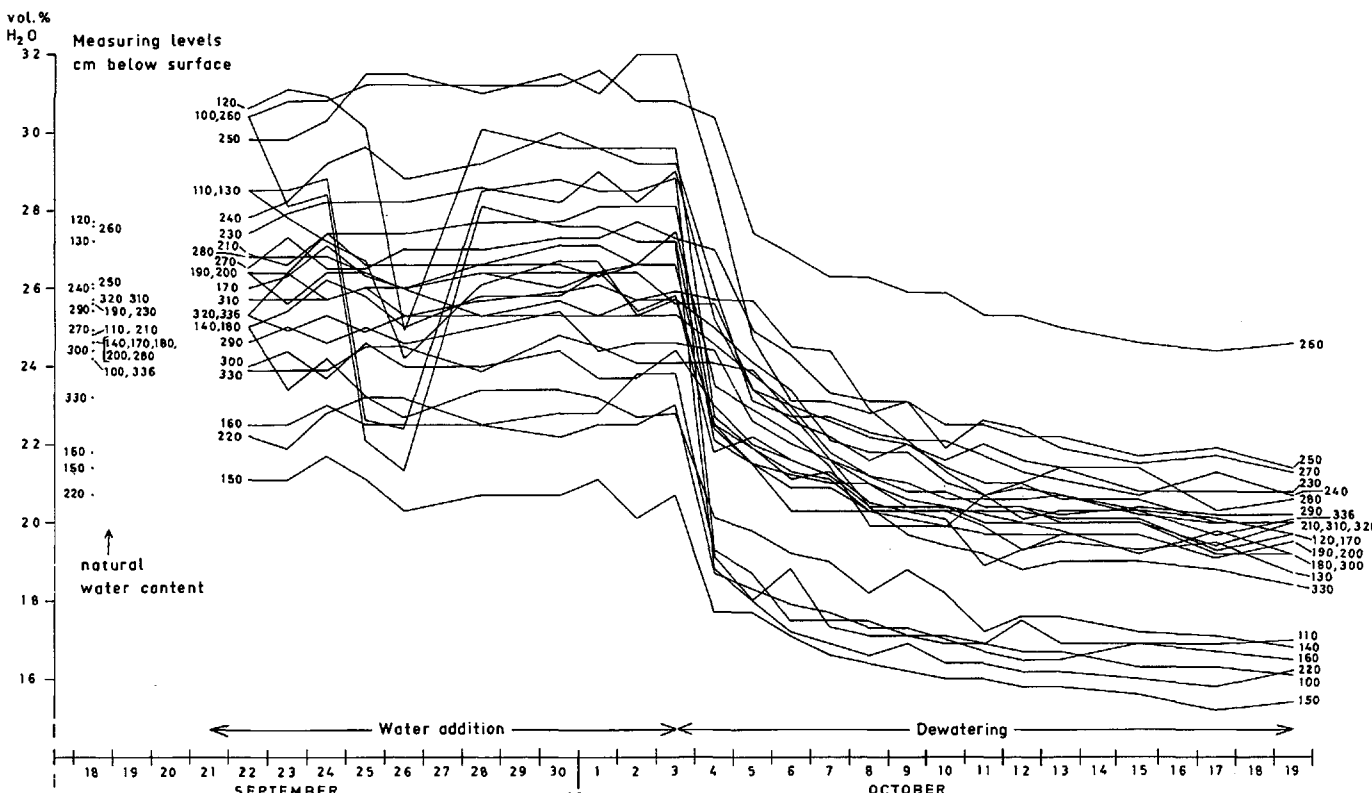
vol.%
H_2O
Measuring levels
cm below surface
natural
water content
Water addition
Dewatering
SEPTEMBER
OCTOBER
1972

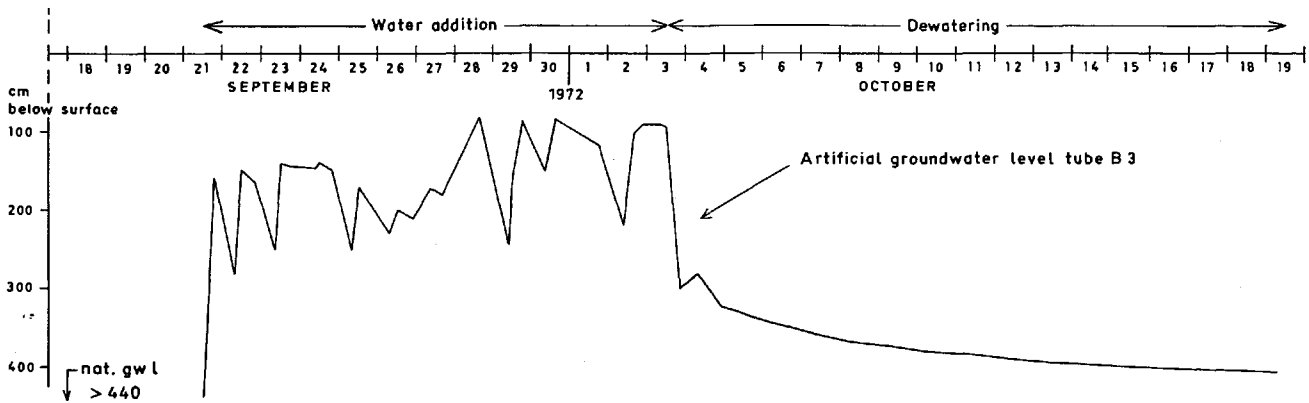

FIG. 7. Tube B 1: water content during water addition and dewatering; measuring levels 100 - 336 cm below surface.

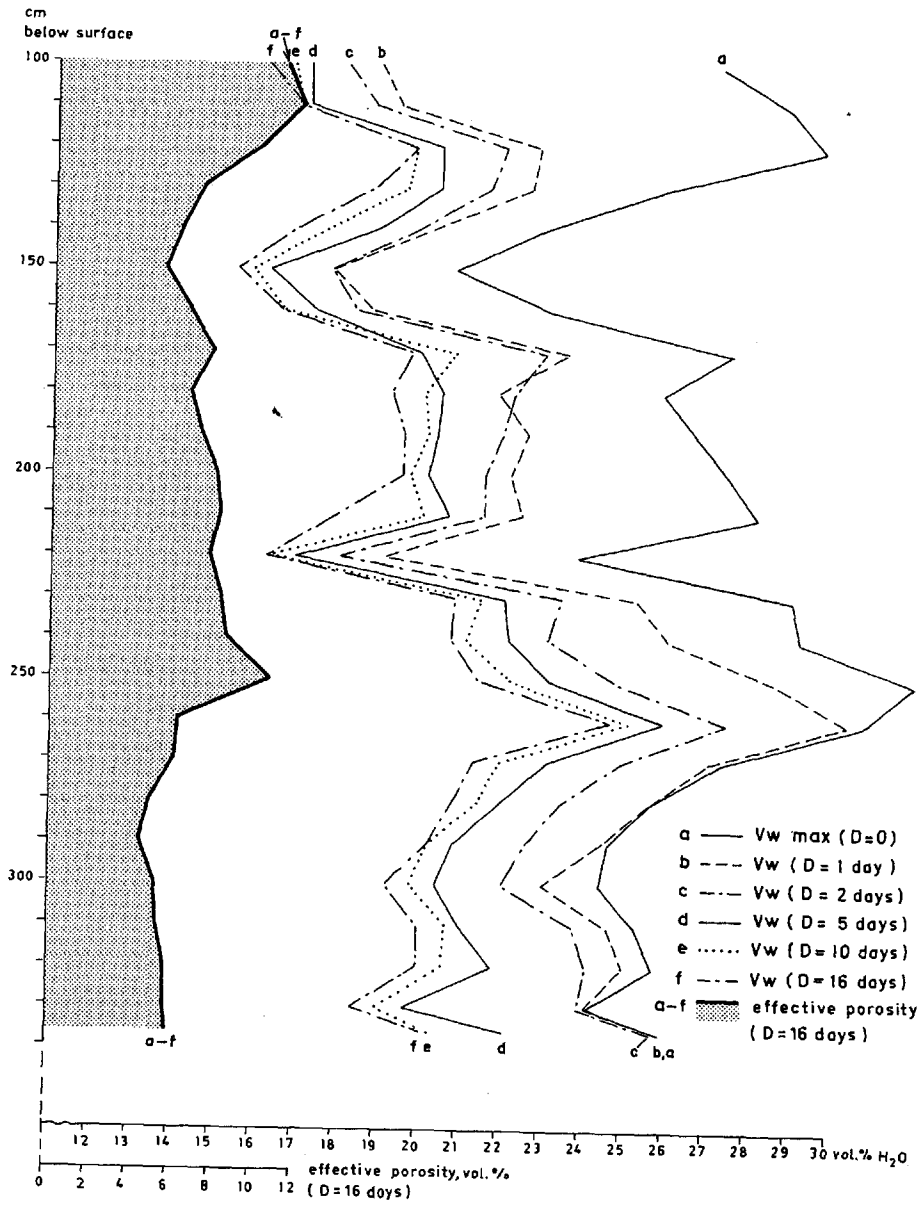

FIG. 8. Tube B 1: water content after different periods of dewatering and effective porosity after 16 days of drainage; note the difference in scale.

After one day of drainage, approximately half the totally withdrawn water from the depth interval 100 - 250 cm had vanished.

From the levels investigated below 250 cm, however, only about 10% was withdrawn in one day (Fig.8). After two days, 30 - 50% of the totally withdrawn water had drained from the depth interval of 260 - 320 cm. Relatively steady conditions were reached after 10 - 15 days.

The value of effective porosity increases with duration of drainage until steady conditions are reached. After 16 days (D = 16 d) the range through the profile is 4.4 - 11.8% with a mean value of 7.2%. There is a trend towards decreasing values of effective porosity with increasing depth.

At the beginning of the dewatering period, the artificial groundwater level fell very rapidly. After one day the level was more than 3 m below the ground surface, and after 16 days the groundwater level had fallen to more than 4 m below the ground surface. Therefore, on the latter occasion, the conditions at the investigated levels are assumed not to be directly influenced by the artificial groundwater.

PLOT B, TUBE B 2 (Figs 9 - 10)

The initial, natural water content, measured in tube B 2, ranges from 17.9 - 30.2%. Total porosity, calculated from the values of water content at saturation, ranges from 21.0 - 28.9% with a mean value of 25.4%. The highest values refer to the levels 200 - 240, 110 - 120 and 370 cm.

After one day of drainage approximately half of the totally withdrawn water from the depth interval of 100 - 260 cm had left that zone. During the second day of drainage a further considerable withdrawal took place, in particular from the levels of 270 - 330 cm. A state of relatively steady conditions was present after 10 - 15 days of dewatering.

The effective porosity, calculated after 16 days of drainage, ranges from 2.8 - 11.0% with a mean value of 7.5%.

DISCUSSION OF RESULTS FROM PLOTS A AND B

The initial, natural water content at the two investigated plots ranges from 17.9 - 32.3%. Because of the initially high groundwater level at plot A, the values of natural water content correspond fairly well with values of saturation. The values at plot B, with a considerably lower groundwater level, were expected to be correspondingly lower. The calculated difference, however, is rather small, which is assumed to be caused by the presence of percolating soil water in the unsaturated zone. Because of earlier rainfalls the water content in the unsaturated zone was above field capacity. This circumstance has been verified by soil-moisture measurements at adjacent stations within the basin. This is also clearly demonstrated by groundwater level variations and precipitation from nearby observation stations (Fig.11).

Values of water content at saturation, i.e. total porosity, at plots A and B range from 17.9 - 32.0%. The mean value for all measurements at plot A is 24.5% and at plot B 25.9%.

The process of drainage is very similar in the four investigated soil profiles. All measured levels at tubes A 1 and A 2 and levels from 100 to

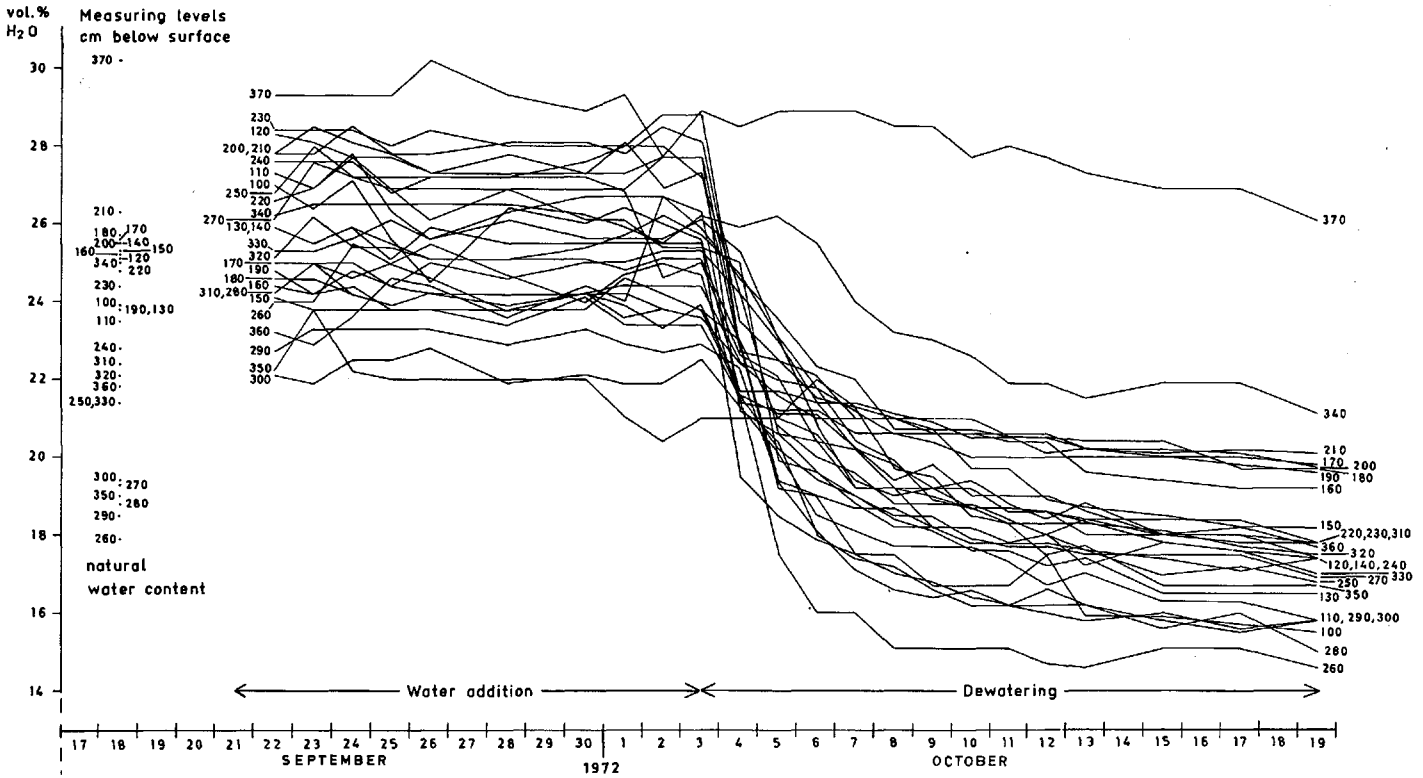
vol.% H_2O
Measuring levels cm below surface
natural water content
Water addition
Dewatering
SEPTEMBER
OCTOBER
1972

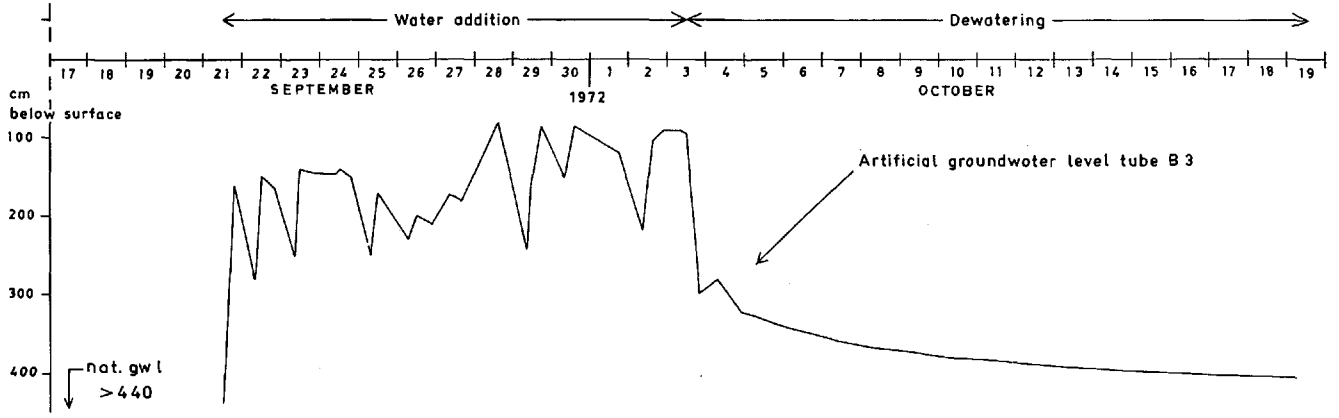

FIG. 9. Tube B 2: water content during water addition and dewatering; measuring levels 100 - 370 cm below surface.

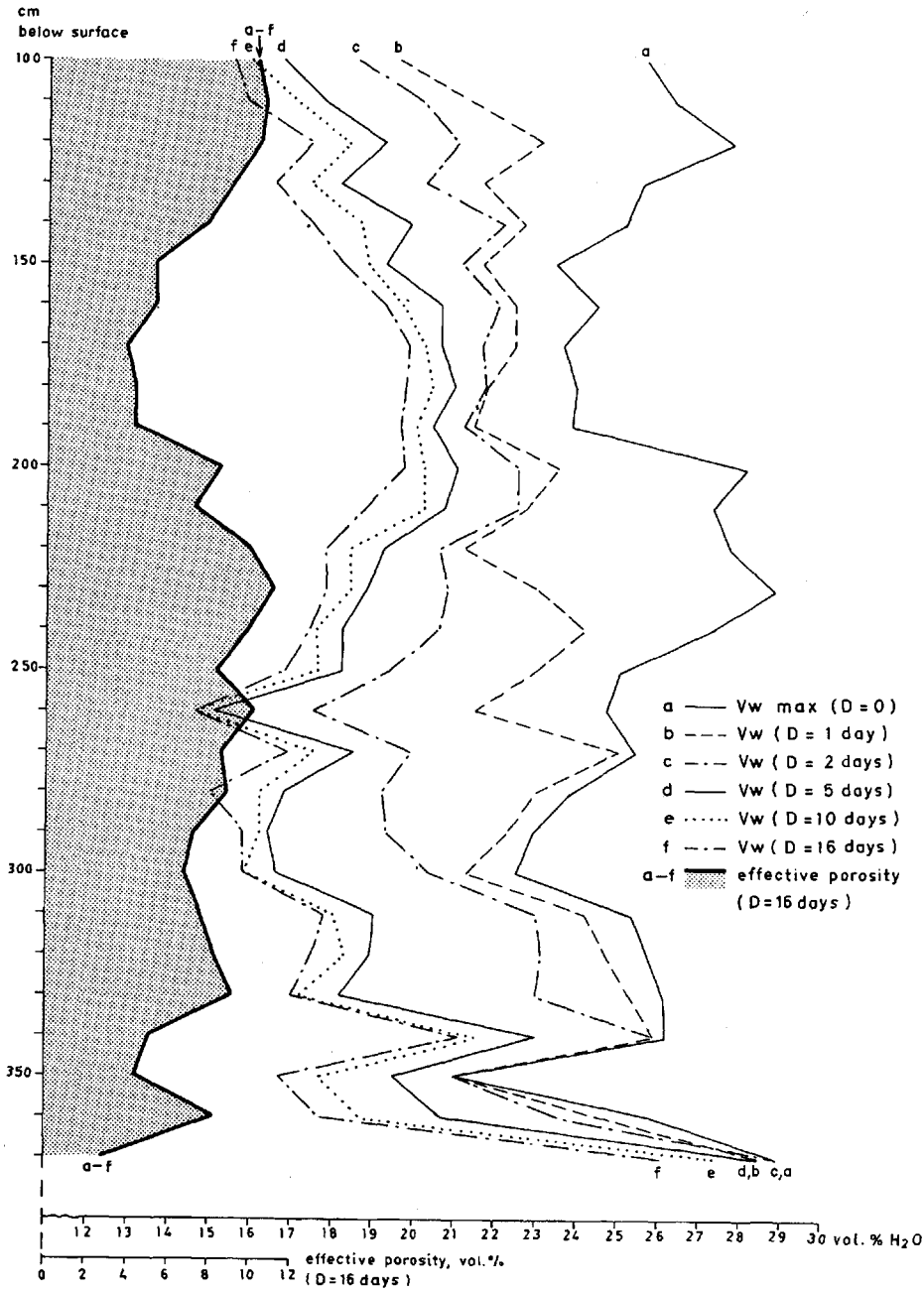

FIG. 10. Tube B 2: water content after different periods of dewatering and effective porosity after 16 days of drainage; note the difference in scale.

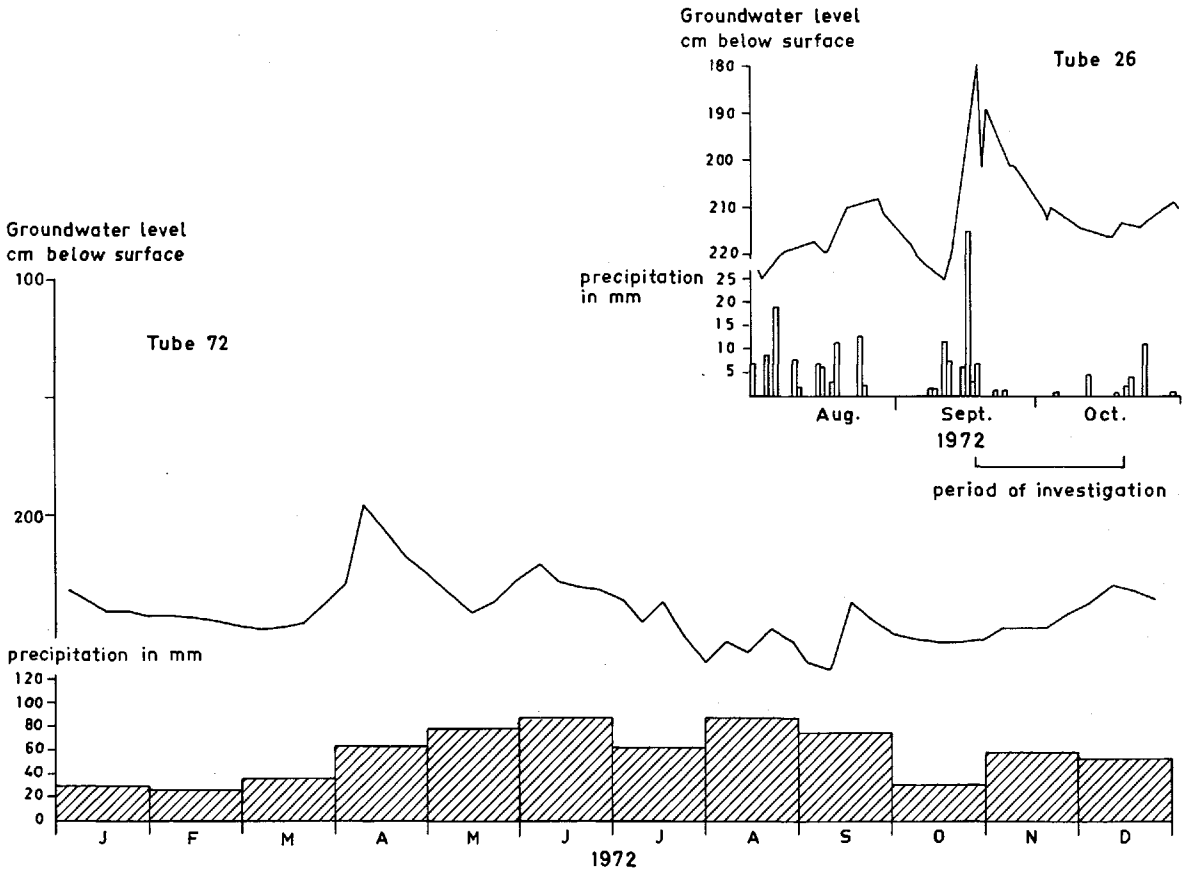

FIG. 11. Precipitation and groundwater level at two stations adjacent to the plots.

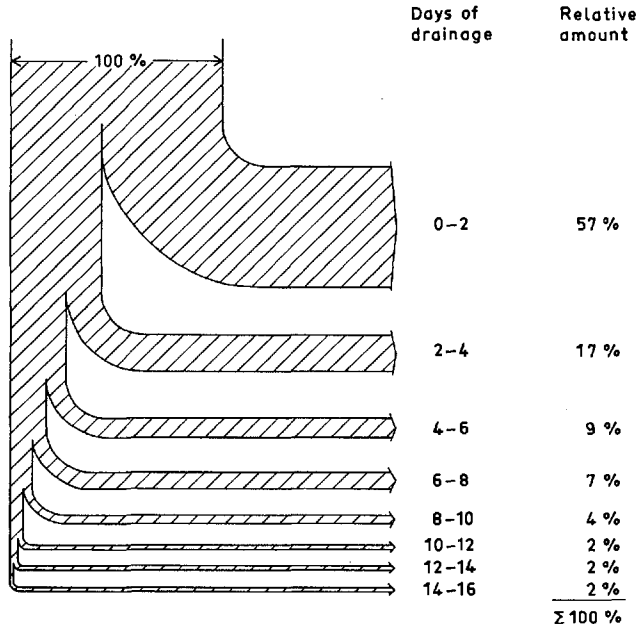

FIG. 12. Sankey diagram of the relative amount of dewatering from 0 to 16 days. The percentage figures are the arithmetic mean of the effective porosity from the whole profiles B 1 and B 2. The arithmetic mean after 16 days of drainage equals 100%.

200 cm at tubes B 1 and B 2 were drained by about half the totally withdrawn volume of water during the first day of dewatering. A corresponding portion of water was drained from the 250 - 330 cm depth interval at tubes B 1 and B 2 in two days. The levels investigated beneath 330 cm were drained by 50% of the totally withdrawn water in three days. A similar time lag in the process of drainage was not discernible at plot A because of the small thickness of the investigated profile.

The process described is visualized in Fig. 12. The arithmetic mean value of the effective porosity from the whole profiles B 1 and B 2 after 16 days of drainage (7.4% by volume) equals 100%. The time of drainage is divided into intervals of two days.

Field capacity is defined in this paper as the "amount of water held in the soil after the excess gravitational water has drained away and after the rate of downward movement of water has materially decreased". To investigate when this state was reached in the soil columns, the process of drainage was recorded for as long a period as 15 and 16 days respectively. It was concluded that steady conditions were approached after 5 - 15 days of drainage (Fig. 13).

The water content was also recorded at 5, 7 and 12 months after the beginning of dewatering; during this period, however, the plots were not sheltered from precipitation. The lower levels at plot B showed continuously decreasing values of water content, amounting to about 0.5 - 1.0% further drainage compared with the state after 16 days of drainage. At higher levels and at plot A the water content increased.

Accordingly, the effective porosity was calculated after 15 days (plot A) and 16 days (plot B). The values of effective porosity at plot A (levels 100 - 170 cm) range from 1.1 - 8.0% with a mean value of 3.4%. The corresponding range at plot B (levels 100 - 370 cm) is 2.8 - 11.8% with a mean value of 7.4%. The frequency distribution of the values obtained is shown in a histogram, Fig. 14, where the material is grouped in classes with one per cent intervals.

The remarkably large difference in effective porosity between plots A and B is tentatively explained by the presence, at plot A, of capillary water due to the high groundwater level. This explanation is supported by the evident similarity with respect to density, natural and maximum water content and drainage characteristics at the two plots. It should be noted, however, that the till in itself, because of its heterogeneous composition, contains a wide range of values of effective porosity even in one limited locality.

No significant difference in the composition of the till was noted when making the excavations. Results of analyses of soil samples from the two plots are shown in Fig. 15. It is clearly demonstrated that the till at the two plots is almost identical in composition. This type of sandy till is representative of large areas in Sweden. Therefore, the values obtained are assumed to have validity also for areas outside the representative basin of Velen.

CONCLUSIONS

The results obtained are assumed to demonstrate that the value of effective porosity varies with the soil-water situation at the moment of gauging and whether the capillary zone influences this situation or not. Effective porosity, calculated from water contents that are influenced by the capillary zone, may reach a higher value when such an influence ceases. A contrary change may take place if conditions are the opposite.

When calculating the effective porosity in the zone of rise of a rising groundwater level, attention might be paid to the soil-water situation in the unsaturated zone, as this situation controls the volume available for the rising groundwater.

When calculating the effective porosity at falling groundwater levels, due attention should be paid to the period of time that has elapsed since the beginning of drainage.

The principle of how the effective porosity is affected by soil-water and groundwater conditions is schematically shown in Fig. 16. Case 1 is assumed to be indicative of plot A, whereas case 2 probably characterizes plot B. This means that higher values of effective porosity should have been obtained at plot A if the groundwater level could have been lowered further during the period of measurements.

Generally speaking, conditions represented by plot A are assumed to be the most common type of situation in the zone of groundwater variation in till. This zone is of the utmost importance for water balance calculations. Nevertheless, conditions represented by plot B are probably present temporarily during the year. Thus it is of interest, when making water balance calculations in moraine terrain, to evaluate the duration of various soil-water and groundwater conditions.

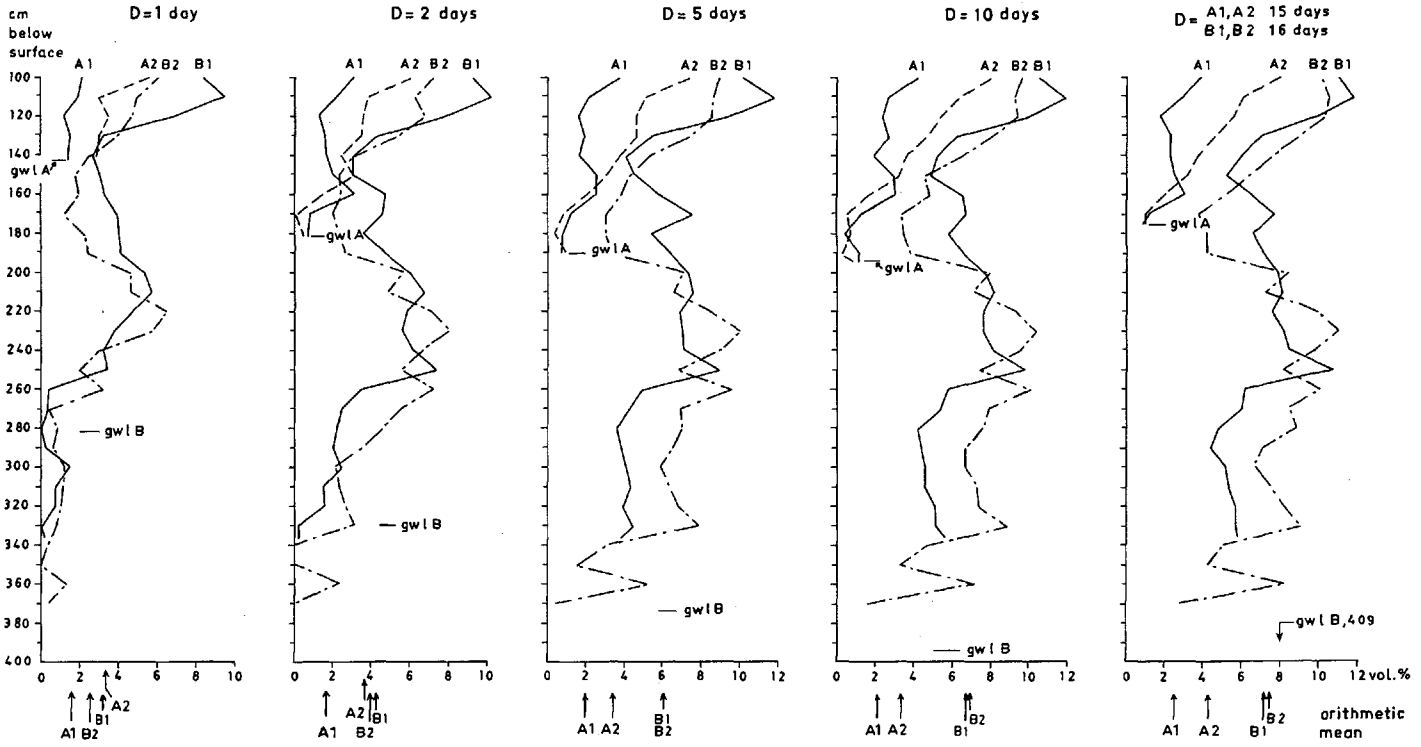

FIG. 13. Effective porosity after different periods of dewatering; note the increase of the arithmetic means from 1 to 15 and 16 days.

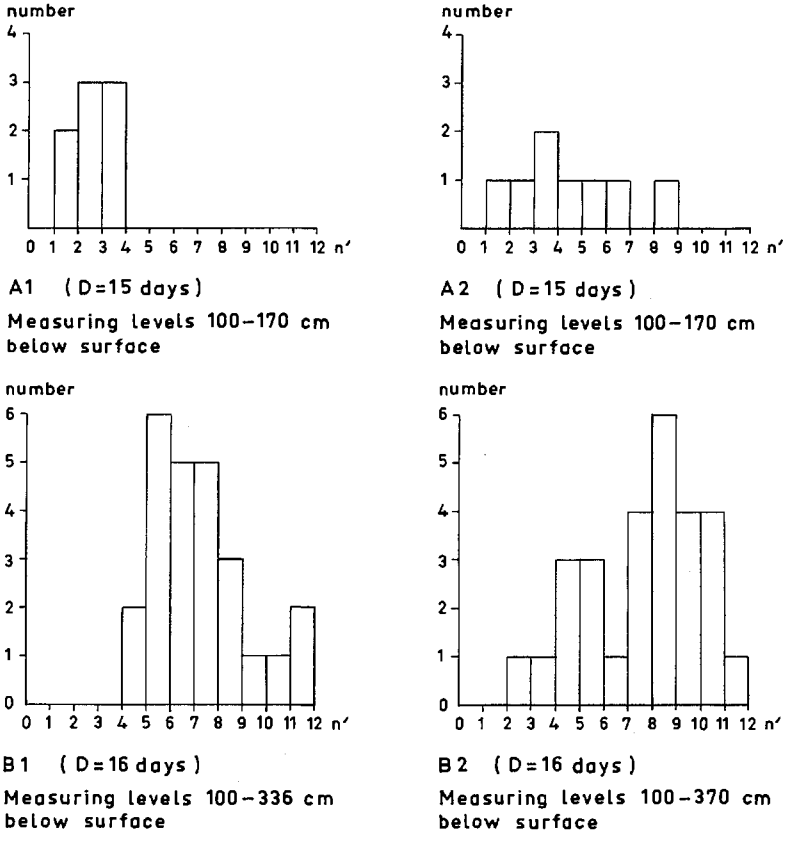

FIG. 14. Histograms of the distribution of the effective porosity: n' = effective porosity (percentage by volume).

PERMEABILITY

In order to obtain information on the permeability of the till, two soil samples were analysed in a compressometer at the Swedish Geotechnical Institute, Stockholm. The k-values were found to be $2.5 \cdot 10^{-6}$ and $2 \cdot 10^{-6}$ m/s respectively. The corresponding dry density was determined as 1.86 and 1.93 g/cm^3 respectively. The k-values indicate that the investigated soil represents a rather permeable variant of till.

CONTROL OF OBTAINED RESULTS

In order to study the influence of disturbances introduced along the access tubes when they were hammered down, the tubes were carefully relieved from the surrounding till by digging after the measurements had finished. This procedure also allowed for a close-up examination of stones and boulders adjacent to the tubes.

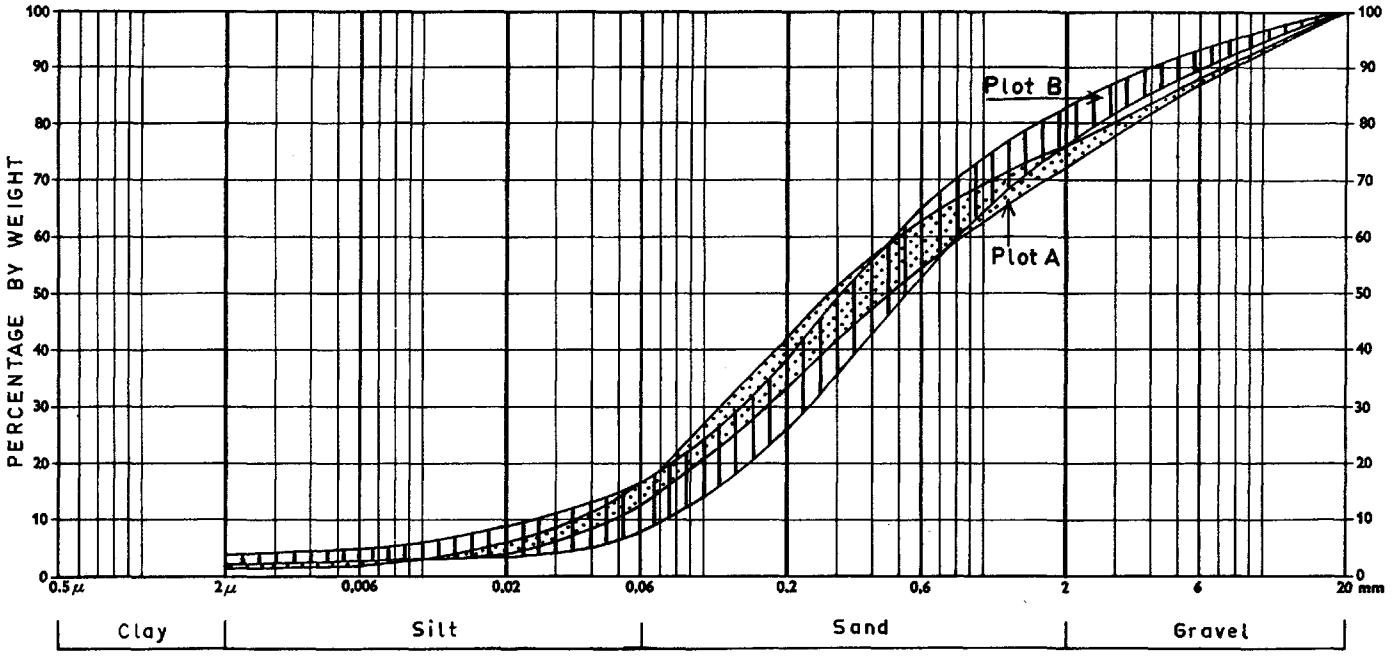

FIG. 15. Field of cumulative curves showing the composition of the till of plots A and B respectively.

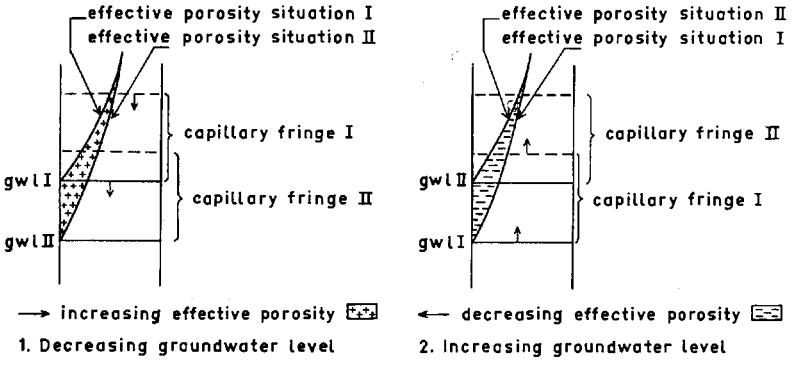

FIG. 16. Sketch showing the variation of the effective porosity with varying conditions of groundwater level and capillary fringe.

Two major disturbances were found along the tubes, the largest being a void space around tube A 2 at the 40 - 100 cm levels. This void, with a maximum width of 5 cm, is assumed to have been caused by swinging vibrations in the tube when it reached underlying bedrock and percussion continued for a short time. The disturbance may have been the cause of the high values of total and effective porosity at the 100 - 120 cm levels. Higher levels were not measured.

A corresponding disturbance, although of less size and extension, at the 90 - 110 cm levels around tube B 1, may have caused the high values of porosity at the 100 - 120 cm levels.

Stones and boulders in close contact with the tubes are generally reflected by a higher value of density at the levels of contact.

The study of structure and texture around the tubes has shown the need for this type of examination. The interpretation of data obtained is highly facilitated by the availability of information on soil structure and texture immediately around the access tubes. Disturbances caused by the installation of tubes are likely to be abundant in till. This has been shown by Nordberg and Modig [2] from previous investigations. Stones and boulders in the till, when hit by the point of the access tube, are easily pushed some way ahead of the tube or to the side, thus creating voids and hollows along the tube.

FURTHER INVESTIGATIONS

Measurements performed with the combined soil moisture/density gauge have produced interesting results. As the effective sphere of measurement is rather large (diameter 20 - 80 cm), an average value of different porosities is obtained. It is desirable that measurements be made in the whole zone of groundwater variation in several tubes. The effects of disturbances along the access tubes should be studied by a careful removal of soil from around the tubes. The present investigation will be continued by laboratory tests on undisturbed soil samples taken from the till columns of plots A and B. This work is underway. The final results of the project are planned to be published in 1974 in publication series C of the Geological Survey of Sweden.

The conventional method of studying effective porosity (= specific yield), i.e. pumping tests, are not very well suited for till, as the inhomogeneities of the soil impair the calculations. In localized areas the till has been found to be very hard, containing thin layers of silt and sand. Water may move rather freely through the layers and along cracks and root channels, whereas the surrounding material has a very low permeability. In such areas the depression cone from pumping, if any, will be completely irregular.

Another method of investigation is offered by an analysis of recession curves of selected rivers or brooks. It can be assumed that a dominating share of the winter discharge of rivers in northern Sweden is made up of groundwater. No replenishment of groundwater takes place because of the frozen ground; precipitation is accumulated as snow. Systematic observation of groundwater levels in a well-defined watershed in moraine terrain, therefore, may contribute information on the water-yielding capacity of the till.

Finally, the water balance method should be mentioned. Changes of the groundwater storage within a basin can be calculated if all other variables of the water balance equation are known. So far, this method is not satisfactory as other variables, e.g. soil-water storage, are insufficiently well calculated.

APPLICATIONS

The results obtained will improve the water balance calculations from the representative basin of Velen. The values presented of effective porosity agree well with previous, qualified assumptions, arrived at by the tentative use of the water balance method. This investigation, however, proposes the use of different values on effective porosity according to the current soil-moisture state of the unsaturated zone. This proposal refers to monthly water balance calculations; for annual calculations this distinction could be omitted.

With the extrapolation of values to northern Sweden, the investigation will furnish material for a better understanding of the volume of groundwater discharge into lakes, rivers and brooks in moraine terrain. In future the knowledge of the effective porosity of till will contribute to the improvement of forecasts of winter discharge of rivers used for hydroelectric power plants.

Knowledge of the quantitative and qualitative behaviour of saturation and dewatering of till facilitates judgements involved in the planning of various types of construction work in moraine terrain.

The investigation has also contributed to the knowledge of how water moves in till. The effective porosity controls the true permeability of the soil. Thus, the investigation has a bearing on the problem of wastewater management in moraine terrain, including judgements on proper and optimal locations of disposal dumps in such terrain.

ACKNOWLEDGEMENTS

The investigation described here was partly financed with grants from the Swedish Natural Science Research Council (the Swedish Committee for

the IHD), and partly from the Geological Survey of Sweden. The work was performed within the framework of the national groundwater network of Sweden, which is a long-term project of the Geological Survey of Sweden.

Å. Hörnsten, chief geologist with the Geological Survey and project leader, has followed this work from the first field-reconnoitring to the present report. He has followed the investigation with great interest and has also critically read the manuscript.

The drawings were made by G. Hellström, U. Skarin, I. Palmaer and A.-C. Sjöberg. The manuscript was typed by K. Brodén.

REFERENCES

[1] TODD, D.K., Ground Water Hydrology, Wiley, New York (1967).

[2] NORDBERG, L., MODIG, S., Försök till bestämning av effektiv porositet i morän (An attempt to determine the effective porosity of till), Swedish Natural Science Research Council, IHD Rep. No. 30, Stockholm (1973).

[3] SOMER, E., "The BASC Combined Soil/Density Equipment produced by NEA, Copenhagen", Int. Symp. on Radiometric Methods and Instruments for the Determination of Density and Moisture of Building Materials and Soils, Brno, 1969.

[4] JENSEN, P.A., SOMER, E., "Scintillation techniques in soil-moisture and density measurements", Isotope and Radiation Techniques in Soil Physics and Irrigation Studies (Proc. Symp., Istanbul, 1967), IAEA, Vienna (1967) 31.

DISCUSSION

A.L. BENTZ: I disagree with your assumption that the volume of trapped air is negligible after "saturation". If one takes your mean dry density value of 1.79 g/cm^3 for tube A 1 and assumes the specific gravity to be about 2.65 g/cm^3, from the formula $n = 1 - \frac{\text{dry density}}{\text{specific gravity}}$ one obtains a total porosity of some 32%. Even below the groundwater level the humidity fluctuates around 26%, giving a degree of saturation of about 80%. Would you care to comment?

L.O. NORDBERG: One should not pay too much attention to the exact dry density values. The disturbances along the tubes, which are mentioned in the paper, may explain part of the discrepancy pointed out by you.

A.L. BENTZ: What is the accuracy of your neutron probe for absolute measurements?

L.O. NORDBERG: It is supposed to be about ±1%.

A.L. BENTZ: Why did the groundwater level of plot A fall to 193 cm on day 10 and rise to 172 cm on day 15?

L.O. NORDBERG: It may have been due to a pump failure at the end of the investigation period.

A.L. BENTZ: What was the shape of the bottoms of the tubes which you hammered into the ground?

L.O. NORDBERG: They were pointed.

A.L. BENTZ: It is a pity that you did not carry out permeability measurements using the auger hole method of Ernst (Wageningen, Netherlands), which is widely used in agriculture for drainage purposes.

L.O. NORDBERG: The groundwater tubes were perforated only at the bottom ends and therefore not very suitable for permeability measurements in the zones investigated by the probe.

J.W. HOLMES: Do you not think that changes in soil porosity and pore size as a result of hammering the access tubes into the ground may significantly affect the measurement of effective porosity?

L.O. NORDBERG: Yes, they may; in fact, I am worried about the effects of disturbances around the tubes. In general, however, the compression around the tubes is restricted to a fairly small fraction of the volume of the effective measuring sphere.

Because of the composition of the till, which includes boulders and stones, it is extremely difficult to use augering methods for installing the tubes, so that an error is introduced. In my opinion, however, greater errors are introduced by the creation of voids around the tubes as they are hammered down, so that it is important to examine in detail the soil profiles along the tubes; such examinations may explain deviating values.

J.P. GAUDET: With regard to the discrepancy found between porosity and maximum water content, I should like to point out that after long experiments on unsaturated zones we have found that the water content attained during gravity flow is always low in relation to the porosity. Your results are therefore representative of what is found in reality.

L.O. NORDBERG: Thank you for your comment.

U. CHANDRA: Figure 8 shows a regular pattern of moisture variation with depth. With the density profiles obtained using the gamma-logging probe one could confirm the stratification of the layers indicated by Fig. 8. Would you care to comment?

L.O. NORDBERG: I did not present density profile values in the paper as they are not very accurate, owing in particular to various disturbances along the tubes. There is, however, good agreement between density and porosity at certain levels; high density, usually caused by an abundance of stones in contact with the tubes, is reflected in low porosity.

HYDRODYNAMIC DISPERSION AS AQUIFER CHARACTERISTIC
Model experiments with radioactive tracers

D. KLOTZ, H. MOSER
Institut für Radiohydrometrie,
Gesellschaft für Strahlen- und
Umweltforschung mbH,
Munich,
Federal Republic of Germany

Abstract

HYDRODYNAMIC DISPERSION AS AQUIFER CHARACTERISTIC: MODEL EXPERIMENTS WITH RADIOACTIVE TRACERS.

About 2500 dispersion tests using radioactive, salt and dye tracers have been performed on column devices of varying diameter and different lengths to determine the dependence of the longitudinal dispersion coefficient on the parameters of the streaming fluid and on the characteristics of the porous medium. Artificial and natural materials were employed differing in grain size, grain shape, grain roughness and angularity, compactness, and having various uniformity coefficients of grain-size distribution. The study generally confirmed the approximately linear relation between dispersion coefficient and distance velocity found in the literature for special conditions. In addition it appeared that in particular the grain size and uniformity coefficient of grain-size distribution substantially affect dispersion, and other parameters also enter into the dispersion coefficient. It is concluded that the dispersion coefficient is a characteristic quantity independent of permeability, which in turn describes the phenomena of tracer spread in aquifers.

1. INTRODUCTION

One of the most important features of hydrological investigations is the observation of water movements in porous aquifers. For this purpose tracer solutions miscible with water are used for following their distribution in the flow. Essentially, this distribution[1] is governed by hydrodynamic dispersion which thereby becomes one of the most significant phenomena of groundwater flow. Knowledge of dispersion has been increasing in practical importance since it plays a decisive part in various problems of groundwater investigations related to protection of the environment. This applies particularly to investigation of pollutants entering groundwater from refuse tips [1, 2], safety problems of nuclear power stations [3, 4] and intrusion of salt water into drinking water galleries [5, 6]. Mainly on the basis of the statistical model of Scheidegger [7], the theory of hydrodynamic dispersion has been developed in detail during the past few years for a variety of boundary conditions [8 - 11].

Laboratory and field experiments involving dispersion have been conducted with widely differing aims dictated in many cases by complex practical problems. Selected model experiments (see Table I) and field tests have

[1] Other distributing mechanisms are molecular diffusion, density convection and osmotic effects, which however, are not dealt with here.

TABLE I. SELECTED MODEL EXPERIMENTS ON COLUMNS TO DETERMINE LONGITUDINAL DISPERSION: d_{50} = effective grain diameter, U = uniformity coefficient of grain-size distribution[a], n = total porosity (according to Ref. [13])

Author		Column dimensions diameter (cm)	length (cm)	Type	Parameters of porous medium d_{50} (mm)	U	n (%)	Tracer
De Jong	[14]	6	20	Glass spheres	0.2	< 1.05	38.5	NaCl
Bear	[15]	10	110	Quartz sand	≈0.5	1.30	33.4	NaCl
Rumer	[16]	14	84	Glass spheres	0.39	1.13	39	NaCl
				Quartz sand	1.65	1.26	39	NaCl
Harleman et al.	[17]	9.8	Variable	Plastic spheres	0.39 - 2	1.00 - 1.15	36 - 40	NaCl
				Quartz sand	0.45 - 1.4	1.08 - 1.15	39 - 40	NaCl
Baetslé	[4]	-	100	Sand	≈0.3	-	-	^{131}I
Andreas	[18]	5.8	205	Quartz sand	0.77	1.8	-	^{82}Br, ^{3}H, Uranin A, Sulforhodamin G
		20	423					
Bertsch	[12]	20	100	Sand	≈0.7	-	-	$SrCl_2$
		40	200					
Kaisersberger	[13]	7.5	210	Sand	0.69	1.6		^{82}Br, ^{131}I, Uranin A
		7.5	421		0.77	1.8		
		20.6	423	Gravel	2.1	1.25		
					9.3	1.55		
				Natural fluvio-glacial soil	≈6	> 10		

[a] Definition: d_n = grain diameter after n weight-per cent passage through a sieve set; $U \doteqdot \frac{d_{60}}{d_{10}}$

been analysed by Lenda and Zuber [10] and Fried [11]. Dependence of dispersion characteristics on distance velocity of the flow, grain diameter, permeabilities of the porous medium as well as on kinematic viscosity of the streaming fluid, was observed and partly explained in the past, although it was not possible to establish a simple relation between dispersion and characteristic parameters of the porous medium and of the flow. Thus application of the results of the laboratory measurements to conditions in the field proved uncertain, and it remained unresolved whether or not dispersion, like permeability or porosity, could be regarded as an independent characteristic parameter in studies of soil physics. The present results, drawing on model experiments, attempt to provide a preliminary answer.

2. MEASURING ARRANGEMENT AND PRELIMINARY TESTS

The experiments were performed with the aid of column devices such as have been used in previous investigations [4, 12 - 17, 21]. Figure 1 shows a schematic drawing of the measuring set-up. The main column is made of Plexiglass. All connections as well as the two tracer distributors at the

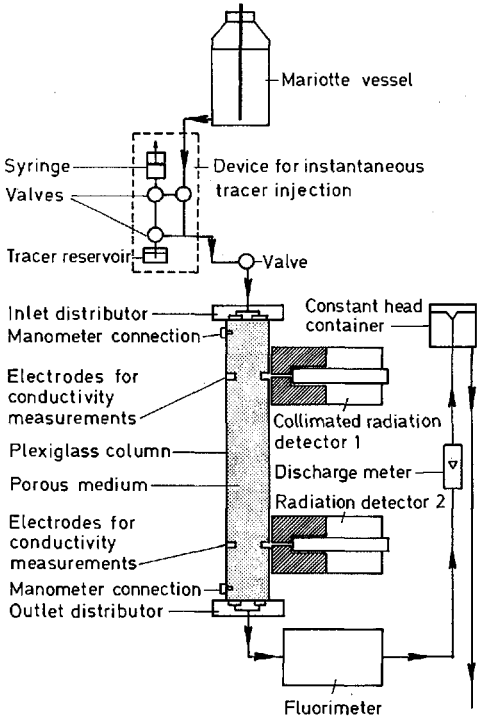

FIG.1. Schematic representation of the column set-up to measure longitudinal dispersion.

top and the bottom of the column are positioned symmetrically with respect to the column centre in order to allow a reversal of the flow direction without changing the configuration of the apparatus. The Mariotte vessel and the constant-head container ensure a constant rate of flow through the column. De-aerated tap water was used for all experiments with the addition of sodium hypochlorite from time to time to inhibit bacteria and algae growth in the column. In all experiments labelling of the streaming fluid was done by pulse injection. The solenoid valve device (Fig. 1) immediately upstream of the inlet distributor ensured that the tracer solution penetrates the porous medium as a thin layer distributed over the column cross-section. In the case of radioactive gamma-emitting tracers, the movement of the tracer was recorded by two or three collimated scintillation detectors fitted along the length of the columns. Besides radioactive tracers such as $NH_4{}^{82}Br$, $Na^{131}I$ and ^{51}Cr-EDTA, solutions of NaCl and fluorescent dye Uranin A were also employed; detection of the electrolyte was done by measuring conductivity in the column, and the fluorescent dye was detected with the help of a fluorimeter at the column outlet or after automatic sampling.

In total, 17 columns with different lengths (500 to 4000 mm) and diameters (10 to 290 mm) were used for tests. Preliminary experiments ascertained the optimum packing of the porous medium in the column, the required column diameter for a given grain size distribution, and the minimum distance of the measuring point from the inlet distributor.

Various methods of packing quartz sand (0.5 - 1.5 mm) in columns (diameter 190 mm, length 1500 mm) were tried which finally led to an optimum method of packing the porous medium. The materials were packed under water in steps of small layers of about 50 mm thickness, and were then evenly compacted with a round rod. Thus the most essential condition of uniform flow through the column by a homogeneous packing for satisfactory dispersion measurements was satisfied.

Comparative measurements on quartz sand (0.5 to 1.5 mm) in columns of varying diameter revealed that, in order to be able to neglect boundary disturbances, the relation between average grain diameter d_{50} and column diameter $\emptyset$ of $\emptyset \geq 25\ d_{50}$ must be maintained.

From measurements with columns with different diameters $\emptyset$ and varying distance 1 between inlet distributor and first measuring point it was found that a relation $1 \geq 2\ \emptyset$ is required to obtain reproducible tracer passage curves.

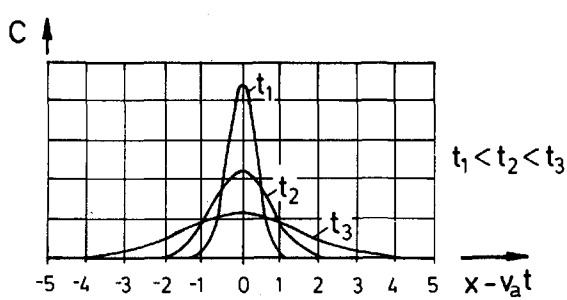

FIG.2. Distribution of a thin layer of tracer after one-dimensional dispersion within a porous medium at different times after injection: c = tracer concentration, x = distance from injection point, v_a = distance velocity, t = time after injection.

3. RESULTS

3.1. Evaluation

As a measure of dispersion, the longitudinal dispersion coefficient D is used in the evaluation of the measured tracer-concentration-time distributions. For one-dimensional flow (in direction x) in an isotropic, homogeneous, porous medium it is defined by the differential equation [9, 7, 12].

$$\frac{\partial c}{dt} = D\frac{\partial^2 c}{\partial x^2} - v_a \frac{\partial c}{\partial x} \tag{1}$$

where c is the concentration of the tracer in the streaming fluid, v_a the distance velocity of the flow in the column and t the time variable.

For the given test arrangement with pulse injection of the tracer, Eq. (1) must be solved under the boundary condition

$$c(x, t = 0) = M\delta(x) \tag{2}$$

M being the tracer amount added, and $\delta(x)$ the delta function ($\int_{-\infty}^{+\infty}\delta(0) = 1$, $\delta(x \neq 0) = 0$). The consequent solution of the Eq. (1) is given by [10, 19]

$$c(x, t) = \frac{M}{F \cdot n_e\sqrt{4\pi Dt}} \cdot \exp\frac{-(x - v_a t)^2}{4\,Dt} \tag{3}$$

where $F \cdot n_e$ is the effective flow cross-section (n_e = effective porosity, F = column cross-section). Equation (3) has been plotted in Fig. 2 for

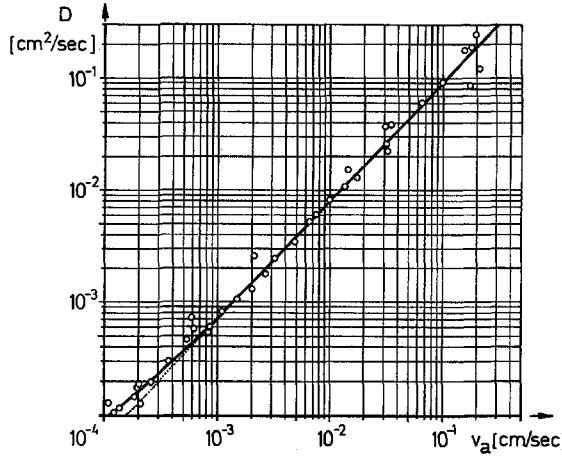

FIG. 3. Longitudinal dispersion coefficient D in relation to distance velocity v_a; porous medium: sand (0.5 - 1.5 mm), effective grain diameter d_{50} = 0.75 mm, uniformity coefficient of grain-size distribution U = 1.85, total porosity n ≈ 0.3, permeability coefficient k = 0.125 cm/s, water temperature T = 20°C.

TABLE II. CORRELATION OF THE LONGITUDINAL DISPERSION COEFFICIENT D AND THE DISTANCE VELOCITY v_a, ACCORDING TO Eq. (4)

Author	Type of porous medium	Range of velocity v_a (cm/s)	Constants in Eq.(4) A	B
Rumer [16]	Sand, glass spheres	$8 \cdot 10^{-3}$ - 5	1.08 - 1.10	0.027 - 0.2
Baetslé [4]	Sand (0.2 - 0.4 mm)	$3 \cdot 10^{-4}$ - $3 \cdot 10^{-3}$	1	0.045 - 0.15
Kaisersberger [13]	Sand and gravel (0.8 mm $< d_{50} < 9.3$ mm)	1.10^{-3} - 2	1.03 - 1.06	0.7 - 1.6
	Fluvioglacial soil ($d_{50} \approx 6$ mm)	$2.5 \cdot 10^{-3}$ - $7 \cdot 10^{-2}$	1.06	7.7
Harleman et al.[a] [17]	Sand ($0.45 < d_{50} < 1.4$ mm) / Plastic spheres ($0.39 < d_{50} < 2$ mm)	$6 \cdot 10^{-3}$ - $2 \cdot 10^{-1}$	1.2	0.03 - 0.21
Bruch and Street[a] [20]	Sand ($d_{50} = 0.92$ mm)	Unknown	1.205	0.26

[a] These authors attempt to correlate the dispersion coefficient D with the Reynolds number R_e and the kinematic viscosity ν: $D = c \cdot \nu \cdot R_e^f$ (c, f = constants). R_e being defined as $d_{50} \cdot v_a/\nu$ the correlations $A = f$ and $B = c \cdot d_{50}^f/\nu^{f-1}$ are used for the quantities A and B in the table.

different values of t. From the standard deviations, $\sqrt{4Dt}$, of the Gauss distribution curves, it is possible to calculate the (longitudinal) dispersion coefficient D. The distance velocity v_a results from the central point of the concentration-time curve and the column length between the measuring points.

An account is given below of the results obtained from about 2500 individual experiments. The test parameters were flow velocity, type of tracer solution and porous medium. "Dispersion" in all cases means longitudinal dispersion.

3.2. Dispersion and flow velocity

Figure 3 shows the dispersion coefficient D as a function of the distance velocity v_a within the range of 10^{-4} cm/sec $< v_a < 2 \cdot 10^{-1}$ cm/s. The porous medium used consisted of sand with a grain size of 0.5 to 1.5 mm, its index properties being given in the caption to the figure. Unless otherwise indicated, $NH_4{}^{82}Br$ solution was employed as the tracer in these and other experiments described below.

In the range of $v_a > 10^{-3}$ cm/s, a relationship

$$\log D = A \cdot \log v_a + \log B \tag{4}$$

with constant values for A and B can be obtained. For the experiments reported here A and B were found to be 1.05 and 0.99 respectively. This approximate linear relation between D and v_a has been used in the theoretical presentations of Lenda and Zuber [10] to normalize D. Comparative results from similar experiments conducted so far by various workers are shown in Table II. The quantity B assumes highly differing values which at first glance seem to have no relation to the test parameters. Below a velocity of $v_a = 10^{-3}$ cm/s, the quantity D attains greater values than expected on account of the linear pattern. This increase is probably due to additional mixing effects which become apparent in the case of limited hydrodynamic dispersion governed, for instance, by molecular diffusion and density convection. As grain size of the porous medium increases, such deviations from pure hydrodynamic dispersion can also be observed at higher velocities (see Fig. 7). An analysis of this effect has not yet been made [10].

3.3. Dispersion and physical properties of the streaming fluid

Figure 4 contains a compilation of the results of column experiments performed with different tracer solutions under identical experimental conditions. Within the range of distance velocity maintained the value of the dispersion coefficient was found to be independent of the tracer used. Preliminary tests were carried out to determine the proper concentrations of the tracers which could be used while avoiding the effects due to variation

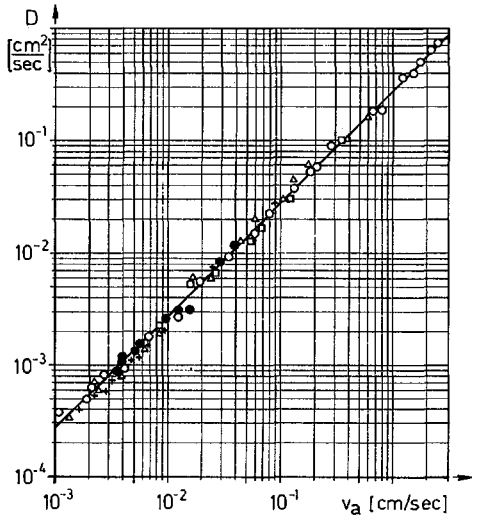

FIG. 4. Longitudinal dispersion coefficient D in relation to distance velocity v_a using different tracer solutions: ○ $NH_4{}^{82}Br$, ● $Na^{131}I$, △ NaCl, □ Uranin A, + ^{51}Cr-EDTA. Porous medium, see Fig. 3, but for a different packing (total porosity n = 0.38).

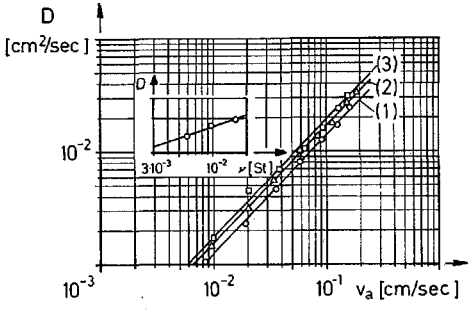

FIG. 5. Longitudinal dispersion coefficient D in relation to distance velocity v_a for different water temperatures T, and in relation to kinematic viscosity ν for $v_a = 10^{-1}$ cm/s: (1) T = 45°C, (2) T = 21°C, (3) T = 5°C. Porous medium: sand (0.9 - 1.12 mm), d_{50} = 1.0 mm, U = 1.85, n = 0.43.

in density or viscosity of the fluid. In the case of an injection volume of about 1 ml, these concentrations amounted to $c \leq 10^{-1}$ mol/l H_2O for the radioactive tracers and the NaCl solution, and to $c \leq 10^{-7}$ g/l H_2O for the dye Uranin A.

Figure 5 reveals that dispersion depends on temperature, i.e. on the viscosity of the streaming fluid. At a lower water temperature, the higher viscosity causes an increase in the value of dispersion coefficient D. The measurements carried out indicate that D is approximately proportional to $\nu^{0.3}$ (ν = kinematic viscosity).

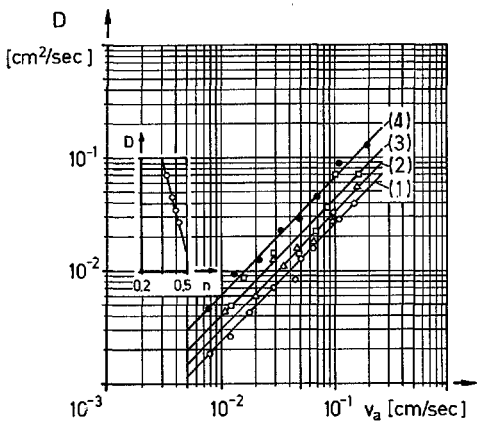

FIG. 6. Longitudinal dispersion coefficient D in relation to distance velocity v_a for different degrees of packing given by total porosity of the porous medium (sand (0.5 - 1.5 mm), d_{50} = 0.75, U = 1.85) and in relation to total porosity n for $v_a = 10^{-1}$ cm/s; water temperature 20°C: (1) n = 0.42, (2) n = 0.40, (3) n = 0.37, (4) n = 0.34.

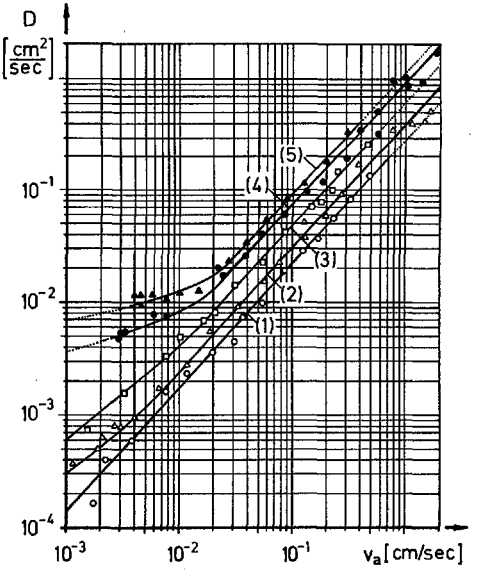

FIG. 7. Longitudinal dispersion coefficient D in relation to distance velocity v_a for like-grained materials (U = 1.5 - 1.8) of different grain size with compact packing (n = 0.31 - 0.35): (1) 0.4 - 0.7 mm, d_{50} = 0.62 mm; (2) 0.5 - 1.5 mm, d_{50} = 0.76 mm; (3) 1 - 2 mm, d_{50} = 1.60 mm; (4) 2 - 3 mm, d_{50} = 2.70 mm, (5) 5 - 7 mm, d_{50} = 6.3 mm.

3.4. Dispersion and index properties of the porous medium

To study the dependence of dispersion on the index properties of the porous medium, systematic measurements were carried out with columns filled with artificial porous media (glass spheres, plastic granules) and natural sands and gravels differing in compactness, grain size, grain shape, grain roughness, grain angularity as well as with varying uniformity coefficients of grain-size distribution. All experiments proved that there exists an approximate linear relation noted in Subsection 3.2 between the dispersion coefficient D and the velocity v_a. In all these series of measurements the quantity A in Eq. (4) was in the range of $1.0 < A < 1.1$.

Figure 6 shows that dispersion increases with decreasing porosity, i.e. with greater compactness. The effect is plausible, since growing compactness leads to a greater branching of the flow paths. The four series of measurements taken show that D is more or less proportional to n^{-3} (n = total porosity).

Figure 7 represents dispersion in the case of like-grained materials of varying grain size with a high degree of compactness whereas all other test conditions remained unaltered. The dispersion coefficient increases with increasing grain size. It is not possible, however, in this instance to represent a relation between D and the average grain diameter d_{50} by a function $D \sim d_{50}^{u}$, since u decreases as grain size becomes larger; although an approximately linear relation ($u \approx 0.8$) is observed up to $d_{50} = 2$ mm between D and d_{50} (agreeing more or less with measurements in Ref. [17] within the range of $0.4 \text{ mm} < d_{50} < 2$ mm, where $u = 1.2$). It can also be seen that with a higher range of particle size ($d_{50} = 2.7$, 6.3 mm), there is only a slight increase in the value of D. This result conforms well with measurements in Ref. [13], where an increase in the average grain diameter from 0.8 mm to 9.3 mm led to a rise in D by some 130% only. It can be said that such comparisons, while dealing with porous media of different grain sizes,

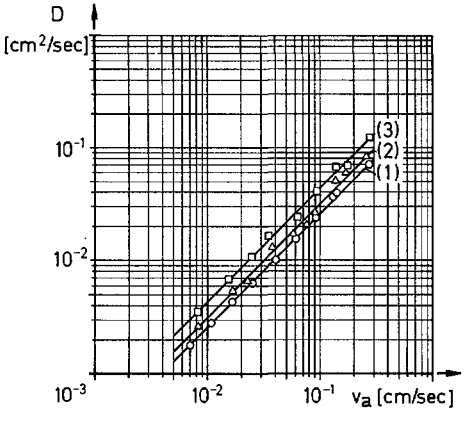

FIG. 8. Longitudinal dispersion coefficient D in relation to distance velocity v_a for porous media of grain sizes 2 - 3 mm ($U \approx 1.5$) with different grain shapes: (1) spherical shape, n = 0.36; (2) lenticular shape, n = 0.32; (3) cylindrical shape, n = 0.33.

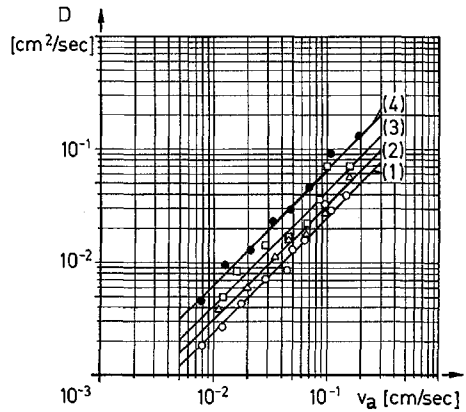

FIG. 9. Longitudinal dispersion coefficient D in relation to distance velocity v_a for sands with a grain size of 0.9 - 1.12 mm (U = 1.1) with varying roughness and angularity of grains: (1) completely rounded (spheres), n = 0.37; (2) well rounded (filter sand), n = 0.38; (3) averagely rounded, n = 0.39; (4) entirely angular (chip material), n = 0.42.

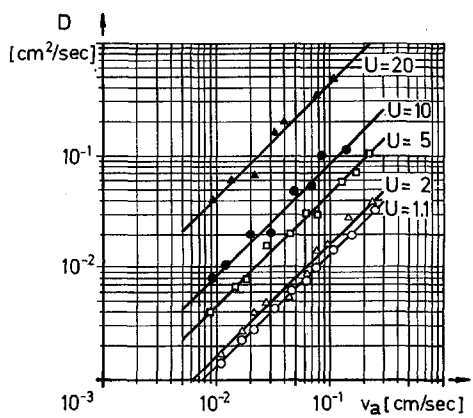

FIG. 10. Longitudinal dispersion coefficient D in relation to distance velocity v_a for sands of effective grain diameter d_{50} = 1.0 mm with different uniformity coefficients U of grain-size distribution; total porosities: n = 0.39 for U = 1.1; n = 0.33 for U = 2; n = 0.31 for U = 5; n = 0.29 for U = 10; n = 0.28 for U = 20.

remain problematical, since it is difficult even in the case of like-grained materials to keep all other soil-physics parameters (porosity, for example) constant. Mention was already made in Subsection 3.2 of the deviations from the linear pattern observed at low velocities.

The influence of grain shape on dispersion is illustrated in Fig. 8. It is seen that the dispersion coefficient increases as the grains vary from a spherical shape. This cannot be explained alone by the change in porosity

TABLE III. CORRELATION OF PERMEABILITY COEFFICIENT k AND DISPERSIVITY $D/v_a = D^+$ WITH FLOW AND AQUIFER PARAMETERS
(↑ increasing, ↓ decreasing, v_a = distance velocity)

Parameter	Permeability coefficient k (cm/s)	Longitudinal dispersivity D^+ (cm)
Kinematic viscosity ν of tracer solution	$\nu\uparrow : k\downarrow$	$\nu\uparrow : D^+\uparrow$
Temperature T of water	$T\uparrow : k\uparrow$	$T\uparrow : D^+\downarrow$
Porosity n	$n\uparrow : k\uparrow$	$n\uparrow : D^+\downarrow$
Effective grain size d_{50}	$d_{50}\uparrow : k\uparrow$	$d_{50}\uparrow : D^+\uparrow$
Deviation sh of grain shape from a sphere	$sh\uparrow : k\downarrow$	$sh\uparrow : D^+\uparrow$
Roughness and angularity C of grains	$C\uparrow : k\downarrow$	$C\uparrow : D^+\uparrow$
Uniformity coefficient U	$U\uparrow : k\downarrow$	$U\uparrow : D^+\uparrow$

due to greater compactness, which becomes apparent particularly in the transition from the lenticular to the cylindrical grain shape.

Figure 9 shows that dispersion increases with decreasing roundness of the grains, i.e. with greater grain roughness and angularity. In the extreme case (from pure spheres to chip material), D increases by about 80%. This is in contrast to measurements in Ref. [16], where an increase of D by a factor of 7 was noted already when changing from glass spheres to like-grained sands. In a similar comparison between glass spheres and like-grained sands [17], however, a growth of some 35% only was observed, which corresponds approximately to our measurements.

Figure 10 reveals that of all index properties of the porous medium the uniformity coefficient of grain-size distribution has the greatest influence on dispersion. The rate of increase of the dispersion coefficient D is accelerated by the increasing uniformity coefficient U. Thus, when passing from U = 1.1 to U = 2, D increases by about 20%; but, from U = 10 to U = 20, D increases by a factor of 5. This agrees well with measurements in Ref. [13] that showed an increase of D by a factor of 5 to 7 in the range of $U < 2$ to $U \approx 20$. Comparison with the results of Fig. 6 shows that the increase of D with increasing U is caused only partly by the decreasing porosity.

4. CONCLUSIONS

The measurements performed indicate roughly that the longitudinal dispersion coefficient D depends linearly on the distance velocity v_a of the streaming fluid so long as the mixing effect is primarily due to hydrodynamic dispersion. The quantity D/v_a ("dispersivity") proposed by Bear [22], with the dimension of length, may therefore be regarded as an index property usable in practice of a porous medium (or an aquifer, for instance), which is well suited to furnish information on spread of a tracer solution in the porous medium. An investigation of the dependence of D/v_a on soil-physics parameters of a porous medium led to the finding that essentially grain size and the uniformity coefficient of grain-size distribution have an influence on dispersion, the effect of grain shape, grain roughness, grain angularity and compactness being not so significant. Measurements to date thus indicate that the dimensionless quotient $D/v_a \cdot d_{50}$ is not capable of uniquely describing the dispersion within a homogeneous isotropic aquifer, which was also noted by Lenda and Zuber [10]. The marked increase of dispersion with increasing uniformity explains the discrepancy which is frequently observed between field tests and laboratory experiments.

The in part complicated relationships between D and soil-physics parameters, and the small number of investigations with respect to the complexity of the problem, do not make it advisable to derive an analytical function for the calculation of D from the characteristics of an aquifer (from grain-size distribution and petrography, for example), as has been attempted repeatedly in the case of permeability.

Finally the question arises whether there is a unique relationship between the dispersion and permeability of an aquifer. In this connection it was stated in Ref. [17], on the basis of dispersion experiments on columns filled with glass spheres and quartz sands, that there exists a simple relation $D \sim K^{0.6}$ between the specific permeability K and the dispersion D.

Table III contains a schematic survey of the dependence of the permeability[2] k and the dispersivity D/v_a on the characteristics of the streaming fluid and the porous medium, as observed in our measurements. It can be seen from this comparison that although a unique relationship may be expected between k and D/v_a for like-grained materials, it is hardly possible to establish such a relationship for natural aquifers. This is because, with the exception of the grain size, the dependence of all other soil-physics parameters on k and D/v_a is inversely related. The dispersion coefficient must therefore be an independent parameter in studies of soil physics.

ACKNOWLEDGEMENT

We wish to thank the Deutsche Forschungsgemeinschaft for supporting these studies financially.

REFERENCES

[1] EXLER, H.J., Ausbreitung und Reichweite von Grundwasserverunreinigungen im Unterstrom einer Mülldeponie, GWF Wasser-Abwasser 113 (1972) 101.
[2] GOLWER, A., MATTHESS, G., SCHNEIDER, E., »Einflüsse von Abfalldeponien auf das Grundwasser", Der Städtetag 2 (1971) 1.
[3] INOUE, Y., KAUFMANN, W.J., Prediction of movement of radionuclides in solution through porous media, Health Phys. 9 (1963) 705.
[4] BAETSLE, L.H., Computational methods for the prediction of underground movement of radionuclides, Nucl. Saf. 8 (1967) 576.
[5] DAY, P.R., Dispersion of a moving salt-water boundary through saturated sand, Trans. Am. Geophys. Un. 37 (1956) 595.
[6] BEAR, J., TODD, D.K., The transition zone between fresh and salt water in coastal aquifers, University of California, Hydraulic Lab., Contract 29 (1960) 1.
[7] SCHEIDEGGER, A.E., "Hydrodynamics in porous media", Handbuch der Physik 8/2 (FLÜGGE, S., Ed.), Springer Verlag, Heidelberg (1963) 625.
[8] HARLEMAN, D.R., RUMER, R.R., Longitudinal and lateral dispersion in an isotropic porous medium, J. Fluid Mech. 16 (1963) 385.
[9] BACHMAT, BEAR, J., The general equations of hydrodynamic dispersion in homogeneous, isotropic porous mediums, J. Geophys. Res. 69 (1964) 2561.
[10] LENDA, A., ZUBER, A., "Tracer dispersion in groundwater experiments", Isotope Hydrology 1970 (Proc. Symp. Vienna, 1970), IAEA, Vienna (1970) 619.
[11] FRIED, J.J., Etudes théorétiques et méthodologiques de la dispersion en milieu poreux naturel, Faculté de Sciences de Bordeaux N°. 348 (1972).
[12] BERTSCH, W., Hydrodynamische Dispersion von $SrCl_2$-Lösung in Einkornsanden bei gesättigtem Fliessen, Dtsche Gewässerkd. Mitt. 14 (1970) 131.
[13] KAISERSBERGER, E., Dispersionuntersuchungen in porösen Medien, Dipl.-Arbeit, Fakultät fur Physik, Univ. München 1972.
[14] De JONG, G. de J., Longitudinal and transverse diffusion in granular deposits, Trans. Am. Geophys. Un. 39 (1958) 67.
[15] BEAR, J., Some experiments in dispersion, J. Geophys. Res. 66 (1961) 2455.
[16] RUMER, R.R., Longitudinal dispersion in steady and unsteady flow, J. Hydraul. Div. 88 (1962) 147.
[17] HARLEMAN, D.R., MEHLHORN, P.F., RUMER, R.R., Dispersion-permeability correlation in porous media, J. Hydraul. Div. Am. Soc. Civ. Engrs 89 (1963) 67.
[18] ANDREAS, G., Dispersion in Tracerlösungen in porösen Medien, Dipl.-Arbeit, Naturwiss. Fakultät, Univ. München 1969.
[19] MACKE, W., Thermodynamik und Statistik, Akademische Verlagsgesellschaft, Leipzig (1962).

---

[2] k is defined by Darcy's Law, $v_f = kI$ (v_f = filter velocity, I = head).

[20] BRUCH, J.C., STREET, R.L., Two-dimensional dispersion, J. Sanit. Engng Div. Am. Soc. Civ. Engrs 6 (1967) 17.
[21] KLOTZ, D., Untersuchungen zur Dispersion in porösen Medien, Z. Dtsch. Geol. Ges., in press.
[22] BEAR, J., On the tensor form of dispersion in porous media, J. Geophys. Res. 66 (1961) 1185.

DISCUSSION

J.B. ROBERTSON: Your experiments are the best laboratory dispersion experiments I have encountered. However, dispersion is a scale-dependent parameter, so that laboratory results do not necessarily apply to large-scale field problems, and caution must be exercised when extrapolating laboratory results to field conditions. The dispersion coefficients for real aquifers are generally a few too many orders of magnitude higher than those observed in the laboratory.

H. MOSER: I agree. Laboratory experiments using like-grained materials give dispersion coefficient values some orders of magnitude too small in comparison with those for real aquifers having the same effective grain size. We believe the reason for this to be the high non-uniformity of grain size distribution in real aquifers. According to measurements, high uniformity coefficients lead to a considerable increase in dispersion coefficient values (see Fig. 10).

J.B. ROBERTSON: I have a further comment and then a question.

It is not surprising that you found D to be dependent on porosity. D, as derived from your Eq. (1), contains a hidden (1/porosity) term.

I should then like to know whether you have extended any of your excellent studies to the other component of two-dimensional dispersion – transverse dispersion.

H. MOSER: We have started investigating dispersion phenomena in three-dimensional models with a view to determining the relationship between longitudinal and transverse dispersion.

H.A. MUNERA: With regard to the paper presented by me (IAEA-SM-182/44)[1], the final slope of the dilution curves leads to an estimated "apparent diffusion" (which takes into account molecular effects, convection, density, etc.) of more than 10^{-1} cm^2/s, the maximum found in your study, which has yielded new information. "Apparent diffusion" values can be as high as 20 cm^2/s, which is in line with what Mr. Robertson just said about real aquifers. As these values relate to vertical diffusion in the presence of a horizontal flow, I should like to know whether you have performed laboratory measurements which might yield additional information about this particular form of vertical diffusion.

H. MOSER: We have carried out laboratory experiments involving measurements of low filter velocities by the point dilution method, and have studied the influence of tracer mixing and concentration within the measurement volume on the measuring process and also diffusion phenomena and convection resulting in dilution of the tracer solution. Apparent diffusion exceeding 1 cm^2/day occurs only if strong convection streams (caused by, for example, density effects) exist (see D. Klotz, H. Moser, Atomkernenergie 14 (1969) 423).

---

[1] MUNERA, H.A., "Modelos matemáticos simplificados para interpretación de resultados de ensayos por el método de marcación de toda la columna piezométrica en pozos de agua", these Proceedings II, IAEA-SM-182/44.

THEORETICAL AND EXPERIMENTAL STUDIES OF TRACER MOVEMENT IN GROUNDWATER

(Session 9)

РАДИОИНДИКАТОРНЫЕ ИССЛЕДОВАНИЯ МОЛЕКУЛЯРНОЙ И КОНВЕКТИВНОЙ ДИФФУЗИИ В НАСЫЩЕННЫХ И НЕНАСЫЩЕННЫХ (ПЕСЧАНО-ГЛИНИСТЫХ) ПОРОДАХ

В.Т.ДУБИНЧУК, З.Г.КОЛЕСНИЧЕНКО,
О.Ф.ЛАПТЕВА, В.С.ГОНЧАРОВ
Всесоюзный научно-исследовательский институт
гидрогеологии и инженерной геологии
Министерства геологии СССР,
Москва,
Союз Советских Социалистических Республик

Abstract–Аннотация

RADIOISOTOPE STUDIES OF MOLECULAR AND CONVECTIVE DIFFUSION IN SATURATED AND NON-SATURATED (SAND-CLAY) ROCK.

The theoretical, technical and methodological aspects of experimental determinations of the characteristics of diffusional transfer of sodium chloride in sand-clay rock are discussed. Knowledge of these characteristics is a prerequisite for the solution of problems relating to the formation and chemical composition of groundwater and interstitial solutions, to applications of hydrogeology in reclamation work and to the efficient use of groundwater and its protection from pollution. Laboratory procedures involving the use of gamma tracers, and more particularly sodium-22, have been developed and tested for studying molecular and convective diffusion in saturated and non-saturated sand-clay rock. Algorithms are discussed for processing the experimental data, taking into consideration methods of successive layers and of open and closed diffusion columns as well as techniques based on non-destructive measurement with collimators. An alternative method is described for field determination of diffusion parameters, developed during the complex hydrogeological survey of territory in the Transvolga steppe that it is proposed to irrigate. A number of unsolved problems requiring more detailed theoretical and methodological study are formulated, more particularly calculation of diffusion characteristics for processes which involve several diffusion mechanisms. Radioisotope methods, which can now be considered as fully developed, make it possible to formulate and, in the very near future, to solve the problem of determining the diffusional transfer characteristics of the main components of groundwater and interstitial water mineralization for the case of typical rock, as a function of such basic conditions as humidity and temperature. As an example of this work, the paper presents the results of some sodium-22 determinations of sodium chloride diffusion.

РАДИОИНДИКАТОРНЫЕ ИССЛЕДОВАНИЯ МОЛЕКУЛЯРНОЙ И КОНВЕКТИВНОЙ ДИФФУЗИИ В НАСЫЩЕННЫХ И НЕНАСЫЩЕННЫХ (ПЕСЧАНО-ГЛИНИСТЫХ) ПОРОДАХ.

Описываются теоретические основы, технические и методические приемы экспериментальных определений характеристик диффузионного переноса хлористого натрия в песчано-глинистых породах. Эти характеристики необходимы для решения проблем формирования химического состава подземных вод и поровых растворов, для целей мелиоративной гидрогеологии, при решении проблем рациональной эксплуатации подземных вод и защиты их от загрязнений. Предложены, разработаны и опробованы лабораторные методики изучения молекулярной и конвективной диффузии в водонасыщенных и ненасыщенных песчано-глинистых породах с применением гамма-трассеров, в частности, ^{22}Na. Обсуждаются алгоритмы обработки экспериментальных данных. Рассмотрены методы последовательных слоев, открытых и закрытых диффузионных колонок, методы, основанные на недеструктивных измерениях с применением коллиматоров. Описывается вариант полевого определения диффузионных параметров, осуществленного в процессе комплексной гидрогеологической съемки на территории предполагаемого орошения в степном Заволжье. Формулируется ряд нерешенных вопросов, требующих более детальных теоретических и методических исследований, в частности, расчета диффузионных характеристик для процессов, в которых проявляются несколько механизмов диффузии. Радиоиндикаторные методы, которые можно считать в настоящее время разработанными, позволяют поставить и в ближайшем будущем решить

задачу определения характеристик диффузионного переноса основных компонент минерализации подземных и поровых вод для типичных пород и в зависимости от таких основных условий как влажность, минерализация и температура. В докладе в качестве примера приводятся результаты некоторых определений диффузии хлористого натрия с применением ^{22}Na.

ВВЕДЕНИЕ

Успешное решение многих научных и практических задач гидрогеологии, гидрологии, гидрогеохимии, агрофизики и мелиорации зависит от разработанности методов исследования процессов диффузии компонентов поровых растворов в грунтах и горных породах [1-6].

Исторически сложилось так, что в гидрогеохимии, гидрологии и мелиоративной гидрогеологии наиболее распространенным способом изучения миграции компонентов веществ, растворенных в почвенных и подземных водах, являются натурные наблюдения [10]. Другим, сравнительно более развитым направлением является разработка априорных теоретических либо полуэмпирических (на основе натурных данных) аналитических методов расчета диффузионного или конвективно-диффузионного переноса макро- и микро-компонентов поровых растворов [11,12].

В гораздо меньшей степени развито направление, которое должно быть связующим (и непременным!) звеном между указанными выше направлениями – это экспериментальное изучение механизма и характеристик диффузионного переноса. Действительно, как бы ни была хороша сама по себе формальная, математическая модель, но если она не учитывает существенных деталей механизма переноса и отсутствуют достаточно точные данные о характеристиках переноса, она не сможет дать достоверных результатов. С другой стороны, одни натурные исследования вследствие многофакторности природных условий и их изменений во времени и пространстве не позволяют добиться однозначной интерпретации данных этих исследований, если характер и степень влияния среды и внешних условий на изучаемый процесс не известны.

Среди наиболее важных факторов, определяющих механизм и характеристики диффузии, можно отметить следующие:

1) ионный состав, концентрация и ее градиенты в почвенных растворах и подземных водах;

2) химический и минералогический состав скелета горных пород и грунтов;

3) структура (геометрия) порового пространства пород, состояние поверхности пор;

4) сорбционные и обменные эффекты (процессы) между раствором и скелетом породы;

5) температура среды, давление;

6) вязкость раствора;

7) степень водонасыщенности пород;

8) воздействие гидродинамических, электромагнитных и гравитационных полей.

Из перечисленного видно, что разработка универсального способа экспериментального исследования диффузионного переноса в поровых растворах представляет весьма сложную задачу. По-видимому, наиболее рациональным является путь разработки методов исследования применительно к конкретным типичным условиям (задачам).

Существенный прогресс в области диффузионных исследований был достигнут в связи со все расширяющимся использованием метода радиоактивных индикаторов, основные преимущества которого по сравнению с другими, например, химико-аналитическими методами, сводятся к следующему:

1) малая трудоемкость и высокая оперативность, объем препаративных и химико-аналитических операций крайне незначителен;

2) при радиоиндикаторных диффузионных экспериментах исследуемый объект не разрушается, отпадает необходимость отбора аналитических проб;

3) эксперименты можно проводить без нарушения процесса диффузии, с использованием внешних регистраторов и практически со сколь угодной временной (или пространственной) детальностью;

4) можно одновременно наблюдать диффузию нескольких компонентов с использованием нескольких радиоактивных индикаторов;

5) и, наконец, самое важное — можно проводить дистанционные натурные эксперименты без отбора проб.

На первом этапе перед нами стояла задача разработать и опробовать экспериментальные радиоиндикаторные методики исследования диффузии хлористого натрия в насыщенных и ненасыщенных водой песчано-глинистых породах.

По завершению этого этапа предполагаются систематические исследования механизма и характеристик диффузионного переноса для наиболее типичных объектов и условий, встречающихся в практике гидрогеологии.

В настоящем докладе излагаются некоторые результаты, полученные на первом этапе указанных исследований.

ТЕОРЕТИЧЕСКИЕ ОСНОВЫ МЕТОДОВ

Любая практическая методика исследования диффузионного переноса базируется на [7,8,9] классическом уравнении вида

$$\frac{dc}{dt} - \nabla(D\nabla c) - \vec{v}\,\mathrm{grad}\,c - \alpha c, \qquad (1)$$

где c — концентрация диффузанта, D — коэффициент диффузии, в общем случае зависящий от концентрации, $\vec{v}$ — скорость конвективного переноса, α — константа сорбции.

Если $v=\alpha=0$, а $D=\mathrm{const}$, то имеем

$$\frac{dc}{dt} = D\frac{d^2c}{dx^2} \qquad (2)$$

В зависимости от принятых начальных, граничных и некоторых других условий, как само уравнение, так и его решение могут быть сведены к тому или иному виду [8,9]. При разработке экспериментального метода обычно стремятся использовать такие условия протекания процесса диффузии, которые обеспечивали бы возможность наипростейшего способа (алгоритма) обработки результатов наблюдений, а, с другой стороны, возможность оперативного контроля за ходом и качеством эксперимента.

Трудности экспериментального исследования диффузии в песчано-глинистых породах состоят в том, что:

а) они имеют нефиксированную структуру;

б) имеют разнообразный минералогический и гранулометрический состав;

в) в них затруднительно получать образцы с равномернораспределенной и заданной влажностью;

г) в них существенную роль играют обменные и сорбционные эффекты, в связи с чем чисто диффузионные процессы можно наблюдать разве что на чистом кварцевом песке.

Когда речь идет об экспериментах, основанных на применении радиоактивных индикаторов, то можно выделить три варианта экспериментов в зависимости от того, в чем и как измеряется активность индикатора:

1) активность измеряется в растворе, вытекающем из образца или омывающем образец;

2) активность измеряется в твердой фазе образца, после отделения тем или иным способом жидкой фазы;

3) активность измеряется непосредственно на образце, содержащем и твердую и жидкую фазу.

В каждом из перечисленных вариантов сорбционные эффекты проявляют себя по-разному.

В принципе возможны обратимые и необратимые реакции, приводящие к связыванию исследуемого компонента и его индикатора. В случае обратимой реакции можно рассмотреть два крайних случая. Первый, когда реакция связывания идет гораздо быстрее диффузии, а количество связанного вещества N прямопропорционально концентрации этого же вещества в поровом растворе, т.е. когда изотерма сорбции

$$N = cR \tag{3}$$

В этом случае суммарная активность диффузанта в образце будет описываться уравнением (2), только вместо D следует поставить

$$D_э = D/(1+R). \tag{4}$$

Параметр R – представляет из себя коэффициент распределения, а $D_э$ – эффективный коэффициент диффузии. Если реакция обратимая, а ее скорость сопоставима со скоростью диффузии, то необходимо учитывать кинетику сорбции (десорбции). Если имеет место реакция 1-го порядка, то процесс диффузии будет описываться уравнением (1), решения которого приводятся в [7,9].

ТЕОРЕТИЧЕСКИЕ МОДЕЛИ ЭКСПЕРИМЕНТОВ

Метод открытых диффузионных колонок. Полное насыщение.

В основу использованной нами методики была положена известная схема одномерной диффузии в ограниченной колонке со связывающими границами (рис.1), на которых концентрация всегда равна нулю. При отсутствии необратимых сорбционных эффектов ($\alpha = 0$) и вынужденного переноса ($v = 0$), при принятых граничных условиях $c(0,t) = c(l,t) = 0$ и начальном условии $c(x,0) = c_0$ нетрудно найти решение уравнения (1),

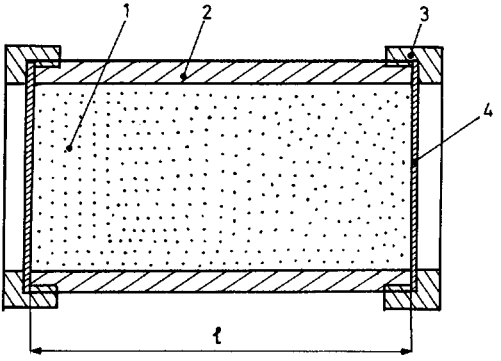

Рис.1. Принципиальная схема определения коэффициента диффузии в водонасыщенных образцах. 1 – образец насыщенной породы с диффузантом; 2 – цилиндрический корпус диффузионной ячейки; 3 – сетка, предохраняющая образец от высыпания и обеспечивающая контакт между образцом и раствором с нулевой концентрацией диффузанта (условие связывания); 4 – навинчивающаяся шайба для удерживания сетки.

см.например [8,9], которое мы не приводим ввиду его общеизвестности. Если длина образца в диффузионной ячейке l, а площадь его поперечного сечения S, то суммарное количество диффузанта, остающегося в ячейке в результате диффузии по истечении произвольного времени t,

$$M = M_0 \sum_0^\infty \frac{8}{[(2k+1)\pi]^2} e^{-[\frac{2k+1}{l}\pi]^2 Dt} \qquad (5)$$

где

$$M_0 = c_0 V = c_0 l S \qquad (6)$$

– полное начальное количество диффузанта в ячейке.

Ряд в формуле (5) быстро сходится и, как показано в работе [8], при $t > 4{,}5 \cdot 10^2 \frac{l^2}{D}$ с погрешностью не более одного процента можно принять, что

$$M = M_0 \frac{8}{\pi^2} e^{-\frac{\pi^2}{l^2} Dt} \qquad (7)$$

Таким образом, экспериментальное определение D состоит из 1) равномерного мечения образца по всему его объему и измерения начальной активности колонки – M_0; 2) внесения колонки в раствор с нулевой концентрацией диффузанта и постоянной температурой; 3) регулярного измерения активности образца M(t) в функции времени; 4) построения графика ln [M(t)] в функции времени t и определения по методу наименьших квадратов тангенса угла наклона экспериментального графика, и, наконец, 6) вычисления коэффициента диффузии по формуле

$$D = \frac{|tg\varphi| l^2}{\pi^2} \qquad (8)$$

Этот метод легко реализуется, если диффундирующее вещество метится гамма-излучающим изотопом.

Метод закрытых колонок. Неполное насыщение.

В основу методики была положена известная схема диффузии из бесконечно тонкого слоя в полуограниченное тело с отражающей поверхностью. Если начальное количество диффузанта в бесконечно тонком слое равно Q, то при граничных и начальных условиях: $\frac{dc}{dx}=0$ при $x=0$, $c=0$ при $x\to\infty$ и $c(x,0)=0$ уравнение (2) имеет как известно решение:

$$c(x,t)=\frac{Q}{\sqrt{\pi Dt}}e^{-\frac{x^2}{4Dt}} \qquad (9)$$

Совершенно очевидно, что если мы диффундирующее вещество пометим радиоактивным изотопом суммарной активности A_0, то для активности единичного слоя образца в диффузионной ячейке имеем зависимость

$$\ln\frac{A(x,t)}{A_0}=-\frac{1}{2}\ln\pi Dt-\frac{x^2}{4Dt} \qquad (10)$$

Таким образом, экспериментальная процедура сводится к следующему: 1) на торец образца тем или иным способом наносится радиоактивная метка в виде тонкого слоя и измеряется ее суммарная активность; 2) образец изолируется; 3) в некоторый момент времени t производится послойное измерение активности в образце; 4) строится график вида $\ln(A/A_0)=f(x^2)$; 5) непосредственно из графика или по методу наименьших квадратов определяют тангенс угла наклона графика; и наконец, 6) определяют коэффициент диффузии по формуле

$$D=\frac{1}{4t/\mathrm{tg}\,\varphi/} \qquad (11)$$

Возможны два варианта практической реализации метода, а именно:

1) разрезание образца на равные последовательные участки и измерение их активности;

2) определение активности детектором гамма-излучения, снабженного коллимирующим устройством, обеспечивающим регистрацию радиоактивного излучения с узкого участка диффузионной колонки.

ЭКСПЕРИМЕНТАЛЬНОЕ ОПРЕДЕЛЕНИЕ КОЭФФИЦИЕНТОВ ДИФФУЗИИ

Полное водонасыщение

Образцы грунта помещались в цилиндрические диффузионные колонки (⌀25мм и l=16мм) с непроницаемой боковой поверхностью и сетчатыми торцами с размером ячеек сетки 0,375мм² (рис.1). Для предохранения грунта от высыпания между образцом и сеткой вставлялся бумажный фильтр.

Затем производилось насыщение образцов в растворе хлористого натрия, меченном натрием-22. Объем раствора V= 1л, а его активность составляла в среднем 4 мкКи/л. Время насыщения определялось путем проведения предварительных опытов по кинетике насыщения. Для разных грунтов оно было, естественно разным, и для песков, супесей, суглинков составляло примерно 90,160 и 500 часов, соответственно. Для определения и контроля пористости и влажности производилось взвешивание колонок до и после насыщения, а также в ходе диффузионного эксперимента. После насыщения колонки помещались в емкость объемом 5л, соединенную с термостатом с объмом рабочего раствора 24л. Таким образом создавались условия нулевой концентрации на границе колонок и поддерживалась заданная температура +15°С. Через определенные интервалы на сцинтилляционной лабораторной установке измерялась суммарная активность колонки, остающаяся к данному времени. По экспериментальным данным строился график вида $\ln [M(t)/M_0] = f(t)$, где M_0 - значение активности при t = 10 часам. Нормирование на эту активность вызвано тем, что определение истинной начальной активности (при t = 0) связано с несколько большими погрешностями, а структура формулы (7) позволяет в принципе производить нормировку на произвольное постоянное значение М.

На экспериментальных графиках наблюдается два характерных участка. Можно предполагать, что уменьшение активности колонки в ходе диффузионного эксперимента контролируется двумя механизмами. На участке 3 процесс контролируется скоростью десорбции диффузанта из материала образца, тогда как на первом участке процесс убывания концентрации контролируется диффузией компонента по поровому пространству с одновременным некоторым влиянием процесса десорбции. В связи с этим можно расчленить суммарную кривую на две составляющие методом последовательного вычитания.

На рис.2 приводится график диффузионной кривой, полученной указанным способом. Определив тангенс угла наклона этого графика, по формуле (8) определялось значение коэффициента молекулярной диффузии. Используя параметры графика на участке 3 можно оценить кинетический коэффициент скорости реакции α и коэффициент распределения R. В табл.I приводятся для примера результаты некоторых определений коэффициента молекулярной диффузии, полученные по описанной выше методике.

Специальные параллельные опыты на одних и тех же образцах показали, что погрешность воспроизводимости результатов определения коэффициента диффузии составляет для песчаносуглинистых грунтов 1-5%.

Неполное насыщение.

Для таких измерений нами применялись разборные секционированные колонки с ϕ25 мм и l = 100 мм, в которые помещался образец, предварительно насыщенный до определенной влажности. На одну из торцевых поверхностей образца помещался бумажный фильтр, равномерно пропитанный раствором хлористого натрия, меченного натрием-22. Удельная активность раствора, в котором насыщались "фильтры", составляла 0,001 мк/л. В зависимости от влажности образца колонки выдерживались при температуре 15°С примерно от 10 до 40 дней. Это время ограничивается, с одной стороны, необходимостью получить достаточно протяженный диффузионный фронт, а, с другой, требованием

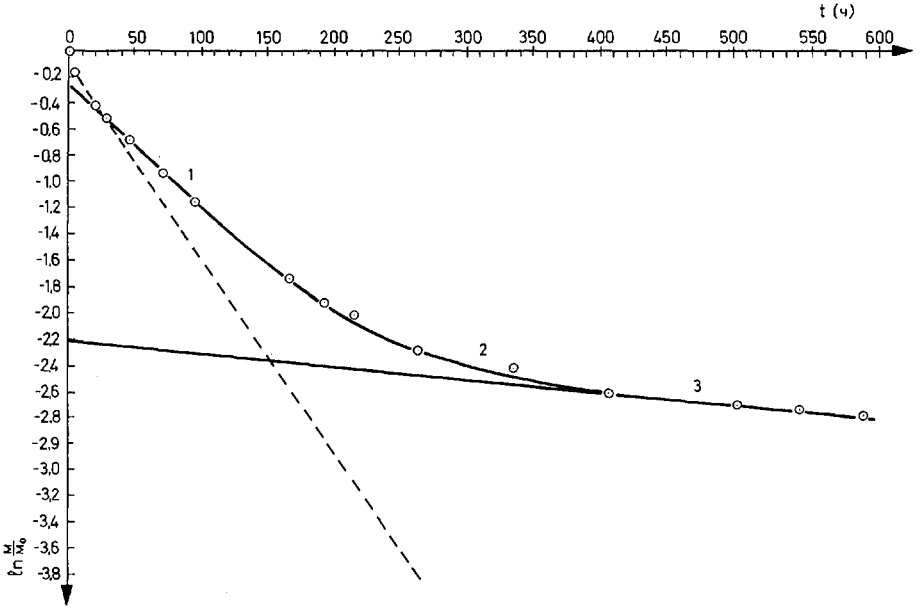

Рис.2. Результаты диффузионного эксперимента при полном водонасыщении образца суглинистого грунта. Скважина 301 Н-4-4,25м, минерализация 8,94 г/л, $D=(1,08\pm0,02)10^{-6}$ см²/с, $\alpha=2,9\cdot10^{-7}c^{-1}$, $R=1,72\cdot10^{-1}$. Пунктирная прямая – результат вычитания из экспериментальной кривой (участки 1,2,3) компоненты, характеризующейся участком 3.

о том, чтобы этот фронт не достиг противоположной границы испытуемого образца. После разборки колонки на секции измерялась удельная активность каждого слоя, а также контролировалась их толщина по весу. Определение коэффициента диффузии производилось согласно приведенного выше алгоритма (10) и (11).

На рис.3 приводится пример экспериментального графика, а в табл.II – значения D, полученные для суглинистых грунтов с различной влажностью. При рассмотрении зависимости нетрудно заметить по данным табл.II, полученным на одном из участков гидрогеологической съемки, что величина D возрастает с увеличением влажности и в первом приближении в исследованном интервале (6-37%) влажностей эту эмпирическую зависимость можно аппроксимировать прямой. Указанная зависимость разумеется не может претендовать на серьезное обобщение, т.к. требуются дополнительные исследования в области малых и максимально возможных для данного типа грунта влажностей.

МЕТОД НЕРАЗБОРНЫХ КОЛОНОК И РЕГИСТРАЦИИ ПРИ ПОМОЩИ КОЛЛИМАТОРОВ

Основными недостатками метода разрезания образца на последовательные слои являются: 1) необходимость разрушения образца и прекращения опыта; 2) некоторая неопределенность в толщине снимаемых

ТАБЛИЦА I. КОЭФФИЦИЕНТЫ МОЛЕКУЛЯРНОЙ ДИФФУЗИИ ХЛОРИСТОГО НАТРИЯ В СУГЛИНИСТЫХ ГРУНТАХ ПОЛНОГО ВОДОНАСЫЩЕНИЯ. ОБРАЗЦЫ ОТОБРАНЫ В РАЙОНЕ ПРЕДПОЛАГАЕМОГО ОРОШЕНИЯ СТЕПНОГО ЗАВОЛЖЬЯ

№№ колонок, дата определения	Диффузионная среда	D см²/с	Минерализация порового раствора, мг/л
№ 4,5 17.VII.72г.	сугл.котлован Н-0,75-1м	$0,89 \cdot 10^{-6}$	-
№ 7,8 6.VI.72г.	сугл.шурф 1-71 Н-1м	$0,89 \cdot 10^{-6}$	-
№ 3,4 28.VIII.72г.	сугл.скв.301 Н-1,75-2,0м	$0,78 \cdot 10^{-6}$	5774
№ 9,10 2.X. 72 г.	сугл.скв.301 Н-4-4,25м	$1,08 \cdot 10^{-6}$	8939
№ 3,6 17.VII.72г.	сугл.скв.302 Н-1,5-1,75м(1)	$0,85 \cdot 10^{-6}$	-
№ 7,8 18.VII.72г.	сугл.скв.302 Н-1,5-1,75м(2)	$0,81 \cdot 10^{-6}$	-
№ 7,8 9.X.72г.	сугл.скв.303 Н-4,65-4,9м	$1,22 \cdot 10^{-6}$	5914
№ 1,2 2.X.72г.	сугл.скв.303 Н-6,75-7,0м	$1,08 \cdot 10^{-6}$	1686
№ 3,4 9.X.72г.	сугл.скв. 4ц Н-3,74-4,0м	$0,98 \cdot 10^{-6}$	-
№ 5,6 9.X.72г.	сугл.скв. 4ц Н-8,8-9,1м	$1,18 \cdot 10^{-6}$	8578
№ 4,5 18.V.72г.	сугл.шурф 28 Н = 1,0м	$0,90 \cdot 10^{-6}$	-
№ 3,6 18.V.72г.	сугл.шурф 28 Н = 4,0м	$1,38 \cdot 10^{-6}$	-

слоев особенно для несвязанных, "зернистых" грунтов, а следовательно, неопределенность в нормировании активности каждого слоя, 3) невозможность (или крайняя затруднительность) в проведении опытов при полном насыщении.

Этих недостатков лишен способ недеструктивных измерений с использованием коллиматоров, обеспечивающих регистрацию излучения индикатора с узких участков диффузионных колонок. Принципиальная схема прибора для таких измерений представлена на рис.4. Нами использовался сферический коллиматор из свинца радиусом 50 мм, с толщиной щели 5 мм.

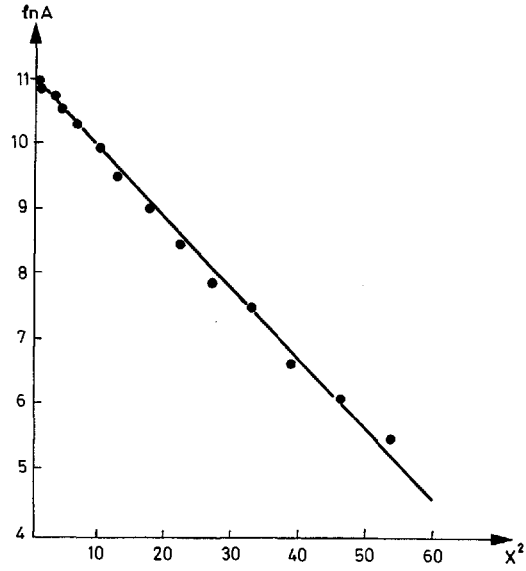

Рис.3. Результаты диффузионного эксперимента при неполном водонасыщении образца суглинистого грунта. Шурф 28 Н-3 м, W – 37,4 %, t – 15 °С, D = (1,65±0,02)10^{-6} см²/с.

ТАБЛИЦА II. КОЭФФИЦИЕНТЫ МОЛЕКУЛЯРНОЙ ДИФФУЗИИ ХЛОРИСТОГО НАТРИЯ В СУГЛИНИСТЫХ ПОРОДАХ НЕПОЛНОГО ВОДОНАСЫЩЕНИЯ. ОБРАЗЦЫ ОТОБРАНЫ В РАЙОНЕ ПРЕДПОЛАГАЕМОГО ОРОШЕНИЯ СТЕПНОГО ЗАВОЛЖЬЯ

№№ п/п	Диффузионная среда	Влажность, вес %	D см²/с	Минерализация порового раствора, мг/л
1.	Суглинок скв.302 Н-4,2-4,4м	5,7	(2,52±0,03) 10^{-7}	-
2.	Суглинок скв.302 Н-1,5-1,75	8,5	(4,55±0,05) 10^{-7}	-
3.	Суглинок скв.302 Н-1,5-1,75	18,6	(1,37±0,02) 10^{-6}	-
4.	Шурф с/х "Родина" Н-1м	6,8	(4,11±0,05) 10^{-7}	-
5.	Шурф 28 Н-3м	6,9	(1,92±0,02) 10^{-7}	-
6.	Шурф 28 Н-3м	37,4	(1,65±0,02) 10^{-6}	-
7.	Шурф 28 Н-5м	5,2	(1,22±0,02) 10^{-7}	-
8.	Шурф 28 Н-5м	36,1	(3,56±0,05) 10^{-6}	-
9.	Скв.303 Н-6,75-7,0м	18,94	(1,42±0,02) 10^{-6}	1686
10.	Скв.303 Н-4,65-4,90м	9,3	(7,0 ±0,1) 10^{-7}	5914
11.	Опытная пл. №188 Н-0,75-1м	12,6	(6,85±0,09) 10^{-7}	-
12.	Скв. 4ц Н-8,8-8,1м	26,9	(2,80±0,04) 10^{-6}	8578

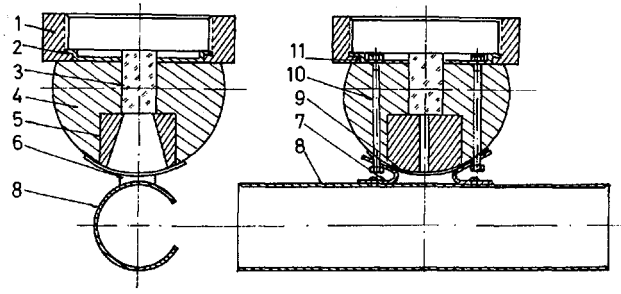

Рис.4. Коллимирующее устройство. 1 – крышка корпуса сцинтилляционного счетчика, 2 – кольцо, 3 – сцинтилляционный кристалл, 4 – сферический свинцовый коллиматор, 5 – цилиндрическая вставка, 6 – подставка, 7 – держатель, 8 – направляющая диффузионной колонки, 9 – прокладка, 10 – крепящий стержень, 11 – гайка.

Решающее значение при использовании коллиматоров имеет разрешающая способность установки в целом, которая зависит от геометрии коллиматора, ширины щели в нем, энергии используемого гамма-изотопа, размеров колонки, плотности упаковки образца и т.д. На рис.5 (кривая 1) приводится кривая чувствительности коллиматора для использованной нами экспериментальной установки с размером щели 5мм. Среднеквадратичное распределение функции чувствительности составляет ~20 мм, а сама функция чувствительности имеет практически вид Гауссова распределения. Это обстоятельство было использовано для расшифровки экспериментальных кривых, получаемых при изучении диффузии на колонках с начальным распределением концентрации в виде δ-функции. В этом случае начальная дисперсия σ_0^2 экспериментальной кривой зависит только от дисперсии функции чувствительности установки. Все последующие диффузионные кривые, которые согласно формуле (9) должны быть гауссианами, имеют дисперсию, являющуюся суммой дисперсии собственно диффузионной кривой и функции разрешения установки. Таким образом, значение коэффициента диффузии может быть оценено по формуле

$$D = \frac{\sigma^2}{2t} = \frac{\sigma^2_{эксп} - \sigma_0^2}{2t}, \qquad (12)$$

где t - время диффузии, $\sigma^2_{эксп}$ - дисперсия экспериментальной диффузионной кривой, а σ_0^2 - дисперсия функции чувствительности. Практически величины σ_0^2 и $\sigma^2_{эксп}$ оценивались путем построения графиков вида $\ln A = f(x^2)$, нахождения тангенса угла наклона прямолинейного участка этого графика и вычисления по формуле

$$\sigma^2 = \frac{1}{2t\,tg\varphi} \qquad (13)$$

Этот способ обработки был нами использован для оценки коэффициента конвективной диффузии. Эксперименты проводились на колонках (ϕ 48 мм и $l = 200$ мм) на суглинистых грунтах при скорости фильтрации порядка $4 \cdot 10^{-3}$ м/сут. В процессе эксперимента через образец

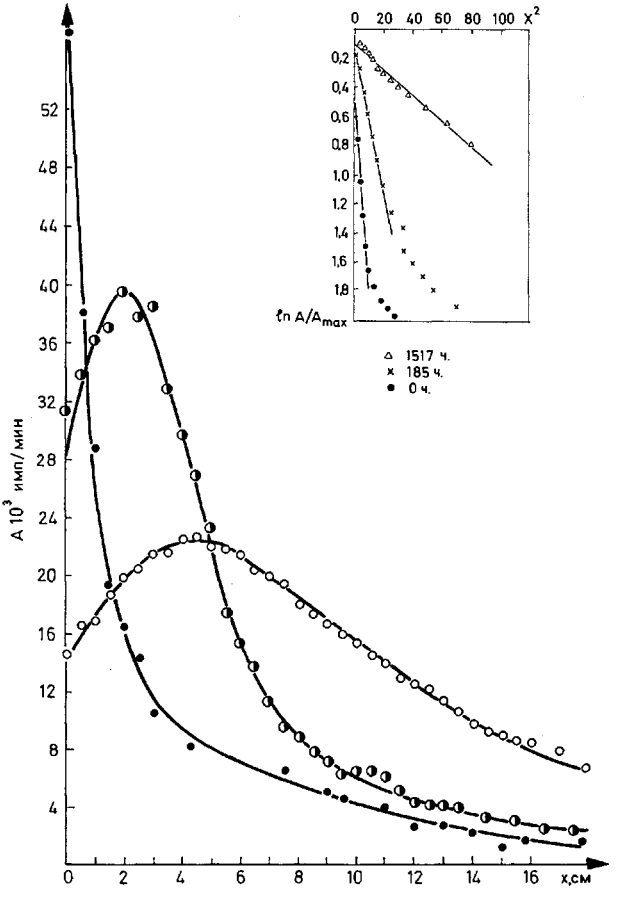

Рис.5. Кривые вынужденной диффузии ^{22}Na при свободном напоре воды 3,5 см для образца суглинистого грунта скв.301 Н-4-4,25м.
● - начальное распределение,
◑ - через 185 ч фильтрации,
○ - через 1517 ч фильтрации.

фильтровался раствор, эквивалентный по своему химическому составу поровому раствору. Результаты одного из таких экспериментов представлены на рис.5. В табл.III представлены полученные значения коэффициентов конвективной диффузии D_K, полученные по описанному выше дисперсионному алгоритму для разных кривых, а также путем сравнения дисперсии соседних кривых. Табл.IV представляет значения D_K, полученные на различных образцах суглинистых грунтов.

Более строго влияние функции чувствительности коллимирующего устройства на экспериментальные распределения можно учесть другим более сложным способом. Действительно, если истинное распределение индикатора вдоль колонки $C(x_i)$, а функция чувствительности $F(x_{ik})$,

ТАБЛИЦА III. РЕЗУЛЬТАТЫ РАСЧЕТА ЭКСПЕРИМЕНТАЛЬНЫХ ЗНАЧЕНИЙ КОЭФФИЦИЕНТА КОНВЕКТИВНОЙ ДИФФУЗИИ ДЛЯ КОЛОНКИ 2 СКВ.301 ГЛУБИНА ВЗЯТИЯ ПРОБЫ 4-4,25м УЧАСТОК 1

$t_{час}$	$tg\varphi$	σ_i^2	$\sigma_{i\,эксп}^2 - \sigma_o^2$	$v \cdot 10^3$ м/сут	$D_K \cdot 10^6$ см²/с
0	$1{,}04 \cdot 10^{-1}$	4,8	0	-	-
t_1 = 185	$5 \cdot 10^{-2}$	10	5,2	$4{,}18 \cdot 10^{-3}$	$3{,}89 \cdot 10^{-6}$
t_2 = 1517	$8{,}33 \cdot 10^{-3}$	56	51,2	$4{,}22 \cdot 10^{-3}$	$4{,}68 \cdot 10^{-6}$
$t_2 - t_1$ = 1332	-	-	56-10=46	$4{,}31 \cdot 10^{-3}$	$4{,}79 \cdot 10^{-6}$
Среднее				4,24±0,04	4,45±0,03

ТАБЛИЦА IV. РЕЗУЛЬТАТЫ ИССЛЕДОВАНИЯ КОНВЕКТИВНОЙ ДИФФУЗИИ ХЛОРИСТОГО НАТРИЯ С ПРИМЕНЕНИЕМ НАТРИЯ-22

Дата	$t_г$	$tg\varphi$	σ^2	D_K см²/с	Примечание
17.9.1971	0	0,266	1,90	-	23,5 часа от начала налива
17.9.-25.9.1971	192	0,19	2,63	$0{,}52 \cdot 10^{-6}$	конец первого налива
21.6.1972		0,16	3,12	-	без налива
2.7.-5.7.1972	72	0,13	3,84	$1{,}40 \cdot 10^{-6}$	72 часа после начала второго налива
2.7.-31.7.1972	696	0,11	4,54	$0{,}28 \cdot 10^{-6}$	окончание 2-го налива
5.7.-31.7.1972	624	-	-	$0{,}16 \cdot 10^{-6}$	

причем ее значения определяют влияние i-го слоя колонки при k-ом положении коллиматора относительно колонки, то экспериментальное распределение регистрируемой скорости счета имеет вид

$$У(x_k) = \sum_{i=1}^{M} F(x_i, x_k)\, C(x_i), \qquad (14)$$

где n - число слоев с толщиной, равной ширине щели коллиматора. В матричной записи имеем:

$$/У/ = /F//C/ \qquad (15)$$

Очевидно, нахождение истинного распределения сводится к решению системы (14) или к нахожд нию матрицы $/F/^{-1}$, обратной матрице $/F/$ и умножению ее слева на члены равенства (15). Действительно,

$$/F/^{-1}/У/ = /F/^{-1}/F//C/ = /C/. \qquad (16)$$

В принципе матрица $/F/^{-1}$ может быть получена путем обращения матрицы /F/, которая в свою очередь получается путем эталонных измерений на колонках с известным распределением концентрации [7]. Дело осложняется тем, что из-за наличия экспериментальных погрешностей уравнения системы (14), вообще говоря, несовместны. Поэтому поставленная задача может быть решена путем переопределения системы (14) и нахождения элементов матрицы /A/ методом наименьших квадратов с последующим ее обращением. Но для этого требуется применение специальных математических приемов и обращение к услугам ЭВЦМ. Кроме того, весьма жесткие требования предъявляются к эталонным измерениям. Построение матрицы позволяет, вообще говоря, проводить диффузионные эксперименты с произвольным начальным распределением. По-видимому, было бы целесообразно также разработать аналогичный алгоритм обработки данных полевых экспериментов, для которых, в связи с ограниченными диаметрами скважин, трудно добиться жесткой коллимации гамма-излучения, поступающего из исследуемой среды.

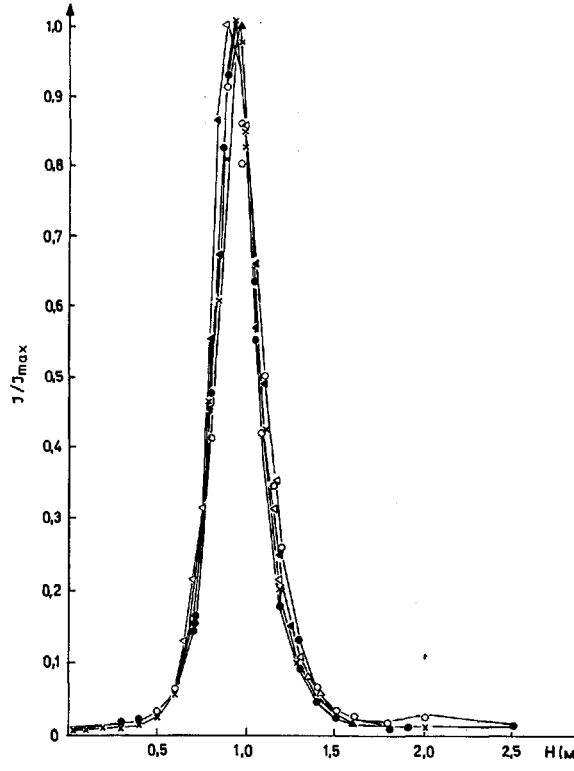

Рис.6. Миграция ^{22}Na при естественном режиме влажности пород:
● - 27.9.71 г., × - 16.12.71 г.,
○ - 19.4.72 г., ▲ - 17.6.72 г., Δ - 16.8.72 г.

ПОЛЕВЫЕ ИССЛЕДОВАНИЯ КОНВЕКТИВНОЙ ДИФФУЗИИ ХЛОРИСТОГО НАТРИЯ

Нами были предприняты предварительные полевые эксперименты с целью оценки практических возможностей радиоиндикаторного способа определения конвективной диффузии хлористого натрия в нарушенных и ненарушенных (гидродинамически) условиях с применением натрия-22.

На участке исследования была оборудована скважина, обсаженная стальной трубой диаметром 89 мм. Вдоль указанной скважины был измерен естественный гамма-фон пород. Затем на расстоянии 0,3 м от наблюдательной скважины по кругу были пробурены 3 шпура и на дно каждого из них было влито 100 мл раствора, содержащего натрий-22 с удельной активностью 1,1 мкКи/мл. После этого шпуры засыпались с послойной утрамбовкой породой, отобранной при их проходке. Через 8 суток было измерено "начальное" распределение радиоактивной метки. Эти измерения проводились с применением коллимированного гамма-детектора дискретно через интервалы 0,05 и 0,1 м. Результаты измерений, проведенных за период с IX.1971г. по VII.1972 г., приведены на рис.6. Эксперимент проводился на суглинистых грунтах степного Заволжья. Для измерения активности индикатора применялся сцинтилляционный детектор, кристалл которого был окружен цилиндрическим свинцовым коллиматором с кольцевой щелью шириной 0,5 см при толщине слоя свинца 1,5 см. В течение срока наблюдения, как видно, уширения распределения концентрации индикатора не наблюдалось. По-види-

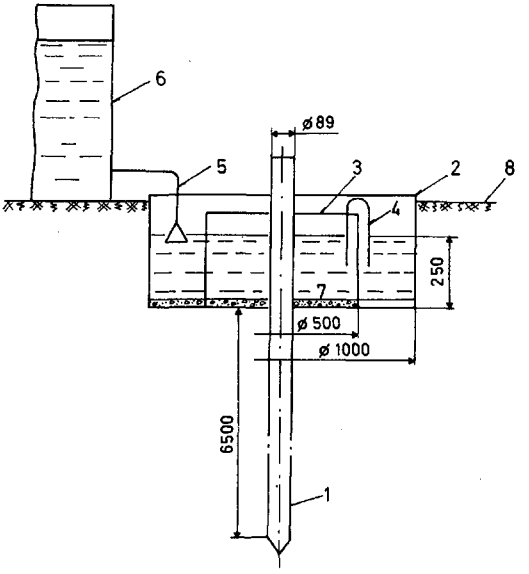

Рис.7. Схема налива в шурф №4. 1 – обсадная труба, 2,3 – двухкольцевой фильтрационный прибор, 4 – сифон, 5 – автоматический регулятор уровня, 6 – источник водоснабжения, 7 – песчано-гравийный фильтр, 8 – порода.

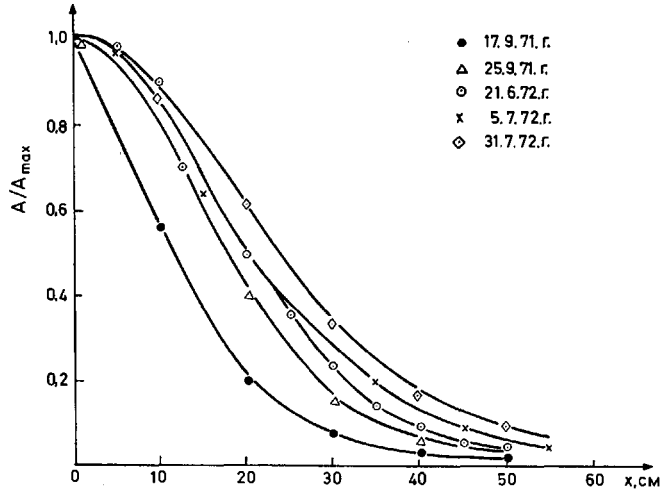

Рис.8. Миграция ^{22}Na при наливе в шурф (концентрации нормированы в максимуме к единице).

мому, на участке исследования создались естественные условия, приведшие к замедлению процесса диффузии. Количество атмосферных осадков в весенне-летний период 1972 г. было значительно ниже среднемноголетней нормы, что обусловило ничтожные инфильтрационные расходы; поэтому в течение эксперимента миграция в масштабах, превышающих погрешности эксперимента, не проявилась.

На том же участке были проведены эксперименты в условиях нарушенного режима влажности. Использованное оборудование для налива приведено на рис.7. В течение первых четырех суток в шурф наливалась чистая вода. Затем были проведены измерения фона радиоактивности пород (гамма-каротаж) и их влажности (нейтронный каротаж). 16 сентября 1971 г. был произведен запуск раствора, содержащего хлористый натрий, меченный натрием-22. Толщина слоя индикатора составила примерно 5 см, что позволяет считать запуск практически мгновенным, а начальное распределение концентрации индикатора δ-образным. После запуска индикатора проводились (начиная с 17 сентября 1971г.) измерения влажности и радиоактивности. Результаты измерения активности представлены на рис.8. По окончании полевых работ сезона 1971 г. шурф был засыпан (27 сентября 1971 г.) породой, а измерения в наблюдательной скважине проводились дважды в зимне-весенний период 1971-1972г.г. В полевой сезон 1972 г. шурф был вскрыт и в него был продолжен налив со 2 июля. В процессе второго налива также проводились измерения гамма-активности (рис.8).

Коэффициент конвективной диффузии оценивался аналогично тому, как это делалось в лабораторных экспериментах.

При обработке результатов первого налива в качестве функции чувствительности детектирующей системы использовалось экспериментальное распределение, полученное 17 сентября 1971 г. При оценке результатов второго налива использовались параметры дисперсии экспериментального распределения активности от 21 июня 1972 г.

ЛИТЕРАТУРА

[1] ПРИКЛОНСКИЙ, В.А., ОКНИНА, Н.А.,"Диффузионные процессы в глинистых породах и их значение в гидрогеологии и инженерной геологии". В сб. Проблемы Гидрогеологии., М., Госгеолтехиздат (1960) 330-334.
[2] ПОЛЯКОВ, В.А., ДУБИНЧУК, В.Т., Приближенные математические расчеты, используемые для решения вопроса о роли диффузии в процессе формирования химического состава подземных вод, VIII конференция младших научных сотрудников, аспирантов и инженеров ВСЕГИНГЕО, часть I. М., 1963, 109с.
[3] ЗАТЕНАЦКАЯ, Н.П., Поровые Воды Глинистых Пород и их Роль в Формировании Подземных Вод, М., изд-во АН СССР, 1963, стр.143.
[4] БОЧЕВЕР, Ф.М., ОРАДОВСКАЯ, А.Е., Гидрогеологическое Обоснование Защиты Подземных Вод и Водозаборов от Загрязнений, "Недра", М., 1972.
[5] СМИРНОВ, С.Н., Происхождение Солености Подземных Вод Седиментационных Бассейнов, "Недра", М., 1971.
[6] ДУБИНЧУК, В.Т., КОЛЕСНИЧЕНКО, З.Г., ЛАПТЕВА, О.Ф., В сб. Материалы Межведомственного Совещания по Мелиоративной Гидрогеологии и Инженерной Геологии, вып.I, часть 1, стр.174-179.
[7] IOST, W., Diffusion Methoden der Messung und Auswerting, 1957.
[8] БОЛТАКС, Б.И., Диффузия в Полупроводниках, М., Физматгиз, 1961, 462с.
[9] CRANK, I., The mathematics of diffusion, 1956, Claredon Press, 347 p.
[10] Методическое руководство по гидрогеологическим и инженерно-геологическим исследованиям для мелиоративного строительства, вып.III, М., 1972, стр.132.
[11] ШЕСТАКОВ, В.М., "О кинетике сорбции на грунтах". В сб. Гидрогеологические Вопросы Подземного Захоронения Промышленных Стоков. Труды ВСЕГИНГЕО, 14(1969) 23-34.
[12] НИКОЛАЕВСКИЙ, В.Н., Конвективная диффузия в пористых средах, Изв. АН СССР, Отдел техн. наук, Прикладная механика и математика, 23 6(1959).
[13] ФРАНК-КАМЕНЕЦКИЙ, Д.А., Диффузия и Теплопередача в Химической Кинетике, Изд. АН СССР, М.-Л., 1947 г., 368 стр.

DISCUSSION

S. GAONA VIZCAYNO: What is the relationship between the values obtained for diffusion and dispersion?

V. T. DUBINCHUK: When the hydrodynamic velocity is zero, one is dealing with molecular diffusion; otherwise one is dealing with what the physicists call "dispersion" and the chemists and hydrogeologists call "convective diffusion"; formally, but not phenomenologically, these are the same process.

S. GAONA VIZCAYNO: What was the soil humidity during the laboratory experiment?

V. T. DUBINCHUK: It varied within the range 5 - 36 wt%.

A. L. BENTZ: Did you encounter any technical difficulties, associated with, for example, adsorption and ion exchange, during your field experiments when using NaCl in heavy clay soils? Hydraulic conductivity is generally reduced by Nah ions in clay soils.

V. T. DUBINCHUK: Yes, we did. The processes mentioned by you were very pronounced, under both field and laboratory conditions.

H. MOSER (Chairman): Is it possible that the deviation, mentioned in your oral presentation, of the dispersion coefficient from the expected value in your experiment is caused by the uniformity coefficient of the soil?

V. T. DUBINCHUK: In principle it is possible. In our laboratory experiments, however, we have tried to achieve uniformity. As for the field experiments, the test plot was as uniform as one can expect under natural conditions.

ANALYSE DES INFORMATIONS FOURNIES PAR LES TRACEURS NATURELS OU ARTIFICIELS DANS L'ETUDE DES SYSTEMES AQUIFERES EN HYDROGEOLOGIE

J. GUIZERIX, R. MARGRITA,
B. GAILLARD, P. COROMPT
CEA, Centre d'études nucléaires
de Grenoble, Grenoble

M. ALQUIER
Institut de mécanique
des fluides, Toulouse,
France

Abstract–Résumé

ANALYSIS OF INFORMATION PROVIDED BY NATURAL OR ARTIFICIAL TRACERS USED TO STUDY AQUIFER SYSTEMS IN HYDROGEOLOGY.

After referring to the use of the transfer function method in the analysis of multivariable linear systems, the authors discuss – on the basis of standard examples – the use of residence time distributions, which are a fundamental kind of information provided by tracers. Measurement of flow rates by Allen's classical method is the first example and illustrates, for confined flows, the method of analysing multivariable systems. The authors examine the conditions for employing this method and introduce the property of pulse response identity, the practical significance of which is considerable. This property, which is established by representing the flow by a Markov chain, is extended to underground flows. In another example, the authors analyse the problem of water transfer between two boreholes. Lastly, they deal with two important sampling problems involving residence time distributions: the dating of water and the study of the kinetics of interactions between pollutants and the medium during their transfer (self-purification).

ANALYSE DES INFORMATIONS FOURNIES PAR LES TRACEURS NATURELS OU ARTIFICIELS DANS L'ETUDE DES SYSTEMES AQUIFERES EN HYDROGEOLOGIE.

Après un rappel sur la méthode des fonctions de transfert pour l'analyse des systèmes linéaires multivariables on traite, en s'appuyant sur des exemples-types, de l'exploitation des distributions des temps de séjour, qui constituent une information fondamentale fournie par les traceurs. La mesure de débits par la classique méthode d'Allen constitue le premier exemple et illustre dans le cas des écoulements confinés la méthode d'analyse des systèmes multivariables. On examine les conditions d'application de cette méthode et introduit la propriété d'identité des réponses impulsionnelles, dont l'incidence sur le plan pratique est d'un grand intérêt. Etablie en représentant l'écoulement par une chaîne de Markov, cette propriété est étendue aux écoulements souterrains. Dans un autre exemple on analyse le problème du transfert de l'eau entre deux forages. On aborde enfin deux problèmes importants d'échantillonnage dans lesquels sont impliquées les distributions des temps de séjour: la datation des eaux et l'étude de la cinétique d'interaction des substances polluantes avec le milieu au cours de leur transfert (autoépuration).

1. INTRODUCTION

Nous définissons la méthode des traceurs dans son application à l'étude des écoulements de la manière suivante: l'objectif étant d'obtenir des informations sur un écoulement donné, on superpose à ce dernier un écoulement de traceur à partir duquel certaines informations sont atteintes. Le

problème est alors de définir les relations qui existent entre ces deux types d'informations afin de déterminer les premières en fonction des secondes (fig. 1). L'écoulement de traceur est provoqué, dans le cas des traceurs artificiels, ou naturellement associé à l'écoulement étudié, dans le cas des traceurs naturels. L'établissement des relations fait intervenir des conditions dont le respect permet une analyse rationnelle du problème posé. Dans le domaine pratique, ces conditions ne sont satisfaites qu'avec certaines approximations dont il convient de conduire l'analyse au terme le plus avancé possible, la limite étant le plus souvent fixée par le temps et des questions financières.

L'information issue des traceurs la plus fréquemment exploitée dans les études de cinématique des systèmes est la distribution des temps de séjour. Le présent mémoire a pour objet de montrer l'exploitation qui en est faite en hydrologie des eaux souterraines, l'accent étant mis sur l'analyse des systèmes. L'exposé s'appuie sur des exemples. Le premier, qui concerne la classique méthode d'Allen pour la mesure des débits en conduite, peut étonner par son choix. Nous l'avons fait parce qu'il illustre parfaitement bien un point important de la théorie des traceurs dont l'exposé

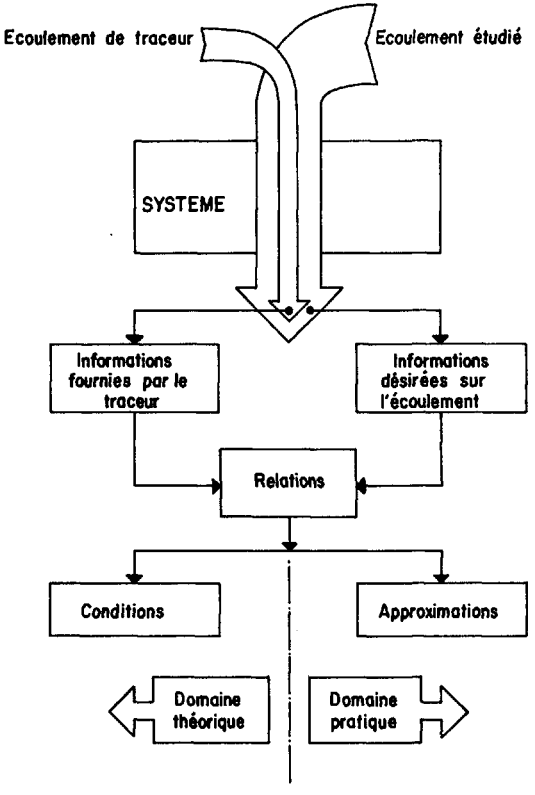

FIG. 1. Illustration de la méthode des traceurs pour l'étude des écoulements de matière dans les systèmes.

est plus simple dans les écoulements confinés; nous verrons que ces résultats sont transposables dans les écoulements souterrains. Quelques points de vue originaux seront développés sur cette méthode. Les autres points originaux de ce mémoire ont trait aux propriétés d'identité et d'isomorphisme des réponses impulsionnelles dont les incidences pratiques, comme nous le verrons dans un autre mémoire présenté à ce Colloque [1], nous paraissent très intéressantes.

Nous rappellerons d'abord quelques points importants de la méthode des fonctions de transfert pour l'étude des systèmes linéaires [2] dans le but, en particulier, de préciser les notations que nous utiliserons.

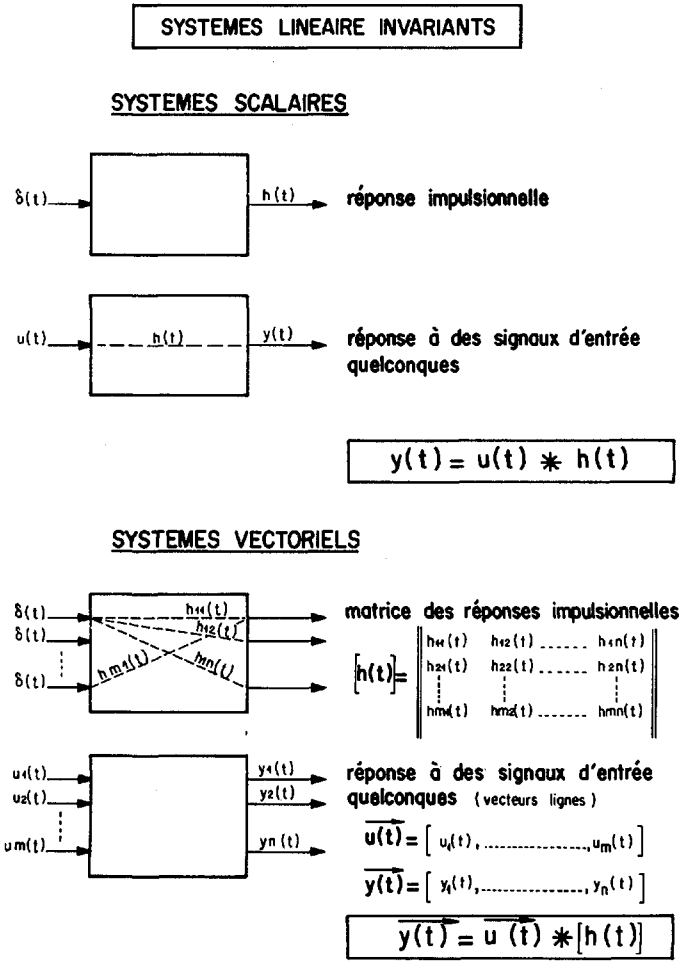

FIG. 2. Réponse des systèmes linéaires invariants.

2. RAPPELS SUR LES SYSTEMES LINEAIRES MULTIVARIABLES

2.1. Définitions

La méthode des fonctions de tranfert pour l'analyse et la synthèse des systèmes est aujourd'hui largement utilisée. Ne considérant que les grandeurs d'entrée et de sortie des systèmes, elle en constitue une théorie extérieure. Un système ne possédant qu'une seule grandeur d'entrée u(t), et une seule grandeur de sortie y(t), est dit univariable ou scalaire. S'il possède plusieurs entrées $u_i(t)$, et plusieurs sorties $y_i(t)$, il est dit multivariable ou vectoriel (fig. 2).

2.2. Principe de superposition et principe de permanence

Si $y_1(t)$, $y_2(t)$, ... $y_n(t)$ sont les réponses d'un sytème à des signaux d'entrée $u_1(t)$, $u_2(t)$, ... $u_n(t)$ agissant séparément, la réponse du système à un signal constitué d'une combinaison linéaire des signaux d'entrée $\Sigma_i a_i u_i(t)$ est la même combinaison des signaux de sortie $\Sigma_i a_i y_i(t)$. Lorsque ce principe est satisfait, le système est dit linéaire.

Le principe de permanence qui permet de définir les systèmes invariants, lorsqu'il est satisfait, s'énonce ainsi: si y(t) est la réponse d'un système à un signal d'entrée u(t) agissant à l'instant t, l'action de ce même signal à $t-\tau$ entraînera une réponse $y(t-\tau)$ (une translation sur l'axe des temps n'affecte pas la réponse).

2.3. Réponse des systèmes linéaires scalaires invariants

La réponse impulsionnelle (nous dirons plus loin: «la distribution des temps de séjour») d'un système linéaire scalaire est sa réponse au signal de Dirac $\delta(t)$, le système étant initialement au repos.

Soit h(t) cette réponse impulsionnelle. Elle permet de déterminer la réponse y(t) à un signal d'entrée quelconque u(t)

$$y(t) = \int_{-\infty}^{+\infty} u(\tau) \cdot h(t-\tau)d\tau \qquad (1)$$

Cette intégrale de superposition ou intégrale de convolution sera ultérieurement notée

$$y(t) = u(t) * h(t)$$

Son écriture signifie que tout signal peut être considéré comme la superposition d'une infinité d'impulsions de Dirac $u(\tau)d\tau$:

$$u(t) = \int_{-\infty}^{+\infty} u(\tau) \cdot \delta(t-\tau)d\tau$$

2.4. Réponse des systèmes linéaires vectoriels invariants

Soit ds un élément de la surface d'entrée d'un système que nous repérons par l'indice i et dσ un élément de la surface de sortie repéré par l'indice j. Nous pouvons définir pour chaque couple ij une réponse impulsionnelle $h_{ij}(t)$.

Nous représentons l'ensemble de ces réponses impulsionnelles par une matrice dite matrice des réponses impulsionnelles:

$$|h(t)| = \begin{vmatrix} h_{11}(t) & h_{12}(t) & \cdots & h_{1m}(t) \\ h_{21}(t) & h_{22}(t) & \cdots & h_{2m}(t) \\ \vdots & \vdots & & \\ h_{m1}(t) & h_{m2}(t) & \cdots & h_{mn}(t) \end{vmatrix}$$

L'ensemble des fonctions d'entrée associées à chaque élément de surface ds est représenté par une matrice $|u(t)|$, comportant une ligne et dont nous considérons que les éléments sont les composantes d'un vecteur $\overrightarrow{u(t)}$. De même, pour les fonctions de sortie on définit $|y(t)|$ et $\overrightarrow{y(t)}$. La réponse d'un système linéaire vectoriel invariant est donnée par

$$\overrightarrow{y(t)} = \overrightarrow{u(t)} * |h(t)| \qquad (2)$$

2.5. Réponse des systèmes linéaires vectoriels variants

Les réponses impulsionnelles sont fonction du temps; la réponse du système est donnée par

$$\overrightarrow{y(t)} = \overrightarrow{u(t)} * |h(t,\tau)| \qquad (3)$$

3. TRANSFERTS DANS UN MILIEU CONFINE – EXEMPLE: METHODE D'ALLEN POUR LA MESURE DES DEBITS

3.1. Définition de la distribution des temps de séjour, marquage et détection idéale

Soit un écoulement, par exemple d'eau, constant dans un système dont nous déterminons l'entrée par une section Σ_1 et la sortie par une section Σ_2 (fig. 3). Soit E_1 l'ensemble des molécules d'eau traversant Σ_1 en un temps court dt; cet ensemble représente un échantillon de l'écoulement et va permettre de le caractériser. Soit $\phi_2(t)$ la fréquence de passage des molécules de E_1 au travers de Σ_2. La distribution des temps de séjour dans le système est

$$h_e(t) = \frac{\phi_2(t)}{\int_{-\infty}^{+\infty} \phi_2(t)\,dt}$$

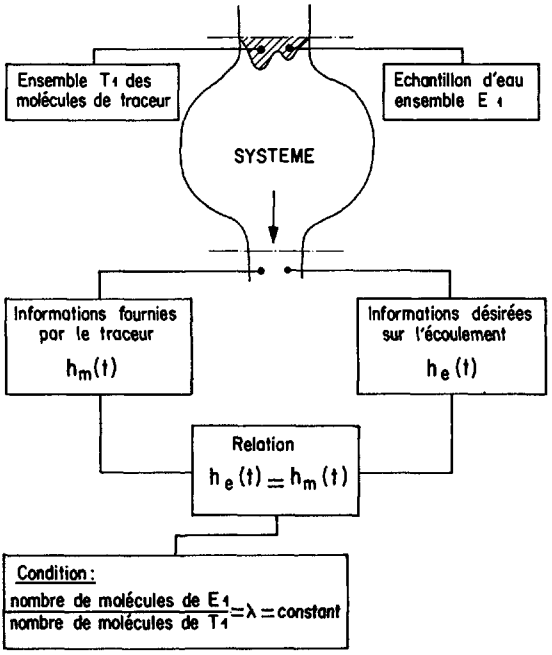

FIG. 3. Détermination de la distribution des temps de séjour à l'aide d'un traceur.

Il y a identité entre réponse impulsionnelle et distribution des temps de séjour. Cette dernière est une loi de densité de probabilité donnant la probabilité qu'a une molécule d'eau de rester dans le système un temps compris entre t et t+dt.

Mélangeons dans E_1 un ensemble T_1 de molécules d'un traceur que nous choisissons pour sa facilité de mesure; nous avons réalisé une injection idéale. Soit $\varphi_2(t)$ la fréquence de passage des molécules de T_1 au travers de Σ_2, supposée déterminée par une détection idéale, la distribution des temps de séjour du traceur dans le système est

$$h_m(t) = \frac{\varphi_2(t)}{\int_{-\infty}^{+\infty} \varphi_2(t)dt}$$

Nous avons $h_e(t) = h_m(t)$ à condition que le rapport

$$\frac{\text{nombre de molécules de } E_1}{\text{nombre de molécules de } T_1} = \lambda = \text{constante} \qquad (4)$$

pour tous les volumes élémentaires intéressant le traceur dans le système.

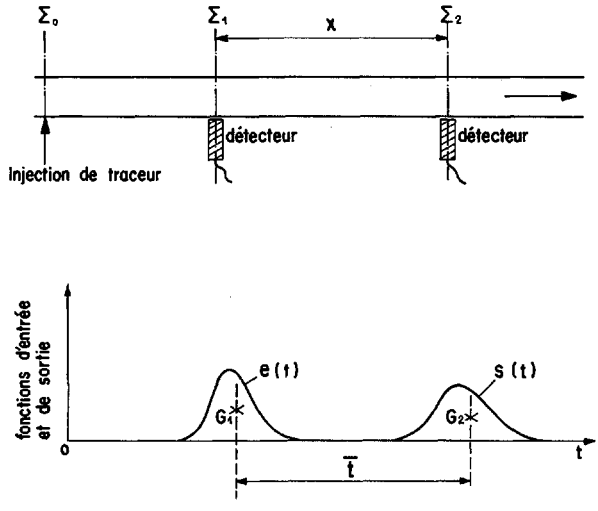

$$Q = \frac{Sx}{\bar{t}}$$

FIG. 4. Méthode d'Allen pour la mesure des débits en conduite.

Nous retrouvons le schéma d'analyse de notre introduction (fig. 1); la relation $h_e(t) = h_m(t)$ est établie lorsque la condition (4) est remplie. Un bon traceur (première définition) est celui qui satisfait à cette relation.

3.2. Méthode d'Allen pour la mesure des débits

La méthode pour la mesure des débits, en général en conduite, dite méthode d'Allen, est déjà ancienne [3]; c'est une très bonne méthode dont le schéma de la figure 4 illustre le processus. Une injection, souvent brève, de traceur est réalisée en un ou plusieurs points d'une section Σ_0. Un ou plusieurs capteurs dans une section Σ_1, en aval, donnent une fonction e(t) (par exemple un seul détecteur nucléaire à l'extérieur de la conduite dans le cas où le traceur est un traceur radioactif). On détermine de même dans une section Σ_2, située en aval de Σ_1, une fonction s(t).

Si la conduite est rectiligne et présente une section d'aire S constante entre les sections Σ_1 et Σ_2 distantes de x, le débit Q est donné par

$$Q = \frac{Sx}{\bar{t}} \tag{5}$$

où $\bar{t}$ représente la différence des abscisses des centres de gravité de e(t) et s(t). Comme nous le verrons, cette relation est exacte. Cependant,

les interprétations qui en sont faites sont le plus souvent inexactes, incomplètes ou trop restrictives. On considère souvent que cette méthode est basée sur une mesure de vitesse en écrivant

$$Q = \frac{S\,x}{\bar{t}} = S\,\bar{v}$$

ce qui est en général inexact sur le plan mathématique. Il faudrait écrire, si l'on veut faire intervenir une vitesse moyenne

$$Q = S\overline{\left(\frac{x}{t}\right)}$$

Soit h(t) la distribution des temps de séjour de l'eau entre Σ_1 et Σ_2; la vitesse considérée étant la vitesse débitante, c'est-à-dire la projection sur l'axe principal de l'écoulement du vecteur vitesse, on a

$$\bar{v} = \overline{\left(\frac{x}{t}\right)} = x\int_{-\infty}^{+\infty} \frac{1}{t}\,h(t)\,dt$$

Cette vitesse moyenne est définie entre Σ_1 et Σ_2. Il est, dans le cas général, incorrect de la multiplier par l'aire de la section de l'écoulement pour obtenir le débit. En effet, dans «débit» il y a une notion de flux et un flux n'intéresse qu'une section et non un volume entre deux sections. Par exemple, il nous importe peu de savoir que, sur une autoroute entre Paris et Lyon, la vitesse moyenne des automobiles est de 120 km/h, alors que la vitesse moyenne est de 2 km/h à la sortie de Paris par suite de l'engorgement de cette voie de communication.

En toute rigueur, la relation $Q = S\,\overline{(x/t)}$ ne s'applique que si la vitesse des molécules d'eau dans leur transfert entre deux sections peut être considérée, pour chaque molécule, comme une variable aléatoire centrée sur une valeur moyenne constante entre ces deux sections. Il n'est pas nécessaire que cette valeur moyenne soit la même pour toutes les molécules. Bien que de telles situations se rencontrent dans la mesure des débits par la méthode d'Allen, nous pensons qu'il est plus général et plus correct de présenter cette méthode comme une application de la propriété suivante:

Si l'écoulement d'un fluide incompressible à débit constant Q a lieu dans un système de volume V, défini entre deux sections Σ_1 et Σ_2, le débit est donné par

$$Q = \frac{V}{\bar{t}} \tag{6}$$

où $\bar{t}$ est le premier moment de la distribution des temps de séjour entre Σ_1 et Σ_2.

$$\bar{t} = \int_{-\infty}^{+\infty} t\,h(t)\,dt$$

L'application de la relation (6) implique que le système soit fermé à la diffusion, à l'entrée et à la sortie, c'est-à-dire que les molécules d'eau ne traversent qu'une fois Σ_1 et Σ_2.

Remarquons que l'application de la relation (5) telle qu'elle est faite d'une manière classique est correcte; en effet, un théorème (théorème d'Aris) nous fait savoir que $\bar{t}$, premier moment de h(t), est égal à la différence des premiers moments des fonctions de sortie s(t) et d'entrée e(t).

Des démonstrations de la relation (6) ont été faites par Danckwerts [4] et Spalding [5]. Nous en donnons, dans le paragraphe suivant, une démonstration qui a l'avantage de montrer les relations existant entre les fonctions concentration-espace et concentration-temps.

Nous établirons, par la suite, les conditions d'application de la méthode d'Allen.

3.3. Démonstration de la relation $Q = V/\bar{t}$

Soit h(t) la distribution des temps de séjour d'un fluide incompressible définie entre Σ_1 et Σ_2, sections d'entrée et de sortie d'un système de volume V, fermé à la diffusion, l'écoulement se faisant à débit constant Q.

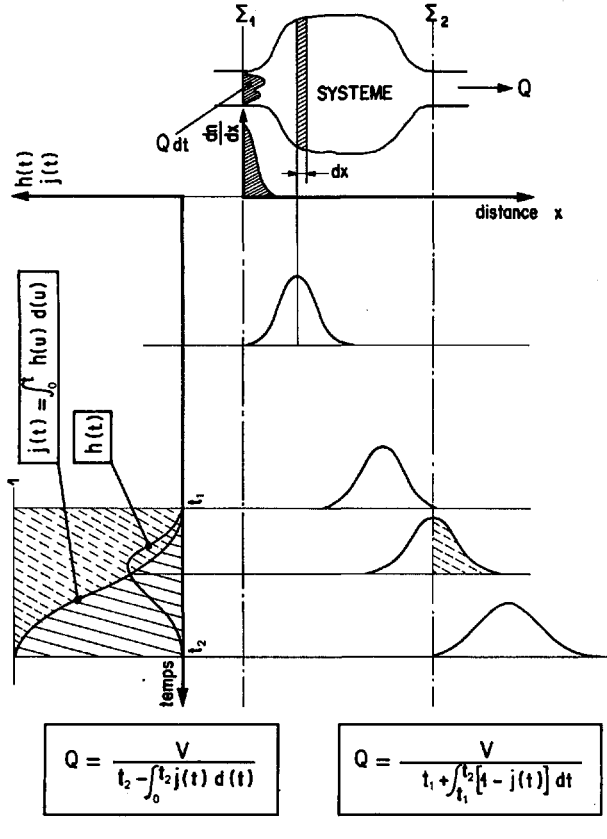

FIG. 5. Démonstration de la relation $Q = V/\bar{t}$.

On définit la réponse indicielle j(t) du système:

$$j(t) = \int_0^t h(u)\,du$$

Considérons l'évolution de l'échantillon de matière E_1 défini plus haut (échantillon entré dans le système entre t_0 et $t_0 + dt$. La première molécule de E_1 sort du système à une date t_1, et la dernière à une date t_2 (fig. 5). t_0 est pris comme origine des temps. La fraction de E_1 déjà ressortie à une date t est

$$\int_0^t [Q\,dt\,h(t)]\,dt = Q\,j(t)\,dt$$

La fraction d'un échantillon entré à une date u et déjà sorti à une date t est

$$Q\,j(t-u)\,du$$

Ecrivons (volume V du système) = (volume du fluide entré entre t = 0 et t_2) - (fraction de ce volume ressorti avant t_2),

$$V = Qt_2 - Q\int_0^{t_2} j(t)\,dt$$

d'où la relation

$$Q = \frac{V}{t_2 - \int_0^{t_2} j(t)\,dt} \tag{7}$$

que l'on peut mettre sous la forme

$$Q = \frac{V}{t_1 + \int_{t_1}^{t_2} [1 - j(t)]\,dt} \tag{8}$$

On montre que ces relations sont identiques à la relation (6) $Q = V/\bar{t}$.

3.4. Détermination pratique des distributions des temps de séjour; condition d'application de la méthode d'Allen

L'application de la méthode d'Allen implique que l'on détermine le premier moment de la distribution des temps de séjour h(t). Nous avons défini au chapitre 2

$$\overrightarrow{y(t)} = \overrightarrow{u(t)} * |h(t)|$$

h(t) est la fonction de sortie du système, pour des injections de traceur réalisées à l'entrée selon des impulsions de Dirac. La masse totale de traceur doit être égale à l'unité et, pour que le marquage soit convenable, les masses de traceur injectées au travers des éléments de surface ds_i doivent être proportionnelles aux débits q_i relatifs à ces éléments de surface. La réponse impulsionnelle du système, h(t), est donc

$$h(t) = y_1(t) + y_2(t) + \ldots y_n(t)$$

et les fonctions d'entrée

$$\begin{aligned} u_1(t) &= \alpha_1 \delta t \\ u_2(t) &= \alpha_2 \delta t \\ &\vdots \\ u_m(t) &= \alpha_m \delta t \end{aligned}$$

$\alpha_1, \alpha_2, \ldots \alpha_m$ sont distribués comme $q_1, q_2, \ldots q_m$ et l'on a

$$\sum_{i=1}^{m} \alpha_i = 1$$

Une bonne approximation à ce marquage idéal consiste à faire des injections multipoints dans la section d'entrée, au travers des surfaces ΔS, par laquelle on admet que q est constant. On trouvera une illustration de cette technique dans la référence [6] pour la détermination des distributions des temps de séjour de tronçons de fleuves, dans le cadre d'une étude sur la pollution thermique des cours d'eau.

Cette procédure n'est pas toujours possible; aussi, d'une manière générale, procède-t-on comme cela a été indiqué par la méthode d'Allen: injection des traceurs dans une section Σ_0 et détermination des fonctions u(t) et y(t) à l'entrée Σ_1 et à la sortie Σ_2 du système.

Nous supposerons, pour faciliter l'exposé, que l'injection dans Σ_0 est une injection $\delta(t)$.

Définissons:

- fonction d'entrée $u(t) = u_1(t) + u_2(t) + \ldots u_m(t)$
- fonction de sortie $y(t) = y_1(t) + y_2(t) + \ldots y_n(t)$.

Nous devons nous poser la question importante suivante: Pouvons-nous écrire

$$y(t) = u(t) * h(t)$$

en d'autres termes, pourrons-nous obtenir h(t) en déconvoluant les fonctions y(t) et u(t)?

Nous recherchons les conditions qui autorisent cette opération.

Supposons, et ce sera une première condition, que la distance entre Σ_0 et Σ_1 soit telle que l'on ait bon mélange en Σ_1: les masses de traceur

passant à travers les éléments de surface ds_i sont distribuées comme les débits correspondants q_i

$$\begin{aligned} u_1(t) &= \alpha_1 f_1(t) \\ u_2(t) &= \alpha_2 f_2(t) \\ &\vdots \\ u_m(t) &= \alpha_m f_m(t) \end{aligned}$$

En général, $f_1(t) \neq f_2(t) \ldots \neq f_m(t)$, mais

$$\int_{-\infty}^{+\infty} f_1(t)\,dt = \int_{-\infty}^{+\infty} f_2(t)\,dt = \ldots = \int_{-\infty}^{+\infty} f_m(t)\,dt = 1$$

Nous avons

$$\begin{aligned} y(t) = {} & \alpha_1 f_1(t) * [h_{11}(t) + h_{12}(t) + \ldots + h_{1n}(t)] \\ & + \alpha_2 f_2(t) * [h_{21}(t) + h_{22}(t) + \ldots + h_{2n}(t)] \\ & \ldots\ldots\ldots\ldots\ldots\ldots\ldots\ldots \\ & + \alpha_m f_m(t) * [h_{m1}(t) + h_{m2}(t) + \ldots + h_{mn}(t)] \end{aligned} \tag{9}$$

Par ailleurs

$$\begin{aligned} u(t) * h(t) = {} & \{\alpha_1 f_1(t) + \alpha_2 f_2(t) + \ldots + \alpha_m f_m(t)\} \\ & * \{\alpha_1 [h_{11}(t) + h_{12}(t) + \ldots + h_{1n}(t)] \\ & + \alpha_2 [h_{21}(t) + h_{22}(t) + \ldots + h_{2n}(t)] \\ & \ldots\ldots\ldots\ldots\ldots\ldots \\ & + \alpha_m [h_{m1}(t) + h_{m2}(t) + \ldots + h_{mn}(t)]\} \end{aligned}$$

Soit, en développant

$$\begin{aligned} u(t) * h(t) = {} & [h_{11}(t) + h_{12}(t) + \ldots + h_{1n}(t)] \\ & * \{\alpha_1\alpha_1 f_1(t) + \alpha_1\alpha_2 f_2(t) + \ldots + \alpha_1\alpha_m f_m(t)\} \\ & + [h_{21}(t) + h_{22}(t) + \ldots + h_{2n}(t)] \\ & * \{\alpha_2\alpha_1 f_1(t) + \alpha_2\alpha_2 f_2(t) + \ldots \alpha_2\alpha_m f_m(t)\} \\ & \ldots\ldots\ldots\ldots\ldots\ldots \\ & + [h_{m1}(t) + h_{m2}(t) + \ldots + h_{mn}(t)] \\ & * \{\alpha_m\alpha_1 f_1(t) + \alpha_m\alpha_2 f_2(t) + \ldots + \alpha_m\alpha_m f_m(t)\} \end{aligned} \tag{10}$$

Pour que les seconds membres des égalités (9) et (10) soient identiques quels que soient les $h_{ij}(t)$, il est nécessaire que

$$\alpha_1 \alpha_1 f_1(t) + \alpha_1 \alpha_2 f_2(t) + \ldots + \alpha_1 \alpha_m f_m(t) = \alpha_1 f_1(t)$$
$$\alpha_2 \alpha_1 f_1(t) + \alpha_2 \alpha_2 f_2(t) + \ldots + \alpha_2 \alpha_m f_m(t) = \alpha_2 f_2(t)$$
$$\cdots\cdots\cdots\cdots\cdots\cdots\cdots\cdots\cdots\cdots$$
$$\alpha_m \alpha_1 f_1(t) + \alpha_m \alpha_2 f_2(t) + \ldots + \alpha_m \alpha_m f_m(t) = \alpha_m f_m(t)$$

c'est-à-dire

$$\alpha_1 f_1(t) + \alpha_2 f_2(t) + \ldots + \alpha_m f_m(t) = f_1(t)$$
$$\alpha_1 f_1(t) + \alpha_2 f_2(t) + \ldots + \alpha_m f_m(t) = f_2(t)$$
$$\cdots\cdots\cdots\cdots\cdots\cdots\cdots\cdots$$
$$\alpha_1 f_1(t) + \alpha_2 f_2(t) + \ldots + \alpha_m f_m(t) = f_m(t)$$

d'où: $f_1(t) = f_2(t) = \ldots = f_m(t)$ étant donné que

$$\sum_{i=1}^{m} \alpha_i = 1$$

Les fonctions d'entrée $f_i(t)$ doivent être identiques. Cette condition est nécessaire si l'on veut obtenir, d'une manière générale, la distribution des temps de séjour par déconvolution de la fonction de sortie par la fonction d'entrée d'un système. Dans l'application de la méthode d'Allen, il n'est pas nécessaire d'expliciter la distribution des temps de séjour et cette condition d'identité des fonctions d'entrée n'est pas nécessaire. Nous allons montrer que la condition à respecter est la condition de bon mélange.

Soit $n(P, t)$ le nombre de particules de traceur en un point P, à l'instant t. Le nombre de particules de traceur dans un volume dV entre t et t+dt est: $n(P, t)dV\,dt$. Le bon mélange s'exprime par la relation

$$\int_0^\infty n(P, t)dt = K = \text{constante (indépendant de P)}$$

Soient:
u(t) le flux de traceur entrant
y(t) le flux de traceur sortant
M(t) le nombre de particules de traceur présentes à l'instant t dans le volume V.

On a

$$u(t) = \int_{\Sigma_1} n(P, t)\, \overrightarrow{V(P)}\, \vec{n}\, ds$$

où $\overrightarrow{V(P)}$ = vecteur vitesse au point P, $\vec{n}$ la normale à ds

$$y(t) = \int_{\Sigma_2} n(P, t)\, \overrightarrow{V(P)}\, \vec{n}\, ds$$

$$M(t) = \int_V n(P, t)dV$$

La relation de bilan s'écrit $\frac{dM}{dt} = u(t) - y(t)$.

Multiplions les deux membres de cette égalité par t et intégrons de 0 à l'infini:

$$\int_V \int_0^\infty t \frac{\partial n(P,t)}{\partial t} dt = \int_0^\infty t\, u(t) dt - \int_0^\infty t y(t) dt$$

Une intégration par parties donne

$$\int_0^\infty t \frac{\partial n(P,t)}{\partial t} dt = [t \cdot n(P,t)]_0^\infty - \int_0^\infty n(P,t) dt$$

Si la condition de bon mélange est respectée, l'expression au deuxième membre de l'égalité est égale à -K. On a ainsi

$$-KV = \int_0^\infty t u(t) dt - \int_0^\infty t y(t) dt$$

Soit: $\bar{t}_1$ le premier moment du flux de traceur entrant et $\bar{t}_2$, le premier moment du flux de traceur sortant:

$$\bar{t}_1 = \frac{\int_0^\infty t u(t)\, dt}{\int_0^\infty u(t)\, dt} \qquad \bar{t}_2 = \frac{\int_0^\infty t\, y(t) dt}{\int_0^\infty y(t) dt}$$

Le flux de traceur étant conservatif:

$$\int_0^\infty u(t) dt = \int_0^\infty y(t) dt$$

d'où

$$\int_{\Sigma_1} \int_0^\infty n(P,t) \overrightarrow{V(P)}\, \vec{n}\, ds\, dt = \int_{\Sigma_2} \int_0^\infty n(P,t) \overrightarrow{V(P)}\, \vec{n}\, ds\, dt$$

La relation définissant le bon mélange étant respectée, on peut écrire

$$\int_0^\infty u(t) dt = \int_0^\infty y(t) dt = K \int_0^\infty \overrightarrow{V(P)}\, \vec{n}\, ds = KQ$$

d'où

$$\frac{V}{Q} = t_2 - t_1$$

Cette relation a été établie en ne supposant que le respect de la condition de bon mélange.

3.5. Existence d'une section pour laquelle le bon mélange est réalisé

On peut trouver en aval de Σ_0 une section Σ_1 pour laquelle $\int_{-\infty}^{+\infty} C(t)dt = \mu \pm \Sigma$, où μ est une constante et Σ peut avoir une valeur aussi petite qu'on le désire. On dit que le bon mélange est réalisé à $100\epsilon/\mu$ % près. Soient, en aval de Σ_0 (section d'injection), des sections S_1, S_2, ... équidistantes. Nous nous intéressons au mouvement d'une molécule d'eau, en aval de Σ_0. Cette molécule traverse chaque élément ds_i de Σ_0 avec des probabilités différentes que nous représentons par un vecteur

$$\vec{\gamma}_0 = (P_1^0, P_2^0, \ldots, P_m^0)$$

Nous représentons également par un vecteur l'ensemble des probabilités de passage de cette molécule dans un élément ds_i d'une section S_σ

$$\vec{\gamma}_\sigma = |P_i^\sigma| \qquad i = 1, 2, \ldots, m$$

Considérons deux sections consécutives S_k et S_{k+1} et repérons par i et j les éléments de surface ds homologues, les deux sections étant supposées identiques.

Représentons par une matrice l'ensemble des probabilités de passage de la molécule d'un élément ds_i de S_k à un élément ds_j de S_{k+1}

$$\Pi = |\alpha_{i,j}^{k,k+1}| \qquad \begin{array}{l} i = 1, 2, \ldots, m \\ j = 1, 2, \ldots, m \end{array}$$

Suppons que cette matrice soit indépendante de K; on traduit ainsi la stationnarité de l'écoulement. Nous pouvons alors considérer que le mouvement de la molécule correspondante se fait selon un processus de Markov homogène du premier ordre.

On a

$$\vec{\gamma}_\sigma = \vec{\gamma}_0 \cdot \Pi^\sigma$$

On démontre que si l'on est dans le cas «positivement régulier», Π^σ tend, lorsque σ croît, vers une matrice dont toutes les lignes sont identiques.

$$\vec{\gamma}_\infty = (P_1^0, P_2^0, \ldots\ldots P_m^0) \times \begin{vmatrix} \alpha_1 & \alpha_2 & \ldots\ldots\ldots\ldots & \alpha_m \\ \alpha_1 & \alpha_2 & \ldots\ldots\ldots\ldots & \alpha_m \\ \ldots & \ldots & \ldots\ldots\ldots\ldots & \ldots \\ \alpha_1 & \alpha_2 & \ldots\ldots\ldots\ldots & \alpha_m \end{vmatrix}$$

On montre que cette convergence vers un «régime permanent» est de caractère exponentiel; elle est donc rapide. Par conséquent on doit pouvoir trouver, en aval de Σ_0, une section S_p, pour laquelle les probabilités de passage

$$\begin{aligned} P_1^p &\cong \alpha_1 \\ P_2^p &\cong \alpha_2 \\ &\cdots \\ &\cdots \\ &\cdots \\ P_m^p &\cong \alpha_m \end{aligned}$$

sont indépendantes des conditions initiales.

Si, au lieu d'une molécule, on considère N molécules en évolution dans le système, les fréquences relatives de passage de ces molécules dans les éléments de surface de S_p convergent (pour $N \to \infty$) en probabilité, vers les probabilités de passage P_1^p, P_2^p, ... Soit q_i le débit associé à l'élément de surface ds_i, on a donc

$$P_i^p = \frac{q_i}{Q} \tag{11}$$

La même analyse peut être faite pour décrire l'évolution des molécules d'un traceur en aval de Σ_0.

Nous dirons que le traceur est un bon traceur (deuxième définition d'un bon traceur) si sa matrice de passage est égale à celle de l'eau.

Si la masse de traceur injectée en Σ_0 est A et si $C_i(t)$ est sa concentration dans l'élément de surface, ds_i de S_p, on a

$$P_i^p = \frac{q_i \int_{-\infty}^{+\infty} C_i(t)dt}{A} \tag{12}$$

(11) et (12) permettent d'écrire

$$\int_{-\infty}^{+\infty} C_i(t)dt = \frac{A}{Q} = \text{constante}$$

3.6. Existence d'une section pour laquelle la condition d'identité des réponses impulsionnelles est satisfaite

Un traceur ayant été injecté dans une section Σ_0, selon une impulsion de Dirac, nous allons montrer qu'il existe une section de l'écoulement Σ_d pour laquelle les réponses impulsionnelles définies entre le point d'injection et les différents éléments de surface ds de cette section sont identiques.

Supposons que l'écoulement est représenté par un ensemble de systèmes élémentaires, associés en série et en parallèle comme le représente la figure 6. Les systèmes, sur chaque ligne, ont même distribution des temps de séjour $h_i(t)$, et nous supposons que le temps de passage d'une ligne à

l'autre est négligeable. Supposons enfin que la probabilité pour une molécule de se trouver aux différents nœuds peut être analysée selon un processus de Markov, homogène dans le temps et «dans le cas régulier». Ces suites de Markov ont la propriété d'ergodicité: les moyennes statistiques convergent vers les probabilités α_i lorsque s tend vers l'infini. Rappelons que la moyenne statistique d'un événement repéré par l'indice i est le rapport du nombre Z_i de ses réalisations et du nombre s de fois où il aurait pu se produire. On a

$$\frac{Z_i}{s} \xrightarrow[s \to \infty]{\text{Prob}} \alpha_i$$

Une molécule arrivant à un nœud quelconque d'une section Σ_d aura séjourné dans les lignes 1, 2, . . . , m avec des fréquences $\alpha_1, \alpha_2, \ldots, \alpha_m$. La réponse impulsionnelle r(t) relative à chaque nœud de Σ_d sera identique et aura pour valeur

$$r(t) = h_1^{*\alpha_1 d} * h_2^{*\alpha_2 d} * \ldots * h_m^{*\alpha_m d}$$

L'exposant $*\alpha_i d$ indique qu'il faut convoluer $\alpha_i d$ fois la fonction par elle-même. Nous avons, depuis 1966, fait de nombreuses vérifications de cette propriété, en hydrologie de surface, sur des fleuves comme la Loire, la Seine et le Rhin. On notera son très grand intérêt sur le plan pratique, étant donné que, dans une section de mesure, on n'est conduit à la détermination que d'une seule réponse impulsionnelle, au lieu de déterminer n réponses impulsionnelles et le champ de vitesse, comme cela est nécessaire si l'on ne peut pas choisir une section de mesure assez éloignée de la section d'injection. La figure 7 représente quatre réponses impulsionnelles identiques, obtenues sur la Loire à 75 km du point d'injection, le débit étant de 108 m^3/s.

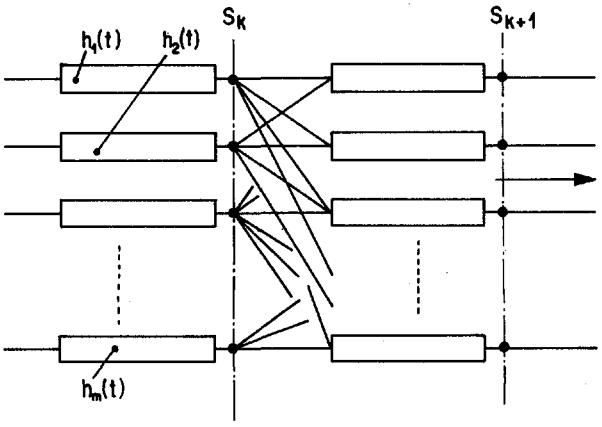

FIG. 6. Modèle utilisé pour la démonstration de l'identité des réponses impulsionnelles.

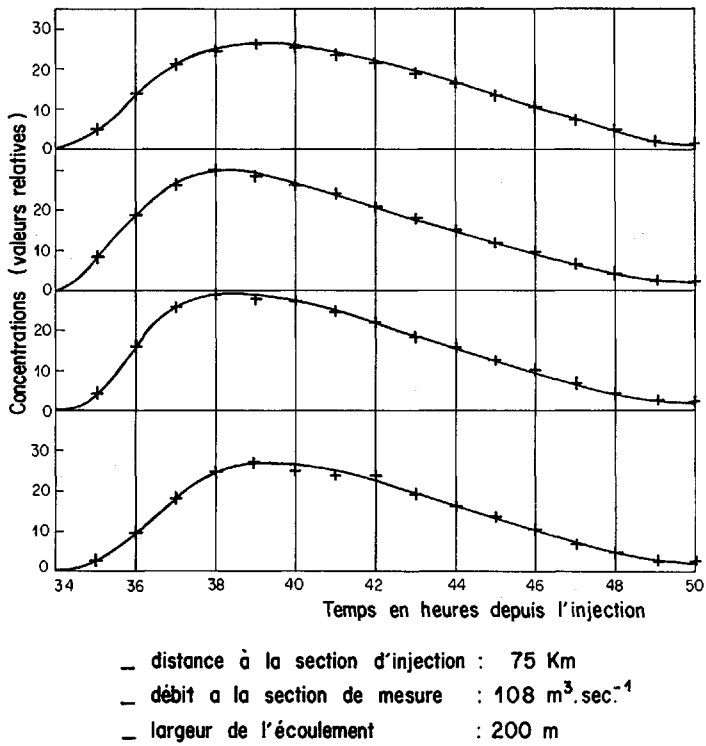

FIG. 7. Réponses impulsionnelles obtenues sur la Loire (pont d'Amboise).

4. TRANSFERT DANS UN MILIEU NON CONFINE ISOMORPHISME DES FONCTIONS $n(P_i, t)$

Le second mémoire que nous présentons à ce Colloque [1] expose dans les détails un problème de transfert dans un milieu non confiné. Les chapitres 5 et 6 du présent mémoire en sont d'autres illustrations. Dans ce chapitre 4, nous établissons une propriété importante sur le plan pratique dans les problèmes de transfert des eaux ou des substances polluantes, dans le milieu souterrain: l'isomorphisme des réponses impulsionnelles.

Pour la simplicité de l'exposé, le traitement est fait dans le cas d'un écoulement bidimensionnel, dans un milieu homogène en grand. Nous supposons que l'écoulement est constitué de bandes parallèles. Chaque bande, de plus, parallèle à l'axe général de l'écoulement, est identique à celle du modèle représenté à la figure 6 et présente un axe de symétrie:

$$h_1(t) = h_m(t)$$
$$h_2(t) = h_{m-1}(t)$$
$$\cdots\cdots\cdots\cdots$$

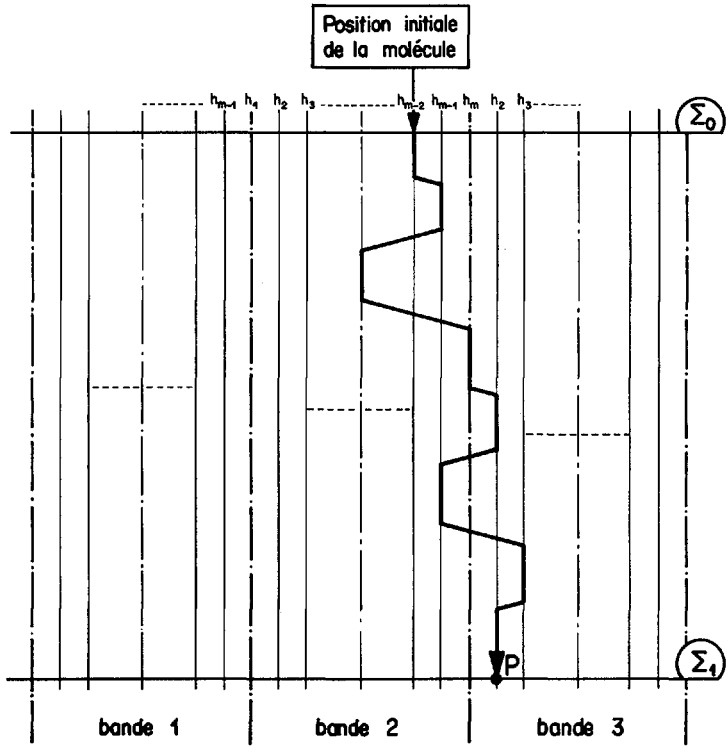

FIG. 8. Modèle d'écoulement bidimensionnel pour la démonstration de l'isomorphisme des fonctions n(P, t).

La frontière de chaque bande est commune à chaque bande; nous aurons, par exemple, des successions de lignes caractérisées par des réponses impulsionnelles.

$$\ldots h_{m-2}(t),\ h_{m-1}(t),\ h_1(t),\ h_2(t), \ldots,\ h_{m-1}(t),\ h_m(t),\ h_2(t),\ h_3(t) \ldots.$$

Dans ces conditions, une molécule se trouvant dans une ligne frontière est dans une situation symétrique et son changement de bande n'a pas d'effet sur sa probabilité ultérieure de se trouver, après un certain nombre d'étapes, dans une ligne d'indice 1, 2, . . . , m. Tout se passe, du point de vue de la probabilité pour la molécule d'arriver dans une ligne d'indice i, à une section Σ_1 perpendiculaire à l'écoulement, comme si cette molécule était restée dans sa bande d'origine (fig. 8).

On peut donc en conclure que les réponses impulsionnelles (distribution des temps de séjour) entre le point de départ et les points d'arrivée dans Σ_1 sont identiques. Nous n'avons pas fait d'hypothèses sur les probabilités d'atteindre un point donné de cette section, il a été seulement montré que, si la molécule atteint un de ces points, la distribution des temps de séjour

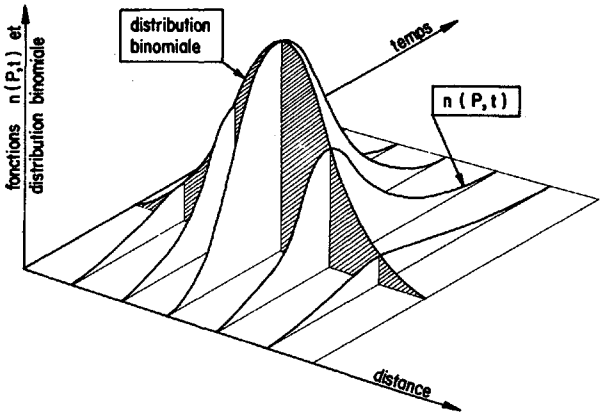

FIG. 9. Isomorphisme des fonctions n(P, t).

correspondante est indépendante de la position de ce point. Comme nous l'indiquons dans [1], la probabilité d'atteindre un point donné de la section Σ_1 est donnée par une loi binomiale.

Les fonctions $n(P_i, t)$ ont même forme (isomorphisme) et sont des affines; le coefficient d'affinité est donné par une distribution binomiale. Les réponses impulsionnelles

$$h_i(t) = \frac{n(P_i, t)}{\int_{-\infty}^{+\infty} n(P_i, t)dt}$$

sont identiques (fig. 9).

L'extension de cette propriété importante à un écoulement tridimensionnel pourrait être faite en imaginant un modèle présentant des symétries dans deux dimensions; il pourrait avoir pour surfaces frontières des cylindres s'appuyant sur un réseau d'hexagones réguliers, dans un plan perpendiculaire à l'écoulement. Le modèle bidimensionnel proposé étant déjà difficile à concevoir, nous pensons que c'est surtout le verdict expérimental qui doit confirmer les propriétés énoncées, c'est ce qui est montré dans [1].

5. TRANSFERTS ENTRE DEUX FORAGES

5.1. Position du problème

Les transferts de masses d'eau entre deux forages intéressant une nappe phréatique concernent, par exemple, des problèmes d'hydrodynamique (calage de modèles mathématiques), des problèmes de pollution d'aquifères

(caractéristiques de transfert de substances polluantes) [1]. La distribution des temps de séjour de l'eau entre deux forages permet, encore à titre d'exemple, de définir la vitesse moyenne de l'écoulement et de la comparer à la vitesse de Darcy efficace (quotient de la vitesse donnée par la loi de Darcy, par la porosité efficace). Dans ce dernier cas, il résulte des remarques faites au paragraphe 3.2 ci-dessus que l'on ne pourra obtenir une vitesse moyenne que si l'on peut faire l'hypothèse que les vitesses de chaque molécule d'eau entre F_1 et F_2 peuvent être considérées comme des variables aléatoires, centrées sur une valeur moyenne constante. Il serait donc incorrect d'exploiter la distribution des temps de séjour, pour une nappe fortement cylindrique, dans le but d'obtenir une vitesse moyenne.

Notre objectif est donc de déterminer la distribution des temps de séjour de l'eau entre deux forages, supposés crépinés sur toute la hauteur, tels que F_1 et F_2 (fig.10). Chaque forage a une entrée constituée par le demi-cylindre immergé amont, et une sortie constituée par le demi-cylindre aval. Il constitue lui-même un système. Le transfert qui nous intéresse est défini entre la surface Σ_0, sortie de F_1, et Σ_1, sortie de F_2. Un traceur est injecté dans F_1 et mesuré lors de son passage dans F_2. La technique qui résulte de l'analyse que nous proposons n'est évidemment pas exclusive.

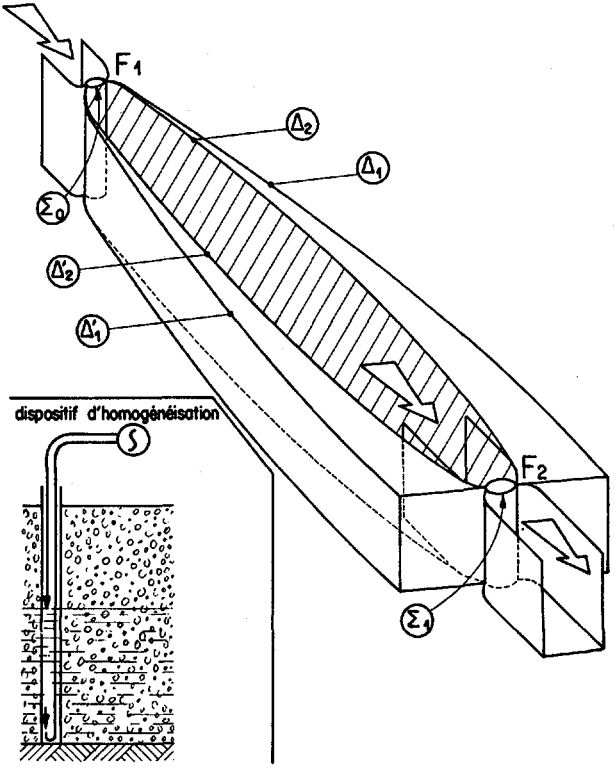

FIG.10. Transfert entre deux forages.

5.2. Injection du traceur

Si le milieu souterrain est, par exemple, constitué de couches de débit unitaire q_i, au niveau du forage d'injection, les quantités de traceur a_i à introduire dans chacune de ces couches doivent alors être proportionnelles à ces débits. Pour réaliser cette opération, la méthode la plus simple, au point de vue technique, consiste à homogénéiser le contenu du forage en lui apportant de l'énergie. On pompe l'eau au fond du forage et on la rejette au toit de la nappe, par exemple. Dans ce cas, la concentration en traceur C(t) de l'eau sortant de ce forage est alors égale à la concentration mesurée à l'intérieur du forage (propriété du mélangeur parfait). Le flux sortant du forage est ainsi Q C(t), c'est-à-dire est proportionnel à C(t) (Q étant égal à Σq_i). Cette homogénéisation dans le forage d'entrée doit être réalisée pendant un temps égal à la réponse impulsionnelle propre du forage. Si cette réponse impulsionnelle présente un temps non négligeable devant la durée du transit entre les deux forages (puits fermiers par exemple), l'injection ne pourra plus être considérée comme instantanée et il sera nécessaire de tenir compte de ce facteur dans l'analyse effectuée au niveau du forage de détection.

5.3. Conditions de mesure du traceur

Si la surface de sortie Σ_1 du système étudié était la surface d'entrée de F_2, les concentrations du traceur relevées au niveau de chacune des couches de terrain devraient être composées par le débit de ces couches q_j, pour obtenir le flux entrant dans ce forage de détection qui serait alors égal à $\Sigma q_j\ C_j(t)$. Pour éviter une telle procédure, impliquant une mesure de la concentration en traceur par couches et la connaissance du débit d'eau de chaque couche, on mesure le flux sortant de ce forage de détection. Ce flux sortant est obtenu en homogénéisant le contenu du forage (par pompage par exemple) et, comme précédemment, est proportionnel à la concentration mesurée à l'intérieur du forage (propriété du mélangeur parfait). Cette homogénéisation doit être effectuée pendant toute la durée de passage de la vague de traceur, dans le cas d'enregistrement continu de la concentration. Par contre, dans le cas où la mesure de la concentration est effectuée par des prélèvements à des dates discrètes, cette condition d'homogénéisation permanente n'est pas impérative. Il suffit alors d'effectuer cette homogénéisation avant le prélèvement, pendant un temps égal à la réponse impulsionnelle propre du forage. La réponse impulsionnelle propre du forage étant du type exponentiel caractérisé par un temps θ de renouvellement, un pompage d'une durée égale à $3\,\theta$, avant la prise d'échantillon, paraît alors suffisante.

Pour chaque forage, les flux d'entrée u(t) et de sortie y(t) sont liés par une intégrale de convolution:

$$y(t) = u(t) * h(t)$$

En effet, le système peut être ici considéré comme scalaire, à condition de réaliser par agitation (pompage) un bon mélange du traceur. C'est donc par une opération de déconvolution que l'on atteindrait u(t), si cela était nécessaire. De telles situations peuvent se présenter au niveau de F_2, par exemple s'il s'agit d'un puits fermier de grand volume.

On choisirait alors pour Σ_1 la face d'entrée de l'eau. h(t) serait alors facile à déterminer, si le système pouvait être considéré comme un mélangeur parfait.

Si la distribution des temps de séjour dans F_1 est trop grande par rapport à celle du transfert entre F_1 et F_2 (et ne peut donc plus être considérée comme une impulsion de Dirac), il faut en tenir compte en déterminant $h_1(t)$ pendant que le système est convenablement mélangé; en utilisant cette fonction comme fonction d'entrée du système F_1 - F_2 et en déconvoluant la fonction de sortie par cette dernière fonction, on obtient la fonction recherchée.

Remarquons enfin que, si les réponses propres des forages F_1 et F_2 sont égales, $h_1(t) = h_2(t)$, on peut facilement montrer que la distribution des temps de séjour déterminée entre les surfaces d'entrée des deux forages est identique à celle qui est déterminée entre leurs surfaces de sortie.

6. IMPORTANCE DE LA DISTRIBUTION DES TEMPS DE SEJOUR DANS LES PROBLEMES D'ECHANTILLONNAGE

Pour illustrer le rôle fondamental de la distribution des temps de séjour dans les problèmes d'échantillonnage, on se propose de commenter les deux exemples suivants:

- datation des eaux;
- transfert de substances polluantes dans les nappes ou les cours d'eau; cinétique d'interaction avec le milieu.

Ces deux exemples peuvent, a priori, paraître différents mais sont, en fait, de même nature quant à leur analyse; ils apparaissent tous deux comme des problèmes d'échantillonnage en relation avec la distribution des temps de séjour.

Soient:

$C_A(t)$ et $C_B(t)$ les variations de concentration au cours du temps d'une substance présente dans l'eau de l'aquifère, respectivement aux points A et B;

$h_{AB}(t)$ la réponse impulsionnelle ou distribution des temps de séjour de l'eau de l'aquifère entre les points A et B.

Supposons que le système entre A et B soit scalaire.

Si la substance considérée a même caractéristique de transfert que l'eau de l'aquifère décrite par la réponse impulsionnelle $h_{AB}(t)$, ces grandeurs $C_A(t)$ et $C_B(t)$ sont liées par l'intégrale de convolution habituelle:

$$C_B(t) = C_A(t) * h_{AB}(t)$$

6.1. Datation des eaux

La datation des nappes par le carbone-14 apparaît comme un cas relevant des hypothèses suivantes:

- il y a apport continu et constant dans le temps à l'eau de l'aquifère du carbone-14 (constante radioactive λ connue) sous forme de bicarbonate de calcium;
- ce bicarbonate de calcium, marqué au carbone-14, présente les mêmes caractéristiques de transfert que l'eau de l'aquifère et est sans interaction avec le milieu; sa disparition résulte uniquement de sa décroissance radioactive.

Dans ces conditions, en utilisant les notations précédentes, on peut écrire

$C_A(t)$ = constante = teneur à l'origine du carbone-14 dans le bicarbonate des eaux notée N_0

La réponse impulsionnelle entre les points A et B pour le bicarbonate marqué au carbone-14 est alors $h_{AB}(t) \exp(-\lambda t)$ où $h_{AB}(t)$ est la réponse impulsionnelle de l'eau entre A et B.

La teneur N_B en carbone-14 au point B est alors obtenue à partir de l'intégrale de convolution précédente qui, dans ce cas, s'écrit

$$N_B = \int_0^t N_0 \; h_{AB}(u) \exp(-\lambda u) du$$

L'expression communément admise

$$N_B = N_0 \quad \exp(-\lambda \tau)$$

qui permet de déterminer l'âge de l'eau τ à partir de la mesure de N_B et de N_0 résulte alors de l'expression ci-dessus, dans le cas et seulement dans le cas où

$$h_{AB}(t) = \delta(t-\tau) \qquad (\delta \text{ notation de Dirac})$$

Ainsi, l'expression habituelle suppose que le transfert de l'eau entre A et B s'effectue sans dispersion, c'est-à-dire comme un piston. Or, en fait, dans les écoulements souterrains, $h_{AB}(t)$ est différent de $\delta(t-\tau)$ et un échantillon d'eau prélevé au point B contient des eaux d'âges différents, dont la proportion est donnée par la distribution des temps de séjour ou réponse impulsionnelle.

La notion d'échantillonnage apparaît ainsi nettement dans cet exemple, et le principe de la datation des eaux par le carbone-14 suppose implicitement que le transfert des eaux dans l'aquifère s'effectue sans dispersion.

Dans le cas du tritium, l'influence de cette distribution des temps de séjour sur «l'âge» des eaux a été étudiée par Nir [7], dans les cas suivants: écoulement du type piston, mélangeur parfait et dispersif.

La réponse impulsionnelle entre deux points A et B peut être convenablement approchée par un modèle du type dispersif unidimensionnel tel que

$$h_{AB}(t) = \frac{1}{2} \frac{v}{\sqrt{\pi D t}} \exp \frac{(L - vt)}{4\,Dt}$$

où v représente la vitesse moyenne de l'écoulement
D le coefficient de dispersion
L la distance entre A et B.

Dans le cas de la datation par le carbone-14, on a alors

$$N_B = N_0 \int_0^\infty \frac{1}{2} \frac{v}{\sqrt{\pi D t}} \exp \frac{(L - vt)^2}{4\,Dt} \exp(-\lambda t)\, dt$$

Cette expression peut se mettre sous une forme adimensionnelle en introduisant le nombre de Peclet $P = vL/D$ et la variable réduite $\theta = t/\tau$ avec $\tau = L/v$.
On obtient ainsi

$$N_B = N_0 \int_0^\infty \frac{1}{2}\sqrt{\frac{P}{\pi\theta}}\ \exp\left[\frac{-P(1-\theta)^2}{4\,\theta}\right] \cdot \exp(-\lambda\tau\theta)d\theta$$

c'est-à-dire après intégration

$$N_B = N_0 \frac{P}{\sqrt{P^2 + 4Ps}} \exp \frac{P - \sqrt{P^2 + 4Ps}}{2}$$

avec $s = 0{,}693\ \tau/T$ (T période du carbone-14).

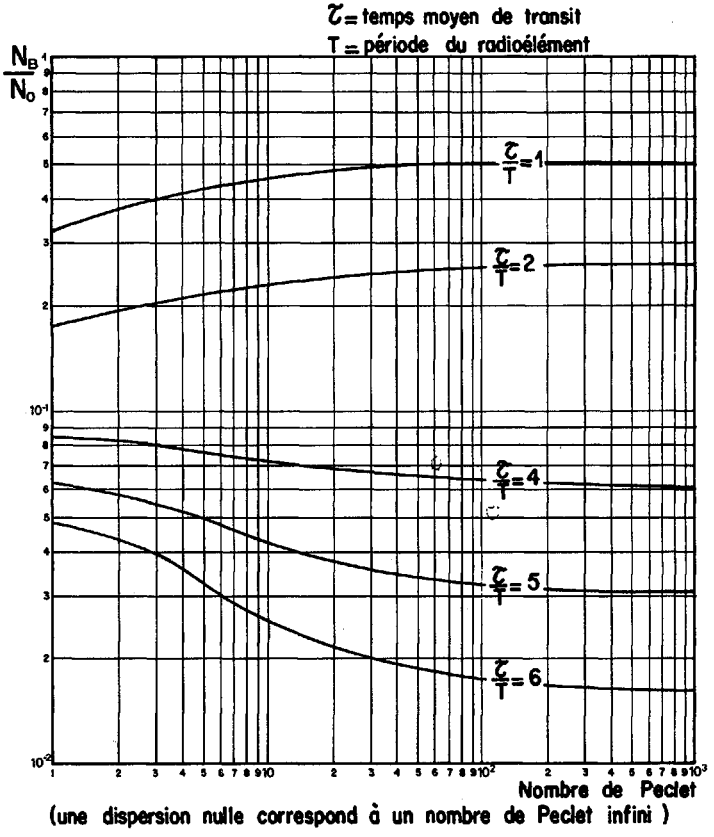

FIG.11. Influence du nombre de Peclet dans les problèmes de datation.

Cette expression montre qu'il est nécessaire de connaître P, nombre de Peclet, pour en déduire le temps moyen τ entre deux forages ou une zone d'alimentation des eaux souterraines et un forage, à partir des mesures de N et N_0.

Quand P est grand ($P > 1000$), l'écoulement peut être considéré comme peu dispersif, et l'expression ci-dessus tend vers la relation habituelle: $N_B = N_0 \exp(-\lambda\tau)$.

La figure 11 montre la valeur du quotient N_B/N_0 en fonction du nombre de Peclet P, pour différentes valeurs du rapport τ/T où τ = temps moyen de transit et T = période du radioélément.

On remarque que, pour des nombres de Peclet supérieurs à 100, il n'y a pratiquement pas de correction à apporter pour la détermination de l'âge moyen.

Citons enfin les valeurs des limites des distributions des temps de séjour, par exemple pour un âge moyen de 10 000 ans en fonction du nombre de Peclet:

Limites de la distribution des temps de séjour pour τ = 10 000 ans		Nombre de Peclet
2 000	23 000	10
4 000	20 000	20
6 000	15 000	75
7 000	14 000	200

Il apparaît que nos connaissances sur la dispersion dans le milieu poreux, dans le cas particulier où intervient la diffusion moléculaire, nécessitent de sérieux amendements afin que l'on puisse parfaire le traitement de la question importante de l'influence des distributions des temps de séjour dans la détermination des âges des eaux souterraines. De plus, on saisira facilement que ce problème se complique grandement si l'on a affaire à un système vectoriel.

6.2. Transfert de substances polluantes; cinétique d'interaction avec le milieu

Le transfert de substances polluantes dans un aquifère ou un cours d'eau relève de la même analyse. Si la substance est sans interaction avec le milieu et si son transfert est identique à celui de l'eau, on peut prévoir sa concentration en un point B, par l'intégrale de convolution précédente.

$$C_B(t) = C_A(t) * h_{AB}(t)$$

Si cette éventualité ne se produit pas, c'est-à-dire, s'il y a interaction de la substance avec le milieu, cette expression doit être modifiée pour tenir compte de la cinétique d'interaction. L'intégrale de convolution modifiée s'écrit alors

$$C_B(t) = C_A(t) * h_{AB}(t)\,\Gamma(t)$$

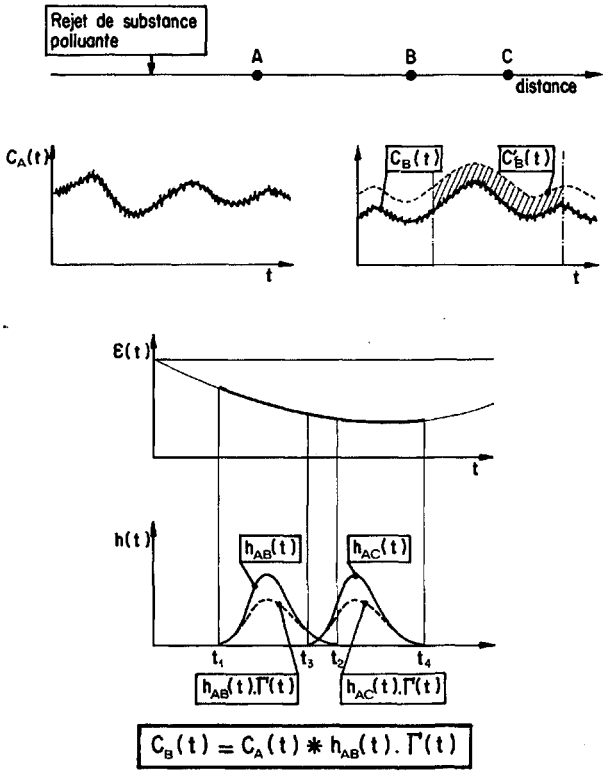

FIG.12. Détermination de la cinétique d'interaction avec le milieu.

où $\Gamma(t)$ rend compte de cette cinétique d'interaction. Cette analyse suppose implicitement que cette cinétique d'interaction de la substance avec le milieu est linéaire vis-à-vis de la concentration, c'est-à-dire que $\Gamma(t)$ est uniquement fonction du temps et non pas des concentrations.

La connaissance de $h_{AB}(t)$ et de $\Gamma(t)$ permet alors de prévoir la concentration en B, à partir de la concentration en A.

Inversement, dans un milieu soumis à pollution, on peut déterminer $\Gamma(t)$ à partir des grandeurs mesurées $C_B(t)$ et $C_A(t)$ et de la réponse impulsionnelle $h_{AB}(t)$, par une opération de déconvolution. A partir de cette information $\Gamma(t)$, on peut alors ultérieurement prévoir la réponse du milieu à une pollution entrante. L'exemple ci-après illustre ce cas.

Considérons (fig. 12) un cours d'eau soumis à une pollution et, soient $C_A(t)$ et $C_B(t)$ les teneurs en fonction du temps de l'oxygène dissous dans les sections A et B (A situé en amont de B). On supposera que l'on a affaire à un écoulement monodimensionnel. La convolution de $C_A(t)$ donnerait la teneur en oxygène en B, s'il n'y avait pas de consommation ou d'apport d'oxygène entre A et B. La comparaison de cette courbe théorique $C'_B(t)$

à la concentration en oxygène mesurée en B, $C_B(t)$, permet d'établir un bilan correct en oxygène. Ce bilan n'est possible qu'en tenant compte de la réponse impulsionnelle traduisant le transfert entre A et B. Ce cas met en évidence l'importance de cette distribution des temps de séjour et souligne l'aspect échantillonnage de ce problème.

D'autre part, à partir des teneurs en oxygène mesurées en A et B et de $h_{AB}(t)$ obtenu par traceur, on peut déterminer la fonction $\Gamma(t)$ (par déconvolution ou optimisation). Cette fonction sera alors définie sur un intervalle de temps (t_1, t_2) correspondant à la durée de la réponse impulsionnelle au point B. Une telle analyse peut être effectuée pour une section C située en aval de B, afin d'obtenir $\Gamma(t)$, sur un autre intervalle de temps (t_3, t_4) correspondant à la durée de la réponse impulsionnelle dans la section C. Cette analyse est toutefois en défaut si les teneurs en oxygène mesurées dans les sections A, B, C... sont constantes dans le temps. En effet, une expression du type

$$C_B = C_A \int_0^t h_{AB}(u)\, \Gamma(u) du$$

ne permet de déterminer $\Gamma(t)$ à partir de $h_{AB}(t)$. La seule possibilité consiste alors à admettre l'approximation $h_{AB}(t) = \delta(t-\tau)$ où τ est le temps moyen de transfert entre A et B, défini par le centre de gravité de la réponse impulsionnelle $h_{AB}(t)$ mesurée par traceur. On obtient alors $C_B = C_A \Gamma(\tau)$, expression permettant de déterminer la valeur de C(t) pour $t = \tau$, à partir des mesures C_B et C_A. La courbe $\Gamma(t)$ peut alors être construite par points, en effectuant des mesures d'oxygène dissous tout au long du cours d'eau et en admettant cette approximation.

L'analyse a été faite ici pour un écoulement monodimensionnel. Nous poursuivons actuellement des études traitant de ce problème pour des écoulements tridimensionnels en hydrologie de surface et en hydrologie des eaux souterraines.

REFERENCES

[1] COROMPT, P., et al., «Méthode pour la détermination des caractéristiques de transfert de substances polluantes dans les nappes aquifères», ces comptes rendus, vol. 2, IAEA/SM-182/41.

[2] LIFERMANN, J., Systèmes linéaires, Variables d'état, Masson et Cie, Paris (1972).

[3] ALLEN, C.M., TAYLOR, E.A., The salt velocity method of water measurement, Am. Soc. Mech. Eng. (Dec. 1923).

[4] DANCKWERTS, P.V., Continuous flow systems, Chem. Eng. Sci. 2 1 (1953) 1.

[5] SPALDING, D.B., A note on mean residence times in steady flow of arbitrary complexity, Chem. Eng. Sci. 9 (1958) 74.

[6] GUIZERIX, J., et al., «Expériences de traceur réalisées en France dans le cadre d'études sur la pollution thermique des cours d'eau», Nuclear Techniques in Environmental Pollution (C.R. Coll. Salzburg, 1970), AIEA, Vienne (1971) 63.

[7] NIR, A., On the interpretation of tritium "age" measurements of ground water, J. Geophys. Res. 69 12 (1964) 2589.

METHODE POUR LA DETERMINATION DE CARACTERISTIQUES DE TRANSFERT DE SUBSTANCES POLLUANTES DANS LES NAPPES AQUIFERES

P. COROMPT, B. GAILLARD, J. GUIZERIX,
R. MARGRITA, J. MOLINARI
CEA, Centre d'études nucléaires
de Grenoble, Grenoble

R. CORDA, N. CRAMPON, D. OLIVIER
Ministère de l'Agriculture
et du développement rural,
Service de l'Aménagement des eaux
de la région lorraine, Metz,
France

Abstract–Résumé

METHOD FOR DETERMINING THE CHARACTERISTICS OF POLLUTANT TRANSFER IN AQUIFERS.

The problems considered relate mainly to the definition of perimeters for the purpose of protecting underground water catchment areas. Use is made of a transition analysis method involving the pulse responses between two (or n) boreholes of a good tracer, the object being to determine minimum pollutant transfer times. Special attention is paid to the linearity conditions of the system, the representativeness of the ground samples between the boreholes, the signals received in the boreholes and transverse dispersion. It is established that the isochronism and isomorphism of the pulse responses relative to boreholes located in a plane perpendicular to the flow lines are of considerable practical significance. Examples drawn from current studies are presented.

METHODE POUR LA DETERMINATION DE CARACTERISTIQUES DE TRANSFERT DE SUBSTANCES POLLUANTES DANS LES NAPPES AQUIFERES.

Les problèmes traités concernent principalement la définition des périmètres de protection d'aires de captage des eaux souterraines. On applique une méthode d'analyse transitoire, dans laquelle sont exploitées les réponses impulsionnelles d'un bon traceur de l'eau obtenues entre deux ou n forages, afin de définir les temps minimums de transfert de substances polluantes. On analyse en particulier les conditions de linéarité du système, la représentativité de l'échantillon de terrain compris entre deux forages, les signaux recueillis dans un forage, la dispersion transversale, et l'on expose une propriété aux incidences pratiques importantes, qui est l'isochronisme et l'isomorphisme des réponses impulsionnelles relatives à des forages situés dans un plan perpendiculaire aux lignes de courant. Des exemples pratiques, tirés d'études en cours, sont donnés.

1. INTRODUCTION

1.1. Généralités

Le problème que nous abordons intéresse:

- la détermination des périmètres de protection des aires de captage des eaux souterraines,
- les dispositions à prendre dans le cas de rejets accidentels de substances polluantes pouvant atteindre ces captages (voies de communication, usines),

– l'implantation de forages de surveillance,
– l'implantation d'ouvrages de protection des captages.

Une solution drastique de ce problème impliquerait que l'on connaisse, pour tous les couples possibles – point de rejet potentiel de substances polluantes-forages ou puits – les chances, pour toutes les substances polluantes possibles, d'atteindre le puits, le temps de transfert correspondant, le temps de passage et les variations de concentration traduisant la contamination.

La méthode d'analyse et la tactique des mesures sur le terrain qui en découle représentent une solution approchée de ce problème.

Nous supposerons acquis les résultats des analyses exposées dans le mémoire IAEA-SM-182/48 [1], présenté à ce Colloque. L'originalité du présent mémoire réside dans les hypothèses simplificatrices initiales, dans la séparation des phénomènes de dispersion longitudinale et transversale, dans la propriété d'isomorphisme des réponses impulsionnelles, qui, liée aux hypothèses précédentes, autorise cette séparation, dans la détermination de la représentativité de l'échantillon de terrain intéressant l'expérimentation et, enfin, dans la tactique générale d'acquisition des informations.

1.2. Définition des périmètres de protection

Un réseau de lignes isopièzes permet de définir une ligne de partage des eaux souterraines (fig. 1). Supposant que celle-ci subit avec le temps des fluctuations, nous retenons la ligne L la plus éloignée de la zone de captage; elle constitue une partie du périmètre de protection recherché. Une correction, cependant, doit théoriquement être faite pour tenir compte de la dispersion transversale. Cette correction consiste à remplacer L par D, lieu des sommets des pseudo-paraboles définissant la limite du panache de dispersion des substances polluantes, l'une des branches de ces pseudo-paraboles passant par le point R de convergence des lignes de partage des eaux, à droite et à gauche du puits, sur la figure 1. Cette frontière D est une ligne limite de partage des eaux; une molécule d'eau lui appartenant a une probabilité faible mais non nulle d'atteindre le ou les puits de captage. En pratique, on adopte, en prenant une certaine distance de sécurité, une ligne Δ à l'extérieur de la surface déterminée par D pour définir, vers l'aval, une partie du périmètre de protection. A l'intérieur de cette courbe Δ, le périmètre de protection est défini par des lignes isochrones d'écoulement: I_1, I_2, I_3, par exemple, correspondant à différents temps minimums d'arrivée de substances polluantes dans les puits de captage. Ayant, à l'aide de traceurs, la possibilité de définir ces lignes avec une bonne précision, l'usage fixera les temps minimums relatifs aux périmètres de protection immédiats, rapprochés et éloignés. Il ne serait pas raisonnable, par exemple, d'adopter un périmètre de protection rapproché au-delà de la ligne correspondant à un temps minimum, t_0, inférieur à huit jours.

2. HYPOTHESES FONDAMENTALES

Supposons qu'une substance polluante ait été déversée, par exemple, à la surface du sol en un point I (fig. 2), et qu'après infiltration dans la

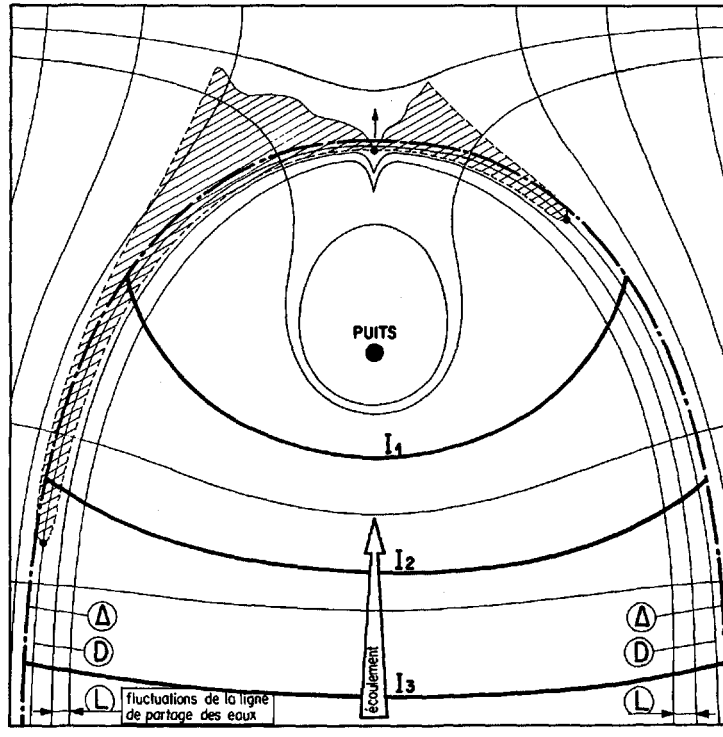

FIG. 1. Définition du périmètre de protection.

zone non saturée et migration dans la zone saturée d'une nappe phréatique, elle apparaisse, en partie, dans un puits P. Nous désirons définir le mode de passage de cette substance de I à P, et, pour résoudre notre problème général, être capable de définir ce transfert, quelle que soit la position du point I.

Au cours de son transfert, la substance polluante sera soumise à divers phénomènes, connus mais difficiles à préciser, ou inconnus: des phénomènes physiques (dispersion, adsorption, ...), physico-chimiques (échange d'ions, ...), chimiques (précipitations, ...), biochimiques, etc. Il est pratiquement impossible de prévoir l'effet global de ces phénomènes, dans l'état actuel de nos connaissances.

Isolons par la pensée la substance polluante rejetée pendant un *intervalle de temps court*, compris entre t_i et $t_i + dt$. Son passage en P est déterminé par une fonction concentration-temps $C_P(t)$. La réponse impulsionnelle correspondante $h^S_{IP}(t)$ est définie par

$$h^S_{IP}(t) = \frac{C_P(t)}{\int_{-\infty}^{+\infty} C_P(t)\,dt}$$

Elle est représentée à la figure 3.

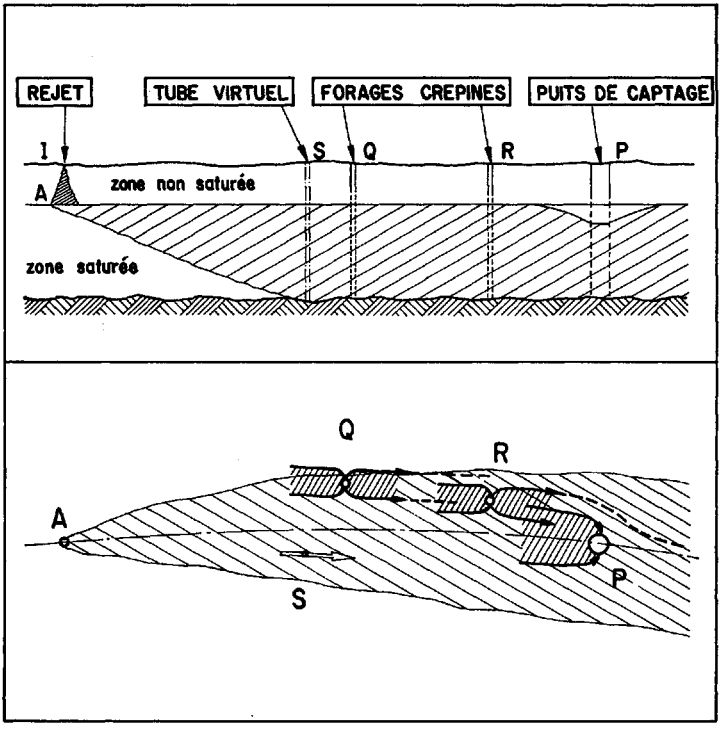

FIG. 2. Schéma de dispersion d'une substance polluante après rejet à la surface du sol.

Nous ne savons pas si le système intéressant le transfert de cette substance est linéaire et si, donc, nous pouvons utiliser $h^S_{IP}(t)$ comme une réponse impulsionnelle, dans une opération de convolution. Cependant, cette fonction est bien définie entre I et P.

Définissons, de même, la réponse impulsionnelle de l'eau, $h^E_{AP}(t)$, vecteur de la pollution, entre les points A et P, A étant situé au toit de la nappe, sur la verticale passant par I. Soit $h^T_{AP}(t)$ la réponse impulsionnelle d'un bon traceur de l'eau, entre A et P. Si nous adoptons une même origine des temps et si t_1, t_2, t_3 sont les dates de début des réponses $h^E_{AP}(t)$, $h^T_{AP}(t)$ et $h^S_{IP}(t)$, nous pouvons faire l'hypothèse que nous aurons le classement

$$t_1 \leqslant t_2 \leqslant t_3$$

En d'autres termes, le traceur peut ne pas être un traceur idéal et présenter un léger glissement par rapport à l'eau dans son transfert; la substance polluante sera retardée par rapport au bon traceur de l'eau. Dans l'évaluation des temps, nous avons négligé son transfert entre I et A, dans la zone non saturée. Nous prenons ainsi un facteur de sécurité favorable à la réalisation de $t_2 \leqslant t_3$.

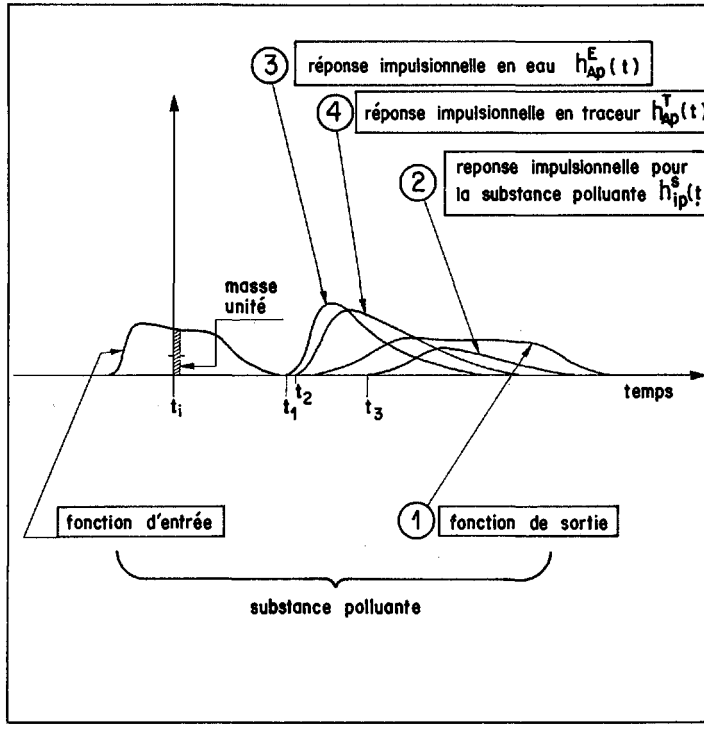

FIG. 3. Différents types de réponses obtenues dans le puits P.

t_2, qui représente le temps minimum d'arrivée de la substance polluante au puits P, est le paramètre essentiel, qui, à notre sens, intéresse les problèmes de pollution des ouvrages de captage pour la définition des périmètres de protection immédiats, rapprochés et éloignés (I_1, I_2, I_3). Son choix, comme nous le verrons, autorise le traitement séparé de l'effet de la diffusion transversale et longitudinale. Par ailleurs, s'il est souhaitable de disposer de l'ensemble des réponses impulsionnelles, de façon à pouvoir comparer les concentrations maximales admissibles et apprécier le temps de contamination d'un puits, nous pensons qu'il est pratiquement impossible de donner, aujourd'hui, une telle solution, étant donné l'état de nos connaissances.

Rappelons et complétons nos hypothèses et conditions initiales:

- la substance polluante est en solution ou en suspension dans l'eau; nous n'envisagerons donc pas le cas particulier important de la pollution des nappes par les hydrocarbures;
- le mouvement des substances polluantes les plus rapides est représenté par celui de l'eau;
- la vitesse de transfert est assez grande pour que l'on puisse négliger la diffusion moléculaire.

Notre problème revient alors à définir le transfert de l'eau, vecteur de la pollution, entre un point tel que A et un forage tel que Q (fig. 2), puis entre deux forages tels que Q et R, et à étudier des conditions d'extrapolation à tout l'espace. Nous traiterons enfin ce problème pour un écoulement à deux dimensions, le transfert étant défini entre deux forages Q et R; cela revient à prendre, pour le temps minimum de transfert, un coefficient supplémentaire de sécurité, dans le cas où le point A n'est pas situé sur l'horizon le plus perméable.

3. POSSIBILITE DE SEPARER LES PHENOMENES DE DISPERSION LONGITUDINALE ET TRANSVERSALE

Rappelons une propriété qui est démontrée dans le mémoire IAEA-SM-182/48 [1]. Un traceur étant injecté en un temps court dans un forage Q, l'observation du passage de ce traceur dans des forages R_1, R_2, ... situés dans un plan perpendiculaire à la ligne de courant passant par Q (fig. 4) fournit après homogénéisation (voir le chapitre 5 de [1]) des fonctions concentration-temps $C_1(t)$, $C_2(t)$, ... Les courbes représentatives de ces fonctions sont des affines et se déduisent donc les unes des autres, par multiplication des ordonnées par des constantes. Elles ont même forme. La figure 5 donne un exemple de vérification expérimentale de cette propriété. Les réponses impulsionnelles définies par

$$h^1_{QR}(t) = \frac{C_1(t)}{\int_{-\infty}^{+\infty} C_1(t)\,dt}$$

sont identiques.

Notre objectif étant d'atteindre t_0, temps minimum de transfert, il en résulte qu'un seul forage R sera nécessaire, en aval du forage Q d'injection du traceur, et que sa position dans un plan perpendiculaire à l'écoulement devra satisfaire aux deux seules conditions:

- d'intéresser le panache de dispersion;
- d'être assez éloignée de Q pour que le système, entre Q et R, puisse être considéré comme homogène en grand; cette dernière condition sera examinée au chapitre suivant.

Il est alors possible de traiter séparément, dans l'analyse, les phénomènes de dispersion transversale et longitudinale dès lors que l'on ne désire pas obtenir la valeur absolue des fonctions concentration-temps dans l'espace. Nous verrons dans le chapitre 4 qu'une conséquence importante de cette méthode d'analyse est de permettre, à l'avenir, lorsque les études sur l'interaction des substances polluantes avec le milieu auront progressé, de pouvoir utiliser des modèles mathématiques complexes qui tiendront compte de ces phénomènes d'interaction. Cela ne serait pas possible, à notre sens, avec les modèles mathématiques diffusionnels classiques.

Rappelons que ces modèles [2-6] visent à l'obtention des valeurs absolues des concentrations dans le temps et dans l'espace, leur écriture traduisant des bilans de matière.

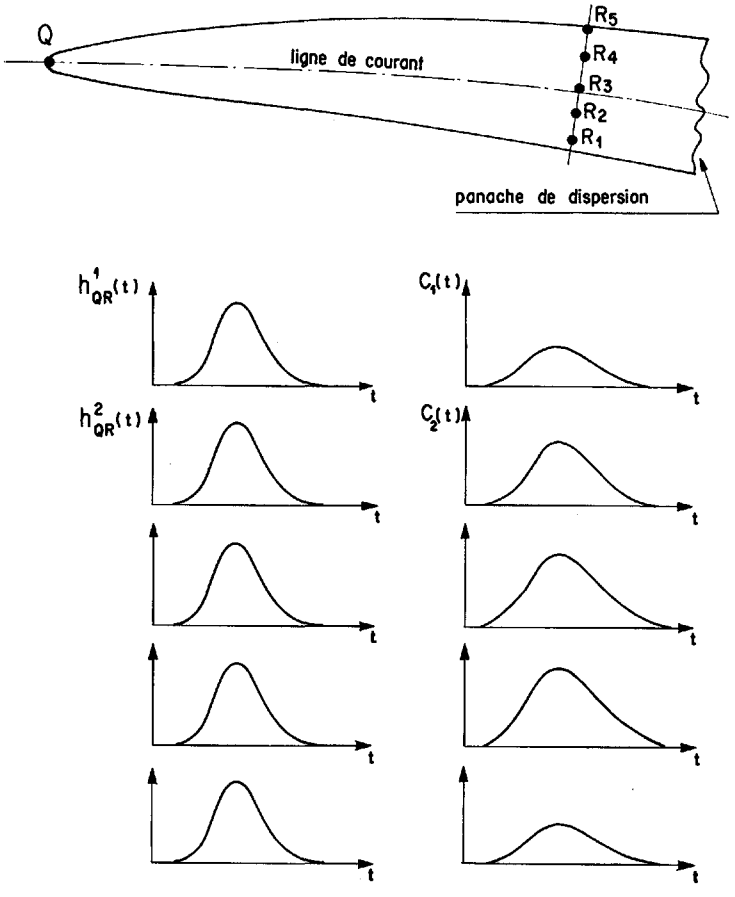

FIG. 4. Identité des réponses impulsionnelles et isomorphisme des fonctions $C_i(t)$.

4. DISPERSION LONGITUDINALE

4.1. Cas d'un gradient hydraulique constant

4.1.1. Détermination de la réponse impulsionnelle entre deux forages

Ce problème est examiné en détail dans [1]. Le traceur est injecté dans un forage tel que Q (fig. 2), l'eau du milieu étant homogénéisée en permanence par apport d'énergie extérieure. On peut, par exemple, à cette fin, utiliser une pompe qui prélève de l'eau au fond du forage et la rejette dans ce dernier au toit de la nappe. On réalise ainsi une injection pondérée par les débits. Dans un forage R, situé en aval, un dispositif analogue d'homogénéisation peut être mis en œuvre et l'on détermine la

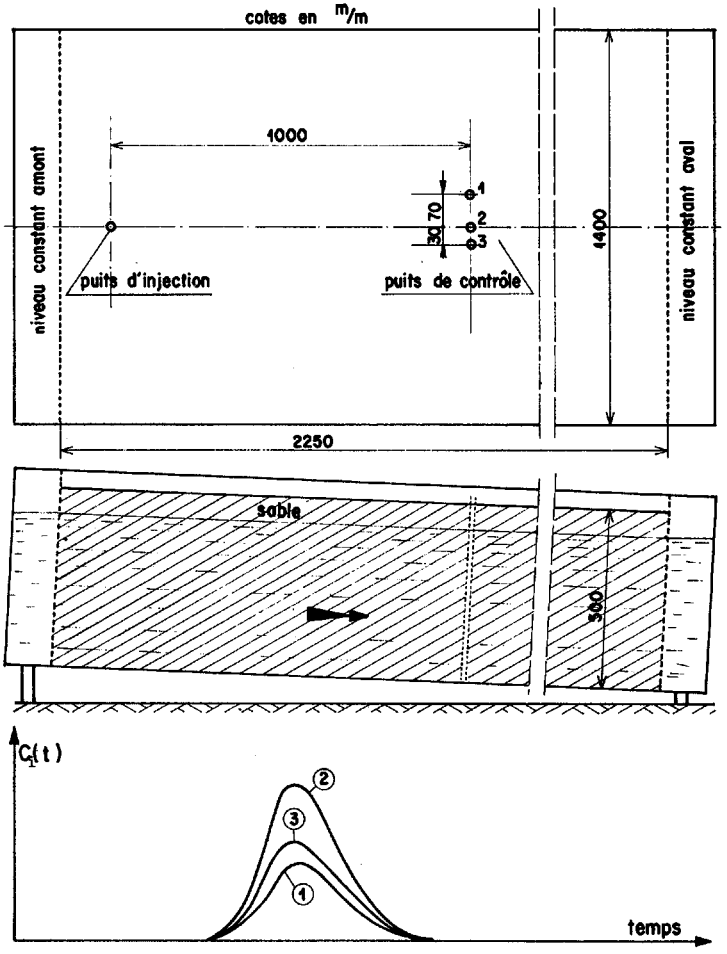

FIG. 5. Vérification expérimentale de l'isomorphisme des fonctions concentration-temps (cuve).

fonction concentration-temps qui permet de calculer la réponse impulsionnelle $h_{QR}(t)$. Si les réponses impulsionnelles propres aux forages Q et R ont une durée non négligeable devant celle de $h_{QR}(t)$ il faut en tenir compte, et cette dernière fonction est obtenue par une opération de déconvolution entre les fonctions de sortie et d'entrée du système. L'homogénéisation dans Q n'est nécessaire, avant le prélèvement d'échantillon, qu'un temps au moins égal à la durée de la réponse impulsionnelle propre de ce forage. Si cette réponse impulsionnelle est exponentielle, on peut adopter un temps d'homogénéisation égal à trois fois la constante de temps.

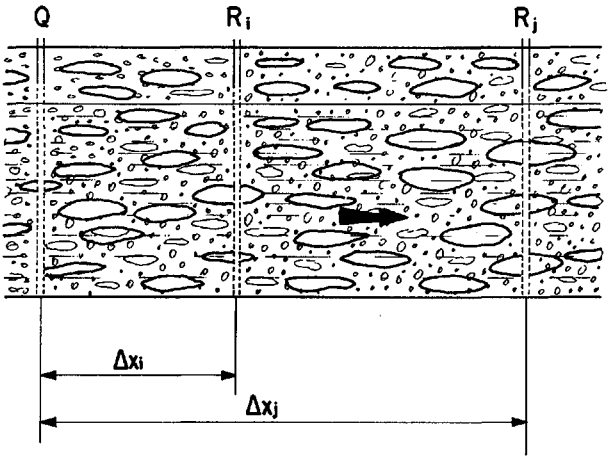

FIG. 6. Notions d'homogénéité en petit et en grand.

4.1.2. Représentativité de l'échantillon de terrain compris entre les deux forages; linéarité du système

Nous développons, dans ce paragraphe, deux notions importantes qui, dans l'examen de notre problème, sont liées. En premier lieu, la notion d'homogénéité en grand et en petit. L'analyse que nous faisons dans ce mémoire suppose que l'on ait affaire à un milieu homogène. Il ne peut être supposé homogène qu'à partir d'une certaine dimension (distance QR) que notre objectif est de déterminer. Le milieu peut, par exemple (fig. 6), comporter des lentilles argileuses et l'intuition nous laisse prévoir, sur cette figure, que la distance Δx_i est trop faible pour que l'on puisse considérer que le système est homogène alors que la distance Δx_j paraît suffisante.

En second lieu, dans l'extrapolation à tout l'espace intéressant le problème de l'information représentée par $h_{QR}(t)$ par des opérations de convolution, comme nous le verrons dans le paragraphe suivant, il est nécessaire que le système constitué par l'ensemble de cet espace soit linéaire. On peut en effet considérer les sous-systèmes comme des opérateurs au sens mathématique du terme, qui permettent de transformer les fonctions d'entrée en fonctions de sortie. Ces opérations doivent être linéaires pour que l'on puisse réaliser ces transformations par des opérations de convolution (voir l'exposé détaillé de cette question dans [1]). Nous pouvons traduire cette condition de la manière suivante: la réponse impulsionnelle $h_{QR}(t)$ doit être stationnaire dans l'espace, c'est-à-dire, quel que soit le couple QR, ou encore, si la distance Δx est suffisante pour que le milieu soit homogène en grand.

La figure 7 illustre la technique que nous proposons pour vérifier que cette condition est réalisée ou, en d'autres termes, que le «pas» d'espace adopté, Δx, est suffisant.

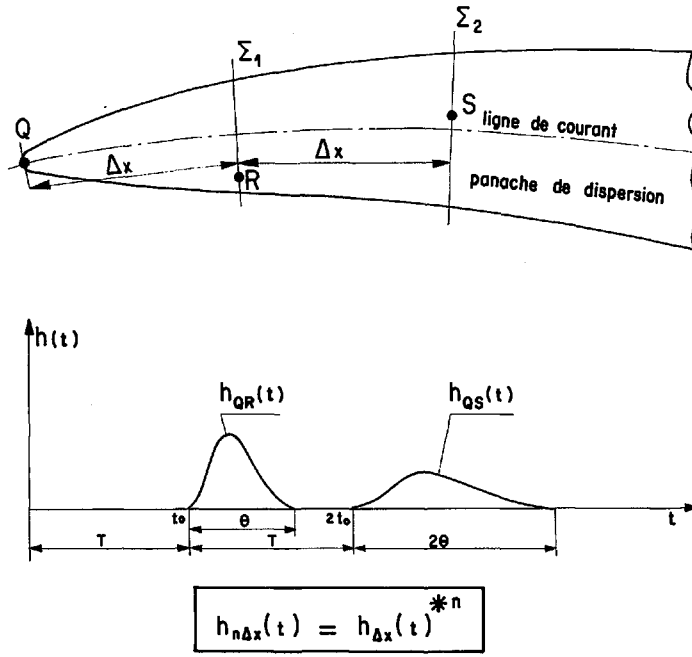

FIG. 7. Vérification de la stationnarité de h(t) dans l'espace.

Il faut disposer, pour cela, de trois forages tels que Q, R, S, équidistants. Après injection du traceur en Q et mesure de ce dernier en R et S, on détermine les réponses impulsionnelles $h_{QR}(t)$ et $h_{QS}(t)$. Il faut vérifier que

$$h_{QS}(t) = h_{QR}(t) * h_{QR}(t)$$

le symbole $*$ représentant une opération de convolution. L'examen géologique du milieu étudié permet de se faire une idée de la grandeur Δx, dans le choix de Q et R, et, éventuellement, du nombre de tests à réaliser si le système est constitué de sous-systèmes qui, seuls, pourront être considérés comme homogènes. La figure 8 donne un exemple de vérification expérimentale obtenue sur un modèle physique.

4.1.3. Extrapolation dans l'espace

Notre objectif étant, rappelons-le, de déterminer t_0, il est nécessaire de connaître les réponses impulsionnelles pour tout l'espace considéré. Dans la zone où le gradient hydraulique est constant, une opération de convolution donne la solution

$$h_{n\Delta x}(t) = h_{\Delta x}(t)^{*n}$$

l'exposant $*n$ signifiant qu'il faut convoluer la fonction n fois par elle-même.

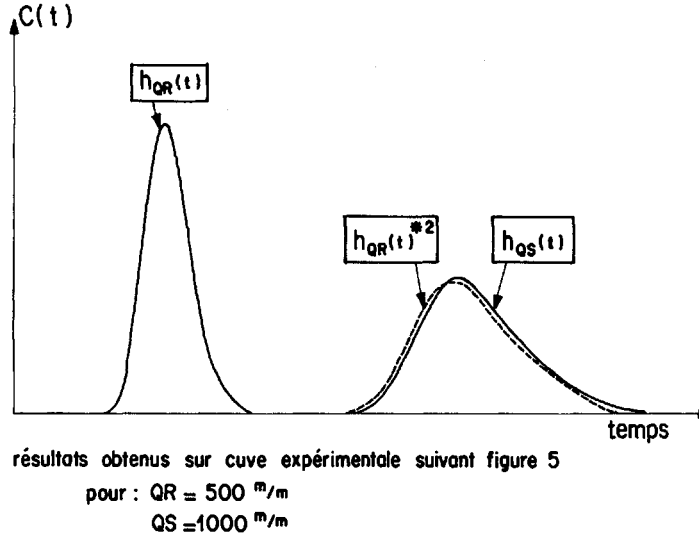

FIG. 8. Exemple expérimental de la stationnarité de h(t) dans l'espace.

Dans le voisinage d'un puits où un pompage est réalisé, le gradient est variable; on peut obtenir une réponse impulsionnelle globale que l'on pourra convoluer pour les réponses impulsionnelles déterminées dans la zone où le gradient est constant, en injectant le traceur dans un forage situé à la limite de la zone perturbée et en le mesurant dans le puits.

Nous avons, dans le cadre de marchés, réalisé de telles expériences [7-9], pour lesquelles nous utilisons comme traceur NaI, $2H_2O$ dosé par voie chimique [10] ou par activation (sensibilité 10^{-9}).

4.2. Cas d'un gradient hydraulique variable

Si la zone étudiée présente un gradient hydraulique variable, la méthode des fonctions de transfert est théoriquement applicable. On a, en effet, affaire à un système qui peut être linéaire et variant dans l'espace [1].

Pour des questions pratiques et économiques, cette méthode ne semble pas la meilleure, nous lui préférons une extrapolation faisant intervenir un modèle diffusionnel simplifié.

L'information particulière que nous désirons, t_0, temps minimum de transfert de l'eau, et la propriété d'isomorphisme des réponses impulsionnelles nous autorisent à traiter le problème dans un écoulement unidimensionnel.

Nous adopterons, par exemple, le modèle piston-diffusion (un paramètre) couramment utilisé dans le domaine du génie chimique.

L'expérience montre qu'un modèle aussi simple permet de fort bien décrire les résponses impulsionnelles observées. La possibilité de traiter le problème en écoulement monodimensionnel laisse la possibilité d'utiliser

des modèles plus complexes et, dans une certaine mesure, plus réalistes tel un modèle du type piston-diffusion avec échange avec des zones mortes (trois paramètres) qui, conçu pour les colonnes à garnissage, en génie chimique, doit fort bien s'appliquer aux écoulements souterrains [11].

La tactique générale que nous proposons est la suivante:

a) Détermination par les méthodes classiques du réseau des isopièzes dont on déduit le réseau des lignes de courant.
b) Expérimentation à l'aide de traceur pour déterminer, entre deux forages Q et R, $h_{QR}(t)$.
c) Ajustement de cette fonction à celle qui est prévue pour un modèle diffusionnel.

Cet ajustement se fait par optimisation mathématique du ou des paramètres du modèle.

Par exemple, dans le cas d'un modèle du type piston-diffusion

$$h_{QR}(t) = \frac{1}{2} \frac{V}{\sqrt{\pi D t}} \exp \frac{-(\Delta x - Vt)^2}{4Dt}$$

où V = vitesse moyenne de l'écoulement
D = coefficient de dispersion
Δx = distance entre les forages Q et R.

La vitesse moyenne est déterminée à partir des données hydrogéologiques classiques (coefficient de Darcy, gradient hydraulique, porosité efficace).

La fonction $h_{QR}(t)$ obtenue à l'aide de traceur permet un recoupement de cette valeur à condition [1] que les vitesses de chaque molécule d'eau puissent être considérées entre Q et R comme des variables aléatoires centrées sur une valeur moyenne constante.

On a alors

$$V = \Delta x \int_{-\infty}^{+\infty} \frac{1}{t} h_{QR}(t)\, dt$$

En adoptant la variable réduite $\theta = t/\tau$ où $\tau = \Delta x/V$, l'expression donnant la réponse impulsionnelle devient

$$h_{QR}(\theta) = \frac{1}{2}\sqrt{\frac{p}{\pi\theta}} \exp \frac{-p(1-\theta)^2}{4\theta}$$

où $p = V\Delta x/D$ est le classique nombre de Peclet.

d) Extrapolation. Sur une ligne de courant, la fonction V(x) étant connue il est nécessaire de définir la loi de variation du coefficient de dispersion avec la vitesse. On adopte une loi linéaire: D = KV [12, 13]. Notre étude sur modèle réduit tend à confirmer cette loi.

Des études sur différents sites, en grandeur réelle, sont en cours pour asseoir cette tactique d'intervention pour la détermination des lignes d'isotemps minimum de transfert des substances polluantes.

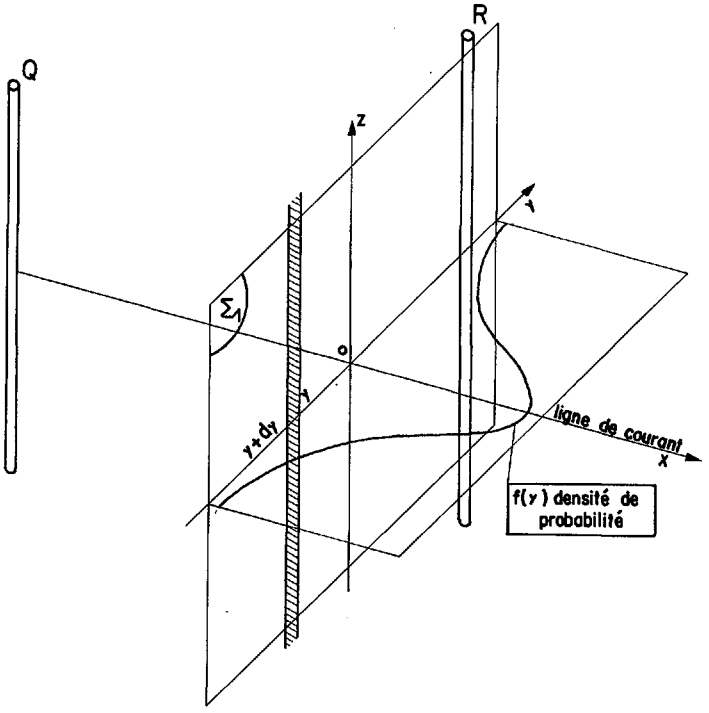

FIG. 9. Définition de la densité de probabilité pour une molécule d'eau issue de Q de traverser un plan perpendiculaire aux lignes de courant.

5. DISPERSION TRANSVERSALE

Il faut tenir compte de la dispersion transversale pour corriger la ligne de partage des eaux, comme nous l'avons vu plus haut. Etant donné, d'une part, l'imprécision dans la détermination de la ligne de partage des eaux et donc de la distance de sécurité qu'il est nécessaire d'adopter, et, d'autre part, la faible importance de la dispersion transversale lorsqu'elle n'est pas due à des mouvements convectifs, nous pensons que sa détermination est d'une importance secondaire. Nous traiterons le problème en termes de probabilité.

5.1. Détermination de la dispersion pour un pas d'expérience Δx à une distance Δx de Q

Soit (fig. 9) un forage Q et un plan Σ_1 perpendiculaire aux lignes d'écoulement, en aval de Q. Soient des axes de coordonnées y, z dans Σ_1. Nous recherchons la loi de densité de probabilité f(y), indépendante du temps, pour une molécule d'eau issue de Q, de traverser Σ_1 dans une bande verticale définie par y et y + dy.

Supposons que le milieu est composé de petites sphères de diamètre égal, empilées selon un réseau imbriqué (modèle classique). Supposons qu'une molécule d'eau arrivant sur une sphère a une chance sur 2 de passer à gauche (probabilité p) et une chance sur 2 d'aller à droite (probabilité q). Après m étapes, la probabilité P_k pour que la molécule soit allée k fois à gauche est donnée par une distribution binomiale

$$P_k = p^k q^{m-k} C_m^k$$

où $C_m^k = \frac{m!}{k!(m-k)!}$ et $p = q = 1/2$.

Il en résulte, selon nos conventions, que la probabilité pour une molécule de traverser Σ_1 dans une bande dy de Σ_1 est une distribution binomiale, à condition que dy soit égal au diamètre des sphères considérées. La distance Δx est égale à $m\lambda dy$, λ étant une constante.

Cette distribution est une distribution discrète et dy n'est pas, jusqu'ici, un élément différentiel. Nous pourrons, pour n assez grand ($n > 20$), la représenter avec une bonne approximation par une loi de Laplace-Gauss de valeur moyenne μ et d'écart-type σ

$$f(y)dy = \frac{1}{\sqrt{2\pi}} \exp\left[-\frac{1}{2}\frac{(y-\mu)^2}{\sigma^2}\right]\frac{dy}{\sigma}$$

Soit un forage tel que R (fig. 9) dans Σ_1, et $C_R(t)$ la fonction concentration-temps d'un traceur, obtenue dans ce forage, après une injection dans Q.

La distribution sur y de $\int_{-\infty}^{+\infty} C_R(t)$, quelle que soit la position de R dans Σ_1, est, à une constante près, égale à f(y).

Nous adopterons l'écart-type $\sigma_{\Delta x}$ pour caractériser la dispersion; l'indice Δx rappelle que cet écart-type est relatif à une distance.

Sur le plan expérimental, on dispose dans Σ_1 trois ou quatre forages et, à la suite d'une injection de traceur en Q, on détermine les fonctions $C_{R1}(t)$, $C_{R2}(t)$, ... dont les intégrales permettent le calcul de f(y).

5.2. Extrapolation à une distance $m\Delta x$

La variance d'une distribution binomiale étant égale à mpq, il en résulte que l'écart-type varie pour des distances $m\Delta x$ comme $\sqrt{m}$

$$\sigma_{m\Delta x} = \sqrt{m}\,\sigma_{\Delta x}$$

Cette propriété peut encore être vue de la manière suivante: Soient, en aval d'un forage Q, deux plans Σ_1 et Σ_2 perpendiculaires aux lignes d'écoulement, à des distances Δx et $m\Delta x$ de Q (fig. 10). Soient $f_1(y)$ et $f_2(y)$ les densités de probabilités de passage, dans des bandes verticales de largeur dy, pour des molécules d'eau issues de Q.

Si l'on fait l'hypothèse que l'on a affaire à un milieu homogène en aval de Q, c'est-à-dire, qu'il y a stationnarité dans l'espace de la « réponse

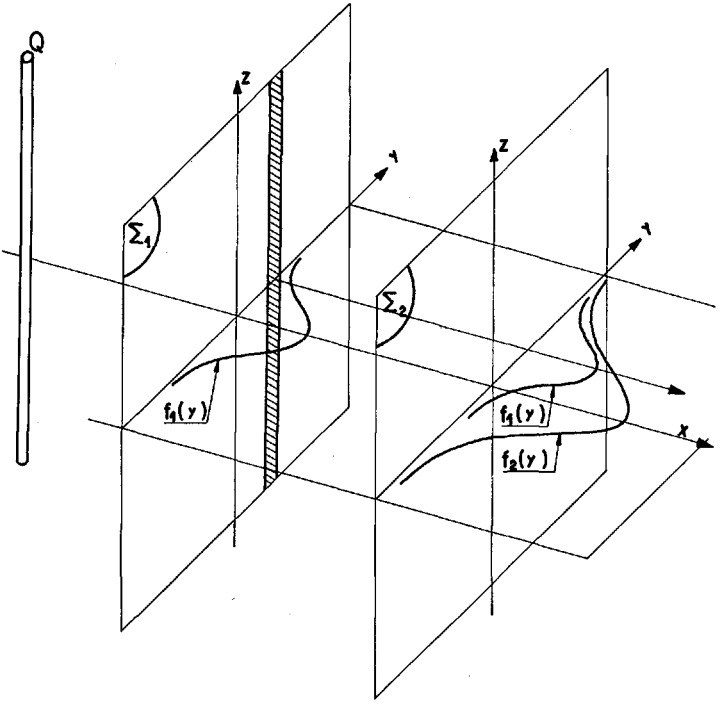

FIG. 10. Variation dans l'espace de l'écart-type de la densité de probabilité.

impulsionnelle» $f_1(y)$, alors $f_2(y)$ peut s'obtenir en convoluant $f_1(y)$ m fois par elle-même

$$f_2(y) = f_1(y)^{*m}$$

Nous connaissons, par ailleurs, la propriété d'additivité des variances dans l'opération de convolution. Si $\sigma_{\Delta x}$ est l'écart type de $f_1(y)$ et $\sigma_{m\Delta x}$ celui de $f_2(y)$, on a

$$\sigma^2_{m\Delta x} = m\,\sigma^2_{\Delta x}$$

Soit

$$\sigma_{m\Delta x} = \sqrt{m}\,\sigma_{\Delta x}$$

Il en résulte qu'un panache de dispersion en milieu poreux présente une allure parabolique, comme le montre la figure 11.

L'étude expérimentale, conduite sur un modèle physique représentant une nappe de 1,40 × 2,25 m a montré en premier lieu que f(y) était représenté avec une excellente approximation par une distribution binomiale.

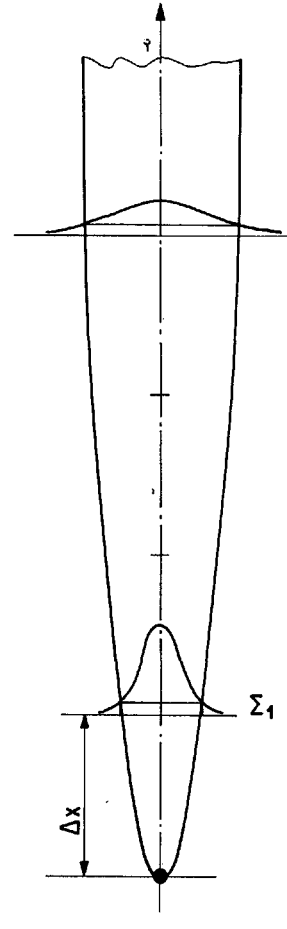

FIG. 11. Forme du panache de dispersion.

Par ailleurs, pour un sable de granulométrie $d_{50} = 0,78$, $\sigma_{2m} = 0,112$. Il en résulte que, pour un milieu identique, à 1 km on aurait

$$\sigma_{1000\,m} = \sqrt{500} \cdot 0,112 = 2,5 \text{ m}$$

En prenant 4σ comme «largeur» de panache de dispersion à 1000 m cette largeur serait seulement de 10 m.

REFERENCES

[1] GUIZERIX, J., et al., «Analyse des informations fournies par les traceurs naturels ou artificiels dans l'étude des systèmes aquifères en hydrogéologie», ces comptes rendus, vol.2, IAEA-SM-182/48.

[2] BACMAT, Y., BEAR, J., The general equation of hydrodynamic dispersion in homogeneous isotopic porous media, J. Geophys. Res. 69 12 (1964) 2561-67.

[3] GELHAR, L.W., COLLINS, M.A., General analysis of longitudinal dispersion in nonuniform flow, Water Resour. Res. USA 7 6 (1971) 1511-21.
[4] FRIED, J.J., COMBARNOU, M.A., Dispersion in porous media, Adv. Hydrosci. USA 7 (1971) 169-282.
[5] SAUTY, J.P., Modèle mathématique de la propagation d'un front de pollution dans une nappe d'eau souterraine, Houille Blanche 8 (1971) 731-35.
[6] SCHEIDEGGER, A.E., General theory of dispersion in porous media, J. Geophys. Res. 66 16 (1961) 3273-78.
[7] GAILLARD, B., Mesure de la vitesse limite de transit de substances polluantes dans la nappe alluviale de la Moselle, Aire de captage de Montigny, DR/AR-G/73-2/BG-MC (janvier 1973) (rapport privé).
[8] GAILLARD, B., Mesure de la vitesse limite de transit de substances polluantes dans la nappe alluviale de la Moselle, Aire de captage de Metz-Sud, DR/AR-G/73-43/BG-MC (octobre 1973) (rapport privé).
[9] GAILLARD, B., Détermination à l'aide de traceur de la vitesse maximale de transit de l'eau de la nappe sur le site du champ de captage des eaux de la ville de Grenoble, DR/AR-G/73-40/BG-EG (septembre 1973) (rapport privé).
[10] GODIN, J.M., ARCHIMBAUD, M., Microdétermination rapide de l'iode dans les eaux, Centre de Pierrelatte, Rapport CEA-R-3145 (1967).
[11] VILLERMAUX, J., VAN SWAAIJ, W.P.M., Modèle représentatif de la distribution des temps de séjour dans un réacteur semi-infini à dispersion axiale avec zones stagnantes, Application à l'écoulement ruisselant dans les colonnes d'anneaux Raschig, Chem. Eng. Sci. 24 7 (1969) 109.
[12] DAY, P.R., Dispersion of a moving salt, Water bondary advancing through satured sand, Trans. Am. Geophys. Union 37 5 (1956) 595-601.
[13] BERTSCH, W., Hydrodynamische Dispersion von $SrCl_2$, Lösung in Einkornsanden bei gesättigtem Fliessen, Dtsch. Gewaesserkd. Mitt. 14 5 (1970) 131-38.

DISCUSSION

S. GAONA VIZCAYNO: In your oral presentation you said that, in the case under consideration, the velocity obtained in the unsaturated zone when using a salt solution should be closer to the true velocity of the water. One must bear in mind, however, that there is going to be a change in the velocities owing to the density difference between the water which was already in the porous medium and the water with the salt tracer, especially in zones where there are air occlusions in the porous medium. Would you care to comment on this point?

J. GUIZERIX: The method presented in our paper is only for transfer in the saturated zone, and I do not think that, given the small amount of tracers employed, there are density currents. The situation is much more complex in the unsaturated zone, and I do not think we shall master the water velocity approach very soon using a tracer method.

H.A. MUNERA: How does your model take into account local variations in the isomorphism of the probability density curves caused by flows in heterogeneous media (with fissures and similar features)?

J. GUIZERIX: If the system between the two boreholes is not "homogeneous on a large scale", in the sense intended in our paper, the pulse response will probably not be isomorphic. This may result from an excessively small "measurement step" (Δx).

H.A. MUNERA: For what kind of medium is the piston-dead waters model most suitable?

J. GUIZERIX: It is suitable for a medium with grain porosity rather than for a fissured medium.

J.B. ROBERTSON: Does your analytical method involve the use of transverse dispersion coefficients?

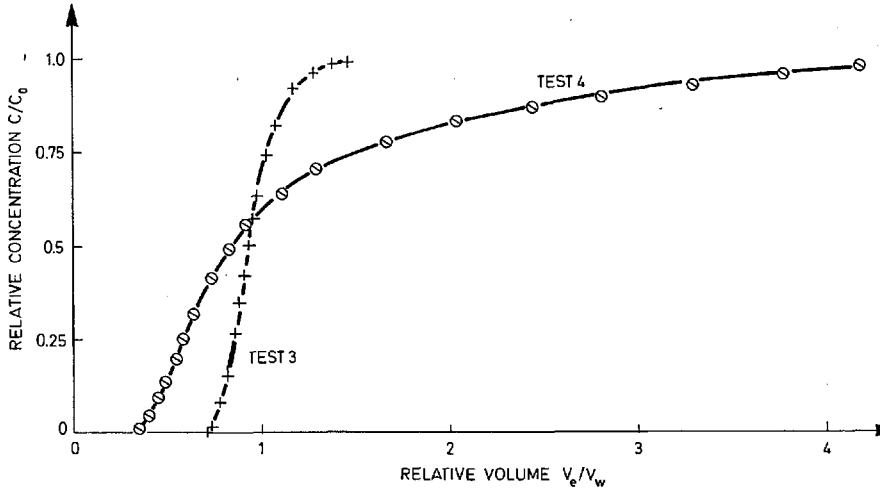

FIG. A. Variation of relative concentration for various water contents.

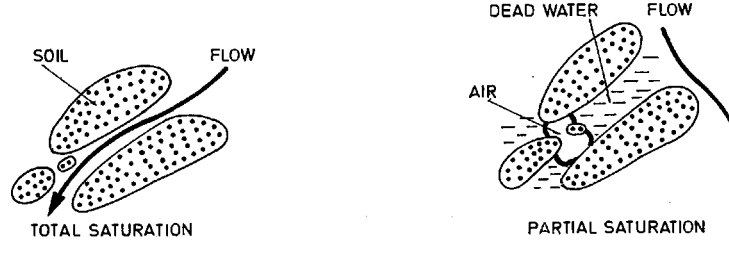

FIG. B. Effect of trapped air on flow.

J. GUIZERIX: No, it does not. In the experiment with the physical model described in Fig. 5, the ratio of the standard deviations of the concentration function in space was close to four.

J. P. GAUDET: I should like to present some results, obtained in our laboratory, relating to the problems of dispersion in the unsaturated zone.

We established a permanent flow of pure water in a vertical sand column, then, at a moment t = 0, we continued the flow with a non-zero constant tracer concentration. The response curves obtained at the column outlet are presented in Fig. A. The water contents, which were constant along the column, were 0.36 cm^3/cm^3 for test 3 and 0.29 cm^3/cm^3 for test 4. The concentration front propagation velocities were the same in both cases, and it was reasonable to expect similar response curves. In the case where the water content was lower, however, the response was very different, partly because the concentration varies more rapidly with time at the bottom of the column and partly because the tail of the curve is

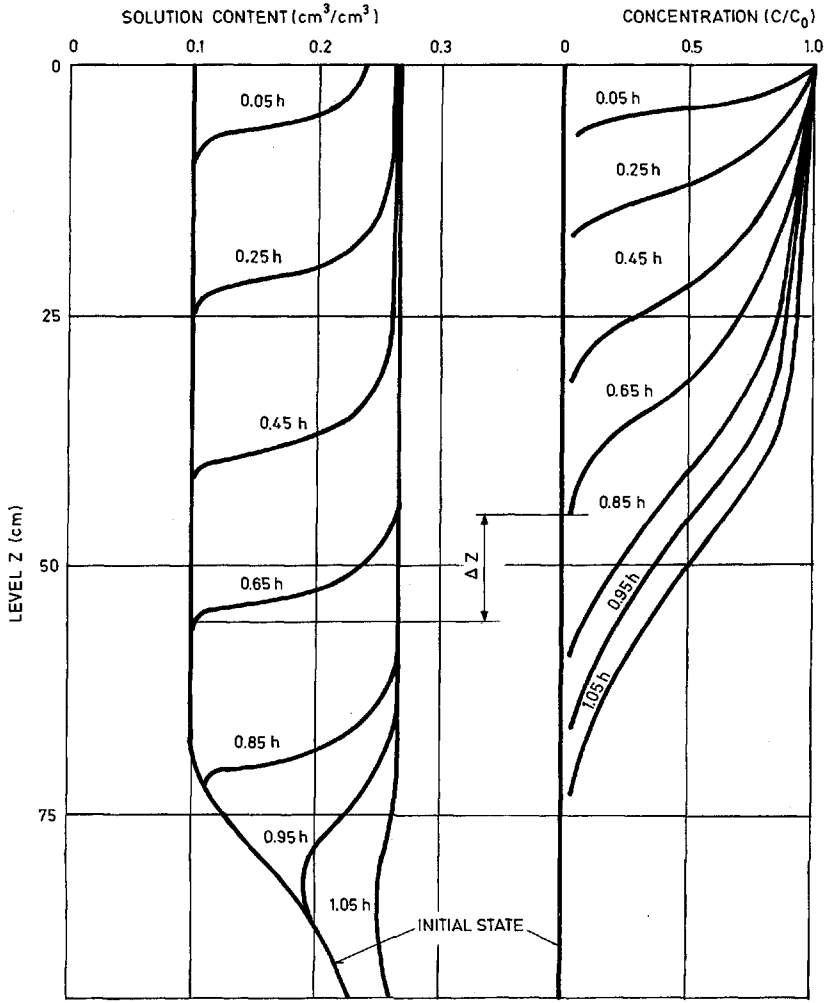

FIG. C. Water and salt transitory flow (q_0 = 13.6q cm/h).

longer. We attribute this phenomenon to the fact that, when the water concentration is not close to the porosity value, occluded bubbles of air block some of the hydraulic pathways, thereby creating "dead-end" pores (see Fig. B). These "dead-end" pores give rise to two liquid phases, a mobile one and one attached to the solid matrix. In any mathematical system explaining the phenomenon, one must therefore take into account tracer transfers between the two phases. We have shown experimentally that in the unsaturated zone one can have very clear separation of the moisture and salinity fronts. The experiment was as follows: we introduced, by infiltration, salt water into a pure water concentration profile obtained by equilibration after drainage; the propagation of the moisture and relative

concentration profiles is illustrated in Fig. C. Thus, we have shown clearly that the diffusion approach must take account of the exchange between mobile water and dead water, and that the tracers in the unsaturated zone do not follow the water exactly.

A. L. BENTZ: With regard to Fig. C presented by Mr. Gaudet, I should like to know whether he advises against using tracers in studies of unsaturated media.

J. P. GAUDET: No, but I recommend extreme caution when one is interpreting the results quantitatively.

A. L. BENTZ: If one can use tracers, how does one allow for lags between the moisture and tracer fronts?

J. P. GAUDET: One has to use a diffusion model with three parameters – the dispersion coefficient, the volume of dead water and a transfer coefficient. At present, these parameters have to be determined for each specific case.

J. GUIZERIX: I should like to add a comment.

Mr. Gaudet has pointed to the important problem of a possible slower movement of the tracer than of the water. Little work has been done on this problem, which deserves to be analysed closely. In this connection I would emphasize that tritium is not the best tracer for water, as is often asserted. From the balance point of view, one can expect to find all the tritium injected into a borehole, but from a kinetic point of view I think it is a bad tracer. We, like other authors, have noticed a considerable lag between the pulse responses of tritium and those of, for example, ^{82}Br or ^{131}I. It is probably due to isotopic exchange.

SOME CONCEPTUAL MATHEMATICAL MODELS AND DIGITAL SIMULATION APPROACH IN THE USE OF TRACERS IN HYDROLOGICAL SYSTEMS

K. PRZEWŁOCKI, Y. YURTSEVER
Department of Research and Isotopes,
International Atomic Energy Agency,
Vienna

Abstract

SOME CONCEPTUAL MATHEMATICAL MODELS AND DIGITAL SIMULATION APPROACH IN THE USE OF TRACERS IN HYDROLOGICAL SYSTEMS.

The use of multi-cell models and of recursive equations based on mass-transport for interpretation of isotopic data in hydrologic systems is discussed with particular emphasis on groundwater aquifers. The effects of both geometry and recharge pattern on the behaviour of aquifers in a tracer case are studied. The digital simulation with multi-cells in series is applied to actual tritium data from two projects.

1. INTRODUCTION

The use of isotopes as tracers in hydrological investigations generally aims at the determination of various characteristics of a given hydrologic system. The observed tracer output from a hydrologic system reflects the response of the system to a known tracer input and, by studying the relation between the two, enables conclusions to be drawn regarding the dynamic behaviour of the system. The general approach in the formulation of such an evaluation usually requires the adoption of certain response functions for the system under consideration, so that the computed tracer output is compared with the actually observed output, to yield interpretation in terms of the hydrodynamic parameters of the system.

Generally, in a real hydrological system, the dispersion and mixing occurring during the flow makes the whole process rather too complex for a full mathematical formulation, and an a priori adoption of the proper system response function is very difficult, and sometimes perhaps impossible. Although certain simplifying assumptions are inevitable in this respect, models adopted for this purpose should describe the process with a reasonable approximation to allow realistic interpretations. Frequently used "completely-mixed-reservoir" and "piston-flow" models in applications of environmental isotopes describe the two limiting cases that may occur in nature, since the former assumes "complete mixing" of the tracer in the system and the latter assumes "no mixing at all". Whereas some hydrological systems may be fairly well approximated by these models, the behaviour of most hydrologic systems, however, lies probably between these two extreme cases and the description of such cases deserves further efforts to be devoted to the development of methods that will enable the simulation of dispersion and mixing in the system.

2. MATHEMATICAL MODEL BASED ON MASS TRANSPORT THROUGH AN INTERCONNECTED SERIES OF CELLS

Cell models or compartmental models are generally employed to describe rather complex natural processes and, in recent years, more attention is being directed towards their use for quantitative evaluations [1-3].

The cell models seem to be quite advantageous in studies concerned with the use of environmental isotopes as tracers in regional hydrological investigations as they enable the study of average properties of the system on a time scale and do not require a detailed description of the parameters and the processes within the system, which are difficult to define in natural hydrologic systems, particularly in the case of dispersion and mixing of tracers.

We are here concerned with interconnected cells in series as a model of a real physical hydrologic system and the application of the principle of conservation of mass to study the characteristics of the system for the tracer case. The tracer is assumed to be an ideal one, that is to say, it is miscible, its physical and chemical properties are identical with those of the traced water and it behaves exactly in the same manner as the water during its transport through the system.

While the methodology presented and the equations given can be used for any macro-scale simulation of dispersion and mixing in a given hydrologic system, groundwater systems are of special concern in this paper.

2.1. The general concept and recursive equation approach

The term "mathematical model" is used in this paper in the same context as defined by R. P. Ibbitt [4]: "... to be an algebraic process which, when applied to an input data sequence, results in an output data sequence". Some idealized conceptual models of flow through the aquifer and dispersion and mixing of tracers can be constructed by a basic transport phenomena approach. Let us consider some hydrologic system or a part of it as being represented by volume "V" as shown on Fig. 1.

If a finite amount of fluid, carrying some amounts of tracer, enters the system, displacing an equal amount of fluid and mixing with the remaining fluid inside the volume, the mass balance of the tracer for such a system may be expressed as:

$$\begin{bmatrix}\text{Net}\\ \text{accumulation}\end{bmatrix} = \begin{bmatrix}\text{input to}\\ \text{the system}\end{bmatrix} - \begin{bmatrix}\text{output from}\\ \text{the system}\end{bmatrix} + \begin{bmatrix}\text{generation}\\ \text{inside the}\\ \text{volume}\end{bmatrix} - \begin{bmatrix}\text{consumption}\\ \text{inside the}\\ \text{volume}\end{bmatrix} \tag{1}$$

The general approach for the solution of the system described above would be to develop the differential equations satisfying the conditions of mass balance and continuity on a finite volume element and integrating the equations for known initial and boundary conditions.

Whereas this general mathematical treatment of the problem is possible for rather simple flow systems with known initial and boundary conditions,

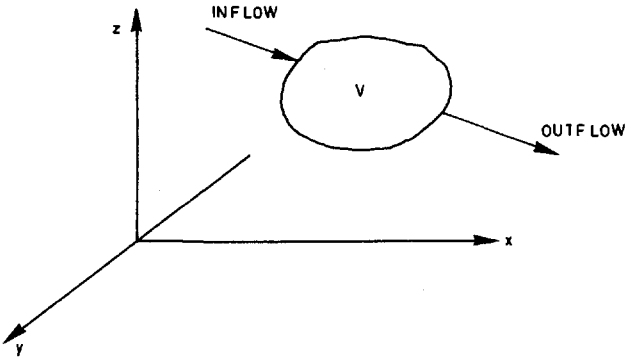

FIG. 1. General concept of the mixing cell.

derivation of equations to describe the time evolution of the tracer in more complex hydrologic systems becomes rather cumbersome and in some cases even impossible. However, Eq. (1) describing the mass balance of the tracer can be applied to studying the time evolution of the tracer for a given hydrologic system with known input conditions, on a discrete time basis. The general concept, therefore, is to apply the mass balance equation successively to each selected finite time increment which will here be referred to as "iteration". Since the state of the system is described at each selected finite time increment, the proposed model is a Finite State Model, where Eq. (1) is applied to each iteration and, therefore, will be referred to as "recursive equation". Hence, the flow through the system is also represented by a sequence of finite inputs and the use of the recursive equation offers the advantage of easy handling with computers.

The use of recursive equations for building mathematical models of aquifers to study the distribution of tracers was first proposed by E. S. Simpson of the University of Arizona during his sabbatical leave with the Agency.

Let us replace the traditionally used parameters to describe the motion of fluid such as: co-ordinates, velocities, densities, etc., by a new concept. Thus, let us assume that the fraction entering volume "V" during each iteration (so-called "BRF" — boundary recharge fraction) will have a size of the fraction of volume. This fraction will carry some concentration of the tracer, "BRC" (boundary recharge concentration), having the size of the tracer mass "M" (in grams, counts per second, tritium units, etc.) over the volume of the carrying fluid. This concept has the advantage that the product of both units is the mass of the tracer in the cell.

$$\text{BRF} * \text{BRC}$$

$$[V] \left[\frac{M}{V}\right]$$

Let us denote the mass of the tracer in the system by "S_T" and call it "state at iteration T". Then using the principle of the mass balance expressed by

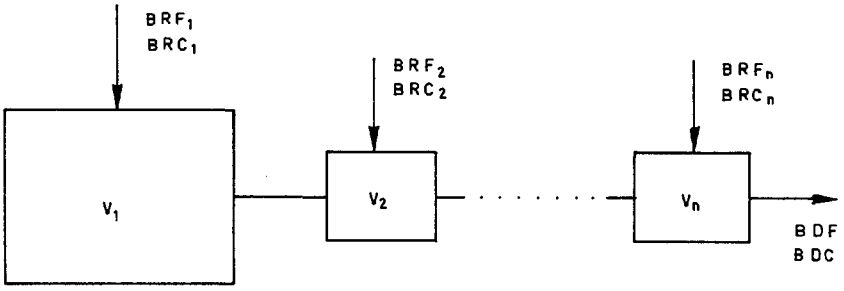

FIG. 2. Multi-cell mixing model.

Eq. (1) one can derive for the case of a non-expandable mixing cell (first cell on Fig. 2) the following recursive equation describing change of the state during unit time:

$$S_{(T+1)} = (S_T + BRF * BRC - BRF * BDC)\, r \qquad (2)$$

where BDC = boundary discharge concentration. For the non-expandable cell BDC = $\frac{S_T}{V}$

$S_{(T+1)}$ = state of the cell at iteration T + 1

r = sink term representing the radioactive decay of the tracer inside the system between two iterations

T = number of iterations

Equation (2) governs the transformation of one mixing cell from one state to another. The unit time is an arbitrary value, which may correspond to any real time unit.

Physically, Eq. (2) describes the process of ideal mixing caused by the instantaneous injection of a portion of the tracer carrying fluid to the system. During the time between two subsequent iterations, a certain amount of fluid enters the cell, displaces an equal amount of fluid with the concentration characteristic of the previous iteration, and then mixes with the remaining fluid, creating inside the cell a state characteristic for the next iteration.

Such a concept, in contrast with the "expandable cell" (recharge-expansion-mixing-discharge) is more versatile, as it permits the simulation not only of mixing, but also of piston flow. This increases the degree of freedom in model making and permits the introduction of the desired amount of mixing.

The application of the recursive equation to a case where the whole aquifer is represented by one mixing cell does not offer significant advantages over the traditionally used analytical model of the completely mixed reservoir. The advantage is clear when one wishes to simulate various degrees of mixing and a gradient of the tracer concentration inside the system.

It is postulated, therefore, that any given aquifer system can be considered as consisting of various sub-component volume elements interconnected with each other. The above recursive equation can be used to study the distribution of the tracer both within the system and at the outflow for a given tracer input, and for the assigned flow rate through the system.

Computations based on the recursive equations require computer facilities. For all computations presented here, the authors used a mini computer Wang 700 c/720, which was sufficient for performing digital simulation for all the models described.

2.2. The case of mixing cells of equal volume in cascade: comparison of the analytical solution with that of the recursive equation

A system consisting of n mixing cells connected in series and cells having equal volumes is one of the simplest cases, Fig. 3. The concentration distribution at the outflow of such a system in steady-state flow conditions and for various values of "n" has been computed using the above recursive equation, taking each cell in the cascade to have unit volume, and initially labelling the first cell with a non-radioactive tracer of unit concentration.

BRF to the first cell arbitrarily chosen was taken to be always 0.1. The concentration distribution curves obtained are shown in Fig. 4 for n = 2, 4 and 6 as an example. For such a system consisting of well-mixed cells in cascade with cells having equal volume and input to the first cell only, the analytical solution for the concentration distribution at the outlet can be obtained from the differential equation describing the simple material balance of tracer on the "n"th cell [5]:

$$\frac{dC_n}{dt} = \frac{Q}{V}(C_{n-1} - C_n) \qquad (3)$$

where C_n = concentration of the "n"th cell
Q = steady flow rate through the system
V = volume of each cell

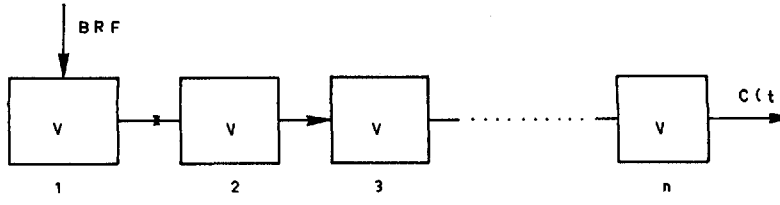

FIG. 3. Mixing cells of equal volume in cascade.

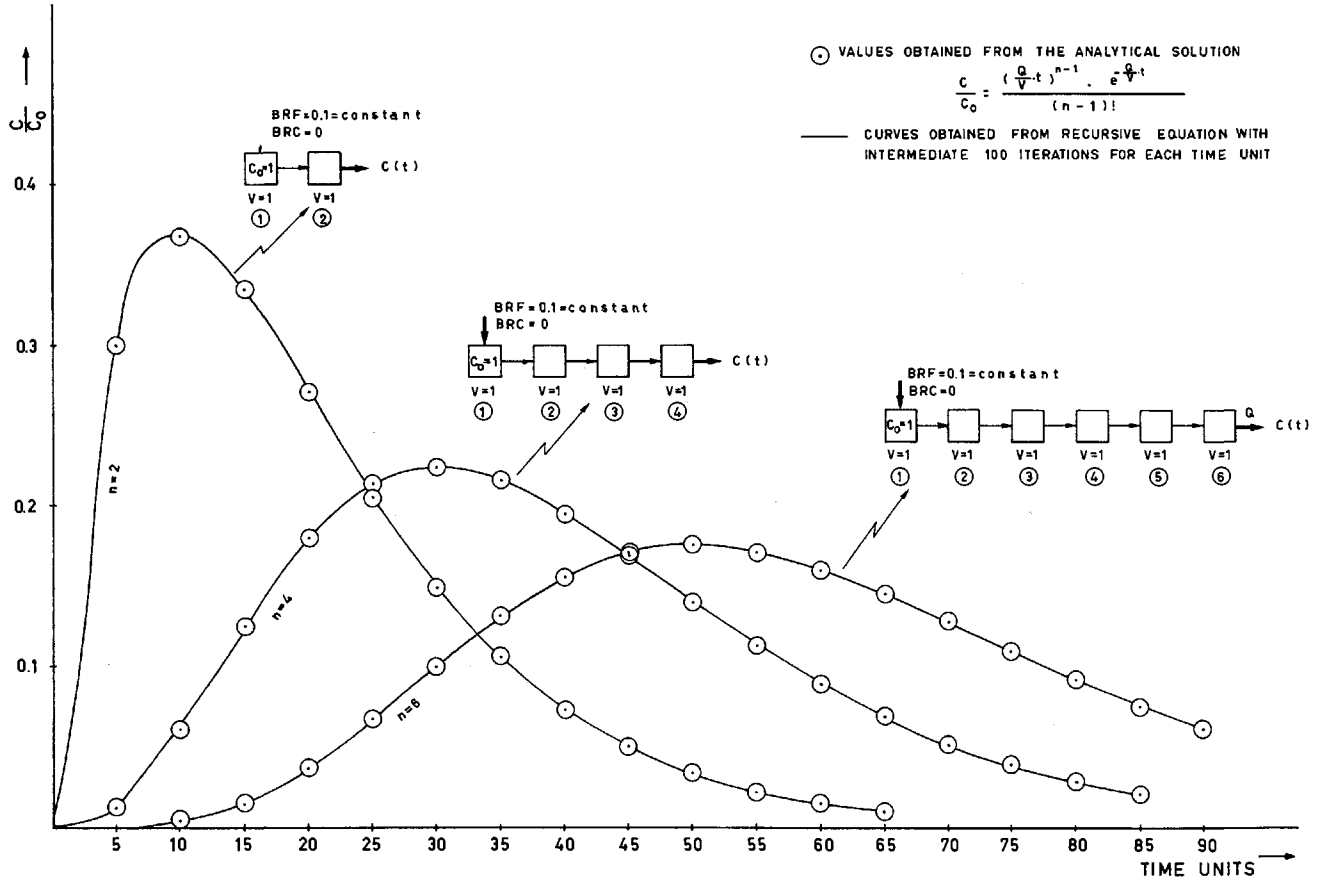

FIG. 4. Typical concentration outflow curves, from a system of mixing cells of equal volume in cascade.

TABLE I. COMPARISON OF RECURSIVE EQUATION SOLUTION WITH ANALYTICAL SOLUTION FOR THE CASE OF MIXING CELLS OF EQUAL VOLUME IN CASCADE — ORDINATES OF CONCENTRATION OUTPUT CURVE

Time units	n = 2		n = 4		n = 6	
	Rec. Eq.	Analyt. Sol.	Rec. Eq.	Analyt. Sol.	Rec. Eq.	Analyt. Sol.
0	0	0	0	0	0	0
5	0.3031	0.3032	0.0125	0.0126	0.0001	0.0001
10	0.3680	0.3678	0.0611	0.0613	0.0030	0.0030
15	0.3348	0.3346	0.1254	0.1255	0.0140	0.0141
20	0.2708	0.2706	0.1804	0.1804	0.0359	0.0360
25	0.2052	0.2052	0.2138	0.2137	0.0667	0.0668
30	0.1493	0.1493	0.2241	0.2240	0.1007	0.1008
35	0.1056	0.1056	0.2159	0.2157	0.1321	0.1321
40	0.0732	0.0732	0.1954	0.1953	0.1563	0.1562
45	0.0499	0.0499	0.1687	0.1687	0.1708	0.1708
50	0.0336	0.0336	0.1404	0.1403	0.1755	0.1754
55	0.0224	0.0224	0.1133	0.1133	0.1714	0.1714
60	0.0148	0.0148	0.0892	0.0892	0.1607	0.1606
65	0.0097	0.0097	0.0688	0.0688	0.1454	0.1453
70	0.0063	0.0063	0.0521	0.0521	0.1277	0.1277
75	0.0041	0.0041	0.0388	0.0388	0.1094	0.1093
80	0.0026	0.0026	0.0286	0.0286	0.0916	0.0916
85	0.0017	0.0017	0.0208	0.0208	0.0752	0.0752
90	0.0011	0.0011	0.0149	0.0149	0.0607	0.0607
95	0.0007	0.0007	0.0106	0.0106	0.0482	0.0482

If the first cell is initially labelled with a concentration of C_0, the solution to the above differential equation is given by [5]:

$$C_n = C_0 \frac{\left(\frac{Q}{V} \cdot t\right)^{n-1} \cdot e^{-\frac{Q}{V} \cdot t}}{(n-1)!} \tag{4}$$

which has the form of a Poisson probability distribution. For the same cases shown on Fig. 4, the solution was obtained by Eq. (4) and the results compared with those obtained by using the recursive equation. The values obtained are given in Table I for both approaches.

Naturally, both solutions yield almost identical results and the insignificant differences observed on the values shown are due to the computational accuracy in the case of the recursive equation which solely depends on the length of the time increment selected for each iteration. For calculations shown on Fig. 4 and on Table I, in the case of recursive equations intermediate 100 iterations were used for each unit time increment. Although the optimization of the necessary number of iterations for the desired accuracy can be worked out, the aim of the above comparison is to show that the use of the recursive equation in a finite state model to study the distribution of the tracer at the outflow of a given system yields results identical with those of the analytical solution. For rather simple systems analytical solutions exist, and therefore there is perhaps no advantage, but the use of the recursive equation is most convenient for more complex cases where the derivation of mathematical equations is rather difficult.

2.3. Evaluation of behaviour of various aquifer systems using recursive equations

The behaviour of a given aquifer system for a tracer case can be studied with the aid of the above-derived recursive equation. The basic characteristic of an aquifer can be described by a function called the "Transit time distribution of water in the system". For any given hydrologic system one can define a function F(t) describing the distribution of transit times in the system, which will also describe the "Age-distribution frequency of water at the outflow". Since this is a continuous function, it can be normalized using the condition that the sum of all fractions of water having transit time "t" is unity.

$$\int_0^\infty F(t) \cdot dt = 1 \tag{5}$$

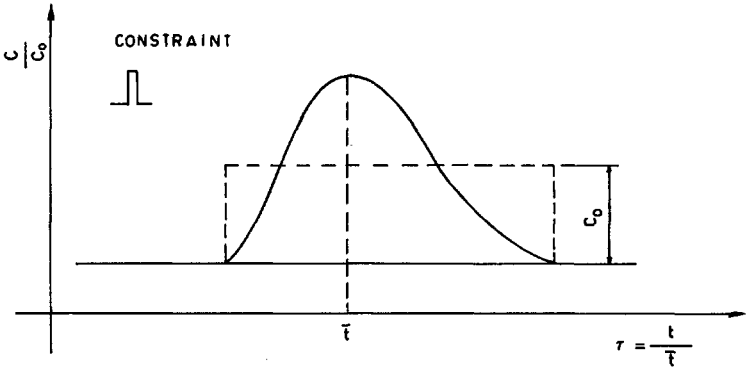

FIG. 5. Dimensionless system response function.

The mean of the transit time distribution "$\bar{t}$" called the "mean residence time" can be found from the first moment of function F(t),

$$\bar{t} = \int_0^\infty t \cdot F(t) \cdot dt \tag{6}$$

The age distribution function and the mean residence time for a steady-state flow system can be experimentally determined from the dimensionless response time curve of the system, which is the concentration distribution at the outflow of the system when a tracer impulse is introduced to the system at time t = 0. The dimensionless response time curve $C(\tau)$, with $\tau = t/\bar{t}$, and with the reference concentration C^0 of the tracer being the concentration of the tracer if uniformly distributed throughout the whole system, is also the normalized "age frequency distribution function" [$F(\tau)$], Fig. 5. This follows from the reasoning that at t = 0, when the impulse of tracer injection occurs, all elements of the water begin to live, and the concentration time curve of the outflow represents the age fraction of water that leaves the system at time t = t, which is identical with the F curve, or

$$C(\tau) = F(\tau) = \bar{t} \cdot F(t) \tag{7}$$

It is this property that enables a study to be made of the behaviour of various aquifers by conducting mathematical simulation experiments to construct the normalized response time curve which is also the age distribution frequency curve at the outflow of the system. It can be shown that the mean residence time of the system for these conditions will be [1]:

$$\bar{t} = \frac{\int_0^\infty t \cdot C(t) \cdot dt}{\int_0^\infty C(t) \cdot dt} \tag{8}$$

In the case of recursive equations, the integral in the above equation can be replaced by a summation and, with the notations already introduced, the mean residence time can be computed from:

$$\bar{t} = \frac{\sum T * BDC_T}{\sum BDC_T} \tag{9}$$

It is worthwhile to mention that the system consisting of a cascade of mixed cells with equal volume used in previous sections for comparison of the analytical solution with that of the recursive equation can be employed as a conceptual mathematical model to simulate a uni-directional dispersion.

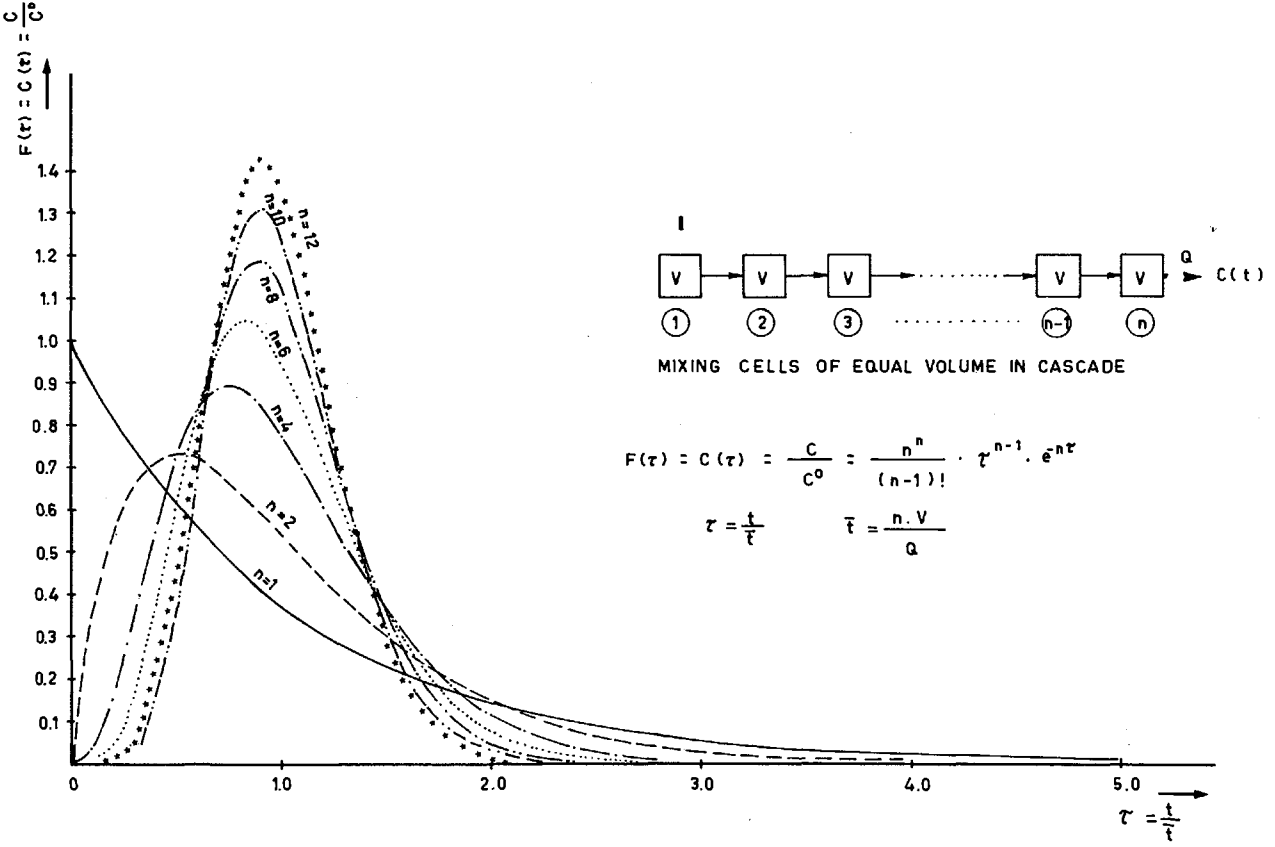

FIG. 6. Age distribution functions computed from Eq. (10).

This can be seen easily from the normalized response-time curve of the system for an impulse injection of the tracer, which can be analytically derived [6] as:

$$C(\tau) = \frac{C}{C^0} = \frac{n^n \tau^{n-1} e^{-n\tau}}{(n-1)!} \tag{10}$$

where $\tau = \frac{t}{\bar{t}}$

$\bar{t} = \frac{n \cdot V}{Q}$

C^0 = initial average concentration of the tracer if uniformly distributed throughout the system

V = volume of each cell

Q = flow rate through the system

The $C(\tau)$ curves for various values of "n" are shown on Fig. 6. As can be seen from Eq. (10) and Fig. 6 for $n = 1$, the $C(\tau)$ curve which, at the same time is the "age distribution function", is an exponential curve.

$$C(\tau) = e^{-\tau} = e^{-\frac{t}{\bar{t}}} \tag{11}$$

As the number of cells increases, they tend to be more and more peaked close to $\tau = 1$. It can be proved [6] from the moments of the distribution curves given by Eq. (10), that as $n \to \infty$ the distribution will be highly peaked at $\tau = 1$ and would correspond to "piston flow". Thus, the so far called "Completely Mixed Reservoir" and "Piston Flow" models can be considered as special cases of the above, more general, conceptual representation of dispersion and mixing by a cascade of mixing cells, where $n = 1$ corresponds to a "Completely Mixed Reservoir" model and $n = \infty$ corresponds simultaneously to a "Piston Flow" model, with the respective uni-directional dispersion coefficient of $D_L = \infty$ and $D_L = 0$. Thus, the adoption of a system response function as given by Eq. (10) could be useful for studying cases where the dispersion and mixing lie between the two extreme cases of complete mixing and piston flow. The number of cells used are quantitatively related to the uni-directional dispersion coefficient of the system [6].

By using the recursive equation, mathematical simulation experiments were carried out to study the effects of both the geometry of the aquifer and the recharge pattern on the age distribution. This necessitates the use of interconnected cells of different sizes and various input patterns to describe the aquifers for some of which analytical solutions do not exist at present. The cases studied are:

(A) Geometry of the aquifer

(i) Rectangular surface-unit width — uniform depth;

(ii) Rectangular surface-unit width — depth linearly increasing along flow direction or radial surface — uniform depth — divergent flow;

(iii) Rectangular surface-unit width — depth linearly decreasing along flow direction or radial surface — uniform depth — convergent flow.

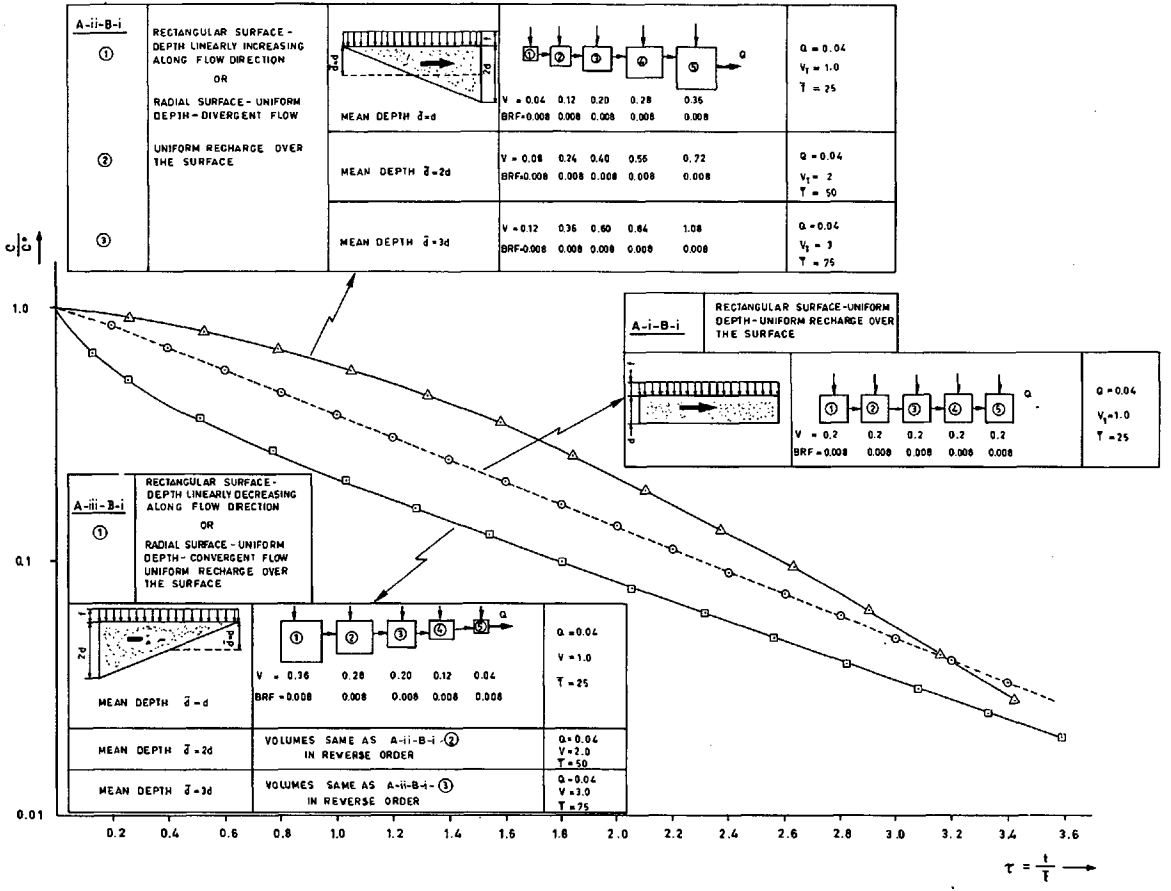

FIG. 7. Dimensionless concentration outflow curves derived for different aquifer systems (uniform recharge).

(B) Recharge pattern

(i) Uniform recharge over the surface;
(ii) Recharge over the surface linearly decreasing along the flow direction.

Figures 7 and 8 give the parameters of the cases studied.

In each of the cases, the aquifer is taken to consist of five mixing cells in series, while the volume of the cells and input to the cells are assigned to represent the various geometric configurations and recharge patterns. Whereas the selected geometric configurations and recharge patterns are rather simple hypothetical cases, the simulation experiments aim at providing more insight into the behaviour of aquifers, and a better understanding of possible effects of these parameters on the age distribution function of the system. In each of the cases, the system is initially assumed to be labelled with unit concentration of a non-radioactive tracer, and the C(t) curves and $\bar{t}$ values are computed with the aid of recursive equations by washing out the tracer from the system with the assigned flow pattern. The flow through the system is, for each case, in a steady state. The dimensionless $C(\tau)$ curves constructed in this way are shown on Figs 7 and 8. It is interesting to note that for cases (A-i—B-i) and (A-iii— B-ii), the age distribution is an exponential one, equivalent to the one mixing cell or "Completely Mixed Reservoir" model (Figs 7 and 8). Obviously, although complete mixing throughout the whole volume of the system does not necessarily take place (as would be in the case of one mixing cell), the behaviour of some systems may be equivalent to that of the "Completely Mixed Reservoir" with an age distribution function of the single exponential type, depending on the input conditions.

With regard to the other cases, the $C(\tau)$ curves have their own characteristic shapes and, apparently, the geometry of the aquifer and the recharge pattern have a significant bearing on the behaviour of the system. Therefore, for a most realistic interpretation of the tracer output curves, these factors have to be taken into account.

It should be noted that in both cases of the aquifers having linearly increasing depth and linearly decreasing depth along the flow direction (with uniform recharge over the entire surface), the shape of their respective dimensionless response curves remains unchanged regardless of the degree of inclination of the aquifer bed. In Fig. 7, i.e. the cases (A-ii—B-i—1) (A-ii— B-i— 2) and (A-ii — B-i— 3) give practically the same normalized concentration outflow curves. This is also true for the cases (A-iii— B-i—1) (A-iii— B-i— 2) and (A-iii— B-i— 3).

Another important finding of the above evaluations is, that for some cases the "mean residence time-$\bar{t}$" is not identical with the "hydrologic turnover time" defined as $\bar{T} = V/Q$ (total volume of the system/discharge). In cases where the age distribution function is of the form $C(\tau) = e^{-\tau}$ (cases (A-i— B-i) and (A-iii— B-ii), the "mean residence time-$\bar{t}$" of the system is equivalent to the "hydrologic turnover time $\bar{T} = V/Q$", a fact which has already been discussed in detail by Eriksson [1] and Bolin and Rodhe [2]. However, in cases where the age distribution is not a simple exponential one, the "mean residence time-$\bar{t}$" for the system is no longer equivalent to the "hydrologic turnover time-$\bar{T}$". The relation between $\bar{t}$ and $\bar{T}$ as developed from the results of the above evaluations are shown on Fig. 9.

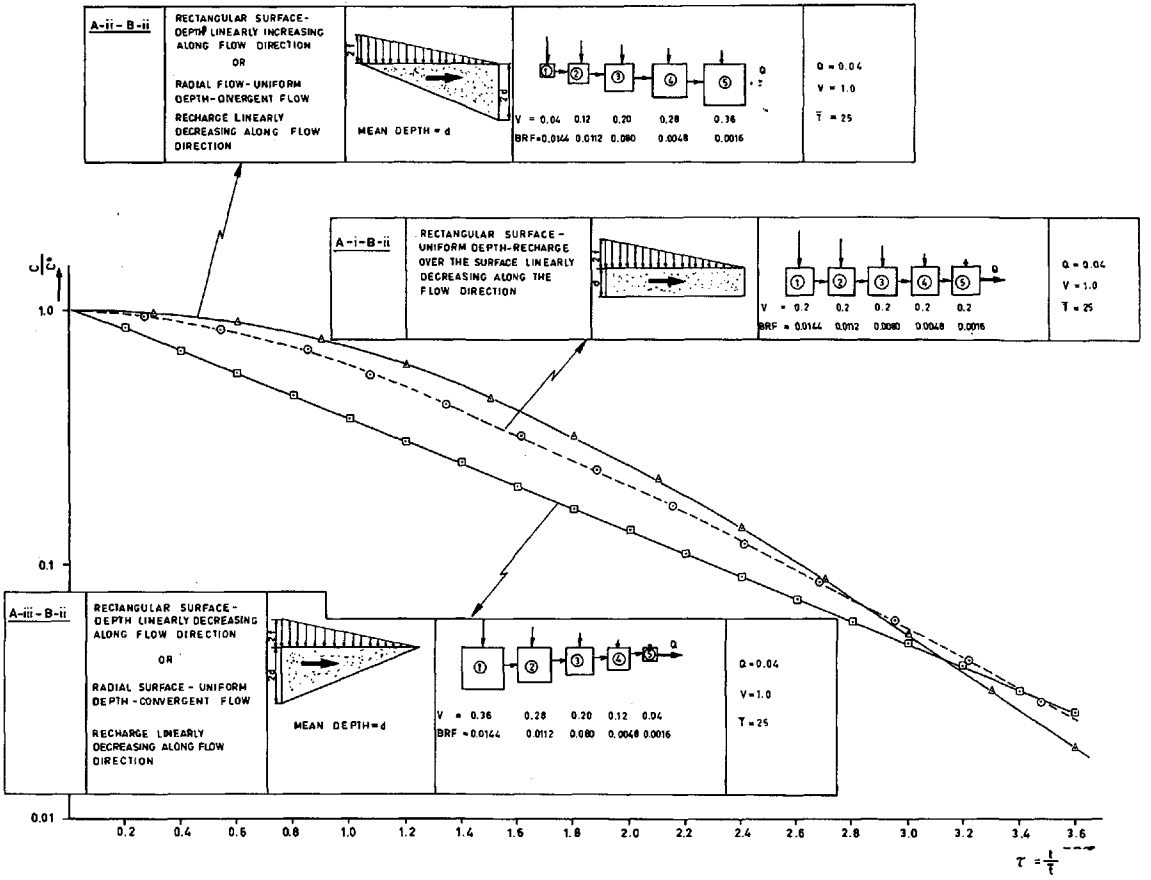

FIG. 8. Dimensionless concentration outflow curves derived for different aquifer systems (variable BRF and volumes).

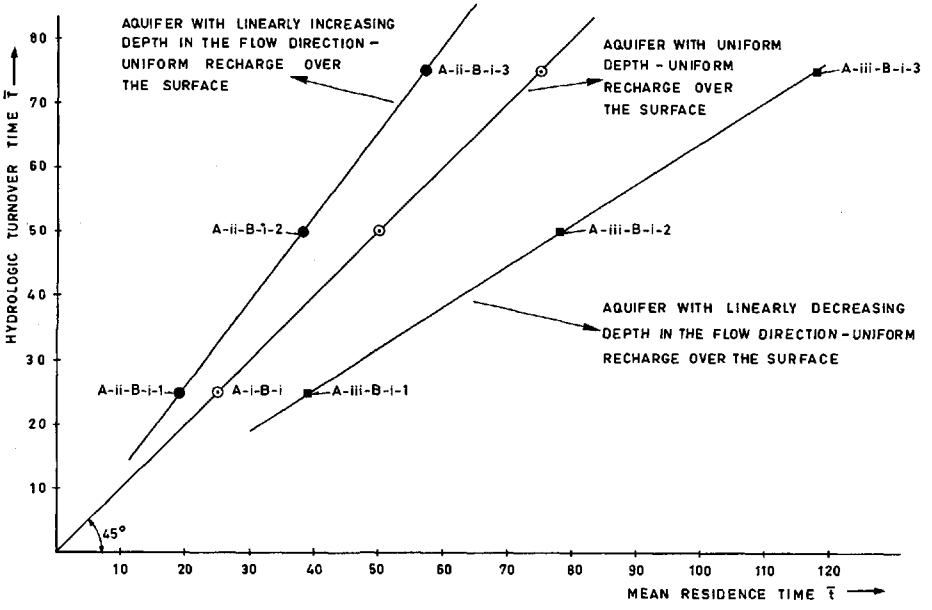

FIG. 9. Relation between mean residence time $\bar{t}$, and hydrological turnover time $\bar{T}$, for the cases studied.

For aquifers with linearly increasing depth along their flow direction and uniform recharge, $\bar{t} < \bar{T}$; and for aquifers with linearly decreasing depth in the flow direction and uniform recharge, $\bar{t} > \bar{T}$. For cases where the recharge is linearly decreasing along the flow direction, $\bar{t} < \bar{T}$ for both aquifers with uniform depth and with depth increasing along the flow direction (Fig. 8, cases A-i – B-ii and A-ii – B-ii respectively). Although the few cases studied here do not enable the development of general quantitative relations between $\bar{t}$ and $\bar{T}$, it is evident that these two mean characteristics can have significantly different values for a given hydrologic system. Whereas the choice between the use of one or the other of these two mean characteristics of a given hydrologic system primarily depends on the type of problem, the realization of a significant difference that may exist regarding their quantitative values is of prime importance, especially in studies dealing with water quality and pollution problems.

All the cases discussed above refer to the behaviour of phreatic aquifers that are recharged over their entire surface area. An attempt has also been made to evaluate the confined aquifer case using mixing cells in series and with an input only to the first cell. Such a representation of the confined aquifer case yields identical results for systems consisting of the same volume elements with equivalent total volume and discharge rate, regardless of the shape of the aquifer. The shape of the dimensionless concentration outflow curves for confined aquifer cases is similar to that given on Fig. 6. Apparently, in systems consisting of a series of mixing cells and with an input to the first cell only, the arrangement (the order) of the cells in the series is irrelevant.

3. PRACTICAL EXAMPLES OF SIMULATION FOR THE INTERPRETATION OF ENVIRONMENTAL ISOTOPE DATA

3.1. Project Grafendorf, Austria

For a hydrological project in Austria, which was carried out jointly by the Society of Hydrological Research in Graz and the International Atomic Energy Agency in Vienna on an area near Grafendorf, Styria, tritium data are available for some mountain springs for the period 1969 to 1973. There is one spring (Code No. St-29) that in 1969 discharged water with an average tritium concentration of more than 500 TU. The spring is located at an altitude of 960m above sea level, not far from the water divide, which in this area is clearly defined by the top of the Massenberger Mountain (1250 m above sea level). The simplified hydrologic situation is shown on Fig. 10a. The sub-catchment area has a surface of about 0.4 km^2.

The results of the monthly measurements of tritium content in precipitation for Vienna, beginning in 1960 and correlated with Ottawa tritium measurements, were used as a basis to determine the input function. The

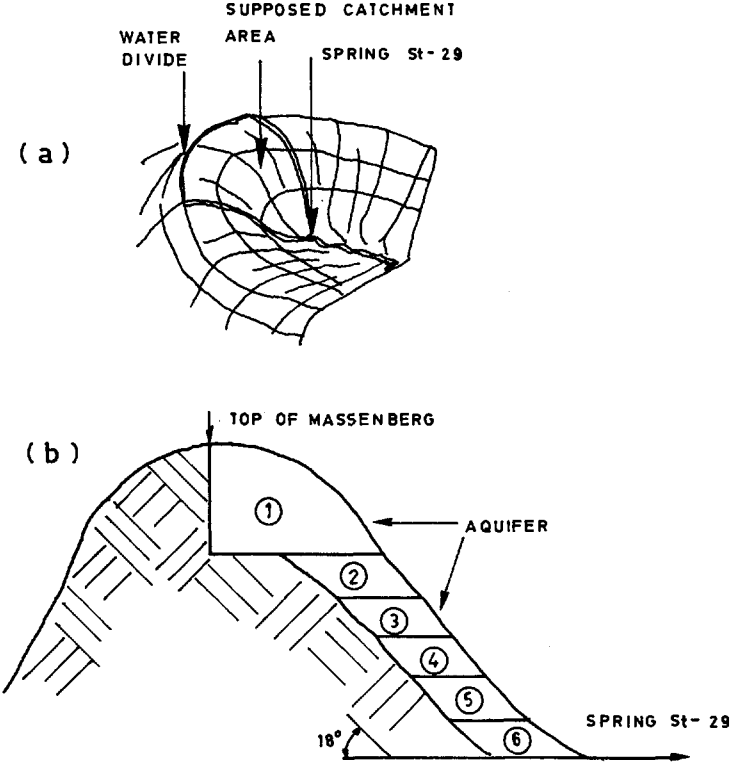

FIG. 10. (a) Schematic representation of the catchment area for spring St-29.
(b) Schematic representation of the mixing cells arrangement.

TABLE II. STAMBACH VALLEY St-29 SPRING (SIMULATION EXPERIMENT)

PSM/1*8/MMCab

rd .986000000

CELL No.		1	2	3	4	5	6	BDC	Experimental value	Year
VOL		2.5000	.7000	.7000	.7000	.7000	.7000			
So		12.000	3.000	3.000	3.000	3.000	3.000			
BRF		.000	.000	.000	.000	.000	.000			
BRC		.0	.0	.0	.0	.0	.0			
C		4.8	4.2	4.2	4.2	4.2	4.2	.0		
BRF		.200	.000	.000	.000	.000	.000			
BRC		10.0	.0	.0	.0	.0	.0			
C	4	5.9	4.9	4.3	4.0	4.0	4.0	4.1		52-53
BRF		.200	.000	.000	.000	.000	.000			
BRC		292.0	.0	.0	.0	.0	.0			
C	8	84.1	34.4	10.7	4.7	3.9	3.8	3.8		53-54
BRF		.200	.000	.000	.000	.000	.000			
BRC		29.0	.0	.0	.0	.0	.0			
C	12	64.9	61.7	40.7	19.2	8.1	4.5	4.0		54-55
BRF		.200	.000	.000	.000	.000	.000			
BRC		77.0	.0	.0	.0	.0	.0			
C	16	65.0	61.8	54.4	39.9	23.5	11.8	9.1		55-56
BRF		.200	.000	.000	.000	.000	.000			
BRC		85.0	.0	.0	.0	.0	.0			
C	20	67.3	62.8	58.0	50.4	38.6	25.4	21.9		56-57
BRF		.200	.000	.000	.000	.000	.000			
BRC		437.0	.0	.0	.0	.0	.0			
C	24	165.4	100.1	67.2	55.4	47.4	37.4	34.8		57-58
BRF		.200	.000	.000	.000	.000	.000			
BRC		552.0	.0	.0	.0	.0	.0			
C	28	263.3	179.7	114.5	75.9	56.7	45.8	43.7		58-59
BRF		.200	.000	.000	.000	.000	.000			
BRC		80.0	.0	.0	.0	.0	.0			
C	32	200.2	210.0	175.6	124.1	83.8	59.8	55.0		59-60
BRF		.200	.000	.000	.000	.000	.000			
BRC		100.0	.0	.0	.0	.0	.0			
C	36	163.0	181.7	185.0	162.9	125.4	89.4	80.8		60-61
BRF		.200	.000	.000	.000	.000	.000			
BRC		442.0	.0	.0	.0	.0	.0			
C	40	231.6	187.2	172.6	167.6	151.2	122.7	115.3		61-62
BRF		.200	.000	.000	.000	.000	.000			
BRC		2070.0	.0	.0	.0	.0	.0			
C	44	724.4	394.8	225.1	172.7	157.2	141.3	138.2		62-63
BRF		.200	.000	.000	.000	.000	.000			
BRC		1581.0	.0	.0	.0	.0	.0			
C	48	924.0	691.4	449.9	276.0	189.2	154.1	149.2		63-64
BRF		.200	.000	.000	.000	.000	.000			
BRC		868.0	.0	.0	.0	.0	.0			
C	52	883.7	811.5	664.0	472.2	310.9	210.3	189.5		64-65
BRF		.200	.000	.000	.000	.000	.000			
BRC		524.0	.0	.0	.0	.0	.0			
C	56	728.5	769.9	739.7	628.5	475.8	332.8	297.8		65-66
BRF		.200	.000	.000	.000	.000	.000			
BRC		255.0	.0	.0	.0	.0	.0			
C	60	563.2	651.5	697.8	677.3	592.2	469.0	437.6		66-67
BRF		.200	.000	.000	.000	.000	.000			
BRC		236.0	.0	.0	.0	.0	.0			
C	64	446.0	521.4	593.4	633.7	621.7	556.6	541.3		67-68
BRF		.200	.000	.000	.000	.000	.000			
BRC		194.0	.0	.0	.0	.0	.0			
C	68	355.2	415.0	482.3	543.1	578.2	572.0	574.6		68-69
BRF		.200	.000	.000	.000	.000	.000			
BRC		171.0	.0	.0	.0	.0	.0			
C	72	287.4	332.1	386.7	445.8	498.4	529.6	544.1	536	69-70
BRF		.200	.000	.000	.000	.000	.000			
BRC		194.0	.0	.0	.0	.0	.0			
C	76	247.8	273.5	311.8	360.1	412.2	458.2	477.3	486	70-71
BRF		.200	.000	.000	.000	.000	.000			
BRC		200.0	.0	.0	.0	.0	.0			
C	80	222.6	235.9	269.1	293.0	335.6	381.4	400.2	-	71-72
BRF		.200	.000	.000	.000	.000	.000			
BRC		200.0	.0	.0	.0	.0	.0			
C	84	205.5	211.6	224.2	245.2	275.4	313.0	328.8	359	72-73
BRF		.200	.000	.000	.000	.000	.000			
BRC		200.0	.0	.0	.0	.0	.0			
C	88	194.0	195.4	201.1	212.8	231.8	258.7	270.9	280	73-74
BRF		.200	.000	.000	.000	.000	.000			
BRC		200.0	.0	.0	.0	.0	.0			
C	92	186.2	184.5	185.8	191.1	201.8	219.1	227.7*		74-75
BRF		.200	.000	.000	.000	.000	.000			
BRC		200.0	.0	.0	.0	.0	.0			
C	96	180.9	177.2	175.5	176.7	181.6	191.4	197.3*		75-76

* Value expected.
BRC and C values expressed in tritium units.
Simulation made by means of the Wang 700 advanced calculator.

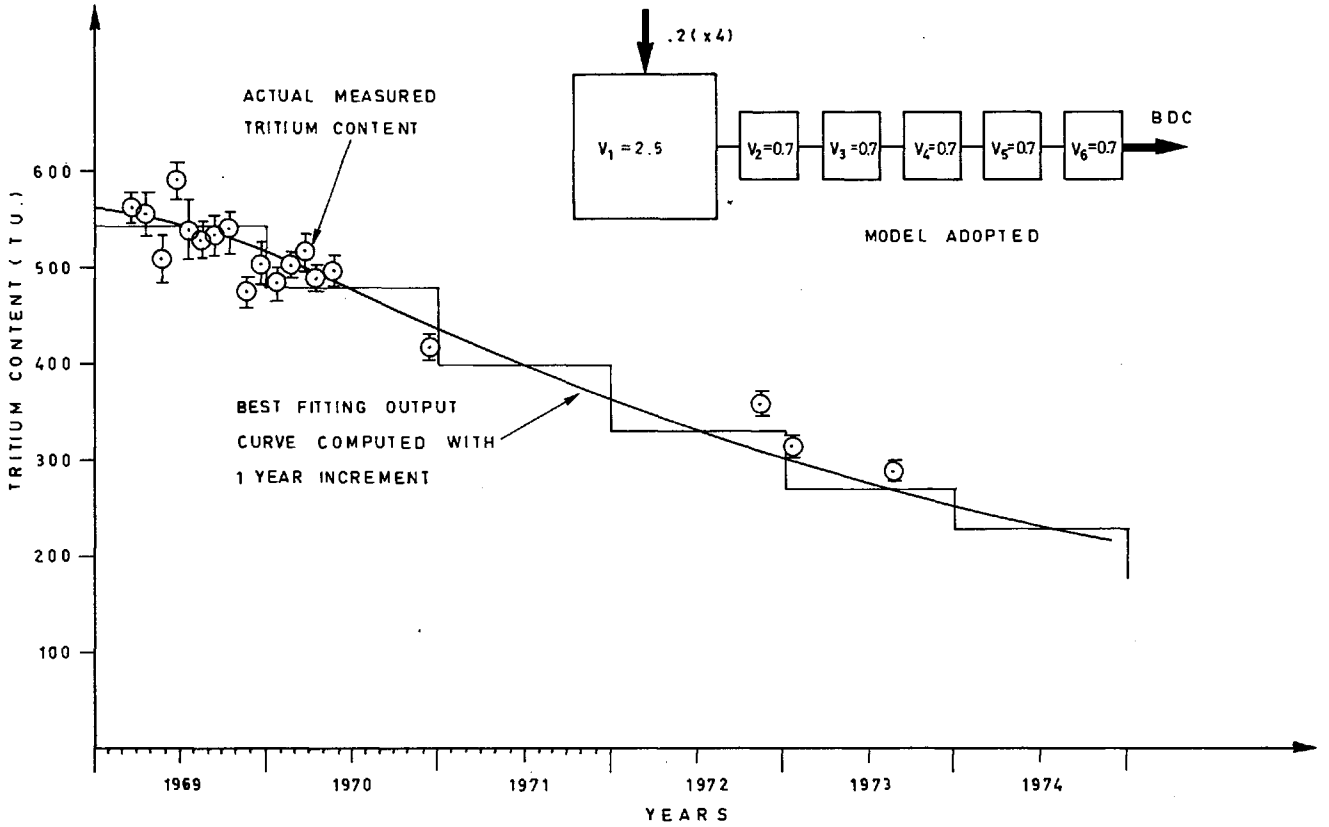

FIG. 11. Best fitting output curve and parameters of the model adopted for Grafendorf.

net potential evapotranspiration for this area was calculated according to the Thornthwaite formula [7], and subtracted from the amount of monthly precipitation characteristic for this area.

The tritium input function was determined by weighting the monthly results of tritium concentration measurements proportionally to the monthly potential recharge.

It was found that in this case neither the exponential nor the binomial model yields acceptable results. More realistic was the reasoning that the basic catchment area is on the top of the mountain and that the flow is stratified. This means, that under the influence of gravity, separate layers of water become lower each year in the direction of outflow almost without mixing (Fig. 10b). This input takes place in the first cell (Cell No. 1) of a relatively high volume. Four instantaneous injections (four iterations per year) with a constant, characteristic for the particular year's concentration, were assumed to take place each year. From this main cell, the water is then discharged to the five adjacent cells which are of a smaller volume and connected in series, in which mixing is much smaller.

Values of the discharge concentration of tritium from the last cell of this model were compared with the average yearly values measured for the same period in the field for spring St-29. The original print of the simulation experiment showing the best coincidence of the simulated and experimental data, is shown in Table II. The state of the system after each iteration was automatically corrected for radioactive decay by the proper adjustment of the program.

Simulation was started for the water year 1952-53 (beginning September, ending August of the next year). The second column on Table II shows the number of iterations performed from the beginning, as four iterations were used for one year period. The best fit was obtained with the following assumed parameters for the model: 6 relative volume units (r.v.u.) for the total volume of the system, and a total discharge (= BRF) that equals 0.8. r.v.u. yearly (Fig. 11). Dividing these two figures each through the other yields 7.5 years for the turnover time of the system.

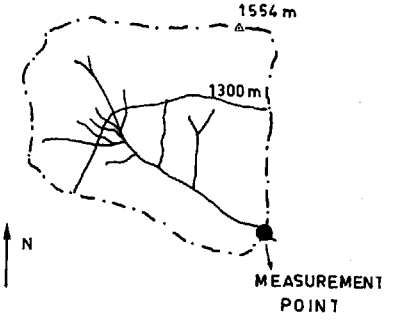

FIG. 12. Catchment basin of Modrý Důl.

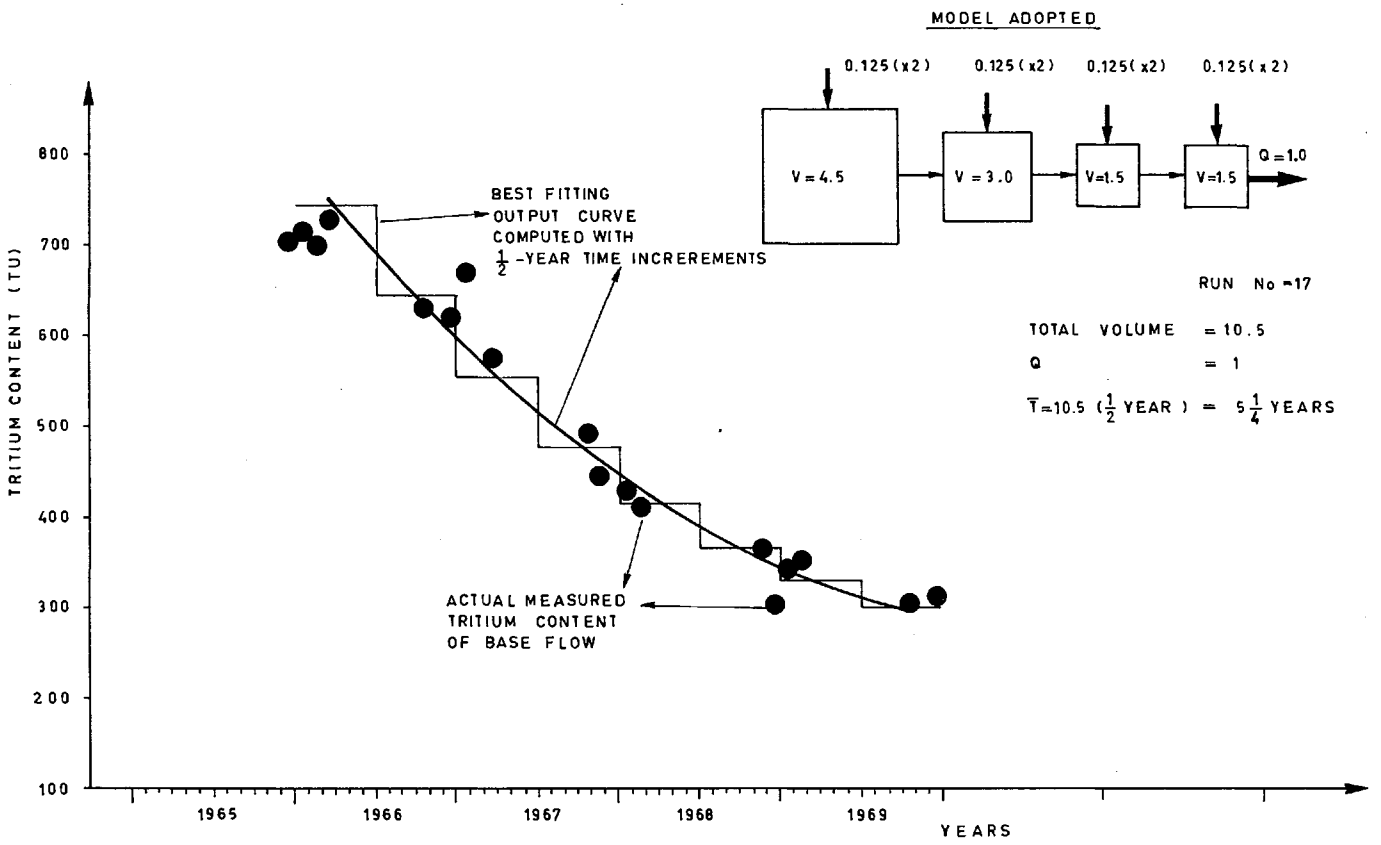

FIG. 13. Best fitting output curve and parameters of the model adopted for the Modrý Důl Basin.

It is also possible to determine the size of an aquifer based on the results obtained by simulation. Since

$$\overline{T} = \frac{V_{model}}{BRF} = \frac{V_{real}}{Q} \qquad (12)$$

where $\overline{T}$ = the turnover time
V_{model} = the total volume of the cells in the model
BRF = the yearly boundary recharge fraction
V_{real} = the volume of water in the real aquifer
Q = yearly average spring discharge (measured)

it is possible to estimate V_{real} from Eq. (12). In the case of spring St-29 it was found that its average yearly discharge is $2.75 \cdot 10^{-3} m^3/s$ [8]. Hence the real volume of the aquifer is about $6.5 \cdot 10^5 m^3$. Estimates of the local hydrologist agree with this value [9].

3.2. The Modrý Důl representative basin, Czechoslovakia

The Modrý Důl watershed in northern Czechoslovakia was selected as a representative basin within the IHD programme, where intensive hydrologic studies were initiated in 1957. Within the scope of the IHD programme, the International Atomic Energy Agency in Vienna, the University of Pisa and the Hydraulic Research Institute in Prague jointly undertook a research project during which extensive basic hydrologic data and environmental isotope data were collected. These data have already been used for a detailed study of the snow-melt process in the catchment area and the results have been published [10]. Evaluations made at that time concerning the transit time of subsurface water in the basin enabled quantitative estimates to be made by using the baseflow tritium measurements of the creek draining the catchment area. However, measurements of the tritium content of the creek continued for a further two years, and observations covering a longer time span are available which justifies another attempt to be made to study the transit time involved in the subsurface flow of the basin.

The Modrý Důl basin is located in the eastern part of the Krkonose mountain in northern Bohemia (Fig. 12), and has a surface area of 2.65 km^2. It belongs to the catchment area of the Elbe river and is a tributary of the Modrý Potok creek. The base flow of the creek draining the basin is 20 - 30 litres/sec. A detailed description of the geological and hydrological features of the basin has already been given [10]. Tritium measurements performed on the samples collected during the base-flow period of the creek cover at present a time span of five years (1965 - 69).

The evaluations presented here concern the application of recursive equations to build a model for studying the transit time of subsurface flow in the catchment. The tritium input function for the area was determined from monthly data of Vienna, since it was found from a correlation of available measurements of monthly rainfall on the catchment area that 1/1 correlation exists with Vienna rainfall tritium data. Tritium values before 1960 were estimated from the Vienna-Ottawa correlation. The evaluations are made taking half a year as a unit time. The tritium input for half-yearly periods, beginning from 1954, was computed by weighting the monthly tritium concentration with the mean monthly distribution of the amount of precipitation throughout a year, as computed from six years of available precipitation data for the catchment area. The tritium input curve obtained is shown on Fig. 13.

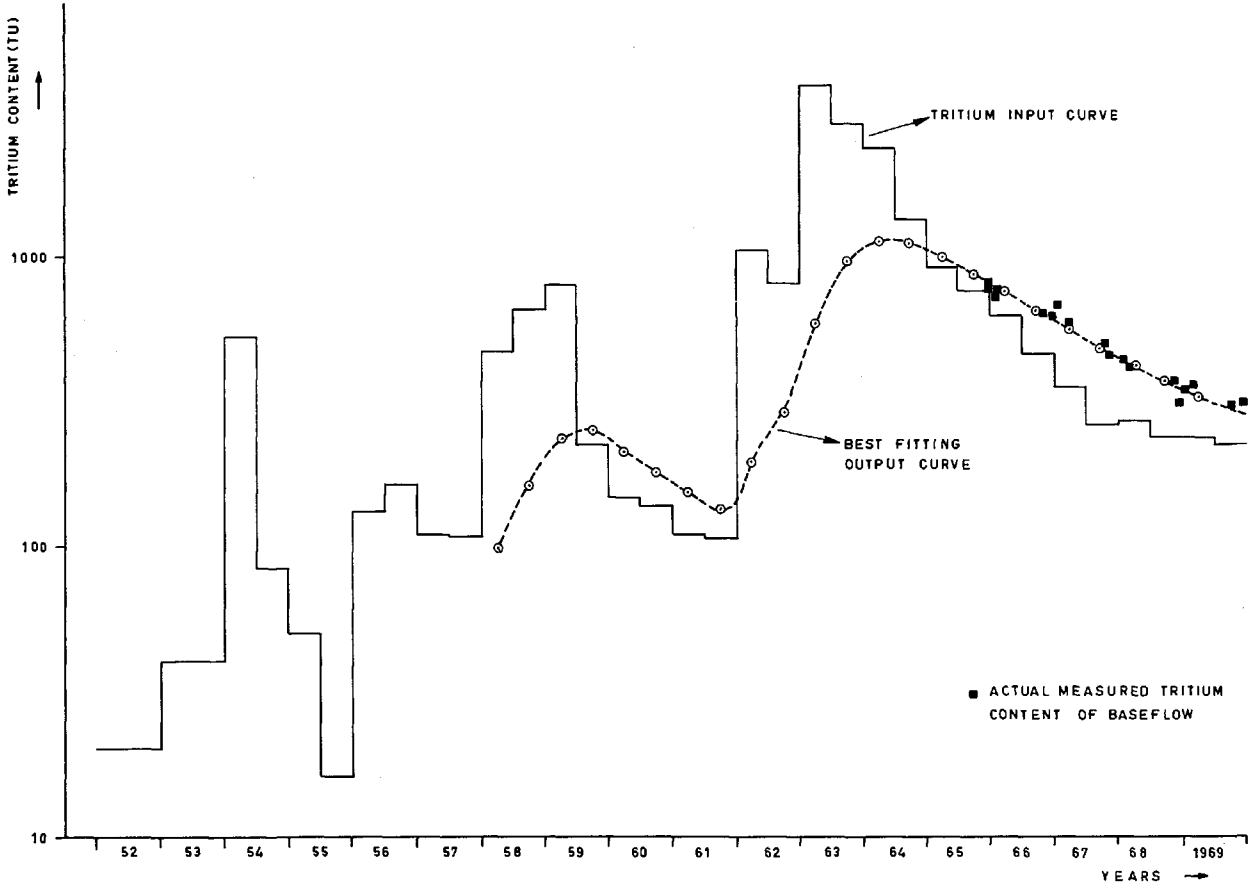

FIG. 14. Tritium input and computed output curve for Modrý Důl.

The mean monthly distribution of precipitation on the catchment area is such that about 50% of the annual precipitation falls during each half year. Thus, evaluations are based on steady-state flow conditions taking half yearly time increments.

The model adopted for the evaluations consists of four mixing cells in series. The shape of the catchment area suggests the use of a decreasing volume of the cells in the flow direction. Since it is expected that the recharge of groundwater in the catchment area would be on its entire surface, input occurs to each mixing cell in the adopted model. Various trial runs had to be conducted to fit the observed tritium values to the adopted model, while changing the volume of the cells at each run, until the best fit was obtained. Figure 14 shows the parameters of the model which resulted in the best fit of the output curve to the observed tritium values. The parameters of the best-fitting model are: Total Volume = 10.5 (r.v.u.) and Q = 1 (per half year). Thus, the turnover time of the subsurface water in the Modrý Důl basin is $\overline{T}$ = 10.5/1 = 10.5 half years or $\overline{T}$ = 5.25 years. The value obtained is about twice that of earlier findings. Dinçer and co-workers [10], using in their evaluation a model where the transit time distribution function is assumed to be of the binomial distribution type, found a value of 2.5 years.

From these two studies, it is clear that the turnover time of the subsurface water in the Modrý Důl catchment area is between 2.5 and 5.25 years. However, in view of the fact that evaluations made here are based on actual tritium measurements covering a longer time span, the value of $\overline{T}$ = 5.25 years is probably a better estimate.

The tritium input function, actually observed tritium values and the best fitting output curve with the adopted model are shown on Fig. 14. It is interesting to note that the apparent mean residence time of the water in the basin is much shorter than 5.25 years. From the relative shift of 1958 and 1963 peaks of input and output (Fig. 13), the apparent mean residence time for the case studied is about one year, compared with an actual turnover time of 5.25 years. It is an important fact that, when mixing of water of different ages occurs in the system, the apparent mean residence time is always smaller than the actual turnover time.

4. DISCUSSION

The use of multi-cell mixing models and the recursive equation approach as discussed above seems to be a quite promising approach for studying the distribution of tracers within a given hydrologic system and at the outflow of the system. They can be employed either as a conceptual mathematical model to simulate dispersion and mixing in a given system or to construct models of real hydrologic systems where the knowledge of the system enables the subdivision of it into physically valid sub-component volume elements. Whereas in all the cases discussed above the system is assumed to be in a steady state, the use of the recursive equation approach can be employed also for non-steady flow systems as the input to the system can be assigned in any desired manner at each subsequent iteration. It should be pointed out that the multi-cell mixing model can be further extended into two and three dimensions to represent the real physical world, and the required computational work for the use of the recursive equation can easily be handled by a computer. The use of two or three such dimensional mixing cells would be

most appropriate, for example, together with groundwater flow models, to obtain a cross-check of the adopted mathematical model with available isotopic or chemical data. A further advantage of the approach is that all other available chemical and physical data can be incorporated in the evaluations to arrive at the most realistic interpretations.

ACKNOWLEDGEMENTS

The authors would like to express their gratitude to Professor E.S. Simpson of the University of Arizona for his fruitful ideas and introduction to recursive programming. We would also like to thank B.R. Payne, Head of the IAEA Isotope Hydrology Section, for his continuous encouragement and constructive discussions, H. Zojer, of the Technical University of Graz, for help in sampling, and our colleagues in the IAEA Isotope Hydrology Laboratory for carrying out the tritium analyses.

REFERENCES

[1] ERIKSSON, E., Compartment models and reservoir theory, Annu.Rev.Ecol.Systematics 2 (1971) 67.
[2] BOLIN, B., RODHE, H., A note on the concepts of age distribution and transit time in natural reservoirs, Tellus 25 (1973) 58.
[3] SHEPPARD, C.W., Basic Principles of the Tracer Method, Wiley, New York (1962).
[4] IBBITT, R.P., Representative Data Sets for Comparative Testing of Conceptual Catchment Models, IAEA Internal Report (1972); available in the IAEA Section of Isotope Hydrology.
[5] BEAR, J., ZASLAVSKY, D., IRMAY, S., Physical Principles of Water Percolation and Seepage, UNESCO (1968).
[6] HIMMELBLAU, D.M., BISCHOFF, K.B., Process Analysis and Simulation — Deterministic Systems, Wiley, New York (1968).
[7] CHOW VEN TE (Ed.), Handbook of Applied Hydrology, McGraw-Hill, New York (1964).
[8] ZOETL, J., Technische Hochschule Graz (private communication).
[9] ZOJER, H., Society of Hydrological Investigations, Graz (private communication).
[10] DINÇER, T., PAYNE, B.R., FLORKOWSKI, T., MARTINEC, J., TONGIORGI, E., Snowmelt runoff from measurements of tritium and oxygen-18, Water Resour.Res. 6 (1970) 110.

DISCUSSION

A. ZUBER: Your very interesting approach enables one to take into account more hydrological parameters than other applied models. However, the number of fitting parameters increases. Could you give the exact number of fitting parameters for the cases described in the paper?

K. PRZEWŁOCKI: We introduced as small a number of fitting parameters as possible and used no complicated models representing real hydrological situations. We also tried to incorporate all available hydrological constraints so as to obtain a realistic estimate of the fitting parameters. In fact, we used two bulk parameters: number of cells and recharge over the volume ratio of the system.

The number of fitting parameters for the cases described in the paper depends on the number of cells selected. In the case of the Graz project, there are four independent fitting parameters: number of cells, recharge, volume of the first cell and volume of the other five equal cells. In the

case of the Modrý Důl basin, there are five independent parameters: constant recharge, number of cells, volume of the first cell, volume of the second cell and volume of the last two equal cells.

J. MARTINEC: I should like to make a few comments regarding the part of your paper which deals with the Modrý Důl basin.

Because of snow accumulation, the distribution of input into a mountain basin differs from the distribution of precipitation during the year. In the Modrý Důl basin, more than 50% of the average annual input from precipitation can be concentrated in April or May, when the snows melt.

The transit time obtained from model calculations is greatly affected by the assumed distribution of recharge. In the earlier study, only winter precipitation (i.e. snowmelt) was considered effective, whereas in the present paper equal importance seems to be ascribed to summer precipitation.

Decreasing compartment volumes were chosen in the light of the shape of the basin. I suggest that the area-elevation curve also be considered in connection with such a choice.

The turnover time of 5.25 years and the assumption of recharge all the year round would imply the existence of a much greater storage capacity than the subsurface storage volume obtained in the previous study, the earlier estimate already being considered surprisingly high.

K. PRZEWŁOCKI: We agree that there is some simplification in the construction of our input function for the Modrý Důl case. We assumed as a reasonable first approximation for practical purposes, that precipitation recharged the aquifer uniformly over the entire year. As a next step one can also test your assumption by modelling no recharge for the second half-year period and taking into account only radioactive decay.

Concerning your remark about compartment volumes, we assumed them to be decreasing in the light of the shape of the basin and did not try to model them in greater detail because of lack of data.

Concerning the turnover time value for Modrý Důl (5.25 years), we believe that this value, which is based on observations over a long period, is a good estimate.

Y. YURTSEVER: As a co-author of this paper I should like to add that the tritium input function adopted for the Modrý Důl area is the mean tritium concentration during each half-year weighted by the mean monthly precipitation amounts derived from five years of precipitation data available for the study area. The difficulty involved in defining the accurate time distribution of actual recharge to a basin is obvious, especially if part of the precipitation is in the form of snow. Since in the early study only winter precipitation (i.e. only snowmelt) was considered, the difference in the estimated turnover time might be partly explained by this fact.

G.B. ALLISON: Using a similar approach to model an unconfined aquifer, we have found that a change in the number of compartments will modify the output generated by the model quite markedly. In your Modrý Důl example you used only four compartments to describe what is quite a large groundwater system in terms of area. Our work suggests that halving (or quartering) the size of each compartment will have quite a significant effect on the output curve generated. Have you studied the effect of compartment size? In practice, I feel that the number of compartments should be increased until the output curve no longer changes with increases in the number of compartments.

K. PRZEWŁOCKI: We have not yet studied the influence of the number of cells on the shape of the output curve. On the basis of physical reasoning we intentionally divided the entire aquifer into four cells in order of decreasing volume; in this way, we hoped to simulate the decreasing amount of mixing within the system. This was, however, a rather intuitive criterion, which we used as a first approach. We therefore appreciate your valuable remarks, which will help in our future work.

Y. YURTSEVER: There is no doubt that the number of components is a parameter which will affect the tracer output curve. As regards the size of the components in the adopted models, although we have not checked the sensitivity of the models, we had, in the Modrý-Důl case for example, more than 30 trial runs with different volumes to obtain the best fit, and from the results of this experiment I can say that slight changes in the size of the components would not significantly change the computed tritium output.

V. T. DUBINCHUK: I am favourably impressed by the authors' approach, for it enables one to employ the tools of finite mathematics, logic and computer technology.

It is perhaps worth noting that the extreme transition gives a Gaussian distribution, so that hydrogeological systems with output curves can be considered by means of this approach; moreover, any other systems consisting of several arbitrary sub-systems can be analysed.

Besides their mathematical treatment, the authors tested their ideas in practice, and I am pleased at their success.

APPLICATION OF DIGITAL MODELLING TO THE PREDICTION OF RADIOISOTOPE MIGRATION IN GROUNDWATER*

J.B. ROBERTSON
US Geological Survey,
National Reactor Testing Station,
Idaho Falls, Idaho,
United States of America

Abstract

APPLICATION OF DIGITAL MODELLING TO THE PREDICTION OF RADIOISOTOPE MIGRATION IN GROUNDWATER.

Recently developed numerical techniques have been adapted to the solution of transient radioactive solute migration problems in groundwater. The differential equations of groundwater movement are first solved by standard finite difference methods, then the differential equations of solute transport are solved by the method of characteristics. Validity of the simulation techniques is demonstrated for real examples of tritium, chloride and ^{90}Sr migration in groundwater at the National Reactor Testing Station, Idaho. This is probably the first documented field-verification of such a model that includes the effects of convective transport, two-dimensional dispersion, radioactive decay and ion exchange. Model results demonstrate the relative sensitivity of groundwater transport systems to various parameters, such as dispersion coefficients and ion-exchange distribution coefficients. The models can be very useful in predicting the behaviour of natural isotopes, artificial tracers or waste in groundwater. The models allow variable hydraulic parameters in space and time, as well as variable chemical parameters. Predictive use of such models is demonstrated for several different conditions in a heterogeneous basaltic aquifer. Thirty-year predictions of tritium and ^{90}Sr migrations are shown with variable hydraulic and chemical influences. Additional methods and potential applications of modelling are suggested, including tracer migration studies and natural isotope distributions in groundwater.

INTRODUCTION

The concentration distributions of migrating dissolved radioisotopes in ground water are difficult to analyze and predict because of many complex, interrelated influences. The significant influences include space and time variations in ground-water flow, hydraulic dispersion, radioactive decay, ion exchange and other chemical reactions. Many different types of problems involve these processes. Among them are: the movement of radioactive wastes in ground water; design and analysis of tracer tests in ground water systems; analysis of natural isotope distributions in ground water.

Recently developed numerical techniques [1, 2] have made possible the analysis of many complex solute migration problems in ground water. These methods have been adapted into a model that can predict the migration of radioisotopes in a heterogeneous aquifer, including the effects of two-dimensional convective transport and hydraulic dispersion, radioactive decay, ion exchange and transient hydraulics. This study demonstrates the applications and usefulness of this type of modeling in a real example of radioactive waste disposal at the U.S. Atomic Energy Commission's National Reactor Testing Station (NRTS), Idaho (U.S.A.). The model has been verified by correctly simulating the observed migration of waste tritium, strontium-90 and chloride in the Snake River Plain aquifer beneath the NRTS [3].

---

* Publication authorized by the Director, US Geological Survey.

THEORY

These types of models consist of two coupled phases--the first simulates the hydraulics and the second simulates solute transport. The hydraulic phase solves the transient, two-dimensional partial differential equation of ground water flow (equation 1) for a bounded, two-dimensional one-layer aquifer, using finite difference techniques (iterative, alternating-direction implicit scheme) as described by Bredehoeft and Pinder [4].

$$\nabla \cdot \vec{\vec{T}} \cdot \nabla h = S \frac{\delta h}{\delta t} + W\ (x,y,t) \qquad (1)$$

where $\nabla = \frac{\delta}{\delta x}\vec{i} + \frac{\delta}{\delta y}\vec{j}$

$\vec{\vec{T}}$ = transmissivity tensor L^2t^1)

h = hydraulic head (L)

S = storage coefficient (L°)

x,y = cartesian coordinates (L)

t = time

W = flux of a source of sink (Lt^{-1})

From the solution of this equation, ground water velocity vectors can be computed for every grid point at any finite time step. These velocities are then transferred to the solute transport phase of the model that solves the transient partial differential equation of transport, equation 2 [3], using the method of characteristics [2, 1].

$$\frac{\delta \varepsilon C_n}{\delta t} = \nabla \cdot \vec{\vec{D}} \cdot \nabla C_n - \nabla \cdot C_n \vec{q} - \varepsilon C_n \alpha_c \frac{\delta p}{\delta t} - QC_s - \lambda_n \varepsilon C_n - \frac{\delta (1-\varepsilon) N_n}{\delta t} \qquad (2)$$

where $\vec{\vec{D}}$ = dispersion coefficient tensor (L^2t^{-1})

C_n = concentration of a particular solute, n, (ML^{-3})

C_s = concentration of solute n in a source or sink (ML^{-3})

$\vec{q}$ = Darcy velocity vector of ground water flow (Lt^{-1})

α_c = compressibility of medium ($M^{-1}Lt^2$)

p = fluid pressure ($Mt^{-2}L^{-1}$)

Q = production rate of source or sink (t^{-1})

ε = effective porosity (L°)

λ_n = radioactive decay constant for solute n (t^{-1})

N_n = concentration of sorbed solute n on solid phase (ML^{-3})

The terms on the right side of the equation include (left to right): hydraulic dispersion, convective transport, aquifer compression factors, sources and sinks, radioactive decay and sorption (or ion exchange). Input for the model includes the usual aquifer hydraulic parameters (transmissivity, storage coefficient and boundaries), hydraulic dispersion coefficients (transverse and

longitudinal), initial concentration distributions, ion exchange distribution coefficient, radioactive decay constant and source-sink inputs. Among the more speculative of these inputs are the dispersion coefficients which are not well understood.

Hydraulic dispersion

Hydraulic dispersion involves transfer of a dissolved constituent from a higher concentration zone to a lower concentration zone by means of mixing and molecular diffusion. Dispersion has been shown in recent studies to be a very significant influence on the migration of solutes in large ground water systems [1, 3]. It involves two orthogonal components--transverse (normal to flow direction) and longitudinal (parallel to flow direction). Dispersion can greatly affect the location and concentration of a tracer interface. It appears that the larger and more heterogeneous an aquifer is, the more prominent are the dispersion effects. These effects are usually quantified by using dispersion coefficients D_T, D_L. In this study the dispersion coefficients are assumed to be proportional to the ground water velocity, v, and the dispersivity (α_T,α_L) so that $D_T = v\alpha_T$ and $D_L = v\alpha_L$ [1].

Dispersion in porous media is a poorly understood process on a large scale; consequently it cannot be exactly quantified and described. It is assumed to obey the Fickian type expression in equation 2.

Radioactive Decay

This process can be described simply and precisely if the decay constant for the isotope is known. It is easily handled in the model.

Ion Exchange

Ion exchange can follow several reaction schemes. When the water chemistry is relatively constant and the isotope of concern is in low concentrations, a simple instantaneous equilibrium, linear adsorption isotherm model may be used. This scheme is quantified by a distribution coefficient, K_d, which is the ratio of the nuclide concentration on the solid phase (pico-curies per cubic centimeter) to its concentration in liquid phase. In this case, equation 2 can be reduced to equation 3 [3].

$$\frac{\delta \varepsilon C_n}{\delta t} = \left(\frac{\varepsilon}{\varepsilon + K_d - \varepsilon K_d}\right) \left[\nabla \cdot \vec{\vec{D}} \cdot \nabla C_n - \nabla \cdot C_n \vec{q} - (\varepsilon C_n \alpha_c) \frac{\delta p}{\delta t} - QC_s - \lambda_n \varepsilon C_n\right] \quad (3)$$

The other factors in equation 2 are either self-explanatory or insignificant.

Method of Characteristics

This scheme of solving equation 3 characterizes the dissolved nuclides by characteristic imaginary particles. It is a rather cumbersome method to use, but works well, once it is properly set up for a particular problem. The method is described more thoroughly by Pinder and Cooper [2].

WASTE DISPOSAL AT THE NATIONAL REACTOR TESTING STATION

The National Reactor Testing Station (NRTS) occupies 894 square miles (2 320 square kilometers) of semiarid land on the eastern Snake River Plain in southeast Idaho (fig. 1) and is operated by the U.S. Atomic Energy Commission (AEC), for testing of various types of nuclear reactors, principally for

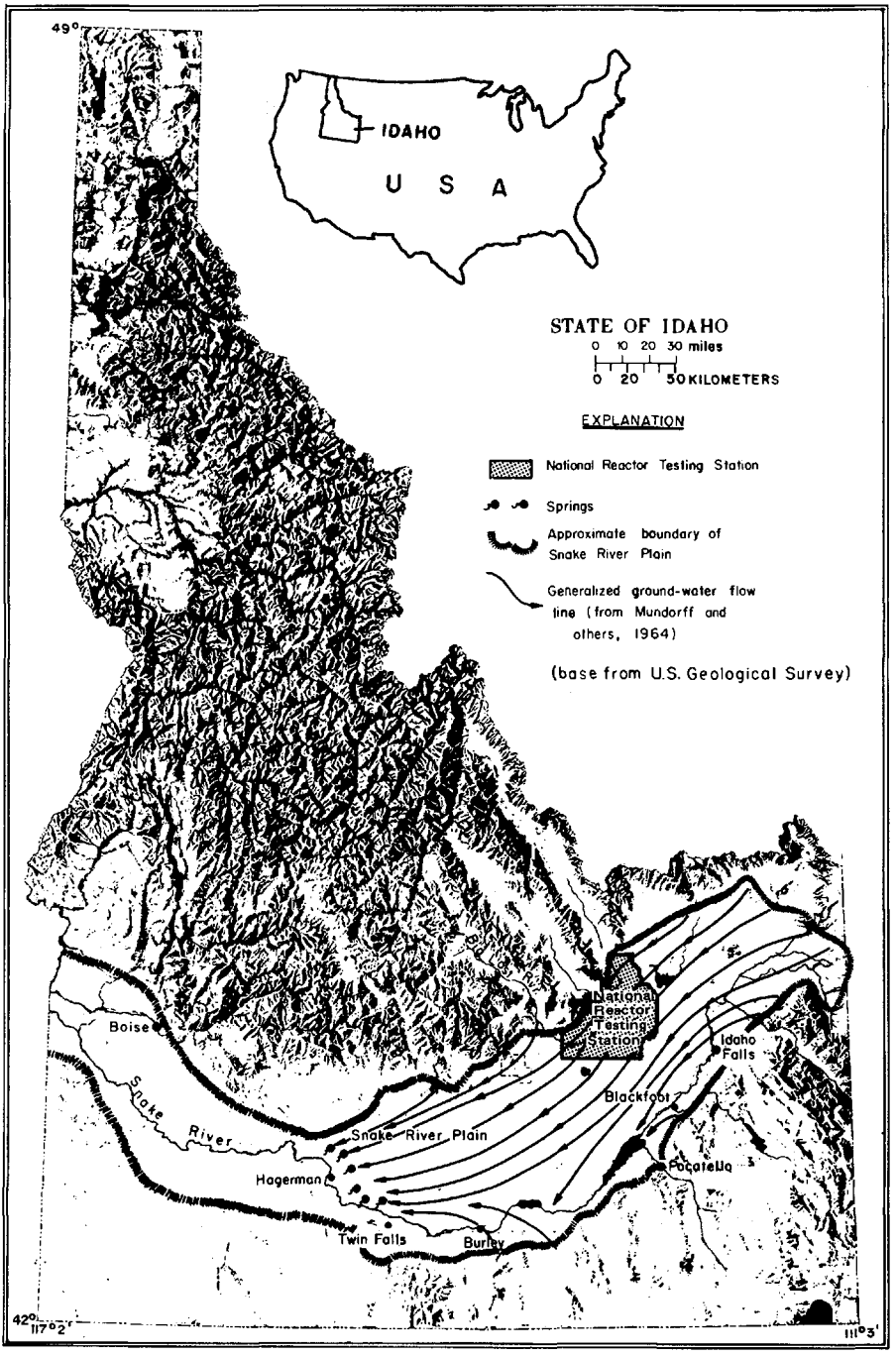

FIG. 1. Relief map of Idaho showing the location of the NRTS, the Snake River Plain, and inferred ground water flow lines of the Snake River Plain aquifer.

peaceful uses. The first NRTS reactor was finished in 1951 and since then, 50 other reactors have been built.

The eastern Snake River Plain is a large structural basin 12 000 square miles (31 000 square kilometers) in area (fig. 1) which has been filled in to its present level with perhaps 5 000 feet (1 500 meters) of thin basaltic lava flows and interbedded sediments. Nearly all of the eastern Snake River Plain is underlain by a vast ground-water reservoir known as the Snake River Plain aquifer, which may contain in excess of 1 billion acre-feet (1 230 cubic kilometers) of water. The flow of ground water in the aquifer is principally to the southwest (fig. 1) at high velocities (generally 5 to 25 feet per day, or 1.5 to 8 meters per day).

Since 1952, dilute or low-level aqueous chemical and radioactive wastes have been discharged to the Snake River Plain aquifer at the NRTS. The wastes migrate with the moving ground water in accordance with complex chemical and hydrologic influences. Although the migration of several waste products has been monitored, their transport mechanisms proved to be so complex, that, until now, rational predictions of the future behavior and migration of wastes have not been made.

The two facilities with the most significant waste discharges, the Test Reactor Area (TRA), and the Idaho Chemical Processing Plant (ICPP) (fig. 2), have discharged wastes continuously since 1952, and are the only ones considered in this study. Discharges from these two facilities comprise 75 percent of the total volume of liquid waste discharged to the ground at NRTS and include 80 percent of the total chemical wastes and more than 90 percent of the total radioactive waste [5].

Test Reactor Area

An average of about 200 million gallons (7.6×10^8 liters) of water per year has been discharged to the TRA radioactive waste seepage ponds since 1952 [3]. Since 1962, the water has contained an annual average of about 460 curies of tritium (^3H), 8 Ci of strontium-90 (^{90}Sr), and 7 Ci of cesium-137 (^{137}Cs) as the most significant long-lived isotopes (Dr. C. Wayne Bills, written communication, 1974).

Waste discharged to the TRA seepage ponds percolates downward to a large perched ground water zone about 150 feet (46 meters) below the ponds. The waste water eventually seeps through that and other perched water zones and enters the Snake River Plain aquifer below the ponds. Tritium (as tritiated water) is the only radionuclide that has entered the Snake River Plain aquifer in detectable quantities. Observed tritium concentrations in the aquifer are well below recommended drinking water standards [5]. All the other nuclides are cationic and appear to be removed from solution by sorption before reaching the water table which is about 450 feet (137 meters) below the ponds. Ordinary sodium chloride has been a significant traceable waste discharge to an adjacent TRA seepage pond.

Idaho Chemical Processing Plant

The Idaho Chemical Processing Plant (ICPP) currently discharges all its low-level or dilute effluents directly into the Snake River Plain aquifer through a 600-foot (180-meter) deep disposal well, CPP-3, (see inset, fig. 2). The disposal well has been in use since 1953. Most of the radioactivity except tritiated water is currently removed from the effluents by distillation and ion exchange before discharge. Small amounts of other significant isotopes, such as strontium-90, have been discharged also. Other wastes carried in the effluent consist primarily of sodium chloride, acids and bases, plus small amounts of heat. The effluent has contained an annual average of 513 Ci of ^3H, 2.3 Ci of ^{90}Sr, and 2.7 Ci of ^{137}Cs (Dr. C. Wayne Bills, written communication, 1974).

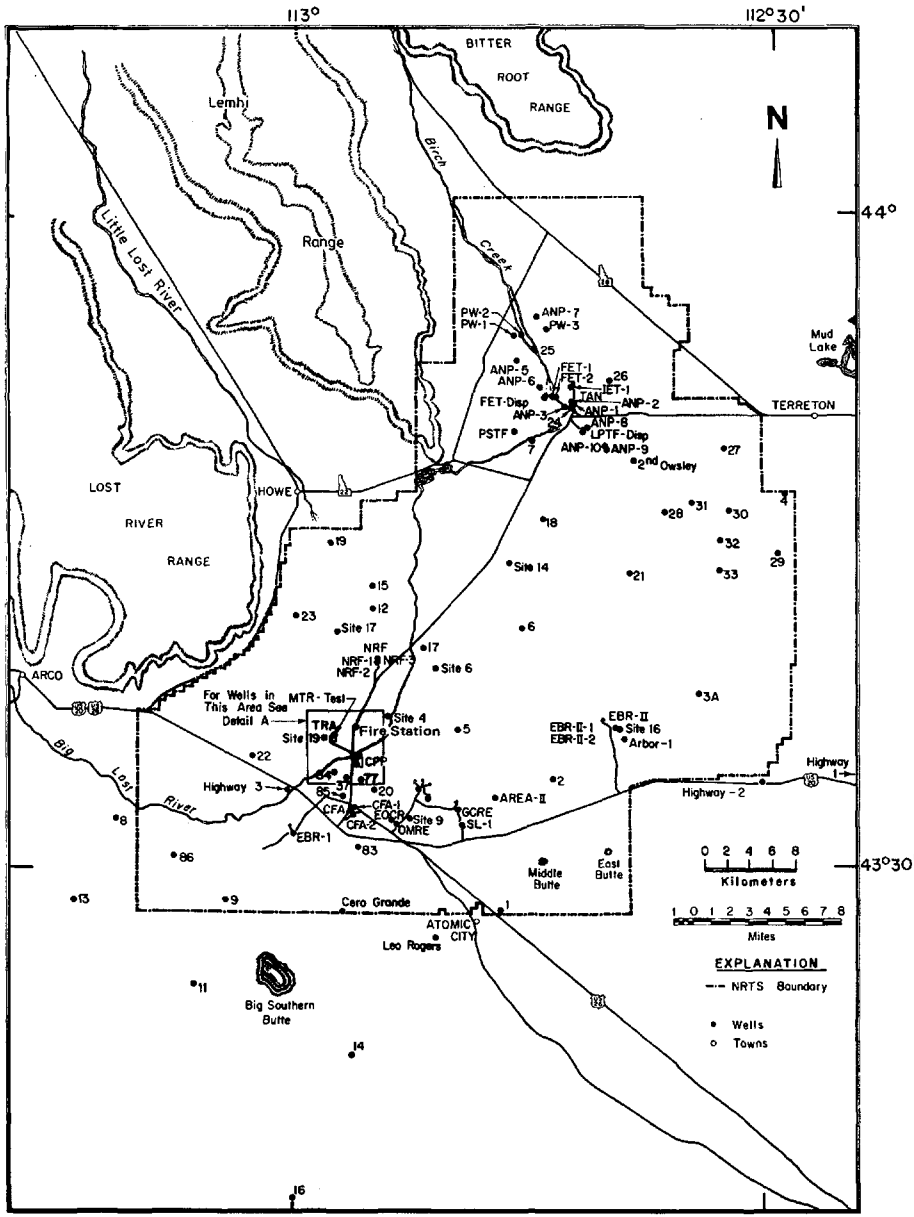
113°
112°30'
44°
43°30'
N
BITTER
ROOT
RANGE
Lemhi
Range
Little Lost River
Birch
Creek
Mud
Lake
TERRETON
LOST
RIVER
RANGE
HOWE
ARCO
Big
Lost
River
Highway 3
Highway 2
Highway 1
PW-2
PW-1
ANP-7
PW-3
25
ANP-5
ANP-6
FET-1
FET-2
26
IET-1
TAN
ANP-2
FET-Disp
ANP-3
24
ANP-1
ANP-8
PSTF
7
LPTF-Disp
ANP-10
ANP-9
2nd Owsley
27
28
31
30
4
32
29
33
18
19
Site 14
21
15
12
23
Site 17
6
NRF
NRF-1
NRF-3
NRF-2
17
Site 6
3A
For Wells in
This Area See
Detail A
MTR-Test
TRA
Site 19
Site 4
Fire Station
5
EBR-II
Site 16
EBR-II-1
EBR-II-2
Arbor-1
22
CPP
84
77
85
37
20
2
AREA-II
CFA-1
CFA
EOCB
Site 9
GCRE
SL-1
CFA-2
OMRE
EBR-1
8
86
83
Middle
Butte
East
Butte
13
9
Cero Grande
1
ATOMIC
CITY
Leo Rogers
Big Southern
Butte
11
14
16
0 2 4 6 8
Kilometers
1 0 1 2 3 4 5 6 7 8
Miles
EXPLANATION
NRTS Boundary
Wells
Towns

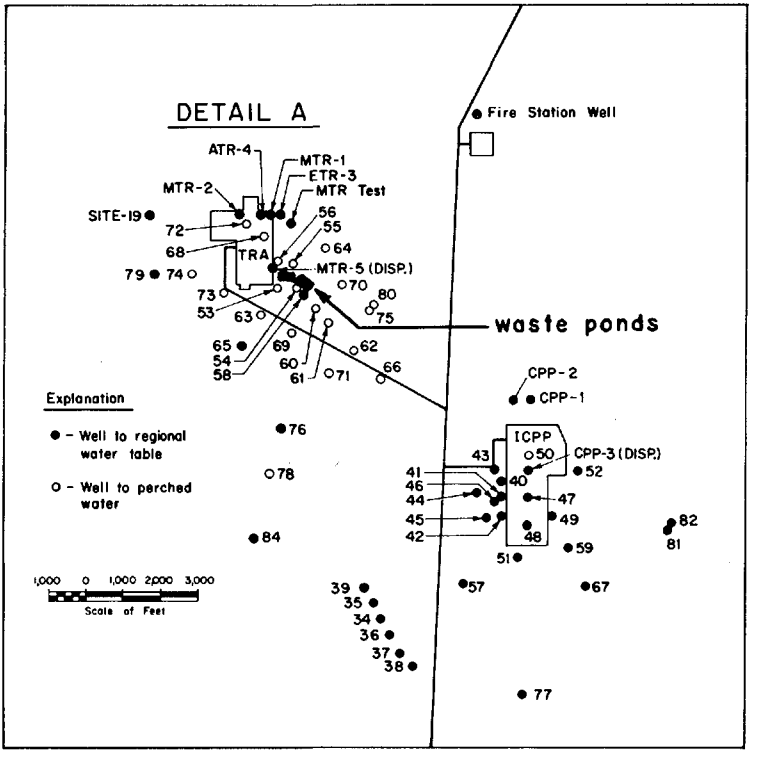

FIG.2. Left: Map of the vicinity of the NRTS showing the numbers and locations of NRTS production and observation wells.

Above: Detail A.

The disposal well extends about 150 feet (46 meters) below the water table. The average annual discharge to the well has been about 300 million gallons (1.1×10^9 liters) per year. More detailed description of NRTS waste discharges are described by Robertson, Schoen, and Barraclough [5], and in AEC reports [6, 7, 8 and 9].

Effects of Waste Disposal

During the 20 years of waste discharge at TRA and ICPP, periodic studies have been made of the migration and distribution of various waste products in the Snake River Plain aquifer [5], based on samples obtained from about 45 observation wells near to and downgradient from points of discharge (fig. 2).

Typical mapped distribution patterns are shown in figures 3, 4, and 5 for chloride, tritium and strontium-90, respectively. The degree of lateral dispersion in the rather rapidly moving chloride and tritium plumes is particularly remarkable. It should be noted that none of the observed concentrations for these waste products in the aquifer have exceeded AEC drinking water standards for a restricted area [5]. The tritium and chloride plumes occupy an area of about 15 square miles (39 square kilometers). The normal analytical detection limit for tritium in water at NRTS is about 2 pCi/ml.

The ^{90}Sr plume occupies an area of only about 1.5 square miles (4 square kilometers). This is due mainly to the effects of sorption (principally ion exchange) that attenuate the concentrations and retard the movement of ^{90}Sr. Mass balances indicate that about 97 percent of the ^{90}Sr discharged down the ICPP well has been adsorbed. The detection limit for ^{90}Sr in NRTS water samples is generally about 0.005 pCi/ml.

Strontium-90 has also been discharged in significant quantities to the TRA ponds, but it is essentially all sorbed out of solution on the sediment and basalt layers between the pond and the aquifer, preventing detectable ^{90}Sr from reaching the aquifer.

Cesium-137 is even more affected by sorption than ^{90}Sr and, for this reason, has never been detected in any aquifer samples near TRA and ICPP.

Studies of waste behavior and aquifer characteristics indicate that the waste plumes shown in the foregoing maps generally remain as relatively thin lenses in about the upper 250 feet (75 meters) of the aquifer. Although there is considerable dispersion laterally and longitudinally, there appears to be little vertically because of low vertical permeability in the layered basalt aquifer.

APPLICATION OF DIGITAL MODEL

Although good documentation has been obtained of changes in waste distribution in the aquifer over the 20-year period of disposal, little quantitative understanding of the processes involved had been obtained until recently. Little could be said as to why the wastes behaved as they had or how they could be expected to behave in the future. It is of particular interest to be able to assess water quality impacts and the effects of possible waste management alternatives. Application of the digital model described herein has enabled both a better understanding of the processes involved as well as a predictive capability.

A valid model of this type requires two forms of verification before it can be used with confidence. First, the hydraulic behavior of the model must accurately correspond to historical observations of the aquifer and, second, the historically observed behavior of waste in the aquifer must be adequately simulated by the model. The verifications must be accomplished using measured values where possible, for the various physical and chemical characteristics and parameters of the system such as transmissivities, dispersivities and distribution coefficients. In the absence of reliable measurements, rational estimates should be used.

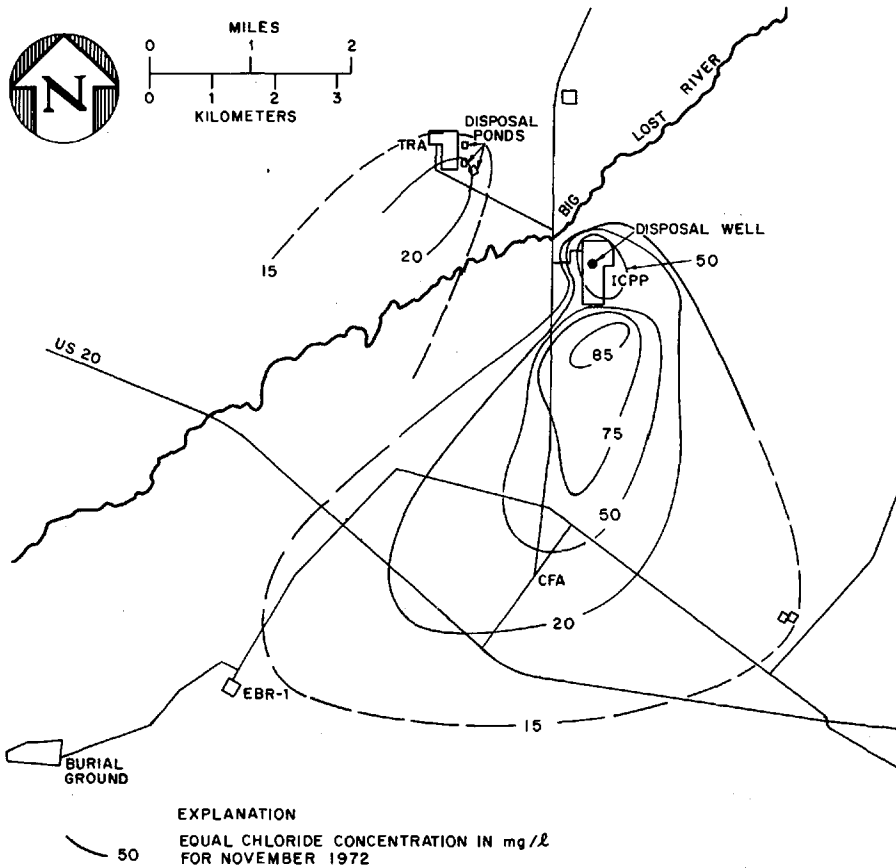

FIG.3. Map of the vicinity of the ICPP-TRA showing distribution of waste chloride in the Snake River Plain aquifer water in 1972.

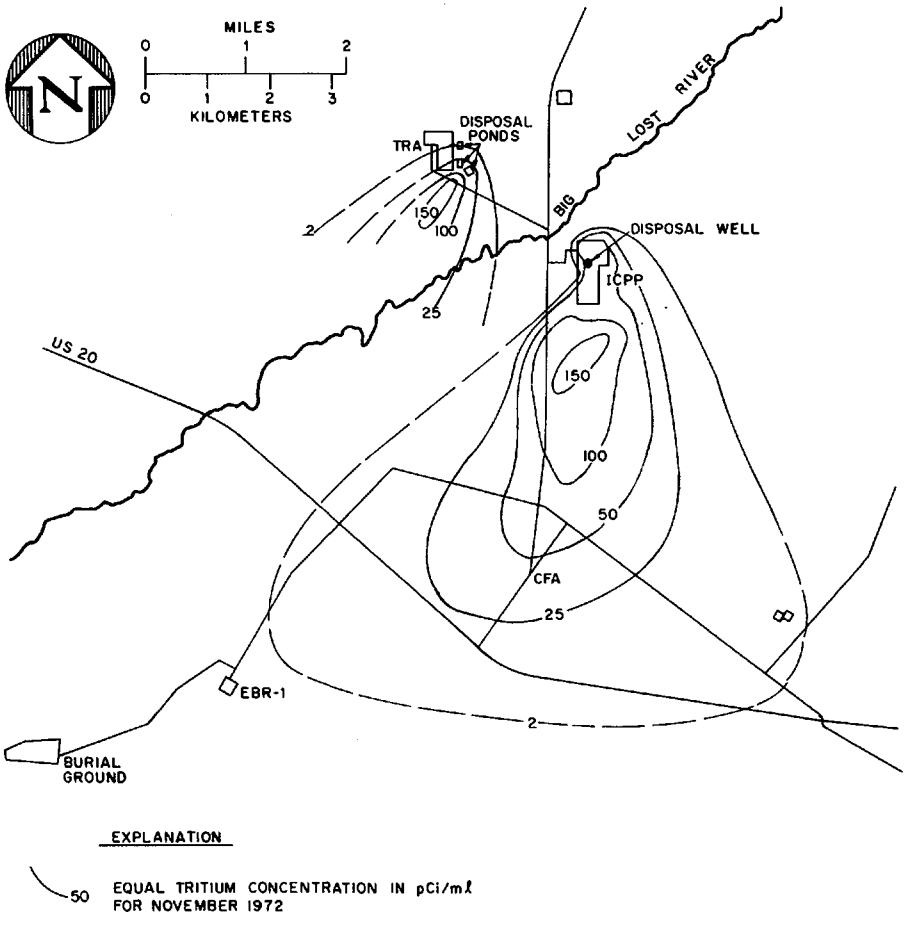

FIG.4. Map of the vicinity of the ICPP-TRA showing distribution of tritium in the Snake River Plain aquifer water in 1972.

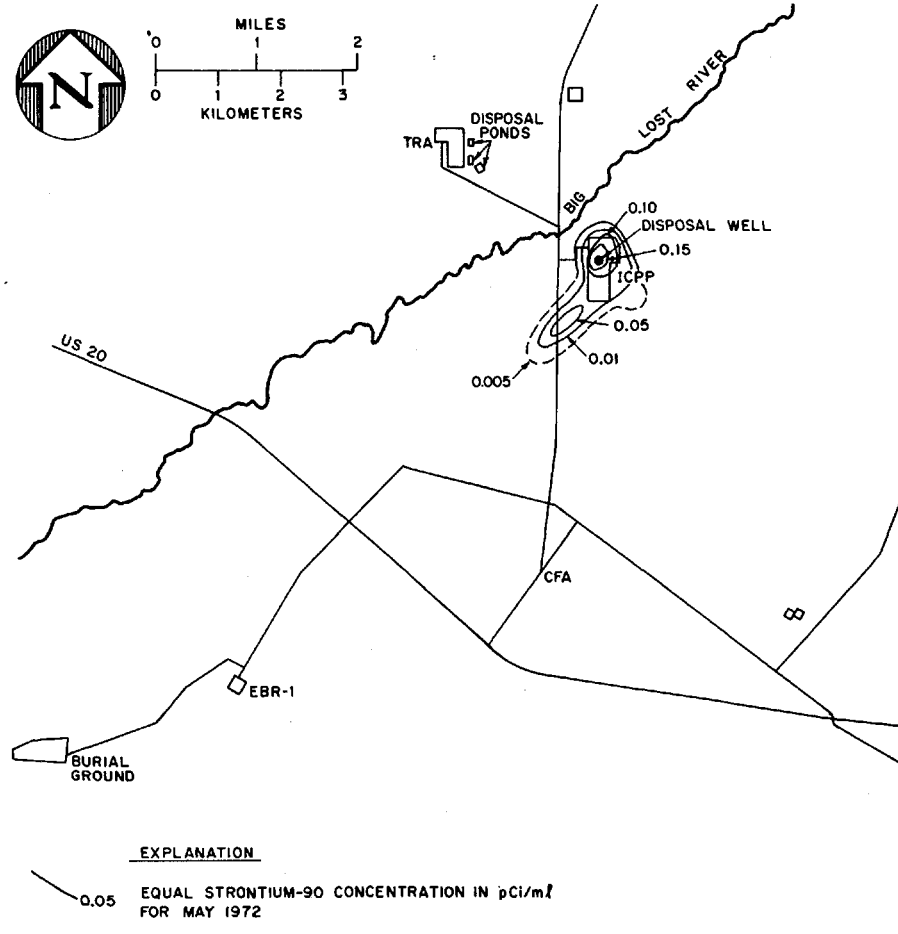

FIG. 5. Map of the vicinity of the ICPP-TRA showing distribution of strontium-90 in the Snake River Plain aquifer water in 1972.

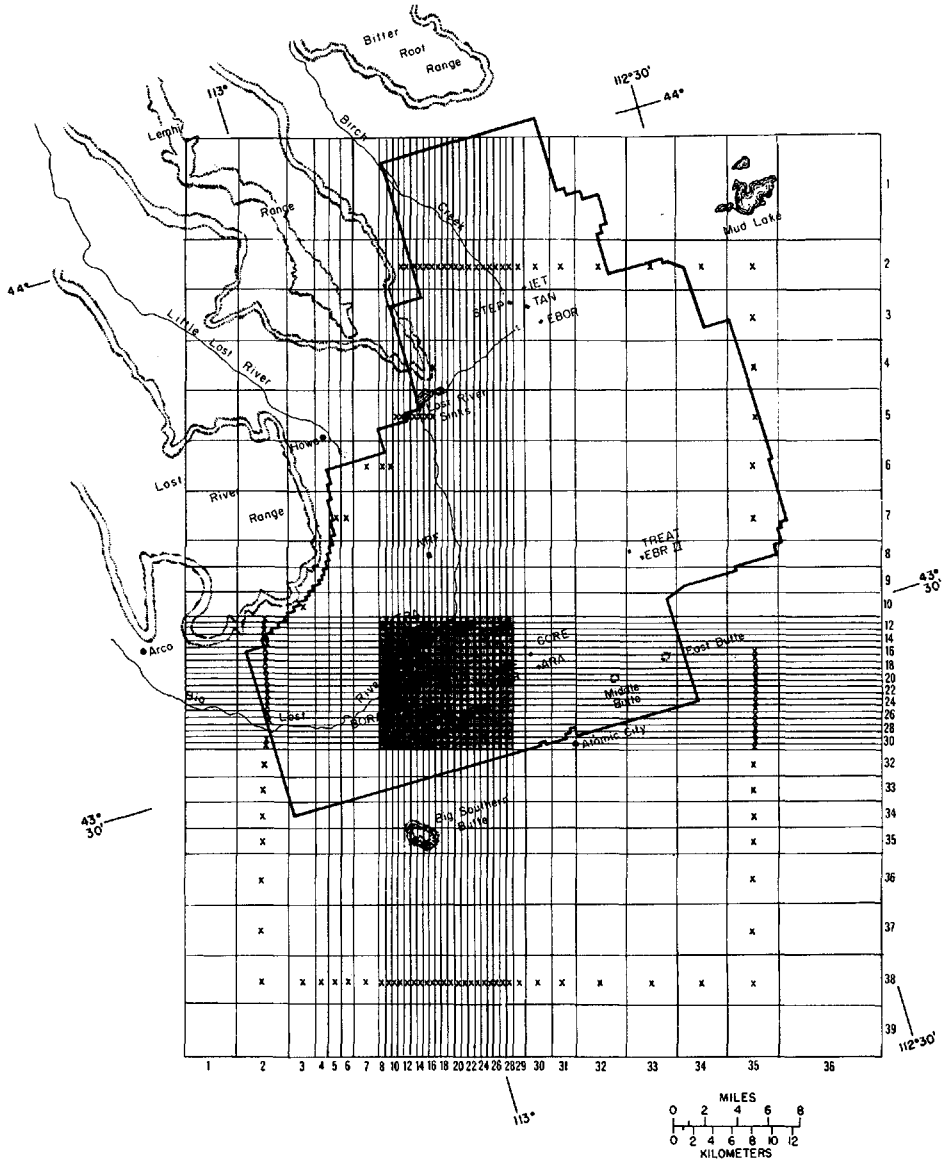

FIG. 6. Finite difference grid map for one version of hydrology and solute transport model. Solute transport model includes only shaded part (smallest nodes). Constant-head boundary nodes are represented by "x"s.

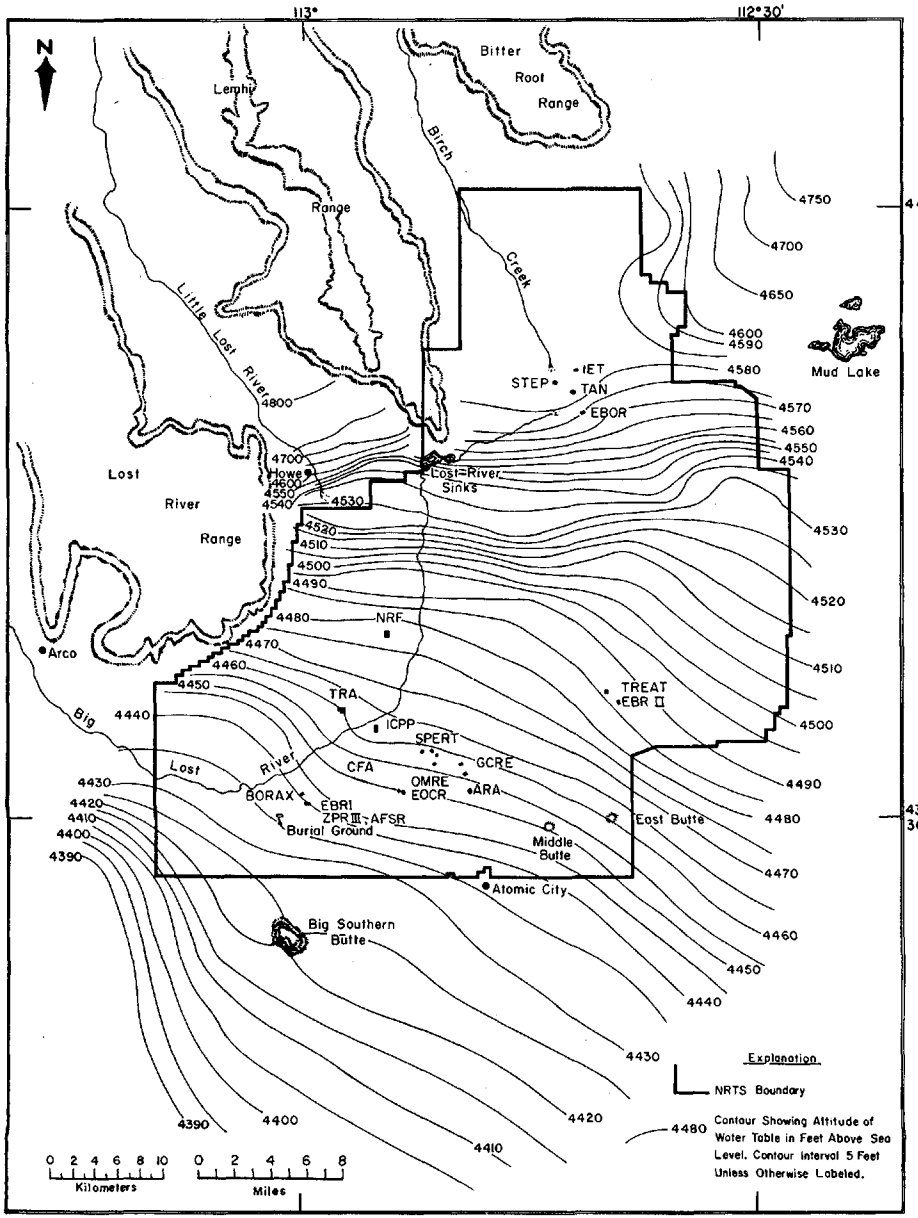

FIG.7. Map of the NRTS and vicinity showing contours on the regional water table, May through June 1965, upon which the steady state verification of the hydrologic model was made.

Hydraulics

The finite grid system for the initial verification model was 36 by 39 nodes (fig. 6) and covered an area of 2 600 square miles (6 600 square kilometers). It is assumed that, for the purposes intended, the model area is large enough to justify neglect of aquifer effects outside the area. The only significant surface-water influence on this portion of the aquifer is on the Big Lost River, whose intermittent recharge is simulated by "recharge wells" at each node along the reach of the river.

Transmissivities for the model were obtained principally by flow net and pumping test analyses and all other physical characteristics were based on the best field information available on the aquifer. Although the real aquifer system is probably more than 1 000 feet (300 meters) thick, a thickness of 250 feet (27 meters) was used in this study based on apparent layering effects in the aquifer. This upper layer appears to be somewhat separated from and more permeable than the lower zones. Details of the hydraulic phase of the model are described by Robertson [10].

Successful verification of the hydraulic model was obtained for both steady state and transient performance of the model. In 1965, a good map of an apparent near steady-state condition of the potentiometric surface of the aquifer was obtained (fig. 7). The model was then given the corresponding head elevations around the constant head boundary nodes and allowed to bring itself to a steady head distribution. After some minor adjustments in transmissivity, the head pattern was nearly identical with that shown in figure 7. The simulated potentiometric surface showed no significant deviations from the well data.

The transient verification was obtained by the accurate simulation of substantial recharge effects from the Big Lost River. With these results, the model was accepted as valid, hydrologically, and verification procedures were applied to the waste transport segment of the model.

Waste Transport

Although the waste transport segment of the model depends directly on the hydraulic segment, the area of concern is much smaller. Solute transport was initially modeled only for the area shown by the shaded grids in figure 6.

Porosity of the aquifer is a critical factor in the waste transport model and was assumed to be 10 percent, based on limited measurements and indirect evidence. The most speculative of the inputs are the dispersivities and distribution coefficients. No effective way is presently practical to measure these coefficients in the field at this site because of the large-scale aquifer inhomogeneities. These parameters must therefore be estimated.

Chloride. Because of its consistent discharge and conservative nature, waste chloride was first used to verify the transport model. It is neither radioactive nor subject to significant sorption so those factors were ignored. Therefore the principal unknowns in modeling chloride transport in the aquifer are the dispersivities.

In comparing simulated chloride plumes with those actually mapped from field data, for 1958 and 1969, the best fits were obtained using dispersivities of α_L = 300 feet (91 meters) and α_T = 450 feet (137 meters). Although the value for α_L appears reasonable, α_T would appear high compared with Bredehoeft and Pinder's [1] value of 60 feet (18 meters) in a limestone aquifer. Good matches were obtained between model-generated chloride plumes and those mapped from field data [3].

Tritium. Using the same dispersivities, good simulations were also made for tritium. Figure 8 demonstrates a typically good fit. The match is not perfect in all details, but for the purpose of this analysis it is considered excellent. Other good tritium matches were also obtained for different years. The radioactive decay part of the model was shown to function properly.

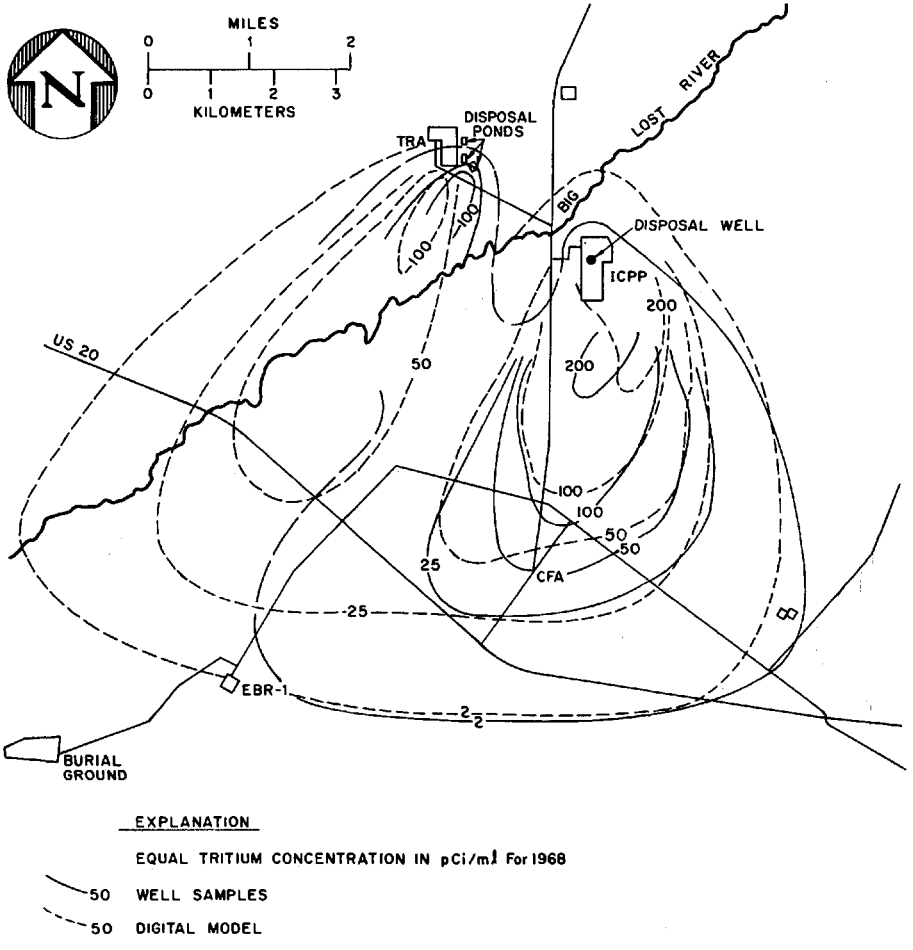

FIG. 8. Comparison of TRA-ICPP waste tritium plumes in the Snake River Plain aquifer for 1968, based on well sample data and the computer model.

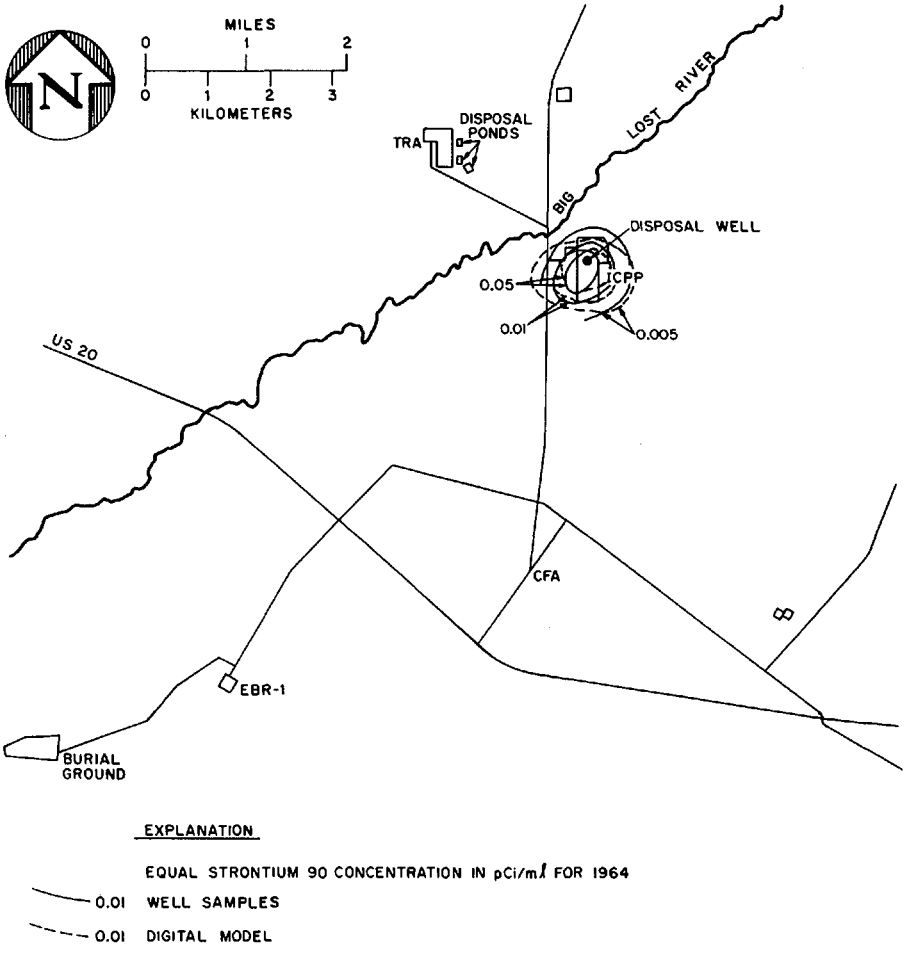

FIG. 9. Comparison of ICPP waste strontium-90 plumes in the Snake River Plain aquifer for 1964, based on well-sample data and the computer model.

Strontium-90. Verification of a sorption routine in the model was obtained with the simulation of ^{90}Sr transport. Because of the small area of contamination by ^{90}Sr, it is more difficult to obtain precisely accurate simulation, due to the coarseness in the model grid. Nevertheless, good matches were obtained for 1964 and 1972 (fig. 9). The results were obtained using a uniform sorption distribution coefficient (K_d) of 3.0. The value of 3.0 for K_d was the estimate based on extrapolation of measured K_d's and mass balances calculated for ^{90}Sr discharged to the aquifer. In a sense, then, the K_d used is a field measurement over a limited area of the aquifer. One of the simplifications used for this model is that the distribution coefficient is uniform throughout the model area. This is certainly not true for the real aquifer, however there is no data available on the spatial variations of K_d, thus necessitating the use of a uniform value. Perhaps better model fits could be forced by varying the K_d spatial distribution in the model, but this was not justified by any quantitative data.

Model Sensitivity

After proper verification, the model may be used to demonstrate the relative sensitivity of the system to the various controlling processes. The model is particularly sensitive to dispersivity values, as shown in the chloride example, figure 10.

If the radioactive decay is relatively fast, such as less than 5 years, the system becomes quite sensitive to that parameter. However, for half-lives of 12 years or longer (such as ^{3}H and ^{90}Sr) this process becomes less effective except in long-term evaluations.

The system is, perhaps, most sensitive to the sorption process. This is demonstrated by comparing the ^{90}Sr plume with those of chloride or tritium (figs. 3, 4 and 5).

Examples of Future Projections

With successful verification, the model is a useful tool for estimating future projections of waste distribution in the aquifer. However, the future behavior of waste in the aquifer is dependent on future hydrologic and waste disposal conditions, which cannot be accurately predicted and must therefore be assumed. Several future projections up to the year 2000 have been made for tritium and ^{90}Sr under various conditions. Because the grid network for the verification model (fig. 6) is too limited in area to make long range projections, an expanded version was adapted for the future projections (fig. 11).

There has been a tendency in recent years to reduce or discontinue NRTS waste disposal to the aquifer. If it is assumed that waste discharges were discontinued in 1973, the simulated 1980 distribution of the previously discharged ^{3}H is shown in figure 12. The projection also assumes no future hydrologic recharge effects from the Big Lost River. Strontium-90 (fig. 13) continues to display a much more limited migration by 1980 than tritium (fig. 12). Although projections to year 2000 have been made for several different conditions of hydrology and waste disposal only a few typical examples are shown in figures 14 and 15 for ^{3}H and ^{90}Sr.

Over a long period, the effects of radioactive decay become more obvious. The tritium plume, for instance, becomes relatively less concentrated than the chloride plume for the year 2000. However the general areal extent of the tritium plume remains similar to that of chloride.

Recharge from the Big Lost River tends to accelerate the southerly movement of the plume and diverts it more to the southeast. Caution must be exercised in interpreting future projections. The longer the projection, the more subject to error it is. In this case study, one source of error is vertical dispersion. For short-term projections it is probably insignificant but for longer ones (perhaps 25 years), vertical dispersion may become very significant.

Text continued on p.475

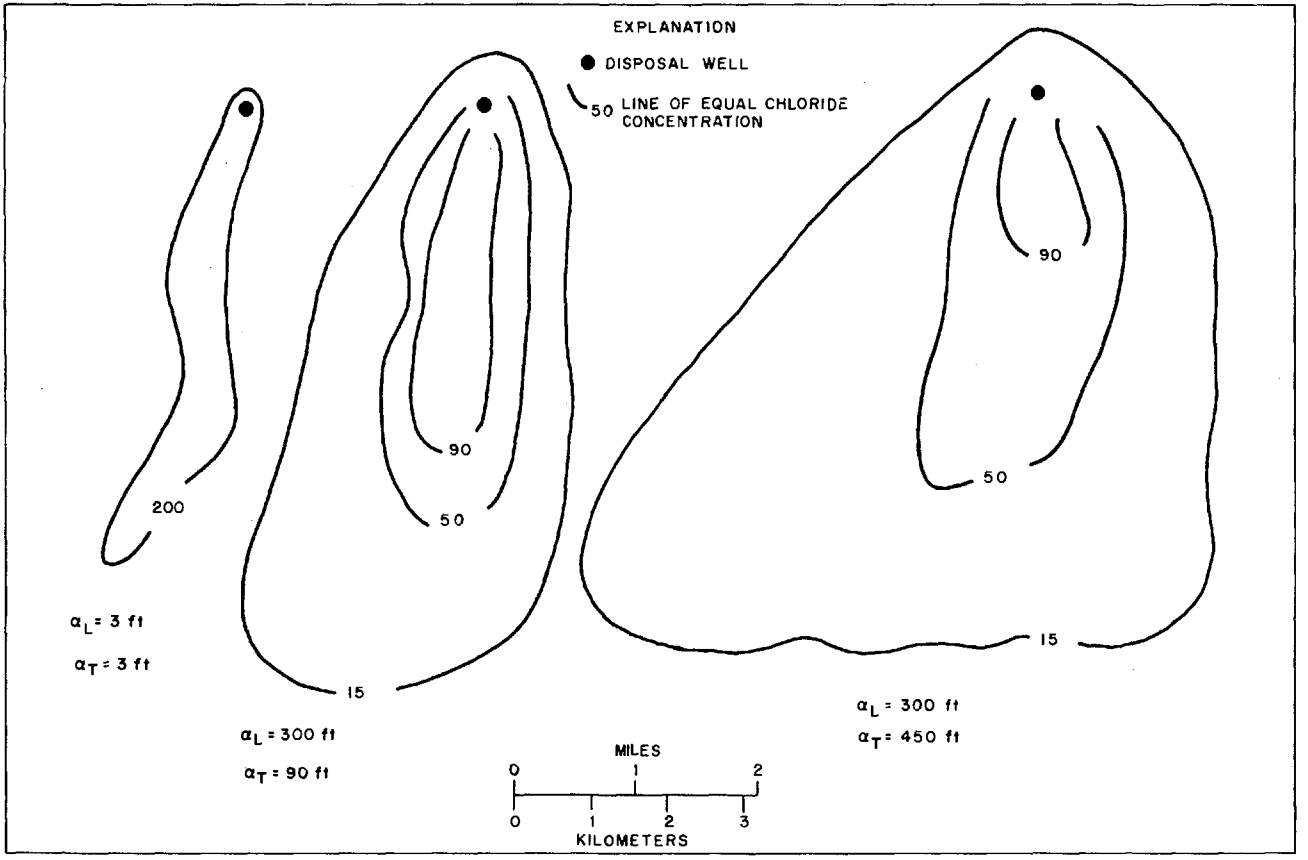

FIG. 10. Model-simulated waste chloride plumes from ICPP for year 1968, showing the effects of varying dispersivities α_L and α_T. Chloride concentrations in mg/l.

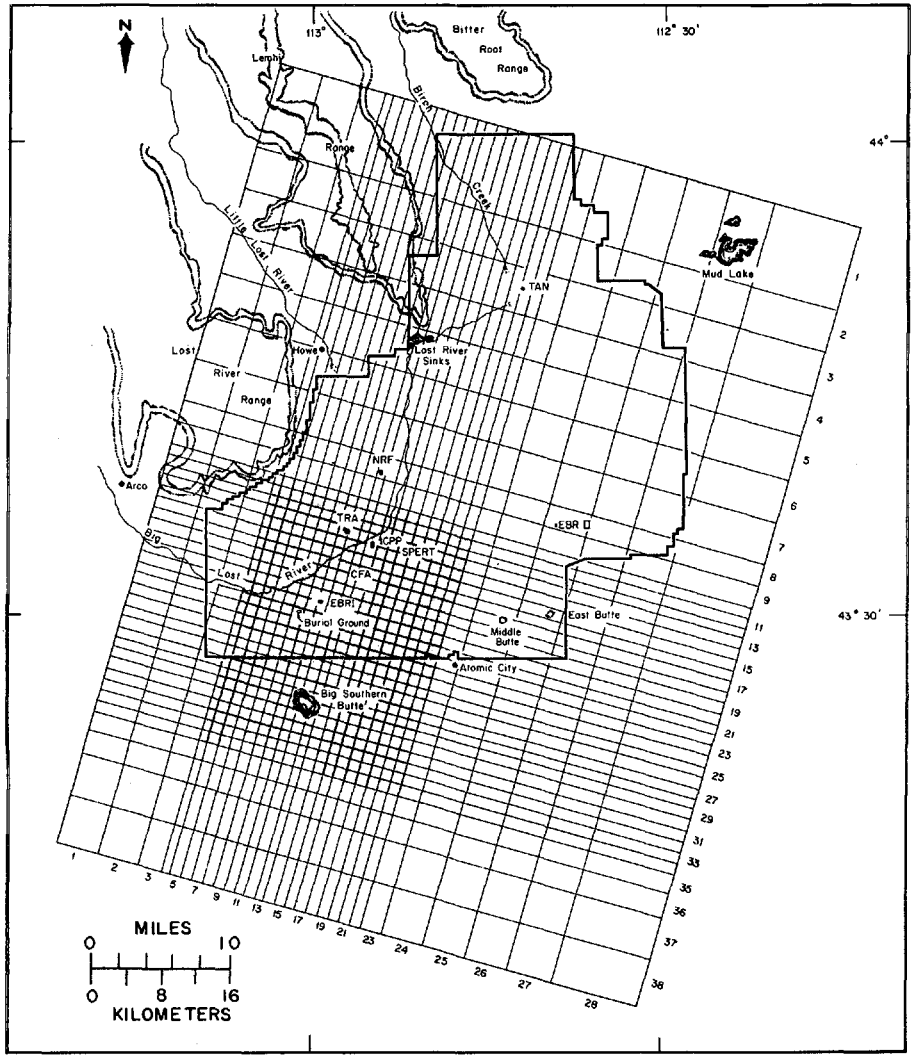

FIG. 11. Finite-difference grid used in second computer model of Snake River Plain aquifer. Shaded area is used for future projections of waste migration.

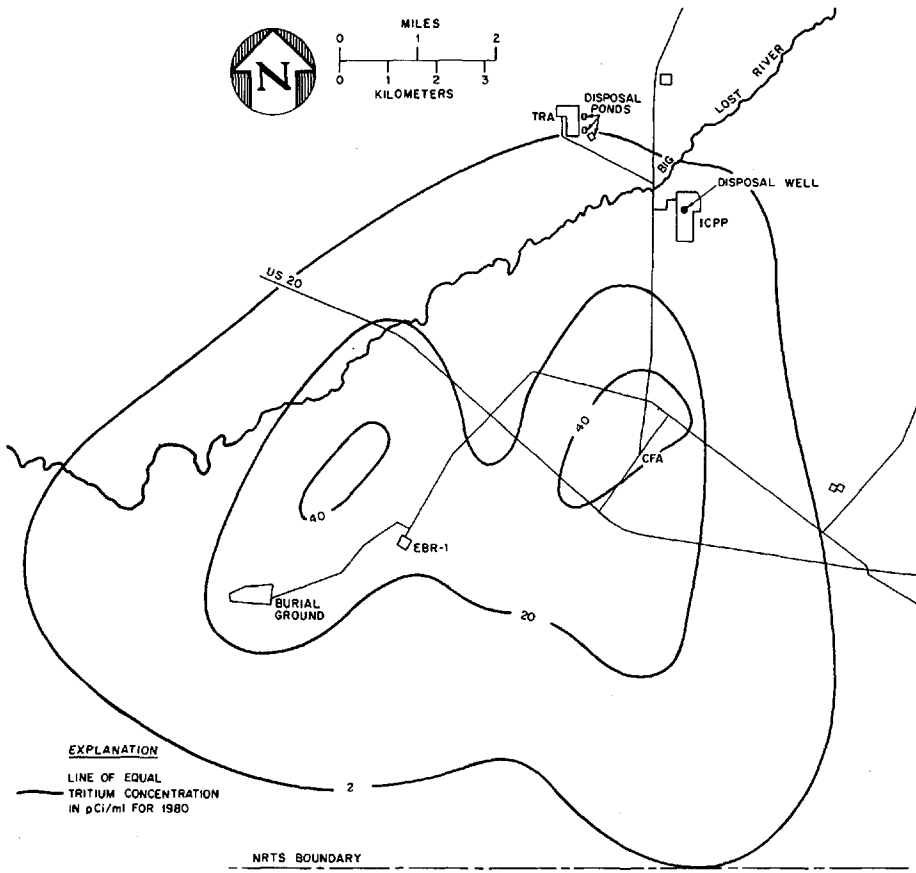

FIG. 12. Model-projected tritium plume for 1980, assuming disposal ceases in 1973 and the Big Lost River does not recharge the aquifer.

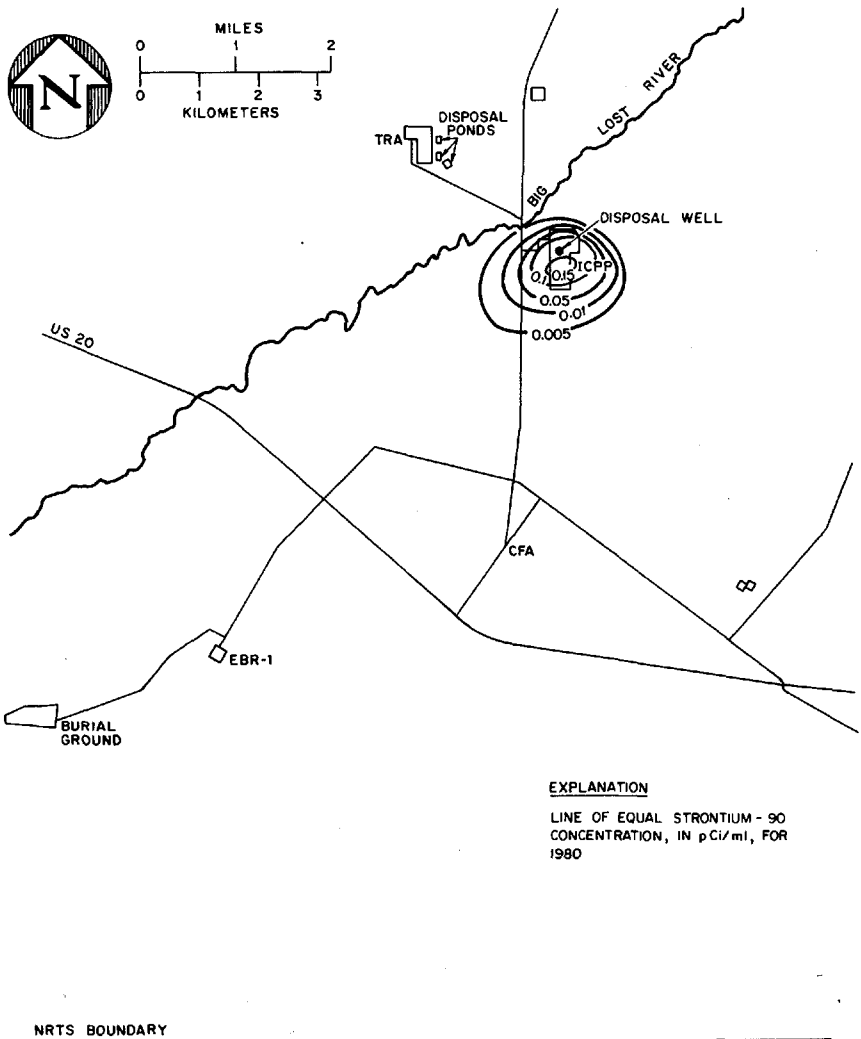

FIG. 13. Model-projected waste strontium-90 plume for 1980, assuming disposal ceases in 1973 and there is no future recharge from the Big Lost River.

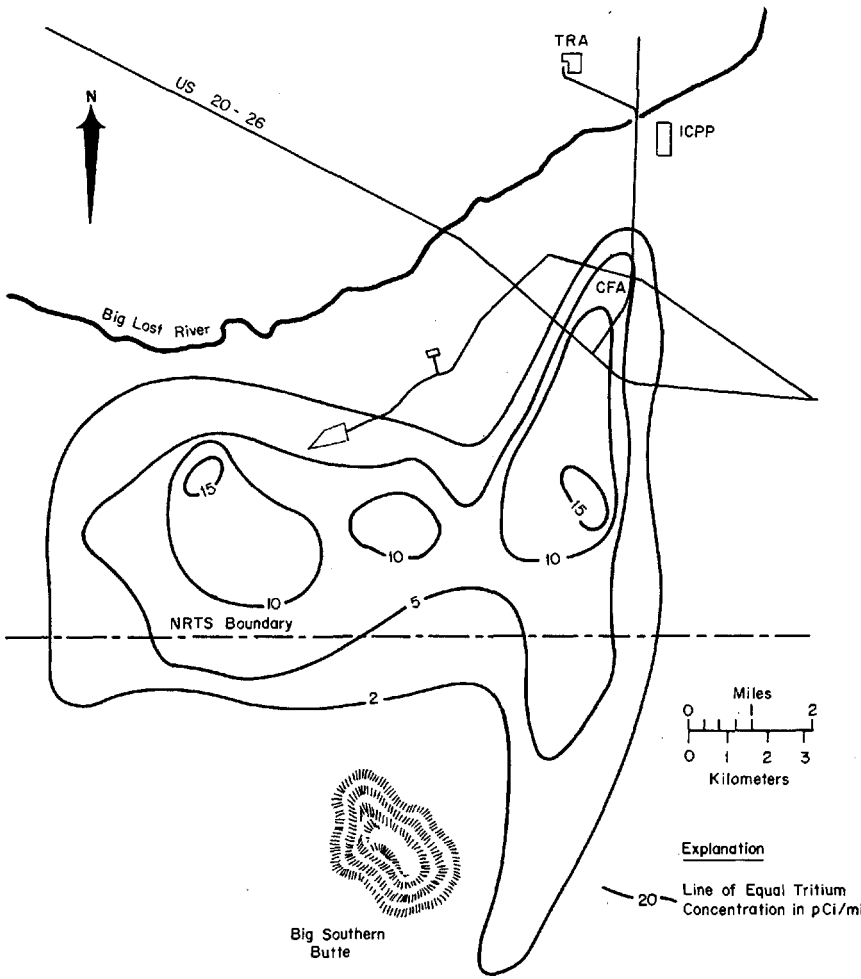
TRA
ICPP
US 20 - 26
N
CFA
Big Lost River
15
15
10
10
10
5
2
NRTS Boundary
Miles
0 1 2
0 1 2 3
Kilometers
Explanation
20 Line of Equal Tritium Concentration in pCi/ml
Big Southern Butte

a

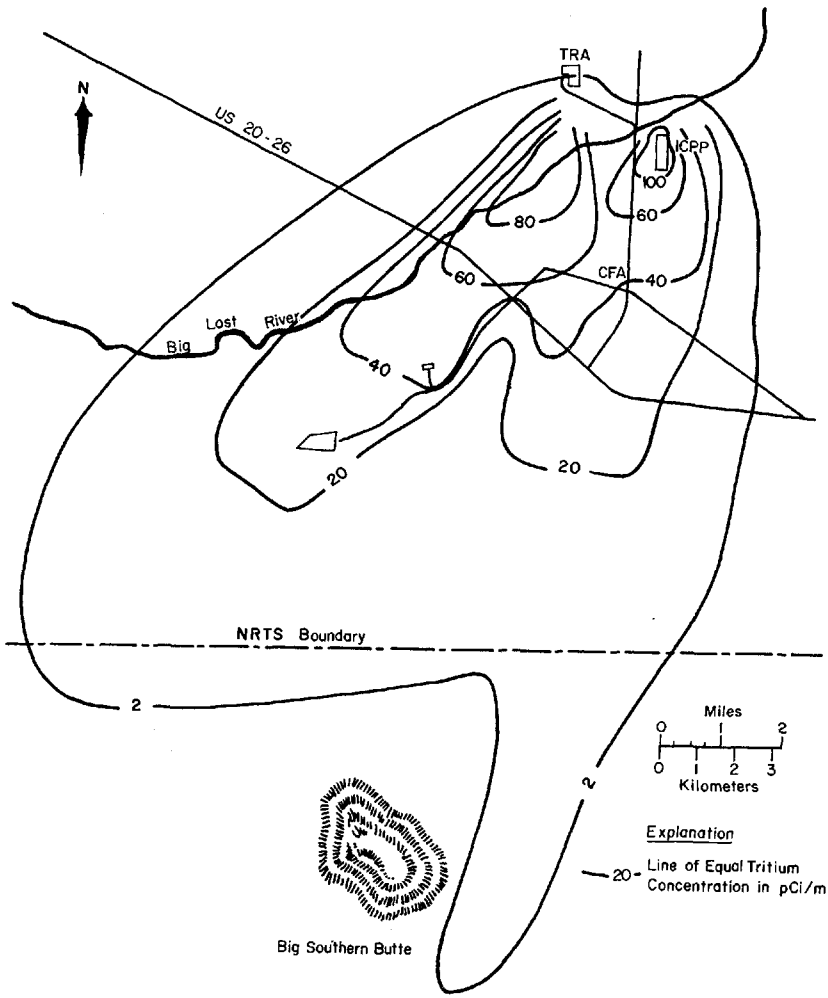

b

FIG. 14. Model-projected waste tritium plumes for year 2000, assuming that there is no future recharge from Big Lost River and that (a) disposal ceases in 1973; and that (b) disposal continues at current rates.

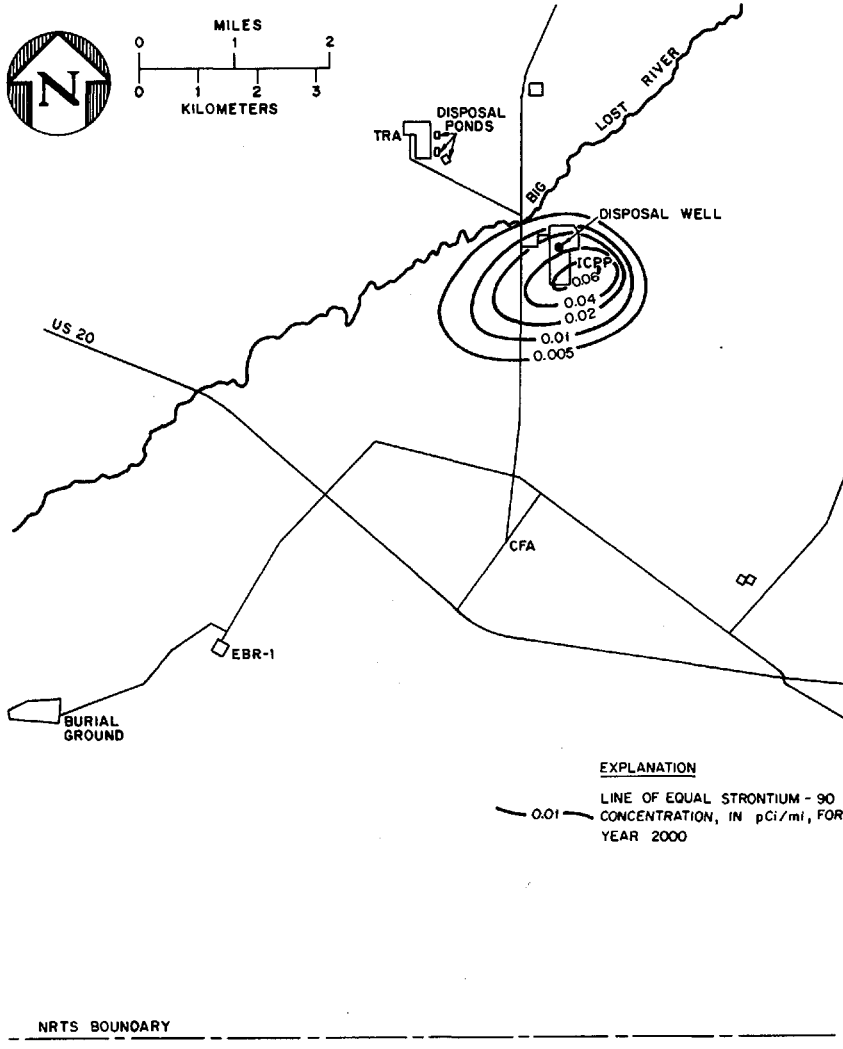

FIG. 15. Model-projected strontium-90 plume for year 2000, assuming disposal ceases in 1973 and there is no future recharge from the Big Lost River.

In that case, the actual extent and concentration of the plume would probably be less than those shown by the model projection. Although there are limitations, the model appears to be useful in a general sense for estimates of future waste distributions, if not too much confidence is placed on exact distribution patterns or exact concentration values at specific locations.

The model, or variations thereof, can be used to study many other NRTS hydrologic and solute transport problems, both real and hypothetical. For example, the effects of an accidental release of waste to the aquifer due to a hypothetical catastrophic event might be studied. Any number of hypothesized future conditions might be analyzed using the model; therefore, no attempt was made to include them all in this study. However, any problems of particular interest could be studied in the future, if desired.

OTHER APPLICATIONS

This report describes real examples of model applications to predicting migration of waste isotopes in ground water. However, these and related techniques have potential application to many other problems, in addition to waste disposal.

For instance, a solute transport model might be applied to the design and analysis of aquifer tracer tests. Tracer tests can be important tools in evaluating aquifer characteristics. Preliminary tests on a proper model could help determine potential effects of dispersion and sorption, observation well locations, test duration, sampling frequencies, proper trace injection concentration and other aspects of the tests. The model would also be helpful in interpreting and evaluating results of tracer tests. With the aid of a model and a proper tracer test with a sorbable tracer, one could actually measure an adsorption distribution coefficient in place, over a fairly large area of the aquifer. The modeling may involve a considerable amount of effort and skill and would therefore require justification based on the magnitude and importance of the tracer tests.

There are potential applications of this type of modeling also to migration-distribution studies of natural and fallout isotopes in ground water. For instance, it may be of interest to study fallout tritium distributions to determine recharge areas of an aquifer. In many complex, heterogeneous systems, it might be infeasible to interpret such distribution without the aid of a model. This would apply even more to studies of sorbable isotopes. There are also several additional applications to waste or contamination problems, such as an accidental spill of high-level liquid radioactive waste into a fresh water aquifer. A valid model could be invaluable in determining the best recovery or decontamination plan, such as the proper location and pump capacity of recovery wells. Potential effects of hypothetical waste discharges or spills could also be evaluated with model aids. This could be particularly useful for environmental impact evaluations for proposed nuclear power, processing or waste facilities.

Although the examples cited in this study use the numerical method of characteristics to solve the transport equation, other numerical methods are adaptable to some types of these problems. For instance, the Galerkin technique has recently been applied successfully to transport models [11, 12]. This method has some advantages over characteristics for certain types of problems. Limitations of this paper do not permit explanation of the Galerkin technique, but the interested reader can refer to the references [11, 12].

CONCLUSIONS

To summarize, it is apparent that nearly any problem involving two-dimensional isotope migration in ground water is amenable to digital modeling. However, the degree of importance of the problem may not justify the application

of modeling. A model can be an invaluable tool for gaining insight and predictive capability for isotope migration problems in ground water, if it is based on adequate and proper information. Generally, a model of this type requires personnel who are intimately familiar with the modeling techniques as well as the hydrologic system they are modeling.

Although a model may be quite useful it also has many limitations which the hydrologist must continually bear in mind. He must avoid the tendency to let the model do his thinking. Neither should he accept all model results without question.

One of the first limitations is simply one of size. These models require large amounts of computer core and time. Thus there are many problems that may be too big to fit a particular machine. Because the finite difference grid must be limited in size, this also limits the extent to which future projections can be made. For the problems described in this study, 500 000 to 600 000 units of computer core were generally required, with central processing unit execution times of 4 to 8 minutes. The computer used was an IBM Model 360/75.

There are many other limitations in the mathematical methods related to finite difference grid size, variability of aquifer physical and chemical parameters, duration of time step, and so forth. These are why the modeler must be familiar with the proper theory and application of these techniques. There are many assumptions that go into these models. The modeler must know the limits within which his assumptions are valid.

As mentioned previously, one of the limiting assumptions in the NRTS model is that of no vertical dispersion, which may not be valid for long-term future projections.

ACKNOWLEDGEMENTS

Most of the development work for the programs used in these models was done by John D. Bredehoeft, U.S. Geological Survey, Denver, Colorado. His help in adapting the technique to the NRTS problems is invaluable. Many staff members of the U.S. Atomic Energy Commission's Idaho Operations Office, Idaho Falls, Idaho, and Headquarters, Washington, D.C. have been helpful with their active support and cooperation in these studies.

REFERENCES

[1] BREDEHOEFT, J.D., PINDER, G.F., Mass transport in flowing ground water, Water Resour. Res. 9 (1973) 144.

[2] PINDER, G.F., COOPER, H.A., Jr., A numerical technique for calculating the transient position of the saltwater front, Water Resour. Res. 6 (1970) 875.

[3] ROBERTSON, J.B., BARRACLOUGH, J.T., "Radioactive and chemical waste transport in ground water at the National Reactor Testing Station, Idaho: 20-year case history and digital model", Proc. International Symposium on Underground Waste Management and Artificial Recharge, New Orleans, 26-30 Sep. 1973, American Association of Petroleum Geologists 1 (1973) 241.

[4] BREDEHOEFT, J.D., PINDER, G.F., Digital analysis of areal flow in multi-aquifer ground-water systems: A quasi three-dimensional model, Water Resour. Res. 6 (1970) 883.

[5] ROBERTSON, J.B., SCHOEN, R., BARRACLOUGH, J.T., The influence of liquid waste disposal on the geochemistry of water at the National Reactor Testing Station, Idaho: 1952-70, US Geol. Survey open-file report (1973).

[6] OSLOOND, J.H., Waste Disposal Data for the National Reactor Testing Station, USAEC Rep. IDO-12074 (1970).

[7] US ATOMIC ENERGY COMMISSION, NRTS radioactive management information for 1971 National Reactor Testing Station, USAEC Rep. IDO-10052 (1973).

[8] US ATOMIC ENERGY COMMISSION, NRTS Radioactive Waste Management Information for 1972, National Reactor Testing Station, USAEC Rep. IDO-10053 (1973).

[9] US ATOMIC ENERGY COMMISSION, National Reactor Testing Station Radioactive Waste Management Information, 1972 summary and record-to-date, USAEC Rep. IDO-10054 (1973).
[10] ROBERTSON, J.B., Digital modeling of radioactive and chemical waste transport in the Snake River Plain aquifer at the National Reactor Testing Station, Idaho, U.S. Geol. Survey open-file report (in press) (1974).
[11] RUBIN, J., JAMES, R.V., Dispersion-affected transport of reacting solutes in saturated porous media: Galerkin method, applied to equilibrium controlled exchange in unidirectional steady water flow, Water Resour. Res. 9 (1973) 1332.
[12] PINDER, G.F., A Galerkin-finite element simulation of ground water contamination on Long Island, New York, Water Resour. Res. 9 (1973) 1657.

DISCUSSION

A. ZUBER: How did you estimate the ^{90}Sr distribution coefficients?

J.B. ROBERTSON: We estimated them on the basis of mass balance calculations for the amount of waste injected in comparison with the amount apparent in the aquifer. The estimates were in good agreement with values obtained by extrapolation from laboratory measurements.

A. ZUBER: What values did you use for the different ions?

J.B. ROBERTSON: We used a uniform value of 3.0 (dimensionless) for the entire area modelled.

A. ZUBER: Is the distribution coefficient value constant along the aquifer body?

J.B. ROBERTSON: No doubt it varies spatially in the real aquifer, but we have no data on the variation. Distribution coefficients for other aquifers can be estimated from aquifer samples, or, even better, on the basis of small-scale tracer injection tests.

J.J. FRIED: The method of characteristics is difficult to apply and the calculation times are long. That being so, why did you use it?

J.B. ROBERTSON: Because it was the best method available at the time we started modelling. Incidentally, it is not as difficult to apply as many people think, and it has worked well with our problem.

J.J. FRIED: In your oral presentation you spoke of modifying the method. What modifications did you have in mind?

J.B. ROBERTSON: The method must be adapted to each individual problem. Such modifications were the only ones which I had in mind.

J.J. FRIED: You spoke of Galerkin and finite elements in your oral presentation. How will you allow for numerical dispersion?

J.B. ROBERTSON: I am not sufficiently acquainted with Galerkin-finite element methods to discuss the numerical dispersion problems involved. I do know, however, that these methods are being used sucessfully by such people as George Pinder and Jacob Rubin in the United States of America.

U. CHANDRA: What are the groundwater velocities encountered in the area?

J.B. ROBERTSON: On average some 3-4 m daily, with large local variations.

U. CHANDRA: Have you any data on ^{137}Cs migration compared with that of ^{90}Sr?

J.B. ROBERTSON: ^{137}Cs is strongly adsorbed in our aquifer, to the extent that no detectable amounts remain in solution. Consequently, migration is very slow and limited in area. We have not found any ^{137}Cs in the aqueous phase of the aquifer.

R.E. ISAACSON: I should like to make a comment in connection with Mr. Chandra's second question. Information on the migration of caesium in basaltic soils is available in the open literature, in reports issued by the Pacific Northwest Laboratories (operated by Battelle Northwest). Caesium migrates at about one tenth of the rate of strontium or about one hundredth of the rate of water.

CHAIRMEN OF SESSIONS

Session 1	D.B. SMITH	Atomic Energy Research Establishment, Harwell, Didcot, Berks, United Kingdom
Session 2	J. GUIZERIX	Centre d'études nucléaires de Grenoble, BP N° 35, Centre de tri, 38041 Grenoble, France
Session 3	J.R. GAT	Isotope Research Department, Weizmann Institute of Science, Rehovot, Israel
Session 4	F.J. PEARSON	US Geological Survey, National Center, Reston, Va. 22092, United States of America
Session 5	I. SAINZ ORTIZ	Secretaría de Recursos Hidráulicos, Mexico 1, DF, Mexico
Session 6	H.A. OESCHGER	35 Giacomettistrasse, 3000 Berne, Switzerland
Session 7	E. SOMER	Danish Isotope Centre, Skelbaekgade 2, 1717 Copenhagen V, Denmark
Session 8	V.T. DUBINCHUK	All-Union Research Institute for Hydrogeology and Engineering Geology, Moscow, USSR
Session 9	H. MOSER	Gesellschaft für Strahlen- und Umweltforschung mbH, Luisenstrasse 37, 8000 Munich 2, Federal Republic of Germany

SECRETARIAT

Scientific Secretary:	R. GONFIANTINI	Division of Research and Laboratories, IAEA
Administrative Secretary:	R. NAJAR	Division of External Relations, IAEA
Editor:	S.M. FREEMAN	Division of Publications, IAEA
Records Officer:	M. DAVIES	Division of Languages and Policy-Making Organs, IAEA

LIST OF PARTICIPANTS

ARGENTINA

Levin Lipsin, M.	Comisión Nacional de Energía Atómica, Facultad de Ciencias Naturales y Museo, Paseo del Bosque, La Plata

AUSTRALIA

Allison, G.B.	CSIRO Division of Soils, Private Bag No.1, P.O. Glen Osmond
Holmes, J.W.	Flinders University of South Australia, Bedford Park, SA 5042
Pettifer, G.R.	Bureau of Mineral Resources, P.O. Box 318, Canberra City, ACT 2601
Spragg, W.T.	Isotope Division, Australian Atomic Energy Commission Research Establishment, Private Mail Bag, Sutherland 01, NSW 2232

AUSTRIA

Bauer, F.	Speläologisches Institut, Hofburg, Bettlerstiege, 1010 Vienna
Buchtela, K.	Atominstitut der Österreichischen Hochschulen, Schüttelstr. 115, 1020 Vienna
Dohlhofer, H.	Bundesministerium für Land- und Forstwirtschaft, Stubenring 1, 1010 Vienna
Frantz, A.M.T.	Federal Institute of Hydrobiology, Kaisermühlen, Schiffmühlenstr. 120, 1050 Vienna
Frevert, E.	Österreichische Studiengesellschaft für Atomenergie mbH, Lenaug. 10, 1080 Vienna
Hacker, P.	Bundesversuchs- und Forschungsanstalt, Arsenal, G 1, 1030 Vienna

Heintschel, H.G.	Hygienisch-bakteriologische Untersuchungsanstalt der Stadt Wien, Feldgasse 9, 1080 Vienna
Kastanek, F.J.	University of Agriculture, Institute for Hydrology, Gregor Mendelstr. 33, 1180 Vienna
Klaghofer, E.	Bundesversuchsinstitut für Kulturtechnik und technische Bodenkunde, Ybbserstr. 18, 3252 Petzenkirchen
Krejsa, P.P.	Österreichische Studiengesellschaft fur Atomenergie mbH, Lenaug. 10, 1082 Vienna
Mairhofer, J.E.	Bundesversuchs- und Forschungsanstalt, Arsenal, Objekt 210, 1030 Vienna
Mayer, P.	Österreichische Studiengesellschaft für Atomenergie mbH, Lenaug. 10, 1082 Vienna
Niel, A.	Bundesministerium für Land- und Forstwirtschaft, Stubenring 1, 1010 Vienna
Nussbaumer, W.	Bundesversuchs- und Forschungsanstalt, Arsenal, Objekt 214, 1030 Vienna
Rainer, V.	Bundesversuchs- und Forschungsanstalt, Arsenal, 1030 Vienna
Rank, D.O.	Bundesversuchs- und Forschungsanstalt, Arsenal, 1030 Vienna
Rötzer, H.	Österreichische Studiengesellschaft für Atomenergie mbH, Lenaug. 10, 1082 Vienna
Sas-Hubicki, J.E.M.	Bundesanstalt für Wasserbiologie und Abwasserforschung, Schiffmühlenstr. 120, 1223 Vienna
Schimpf, H.	Hydrographisches Zentralbüro, Marxerg. 2, 1030 Vienna
Schleifer, H.O.	Bundesministerium für Land- und Forstwirtschaft, Abt. 10, Stubenring 1, 1010 Vienna
Schmidt, F.	Bundesministerium für Land- und Forstwirtschaft, Stubenring 1, 1010 Vienna

Wiederstein, F.X.	Hydrographisches Zentralbüro, Marxerg. 2, 1030 Vienna
Zellhofer, O.	Bundesministerium für Wissenschaft und Forschung, Währingerstr. 28, 1090 Vienna
Zojer, H.	Vereinigung für Hydrogeologische Forschungen, Rechbauerstr. 12, 8010 Graz

BELGIUM

Beken, A.M.L. van der	Vrije Universiteit Brussel, A. Buyllaan 105, 1050 Brussels
Constant, R.J.	Institut national des radioéléments, c/o CEN, Boeretang 200, 2400 Mol
Depoitier, J.	Institut national des radioéléments, c/o CEN, Boeretang 200, 2400 Mol
Gilot, E.E.	Université de Louvain, Laboratoire de chimie nucléaire, chemin du Cyclotron 2, 1348 Louvain-la-Neuve

BRAZIL

Salati, E.	Centro de Energía Nuclear na Aggricultura, P.O. Box 96, Piracicaba, S.P.

CANADA

Bentz, A.L.	Université Laval, Département des sols, Québec, Que. G1K 7P4
Brown, R.M.	Atomic Energy of Canada Ltd, Chalk River Nuclear Laboratories, Chalk River, Ontario K0J 1J0
Fritz, P.	Department of Earth Sciences, University of Waterloo, Waterloo, Ont.
Merritt, W.F.	Atomic Energy of Canada Ltd, Chalk River Nuclear Laboratories, Chalk River, Ontario K0J 1J0

Vonhof, J. A.	Inland Waters Directorate, Environmental Management Services, Environment Canada, 3303-33 St., N. W., Calgary, Alberta T2L 2A7

CHILE

Silva, C. A.	Comisión Chilena de Energía Nuclear, Salvador 943, Santiago

COLOMBIA

Múnera, H. A.	Instituto de Asuntos Nucleares, A. A. 8595, Bogotá, D.E.
Marulanda, T.	Permanent Mission of Colombia to the IAEA, Stadiong. 6-8, 1010 Vienna, Austria

CUBA

Arellano Acosta, Daniela M.	Grupo Hidráulico Nacional, Humboldt 106 esq., P. Veclado, Habana

CZECHOSLOVAK SOCIALIST REPUBLIC

Hulla, J.	Slovak Technical University, Faculty of Construction, Gottwaldovo nám. 52, 80000 Bratislava
Šilar, J.	Department of Hydrogeology and Engineering Geology, Faculty of Natural Sciences, Charles University, Albertov 6, Prague 2
Trýzna, P.	Laboratory of Applied Nuclear Physics, 43437 Most

DENMARK

Andersen, L. J.	Geological Survey of Denmark, 31 Thoravej, 2400 Copenhagen NV
Sevel, T.	Danish Isotope Centre, Skelbaekgade 2, 1717 Copenhagen V
Somer, E.	Danish Isotope Centre, Skelbaekgade 2, 1717 Copenhagen V

FINLAND

Kasi, S.S.H.	Helsinki University of Technology, 02150 Otaniemi
Kuoppamäki, R.J.	Reactor Laboratory, Technical Research Centre of Finland, 02150 Otaniemi
Salonen, P.O.	Reactor Laboratory, Technical Research Centre of Finland, 02150 Otaniemi
Soveri, J.H.	Hydrological Office, Vuorikatu 24, Helsinki 10

FRANCE

Bakalowicz, M.	Centre national de la recherche scientifique, Laboratoire souterrain, 09410 Moulis
Castany, G.	Service géologique national, B.P. 6009, 45018 Orléans Cédex
Conrad, G.	Laboratoire de géologie, Faculté des sciences, Université de Rouen, 76130 Mont-Saint-Aignan
Coppens, R.	Institut national polytechnique, Ecole nationale supérieure de géologie appliquée et de prospection minière, Centre de recherches radiogéologiques, B.P. 452, 54501 Nancy Cédex
Evin, J.	Laboratoire du radiocarbone, Département de géologie, Université de Lyon I, I.P.N., 43 bd. du 11 Novembre 1918, 69100 Villeurbanne
Fontes, J.Ch.	Laboratoire de géologie dynamique, Université de Paris VI, 4 pl. Jussieu, 75230 Paris Cédex 05
Fried, J.J.	Institut de mécanique des fluides, Université de Strasbourg, 2 rue Boussingault, 6700 Strasbourg
Gaillard, B.	CEA, Centre d'études nucléaires de Grenoble, B.P. 85, Centre de tri, 38041 Grenoble Cédex
Gaudet, J.P.	Institut de mécanique, B.P. 53, Centre de tri, 38041 Grenoble Cédex
Guizerix, J.	CEA, Centre d'études nucléaires de Grenoble, B.P. 85, Centre de tri, 38041 Grenoble Cédex

Jouzel, J.	CEA, Centre d'études nucléaires de Saclay, B.P. 2, 91190 Gif-sur-Yvette
Lerman, J.C.	Centre des faibles radioactivités, Laboratoire mixte CNRS-CEA, B.P. 1, 91190 Gif-sur-Yvette; Laboratoire de géologie dynamique, 4 pl. Jussieu, 75230 Paris Cédex 05
Létolle, R.	Laboratoire de géologie dynamique, Département des sciences de la terre, Université de Paris VI, 4 pl. Jussieu, 75230 Paris Cédex 05
Lévêque, P.Ch.	Laboratoire de radiogéologie et de mécanique des roches, Université de Bordeaux I, av. des Facultés, 33405 Talence
Mangin, A.	Centre national de la recherche scientifique, Laboratoire souterrain, 09410 Moulis
Maurin, Catherine	Laboratoire de radiogéologie et de mécanique des roches, Université de Bordeaux I, av. des Facultés, 33405 Talence
Molinari, J.	CEA, Centre d'études nucléaires de Grenoble, B.P. 85, Centre de tri, 38041 Grenoble Cédex
Peyrus, J.C.	CEA, Centre d'études nucléaires de Saclay, B.P. 2, 91190 Gif-sur-Yvette
Sarrot-Reynauld, J.A.P.	Laboratoire de géologie, Institut Dolomieu, rue Maurice Gignoux, 38000 Grenoble
Severac, J.	Laboratoire de radiogéologie et de mécanique des roches, Université de Bordeaux I, av. des Facultés, 33405 Talence
Téhel, J.F.	Institut de mécanique, B.P. 53, Centre de tri, 38041 Grenoble
Viguier, Cl.	Laboratoire de radiogéologie et de mécanique des roches, Université de Bordeaux I, av. des Facultés, 33405 Talence

GERMANY, FEDERAL REPUBLIC OF

Drost, W.	Gesellschaft für Strahlen- und Unmweltforschung mbH, Institut für Radiohydrometrie, Luisenstr. 37, 8000 Munich 2
Faber, E.	Bundesanstalt für Bodenforschung, Stilleweg 2, 3000 Hanover

Jakubick, A.T.	Kernforschungszentrum, Postfach 3640, 7500 Karlsruhe
Kussmaul, H.	Bundesgesundheitsamt, Auf'm Hennekamp 70, 4000 Düsseldorf
Lieser, K.H.	Technische Hochschule, Hochschulstr., 6100 Darmstadt
Matthess, G.	Geologisch-Palaeontologisches Institut, Universität Kiel, Olshausenstr. 40/60, 2300 Kiel
Möller, P.	Hahn-Meitner Institut für Kernforschung GmbH, Glienicker Str. 100, 1000 Berlin 39
Moser, H.	Gesellschaft für Strahlen- und Umweltforschung mbH, Institut für Radiohydrometrie, Luisenstr. 37, 8000 Munich 2
Mundschenk, H.	Bundesanstalt für Gewässerkunde, Kaiserin-Augusta-Anlage 15, 5400 Koblenz
Neumaier, F.	Gesellschaft für Strahlen- und Umweltforschung mbH, Institut für Radiohydrometrie, Luisenstr. 37, 8000 Munich 2
Rauert, W.	Gesellschaft für Strahlen- und Umweltforschung mbH, Institut für Radiohydrometrie, Luisenstr. 37, 8000 Munich 2
Roether, W.	Zweites Physikalisches Institut der Universität Heidelberg, Philosophenweg 12, 6900 Heidelberg
Stahl, W.	Bundesanstalt für Bodenforschung, Stilleweg 2, 3000 Hanover
Stephan, H.	Institut für Radiochemie, FH Nürnberg, Kesslerstr. 40, 8500 Nuremberg
Stichler, W.	Gesellschaft für Strahlen- und Umweltforschung mbH, Institut für Radiohydrometrie, Luisenstr. 37, 8000 Munich 2

GHANA

Quist, L.G.	Water Resources Research Unit, Box M. 32, Accra

GREECE

Dimitroulas, C.	N.R.C. Demokritos, Aghia Paraskevi, Attikis, Athens
Leontiadis, J.	N.R.C. Democritos, Aghia Paraskevi, Attikis, Athens

HUNGARY

Csürös, M.	Institute of Isotopes, Konkoly Th. u., Budapest XII
Déak, J.	Research Institute for Water Resources Development, Rákóczi út 41, 1088 Budapest
Papp, B.	Research Institute for Water Resources Development, Rákóczi út 41, 1088 Budapest

INDIA

Chandra, U.	Bhabha Atomic Research Centre, Bombay 400085

IRAN

Movahhed, M.A.	Centre of Research and Laboratories, Ministry of Water and Power, Varzesh Ave., Tehran

ISRAEL

Gat, J.R.	Isotope Research Department, Weizmann Institute of Science, Rehovot
Mazor, E.	Isotope Department, Weizmann Institute of Science, Rehovot
Wakshal, E.	Groundwater Research Centre, School of Applied Science and Technology, The Hebrew University of Jerusalem, Jerusalem

ITALY

Bertolami, G.	Istituto di Geologia, 5, Via Accademia delle Scienze, Turin
Crema, G.	ENI Group (Idrotecnico), 61047 S. Lorenzo in Campo (Pesaro)

Dall'Aglio, M.	Comitato Nazionale Energia Nucleare, C.S.N. Casaccia, 00060 S. Maria di Galeria (Roma)
Ferrara, G.C.	ENEL – Centro Ricerca Geotermica, Piazza B. Sassoferrato 14, Pisa
Magri, G.	Comitato Nazionale Energia Nucleare, Traversa 199 Re David 55, 70125 Bari
Noto, P.	Istituto Internazionale Ricerche Geotermiche, C.N.R., Lungarno Pacinotti 55, Pisa
Nuti, S.	Istituto Internazionale Ricerche Geotermiche, C.N.R., Lungarno Pacinotti 55, Pisa
Panichi, C.	Istituto Internazionale Ricerche Geotermiche, C.N.R., Lungarno Pacinotti 55, Pisa
Tazioli, G.S.	Istituto di Geologia Applicata e Geotecnica, Università di Bari, Via Re David 200, 70125 Bari
Zuppi, G.M.	Laboratoire de géologie dynamique, Département des sciences de la terre., Université de Paris VI, 4 pl. Jussieu, 75230 Paris Cédex 05, France

LIBYAN ARAB REPUBLIC

Abufila, T.M.	General Water Authority, Eshatte Street, Tripoli

MEXICO

Gálvez Cruz, L.	Instituto Nacional de Energía Nuclear, Insurgentes Sur 1079, 3 Piso, México 18, D.F.
Gaona Vizcayno, S.	Instituto de Física, UNAM, México 20-364
Latorre Díez, C.	Secretaría de Recursos Hidráulicos, Grupo de Física, Versalles 19, 4 Piso, México, D.F.
Ortiz Aguilar, J.L.	Secretaría de Recursos Hidráulicos, Sierra Gorda 23, México 10, D.F.
Sainz Ortiz, I.	Secretaría de Recursos Hidráulicos, Reforma 69, México 1, D.F.

MOROCCO

Bentayeb, A.	Direction de l'hydraulique, B.P. 535, Rabat-Chellah
Guessab, D.	Direction de l'hydraulique, B.P. 535, Rabat-Chellah

NETHERLANDS

Groeneveld, D.J.	Natuurkundig Laboratorium, Westersingel 34, Groningen
Mook, W.G.	Physics Laboratory, University of Groningen, Westersingel 34, Groningen
Romijn, E.	Government Institute for Water Supply, Parkweg 13, The Hague
Vermeulen, H.R.	Delft University of Technology, Civil Dept., 1 Stevinweg, Delft
Wart, R. van der	Scientific Council for Nuclear Affairs, Duinweg 24, P.O. Box 5086, The Hague

NORWAY

Ellingsen, K.	National Institute of Public Health, Postuttale, Oslo 1
Englund, J.-O.	Agricultural University of Norway, 1432 Ås-NLH
Haagensen, U.H.	Institutt for Atomenergi, P.O. Box 40, 2007 Kjeller
Kirkhusmo, L.A.	Oscars Gt. 63, Oslo 2
Østmo, S.R.	Norges geologiske undersökelse, Eilert Sundtsgt. 32, Oslo 2
Steenberg, K.	Isotope Laboratory, Agricultural University, 1432 Ås-NLH

PHILIPPINES

Kagahastian, L.D.	Bureau of Public Works, Port Area, Manila

POLAND

Czauderna, K.	Hydrological Enterprise Hydrokop, ul. Łokietka 19, Cracow

Dowgiałło, J.	Institute of Geological Sciences, Polish Academy of Sciences, Zwirki 1 Wigury 93, Warsaw
Florkowski, T.	Institute of Nuclear Techniques, Academy of Mining and Metallurgy, Al. Mickiewicza 30, Cracow
Lenda, A.M.	Institute of Nuclear Techniques, Academy of Mining and Metallurgy, Al. Mickiewicza 30, Cracow
Różkowski, A.	Institute of Geology, Bialego 5, 41-200 Sosnowiec
Smietanski, Z.	Academy of Mining and Metallurgy, Cracow
Zuber, A.	Institute of Nuclear Physics, Radzikowskiego 132, Cracow

SAUDI ARABIA

Aldalooj, A.E.	Hydrology Division, Ministry of Agriculture and Water, Riyadh
Dinçer, T.	c/o FAO-UNDP, P.O. Box 558, Riyadh
Javed, A.R.K.	Geology Division, Water Resources Development Department, Ministry of Agriculture and Water, Riyadh
Noory, M.	Geology Division, Water Resources Development Department, Ministry of Agriculture and Water, Riyadh

SOUTH AFRICA

Botha, B.J.	University of the Orange Free State, Bloemfontein
Henzen, M.R.	Water Research Commission, P.O. Box 824, Pretoria
Schutte, J.M.	Hydrological Research Institute, Dept. of Water Affairs, Private Bag X 313, 0001 Pretoria
Sellschop, J.P.F.	Nuclear Physics Research Unit, University of the Witwatersrand, Johannesburg
Verhagen, B.T.	Nuclear Physics Research Unit, University of the Witwatersrand, Johannesburg
van Wyk, W.L.	Department of Water Affairs, Private Bag X 313, 0001 Pretoria

SPAIN

Baonza del Prado, E.	Ministry of Public Works, Laboratory of Isotope Hydrology, Paseo Bajo Virgen del Puerto 3, Madrid 5
Escolano Bueno, A.	Ministerio de Obras Públicas, Comisaría Aguas, Po. Reding-6, Malaga
Custodio Gimena, E.	Water Agency of the Eastern Pyrenees, calle Beethoven 15, 3 Barcelona 3
Plata Bedmar, A.	Ministry of Public Works, Paseo Bajo Virgen del Puerto 3, Madrid 5

SUDAN

Iskander, W.	Rural Water and Development Corporation, P.O. Box 381, Khartoum

SWEDEN

Carlsson, L.F.	Department of Water Supply and Sewerage, Chalmers University of Technology, Fack 40220 Gothenburg 5
Nordberg, L.O.	Geological Survey of Sweden, Fack 10405 Stockholm
Persson, G.	Geological Survey of Sweden, Fack 10405 Stockholm

SWITZERLAND

Emmenegger, C.	Office fédéral de l'économie hydraulique, Bollwerk 27, 3001 Berne
Gugelmann, A.A.	Physikalisches Institut, Sidlerstr. 5, 3012 Berne
Hardy, E.E.	Nordostschweizerische Kraftwerke, Baden
Imboden, D.	Swiss Federal Institute for Water Resources and Water Pollution Control, Überlandstr. 133, 8600 Dübendorf
Loosli, H.H.	Physikalisches Institut, Sidlerstr. 5, 3012 Berne
Martinec, J.	Federal Institute for Snow and Avalanche Research, 7260 Weissfluhjoch/Davos
Oeschger, H.	35 Giacomettistr., 3000 Berne
Schotterer, U.	University of Berne, Sidlerstr. 5, 3012 Berne

Schweizer, H.U.	Eidgenössisches Amt für Umweltschutz, Monbijoustr. 8, 3000 Berne
Siegenthaler, U.	Physikalisches Institut, Sidlerstr. 5, 3012 Berne
Wiest, W.	University of Berne, Sidlerstr. 5, 3012 Berne

USSR

Dimaksyan, A.M.	State Hydrological Institute, Leningrad
Dubinchuk, V.T.	All-Union Research Institute for Hydrogeology and Engineering Geology, Moscow

UNITED KINGDOM

Edmunds, W.M.	Institute of Geological Sciences, Exhibition Rd., South Kensington, London, S.W. 7
Smith, D.B.	AERE, Harwell, Didcot, Berks.

UNITED STATES OF AMERICA

Bradley, E.	US Geological Survey, National Center, Reston, Va. 22092
Cowart, J.B.	Department of Geology, Florida State University, Tallahassee, Fla. 32306
Davis, G.H.	US Geological Survey, National Center, Reston, Va. 22092
Deines, P.	Mineral Sciences Bldg, Room 19, Department of Geosciences, University Park, Pa. 16802
Hufen, T.H.	Water Resources Research Center, Holmes Hall, University of Hawaii, Honolulu, Hawaii 96822
Isaacson, R.E.	Atlantic Richfield Hanford Co., P.O. Box 250, Richland, Wash. 99332
Pearson, F.J.	US Geological Survey, National Center, Reston, Va. 22092
Rightmire, C.T.	US Geological Survey, National Center, Reston, Va. 22092
Robertson, J.B.	US Geological Survey, P.O. Box 2230, Idaho Falls, Idaho 83401

Swarzenski, W.V.	US Geological Survey, W.R.D., Washington, D.C.
Winograd, I.J.	US Geological Survey, National Center, Reston, Va. 22092

YUGOSLAVIA

Anovski, T.	Center for Application of Radioisotopes in Science and Industry, 91000 Skopje
Kirkov, P.	Center for Application of Radioisotopes in Science and Industry, 91000 Skopje
Pirš, M.	Institute J. Stefan, Jamova 39, Ljubljana
Tolev, M.	Center for Application of Radioisotopes in Science and Industry, 91000 Skopje

ZAIRE

Lumu, B.M.	Commissariat des sciences nucléaires, Centre régional d'études nucléaires, B.P. 868, Kinshasa 11

ORGANIZATIONS

ASSOCIATION INTERNATIONALE DES HYDROGEOLOGUES (AIH)

Castany, G.	BRGM, 74 rue de la Fédération, 75739 Paris Cédex 15

FOOD AND AGRICULTURE ORGANIZATION OF THE UNITED NATIONS (FAO)

Barrada, Y.	c/o IAEA
Chapond, G.	B.P. 3216, Beirut, Lebanon
Hachache, A.	B.P. 3216, Beirut, Lebanon
Thomas, R.B.	FAO, Viale delle Terme di Caracalla, 00100 Rome

FORUM ATOMIQUE EUROPEEN (FORATOM)

Mayer, P.	Österreichische Studiengesellschaft für Atomenergie, Lenaug. 10, 1082 Vienna, Austria (see also under Austria)

INTERNATIONAL ATOMIC ENERGY AGENCY (IAEA)

Payne, B.R.	Division of Research and Laboratories, IAEA, P.O. Box 590, 1011 Vienna, Austria
Przewłocki, K.	Division of Research and Laboratories, IAEA, P.O. Box 590, 1011 Vienna, Austria
Sauzay, G.	c/o CEN de Scalay, DCA-SARR, B.P. 2, 91190 Gif-sur-Yvette, France
Saxena, R.K.	c/o Div. of Hydrology, Dept. of Physical Geography, University of Uppsala, Box 554, 751 22 Uppsala, Sweden
Taylor, C.B.	Division of Research and Laboratories, IAEA, P.O. Box 590, 1011 Vienna, Austria
Yurtsever, Y.	Division of Research and Laboratories, IAEA, P.O. Box 590, 1011 Vienna, Austria

UNITED NATIONS EDUCATIONAL, SCIENTIFIC AND CULTURAL ORGANIZATION (UNESCO)

Gilbrich, W.H.	Unesco, Office of Hydrology, pl. de Fontenoy, 75 Paris

AUTHOR INDEX

(including participants in discussions)

Roman numbers are volume numbers. Arabic numbers underlined indicate the first page of a paper by an author. Other Arabic numbers denote the page numbers of discussion comments. Literature references are not indexed.

Airey, P.L.: I 115
Allison, G.B.: I 19, 57, 70, 71, 95, 155, 314; II 67, 449
Alquier, M.: II 377
Andersen, L.J.: I 3, 18, 19, 20, 55
Anovski, T.: I 465
Atakan, Y.: I 21
Aust, H.: I 317
Babushkin, V.D.: I 399
Back, W.: II 191
Bentz, A.L.: I 114; II 339, 375, 424
Bradley, E.: I 155, 396
Bredenkamp, D.B.: I 73
Brouwn, A.E.: I 145
Brown, L.J.: I 169
Brownell, L.E.: I 97
Buddemeier, R.W.: II 111
Calf, G.E.: I 115
Castany, G.: I 243, 257, 258
Celati, R.: II 3
Chandra, U.: I 18; II 254, 340, 477
Chapond, G.: I 224, 338
Conrad, G.: I 227, 240, 241; II 126, 220
Coppens, R.: II 149
Corda, R.: II 405
Corompt, P.: II 377, 405
Cotecchia, V.: I 445
Cowart, J.B.: II 131, 149
Crampon, N.: II 405
Crema, G.: II 220
Custodio Gimena, E.: II 91, 311
Czauderna, K.: II 295
Davis, G.H.: I 240, 241, 338; II 28
Deák, J.: I 157, 166
Derekoy, A.M.: I 293
Dinçer, T.M.: I 55, 71, 72, 143, 155, 241, 293, 315, 363, 479; II 109
Dounas, A.: I 317
Dowgiałło, J.: I 166, 201, 240, 337, 338, 429, 462; II 68, 206
Drimmie, R.J.: I 379
Drost, W.: II 241, 253, 254
Dubinchuk, V.T.: I 257, 399, 429, 501; II 46, 126, 359, 375, 450
Du Toit, G.J.: I 73
Edmunds, W.M.: I 70
Farlekas, G.M.: II 69
Ferronskij, V.I.: I 285
Florkowski, T.: I 188, 201; II 46, 189
Fontes, J.Ch.: I 143, 154, 227, 241, 341, 361, 398, 442; II 45, 92
Fried, J.J.: II 477
Fritz, P.: I 70, 154, 155, 224, 257, 315, 379, 396, 397, 398; II 45, 91, 207, 220
Gaillard, B.: II 377, 405
Gaona Vizcayno, S.: I 143, 443; II 253, 254, 375, 421
Gat, J.R.: I 43, 70, 283, 315, 316; II 51, 59, 68, 177
Gaudet, J.P.: II 312, 340, 422, 423, 424
Goncharov, V.S.: II 359
Gonfiantini, R.: I 227, 241, 293, 314, 315
Groeneveld, D.J.: I 145

Gros, J.Cl.: II 223
Gugelmann, A.: II 179
Guizerix, J.: II 377, 405, 421, 422, 424
Hanshaw, B.B.: II 191
Hartley, P.E.: I 115
Henzen, M.R.: I 95
Holmes, J.W.: I 19, 95, 166, 167, 282; II 340
Hufen, T.H.: II 111, 126
Hughes, M.W.: I 57
Hutton, L.G.: I 203
Isaacson, R.E.: I 97, 114, 224; II 108, 254, 478
Isaev, N.V.: I 285
Javed, A.R.K.: I 363
Kačurkov, D.: I 465
Karasev, B.V.: I 399
Kashkovskij, G.N.: I 399
Kasi, S.S.H.: II 294
Kirkov, P.: I 18, 125, 166, 224, 257, 442, 465, 478, 479
Klotz, D.: II 341
Kolesnichenko, Z.G.: II 359
Kreft, A.: II 295
Kuptsov, V.M.: I 399
Lapteva, O.F.: II 359
Lau, L.S.: II 111
Lenda, A.: II 295, 311, 312
Lerman, J.C.: I 224, 225, 258, 398; II 189
Létolle, R.R.: I 341, 461; II 45, 209, 219, 220
Lévêque, P.Ch.: II 176, 223, 238
Levin Lipsin, M.: I 462, 463; II 46
Loosli, H.: II 179
Lumu, B.M.: I 126
Magri, G.: I 445
Marce, A.: I 243
Margat, J.: I 243
Margrita, R.: II 377, 405
Mariotti, A.: II 209
Martinec, J.: I 129, 142, 143; II 449
Matthess, G.: I 21
Maurin, Catherine: II 223
Mazor, E.: I 71, 203, 224, 339; II 29, 45, 46, 190, 206, 220
Mendes Campos, M.: I 259
Menezes Leal, J.: I 259
Modig, S.: II 313
Molinari, J.P.A.: I 155, 201, 361; II 190, 405
Mook, W.G.: I 18, 145, 154, 155, 201; II 46, 68, 108, 219
Moser, H.: II 274, 341, 355, 375
Moussu, H.: I 243
Múnera, H.A.: II 255, 274, 275, 355, 421
Münnich, K.-O.: I 21
Nechaev, V.I.: I 399
Negreanu, E.: II 29
Nelson, R.W.: I 97
Neumaier, F.: II 241
Noory, M.: I 363
Nordberg, L.O.: II 313, 339, 340
Noto, P.: II 3
Nuti, S.: I 363
Oeschger, H.: I 129, 397, 398, 429; II 45, 91, 179, 189, 190
Olivier, D.: II 405
Osmond, J.K.: II 131
Panichi, C.: II 3, 28
Payne, B.R.: I 71, 193, 201, 227, 338, 396, 443; II 190
Pearson, F.J.: II 46, 92, 95, 108, 109, 191, 207
Persson, G.N.: I 45, 55, 56
Plata Bedmar, A.: I 282; II 59, 67, 253, 274
Polyakov, V.A.: I 285, 399
Przewłocki, K.: I 429, 481; II 148, 176, 425, 448, 449, 450
Quist, L.G.: I 224, 396
Rauert, W.: I 431, 442, 443
Render, F.W.: I 379
Rightmire, C.T.: II 191, 206, 207
Robertson, J.B.: I 397; II 355, 421, 451, 477
Robins, N.S.: I 203
Roether, W.: I 21, 43
Roetman, E.L.: I 97
Roman, D.: I 115
Różkowski, A.: I 282, 396, 481, 501, 502
Rye, R.O.: II 191
Sainz Ortiz, I.: I 70, 142, 201, 202; II 109, 312
Salati, E.: I 259, 282
Sarrot-Reynauld, J.A.P.: I 361; II 149, 207
Sauzay, G.: I 227; II 58, 61, 67, 68, 109, 294

Schotterer, U.: II 179, 190
Schutte, J.M.: I 73, 95
Seletskij, Yu.B.: I 285, 399
Sellschop, J.P.F.: I 203
Sevel, T.: I 3, 19, 20
Sévérac, J.: II 223
Siegenthaler, U.: I 20, 129, 143; II 68, 179
Šilar, J.: I 56, 339, 501; II 126
Smietanski, Z.: I 429
Smith, D.B.: I 18, 153, 442; II 46, 294
Spragg, W.T.: I 115, 125, 126
Squarci, P.: II 3
Stahl, W.: I 317, 338, 339, 501
Stichler, W.: I 431
Swarzenki, W.V.: II 95
Taffi, L.: II 3
Taylor, C.B.: I 43, 126, 169, 188, 189, 397; II 59
Tazioli, G.S.: I 445, 461, 462, 463; II 238
Thomas, R.B.: I 70; II 108, 176, 177
Tolev, M.: I 465
Tongiorgi, E.: I 363, II 3
Turek, B.: II 295
Van Ganswijk, A.J.: I 145
Verhagen, B.T.: I 56, 114, 154, 203, 315, 442, 462; II 29, 59, 189
Viguier, Cl.: II 223
Vuillaume, Y.: I 243
Wakshal, E.: II 151, 176, 177
Wiest, W.: II 179
Winograd, I.J.: I 397; II 69, 91, 92, 93, 312
Yakubovskij, A.V.: I 285
Yaron, F.: II 151
Yurtsever, Y.: I 193, 478; II 425, 449, 450
Zuber, A.: I 19, 143, 201, 397; II 277, 294, 295, 312, 448, 477
Zuppi, G.M.: I 341

HOW TO ORDER IAEA PUBLICATIONS

Exclusive sales agents for IAEA publications, to whom all orders and inquiries should be addressed, have been appointed in the following countries:

UNITED KINGDOM	Her Majesty's Stationery Office, P.O. Box 569, London SE 1 9NH
UNITED STATES OF AMERICA	UNIPUB, Inc., P.O. Box 433, Murray Hill Station, New York, N.Y. 10016

In the following countries IAEA publications may be purchased from the sales agents or booksellers listed or through your major local booksellers. Payment can be made in local currency or with UNESCO coupons.

ARGENTINA	Comisión Nacional de Energía Atómica, Avenida del Libertador 8250, Buenos Aires
AUSTRALIA	Hunter Publications, 58 A Gipps Street, Collingwood, Victoria 3066
BELGIUM	Office International de Librairie, 30, avenue Marnix, B-1050 Brussels
CANADA	Information Canada, 171 Slater Street, Ottawa, Ont. K 1 A OS 9
C.S.S.R.	S.N.T.L., Spálená 51, CS-11000 Prague Alfa, Publishers, Hurbanovo námestie 6, CS-80000 Bratislava
FRANCE	Office International de Documentation et Librairie, 48, rue Gay-Lussac, F-75005 Paris
HUNGARY	Kultura, Hungarian Trading Company for Books and Newspapers, P.O. Box 149, H-1011 Budapest 62
INDIA	Oxford Book and Stationery Comp., 17, Park Street, Calcutta 16
ISRAEL	Heiliger and Co., 3, Nathan Strauss Str., Jerusalem
ITALY	Libreria Scientifica, Dott. de Biasio Lucio "aeiou", Via Meravigli 16, I-20123 Milan
JAPAN	Maruzen Company, Ltd., P.O.Box 5050, 100-31 Tokyo International
NETHERLANDS	Marinus Nijhoff N.V., Lange Voorhout 9-11, P.O. Box 269, The Hague
PAKISTAN	Mirza Book Agency, 65, The Mall, P.O.Box 729, Lahore-3
POLAND	Ars Polona, Centrala Handlu Zagranicznego, Krakowskie Przedmiescie 7, Warsaw
ROMANIA	Cartimex, 3-5 13 Decembrie Street, P.O.Box 134-135, Bucarest
SOUTH AFRICA	Van Schaik's Bookstore, P.O.Box 724, Pretoria Universitas Books (Pty) Ltd., P.O.Box 1557, Pretoria
SPAIN	Nautrónica, S.A., Pérez Ayuso 16, Madrid-2
SWEDEN	C.E. Fritzes Kungl. Hovbokhandel, Fredsgatan 2, S-10307 Stockholm
U.S.S.R.	Mezhdunarodnaya Kniga, Smolenskaya-Sennaya 32-34, Moscow G-200
YUGOSLAVIA	Jugoslovenska Knjiga, Terazije 27, YU-11000 Belgrade

Orders from countries where sales agents have not yet been appointed and requests for information should be addressed directly to:

Publishing Section,
International Atomic Energy Agency,
Kärntner Ring 11, P.O.Box 590, A-1011 Vienna, Austria

74- 06170

INTERNATIONAL
ATOMIC ENERGY AGENCY
VIENNA, 1974

PRICE: US $24.00
Austrian Schillings 440,-
(£10.00; F.Fr. 118,-; DM 61,-)

SUBJECT GROUP: IV
Chemistry, Geology and Raw Materials/
Hydrology